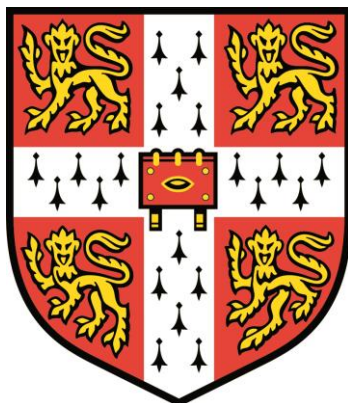**UNIVERSITY OF CAMBRIDGE**
Department of Chemistry

Multivalent Supramolecular Systems

by

Petr Motloch

Jesus College

This dissertation is submitted for the degree of Doctor of Philosophy.

September 2019

to my parents

for all their love and support

Declaration

This dissertation is the result of my own work and includes nothing which is the outcome of work done in collaboration except as declared in the Preface and specified in the text.

It is not substantially the same as any that I have submitted, or, is being concurrently submitted for a degree or diploma or other qualification at the University of Cambridge or any other University or similar institution except as declared in the Preface and specified in the text. I further state that no substantial part of my dissertation has already been submitted, or, is being concurrently submitted for any such degree, diploma or other qualification at the University of Cambridge or any other University or similar institution except as declared in the Preface and specified in the text.

It does not exceed the prescribed word limit for the relevant Degree Committee.

Petr Motloch

Multivalent Supramolecular Systems

Petr Motloch

Nature uses multivalency as one of the most important governing principles to control selective molecular recognition and assembly. By combining a large number of weak interactions, it is possible to obtain high affinity, selective and reversible non-covalent binding processes. Multivalency has also become an important tool in the design of synthetic molecular systems. The result of multiple binding events is not just a simple sum of individual contributions due to cooperative interactions between binding sites.

The main part of this thesis deals with the study of chelate cooperativity in multivalent supramolecular systems. Firstly, a well-known H-bonded rosette system was revisited and the effective molarity was determined experimentally by ^{1}H NMR titrations to be around 2 M, which is a high chelate cooperativity compared to other supramolecular systems. Moreover, the concept of peripheral crowding in solution was revisited, since rosettes based on less bulky pyrimidines showed higher stabilities and effective molarities than the rosettes based on bulky pyrimidines.

The following two chapters deal with efforts towards a supramolecular system inside a porphyrin nanoring. The porphyrin nanoring shows the highest value of effective molarity reported in the literature and is, therefore, a great system to study the cooperative behaviour when a covalent ligand is replaced with a supramolecular system. The first studied system was based on small molecules containing simple hydrogen-bond acceptors and donors. Unfortunately, solubility issues led to the termination of the project. The second system used the hydrogen-bonded rosette motif. A number of different pyridine-pyrimidine and pyridine-barbiturate ligands were synthesised and their assembly inside the porphyrin nanoring was studied in detail by UV-vis-NIR experiments. The effective molarities for the sequential binding of the rosette systems to 6-ring were determined to range from 0.23 to 3.7 M, which is significantly lower compared to the system that utilised a covalent hexadentate ligand (126 M).

The final part of the thesis introduces a new class of hybrid hydrogen-bonded/metal-coordinated cages based on the rosette motif. These complexes are a rare example of architectures where both hydrogen-bonding and metal-coordination form the crucial part of the topology of the complex since if either is removed, the architecture changes drastically.

Contents

List of abbreviations

Ac	acetyl
ACN	acetonitrile
AIBN	azobisisobutylnitrile
br	broad
CCDC	Cambridge Crystallographic Data Centre
CPME	cyclopentyl methyl ether
d	doublet
DBA	dibenzylideneacetone
DCE	1,2-dichloroethane
DBU	1,8-diazabicyclo[5.4.0]undec-7-ene
dd	doublet of doublets
DDQ	dichlorodicyanobenzoquinone
DIPA	disopropylamine
DIPEA	diisopropylethylamine
DCM	dimethyl choride
DMF	dimethyl formamide
DMSO	dimethyl sulfoxide
DOSY	diffusion ordered spectroscopy
EA	elemental analysis
EM	effective molarity
Et	ethyl
ESI	electrospray ionisation
FT-IR	Fourier transform infrared spectroscopy
GPC	gel permeation chromatography
HPLC	high-performance liquid chromatography
HR-MS	high-resolution mass spectrometry
*i*Bu	*iso*-butyl
*i*Pr	*iso*-propyl
J	coupling constant
LCMS	liquid chromatography coupled with mass spectrometry
m	multiplet
M	molecule

MALDI (MS)	matrix-assisted laser desorption/ionisation (mass spectrometry)
Me	methyl
MP	melting point
Ms	mesyl
MTBE	methyl *tert*-butyl ether
MW	microwave
NBS	*N*-bromosuccinimide
n-Bu	*n*-butyl
NMR	nuclear magnetic resonance
n-Hex	*n*-hexyl
NOE	nuclear Overhauser effect
NOESY	nuclear Overhauser effect spectroscopy
obs	observed
Ph	phenyl
pred	predicted
PTFE	polytetrafluorethylene
Py	pyridine
s	singlet
S	solvent
SEC	size-exclusion chromatography
t	triplet
TEBAC	benzyltriethylammonium chloride
*t*Bu	*tert*-butyl
TBAF	tetra-*n*-butylammonium fluoride
TFA	trifluoroacetic acid
THF	tetrahydrofuran
THS	tri(*n*-hexyl)silyl
TMEDA	tetramethylethylenediamine
urotropine	hexamethylenetetramine
UV-vis-NIR	ultra-violet/visible/near infra-red
VPO	vapor pressure osmometry
Xantphos	4,5-bis(diphenylphosphino)-9,9-dimethylxanthene
Y	J. Young valve

"two plus two equals five"[‡]

George Orwell: 1984

I

Introduction

This thesis deals with several topics and thus they will be introduced separately. The first part of the introduction describes multivalent systems and different types of cooperativity and its quantification. The second part deals with porphyrin nanorings, followed by a section that discusses a hydrogen-bonded rosette motif and the last part introduces different molecular containers.

1.1. Multivalency, cooperativity and effective molarity

1.1.1. General

Nature uses multivalency as one of the most important governing principles to control selective molecular recognition and assembly. By combining a large number of weak interactions, it is possible to obtain high affinity, selective and reversible non-covalent binding processes. Multivalency has also become an important tool in the design of synthetic molecular systems.[1-3] The result of multiple binding events is not just a simple sum of individual contributions due to cooperative interactions between binding sites.[4,5] Two types of cooperativity can be identified in multivalent systems: allosteric and chelate cooperativity. Allosteric cooperativity relates to a change in the intrinsic interaction properties of one binding site as a consequence of an intermolecular interaction at another nearby binding site. Chelate cooperativity relates to an increase in binding affinity due to the formation of multiple interactions between two molecules compared with simple monovalent interactions.[6] The term "chelate" was first used by Morgan and Drew in 1920 to describe the binding of a divalent ligand in coordination complexes.[7] The chelate effect describes the increased stability observed for complexes formed with multivalent ligands compared with complexes formed with monodentate ligands. Although the term chelate has its origins in the field of coordination chemistry, it is generally used to describe cooperative multivalent binding in different areas of chemistry. Chelate cooperativity is quantified by the effective molarity. The text below describes its origins as well as shows its application in supramolecular chemistry.

It has been known empirically for a long time that intramolecular reactions are usually faster than intermolecular reactions. In 1934, Stoll proposed that the cyclisation constant (C) defined in Equation 1.1 could be used to quantify this phenomenon.[8] In the same year, Kuhn suggested that a theoretical parameter C_{eff} could be used to predict the rate constant for an

intramolecular reaction from the rate constant k_{inter} for an intermolecular reaction using the same relationship.[9]

$$C = \frac{k_{intra}}{k_{inter}} \tag{1.1}$$

where k_{intra} is the rate constant for the intramolecular reaction (cyclisation) and k_{inter} is the rate constant for the bimolecular reaction (polymerisation).

The constant C has units of concentration and denotes the concentration at which the intramolecular and intermolecular reactions have the same rate. In the 1970s, the term effective molarity (EM) was widely adopted to describe this parameter and to characterise the rate enhancements observed for intramolecular reactions.[10-12] The effective molarity defined by Equation 1.1 is a kinetic EM, because it is based on the ratio of two reaction rates, but it is possible to define a thermodynamic EM in the same way, if equilibrium constants are substituted for rate constants (Equation 1.2).

$$EM = \frac{K_{intra}}{K_{inter}} \approx \frac{K_{intra}}{K_{ref}} \tag{1.2}$$

where K_{inter} is the equilibrium constant for formation of an intermolecular bond, K_{intra} is the equilibrium constant for formation of an intermolecular bond, and K_{ref} is the equilibrium constant for formation of an intermolecular bond in a closely related reference system.

The application of the EM concept to supramolecular complexes is illustrated in Figure 1.a. The first A•B interaction is an intermolecular process associated with an equilibrium constant K_{inter} leading to the singly bound open complex *o*-AA•BB. This intermediate can either cyclise *via* an intramolecular process to form the doubly bound closed complex *c*-AA•BB with an equilibrium constant K_{intra}, or it can form higher order complexes *via* intermolecular binding processes. In most cases, K_{inter} cannot be measured directly, and the experimental parameter that is commonly reported is the global equilibrium constant K_f for assembly of the closed complex *c*-AA•BB from AA and BB (Figure 1.b). Thus a different approach is required to determine K_{inter}. Reference systems that form monovalent A•B interactions are commonly used to measure K_{ref} (Figure 1.c), and this parameter is assumed to be equivalent to K_{inter} in Equation 1.2. However, it is clearly important that an appropriate reference system is used and that any contributions from allosteric cooperativity in the multivalent system can be quantified.[6] The effective molarity for the system shown in Figure 1.1 is then given by Equation 1.3.
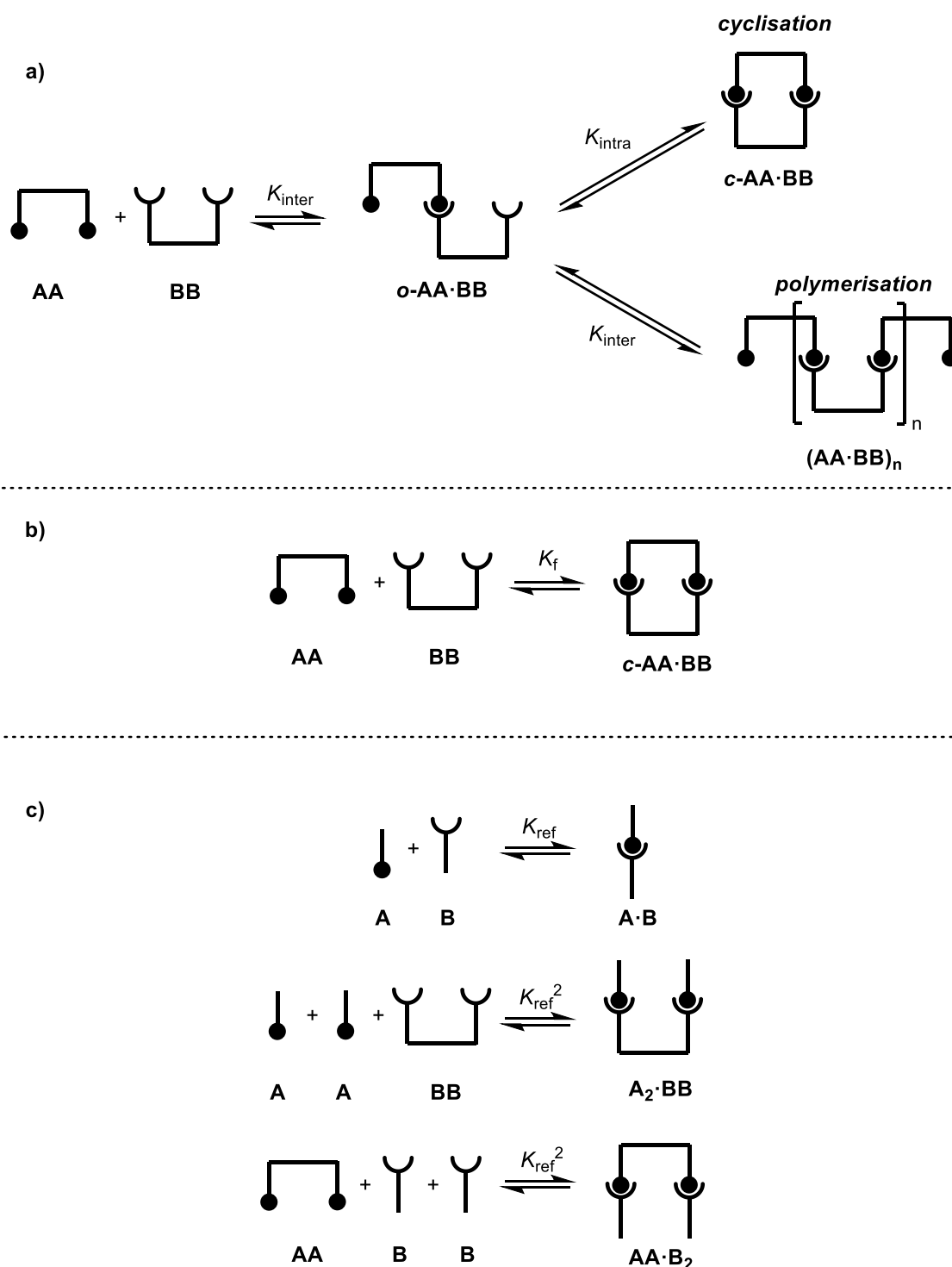
Figure 1.1. (a) Stepwise assembly of a cooperative supramolecular complex with two binding interactions c-AA•BB. The first intermolecular equilibrium leads to the open o-AA•BB complex with one intermolecular interaction. This complex can cyclise *via* an intramolecular interaction (K_{intra}) or polymerise *via* a series of intermolecular interactions (K_{inter}). (b) The overall equilibrium observed for formation of the closed complex c-AA•BB. (c) Reference systems that can be used to measure K_{ref} for a monovalent interaction, which serve as an estimates for K_{inter} in (a).

$$\text{EM} = \frac{K_\text{f}}{K_{ref}^2} \qquad (1.3)$$

The value of EM obtained from Equation 1.3 includes a contribution from the statistical degeneracies of the complexes in Figure 1.1. It is possible to correct the value of EM for this contribution by using a statistical factor K_σ, which can be estimated based on the symmetry of the complex (Equation 1.4).[13-16] Both statistically corrected and uncorrected values of EM are commonly reported.

$$\text{EM} = K_\sigma \frac{K_\text{f}}{K_{ref}^2} \qquad (1.4)$$

Equation 1.4 can be generalised to multivalent systems that make multiple non-covalent interactions (Equation 1.5).

$$\prod_{i=1}^{n-1} \text{EM}_i = K_\sigma \frac{K_\text{f}}{\prod_{i=1}^{n} K_i} \qquad (1.5)$$

where n is the number of intermolecular binding interactions made in the multivalent complex, EM_i are the effective molarities for each of the intramolecular interactions made in the multivalent complex, K_f is the equilibrium constant for formation of the multivalent complex and K_i are the equilibrium constants for formation of the corresponding monovalent interactions in the appropriate reference systems.

The equilibrium constant for formation of the intramolecular interaction in Figure 1.1a is $K_\text{ref} \times \text{EM}$, so this parameter is the most important indicator of chelate cooperativity in supramolecular systems. When the product $K_\text{ref} \times \text{EM}$ is much larger than one, cooperative assembly of the closed complex occurs, but when $K_\text{ref} \times \text{EM}$ is less than one, the intramolecular interaction is not formed.

## 1.1.2. Distribution of effective molarities and extreme values

Figure 1.2 shows a distribution of thermodynamic effective molarities in supramolecular systems. The median value is 100 mM and EM $> 10^2$ M are considered to be extremely high, since less than 5% of the reviewed supramolecular systems showed the values of this magnitude.[17]
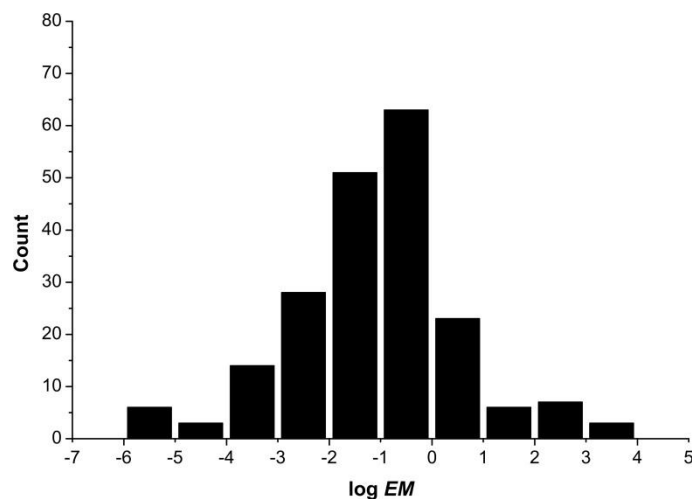
Figure 1.2. Distribution of thermodynamic effective molarities in supramolecular systems.[17]

Examples of complexes with unusually large values of EM are discussed below. As expected, these systems are rigid and highly preorganised, so that losses in conformational entropy on formation of cooperative intramolecular interactions are minimised. However, the two examples discussed below also highlight the sensitivity of systems that have exceptionally high EM values to subtle changes in molecular structure.

The Anderson group has measured EM values for a range of cyclic zinc porphyrin oligomers binding to oligopyridine ligands that were used as templates in the synthesis.[18-20] An exceptionally high value of EM (126 M) was found for the complex shown in Figure 1.3a. This value of EM is actually the average EM for five intramolecular interactions. Anderson used a series of ligands with two, three, four, and five pyridine binding sites to determine stepwise EMs for each binding interaction in the hexamer.[21] The value of EM for the first intramolecular binding interaction is 100 mM, which is comparable to the value found for the majority of supramolecular complexes (see Figure 1.2). However, all four subsequent intramolecular binding interactions have exceptionally high values of EM of 10^3 M. Presumably, the first intramolecular binding interaction organises the complex in a rigid geometry that is a precise match for subsequent binding interactions.
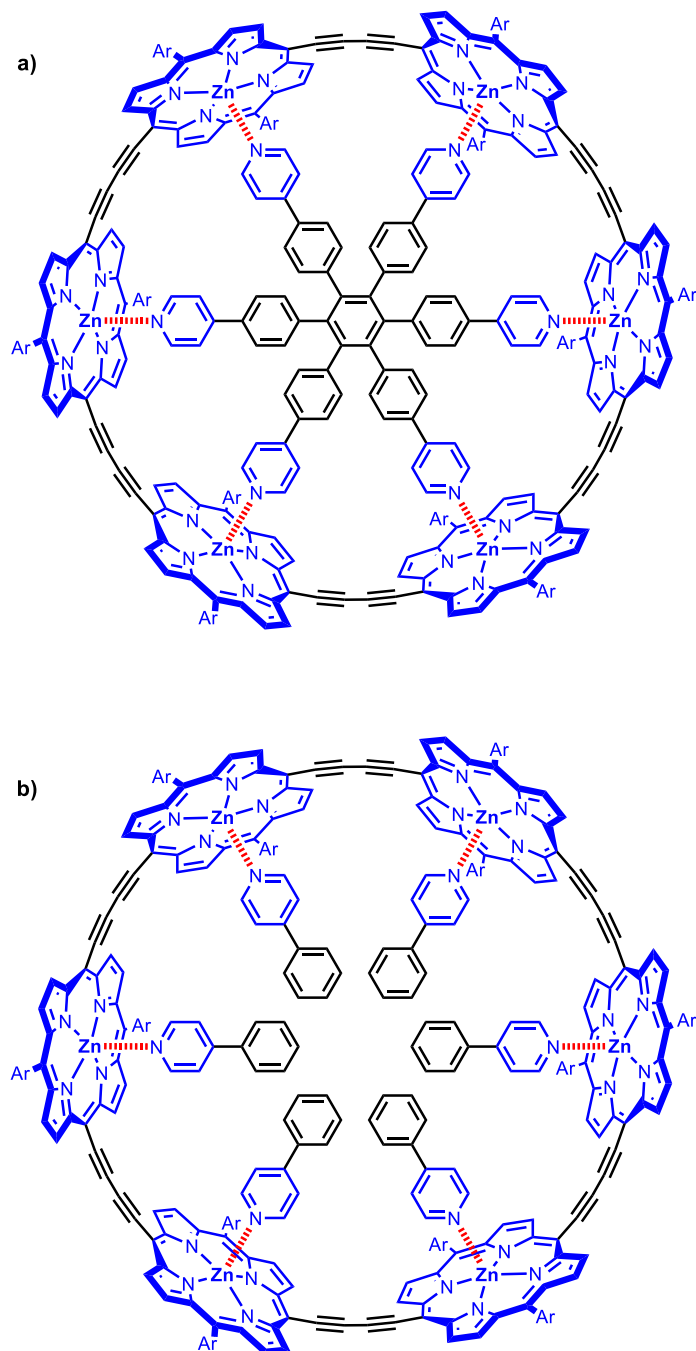
Figure 1.3. (a) Anderson's zinc porphyrin-pyridine complex which has a very high binding affinity ($K_f = 1.3 \times 10^{36}$ M^{-1}) and (b) the reference system (Ar are solubilising groups).

The González-Rodríguez group have studied the self-assembly of cyclic hydrogen-bonded tetramers based on nucleic acid base-pairs (Figure 1.4).[22] The tetramer is extremely stable and persists in very competitive solvent environments (33% dimethylsulfoxide in chloroform). The value of EM for cyclisation interaction leading to the tetramer shown in Figure 1.4a is 860 M. It is interesting to note that the exceptionally high EM observed for this system depends critically on the base-pairing system. The corresponding cyclic hydrogen-bonded tetramer prepared using 2-aminoadenine-uracil base-pairs (Figure 1.4c) in place of the guanine-cytosine base-pairs in Figure 1.4a has an EM of 100 mM, which is comparable to the value found for the majority of supramolecular complexes (see Figure 1.2).[23] In the following work, they showed that also conformational equilibria and the length of the monomer have a significant effect on the chelate cooperativity of these systems.[24,25]
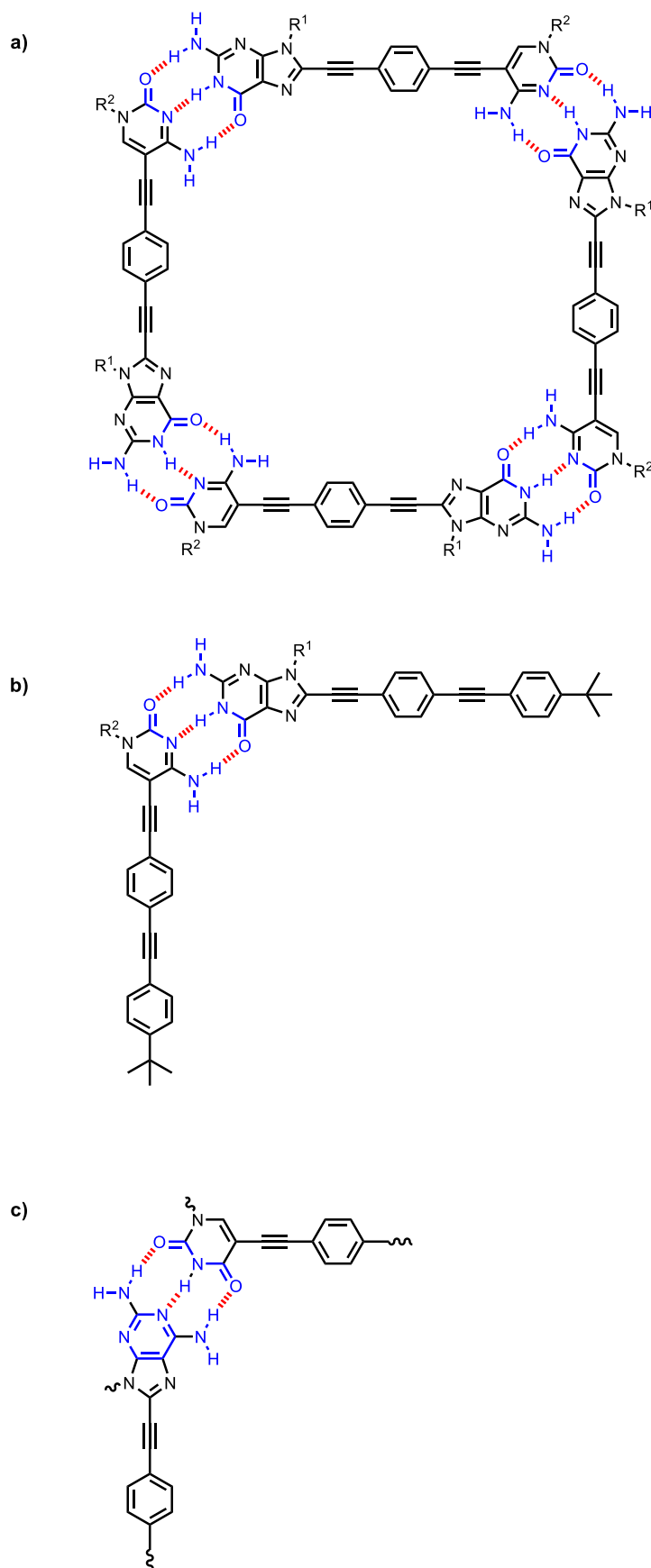
Figure 1.4. (a) González-Rodríguez's cyclic hydrogen-bonded tetramer based on guanine-cytosine base-pairing and (b) the reference system (R[1] and R[2] are solubilizing groups). (c) An alternative base-pairing system based on 2-aminoadenine-uracil.

9

1.2. Porphyrin nanorings

Two important findings started the recent flourishing development in the field of porphyrin nanorings.[26] Firstly, Anderson and Sanders showed in 1990 that the addition of feasible multivalent pyridine ligand can result in the template synthesis of specific cyclic porphyrin oligomers (Figure 1.5).[27] By using a bidentate pyridine ligand, the yield of the dimer increased by approximately 50 percentage points to 70% compared to a reaction with no template present at all. Similarly, when a tridentate ligand was used, the trimer was prepared with a yield of 50%, whereas the yield for the reaction without any template was 30-35%.
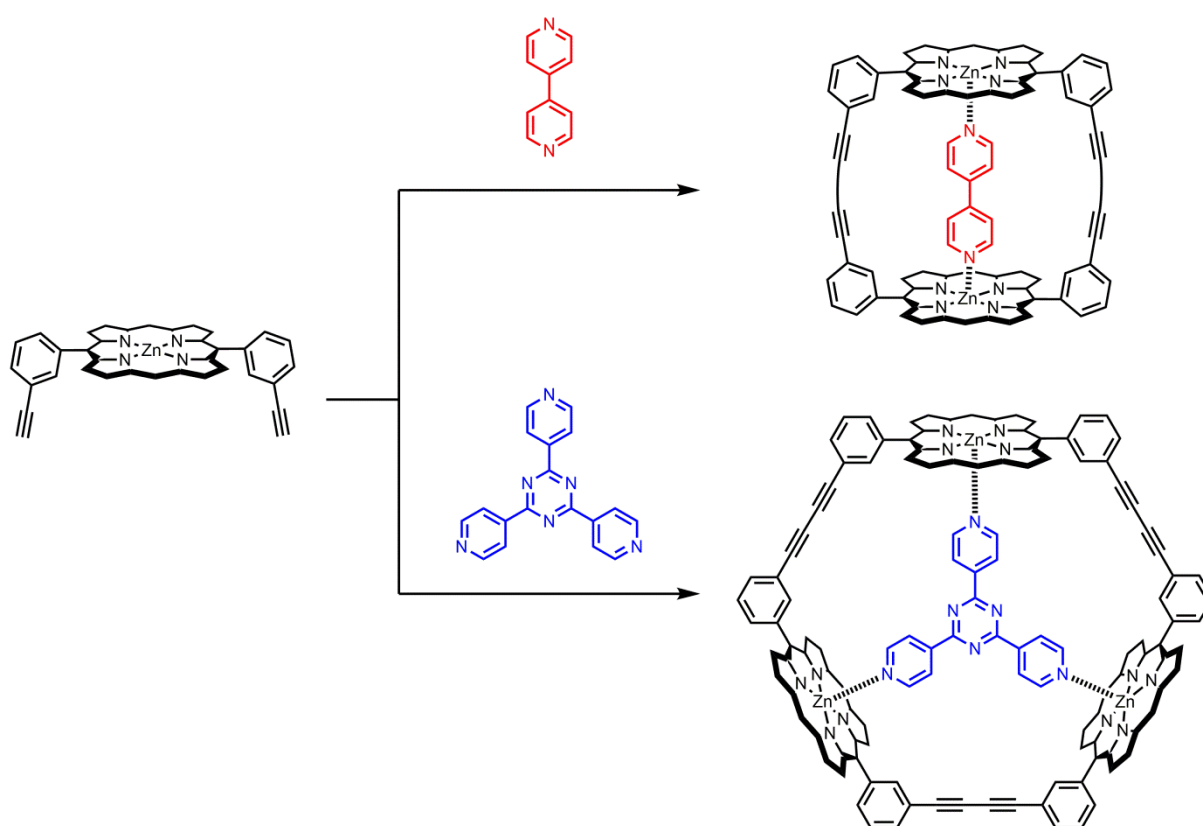

Figure 1.5. Simplified scheme for template synthesis of cyclic porphyrin oligomers. Reaction conditions: CuCl, TMEDA, DCM, air.

The second finding was the creation of *meso*-alkynyl porphyrins chemistry. Anderson synthesised the first of these in 1992 (Figure 1.6a).[28] After that, the Anderson group prepared a large number of various linear oligomers and extensively studied their supramolecular behaviour (Figure 1.6b),[29] as well as their optical properties, since these molecules are highly π-conjugated.[30]

a)
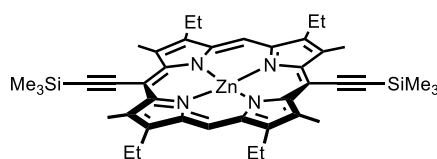
b)
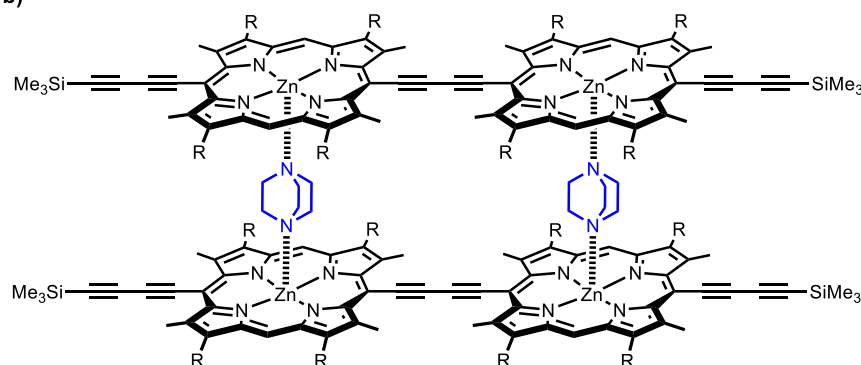

Figure 1.6. *Meso*-alkynyl porphyrins prepared by the Anderson group: (a) the first example prepared and (b) porphyrin ladder.

In 2007, the Anderson group connected the two concepts. They used a linear porphyrin octamer based on a *meso*-alkynyl porphyrin and an octadentate pyridine ligand for the first reported synthesis of a porphyrin nanoring (Scheme 1.1). The cyclic oligomers prepared by Anderson and Sanders 17 years before this contribution (Figure 1.5) cannot be considered as genuine rings, since their diphenylethyne arms are perpendicular to the porphyrins and therefore these molecules lack the circular π-conjugation that is found in the porphyrin rings.

Since this seminal paper, the Anderson group has used the template method for the synthesis of various porphyrin nanorings (5-ring,[31] 6-ring,[19] 7-ring,[20] 10-ring,[32] and many others up to a 40-ring[33]) as well as complex structures such as a "Russian dolls" complex that resembles a natural bacterial photosynthetic system,[34] fused nanorings,[35] nanoballs,[36] and nanotubes.[37,38]
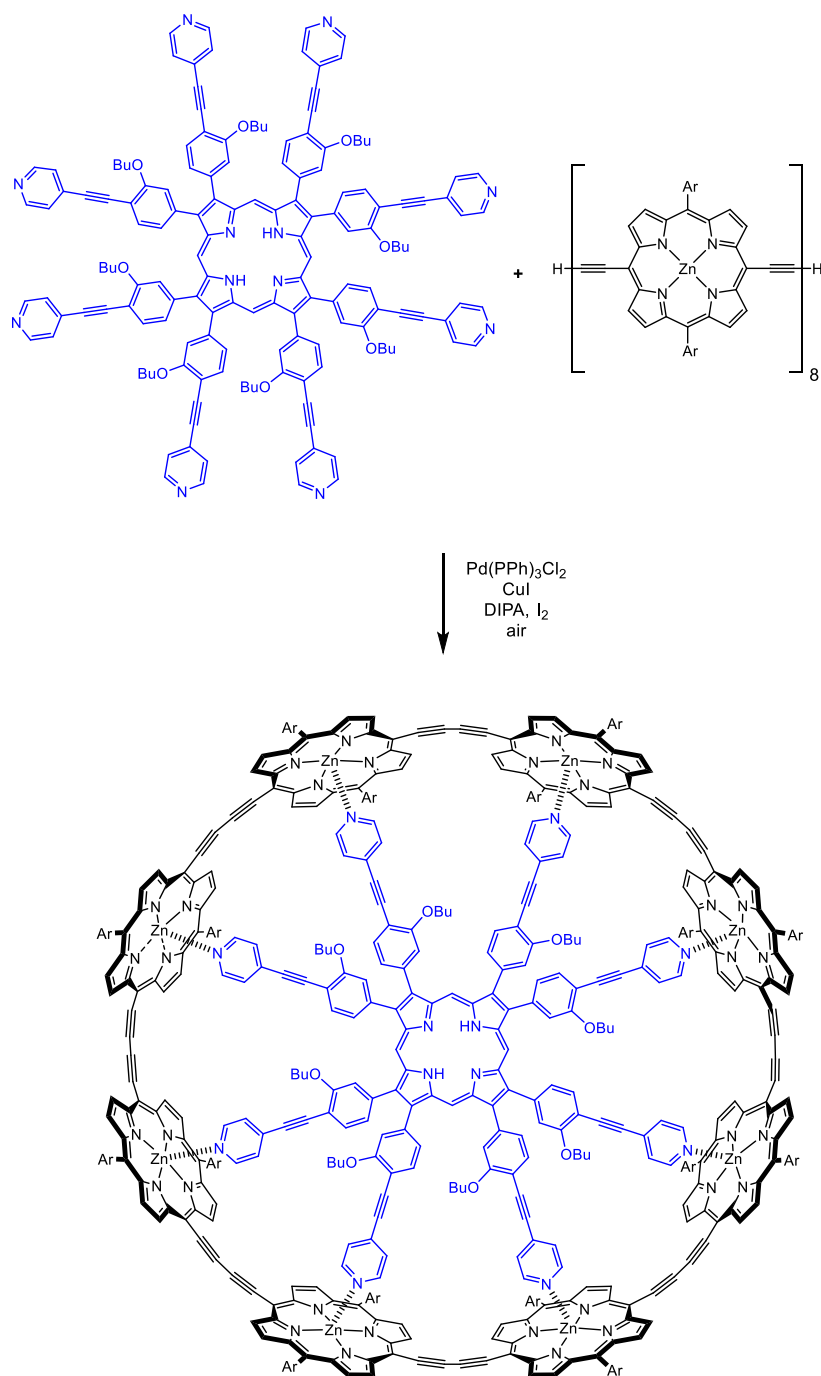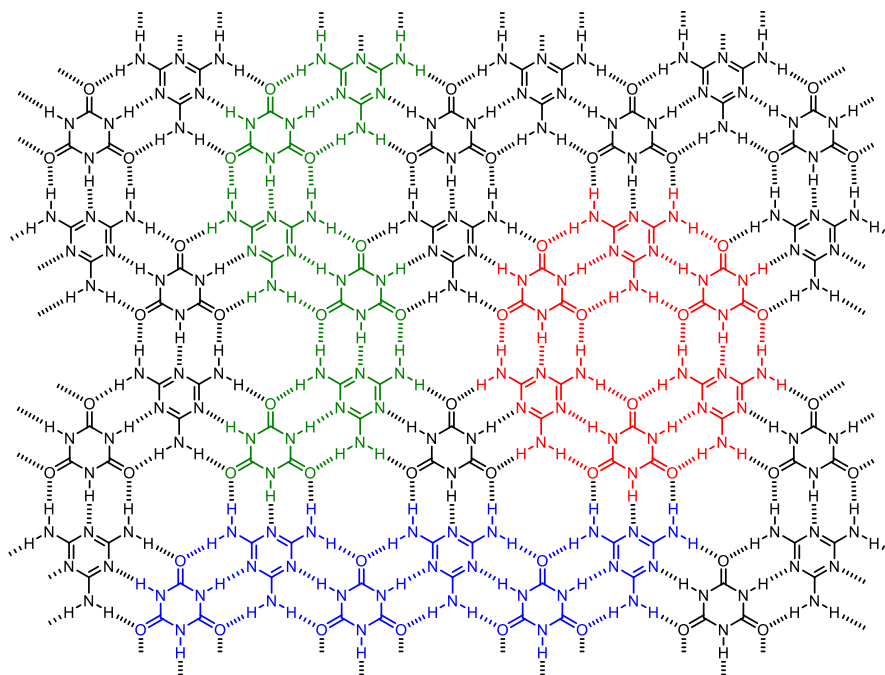
Scheme 1.1. First reported synthesis of a porphyrin nanoring.

1.3. Rosette motif

1.3.1. General

The rosette motif is derived from the lattice of melamine and cyanuric acid complex mixed in a 1:1 ratio as shown in red in Figure 1.7.[39] There are other two motifs that can be derived from this lattice – a linear tape (blue) and crinkled tape (green).

Figure 1.7. The melamine•cyaunuric acid lattice showing rosette (red), linear tape (blue) and crinkled tape (green) structures.

The group of Whitesides pioneered the use of different compounds based on melamine together with derivates of cyanuric and barbituric acids, to prepare many complexes exhibiting all the structural motifs shown in Figure 1.7.[39] A system based on melamine **M** and barbiturate **B** that forms the rosette $M_3 \cdot B_3$ is shown as an example in Figure 1.8.[40] This complex is probably the most studied and best characterised system of all.
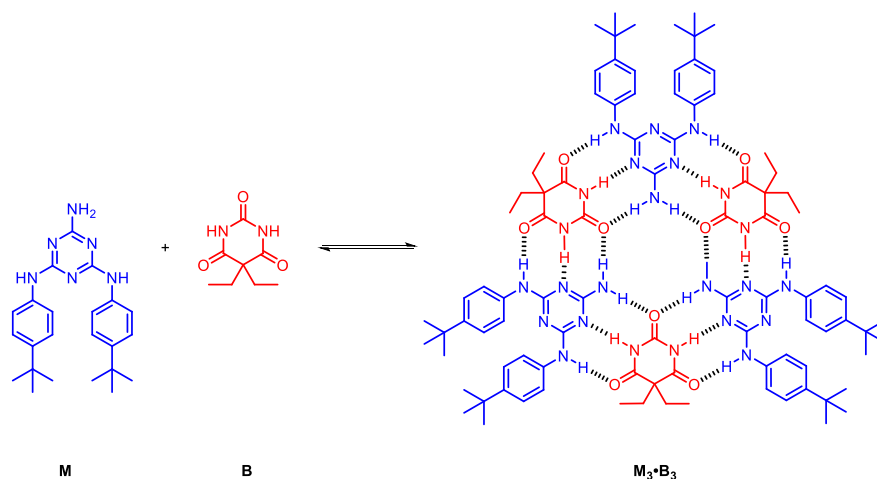
Figure 1.8. Rosette **M₃•B₃** formation from a barbiturate **B** and a melamine **M**.

The Whitesides group used non-polar solvents, such as chloroform, to study these complexes in solution. To characterise the complexes, several techniques have to be used.[39] The first hint of a successful formation of a rosette complex is a change in solubility. Both of the rosette building blocks (melamine and cyanuric/barbituric acids derivates) are usually poorly soluble in chloroform. They have to be dissolved in more polar solvent first, such as methanol and mixed together. After removal of methanol, the solubility of formed complex in chloroform is increased significantly compared to the respective building blocks, especially when the ratio is 1:1. Most of the time, this process has to be used to prepare the target complexes.[39]

Once in solution, these complexes are investigated by ^{1}H NMR spectroscopy. Fortunately, formation of a rosette results in the appearance of characteristic peaks – NH of a barbiturate/cyanurate in a region δ 13 – 16 ppm and the NH and NH₂ from melamine in the region δ 8 – 11 ppm as depicted in Figure 1.9. The observation of these peaks is normally used for a judgment if the rosette is formed or not. ^{1}H NMR titrations are used also to determine the complex stoichiometry, which is also shown in Figure 1.9.
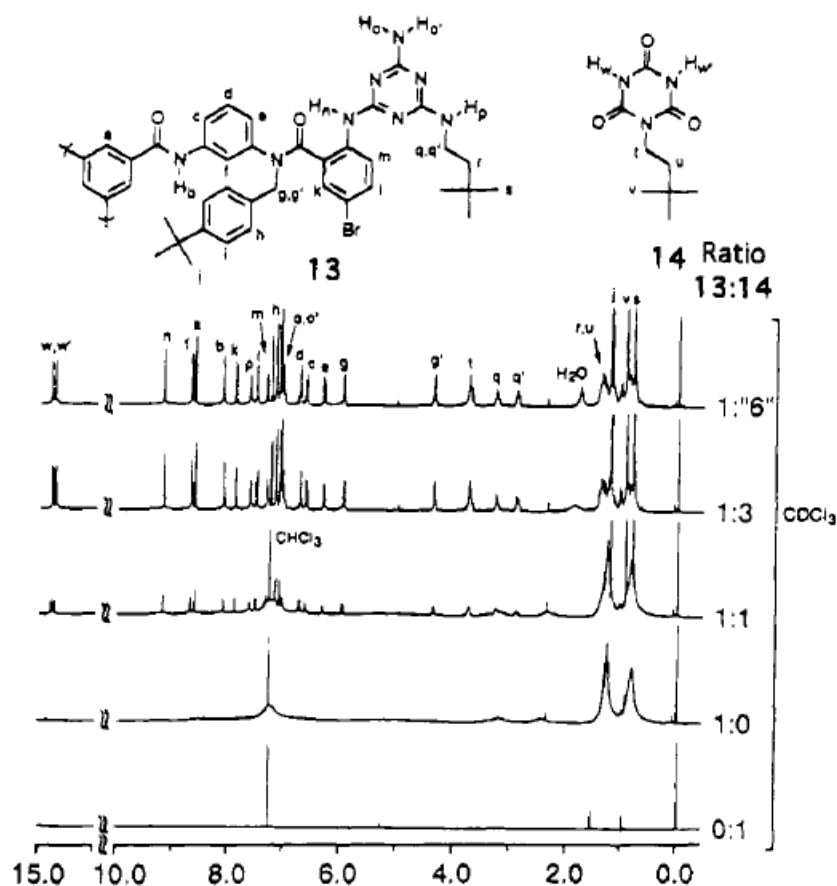
Figure 1.9. ^{1}H NMR spectra showing characteristic rosette peaks and titrations used to determine the stoichiometry. Reprinted with permission from reference 39. ©1995 American Chemical Society

Other methods used for characterisation of rosettes are GPC and VPO that determine the molecular size or weight of the complexes. Occasionally, it has been possible to obtain an X-ray structure that shows the rosette motif. One of the systems where this was successful is **$M_3 \cdot B_3$** from Figure 1.8.[41] Interestingly, the X-ray structure of melamine•cyanuric acid complex that contains the lattice, shown in Figure 1.7, was obtained only after the main part of the work on rosettes was conducted.[42] The crystallisation required drastic hydrothermal conditions, which demonstrates the difficulty of obtaining a suitable crystal for these systems.

As these complexes are non-covalent, the utilisation of mass spectrometry for their characterisation has been limited. The group of Lehn used benzo[18]crown-6 functionalised melamines as a binding site for K^+ that was then characterised by ESI-MS.[43] The Whitesides group used Cl^- labelling that worked only for a special melamine derivative.[44] The most elegant approach was from Timmerman *et al.*; they used Ag^+ as a label for the rosette

15

complexes that were then characterised by MALDI-TOF mass spectrometry.[45] Unfortunately, as the Ag^+ binds to the aromatic parts on the periphery of the molecules, this method works only for molecules containing these aromatic parts.

The groups of Whitesides, Reinhoudt and others extended the work to the preparation of complexes with more than one rosette.[39,46] The Whitesides group prepared a complex with three rosettes that was assembled from 10 molecules (Figure 1.10).[47] The Reinhoudt group used calix[4]arene dimelamines to prepare various double to tetra rosette complexes. They were able to obtain an X-ray structure of the double rosette complex with three guest molecules inside the cavity.[48]
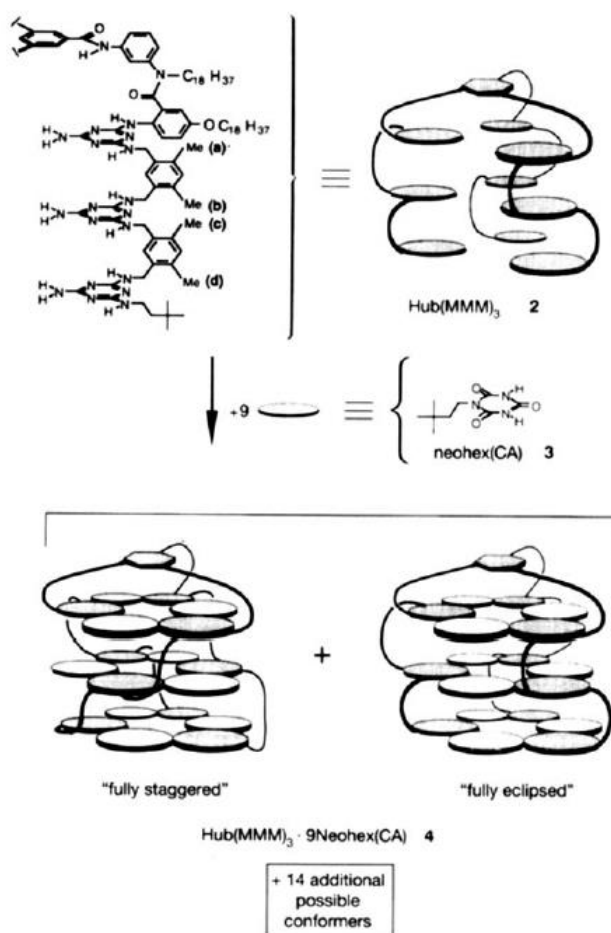

Figure 1.10. Triple rosette complex prepared by the group of Whitesides. Reproduced with permission from reference 47.

1.3.2. Thermodynamic stability

Firstly, a strong influence of concentration and temperature has been determined for the rosette complexes. The higher concentration, the more stable they are, as indicated by the improved resolution of peaks in the ^{1}H NMR spectra, as shown in Figure 1.11. The Whitesides group used the concentration of 4 mM as a threshold between the formation of a rosette and other structural motifs for systems based on single rosettes.[23,40] Others have found that this can be different if increased bulky molecules are used.[49] The rosette complexes are usually more stable at lower temperatures as shown in Figure 1.12.
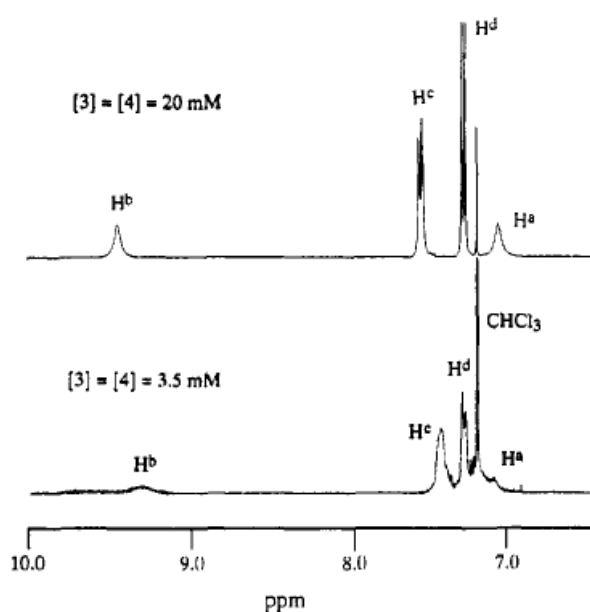

Figure 1.11. Effect of concentration on the rosette assembly, as showed by partial ^{1}H NMR (400 MHz, CDCl$_3$) spectra of 1:1 complex of **M** (**4**) and **B** (**3**) at concentrations of 20 mM (top) and 3.5 mM (bottom). H^b and H^a are NH and NH$_2$ of melamine, respectively. Adapted with permission from reference 40. ©1994 American Chemical Society
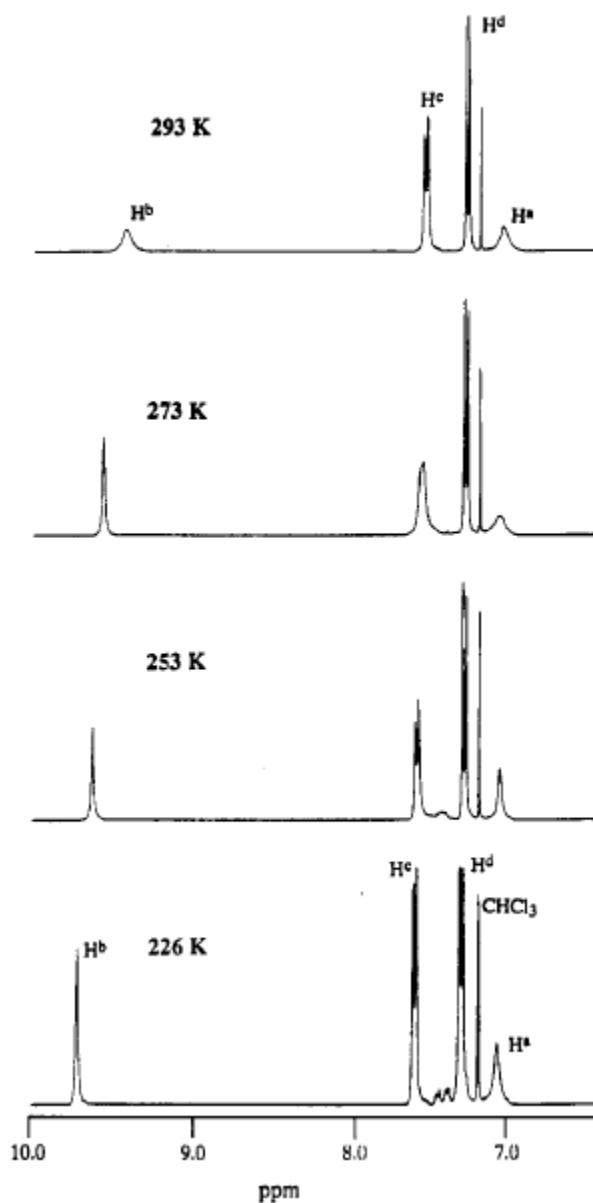
Figure 1.12. Effect of temperature on the rosette assembly, as showed by partial variable temperature ^{1}H NMR (400 MHz, CDCl$_3$) spectra of 1:1 complex of **M** and **B** ([**M**] = [**B**] = 3 mM). H^b and H^a are NH and NH$_2$ of melamine, respectively. Adapted with permission from reference 40. ©1994 American Chemical Society

In order to predict the stability of rosette complexes, the Whitesides group came up with an empirical parameter HB/(N–1), where HB is the number of hydrogen bonds in the complex related to the enthalpy of formation of the complex, and N is the number of molecules needed for the assembly of the complex. N–1 is associated with the loss in entropy.[39] The larger this parameter, the more stable a rosette complex should be. Therefore more hydrogen bonds (for example, in double rosettes) and using fewer molecules to assemble the system (by joining some of them into one molecule), should result in the increased stability of the rosette complexes. Whitesides stated that complexes with an empirical parameter of > 5 seem to be stable in chloroform and the ones with a value > 9 are stable in 20% methanol in chloroform solutions. In later work,[50] Whitesides renamed this parameter to I_{Tm} to indicate a melting point index and introduced additional two "rule of thumb" parameters. These were I_G and I_G/(N–1), where I_G is a free energy index and is determined as 2.8HB–16(N–1) and I_G/(N–1) index is then equal to 2.8HB/(N–1)–16, which corresponds conceptually to a free energy of association per particle. They showed that these parameters correlate well to the experimental observations with $\chi_{1/2}^{DMSO}$ being the general experimental indicator of stability of an assembly. It describes the amount of DMSO that is needed for 50% of the assembly being present in solution.

Interestingly, there are only few studies of the actual thermodynamic values for the rosette formation. In 2001, the group of Timmerman conducted a detailed study of thermodynamics of barbiturate/melamine system in CDCl$_3$ by ^{1}H NMR spectroscopy at 297 K and by VPO in 1,2-dichloroethane at 308 K.[51] They used blocked barbiturates and melamines to measure reference intermolecular association constants K_0 as depicted in Figure 1.13a. By using a model bis(melamine) system that should resemble a rosette based on the examination of molecular models (Figure 1.13b), they determined an effective molarity of rosette formation from measuring K_{plug} of the model assembly. Using $K_{plug} = 4 \times EM \times K_0$, they calculated the effective molarity of the rosette formation to be 0.18 ± 0.05 M. We believe that this model does not provide a realistic view of the rosette cyclisation, because of the phenyl hydrogen highlighted in Figure 1.13b, which is not present in the rosette motif. Additional interactions with the barbiturate carbonyl group could, therefore, affect the stability of the model complex in comparison to the rosette.
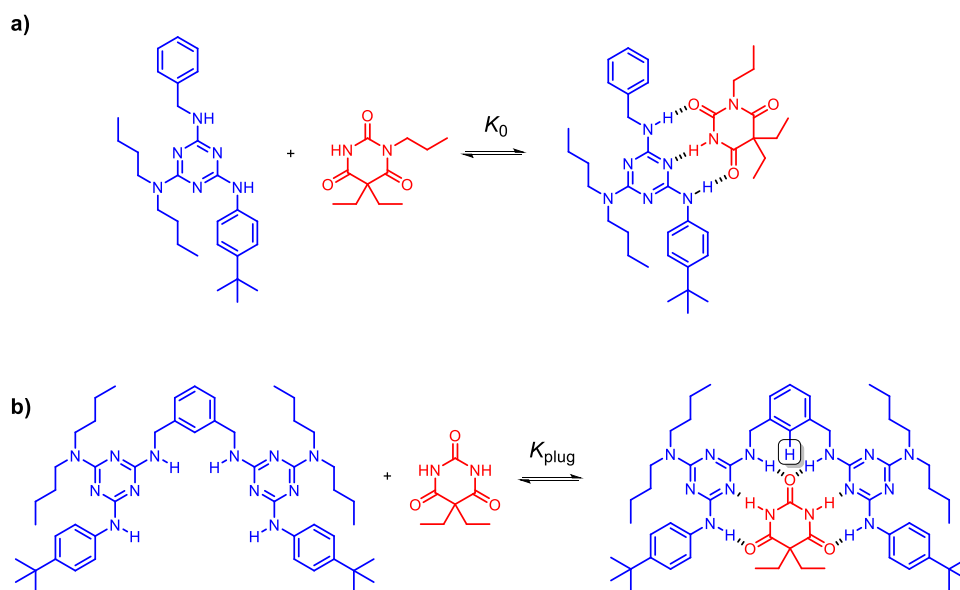
Figure 1.13. Equilibria used by the Timmerman group to study chelate cooperativity of the rosette motif. (a) Reference intermolecular interaction using blocked melamine and barbiturate. (b) Using bis(melamie) to simulate the rosette motif to obtain the effective molarity of rosette cyclisation. Highlighted hydrogen can affect the stability of the complex compared to the rosette motif.

In 2004, Crego-Calama, Reinhoudt and co-workers studied the formation of different single and double rosette complexes by ITC in 1,2-dichloroethane at 298 K.[52] They determined rosette equilibrium constants for the first time and provided thermodynamic values that explain some previous empirical observations, i.e. rosettes based on cyanurates are more stable than those based on barbiturates as shown in Figure 1.14.
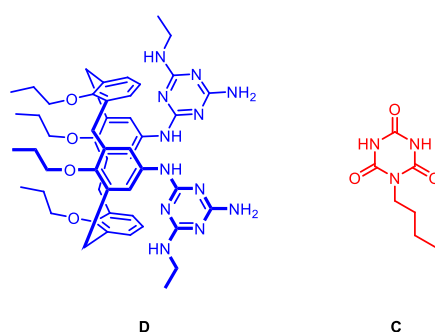
Rosette	K_f
$M_3 \cdot C_3$	$(1.4 \pm 0.3) \times 10^{20}\,M^{-5}$
$D_3 \cdot B_6$	$(1.5 \pm 0.6) \times 10^{31}\,M^{-8}$
$D_3 \cdot C_6$	$(2.7 \pm 2.0) \times 10^{43}\,M^{-8}$

Figure 1.14. Rosette and double rosette formation constants determined in 1,2-DCE by ITC at 298 K.[52]

20

1.3.3. Concepts of preorganisation and peripheral crowding

Originating from a study of a large diverse set of rosette complexes and their stability in solution, the Whitesides group postulated a concept of preorganisation.[39] They connected several melamine units into one molecule. This decreased the entropy contribution and these rosette complexes were much more stable compared to a simple rosette. This is also the reason why Whitesides and co-workers were successful in assembling complexes with three rosettes that were shown above in Figure 1.10.

Another concept that was postulated by Whitesides group is peripheral crowding.[21] This originated from using various substituent on the periphery of melamine that provide different structural motifs in the solid state (Figure 1.15), and their investigation of stability in solution by ^{1}H NMR spectroscopy as judged by the observation of the characteristic rosette peaks of N-Hs or not.[40,41,53] The concept postulates that molecules with bulky groups on the periphery destabilise other possible structures and therefore a formation of a rosette is preferred as shown in Figure 1.16. For less bulky melamines, the crinkled tape is preferred in the solid state, and the least bulky melamines crystalise in a form of linear tapes.

However, the peripheral crowding concept was questioned by the work of the Timmerman group.[51] They argued that obtaining different structures in the solid state can originate simply from a different solubility of competing species – the least soluble complex crystallises from the solution first, no matter what its stability in solution is. As a rosette motif has all polar groups bound, it should have higher solubility in non-polar solvents compared to structures based on a linear or crinkled tape.

Interestingly, even the work from the Whitesides group can be used to point out some discrepancies of the concept of peripheral crowding. In one of their studies, they used the same bulky melamine (**M**) for two different partners – one based on barbiturate **B** and the second on cyanurate **CYA** (Figure 1.17).[40] They stated that only the complex based on **B** forms the rosette as judged by ^{1}H NMR spectroscopy, even though the rosettes based on a cyanurate are significantly more stable. Moreover, the original paper reporting the successful system **M₃•B₃** did not report a well-defined characteristic rosette barbiturate N-H peak in the expected region, but only very broad one.[40] This again shows how difficult the characterisation of these systems can be.
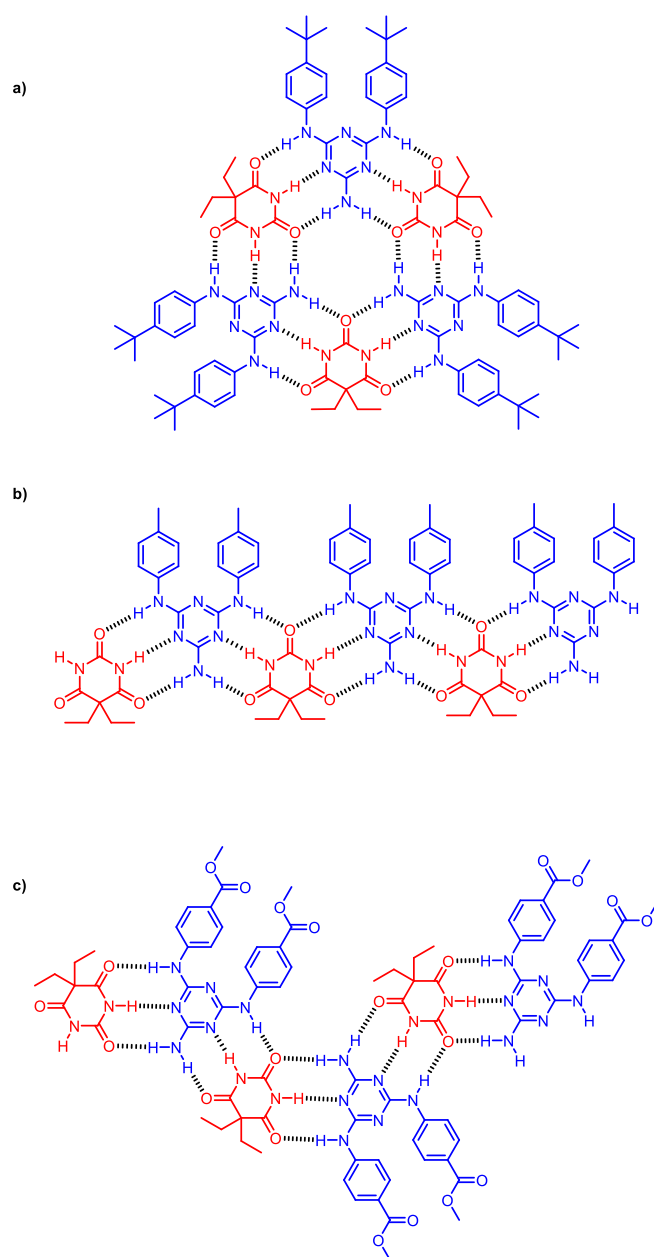
Figure 1.15. Different structures of barbiturate/triaminotriazines complexes in solid state; a) rosette, b) linear tape and c) crinkled tape.
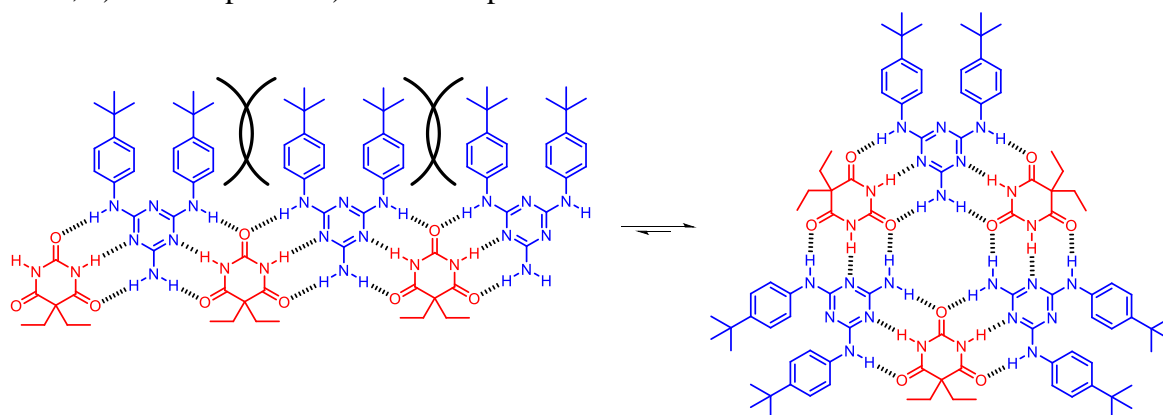
Figure 1.16. Concept of peripheral crowding. The bulkiness of the periphery of melamines leads to a preferable formation of the rosette structure.
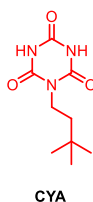
Figure 1.17. Cyanurate **CYA** that does not form a rosette with melamine **M** according to the Whitesides group.

1.4. Molecular containers

1.4.1. General

The topic of molecular containers includes a large number of different architectures of various sizes, shapes and functionalities.[54] By and large, any discrete molecule or complex that has either an inner void volume that shows different properties compared to the outside of the species or a separation of the inside to the rest can be considered a molecular container. Traditionally, self-assembled molecular containers have been divided into two main categories: metal-coordinated cages and hydrogen-bonded capsules. Both types have been studied extensively for their host-guest,[55-57] guest-guest,[58,59] catalytic,[60,61] and stimuli-responsive behaviour.[62,63]

1.4.2. Metal-coordinated cages

Metal-coordinated cages have been developed by the efforts of several groups, namely Fujita,[64] Stang,[65] Raymond,[66] and others. An example from Fujita group is shown in Figure 1.18 in which they used bipyridine and palladium and platinum salts to prepare square complexes that were able to encapsulate various molecules in aqueous media.[67] Over the years, initial simple 2D complexes have been extended to 3D architectures, since the geometry of both the ligand and metal centre allows one to rationally design and prepare complexes of target architectures as depicted in Figure 1.19.[68]

Over the years, many other suitable ligands and metal systems have been explored. The illustration of the state of the art comes again from the Fujita group. In 2016, they published the biggest self-assembled supramolecular cage ever described, formed from 144 small components.[69]
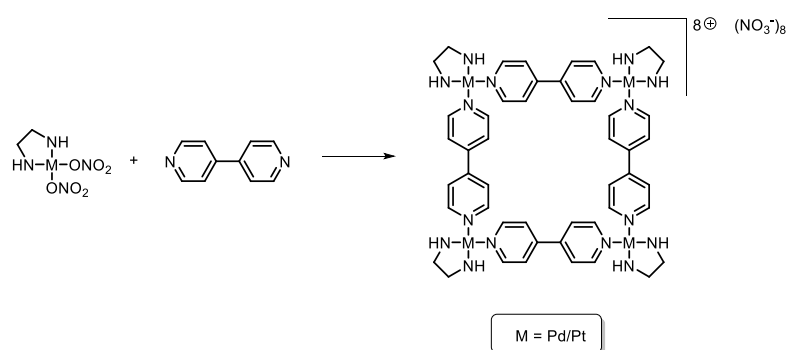
**Figure 1.18.** Self-assembly of bipyridine and palladium or platinum salts to form square complex.[67]
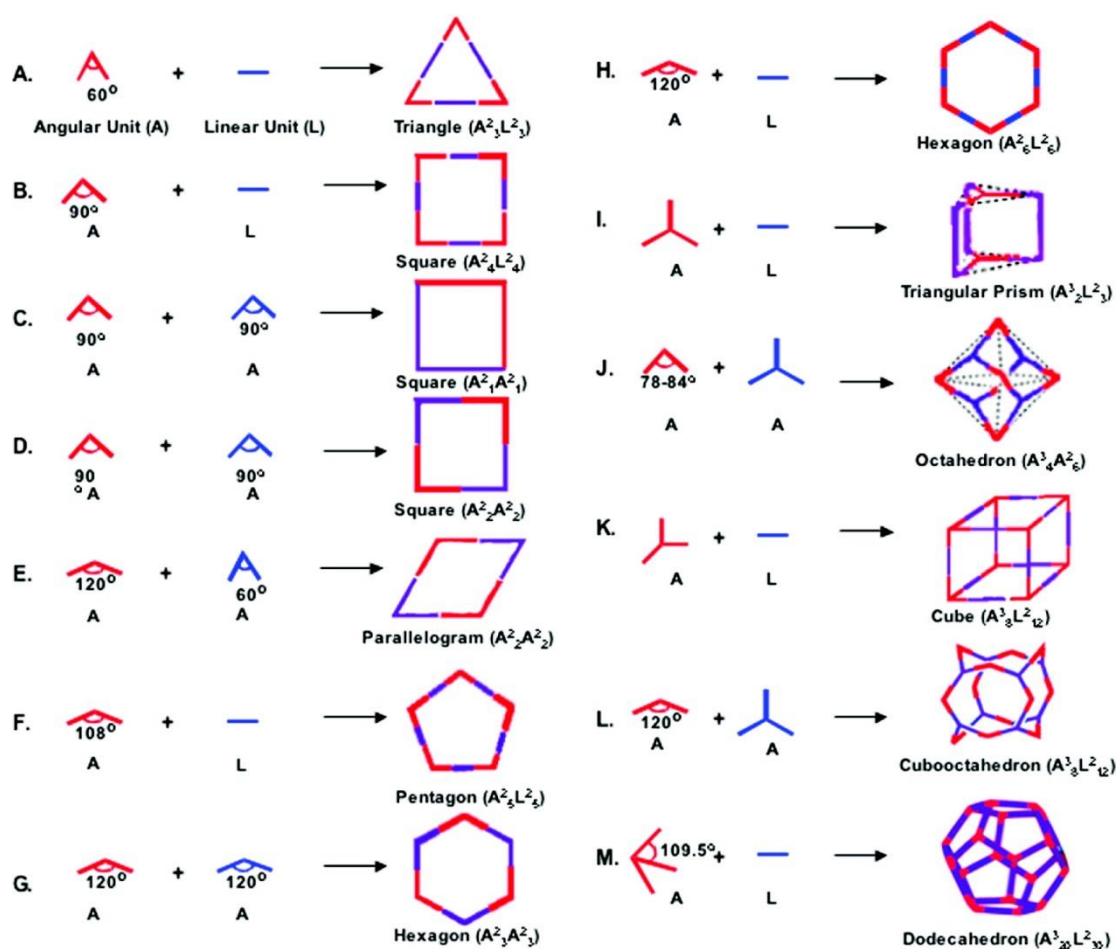
Figure 1.19. Combination of angular and linear building blocks (metal centres and ligands) to assembly different 2D and 3D architectures. Reprinted with permission from reference 68. ©2009 American Chemical Society.
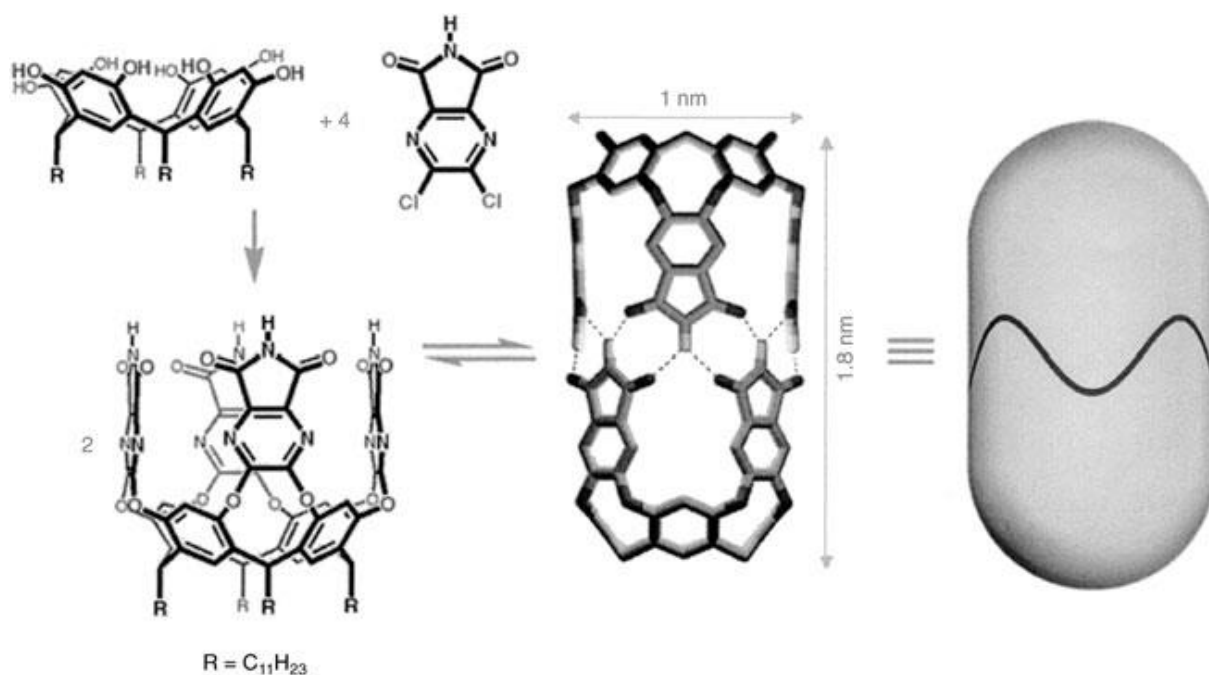
1.4.3. Hydrogen-bonded capsules

The chemistry of hydrogen-bonded capsules was pioneered in the group of Rebek in 1993.[58,70] They prepared a molecule shown in Figure 1.20a by condensing two molecules of diphenyl glycoluril with durene tetrabromide. This molecule self-assembles into the form of a tennis ball through eight hydrogen bonds (Figure 1.20b) in $CDCl_3$ and benzene, and is able to encapsulate methane and other small molecules.[71]
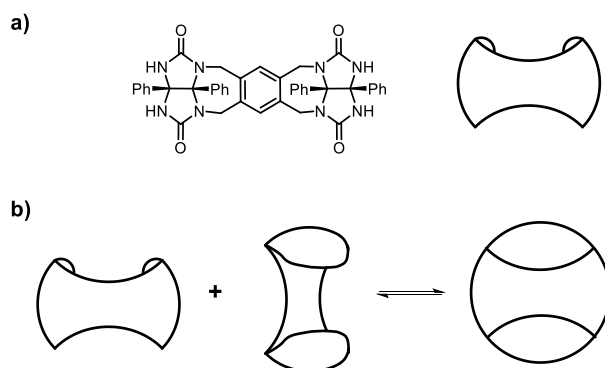
Figure 1.20. (a) Molecule prepared in the group of Rebek, (b) that assembles in the tennis ball fashion.

Since then, the Rebek group has used the same type of molecules to prepare larger semi-spherical structures that were used to study the encapsulation of different guest molecules.[72,73] Their efforts resulted in the synthesis of non-spherical capsule shown in Figure 1.21 that was further utilised to study various topics, ranging from isomerism to catalysis inside the cavity.[58]

Figure 1.21. Non-spherical capsule from the Rebek group. Reproduced with permission from reference 58.

As mentioned above, the rosette motif has been used for the preparation of various hydrogen-bonded capsules that contain two to four rosettes. The best characterised example is the double rosette from Reinhoudt group shown in Figure 1.22a.[48] This complex is able to encapsulate three guest molecules to form a well-defined hydrogen-bonded system inside its cavity as depicted in Figure 1.22b. They were able to characterise this host-guest system by X-ray studies and this is an exception in the rosette chemistry, as stated above. When a cyanurate is added to the complex, a more stable cyanurate-triazine rosette is formed that leads to the release of the guest molecules. The Reinhoudt group extended this work to prepare a tetra rosette complex that was able to encapsulate six guest molecules as shown in Figure 1.23.[74]

Other types of hydrogen-bonded capsules utilise peptide-based systems, cyclodextrines, calix[4]arenes, resorcinol and others.[75]
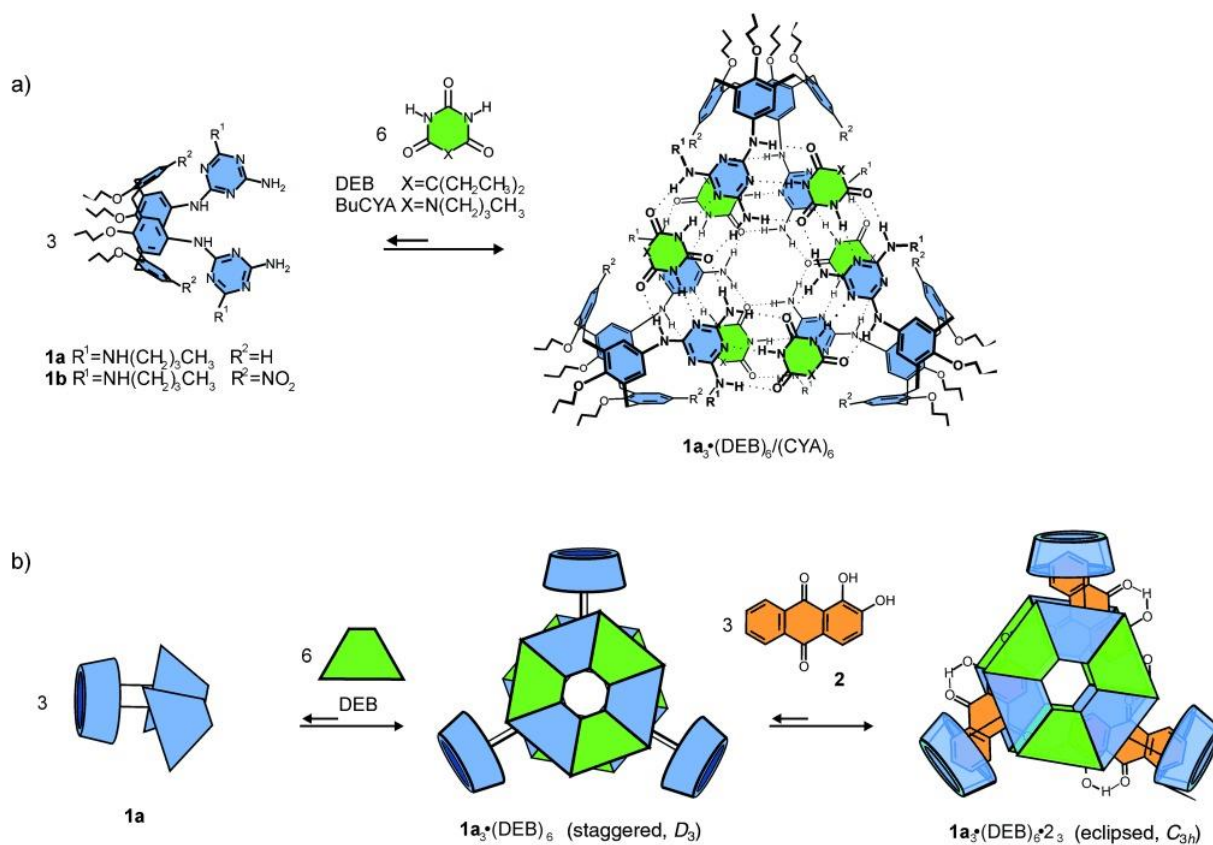
Figure 1.22. (a) Self-assembly of melamine calix[4]arene with barbiturate to form a double rosette complex and (b) encapsulation of three guest molecules. Reproduced with permission from reference 48.
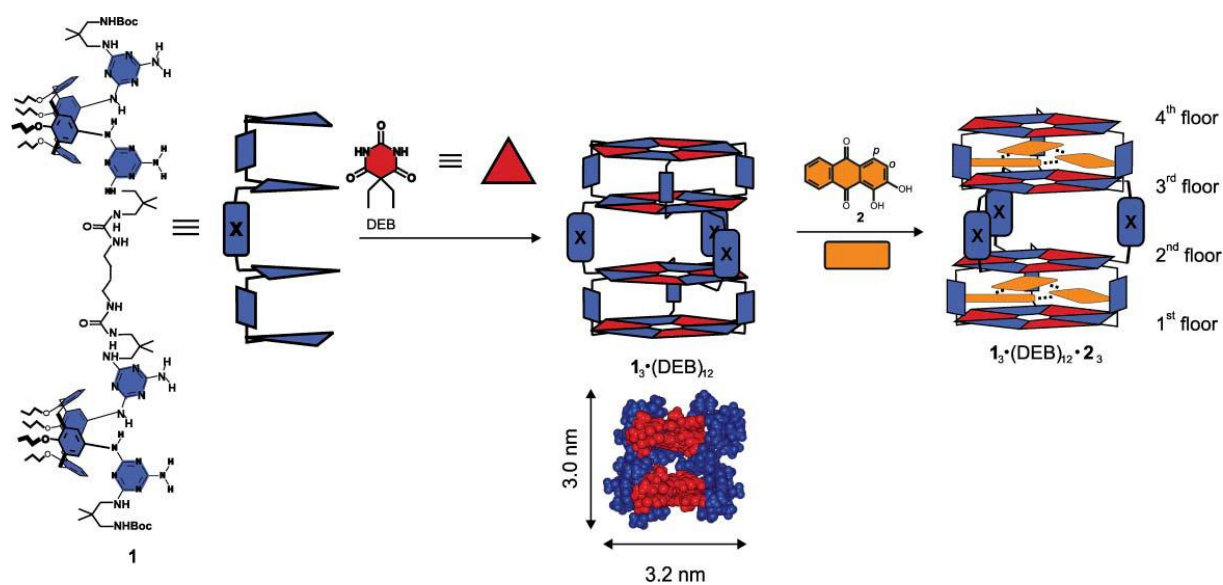

Figure 1.23. Tetra rosette complex that is capable to accommodate 6 guest molecules. Reproduced from Ref. 74 with permission from The Royal Society of Chemistry.

27

1.4.4. Hybrid molecular containers

Ever since the initial development of metal-coordinated cages and hydrogen-bonded capsules, hybrid systems have been studied.[76] Conversely, discrete well-defined 3D examples are rare. Moreover, there have been only a few reported systems where both types of the bonding form the crucial part of the structure, since many other system have one of them only on the periphery of the container backbone. In other words, we define a true hybrid system as a system where removal of one part (hydrogen-bonding or metal-coordination) leads to a change of the topology of the complex. Only the genuine discrete 3D hybrid examples will be discussed here. This strict definition excludes some examples of systems based on porphyrins and salen ligands,[77-79] since the removal of just the metal would not lead to a change of the topology of the complex, and also complexes where the second type of binding only results in higher stability of the complex.[79,80] Moreover, some of the complexes presented below are on the borderline of being considered a container, but we decided to include them since the number of examples is very limited.

Appavoo and co-workers prepared an arene ruthenium rectangle using 2-ureido-4-[1H]-pyrimidinone as the hydrogen-bonding motif, which is one of the most popular hydrogen-bonding motif for the preparation of supramolecular systems (Figure 1.24).[81]
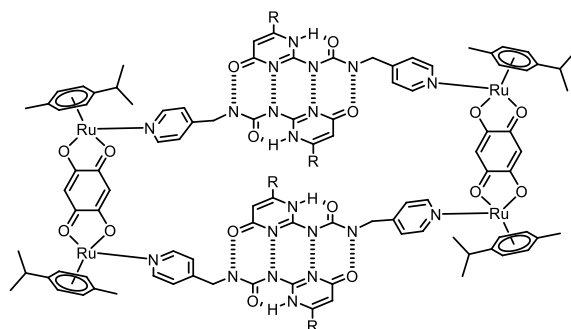

Figure 1.24. Structure of hybrid ruthenium/2-ureido-4-[1H]-pyrimidinone complex from Appavoo and co-workers (R is a solubilising group).[81]

The group of Houlton synthesised a cationic nucleobase duplex mimic using a tetrahedral bis(adeninyl)–Cu(I) complex that self-associated by hydrogen-bonding in polar solvents and solid phase as proven by the X-ray structure (Figure 1.25).[82] Similarly, Kokan and co-workers showed a dimerisation of palladium complex (Figure 1.26) by hydrogen bonding in chlorinated solvents.[83]
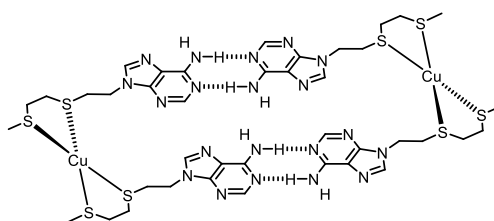
Figure 1.25. Structure of hybrid complex formed by a combination of hydrogen-bonding and copper(I) coordination.[82]
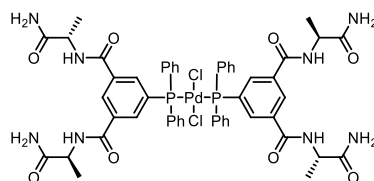

Figure 1.26. Structure of palladium complex from Kokan *et al.* that dimerise by hydrogen-bonding.[83]

In 2003, Alam and co-workers published a synthesis of hybrid container by a combination of hydrogen-bonding and copper(II) coordination using a ligand showed in Figure 1.27a. The capsule formed from eight copper atoms and eight molecules of ligand was able to accommodate four pyridine molecules inside the cavity as was shown by single X-ray analysis (Figure 1.27b).[84]

The group of Li prepared a strapped zinc porphyrin cyanuric acid and mixed it with a melamine and a pyridine-substituted barbiturate to prepare a hybrid container shown in Figure 1.28.[49] The removal of metal-coordinated fragment from the double rosette complex would lead to the disassembly and produce a single rosette complex. Unfortunately, they characterised this cage only by simple ^{1}H NMR spectroscopy and did not explore the host-guest and stimuli-responsive behaviour.

a)

b)
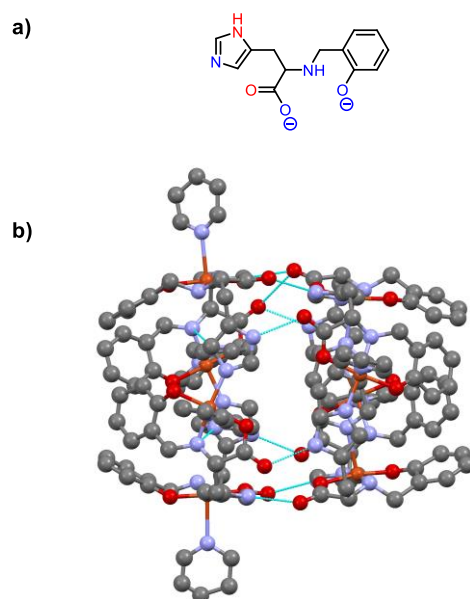
Figure 1.27. (a) Structure of the tetradentate ligand (the atoms that participate in hydrogen-bonding are in red and atoms that participate in copper(II) coordination are in blue) used for the preparation of (b) hybrid molecular capsule showing the X-ray structure (CCDC 197602) with trapped pyridine molecules inside the cavity (the hydrogens were omitted for clarity). Colouring of the atoms: C (grey), N (blue), O (red), Cu (orange) and the turquoise dashed line indicates a hydrogen bond.[84]
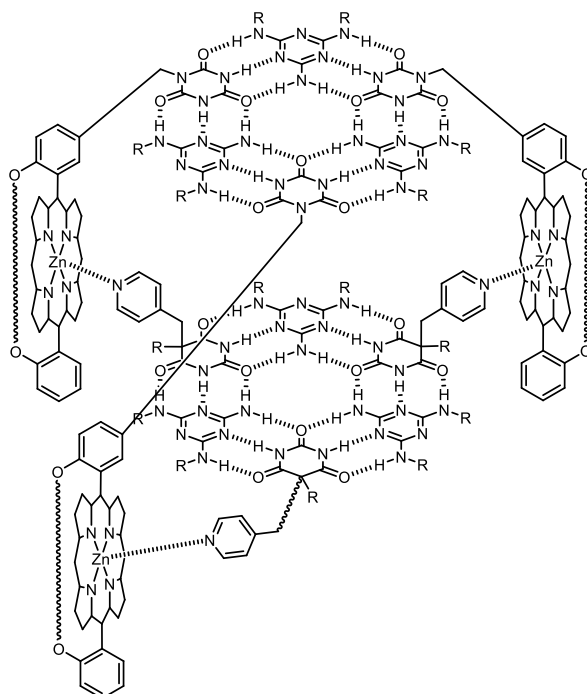
Figure 1.28. Hybrid rosette container based on zinc porphyrin and rosette motif from the Li group (R is a substituent).[49]

1.5. Conclusion

Multivalent supramolecular complexes show some degree of cooperativity in most of the cases. Two types of cooperativity exist: allosteric and chelate cooperativity. The chelate cooperativity has been studied extensively in a large number of systems. In spite of this, there is no predictor for it and even a small alternation of the studied system can lead to drastic changes in chelate cooperativity. Therefore each system has to be studied separately. The largest value of effective molarity that is used to quantify the chelate cooperativity is seen at highly rigid and preorganised systems, such as porphyrin nanorings from the Anderson group or cyclic hydrogen-bonded tetramers from the group of González-Rodríguez.

The rosette motif has been investigated enormously in the last 30 year and became one of the textbook examples of hydrogen-bonded supramolecular systems. Several concepts originated from the research and they are used in other areas as well. The motif has been also used for the preparation of hydrogen bonded capsules that were able to encapsulate guest molecules. Literature provides an overwhelming number of other hydrogen-bonded capsules as well as metal-coordinated cages, but systems where these two would be connected to form a genuine hybrid molecular container while using both as the crucial part of the architecture are rare.

1.6. References

(1)   Fasting, C.; Schalley, C. A.; Weber, M.; Seitz, O.; Hecht, S.; Koksch, B.; Dernedde, J.; Graf, C.; Knapp, E.-W.; Haag, R. *Angew. Chem. Int. Ed.* **2012**, *51*, 10472-10498.

(2)   Muller, C.; Despras, G.; Lindhorst, T. K. *Chem. Soc. Rev.* **2016**, *45*, 3275-3302.

(3)   Mulder, A.; Huskens, J.; Reinhoudt, D. N. *Org. Biomol. Chem.* **2004**, *2*, 3409-3424.

(4)   Mahadevi, A. S.; Sastry, G. N. *Chem. Rev.* **2016**, *116*, 2775-2825.

(5)   Williamson, J. R. *Nat. Chem. Biol.* **2008**, *4*, 458-465.

(6)   Hunter, C. A.; Anderson, H. L. *Angew. Chem. Int. Ed.* **2009**, *48*, 7488-7499.

(7)   Morgan, G. T.; Drew, H. D. K. *J. Chem. Soc., Trans.* **1920**, *117*, 1456-1465.

(8)   Stoll, M.; Rouvé, A.; Stoll-Comte, G. *Helv. Chim. Acta* **1934**, *17*, 1289-1308.

(9)   Kuhn, W. *Kolloid. Zh.* **1934**, *68*, 2-15.

(10)   Kirby, A. J. *Adv. Phys. Org. Chem.* **1980**, *17*, 183-278.

(11)   Mandolini, L. *Adv. Phys. Org. Chem.* **1986**, *22*, 1-111.

(12)   Illuminati, G.; Mandolini, L. *Acc. Chem. Res.* **1981**, *14*, 95-102.

(13)   Benson, S. W. *J. Am. Chem. Soc.* **1958**, *80*, 5151-5154.

(14)   Bishop, D. M.; Laidler, K. J. *J. Chem. Phys.* **1965**, *42*, 1688-1691.

(15)   Bailey, W. F.; Monahan, A. S. *J. Chem. Educ.* **1978**, *55*, 489-493.

(16)   Ercolani, G.; Piguet, C.; Borkovec, M.; Hamacek, J. *J. Phys. Chem. B* **2007**, *111*, 12195-12203.

(17)   Motloch, P.; Hunter, C. A. *Adv. Phys. Org. Chem.* **2016**, *50*, 77-118.

(18)   Hoffmann, M.; Wilson, C. J.; Odell, B.; Anderson, H. L. *Angew. Chem. Int. Ed.* **2007**, *46*, 3122-3125.

(19)   Hoffmann, M.; Kärnbratt, J.; Chang, M.-H.; Herz, L. M.; Albinsson, B.; Anderson, H. L. *Angew. Chem. Int. Ed.* **2008**, *47*, 4993-4996.

(20)   Liu, P.; Neuhaus, P.; Kondratuk, D. V.; Balaban, T. S.; Anderson, H. L. *Angew. Chem. Int. Ed.* **2014**, *53*, 7770-7773.

(21)   Hogben, H. J.; Sprafke, J. K.; Hoffmann, M.; Pawlicki, M.; Anderson, H. L. *J. Am. Chem. Soc.* **2011**, *133*, 20962-20969.

(22)   Montoro-García, C.; Camacho-García, J.; López-Pérez, A. M.; Bilbao, N.; Romero-Pérez, S.; Mayoral, M. J.; González-Rodríguez, D. *Angew. Chem. Int. Ed.* **2015**, *54*, 6780-6784.

(23)   Montoro-García, C.; Camacho-García, J.; López-Pérez, A. M.; Mayoral, M. J.; Bilbao, N.; González-Rodríguez, D. *Angew. Chem. Int. Ed.* **2016**, *55*, 223-227.

(24) Montoro-García, C.; Bilbao, N.; Tsagri, I. M.; Zaccaria, F.; Mayoral, M. J.; Fonseca Guerra, C.; González-Rodríguez, D. *Chem. Eur. J.* **2018**, *24*, 11983-11991.

(25) Montoro-García, C.; Mayoral, M. J.; Chamorro, R.; González-Rodríguez, D. *Angew. Chem. Int. Ed.* **2017**, *56*, 15649-15653.

(26) Wang, S.-P.; Shen, Y.-F.; Zhu, B.-Y.; Wu, J.; Li, S. *Chem. Commun.* **2016**, 10205-10216.

(27) Anderson, H. L.; Sanders, J. K. M. *Angew. Chem. Int. Ed.* **1990**, *29*, 1400-1403.

(28) Anderson, H. L. *Tetrahedron Lett.* **1992**, *33*, 1101-1104.

(29) Anderson, H. L. *Inorg. Chem.* **1994**, *33*, 972-981.

(30) Pawlicki, M.; Collins, H. A.; Denning, R. G.; Anderson, H. L. *Angew. Chem. Int. Ed.* **2009**, *48*, 3244-3266.

(31) Liu, P.; Hisamune, Y.; Peeks, M. D.; Odell, B.; Gong, J. Q.; Herz, L. M.; Anderson, H. L. *Angew. Chem. Int. Ed.* **2016**, *55*, 8358-8362.

(32) Liu, S.; Kondratuk, D. V.; Rousseaux, S. A. L.; Gil-Ramírez, G.; O'Sullivan, M. C.; Cremers, J.; Claridge, T. D. W.; Anderson, H. L. *Angew. Chem. Int. Ed.* **2015**, *54*, 5355-5359.

(33) Kondratuk, D. V.; PerdigãoLuís, M. A.; EsmailAyad, M. S.; O'Shea, J. N.; Beton, P. H.; Anderson, H. L. *Nat. Chem.* **2015**, *7*, 317-322.

(34) Rousseaux, S. A. L.; Gong, J. Q.; Haver, R.; Odell, B.; Claridge, T. D. W.; Herz, L. M.; Anderson, H. L. *J. Am. Chem. Soc.* **2015**, *137*, 12713-12718.

(35) Favereau, L.; Cnossen, A.; Kelber, J. B.; Gong, J. Q.; Oetterli, R. M.; Cremers, J.; Herz, L. M.; Anderson, H. L. *J. Am. Chem. Soc.* **2015**, *137*, 14256-14259.

(36) Cremers, J.; Haver, R.; Rickhaus, M.; Gong, J. Q.; Favereau, L.; Peeks, M. D.; Claridge, T. D. W.; Herz, L. M.; Anderson, H. L. *J. Am. Chem. Soc.* **2018**, *140*, 5352-5355.

(37) Neuhaus, P.; Cnossen, A.; Gong, J. Q.; Herz, L. M.; Anderson, H. L. *Angew. Chem. Int. Ed.* **2015**, *54*, 7344-7348.

(38) Haver, R.; Anderson, H. L. *Helv. Chim. Acta* **2019**, *102*, e1800211.

(39) Whitesides, G. M.; Simanek, E. E.; Mathias, J. P.; Seto, C. T.; Chin, D.; Mammen, M.; Gordon, D. M. *Acc. Chem. Res.* **1995**, *28*, 37-44.

(40) Mathias, J. P.; Simanek, E. E.; Zerkowski, J. A.; Seto, C. T.; Whitesides, G. M. *J. Am. Chem. Soc.* **1994**, *116*, 4316-4325.

(41) Zerkowski, J. A.; Seto, C. T.; Whitesides, G. M. *J. Am. Chem. Soc.* **1992**, *114*, 5473-5475.

(42) Ranganathan, A.; Pedireddi, V. R.; Rao, C. N. R. *J. Am. Chem. Soc.* **1999**, *121*, 1752-1753.

(43) Russell, K. C.; Leize, E.; Van Dorsselaer, A.; Lehn, J.-M. *Angew. Chem. Int. Ed.* **1995**, *34*, 209-213.

(44) Cheng, X.; Gao, Q.; Smith, R. D.; Simanek, E. E.; Mammen, M.; Whitesides, G. M. *J. Org. Chem.* **1996**, *61*, 2204-2206.

(45) Timmerman, P.; Jolliffe, K. A.; Crego Calama, M.; Weidmann, J.-L.; Prins, L. J.; Cardullo, F.; Snellink-Ruël, B. H. M.; Fokkens, R. H.; Nibbering, N. M. M.; Shinkai, S.; Reinhoudt, D. N. *Chem. Eur. J.* **2000**, *6*, 4104-4115.

(46) Timmerman, P.; Prins, L. J. *Eur. J. Org. Chem.* **2001**, *2001*, 3191-3205.

(47) Mathias, J. P.; Simanek, E. E.; Seto, C. T.; Whitesides, G. M. *Angew. Chem. Int. Ed.* **1993**, *32*, 1766-1769.

(48) Kerckhoffs, J. M. C. A.; van Leeuwen, F. W. B.; Spek, A. L.; Kooijman, H.; Crego-Calama, M.; Reinhoudt, D. N. *Angew. Chem. Int. Ed.* **2003**, *42*, 5717-5722.

(49) Shao, X.-B.; Jiang, X.-K.; Zhu, S.-Z.; Li, Z.-T. *Tetrahedron* **2004**, *60*, 9155-9162.

(50) Mammen, M.; Simanek, E. E.; Whitesides, G. M. *J. Am. Chem. Soc.* **1996**, *118*, 12614-12623.

(51) Bielejewska, A. G.; Marjo, C. E.; Prins, L. J.; Timmerman, P.; de Jong, F.; Reinhoudt, D. N. *J. Am. Chem. Soc.* **2001**, *123*, 7518-7533.

(52) ten Cate, M. G. J.; Huskens, J.; Crego-Calama, M.; Reinhoudt, D. N. *Chem. Eur. J.* **2004**, *10*, 3632-3639.

(53) Zerkowski, J. A.; Seto, C. T.; Wierda, D. A.; Whitesides, G. M. *J. Am. Chem. Soc.* **1990**, *112*, 9025-9026.

(54) Ballester, P.; Fujita, M.; Rebek, J. *Chem. Soc. Rev.* **2015**, *44*, 392-393.

(55) Chakrabarty, R.; Mukherjee, P. S.; Stang, P. J. *Chem. Rev.* **2011**, *111*, 6810-6918.

(56) Han, M.; Engelhard, D. M.; Clever, G. H. *Chem. Soc. Rev.* **2014**, *43*, 1848-1860.

(57) Rebek, J. J. *Chem. Commun.* **2000**, 637-643.

(58) Rebek Jr., J. *Angew. Chem. Int. Ed.* **2005**, *44*, 2068-2078.

(59) Custelcean, R. *Chem. Soc. Rev.* **2014**, *43*, 1813-1824.

(60) Brown, C. J.; Toste, F. D.; Bergman, R. G.; Raymond, K. N. *Chem. Rev.* **2015**, *115*, 3012-3035.

(61) Pappalardo, A.; Puglisi, R.; Trusso Sfrazzetto, G. *Catalysts* **2019**, *9*, 630.

(62) McConnell, A. J.; Wood, C. S.; Neelakandan, P. P.; Nitschke, J. R. *Chem. Rev.* **2015**, *115*, 7729-7793.

(63)   Díaz-Moscoso, A.; Ballester, P. *Chem. Commun.* **2017**, *53*, 4635-4652.

(64)   Fujita, M.; Tominaga, M.; Hori, A.; Therrien, B. *Acc. Chem. Res.* **2005**, *38*, 369-378.

(65)   Seidel, S. R.; Stang, P. J. *Acc. Chem. Res.* **2002**, *35*, 972-983.

(66)   Caulder, D. L.; Raymond, K. N. *Acc. Chem. Res.* **1999**, *32*, 975-982.

(67)   Fujita, M.; Yazaki, J.; Ogura, K. *J. Am. Chem. Soc.* **1990**, *112*, 5645-5647.

(68)   Stang, P. J. *J. Org. Chem.* **2009**, *74*, 2-20.

(69)   Fujita, D.; Ueda, Y.; Sato, S.; Mizuno, N.; Kumasaka, T.; Fujita, M. *Nature* **2016**, *540*, 563-566.

(70)   Wyler, R.; de Mendoza, J.; Rebek Jr., J. *Angew. Chem. Int. Ed.* **1993**, *32*, 1699-1701.

(71)   Branda, N.; Wyler, R.; Rebek, J. *Science* **1994**, *263*, 1267-1268.

(72)   Meissner, R. S.; Rebek, J.; de Mendoza, J. *Science* **1995**, *270*, 1485-1488.

(73)   Kang, J.; Rebek, J. *Nature* **1996**, *382*, 239-241.

(74)   Mateos-Timoneda, M. A.; Kerckhoffs, J. M. C. A.; Reinhoudt, D. N.; Crego-Calama, M. *Org. Biomol. Chem.* **2007**, *5*, 447-449.

(75)   Conn, M. M.; Rebek, J. *Chem. Rev.* **1997**, *97*, 1647-1668.

(76)   Burrows, A. D.; Chan, C.-W.; Chowdhry, M. M.; McGrady, J. E.; Mingos, D. M. P. *Chem. Soc. Rev.* **1995**, *24*, 329-339.

(77)   Drain, C. M.; Fischer, R.; Nolen, E. G.; Lehn, J.-M. *J. Chem. Soc., Chem. Commun.* **1993**, 243-245.

(78)   Park, J.; Lang, K.; Abboud, K. A.; Hong, S. *J. Am. Chem. Soc.* **2008**, *130*, 16484-16485.

(79)   Fujimoto, K.; Toyoshi, T.; Doi, Y.; Inouye, M. *Mater. Sci. Eng. C* **2007**, *27*, 142-147.

(80)   McKinlay, R. M.; Thallapally, P. K.; Cave, G. W. V.; Atwood, J. L. *Angew. Chem. Int. Ed.* **2005**, *44*, 5733-5736.

(81)   Appavoo, D.; Raja, N.; Deschenaux, R.; Therrien, B.; Carnevale, D. *Dalton Trans.* **2016**, *45*, 1410-1421.

(82)   Galindo, M. A.; Amantia, D.; Clegg, W.; Harrington, R. W.; Eyre, R. J.; Goss, J. P.; Briddon, P. R.; McFarlane, W.; Houlton, A. *Chem. Commun.* **2009**, 2833-2835.

(83)   Kokan, Z.; Kovačević, B.; Štefanić, Z.; Tzvetkova, P.; Kirin, S. I. *Chem. Commun.* **2018**, *54*, 2094-2097.

(84)   Alam, M. A.; Nethaji, M.; Ray, M. *Angew. Chem. Int. Ed.* **2003**, *42*, 1940-1942.

II

Aims

The general aim of this work is to study chelate cooperativity in multivalent supramolecular systems to increase the understanding of this fundamental phenomenon.

As described in Chapter I, porphyrin nanorings show the highest values of effective molarity reported in the literature, particularly the 6-ring that was explored in great detail. The goal is to study if the extreme values of effective molarity found out for the 6-ring can stabilise a H-bonded system inside the 6-ring cavity. This would provide new insights about these extreme values of effective molarity and answer whether additional flexibility and different nature of the supramolecular ligand system compared to the one-molecule covalent ligand can be beneficial or not. The designed system would keep the pyridine units as the molecular recognition for the zinc porphyrins (Figure 2.1).
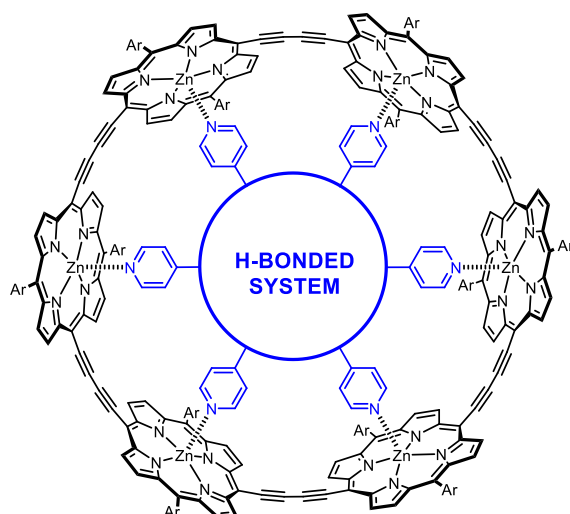
Figure 2.1. H-bonded supramolecular system inside the porphyrin nanoring.

Two different systems will be explored. The first one is based on a H-bonded system that utilises phenols as H-bond acceptors and phosphine oxides as H-bond donors (Figure 2.2a). This would presumably provide strong H-bonding according to the molecular recognition toolbox. The second system is based on a H-bonded rosette motif that employs barbiturates and pyrimidines (Figure 2.2b).
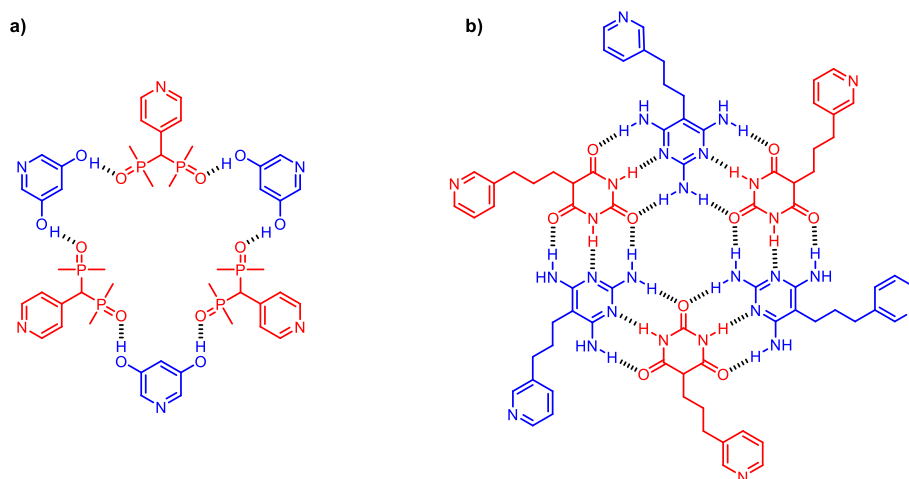
Figure 2.2. (a) H-bonded supramolecular system based on phenols and phosphine oxides, (b) H-bonded supramolecular system based on the rosette motif.

In order to fully quantify the binding of the rosette system inside the porphyrin nanoring, the chelate cooperativity of the rosette motif has to be studied initially, as this has not been reported so far, as was shown in Chapter I.

In addition, we hypothesised that the aforementioned molecules could be used to explore the preparation of a new class of hybrid H-bonded/metal-coordinated cages (Figure 2.3) as they feature the H-bonded component (rosette) as well as the metal-coordinated part (utilising the pyridines). Due to their hybrid character, these cages should potentially show an interesting stimuli-responsive behaviour.
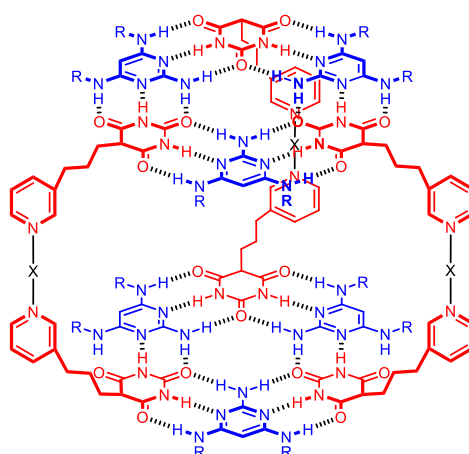
Figure 2.3. Hybrid H-bonded/metal-coordinated cages (X is a metal).

III
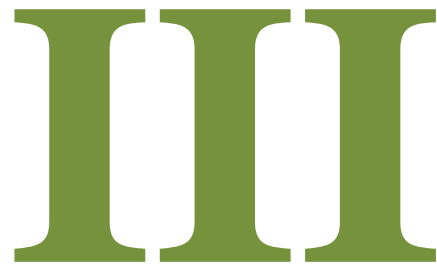
Rosette motif revisited

3.1. Introduction

The study of thermodynamic parameters of different multivalent supramolecular systems plays an important role in their understanding, and as a foundation stone for the design of new systems with desirable behaviour. Significant attention is paid to the competition of cyclisation and polymerisation of these systems through ring-chain equilibria.[1-3] When the cyclisation is preferred, a system shows chelate cooperativity, which is quantified by the effective molarity (EM). Many multivalent supramolecular systems have been studied in great detail and their EMs have been determined,[2] such as porphyrin nanorings from the Anderson group,[4] H-bonded systems based on G-C dinucleoside monomers from the group of González-Rodríguez,[5] and complexes of zinc porphyrins with various pyridine ligands from the Hunter group.[6]

Even though the rosette motif has been studied extensively by many groups over the last 30 years,[7-9] the thermodynamics of its self-assembly has only been studied scarcely. The groups of Crego-Calama and Reinhoudt studied the formation of different single and double rosette complexes by ITC in 1,2-dichloroethane at 298 K.[10] For the rosette shown in Figure 3.1, they determined an association constant to be $(1.4 \pm 0.3) \times 10^{20}\,\text{M}^{-5}$.
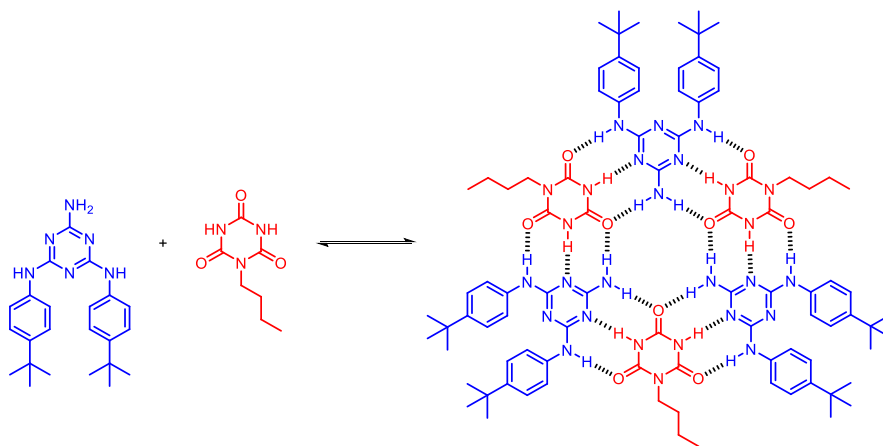
Figure 3.1. Rosette formation from a cyanurate and a triaminotriazine.

The group of Timmerman conducted a detailed study of the thermodynamics of barbiturate/triaminotriazine system in $CDCl_3$ by ^{1}H NMR at 297 K and by VPO in 1,2-dichloroethane at 308 K.[11] They used blocked barbiturates and triaminotriazines to measure reference intermolecular association constants K_0 as depicted in Figure 3.2a. By using a model bis(triaminotriazine) system that should resemble a rosette based on the examination of molecular models (Figure 3.2b), they determined an effective molarity of rosette formation

from measuring K_{plug} of the model assembly. Using $K_{plug} = 4 \times EM \times K_0$, they calculated the effective molarity of the rosette formation to be 0.18 ± 0.05 M. We believe that this model does not provide a realistic view of the rosette cyclisation, because of the phenyl hydrogen highlighted in Figure 3.2b, which is not present in the rosette motif. Additional interactions with the barbiturate carbonyl group could, therefore, affect the stability of the model complex in comparison to the rosette. We decided to revisit the thermodynamics of the rosette self-assembly in detail and determine its effective molarity using a more suitable system.
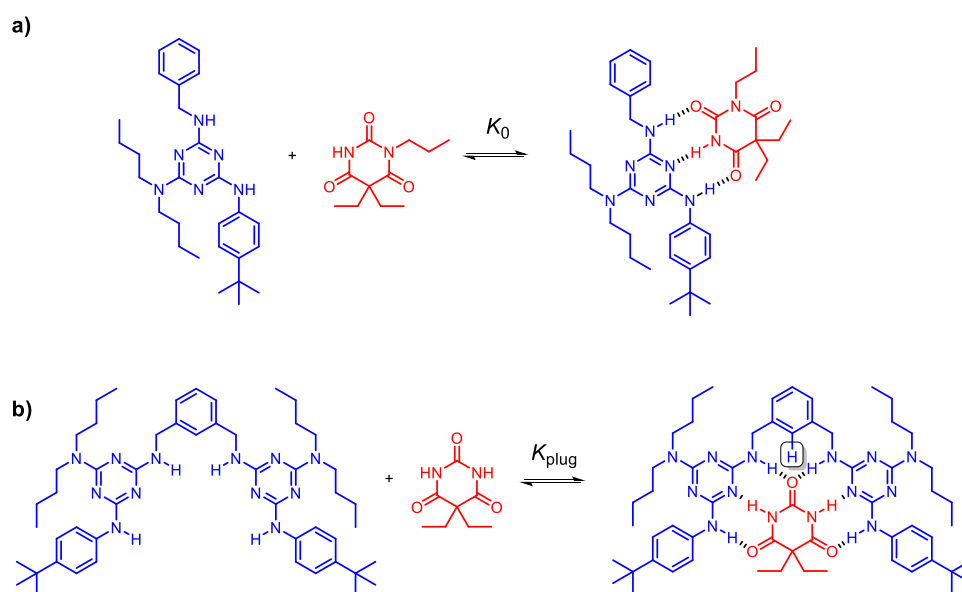
Figure 3.2. Equilibria used by the Timmerman group to study chelate cooperativity of the rosette motif. (a) Reference intermolecular interaction using blocked triaminotriazine and barbiturate. (b) Using bis(triaminotriazine) to simulate the rosette motif to obtain the effective molarity of rosette cyclisation. Highlighted hydrogen can affect the stability of the complex compared to the rosette motif.

The extensive investigation of the rosette motif has led to two general concepts, preorganisation and peripheral crowding.[7] The concept of peripheral crowding originated from the research of the Whitesides group. They obtained a series of X-ray structures with different substituents on the periphery of triaminotriazines that crystallise in different architectures: rosettes, linear tapes and crinkled tapes (Figure 3.3). From these results, they postulated that triaminotriazines with bulky substituents in a periphery form rosettes because of "peripheral crowding" that destabilise the other topologies (Figure 3.3a) both in solid phase and solution. However, this concept was questioned by the work of the Timmerman group,[11] who argued that the selectivity can originate simply from a different solubility of the

competing species – the least soluble complex crystallises first, no matter what the relative stability of the species in solution is. Nobody continued in this work to fully proof their hypothesis experimentally and Whitesides concept is still being used for both solid an solution phases.[12] We therefore decided to revisit the concept of peripheral crowding in solution as well.
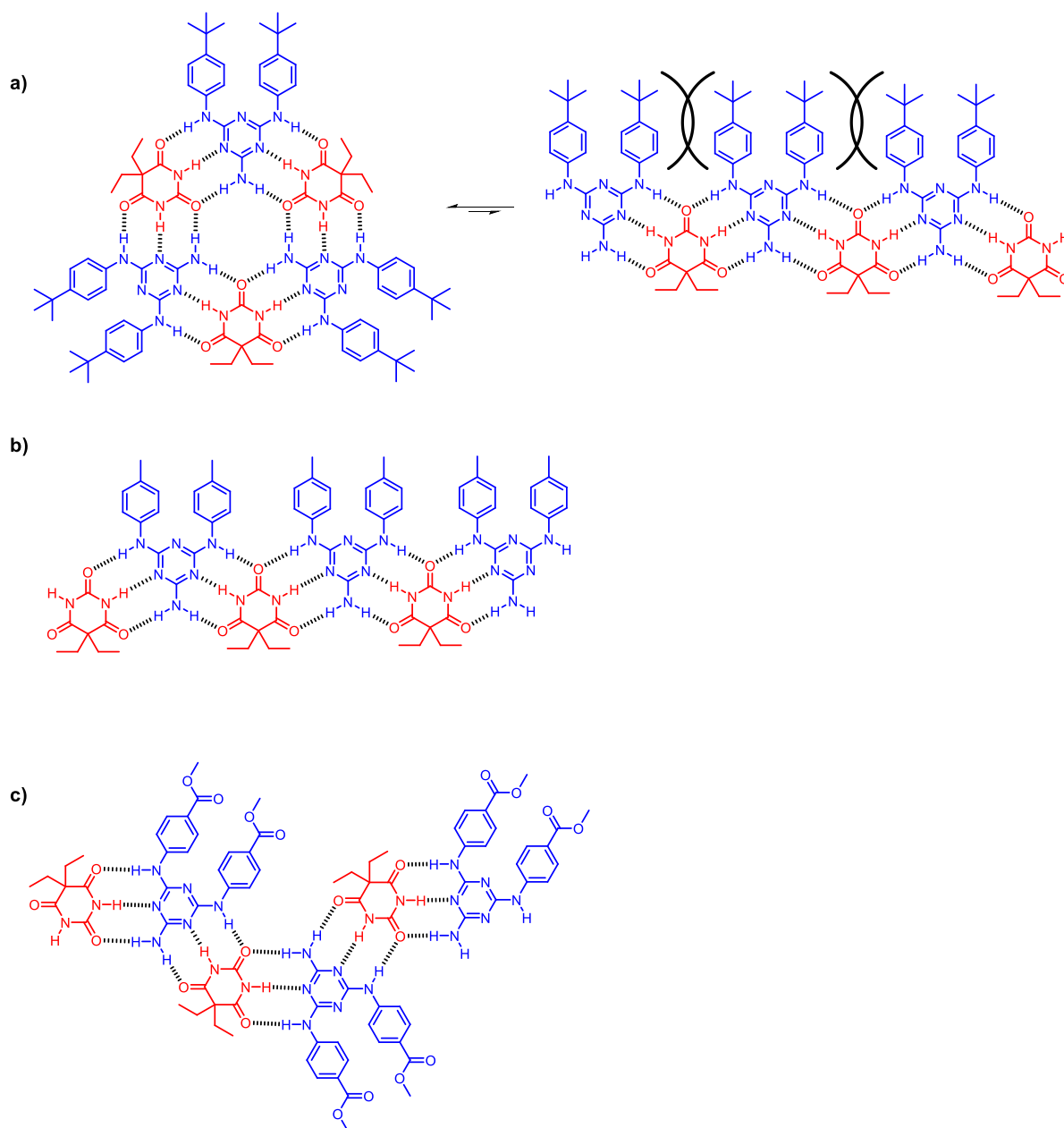
Figure 3.3. Different architectures of barbiturate/triaminotriazines complexes in the solid state; a) rosette, (b) linear tape and (c) crinkled tape. (a) Also shows the concept of peripheral crowding. The bulkiness of the periphery of triaminotriazine leads to a preferable formation of the rosette.

3.2. Approach

Most of the work done by the groups of Whitesides, Reinhoudt and others used 1,3,5-triaminotriazines for the construction of rosettes.[7-9] These molecules provide some great advantages, such as modular synthesis.[13] It is possible to selectively exchange the three chlorine atoms in cyanuric acid by a wide range of nucleophiles by simply changing the temperature (Figure 3.4a). On the other hand, triaminotriazines form rotamers that exchange slowly on the ^{1}H NMR time-scale and complicate the NMR analysis of these molecules and their supramolecular complexes (Figure 3.4b).[11,14]
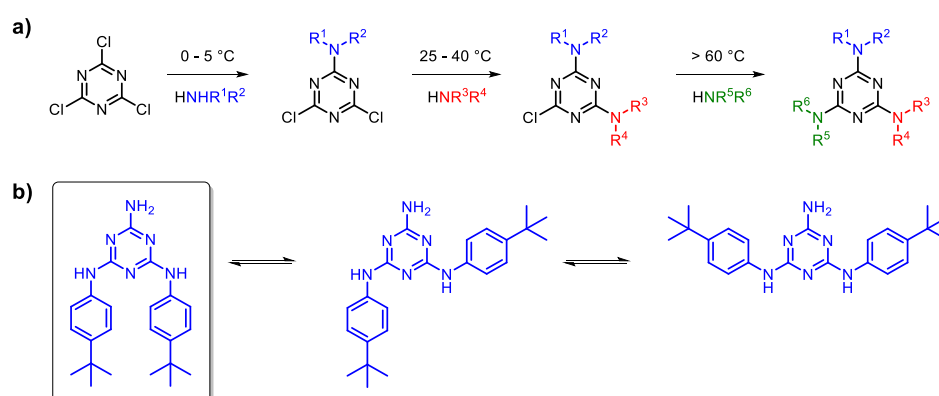
Figure 3.4. (a) Modular synthesis of triaminotriazines (R are substituents). (b) Rotamers of triaminotriazines; only the highlighted rotamer can form a rosette.

In this work, we decided to replace triazines with pyrimidines, which also allow for step-wise functionalisation while avoiding the formation of multiple rotamers on the NMR time-scale. In addition, the aromatic C-H of the pyrimidines should provide an additional NMR probe for studying supramolecular self-assembly. Moreover, the ^{1}H NMR chemical shift of this aromatic C-H is around 6 ppm,[15] which should not overlap with any other resonances and, therefore, greatly simplify the NMR analysis. Surprisingly, the use of pyrimidines to form rosettes has not been widely explored in the literature. There is only one example of using a pyrimidine successfully to form the rosette. However, this was mass spectrometry study.[15] The group of Lehn has used pyrimidines to obtain supramolecular strands based on barbiturates.[16] Lately, pyrimidines have been used in the origin of life research that explores the rosette motif in water.[17]

To be able to determine the effective molarity of the rosette system, the intramolecular and intermolecular equilibrium constants K_{intra} and K_{inter}, respectively, outlined in Figure 3.5 have to be measured.
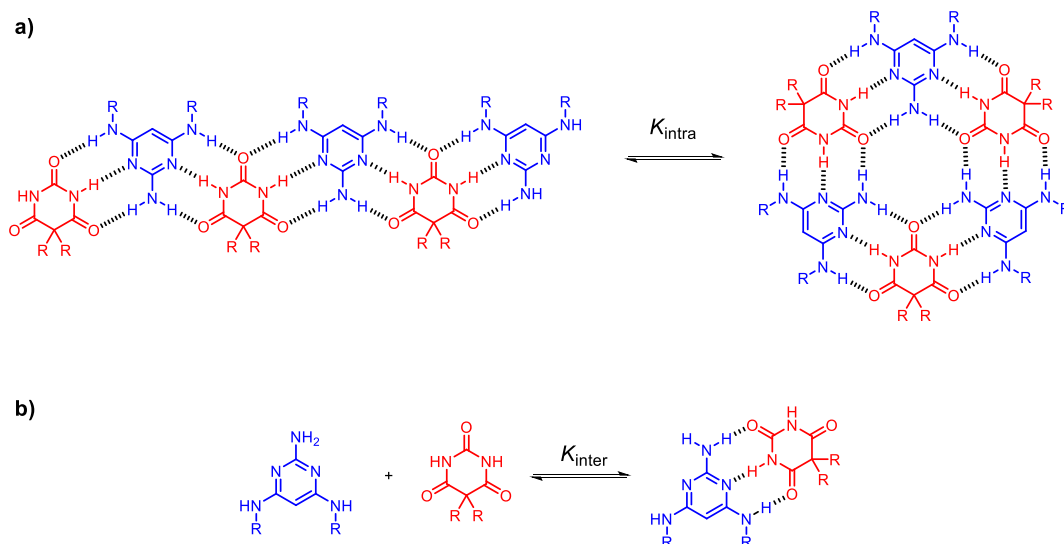
Figure 3.5. (a) Intramolecular cyclisation of a linear oligomer to form a rosette. (b) Intermolecular binding of triaminotriazine and barbiturate. (R is a substituent).

The effective molarity for the intramolecular interaction involved in cyclisation of rosette is given by Equation 3.1.

$$\text{EM} = \frac{K_{intra}}{K_{inter}} \tag{3.1}$$

Unfortunately, neither equilibrium constant depicted in Figure 3.5 can be measured directly. This is usually overcome by measuring the overall equilibrium constant for the formation of the target complex, and using a suitable reference system that provides the equilibrium constants for the corresponding intermolecular interaction. The overall equilibrium constant for the formation of the rosette from its components can be measured easily (Figure 3.6a). We decided to employ blocked rosette building blocks to be able to measure the reference intermolecular association constant, which was also used by the group of Timmerman. The blocking is done by the substitution of N-H in the barbiturate or the pyrimidine for an alkyl group. Since the blocked species have only one site that is able to form a triply H-bond complex, which is significantly more stable than a doubly H-bond complex (Figure 3.7),[9] these systems form only the desired 1:1 reference intermolecular

complex (Figure 3.6b). The effective molarity for the intermolecular interaction involved in cyclisation of rosette is given by Equation 3.2.

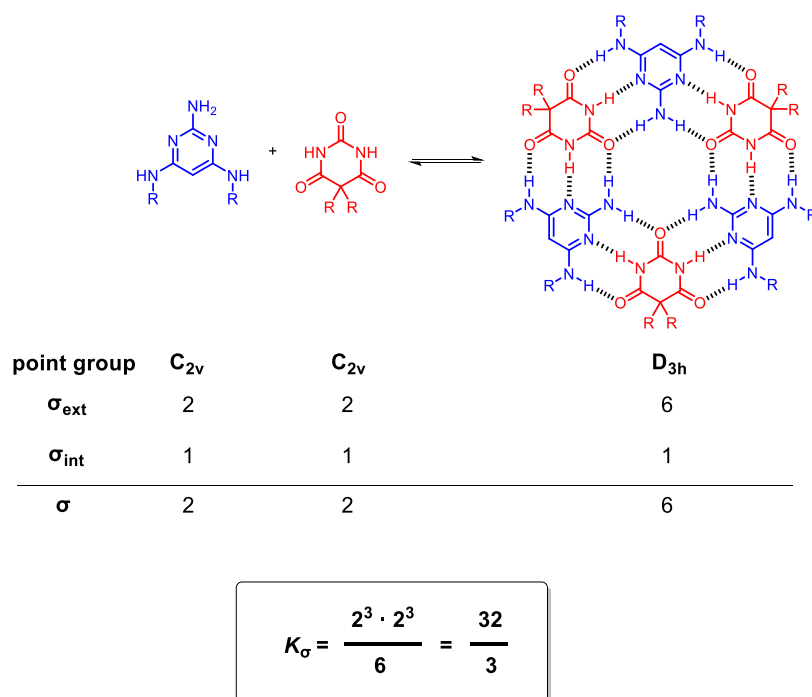$$EM = \frac{K_{rosette}}{K_\sigma \times (K_{ref})^6} \qquad (3.2)$$

where the statistical factor K_σ is based on the symmetry of the involved species.[18-21] Figure 3.8 shows that K_σ for the rosette formation is $\frac{32}{3}$ as calculated by the symmetry number method from internal and external symmetry of each component.
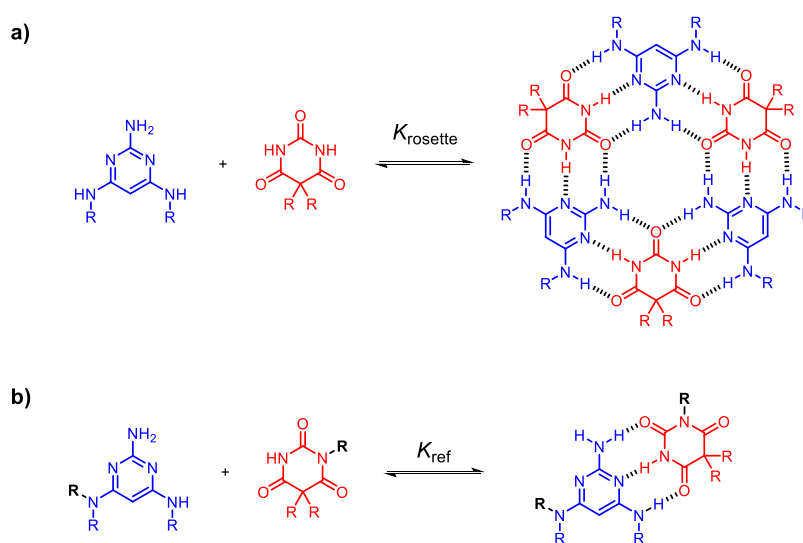
Figure 3.6. (a) Assembly of a pyrimidine and barbiturate to form a rosette. (b) Reference intermolecular equilibrium using blocked building blocks. (R is a substituent).

$K = 10^4 - 10^5\ M^{-1}$ $K = 100 \pm 20\ M^{-1}$
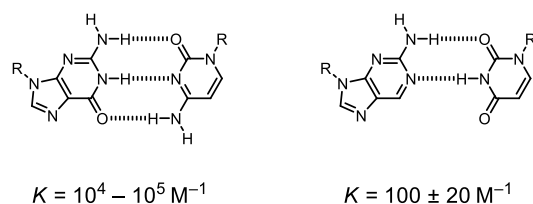
Figure 3.7. Association constants (CHCl₃, 298K) for a triply H-bonded complex (left) and doubly H-bonded complex (right) using nucleic acid derivatives (R is a substituent).[22]

47

point group	C_{2v}	C_{2v}	D_{3h}
σ_{ext}	2	2	6
σ_{int}	1	1	1
σ	2	2	6

$$K_\sigma = \frac{2^3 \cdot 2^3}{6} = \frac{32}{3}$$

Figure 3.8. Determination of the statistical factor K_σ for the rosette assembly (R is a substituent).

To check if there is some allosteric cooperativity associated with multiple H-bond interactions with each component in the rosette, reference 1:2 complexes are also required (Figure 3.9). They can be described in two steps with two different macroscopic equilibrium constants $K_{1,obs}$ and $K_{2,obs}$. In order to obtain the microscopic equilibrium constants K_1 and K_2 that describe the intrinsic thermodynamic properties of the interactions, statistical factor have to be included (Figure 3.10), which translate to $K_{1,obs} = 2 \times K_1$ and $K_{2,obs} = \frac{1}{2} K_2$. The allosteric cooperativity α is then given by Equation 3.3.

$$\alpha = \frac{K_2}{K_1} \tag{3.3}$$

a)

b)
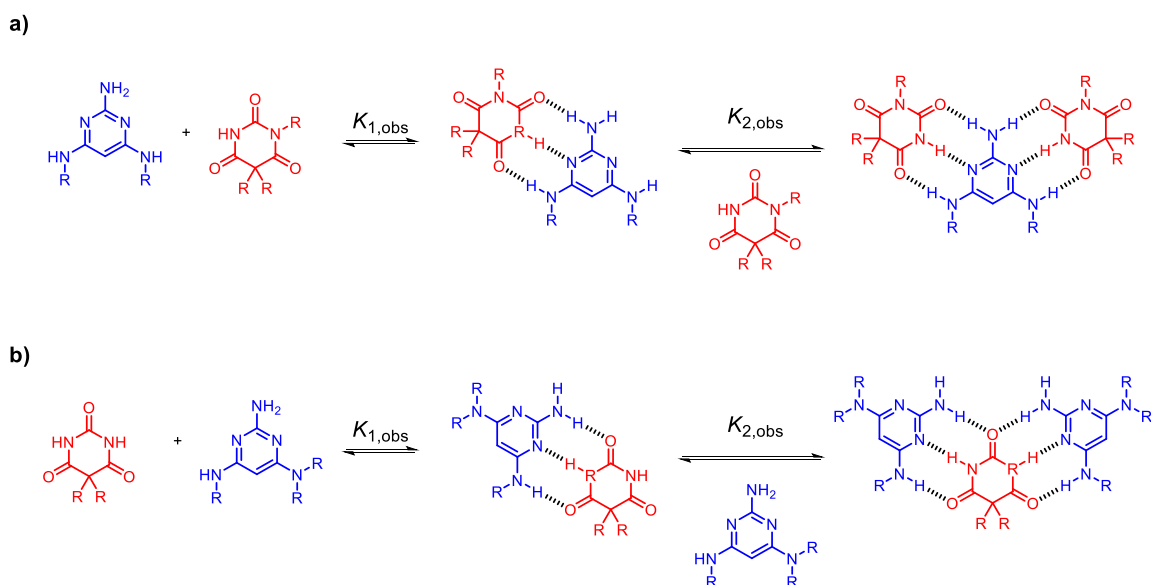
Figure 3.9. Reference 1:2 equilibria using (a) pyrimidine and blocked-barbiturate and (b) barbiturate and blocked-pyrimidine (R is a substituent).

We also decided to include cyanurates that are sometimes used instead of barbiturates in the preparation of rosettes. All the equations and statistical factors derived above for the barbiturates can also be applied to the cyanurates thanks to their analogous symmetry. In addition, the concept of peripheral crowding originated mostly from the solid state. Because of that, we decided to revisit this concept in the solution by employing both bulky (with *p-tert*-butylphenyl being the best candidate based on the results from the Whitesides group) as well as a less bulky pyrimidine – one having only flexible alkyl groups.

To study these equilibria, a non-polar solvent has to be used, as these H-bonded systems would be disrupted in polar solvents such as methanol. We decided to employ chloroform, because these compounds are quite polar and usually hard to dissolve. Chloroform provides a good balance between the H-bond strength and solubility. The less polar toluene would increase the H-bonding, but the solubility in toluene is significantly lower.[23] We tried to increase the solubility in non-polar solvents as much as possible by introducing alkyl chains into these molecules.

point group	C_{2v}	C_{1v}	C_{1v}
σ_{ext}	2	1	1
σ_{int}	1	1	1
σ	2	1	1

$$K_{\sigma} = \frac{2 \cdot 1}{1} = 2$$

point group	C_{1v}	C_{1v}	C_{2v}
σ_{ext}	1	1	2
σ_{int}	1	1	1
σ	1	1	2

$$K_{\sigma} = \frac{1 \cdot 1}{2} = \frac{1}{2}$$
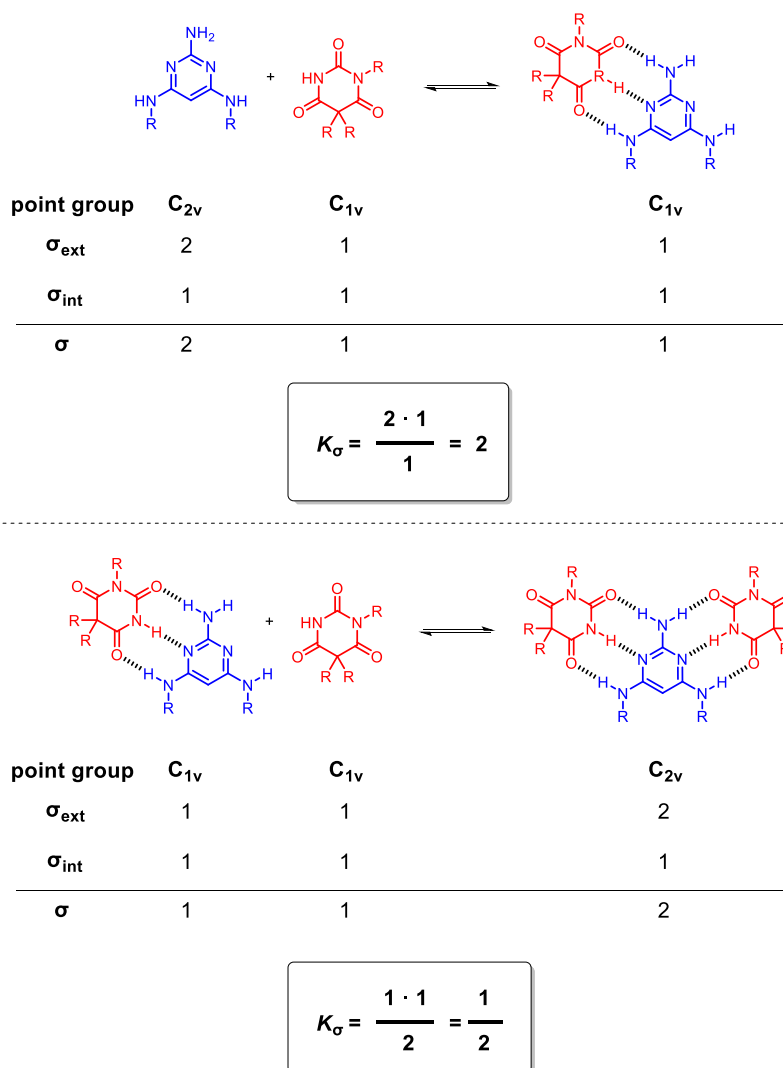
Figure 3.10. Determination of the statistical factors for the reference 1:2 systems. The statistical factors are identical for the corresponding system based on a barbiturate and blocked-pyrimidines.

3.3. Synthesis

Alkyl triaminopyrimidine **PA** and bulky *tert*-butylphenyl triaminopyrimide **PB** were synthesised in one step syntheses in good yields from commercially available 4,6-dichloropyrimidin-2-amine at 130 – 150 °C under microwave irradiation (Scheme 3.1). Slightly harsher conditions had to be used to obtain **PB** as the aniline is less reactive. Different conditions using *iso*-propyl alcohol as a solvent and diisopropylethylamine as a base were therefore used.
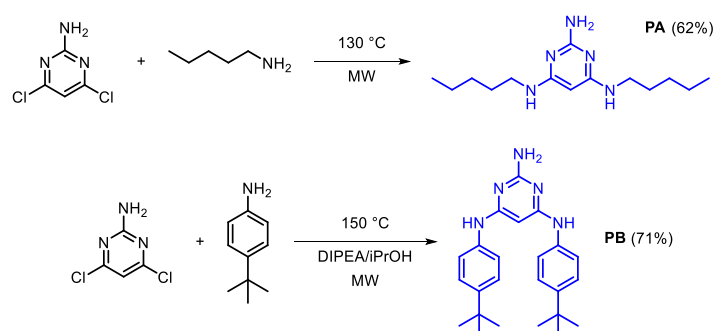
Scheme 3.1. Synthesis of triaminopyrimidines **PA** and **PB**.

To prepare blocked-pyrimidines **bPA** and **bPB**, a modular synthesis was utilised (Scheme 3.2). Reacting 4,6-dichloropyrimidin-2-amine with *N*-methylpenthylamine and K$_2$CO$_3$ as a base in *tert*-butanol at 60 °C provided the singly substituted product **bPA-Cl**. It was then converted to final product **bPA** by heating in neat *n*-penthylamine at 160 °C under microwave irradiation. For the synthesis of **bPB**, blocked *tert*-butylphenyl aniline **bTBA** had to be prepared first. This was achieved by a reaction of *tert*-butyl aniline with acetic anhydride followed by reduction using LiAlH$_4$. The blocked aniline was then used for the synthesis of the singly substituted product **bPB-Cl** that was converted to target compound **bPB** simply by heating in neat *tert*-butyl aniline at 160 °C under microwave irradiation.

Commercially available diethyl-barbiturate was not soluble enough in chloroform for NMR titrations, and therefore barbiturate **B** with longer alkyl chains was synthesised from urea (Scheme 3.3). The cyanurate **C** with *n*-pentyl was prepared from cyanuric acid by nucleophile substitution with iodopentane. The reaction also provided blocked-cyanurate **bC** (Scheme 3.3). Blocked barbiturate **bB** was synthesised in the same fashion as barbiturate **B** using *N*-methylurea instead of urea (Scheme 3.3).

a)

bPA-Cl (75%)   bPA (84%)

b)

bTBA (88% two steps)   bPB-Cl (85%)   bPB (66%)
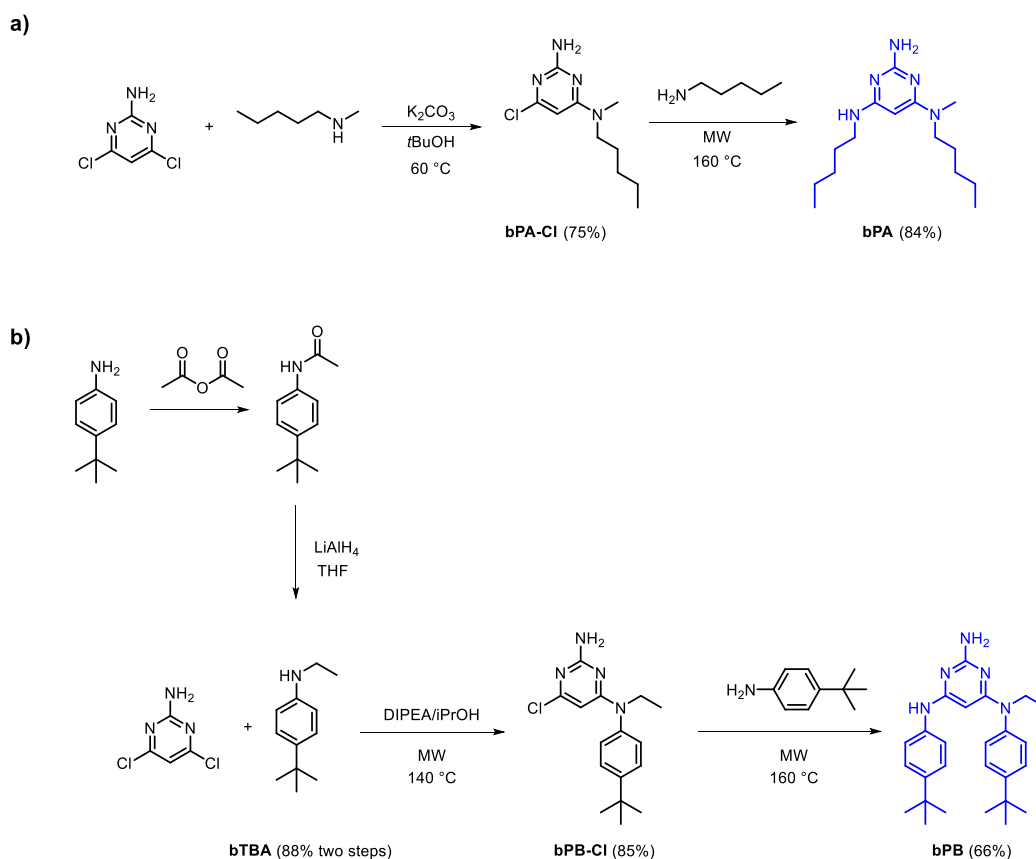
Scheme 3.2. Synthesis of blocked-pyrimidines (a) **bPA** and (b) **bPB**.

B (32%)

C (13%)   bC (15%)

bB (97%)
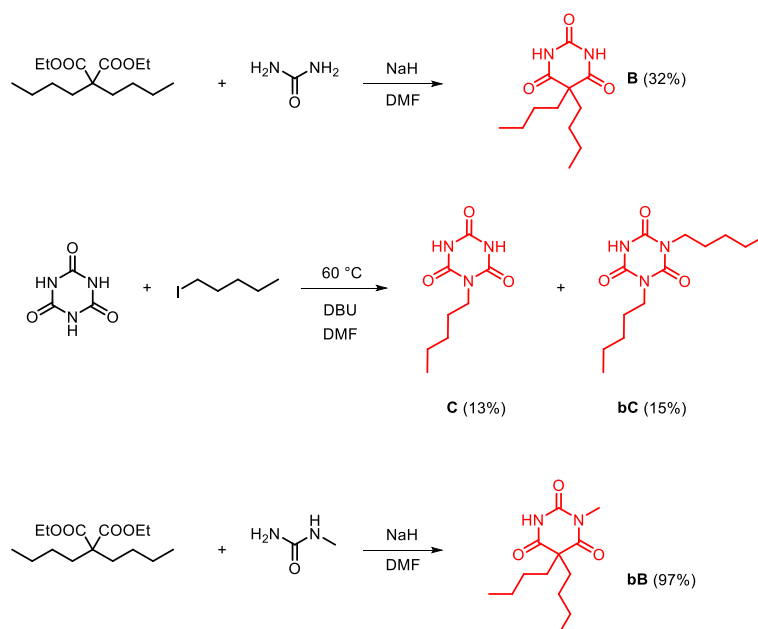
Scheme 3.3. Synthesis of barbiturate **B**, cyanurate **C**, blocked-cyanurate **bC** and blocked-barbiturate **bB**.

3.4. Characterisation of rosettes

To study rosette formation, all possible combinations (namely **PA•B**, **PB•B**, **PA•C** and **PB•C**) were prepared in CDCl$_3$ at 3 mM concentration of each component and then investigated by NMR spectroscopy at 298 K and 233 K (Figure 3.11). At 233 K, all of the complexes showed the characteristic peak of rosettes in the region of δ 14 − 15 ppm corresponding to bound N-H from the barbiturate/cyanurate and two peaks in the region δ 8 − 11 ppm from the N-H and NH$_2$ in pyrimidines.[7] At 298 K, only complexes containing cyanurate **C** showed the characteristic rosette peaks. They were broad as the rosette is less stable at 298 K. The reason why the rosettes based on barbiturate **B** are not visible at 298 K is probably because of an intermediate exchange of the free components and assemblies on the ^{1}H NMR time-scale.
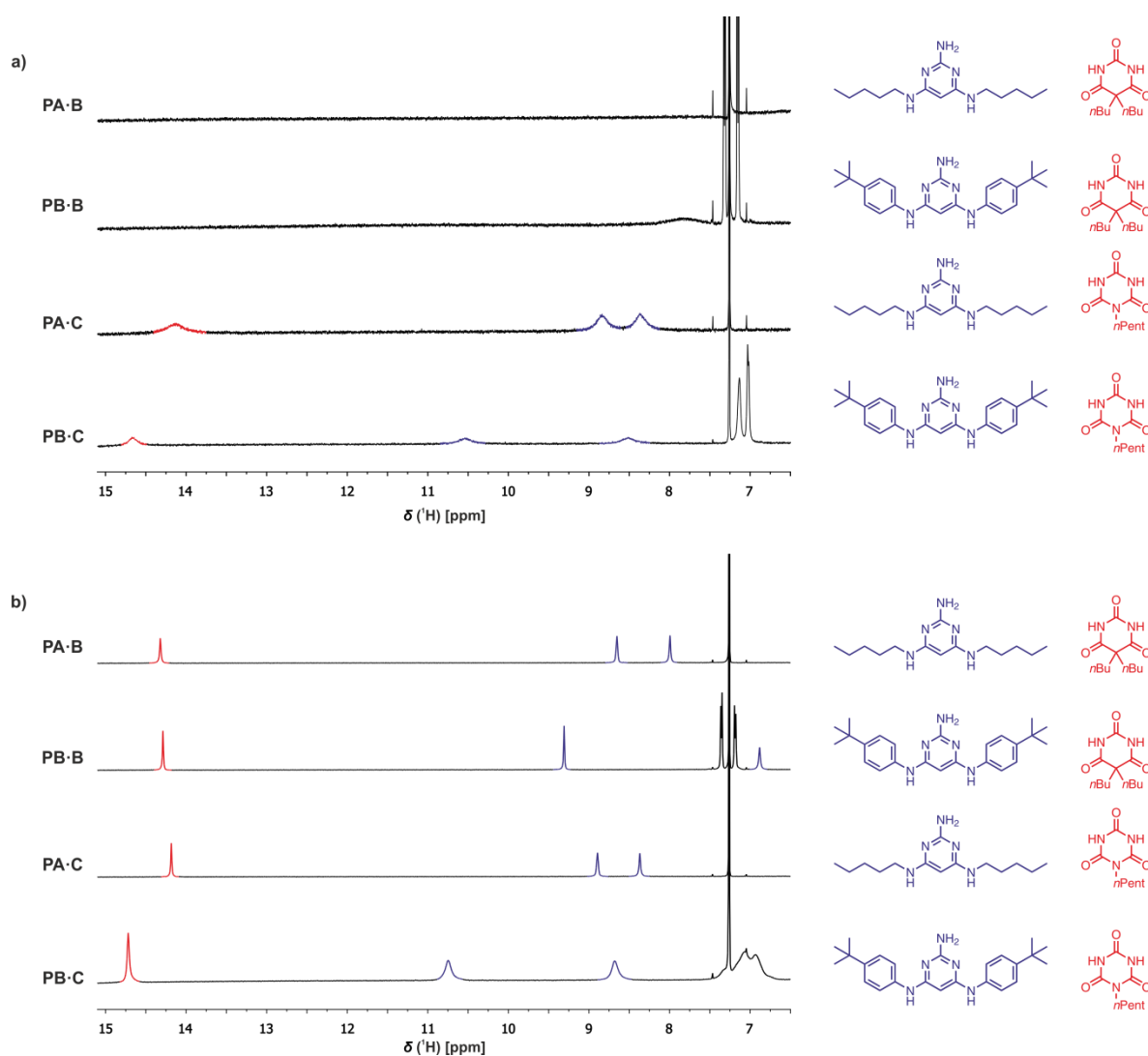
Figure 3.11. Partial ^{1}H NMR spectra (500 MHz, CDCl$_3$) of rosette assemblies at (a) 298 K and (b) 233 K; from top to bottom: **PA•B**, **PB•B**, **PA•C** and **PB•C** with concentration of 3 mM of each component. Barbiturate/cyanurate N-H in red, pyrimidine NH/NH$_2$ in blue.
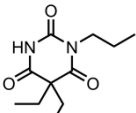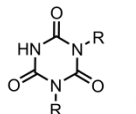
3.5. Dilution experiments

First of all, the self-association of rosette building blocks had to be checked, as this could highly influence the apparent stability of the rosette. For barbiturates and cyanurates, this was already done by the group of Timmerman (Table 3.1).[11] Triaminopyrimidine **PA** and blocked-pyrimidine **bPB** were chosen to study pyrimidine self-association in chloroform (Figure 3.12). It was possible to follow the changes in the aromatic C-H and both N-H peaks. A dimerisation isotherm was fitted to the obtained experimental data. All of the rosette components self-associate with $K < 10 \, M^{-1}$ (Table 3.1). Provided that the concentrations do not significantly exceed 10 mM, self-association will not affect the titration experiments.
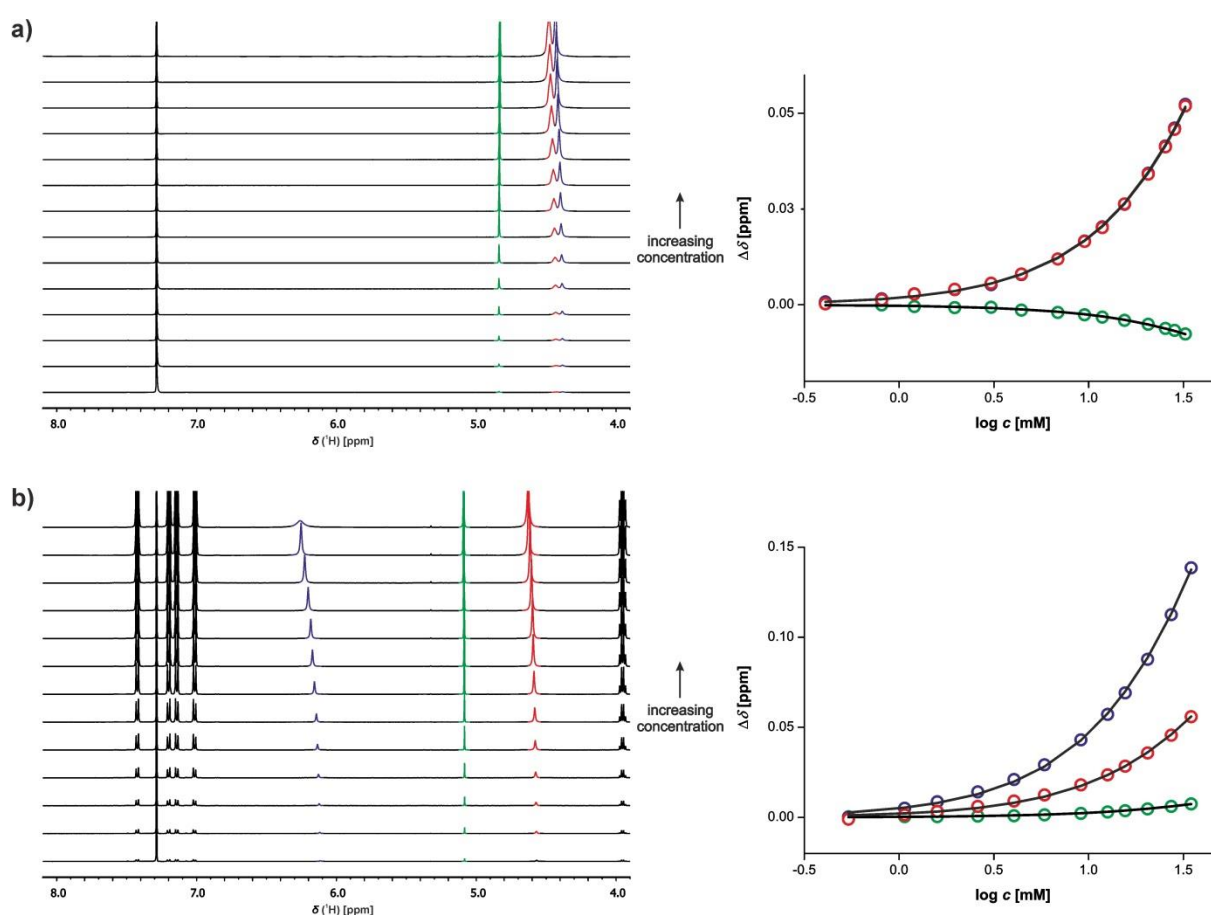
Figure 3.12. ^{1}H NMR (500 MHz, CDCl$_3$, 298 K) dilution experiments for (a) triaminopyrimidine **PA** and (b) blocked-pyrimidine **bPB**. The ^{1}H NMR spectra are shown on the left (pyrimidine C-H signal green, N-H signals blue and red). On the right are shown the experimental data (circles) and calculated values (lines) based on a dimerisation isotherm.

Table 3.1. Dimerisation constants in CDCl$_3$ at 298 K, measured by ^{1}H NMR dilutions.

Compound	K_{dim} [M^{-1}]
(a)	1.7 ± 0.5
(a)	7.4 ± 0.09
PA[b]	2 ± 1
bPB[b]	1 ± 2

[a]Measured by Timmerman group at 297 K.
[b]Errors are quoted as two times the standard
deviation based on two repetitions.
R = p-[C$_6$H$_4$]CH(CH$_3$)$_2$

3.6. Reference intermolecular titrations

To determine reference intermolecular association constants, we conducted ^{1}H NMR titrations in CDCl$_3$ at 298 K using blocked-pyrimidines **bPA** and **bPB** as hosts and blocked-barbiturate **bB** and blocked-cyanurate **bC** as guests, respectively. Again, it was possible to follow both the aromatic C-H and both N-H peaks of pyrimidine. The titration of **bB** into **bPA** is depicted in Figure 3.13, and all the remaining titrations data can be found in the Experimental section. A 1:1 binding isotherm was used to fit the experimental data. The results from these titrations are summarised in Table 3.2.
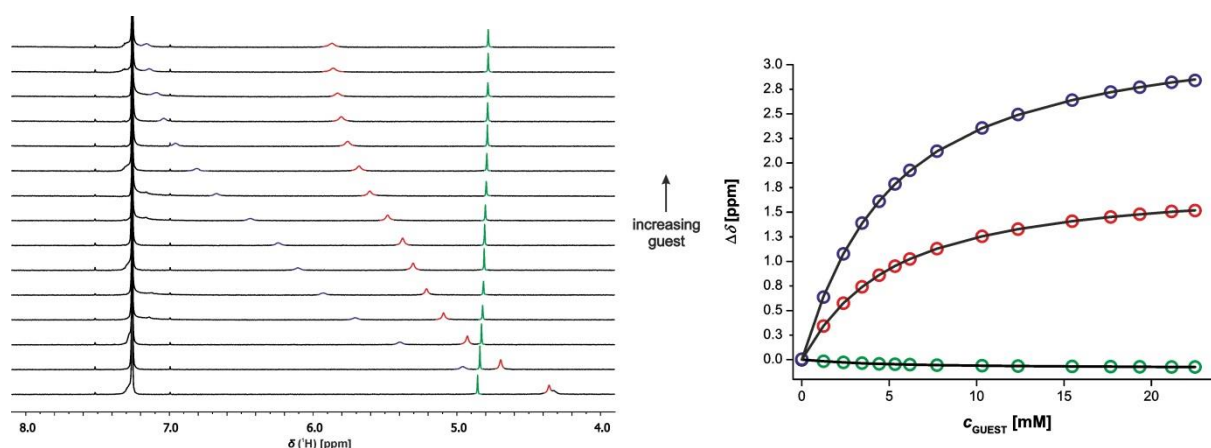
Figure 3.13. ^{1}H NMR (400 MHz, CDCl$_3$, 298 K) titration of **bB** into **bPA** (1.4 mM). ^{1}H NMR spectrum is shown on the left (pyrimidine C-H signal green, N-H signals blue and red). On the right are shown the experimental data (circles) and calculated values (lines) based on a 1:1 binding isotherm.

Table 3.2. Association constants in CDCl$_3$ at 298 K, measured by ^{1}H NMR titrations.[a]

Complex	K_{ref} [M^{-1}]
bPA•bB	240 ± 5
bPB•bB	200 ± 10
bPA•bC	3200 ± 40
bPB•bC	1200 ± 200

[a]Errors are quoted as two times the standard deviation based on two repetitions.

The results show two general trends. Firstly, the association constant measured with cyanurate **C** is approximately one order of magnitude higher than the corresponding value for barbiturate **B** no matter which pyrimidine is used as a partner.[11] Secondly, the association constants for the alkyl pyrimidine **PA** is higher than the corresponding values for the bulky **PB**.

3.7. Measurement of allosteric cooperativity

To quantify allosteric cooperativity in the assembly of rosettes, ^{1}H NMR titrations were carried out to measure the stability of the reference 1:2 complexes shown in Figure 3.9. The titration of **bB** into **PA** is depicted in Figure 3.14 and all the remaining titration data can be found in the Experimental section. We decided to employ several different ways of analysis. The first was using a non-cooperative binding isotherm that assumes that both binding sites are independent and identical. In this analysis, $K_1 = K_2 = K_{nc}$ and the change in chemical shift for formation of the 1:1 complex is identical to the subsequent change in chemical for formation of the 1:2 complex. This fitting provided values of association constants K_{nc} as shown in Table 3.3, which were similar to the corresponding reference intermolecular association constants K_{ref} determined for the 1:1 complexes in Table 3.2. The only outlier was complex **B•bPB$_2$**, that also provided the worst description of the experimental data as judged by the global error E of the fit. These results suggested that there is no allosteric cooperativity, so we decided to check if a 1:2 binding isotherm with K_{nc} fixed to the corresponding K_{ref}, but allowing the changes in chemical shifts for both the first and second binding event to be variables, can be fitted well to the experimental data. When this method was used, all the experimental data were described well as shown in Table 3.3. The third method of fitting used $K_1 = K_{ref}$ and K_2 as a variable that was optimised along with the changes in chemical shifts for both the first and second binding events. Since this method uses

more variables, it provides better fits. However, the values of K_2 are similar to the corresponding K_{ref}. In conclusion, there is no allosteric cooperativity in this system and the values of intermolecular reference association constants K_{ref} can be used for the following calculations of rosette chelate cooperativity.

Table 3.3. Association constants and global error E of the fits in CDCl$_3$ at 298 K, measured by ^{1}H NMR titrations.[a]

Complex	Reference Complex	K_{ref} [M^{-1}]	Non-cooperative isotherms			Cooperative isotherm	
			K_{nc} [M^{-1}] [b]	E [%] [b]	E [%] [c]	K_2 [M^{-1}] [d]	E [%] [d]
PA•bB$_2$	**bPA•bB**	240 ± 5	200 ± 10	0.68^e	$0.65 - 0.69$	334 ± 5	$0.09 - 0.23$
PB•bB$_2$	**bPB•bB**	200 ± 10	220 ± 20	$0.82 - 1.2$	$0.73 - 1.1$	320 ± 40	$0.04 - 0.63$
PA•bC$_2$	**bPA•bC**	3200 ± 40	3700 ± 200	$2.1 - 2.2$	$1.4 - 1.6$	1600 ± 10	$0.40 - 0.57$
PB•bC$_2$	**bPB•bC**	1200 ± 200	690 ± 100	$0.52 - 0.55$	$0.08 - 0.20$	1200 ± 30	$0.08 - 0.19$
B•bPB$_2$	**bPB•bB**	200 ± 10	1400 ± 250	$3.7 - 4.0$	$1.3 - 1.5$	200 ± 50	$1.3 - 1.5$

[a]Errors are quoted as two times the standard deviation based on two repetitions.
[b]Using a non-cooperative isotherm where K_{nc} was optimised.
[c]Using a non-cooperative isotherm where $K_{nc} = K_{ref}$ was fixed.
[d]Using a cooperative isotherm where $K_1 = K_{ref}$ was fixed.
[e]No error for the significant numbers used.
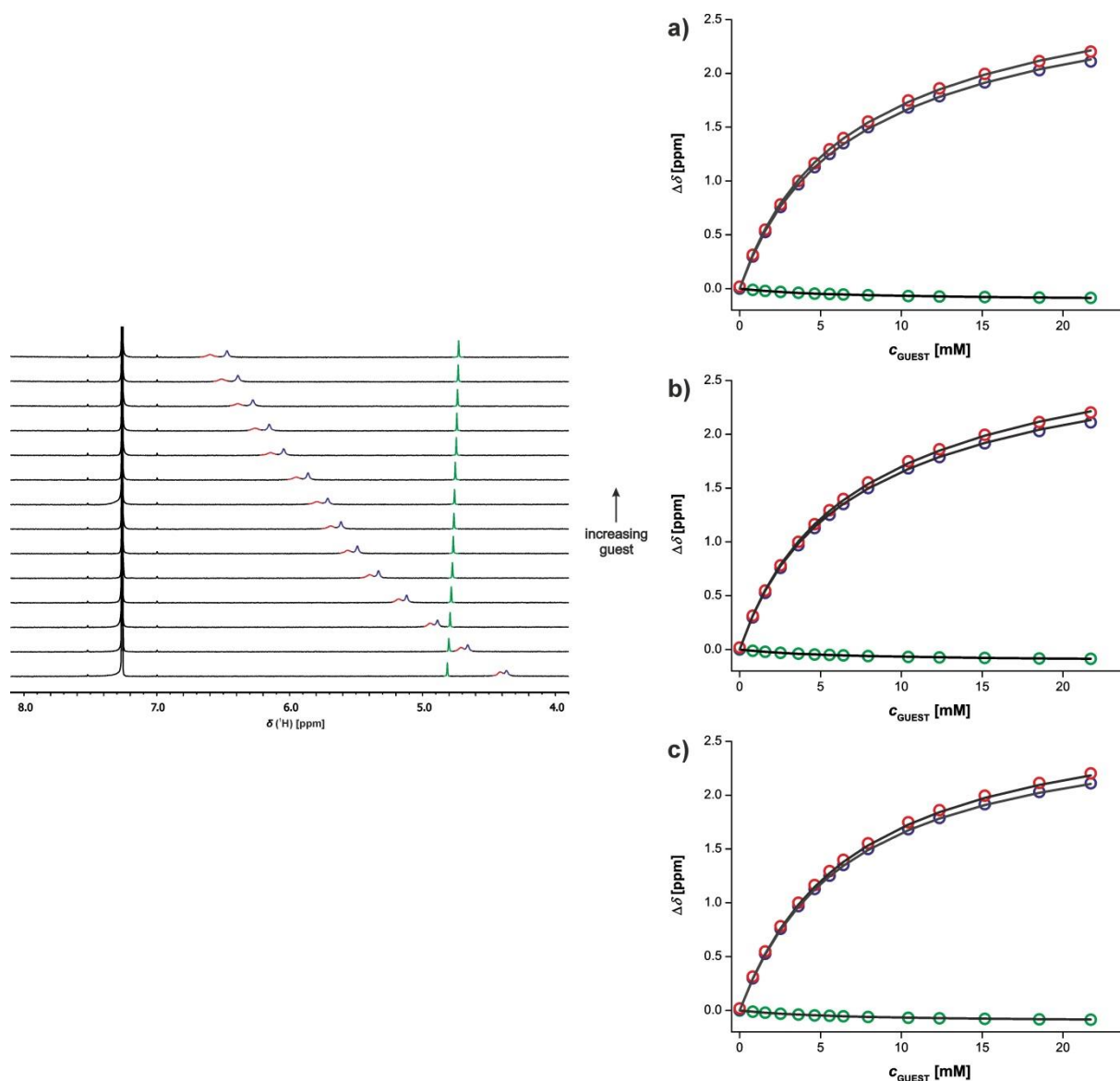
Figure 3.14. ^{1}H NMR (400 MHz, CDCl$_3$, 298 K) titration of **bB** into **PA** (0.99 mM). ^{1}H NMR spectrum is shown on the left (pyrimidine C-H signal green, N-H signals blue and red). On the right are shown the experimental data (circles) and calculated values (lines) based on a 1:2 binding isotherms using (a) non-cooperative model using identical binding sites, (b) non-cooperative model where K_1 and K_2 were fixed to be the appropriate K_{ref} and (c) cooperative isotherm where K_1 was fixed to be the appropriate K_{ref}.

3.8. Measurement of chelate cooperativity

Finally, we determined the macroscopic equilibrium constants for assembly of the rosette. The titration of **B** into **PA** is depicted in Figure 3.15. Using pyrimidines instead of triazines proved to be important as the pyrimidine N-H peaks became very broad after a few additions of guest as shown in Figure 3.15. In comparison, the aromatic C-H of pyrimidine stayed sharp for the whole titration. All the remaining titrations can be found in the Experimental section. A 3:3 binding isotherm was used to fit the experimental data. We tried to include also opening to 1:2 complexes in the presence of excess guest, but this did not change the association constant much as the 1:2 complexes were populated in only 10-20%. The results of these titrations are summarised in Table 3.4.
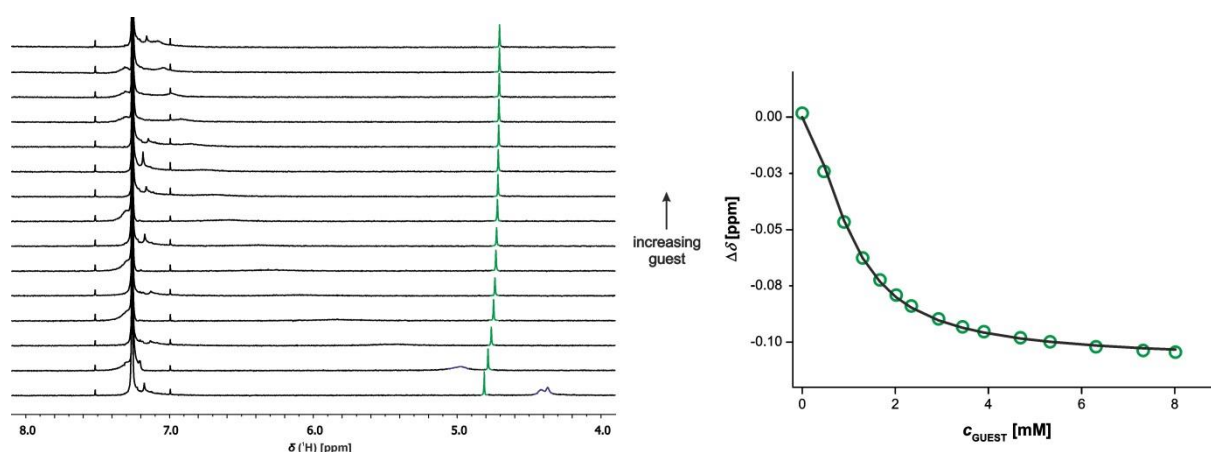
Figure 3.15. ^{1}H NMR (400 MHz, CDCl$_3$, 298 K) titration of **B** into **PA** (0.88 mM). The ^{1}H NMR spectrum is shown on the left (pyrimidine C-H signal green, N-H signals blue). On the right are shown the experimental data (circles) and calculated values (line) based on a 3:3 binding isotherm.

Table 3.4. Macroscopic equilibrium constants for the formation of rosettes in CDCl$_3$ at 298 K, measured by ^{1}H NMR titrations.[a]

Complex	$K_{rosette}$ [M^{-5}]
PA$_3$•B$_3$	$(6.3 \pm 0.1) \times 10^{15}$
PB$_3$•B$_3$	$(8.4 \pm 0.4) \times 10^{14}$
PA$_3$•C$_3$	$(2.7 \pm 0.2) \times 10^{22}$
PB$_3$•C$_3$	$(3.0 \pm 0.1) \times 10^{19}$

[a]Errors are quoted as two times the standard deviation based on two repetitions.

As expected from the literature, rosettes based on cyanurates are more stable than rosettes based on barbiturates. The results for cyanurate **C** show similar values to the value $(1.4 \pm 0.3) \times 10^{20}\,M^{-5}$ determined by the groups of Crego-Calama and Reinhoudt in 1,2-dichloroethane by ICT at 298 K.[10] The rosettes formed by alkyl pyrimidine **PA** show higher stability than bulky **PB** (one order of magnitude for the barbiturate and two orders of magnitude for the cyanurate, respectively).

These results allowed us to calculate the effective molarities for each rosette by using Equation 3.2 and association constants for appropriate reference intermolecular systems from Table 3.2. The values of rosette effective molarities are shown in Table 3.5.

Table 3.5. Effective molarities for rosettes in $CDCl_3$ at 298 K.[a]

Rosette	Reference complex	EM [M]	K_{ref} EM
PA₃•B₃	**bPA•bB**	3.1 ± 0.4	740 ± 80
PB₃•B₃	**bPB•bB**	1.2 ± 0.4	250 ± 60
PA₃•C₃	**bPA•bC**	2.4 ± 0.2	7500 ± 700
PB₃•C₃	**bPB•bC**	1.0 ± 0.9	1100 ± 900

[a]Errors are quoted as two times the standard deviation based on two repetitions.

The determined effective molarities cluster around the value of 2 M, which is an order of magnitude higher compared to the value 0.18 ± 0.05 M determined by the Timmerman group. By comparing our determined value to the literature values of effective molarity for other supramolecular systems, rosette motif shows a high degree of chelate cooperativity.[2] The high value of rosette effective molarity can be used to explain why this system shows "*...a surprisingly high degree of stability...*".[24] Moreover, the results for **PA** and **PB** are similar for both the barbiturate and cyanurate, which provides additional proof that the reference systems used were well suited for their purpose. The results for less bulky alkyl pyrimidine **PA** are slightly higher (approximately twice) compared to the values for bulky pyrimidine **PB**. In addition, the chelate cooperativity connected to rosette formation is quantified by the product K_{ref} EM, which is the equilibrium constant between open and closed 3:3 complexes. These values are shown in Table 3.5. Since the values are $10^2 - 10^3$ for rosettes based on barbiturates and $10^3 - 10^4$ for rosettes based on cyanurates, less than 1% of the species present are not in the form of fully assembled rosettes.

3.9. Conclusion

In this chapter, we revisited the thermodynamics of the self-assembly of the rosette motif. For that, we used pyrimidines rather than commonly used triaminotriazines, which allowed us to easily study all the equilibria by ^{1}H NMR following the aromatic C-H of pyrimidines. We studied rosettes based on both barbiturates and cyanurates as well as a bulky pyrimidine and a pyrimidine with little bulk to revisit the concept of peripheral crowding in solution. We determined the equilibrium constants for the formation of the rosettes of all possible combinations from the listed building blocks. We determined no allosteric cooperativity in the system. Our results show that the effective molarity of rosette is around 2 M, which is a high chelate cooperativity compared to other supramolecular systems. We also found out that rosettes based on the less bulky alkyl pyrimidine show higher stability as well as effective molarity compared to rosettes based on the bulky pyrimidine. This was an unexpected result, since the literature predicts rosettes based on less bulky pyrimidines not to be formed. This study therefore brings new insights into the concept of peripheral crowding as our results show that this concept does not hold true in solution. The chelatecooperativity associated with the intramolecular interactions required to cyclise the rosette was quantified by the effective molarity, which is approximately 2 M for all four rosettes studied, and the product K_{ref} EM is $10^{2} - 10^{4}$ indicating that rosette self-assembly is highly cooperative with no other species populated to a significant extent in these systems.

3.10. Experimental section

3.10.1. General

The chemicals were purchased from commercial suppliers and used without further purifications unless stated otherwise. Solvents were either distilled before use or used as obtained. For chromatography, automatic chromatography systems CombiFlash R_f^+ and CombiFlash R_f^+ Lumen (with UV light detection at 254 nm and 280 nm and evaporative light scattering detector for Lumen) with pre-packed puriFlash columns from Interchim (silica, 25 μm) with a loading of mixtures on Celite were used. The microwave used was Biotage Initiator$^+$. The reactions were monitored by LSMS Waters Acquity H-class UPLC coupled with a single quadrupole Waters SQD2 with the conditions as follows: UPLC Column (see below), solvent A: Water + 0.1% formic acid; solvent B: acetonitrile od THF (see below) + 0.1% formic acid; gradient and flow rate (see below); column temperature of 40 °C, the signal was monitored at 254 nm and 280 nm.

Column
     Col3: ACQUITY UPLC HSS T3 Column, 100Å, 1.8 μm, 2.1 mm X 50 mm
Methods
     MeCN-FAST: Gradient: 0 – 2 minutes 5% – 100%B + 1 minute 100%B
         Flow rate: 0.6 ml/min
     MeCN-SLOW: Gradient: 0 – 4 minutes 5% – 100%B + 1 minute 100%B
         Flow rate: 0.6 ml/min

^{1}H and ^{13}C NMR spectra were recorded on Bruker 400 MHz Avance III HD SmartProbe Spectrometers at 400 MHz for ^{1}H and 101 MHz for ^{13}C or on a Bruker 500 MHz Avance TCI CryoProbe Spectrometer and Bruker 500 MHz AVIII HD SmartProbe Spectrometer at 500 MHz for ^{1}H and 126 MHz for ^{13}C. The variable temperature NMR spectra were measured on a Bruker 500 MHz Avance III HD SmartProbe Spectrometer at 500 MHz for ^{1}H. All chemicals shift are quoted in ppm and were referenced to the residual peaks of used solvents: CDCl$_3$ (^{1}H: 7.26 ppm; ^{13}C: 77.00 ppm), CD$_3$OD (^{1}H: 3.31 ppm; ^{13}C: 49.00 ppm) or d^6-DMSO (^{1}H: 2.50 ppm; ^{13}C: 39.52 ppm). Coupling constants J are stated in Hz. FT-IR spectra were measured on a Bruker Alpha spectrometer. HR-MS spectra were obtained on a Waters Xevo G2-S, Waters Vion IMS Qtof or Waters LCT Premier by electrospray-ionisation of samples. Melting points were recorder on a Mettler-Toledo MP90 system. Elemental analysis was performed by the Microanalysis facility at the Department of Chemistry at the University of Cambridge.

3.10.2. Synthesis

Synthesis of PA
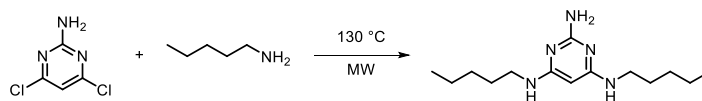
4,6-Dichloropyrimidin-2-amine (210 mg, 1.28 mmol) was flushed with nitrogen in a MW vial. Amylamine (2.5 mL, 21.4 mmol) was added and the mixture was heated at microwave at 130 °C for 14 hours. The remaining amylamine was removed under reduced pressure and the residue was loaded on Celite. A combiflash of the residue on silica (EtOAc/MeOH: MeOH 0%→5%→10%) provided the title compound (210 mg, 62% yield) as a slightly-pale-brown solid.

^{1}H NMR (CDCl$_3$, 400 MHz, 298 K): δ 4.81 (s, 1H), 4.45 – 4.41 (m, 4H), 3.14 (dd, J = 13.0, 7.0 Hz, 4H), 1.62 – 1.54 (m, 4H), 1.40 – 1.30 (m, 8H), 0.92 – 0.89 (m, 6H).
^{13}C NMR (CDCl$_3$, 101 MHz, 298 K): δ 164.3, 162.3, 71.9, 41.7, 29.1, 29.1, 22.4, 14.0.

HR-MS (ESI): Calculated for C$_{14}$H$_{28}$N$_5$ [M+H]$^+$ 266.2345, found: 266.2348 (Δ = 1.1 ppm)

FT-IR (thin film): 3310, 2955, 2928, 2858, 1580, 1433, 1368 cm^{-1}.

MP: 85 – 87 °C

EA: Required for C$_{14}$H$_{27}$N$_5$: C 63.36, H 10.25, N 26.39; found: C 63.28, H 10.34, N 26.04.

LCMS Method: Col3-MeCN-SLOW

^{1}H NMR

7.26

4.81
4.45
4.40

3.17
3.15
3.14
3.12

1.59
1.59
1.58
1.56
1.37
1.36
1.35
1.34
1.33
0.92
0.91
0.90
0.89

1.00
3.79
3.90
3.99
7.86
5.94

10.0 9.5 9.0 8.5 8.0 7.5 7.0 6.5 6.0 5.5 5.0 4.5 4.0 3.5 3.0 2.5 2.0 1.5 1.0 0.5 0.0
f1 (ppm)

^{13}C NMR

164.31
162.32

77.32
77.00
76.68
71.91

41.68

29.13
29.08

22.39

13.98

200 190 180 170 160 150 140 130 120 110 100 90 80 70 60 50 40 30 20 10 0
f1 (ppm)

64
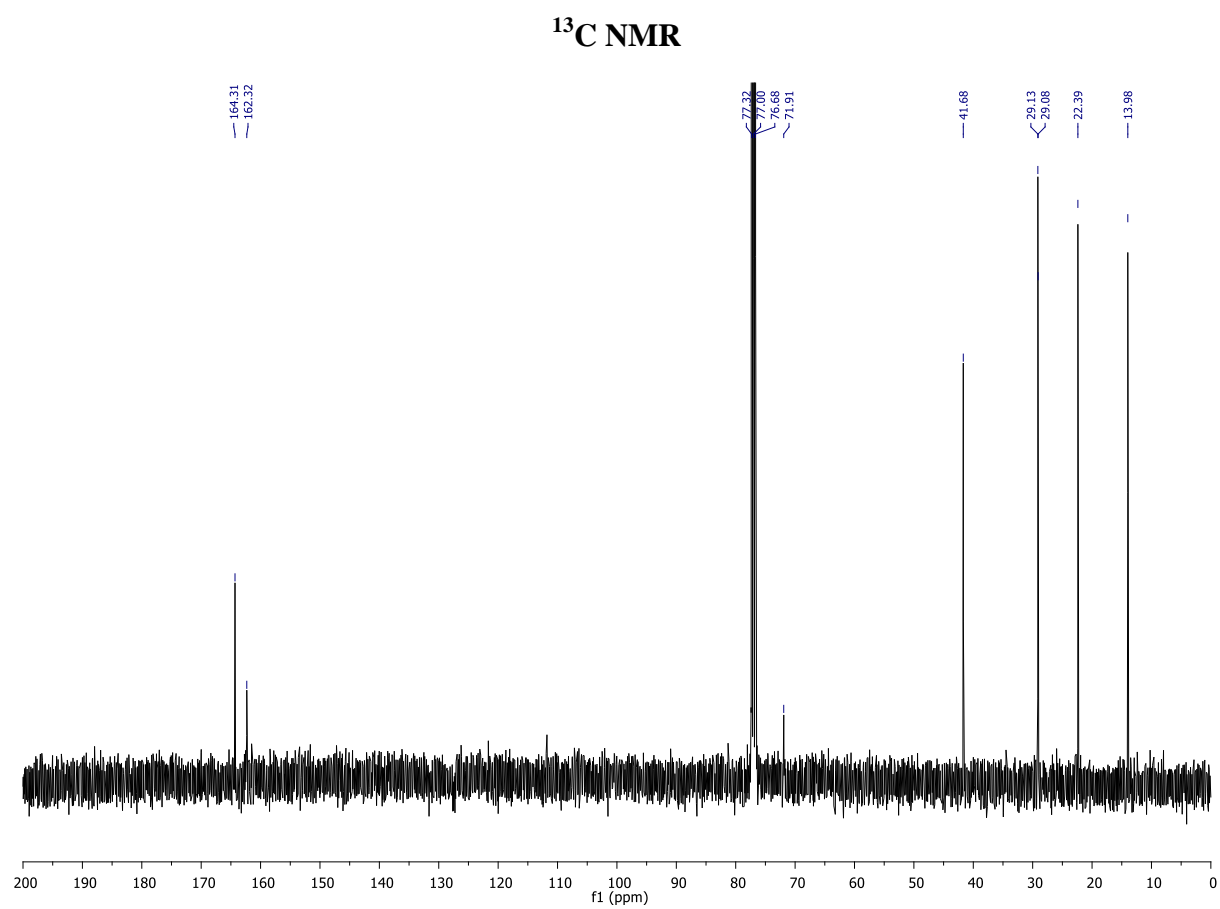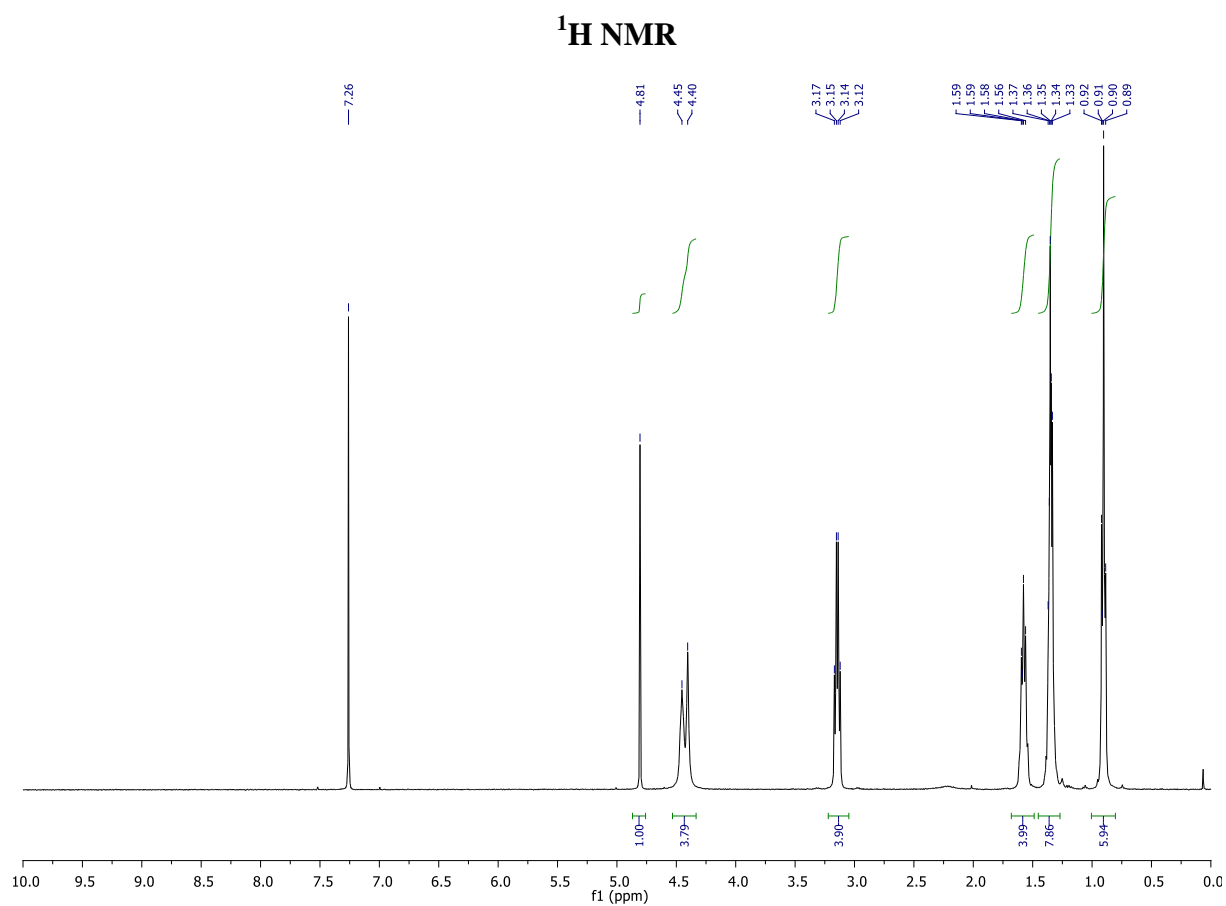
Synthesis of PB

4,6-Dichloropyrimidin-2-amine (178 mg, 1.06 mmol) was flushed with nitrogen in a MW vial. *N,N*-diisopropylethylamine (0.5 mL, 2.48 mmol), isopropyl alcohol (1.0 mL) and 4-*tert*butylaniline (0.6 mL, 562 mg, 3.77 mmol) were added and the mixture was heated in microwave at 150 °C for 1 hours. Then, additional 4-*tert*-butylaniline (0.5 μL, 467 mg, 3.14 mmol) was added under nitrogen atmosphere and the mixture was heated in microwave at 170 °C for 10 hours. A saturated solution of $NaHCO_3$ (20 mL) and water (20 mL) were added and the mixture was extracted with CH_2Cl_2/MeOH (10:1; 2×50 mL) and CH_2Cl_2 (2×50 mL). The organic phase was dried over $MgSO_4$, evaporated and loaded to Celite. A combiflash of the residue on silica (CH_2Cl_2/MeOH: MeOH 0%→10%) provided the title compound (294 mg, 71% yield) as a pale-pink solid.

^{1}H NMR (d[6]-DMSO, 400 MHz, 298 K): δ 8.52 (s, 2H), 7.44 (d, J = 8.5 Hz, 4H), 7.25 (d, J = 8.5 Hz, 4H), 5.80 (s, 2H), 5.50 (s, 1H), 1.26 (s, 18H).

MP: 281 − 284 °C

EA: Required for $C_{24}H_{31}N_5$: C 74.00, H 8.02, N 17.98; found: C 73.75, H 8.14, N 17.66.

LCMS Method: Col3-MeCN-SLOW

The observed data was in agreement with the reported values.[15]

Synthesis of bPA-Cl
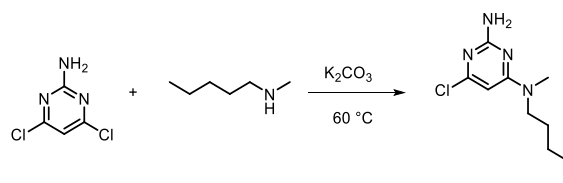
A mixture of 4,6-dichloropyrimidin-2-amine (344 mg, 2.06 mmol), *N*-methylpentylamine (0.4 mL, 290 mg, 2.9 mmol), K$_2$CO$_3$ (430 mg, 3.11 mmol) and *t*BuOH (15 mL) were heated at 60 °C for 3 days. The mixture was evaporated and water (20 mL) was added. The mixture was then sonicated for 20 minutes. Solid was collected by suction and dried overnight in vacuum oven at 40 °C to provide the title compound (347 mg, 75% yield) as a yellowish solid.

^{1}H NMR (CD$_3$OD, 400 MHz, 298 K): δ 5.94 (s, 1H), 3.47 (s, 2H), 3.00 (s, 3H), 1.61 − 1.54 (m, 2H), 1.42 − 1.25 (m, 4H), 0.92 (t, *J* = 7.0 Hz, 3H).
^{13}C NMR (CD$_3$OD, 101 MHz, 298 K): δ 164.9, 163.9, 160.0, 92.3, 50.3, 35.9, 30.1, 28.0, 23.6, 14.4.

HR-MS (ESI): Required for C$_{10}$H$_{18}$N$_4$Cl [M+H]$^+$ 229.1220, found: 229.1218 (Δ = 0.9 ppm).

FT-IR (thin film): 3304, 3204, 2955, 2930, 2859, 2406, 1575, 1498, 1465, 1405, 1367, 974, 785 cm^{-1}.

MP: 96 − 98 °C

^{1}H NMR
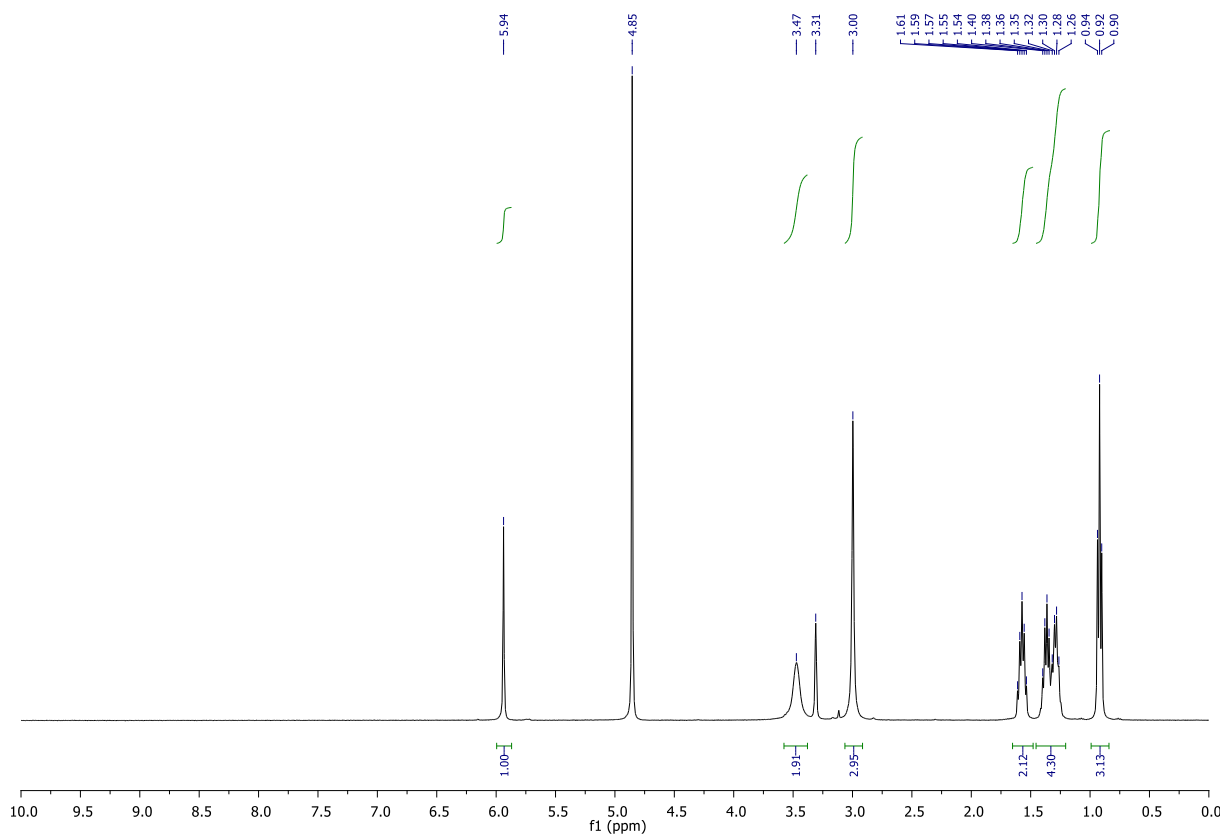
^{13}C NMR
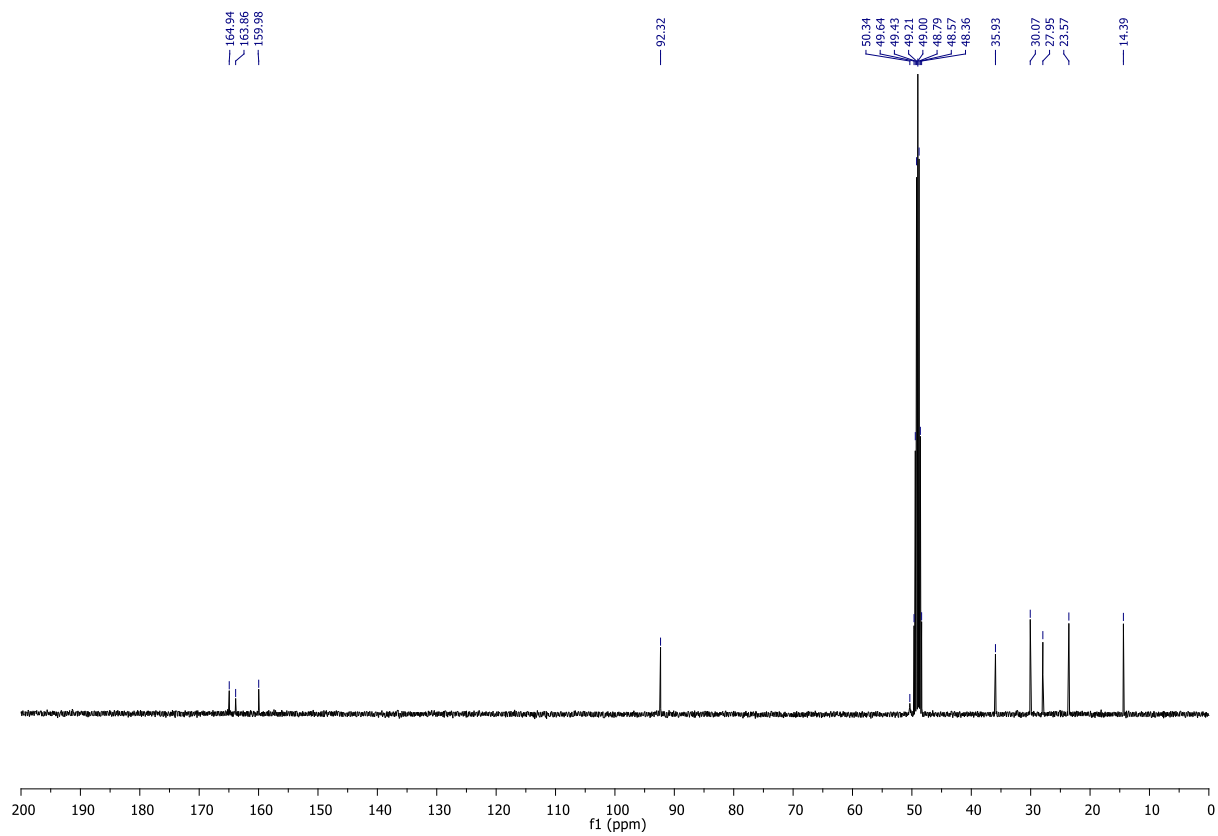
Synthesis of bPA
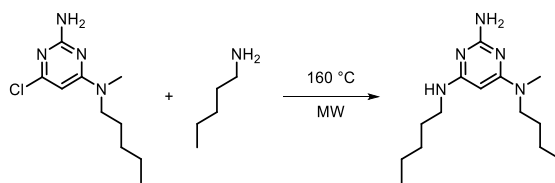
bPA-Cl (198 mg, 1.89 mmol) was flushed with nitrogen in a MW vial. *n*-Pentylamine (1 mL, 0.75 g, 8.6 mmol) was added and the mixture was heated in microwave at 160 °C for 10 hours. A saturated solution of $NaHCO_3$ (20 mL) was added and the mixture was extracted with CH_2Cl_2 (4 × 50 mL). The organic phase was dried over $MgSO_4$, evaporated and loaded to Celite. A combiflash of the residue on silica (CH_2Cl_2/MeOH: MeOH 0%→10%) provided the title compound (178 mg, 84% yield) as reddish oil.

¹H NMR (CDCl₃, 400 MHz, 298 K): δ 4.85 (s, 1H), 4.38 (s, 2H), 4.35 (s, 1H), 3.42 − 3.38 (m, 2H), 3.14 (dd, *J* = 12.0, 7.0 Hz, 2H), 2.96 (s, 3H), 1.62 − 1.51 (m, 4H), 1.39 − 1.23 (m, 8H), 0.90 (t, *J* = 7.0 Hz, 6H).

¹³C NMR (CDCl₃, 101 MHz, 298 K): δ 164.1, 163.9, 162.2, 72.0, 49.2, 41.7, 35.4, 29.2, 29.1, 29.1, 27.0, 22.5, 22.4, 14.1, 14.0.

HR-MS (ESI): Required for $C_{15}H_{30}N_5$ [M+H]$^+$ 280.2501, found: 280.2502 (Δ = 0.4 ppm).

FT-IR (thin film): 3315, 2954, 2927, 2857, 1558, 1507, 1434, 1400, 1360, 1196 cm^{-1}.

LCMS Method: Col3-MeCN-SLOW/Col3-MeCN-FAST

¹H NMR
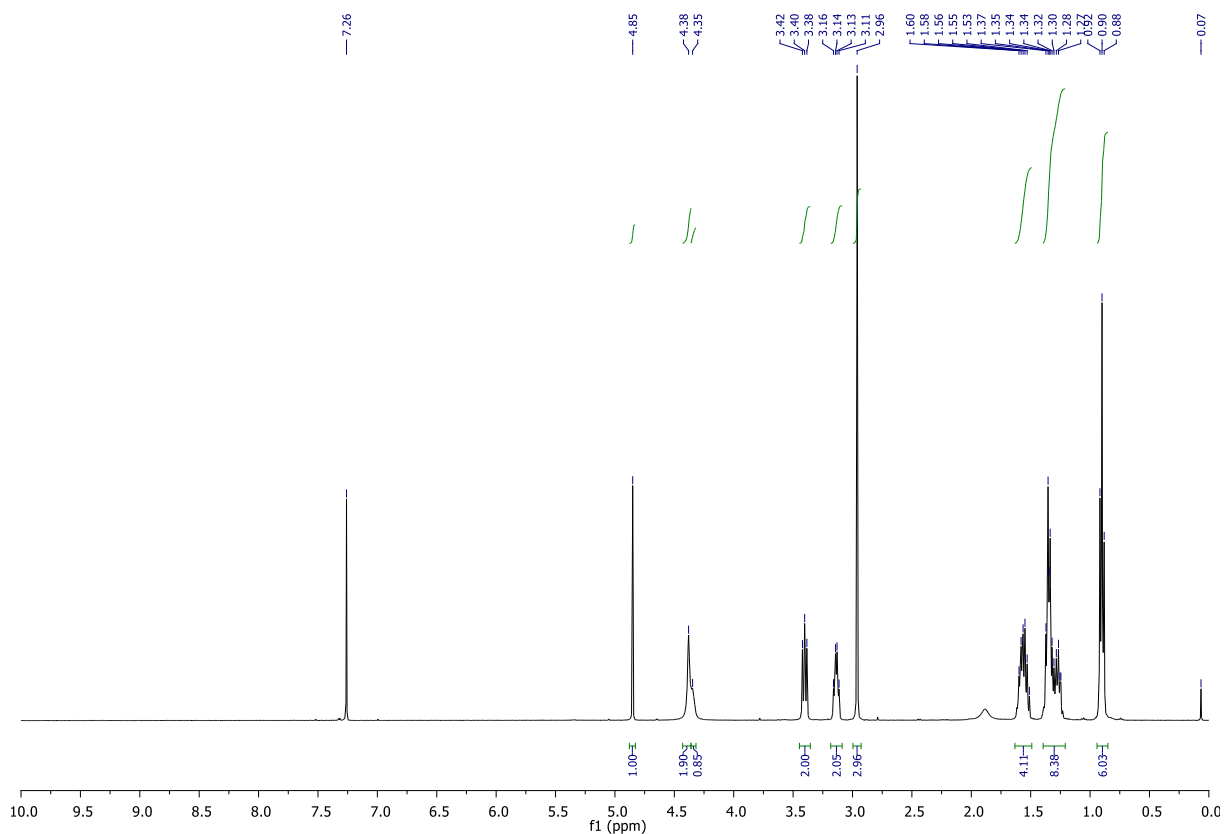
¹³C NMR
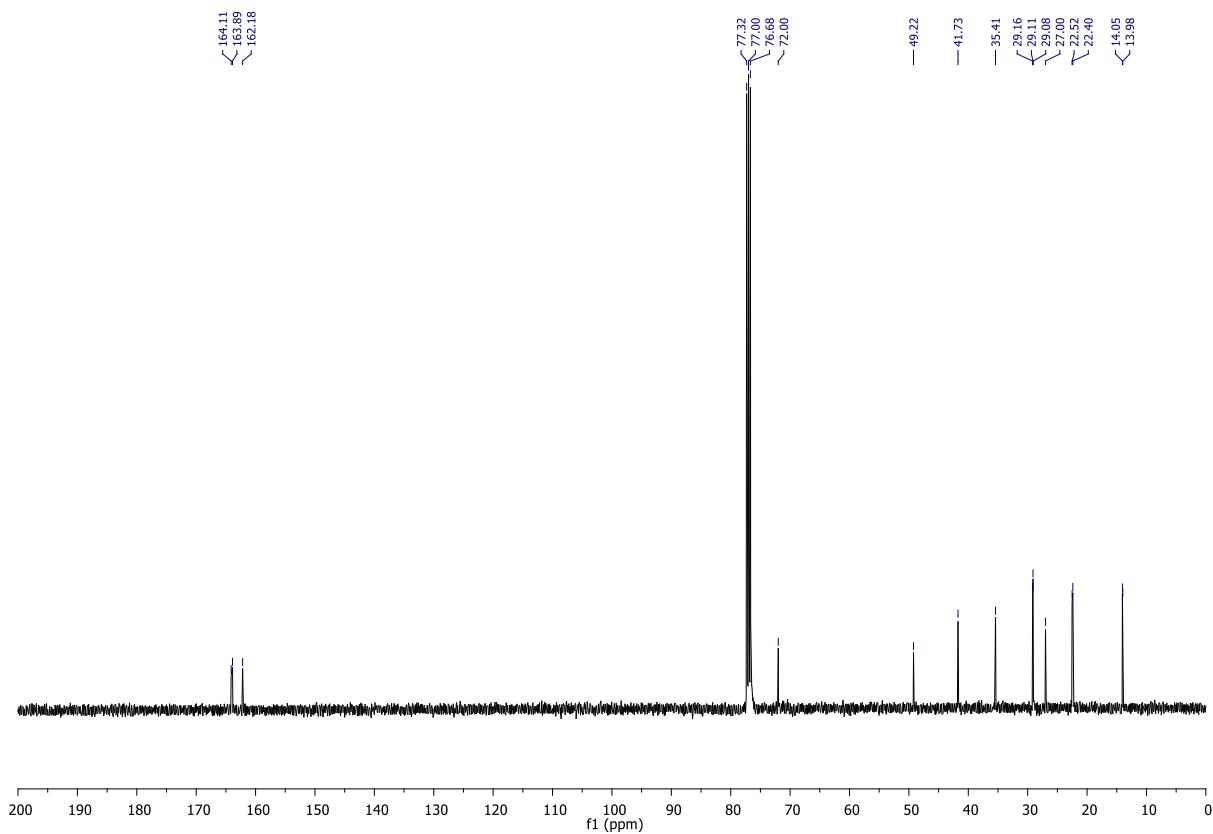
Synthesis of bTBA
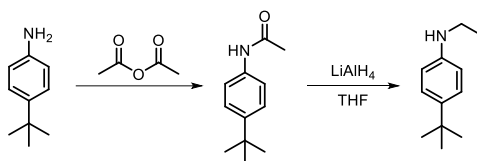
4-*tert*-Butylaniline (0.60 mL, 0.56 g, 3.77 mmol) and acetic anhydride (2.0 mL, 2.2 g, 21.6 mmol) were left stirring for 3 hours at RT. A saturated solution of NH_4Cl (20 mL) was then added with cooling to 0 °C. The mixture was extracted with (3 × 50 mL). The collected organic phase was dried over $MgSO_4$ and the solvents were removed under reduced pressure to provide after drying in vacuum oven overnight the title product (724 mg, *quantitative*) as a white crystalline solid.

^{1}H NMR (CDCl$_3$, 400 MHz, 298 K): δ 7.40 (d, J = 8.5 Hz, 2H), 7.33 (d, J = 8.5 Hz, 2H), 7.11 (bs, 1H), 2.17 (s, 3H), 1.30 (s, 9H).

MP: 172 – 174 °C

The observed data was in agreement with the reported values.[25]

This compound (499 mg, 2.61 mmol) was flushed with N_2 and THF (10 mL) was added and the mixture was cooled to 0 °C. A solution of $LiAlH_4$ (1.0 M in THF, 6 mL, 6 mmol) was added dropwise at 0 °C. After 1 hour, the cooling bath was removed and the mixture was left stirring overnight at RT. Then, a saturated solution of $NaHCO_3$ (10 mL) was added at 0 °C and the mixture was extracted with CH_2Cl_2 (4 × 50 mL). The organic phase was dried over $MgSO_4$ and evaporated to produce the title product (407 mg, 88% yield) as reddish oil.

^{1}H NMR (CDCl$_3$, 400 MHz, 298 K): δ 7.23 – 7.19 (m, 2H), 6.60 – 6.56 (m, 2H), 3.42 (bs, 1H), 3.15 (q, J = 7.0 Hz, 2H), 1.28 (s, 9H), 1.25 (t, J = 7.0 Hz, 3H).

The observed data was in agreement with the reported values.[26]

Synthesis of bPB-Cl
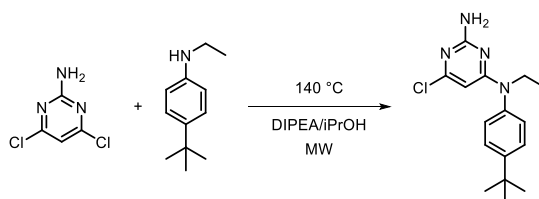
4,6-Dichloropyrimidin-2-amine (229 mg, 1.40 mmol) was flushed with nitrogen in a MW vial. **bTBA** (585 g, 3.31 mmol), isopropyl alcohol (1.5 mL), DIPEA (1 mL) were added and the mixture was heated at microwave at 140 °C for 44 hours. A saturated solution of $NaHCO_3$ (30 mL) was added and the mixture was extracted with CH_2Cl_2 (3 × 50 mL). The organic phase was dried over $MgSO_4$, evaporated and loaded to Celite. A combiflash of the residue on silica (CH_2Cl_2/MeOH: MeOH 0%→5%) provided the title compound (363 mg, 85% yield) as a pale-yellowish solid.

¹H NMR (CDCl₃/CD₃OD, 400 MHz, 298 K): δ 7.48 (d, J = 8.5 Hz, 2H), 7.10 (d, J = 8.5 Hz, 2H), 5.45 (s, 1H), 3.89 (q, J = 7.0 Hz, 2H), 1.35 (s, 9H), 1.15 (t, J = 7.0 Hz, 3H). (*referenced to methanol*)
¹³C NMR (CDCl₃/CD₃OD, 101 MHz, 298 K): δ 164.7, 163.4, 159.0, 151.7, 140.5, 128.5, 127.7, 94.4, 45.6, 35.3, 31.7, 13.2. (*referenced to methanol*)

HR-MS (ESI): Required for $C_{16}H_{21}N_4Cl$ [M+H]$^+$ 305.1533, found: 305.1533 (Δ = 0.0 ppm).

FT-IR (thin film): 3314, 2920, 2851, 1651, 1546, 1519, 1260, 1111 cm^{-1}.

MP: 198 – 202 °C

LCMS Method: Col3-MeCN-SLOW

^{1}H NMR

^{13}C NMR
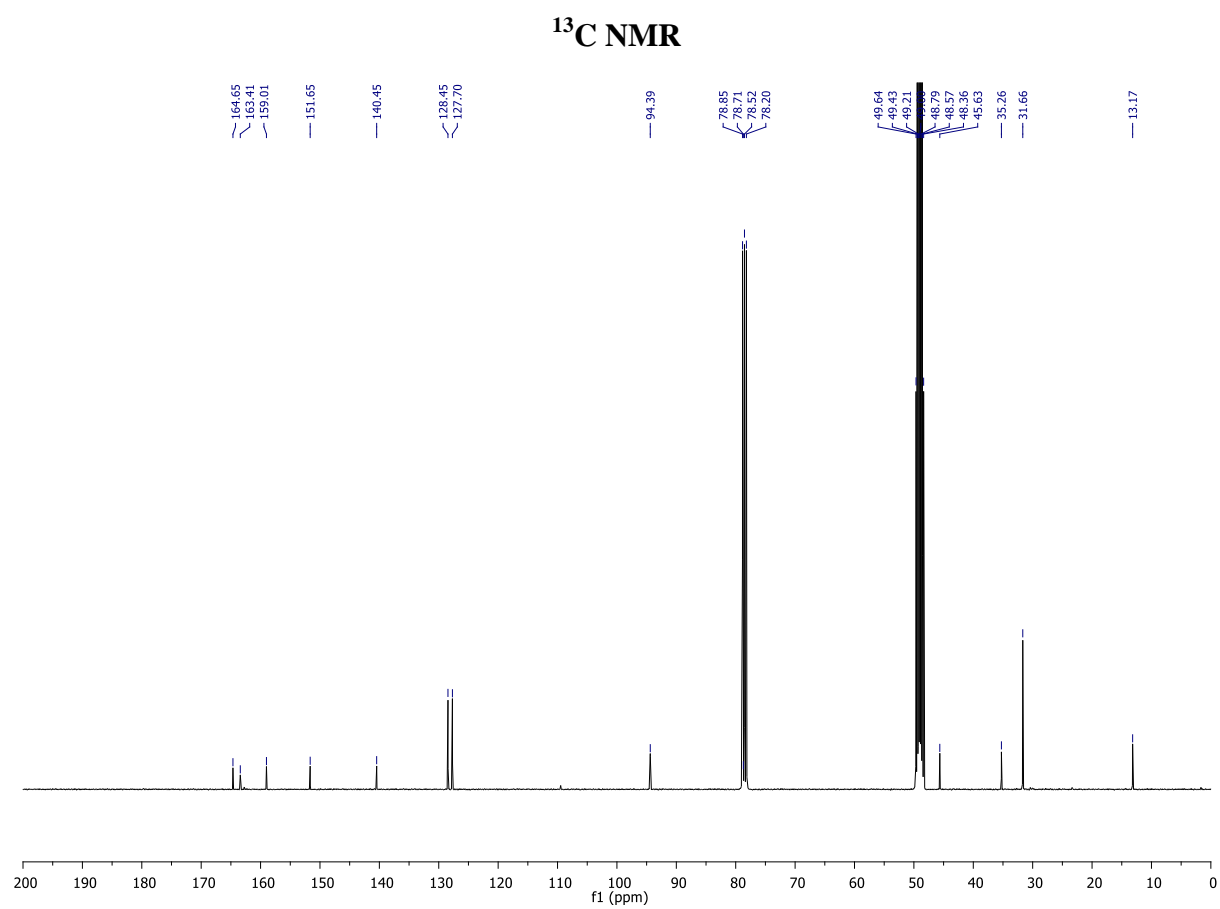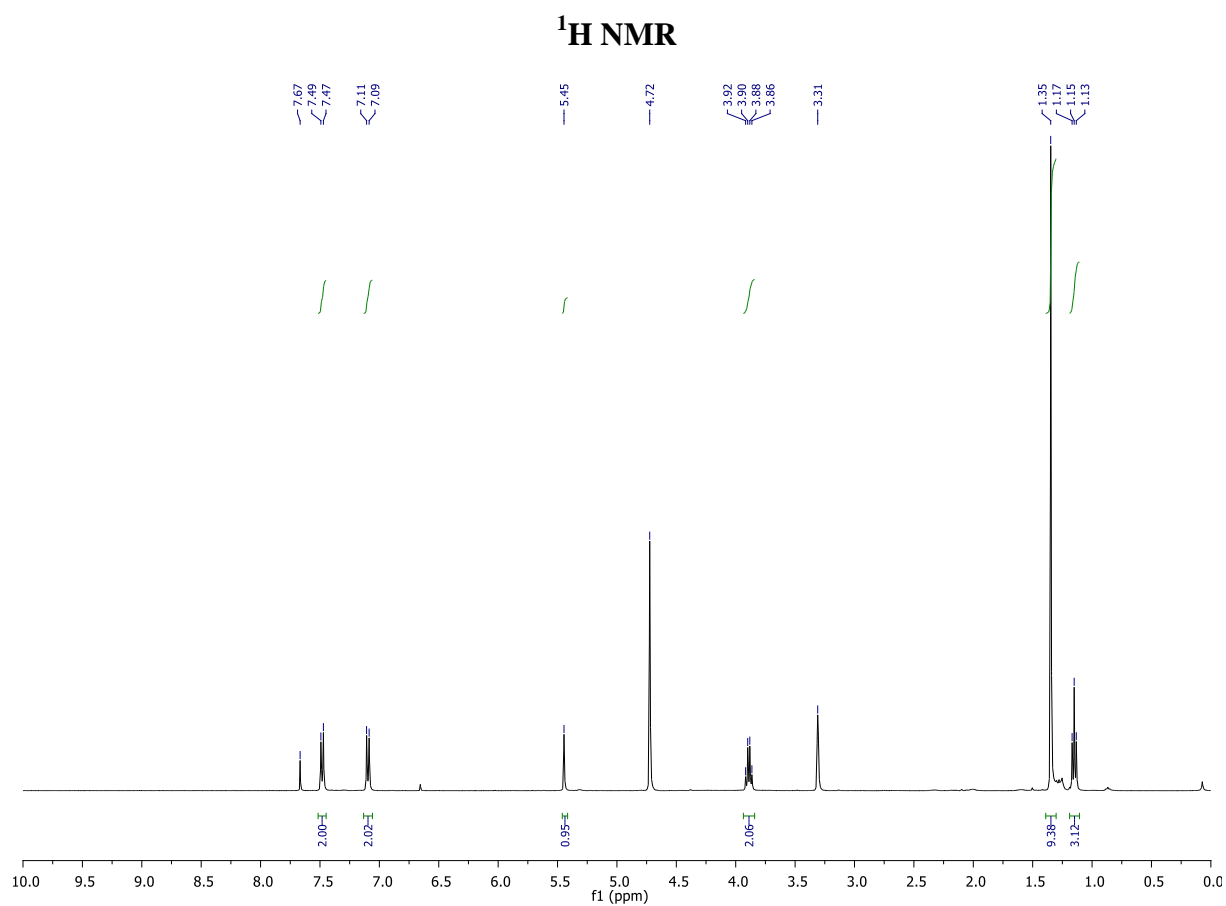
Synthesis of bPB
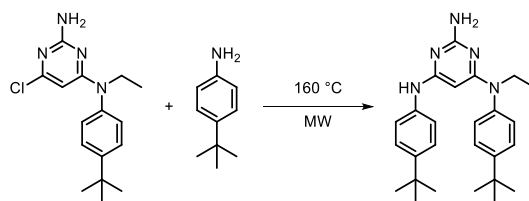
bPB-Cl (83 mg, 0.272 mmol) was flushed with nitrogen in a MW vial. 4-*tert*-Butylaniline (0.6 mL, 0.56 g, 3.8 mmol) was added and the mixture was heated in microwave at 160 °C for 2 hours. A saturated solution of $NaHCO_3$ (5 mL) was added and the mixture was extracted with CH_2Cl_2/MeOH (20:1, 2 × 50 mL) and CH_2Cl_2 (2 × 50 mL). The organic phase was dried over $MgSO_4$, evaporated and loaded to Celite. A combiflash of the residue on silica (CH_2Cl_2/MeOH: MeOH 0%→10%) provided the title compound (75 mg, 66% yield) as a pale purple solid.

^{1}H NMR (CDCl$_3$, 400 MHz, 298 K): δ 7.42 – 7.38 (m, 2H), 7.19 – 7.16 (m, 2H), 7.13 – 7.10 (m, 2H), 7.00 – 6.98 (m, 2H), 6.15 (s, 1H), 5.06 (s, 1H), 4.57 (s, 2H), 3.92 (d, $J = 7.0$ Hz, 2H), 1.33 (s, 9H), 1.24 (s, 9H), 1.17 (t, $J = 7.0$ Hz, 3H).
^{13}C NMR (CDCl$_3$, 101 MHz, 298 K): δ 164.4, 162.6, 160.9, 149.6, 145.6, 141.0, 137.0, 127.9, 126.3, 125.6, 120.5, 77.2, 44.0, 34.5, 34.2, 31.4, 31.3, 13.6.

HR-MS (ESI): Required for $C_{26}H_{36}N_5$ [M+H]$^+$ 418.2971, found: 418.2962 (Δ = 2.2 ppm).

FT-IR (thin film): 3456, 3343, 3229, 2953, 2918, 2850, 1629, 1573, 1540, 1429, 1359, 1256, 1229, 1018, 791 cm^{-1}.

MP: 180 – 182 °C

EA: Required for $C_{26}H_{35}N_5$: C 74.78, H 8.45, N 16.77; found: C 74.62, H 8.53, N 16.32.

LCMS Method: Col3-MeCN-FAST

^{1}H NMR

^{13}C NMR
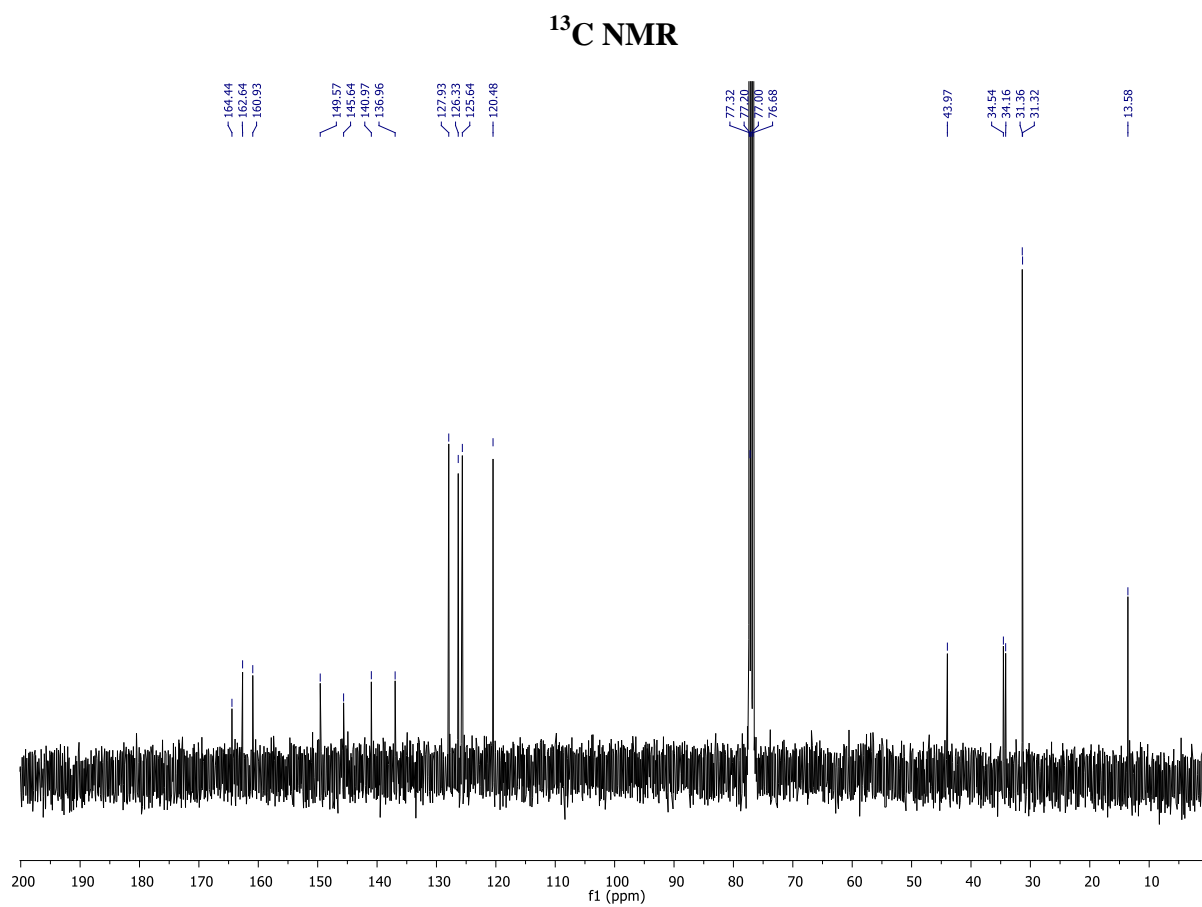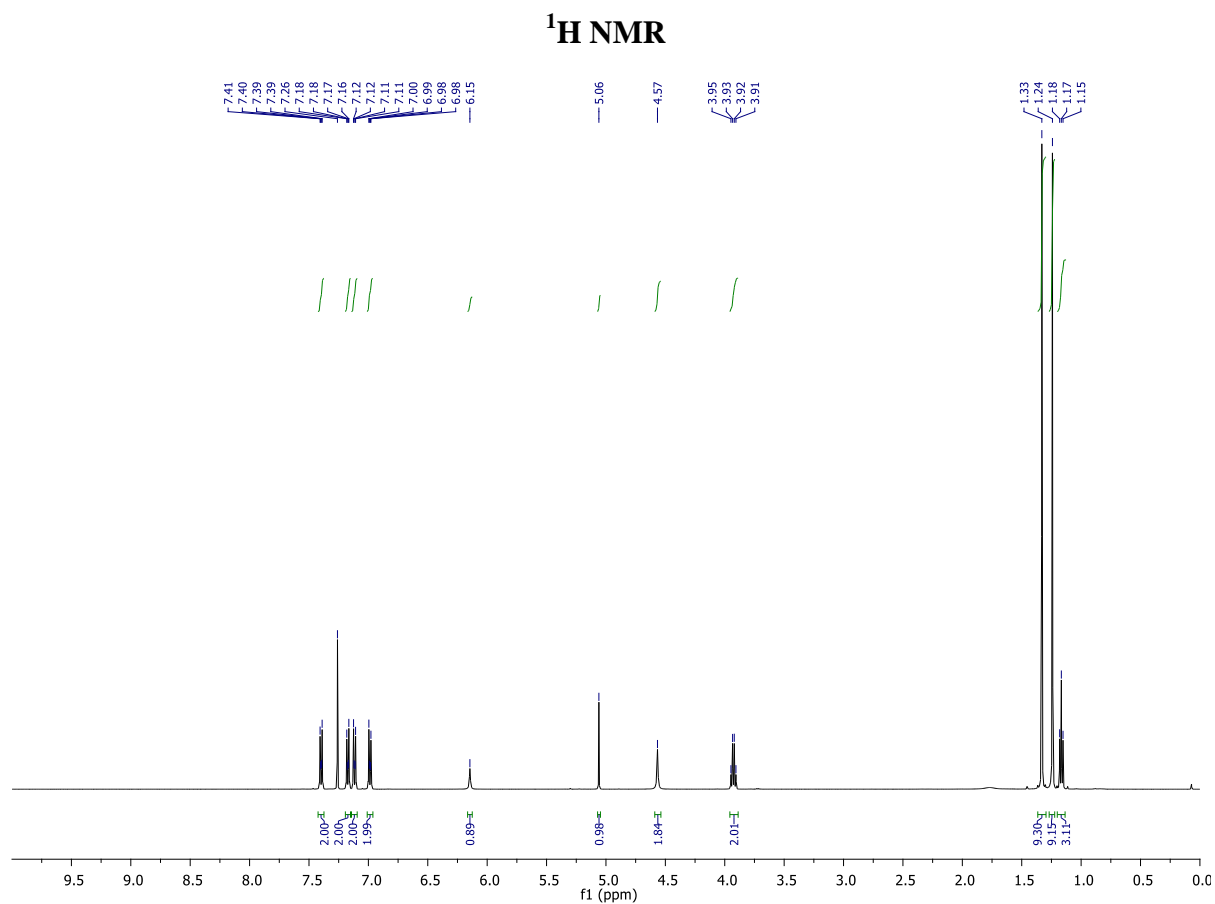
Synthesis of B
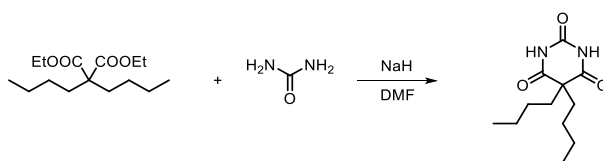
NaH (60% in mineral oil, 140 mg, 3.5 mmol) was flushed with nitrogen and DMF (6 mL) was added. The mixture was cooled to 0 °C and urea (418 mg, 7.0 mmol) was added. After 2 hours of stirring, diethyl dibutylmalonate (0.5 mL, 473 mg, 1.73 mmol) was added dropwise at 0 °C. The mixture was stirred overnight at RT and a saturated solution of NH_4Cl (10 mL) was added with cooling to 0 °C. Water (15 mL) was added and the mixture was extracted with CH_2Cl_2/MeOH (10:1, 40 mL) CH_2Cl_2 (2 × 50 mL). The collected organic phase was dried over $MgSO_4$ and the solvents were removed under reduced pressure (60 °C, <20 mBar). A combliflash of the residue on silica (Celite loading, PE/DCM, DCM: 0%→100%) provided after drying in vacuum oven overnight the title product (135 mg, 32% yield) as a white crystalline solid.

^{1}H NMR (CD$_3$OD, 400 MHz, 298 K): δ 1.92 − 1.88 (m, 4H), 1.33 − 1.24 (m, 4H), 1.20 − 1.12 (m, 4H), 0.88 (t, J = 7.5 Hz, 6H).

MP: 154 − 155 °C

EA: Required for $C_{12}H_{20}N_2O_3$: C 59.87, H 8.39, N 11.66; found: C 59.13, H 8.25, N 11.38.

The observed data was in agreement with the reported values.[16]

Synthesis of bC and C
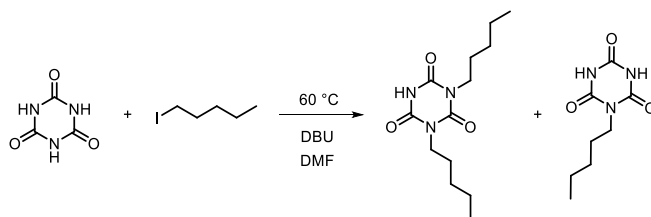
Cyanuric acid (4.2 g, 32.5 mmol) and 1,8-diazabicyclo[5.4.0]undec-7-ene (0.57 mL, 0.58 g, 3.8 mmol) were flushed with N_2. DMF (10 mL) and 1-iodopentane (0.5 mL, 0.79 g, 3.96 mmol) were added and the mixture was heated at 60 °C for 5 days. The solvents was then removed under reduced pressure and a combiflash of the residue on silica (Celite loading, CH_2Cl_2/MeOH, MeOH: 0%→5%) provided the title products **bC** (164 mg, 15% yield) and **C** (99 mg, 13% yield) as white crystalline solids.

Compound **bC**:
^{1}H NMR (CD$_3$OD, 400 MHz, 298 K): δ 3.78 – 3.75 (m, 4H), 1.66 – 1.58 (m, 4H), 1.42 – 1.27 (m, 8H), 0.92 (t, $J = 7.0$ Hz, 6H).
^{13}C NMR (CD$_3$OD, 101 MHz, 298 K): δ 151.7, 150.5, 49.6, 43.0, 29.9, 28.5, 23.4, 14.3.

HR-MS (ESI): Required for $C_{13}H_{24}N_3O_3$ [M+H]$^+$ 270.1818, found: 270.1812 ($\Delta = 2.2$ ppm).

FT-IR (thin film): 3218, 3116, 2955, 2926, 2871, 2859, 1741, 1660, 1482, 1444, 1379 cm^{-1}.

MP: 98 – 101 °C

EA: Required for $C_{13}H_{23}N_3O_3$: C 57.97, H 8.61, N 15.60; found: C 58.87, H 8.64, N 14.32.

Compound **C**:
^{1}H NMR (CD$_3$OD, 400 MHz, 298 K): δ 3.79 – 3.75 (m, 2H), 1.66 – 1.58 (m, 2H), 1.42 – 1.27 (m, 4H), 0.92 (t, $J = 7.0$ Hz, 3H).

MP: 229 – 232 °C

EA: Required for $C_8H_{13}N_3O_3$: C 48.23, H 6.58, N 21.09; found: C 48.27, H 6.55, N 20.92.

The observed data was in agreement with the reported values.[27]

bC: ^{1}H NMR

4.88
4.85

3.79
3.77
3.75

3.31
3.31
3.31

1.66
1.64
1.62
1.60
1.58
1.40
1.38
1.37
1.35
1.35
1.34
1.33
1.31
1.30
1.29

0.94
0.92
0.90

3.95

3.97
8.37
6.00

f1 (ppm)

bC: ^{13}C NMR

151.67
150.50

49.64
49.43
49.21
49.00
48.79
48.57
48.36
43.01

29.93
28.45

23.35

14.28

f1 (ppm)
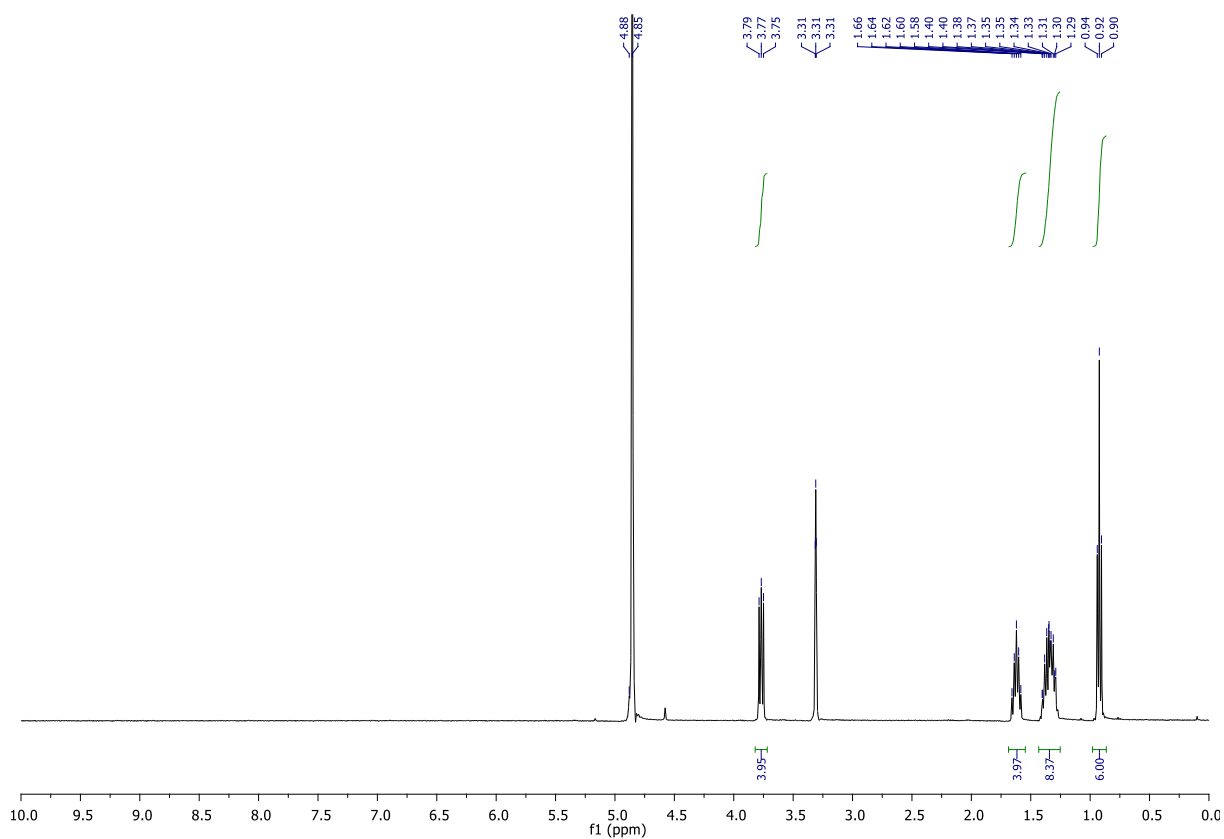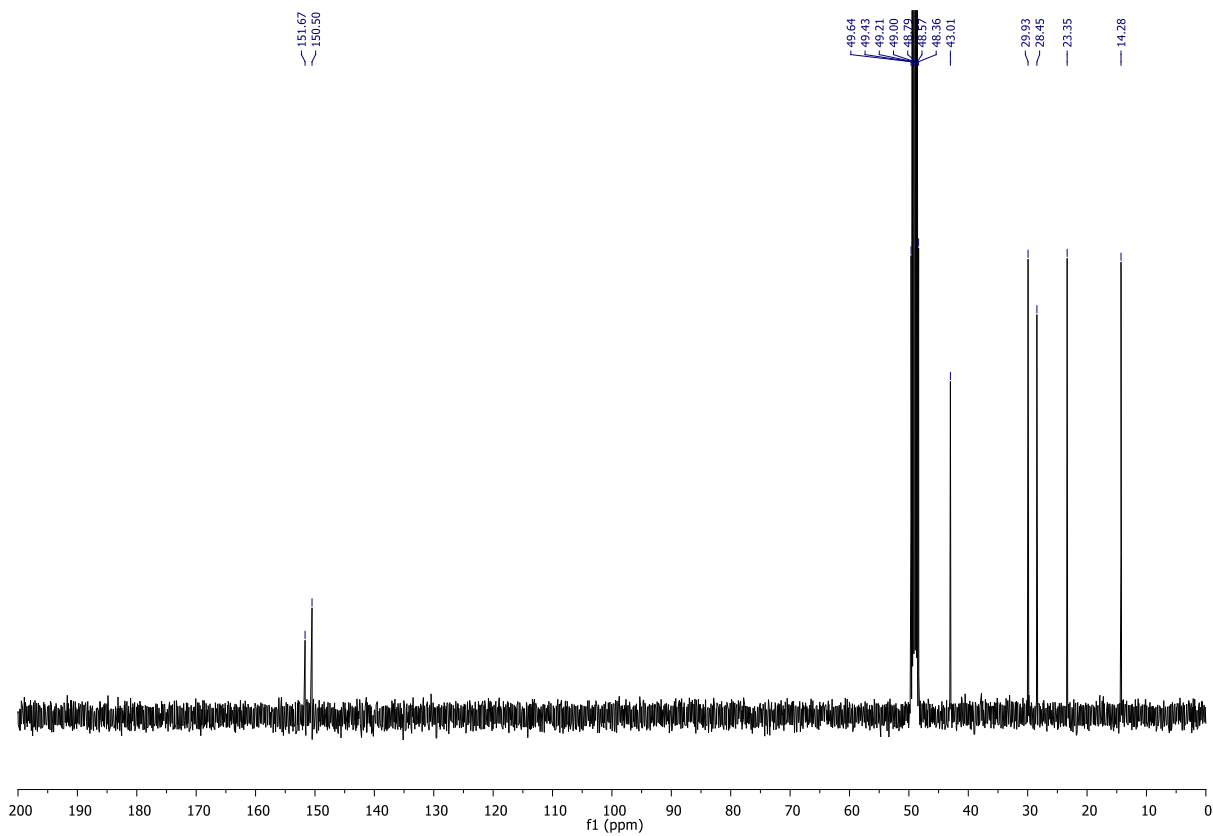
Synthesis of bB
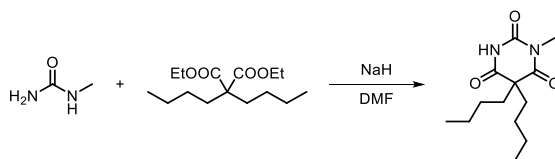
NaH (60% in mineral oil, 266 mg, 6.65 mmol) was flushed with nitrogen and DMF (10 mL) was added. The mixture was cooled to 0 °C and *N*-methylurea (1.25 g, 16.9 mmol) was added. After 3 hours of stirring, diethyl butylmalonate (0.55 mL, 541 mg, 1.99 mmol) was added at 0 °C. The mixture was stirred overnight at 60 °C. Then a saturated solution of NH$_4$Cl (15 mL) was added at 0 °C. Water (20 mL) was added and the mixture was extracted with dichloromethane (4 × 50 mL). The collected organic phase was dried over MgSO$_4$ and the solvents were removed under reduced pressure. A combliflash of residue on silica (Celite loading, PE/CH$_2$Cl$_2$, CH$_2$Cl$_2$: 0%→100%) provided the title product (473 mg, 97% yield) as a white solid.

^{1}H NMR (CDCl$_3$, 400 MHz, 298 K): δ 8.04 (s, 1H), 3.31 (s, 3H), 2.03 – 1.92 (m, 4H), 1.31 – 1.22 (m, 4H), 1.19 – 0.99 (m, 4H), 0.85 (t, J = 7.5 Hz, 6H).
^{13}C NMR (CD$_3$OD, 101 MHz, 298 K): δ 174.6, 174.0, 151.7, 57.6, 40.4, 28.2, 27.7, 23.7, 14.0.

HR-MS (ESI): Required for C$_{13}$H$_{21}$N$_2$O$_3$ [M–H]$^-$ 253.1552, found: 253.1549 (Δ = 3.3 ppm).

FT-IR (thin film): 3237, 3127, 2959, 2873, 2862, 1751, 1710, 1683, 1442, 1383, 1358, 1267, 1190 cm^{-1}.

MP: 97 – 98 °C

EA: Required for C$_{13}$H$_{22}$N$_2$O$_3$: C 61.39, H 8.72, N 11.01; found: C 61.55, H 8.73, N 10.93.

^{1}H NMR
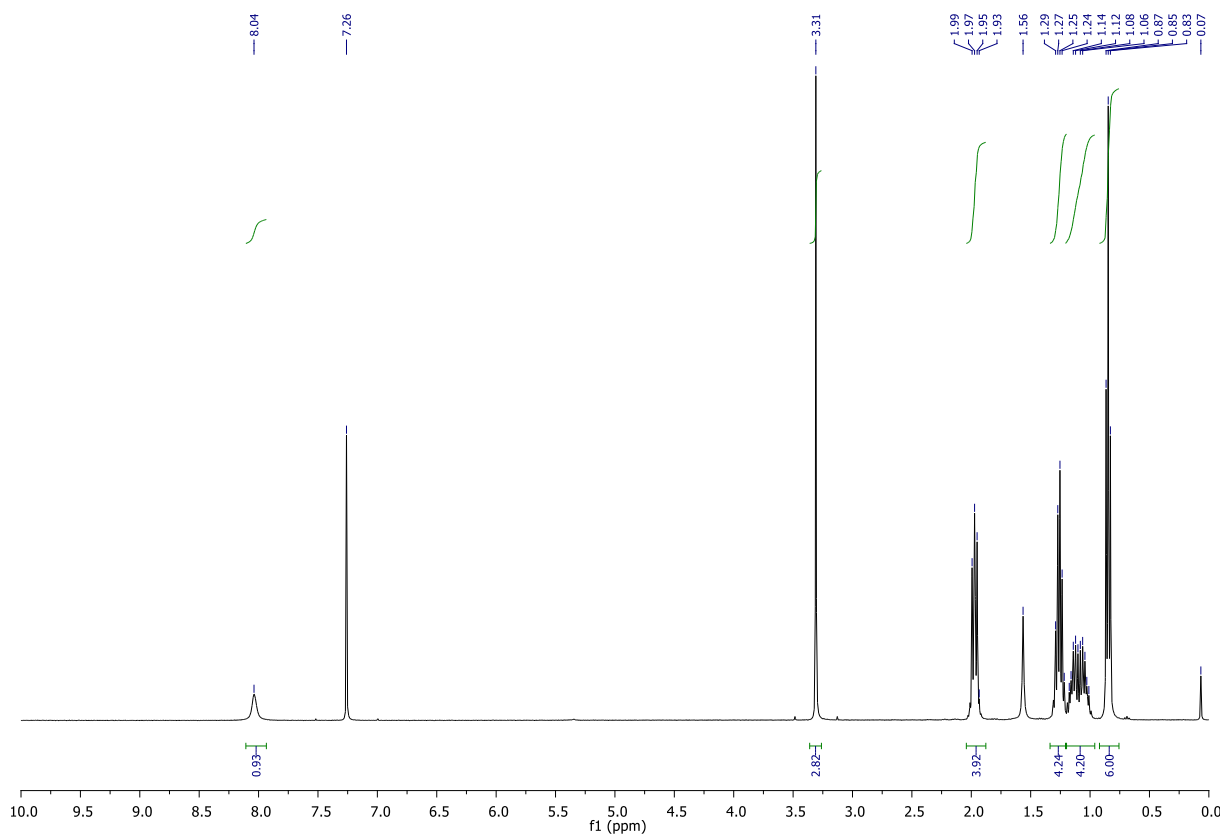
^{13}C NMR
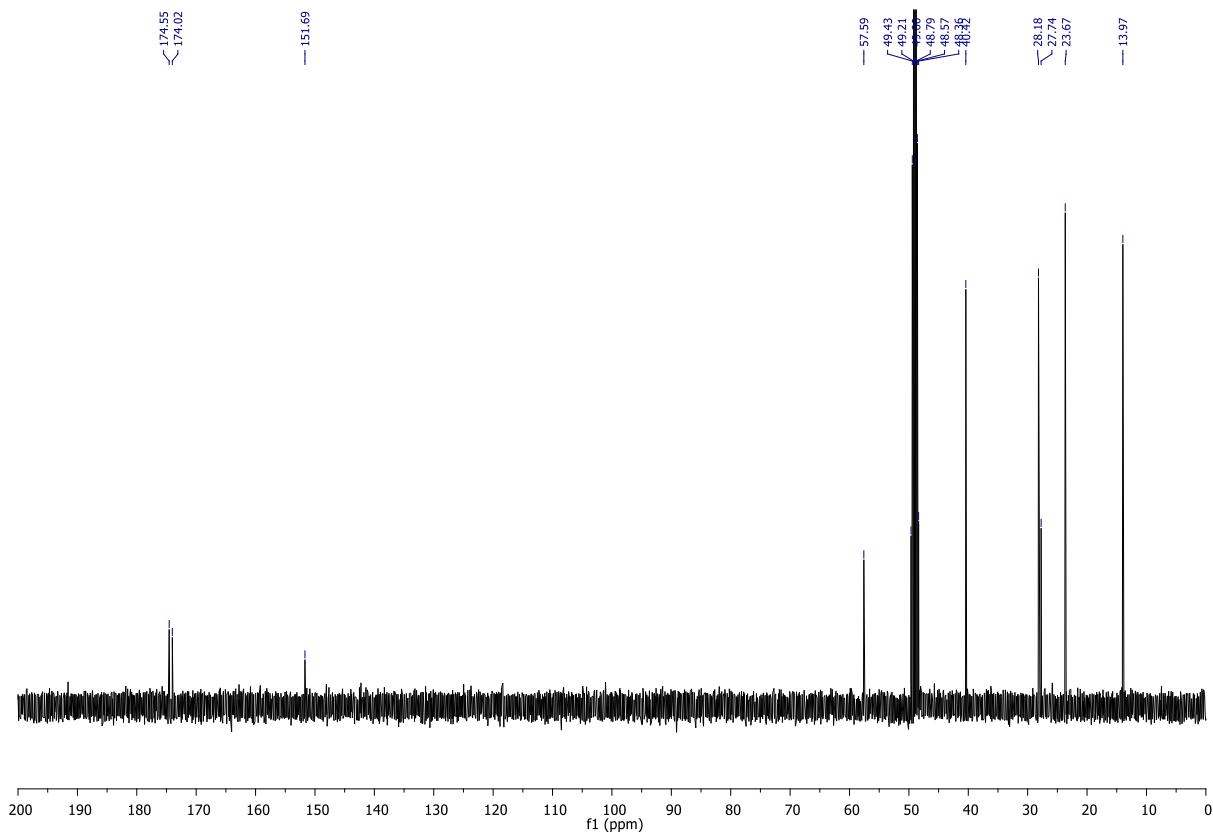
3.10.3. Variable temperature NMR experiments
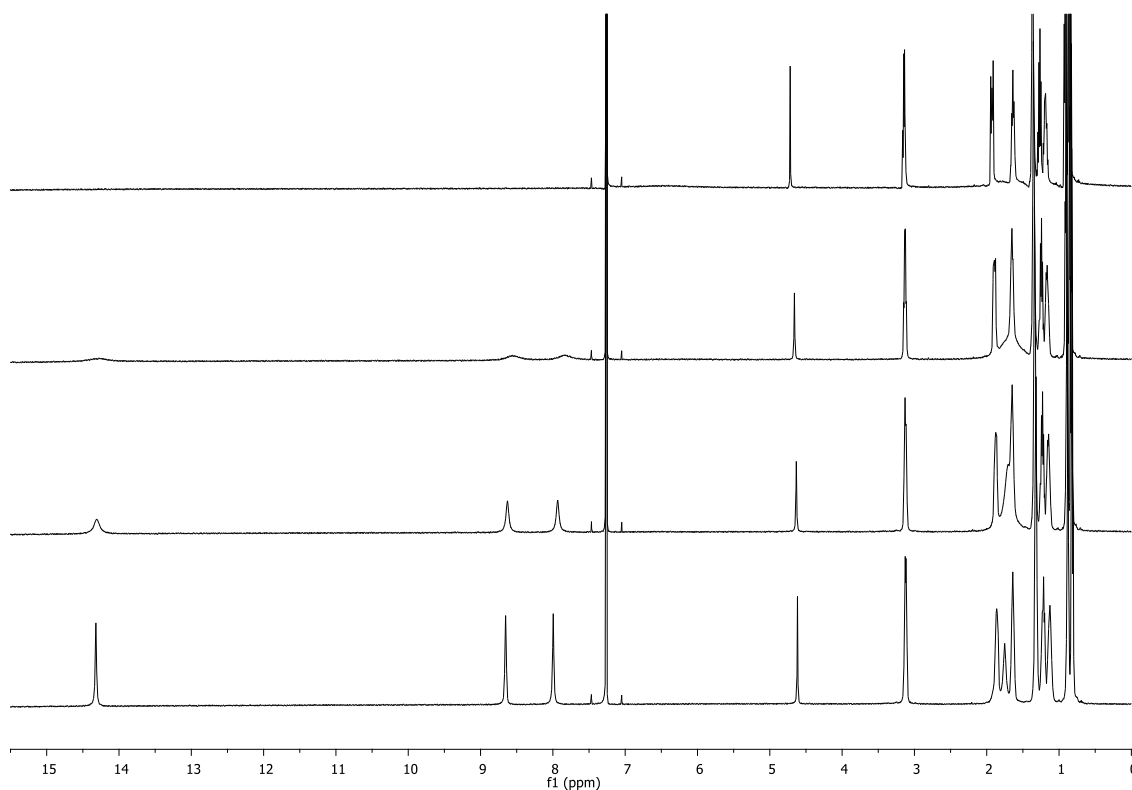
Figure 3.E1. ^{1}H NMR (500 MHz, CDCl$_3$) spectra of **PA•B** at 298 K, 273 K, 253 K and 233 K (from top to bottom) with $c(\textbf{PA}) = c(\textbf{B}) = 3$ mM.
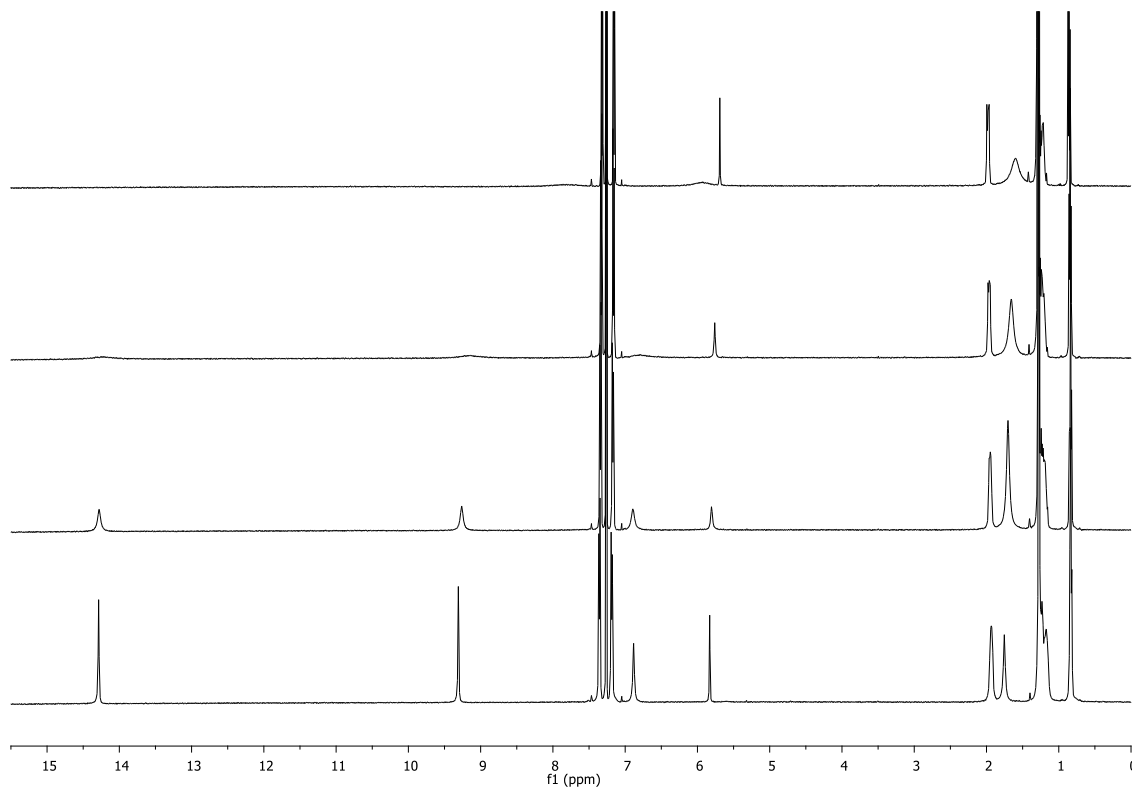
Figure 3.E2. ^{1}H NMR (500 MHz, CDCl$_3$) spectra of **PB•B** at 298 K, 273 K, 253 K and 233 K (from top to bottom) with $c(\textbf{PB}) = c(\textbf{B}) = 3$ mM.
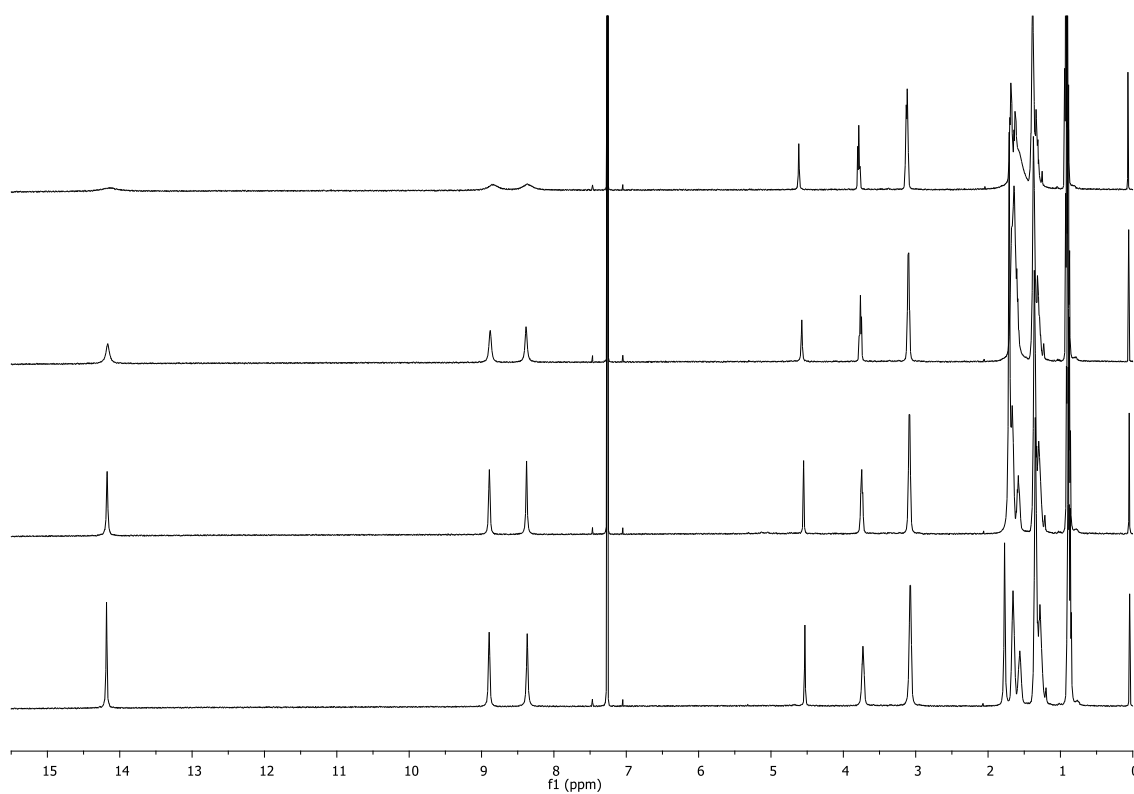
Figure 3.E3. ^{1}H NMR (500 MHz, CDCl$_3$) spectra of **PA•C** at 298 K, 273 K, 253 K and 233 K (from top to bottom) with $c(\textbf{PA}) = c(\textbf{C}) = 3$ mM.
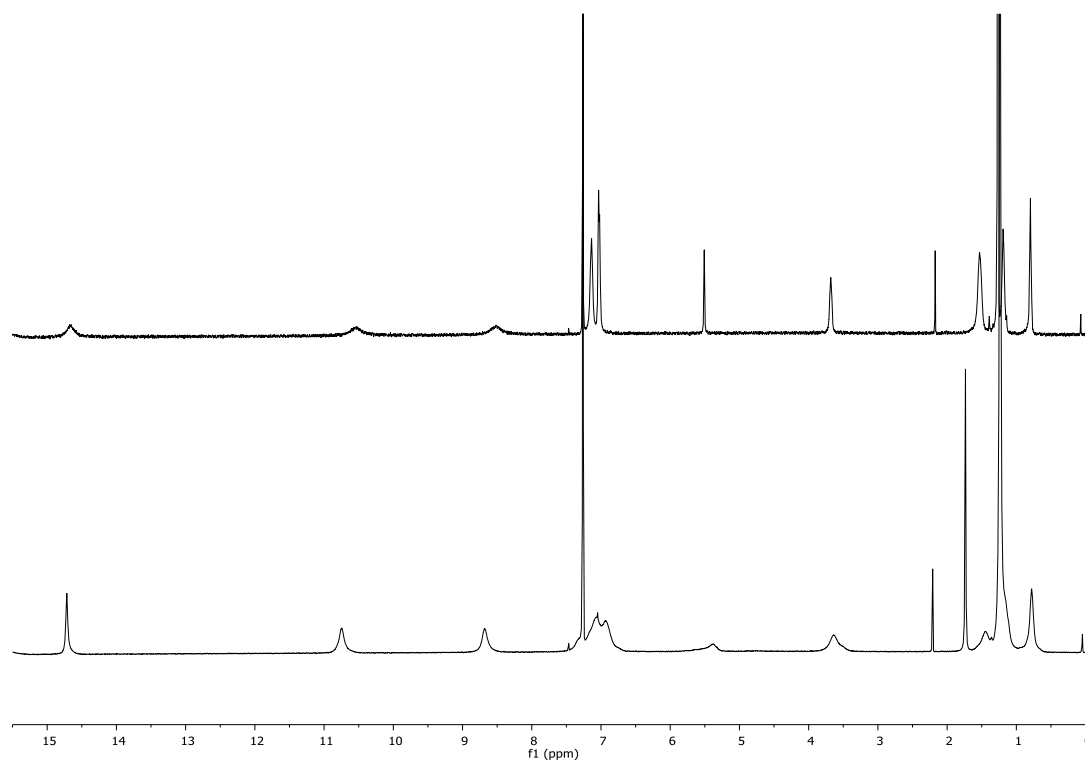
Figure 3.E4. ^{1}H NMR (500 MHz, CDCl$_3$) spectra of **PB•C** at 298 K (top) and 233 K (bottom) with $c(\textbf{PB}) = c(\textbf{C}) = 3$ mM.

81

3.10.4. NMR dilutions and titrations

General

The NMR titrations were recorded on a Bruker 400 MHz Avance III HD Smart Probe at 400 MHz and on a Bruker 500 MHz AVIII HD SmartProbe Spectrometer at 500 MHz at 298 K with CDCl₃ as a solvent. A host solution with known concertation was prepared and a fraction of this solution (500/600 µL) was transferred into a NMR tube. Then, the guest solution was prepared by dissolving a known amount of guest in the host stock solution in a volumetric flask. A change of chemicals shifts of ^{1}H upon addition of aliquots of guest solution were followed. For dilution experiments, a solution with known concentration of a compound was prepared and aliquots of this solution were added to a NMR tube containing only the solvent (500 µL/600 µL) and the change of chemicals shifts of ^{1}H upon addition was followed. The observed changes of chemical shifts were analysed using a purpose-written fitting macro in Microsoft Excel (written by Professor Hunter). A dimerisation isotherm, 1:1 binding isotherm, different 1:2 binding isotherms (see below) and 3:3 binding isotherm were used to fit the experimental data. The experiments were measured at least two times on two different days with freshly prepared solutions in order to eliminate possible systematic errors. The results are stated as average values and errors are quoted as two times the standard deviation.

1:2 binding isotherms

a) Non-cooperative model using identical binding sites:

$K_1 = K_2 = K_{nc}$ and the change in chemical shift for formation of the 1:1 complex is identical to the subsequent change in chemical for formation of the 1:2 complex

b) Non-cooperative model where K_1 and K_2 were fixed to be the appropriate K_{ref}

c) Cooperative isotherm where K_1 was fixed to be the appropriate K_{ref}

Global error of the fit

$$E = \frac{\sum_{i=0}^{N-1}\left(\delta_{i,calc} - \delta_{i,obs}\right)^2}{\sum_{i=0}^{N-1}\left(\delta_{0,obs} - \delta_{i,obs}\right)^2}$$

where $\delta_{i,calc}$ is the calculated chemical shift, $\delta_{i,obs}$ is the observed chemical shift and $\delta_{0,obs}$ is the observed chemical shift for the first point in the titration, N is the total number of data points recorded
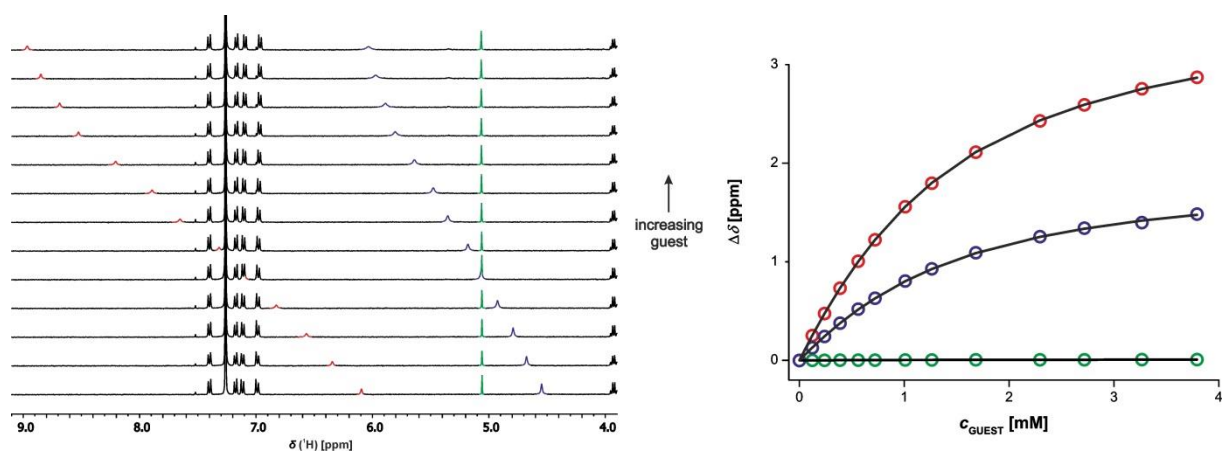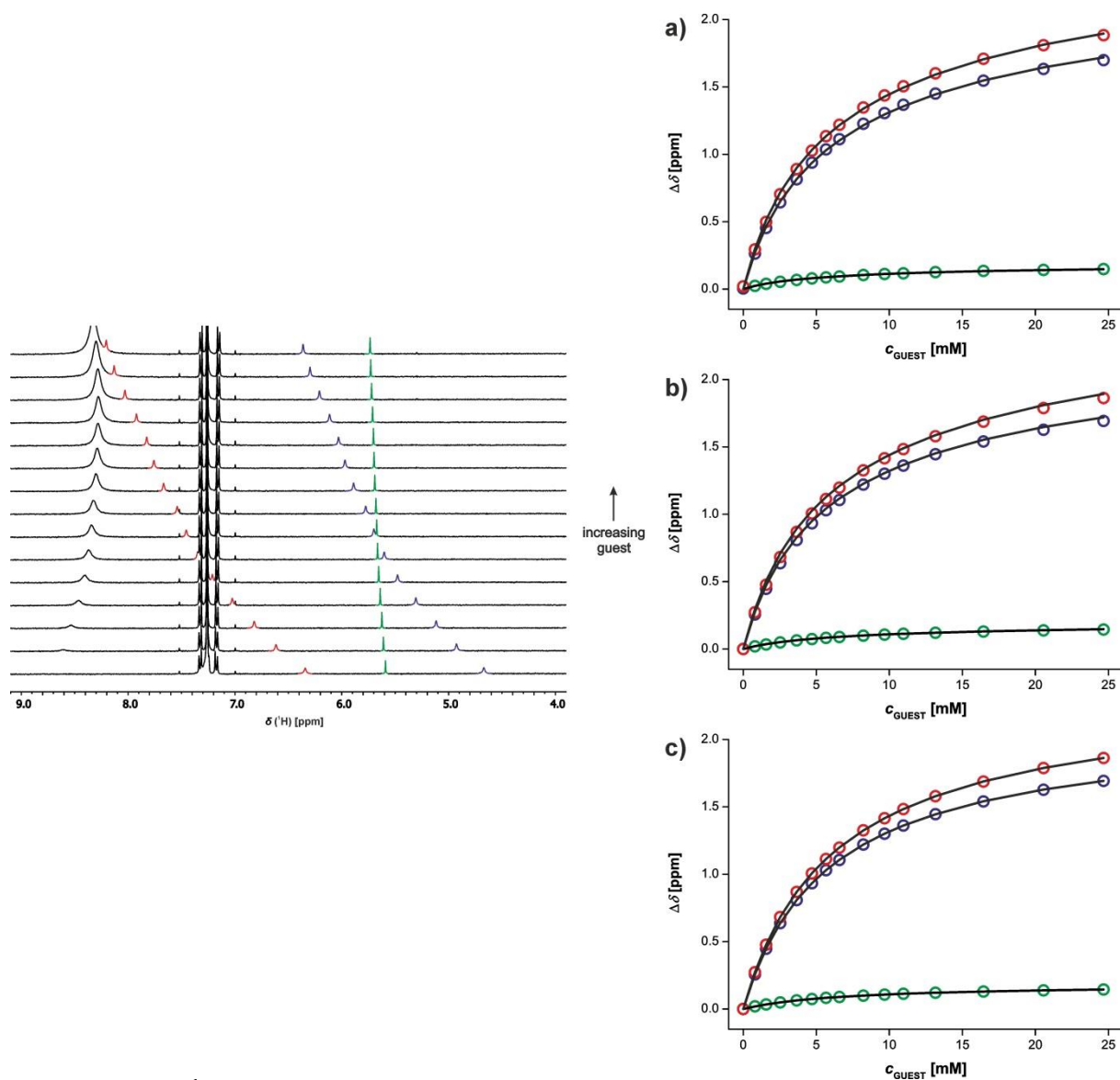
NMR titrations
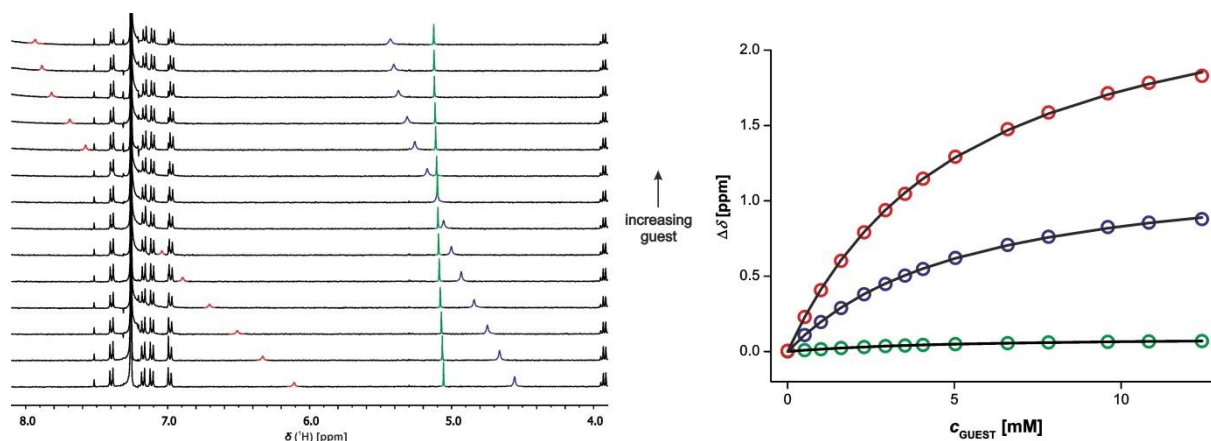
Figure 3.E5. ^{1}H NMR (400 MHz, CDCl$_3$, 298 K) titration of **bB** into **bPB** (0.53 mM). ^{1}H NMR spectrum is shown on the left (pyrimidine C-H signal green, N-H signals blue and red). On the right are shown the experimental data (circles) and calculated values (lines) based on a 1:1 binding isotherm.
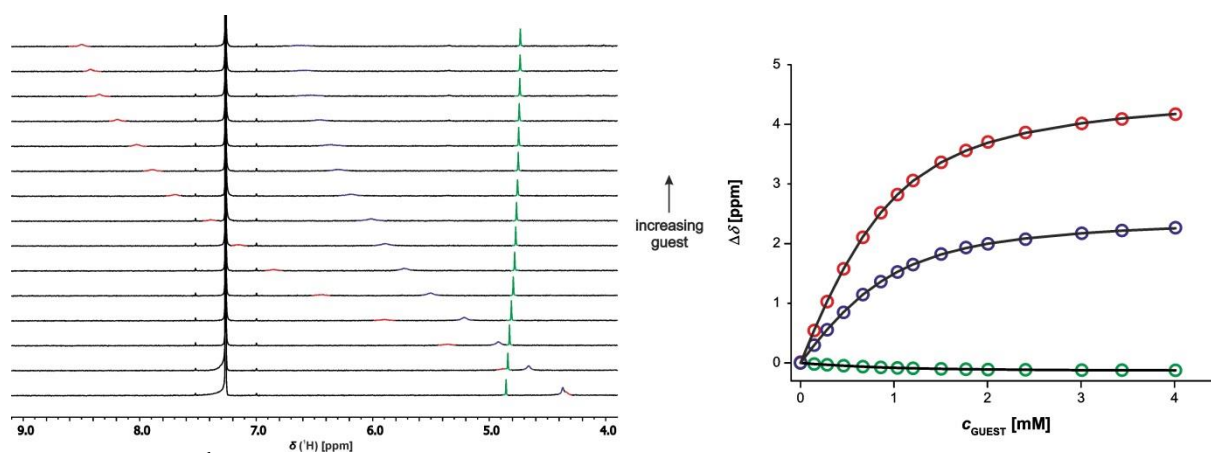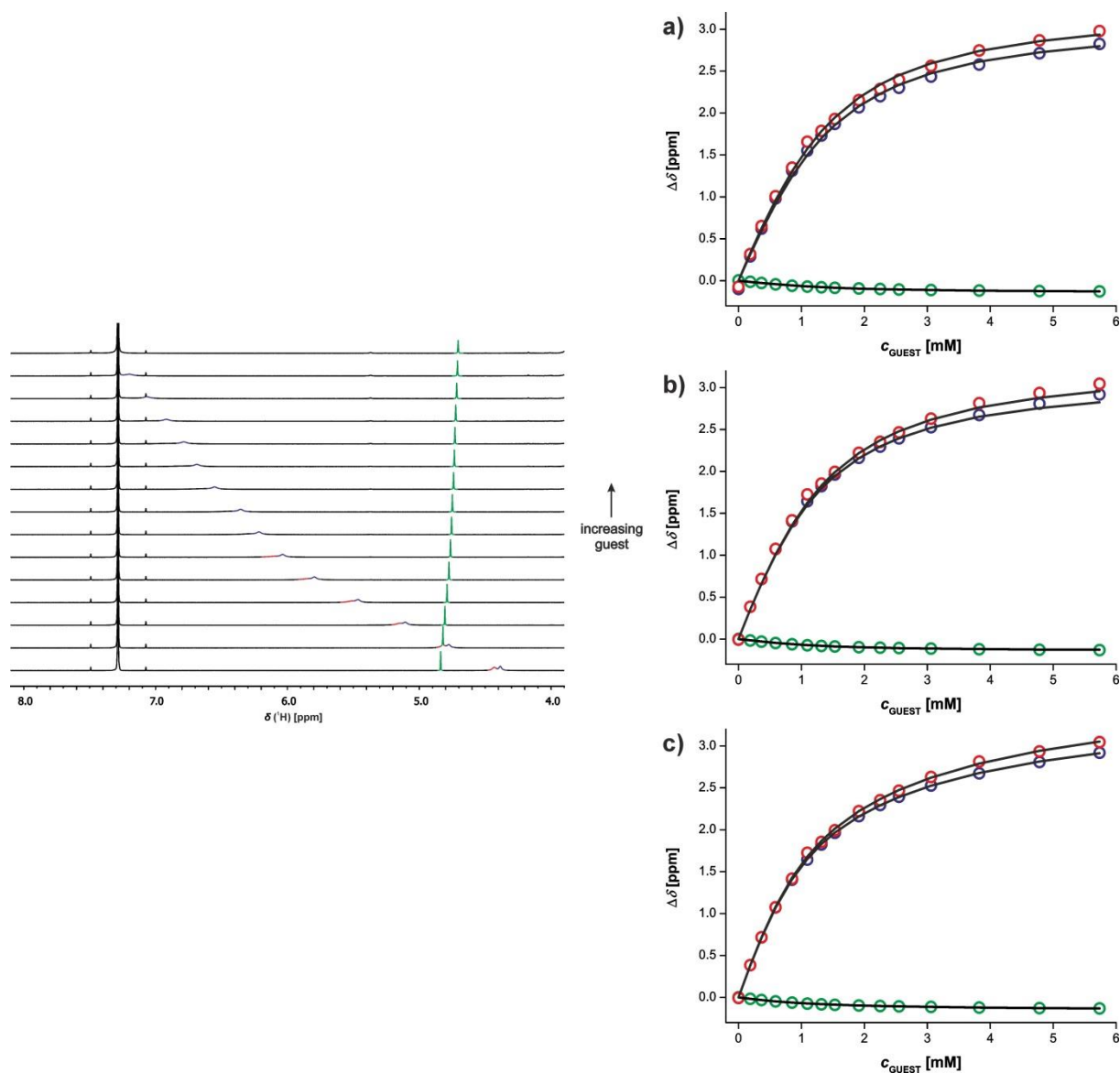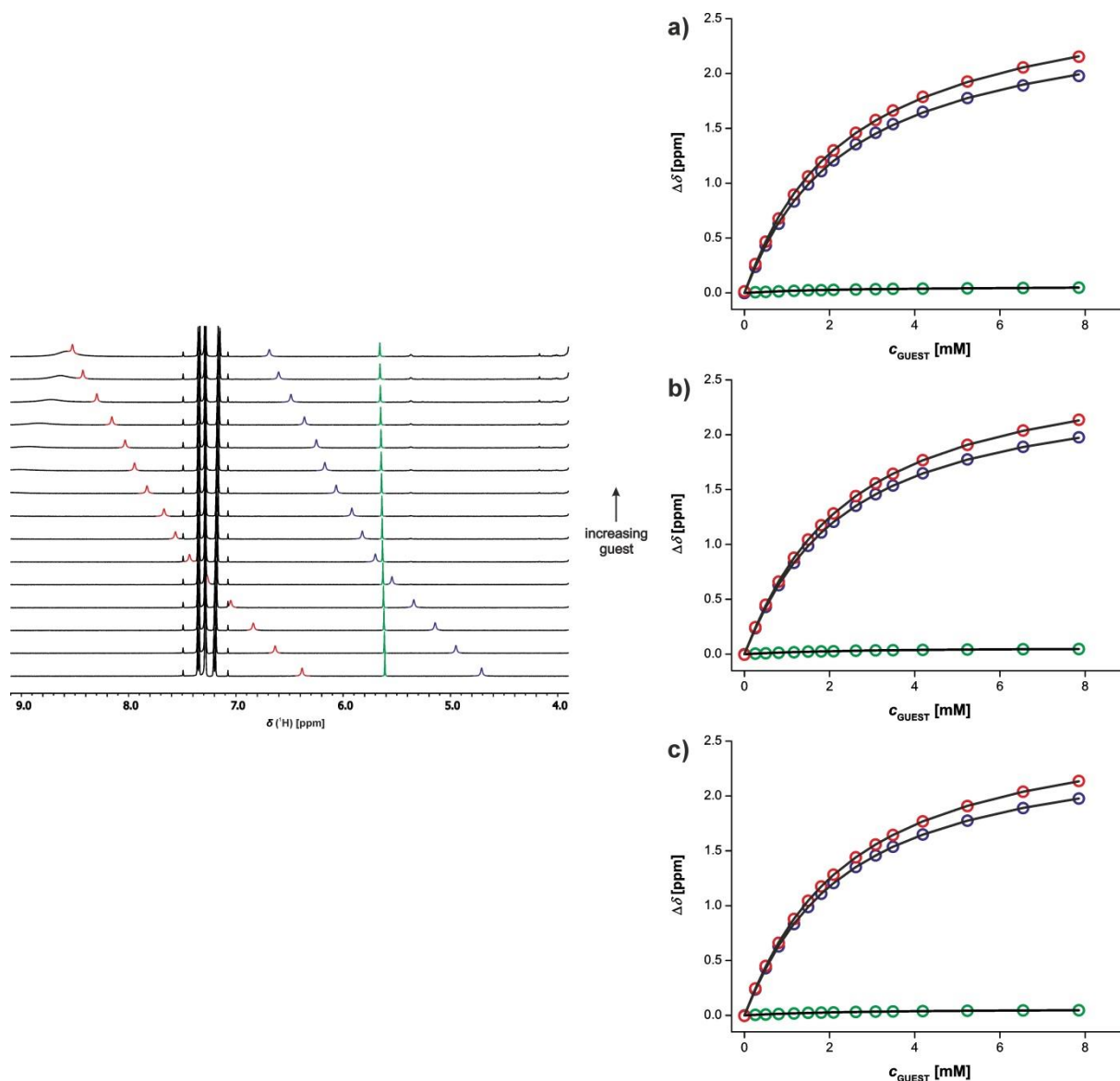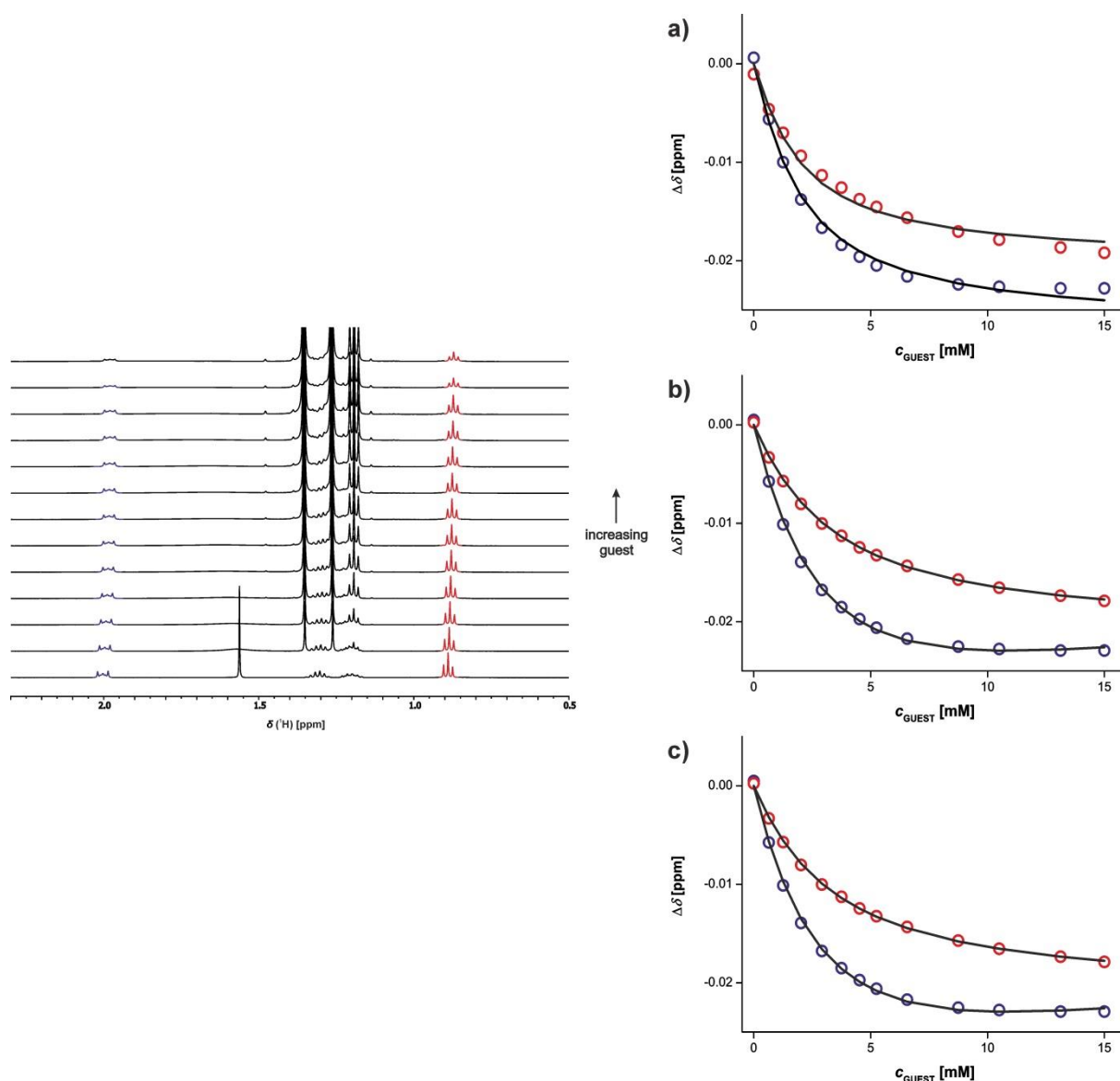

Figure 3.E6. ^{1}H NMR (400 MHz, CDCl$_3$, 298 K) titration of **bC** into **bPA** (0.86 mM). ^{1}H NMR spectrum is shown on the left (pyrimidine C-H signal green, N-H signals blue and red). On the right are shown the experimental data (circles) and calculated values (lines) based on a 1:1 binding isotherm.

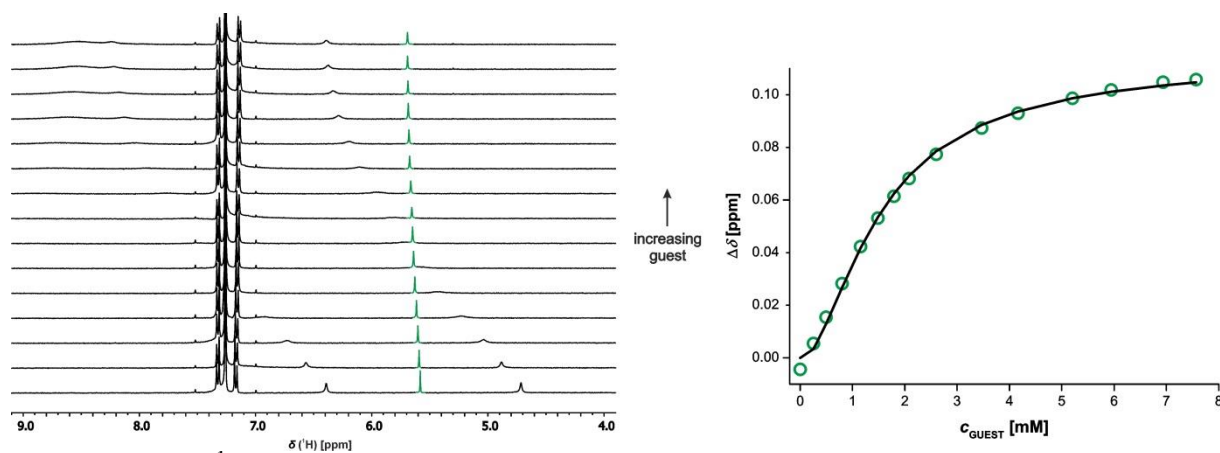**Figure 3.E7**. ^{1}H NMR (400 MHz, CDCl$_3$, 298 K) titration of **bC** into **bPB** (0.83 mM). ^{1}H NMR spectrum is shown on the left (pyrimidine C-H signal green, N-H signals blue and red). On the right are shown the experimental data (circles) and calculated values (lines) based on a 1:1 binding isotherm.

Figure 3.E8. ^{1}H NMR (400 MHz, CDCl$_3$, 298 K) titration of **bB** into **PB** (0.53 mM). ^{1}H NMR spectrum is shown on the left (pyrimidine C-H signal green, N-H signals blue and red). On the right are shown the experimental data (circles) and calculated values (lines) based on a 1:2 binding isotherms using (a) non-cooperative model using identical binding sites, (b) non-cooperative model where K_1 and K_2 were fixed to be the appropriate K_{ref} and (c) cooperative isotherm where K_1 was fixed to be the appropriate K_{ref}.

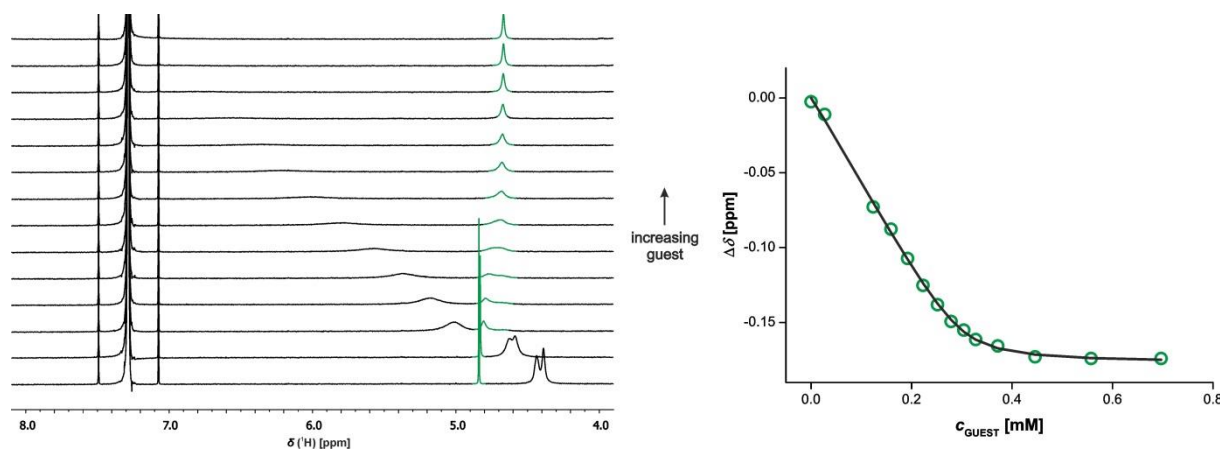**Figure 3.E9**. ^{1}H NMR (500 MHz, CDCl$_3$, 298 K) titration of **bC** into **PA** (0.77 mM). ^{1}H NMR spectrum is shown on the left (pyrimidine C-H signal green, N-H signals blue and red). On the right are shown the experimental data (circles) and calculated values (lines) based on a 1:2 binding isotherms using (a) non-cooperative model using identical binding sites, (b) non-cooperative model where K_1 and K_2 were fixed to be the appropriate K_{ref} and (c) cooperative isotherm where K_1 was fixed to be the appropriate K_{ref}.

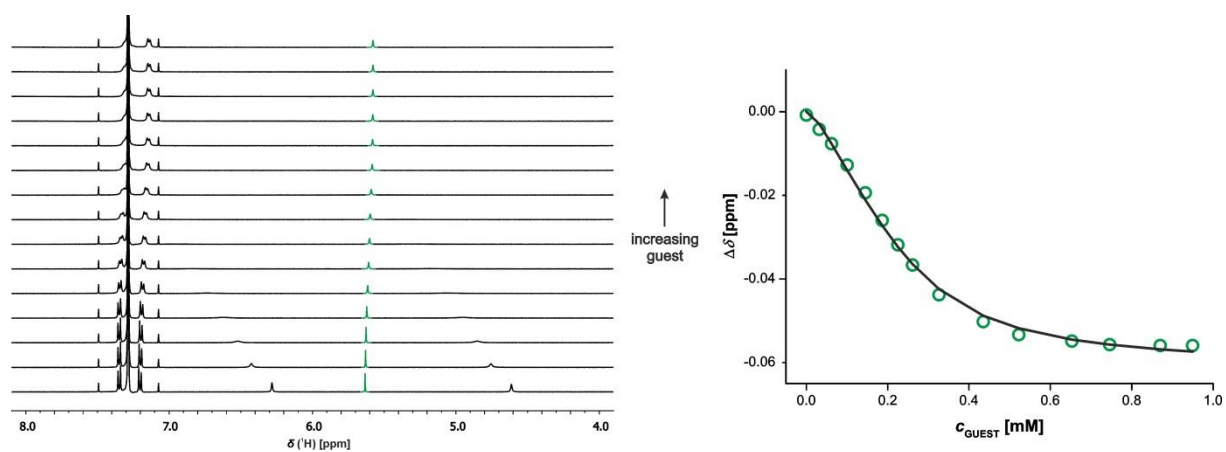**Figure 3.E10**. ^{1}H NMR (500 MHz, CDCl$_3$, 298 K) titration of **bC** into **PB** (0.65 mM). ^{1}H NMR spectrum is shown on the left (pyrimidine C-H signal green, N-H signals blue and red). On the right are shown the experimental data (circles) and calculated values (lines) based on a 1:2 binding isotherms using (a) non-cooperative model using identical binding sites, (b) non-cooperative model where K_1 and K_2 were fixed to be the appropriate K_{ref} and (c) cooperative isotherm where K_1 was fixed to be the appropriate K_{ref}.

Figure 3.E11. ^{1}H NMR (500 MHz, CDCl$_3$, 298 K) titration of **bPB** into **B** (0.90 mM). ^{1}H NMR spectrum is shown on the left (CH$_3$ signal red, (C=O)$_2$C(CH$_2$)$_2$ signal blue). On the right are shown the experimental data (circles) and calculated values (lines) based on a 1:2 binding isotherms using (a) non-cooperative model using identical binding sites, (b) non-cooperative model where K_1 and K_2 were fixed to be the appropriate K_{ref} and (c) cooperative isotherm where K_1 was fixed to be the appropriate K_{ref}.

Figure 3.E12. ^{1}H NMR (400 MHz, CDCl$_3$, 298 K) titration of **B** into **PB** (1.1 mM). The ^{1}H NMR spectrum is shown on the left (pyrimidine C-H signal green). On the right are shown the experimental data (circles) and calculated values (line) based on a 3:3 binding isotherm.

Figure 3.E13. ^{1}H NMR (500 MHz, CDCl$_3$, 298 K) titration of **C** into **PA** (0.30 mM). The ^{1}H NMR spectrum is shown on the left (pyrimidine C-H signal green). On the right are shown the experimental data (circles) and calculated values (line) based on a 3:3 binding isotherm. The weight averaging was used to obtain the average chemical shift of pyrimidine C-H signal.

Figure 3.E14. ^{1}H NMR (500 MHz, CDCl$_3$, 298 K) titration of **C** into **PB** (0.26 mM). The ^{1}H NMR spectrum is shown on the left (pyrimidine C-H signal green). On the right are shown the experimental data (circles) and calculated values (line) based on a 3:3 binding isotherm.

3.11. References

(1)   Hunter, C. A.; Anderson, H. L. *Angew. Chem. Int. Ed.* **2009**, *48*, 7488-7499.

(2)   Motloch, P.; Hunter, C. A. *Adv. Phys. Org. Chem.* **2016**, *50*, 77-118.

(3)   Di Stefano, S.; Ercolani, G. In *Adv. Phys. Org. Chem.* **2016**, *50*, 1-76.

(4)   Hogben, H. J.; Sprafke, J. K.; Hoffmann, M.; Pawlicki, M.; Anderson, H. L. *J. Am. Chem. Soc.* **2011**, *133*, 20962-20969.

(5)   Montoro-García, C.; Camacho-García, J.; López-Pérez, A. M.; Bilbao, N.; Romero-Pérez, S.; Mayoral, M. J.; González-Rodríguez, D. *Angew. Chem. Int. Ed.* **2015**, *54*, 6780-6784.

(6)   Jinks, M. A.; Sun, H.; Hunter, C. A. *Org. Biomol. Chem.* **2014**, *12*, 1440-1447.

(7)   Whitesides, G. M.; Simanek, E. E.; Mathias, J. P.; Seto, C. T.; Chin, D.; Mammen, M.; Gordon, D. M. *Acc. Chem. Res.* **1995**, *28*, 37-44.

(8)   Timmerman, P.; Prins, Leonard J. *Eur. J. Org. Chem.* **2001**, *2001*, 3191-3205.

(9)   Prins, L. J.; Reinhoudt, D. N.; Timmerman, P. *Angew. Chem. Int. Ed.* **2001**, *40*, 2382-2426.

(10)   ten Cate, M. G. J.; Huskens, J.; Crego-Calama, M.; Reinhoudt, D. N. *Chem. Eur. J.* **2004**, *10*, 3632-3639.

(11)   Bielejewska, A. G.; Marjo, C. E.; Prins, L. J.; Timmerman, P.; de Jong, F.; Reinhoudt, D. N. *J. Am. Chem. Soc.* **2001**, *123*, 7518-7533.

(12)   Anslyn, E. V.; Dougherty, D. A.; Dougherty, E. V.; Books, U. S. *Modern Physical Organic Chemistry*; University Science Books, 2006.

(13)   Bann, B.; Miller, S. A. *Chem. Rev.* **1958**, *58*, 131-172.

(14)   Birkett, H. E.; Harris, R. K.; Hodgkinson, P.; Carr, K.; Charlton, M. H.; Cherryman, J. C.; Chippendale, A. M.; Glover, R. P. *Magn. Reson. Chem.* **2000**, *38*, 504-511.

(15)   Timmerman, P.; Jolliffe, K. A.; Crego Calama, M.; Weidmann, J.-L.; Prins, L. J.; Cardullo, F.; Snellink-Ruël, B. H. M.; Fokkens, R. H.; Nibbering, N. M. M.; Shinkai, S.; Reinhoudt, D. N. *Chem. Eur. J.* **2000**, *6*, 4104-4115.

(16)   Lehn, J.-M.; Mascal, M.; Decian, A.; Fischer, J. *J. Chem. Soc., Chem. Commun.* **1990**, 479-481.

(17)   Hud, N. V. *Synlett* **2017**, *28*, 36-55.

(18)   Benson, S. W. *J. Am. Chem. Soc.* **1958**, *80*, 5151-5154.

(19)   Bishop, D. M.; Laidler, K. J. *J. Chem. Phys.* **1965**, *42*, 1688-1691.

(20)   Bailey, W. F.; Monahan, A. S. *J. Chem. Educ.* **1978**, *55*, 489.

(21)   Ercolani, G.; Piguet, C.; Borkovec, M.; Hamacek, J. *J. Phys. Chem. B* **2007**, *111*, 12195-12203.

(22)   Kyogoku, Y.; Lord, R. C.; Rich, A. *Biochim. Biophys. Acta* **1969**, *179*, 10-17.

(23)   Hunter, C. A. *Angew. Chem. Int. Ed.* **2004**, *43*, 5310-5324.

(24)   Mathias, J. P.; Simanek, E. E.; Zerkowski, J. A.; Seto, C. T.; Whitesides, G. M. *J. Am. Chem. Soc.* **1994**, *116*, 4316-4325.

(25)   Franzmann, P.; Beil, S. B.; Schollmeyer, D.; Waldvogel, S. R. *Chem. Eur. J.* **2019**, *25*, 1936-1940.

(26)   Yu, X.; Zhao, R.; Wan, H.; Yang, Y.; Wang, D. *Tetrahedron Lett.* **2016**, *57*, 4588-4591.

(27)   Close, W. J. *J. Am. Chem. Soc.* **1953**, *75*, 3617-3618.

IV

Towards supramolecular system inside porphyrin nanoring

4.1. Introduction

In nature, most of the biological systems are multivalent. Due to cooperativity, the product of multiple bindings is usually not just a simple sum of individual binding contributions.[1] In multivalent supramolecular systems, two types of cooperativity exist: allosteric and chelate cooperativity. Allosteric cooperativity happens when a first binding influences the strength of the second binding. Chelate cooperativity originates from the binding of a multivalent host and guest which leads to the change of the "effective concentration" for the second binding. Nowadays, the term effective molarity is used for the quantification of chelate cooperativity. A model divalent system is described in Figure 4.1. The first binding is always intermolecular with an equilibrium constant K_{inter}. For second binding, two different pathways are possible: intramolecular cyclisation with an equilibrium constant K_{intra} (that usually differs from K_{inter}) or intermolecular interaction with an equilibrium constant K_{inter} resulting in oligomerisation.
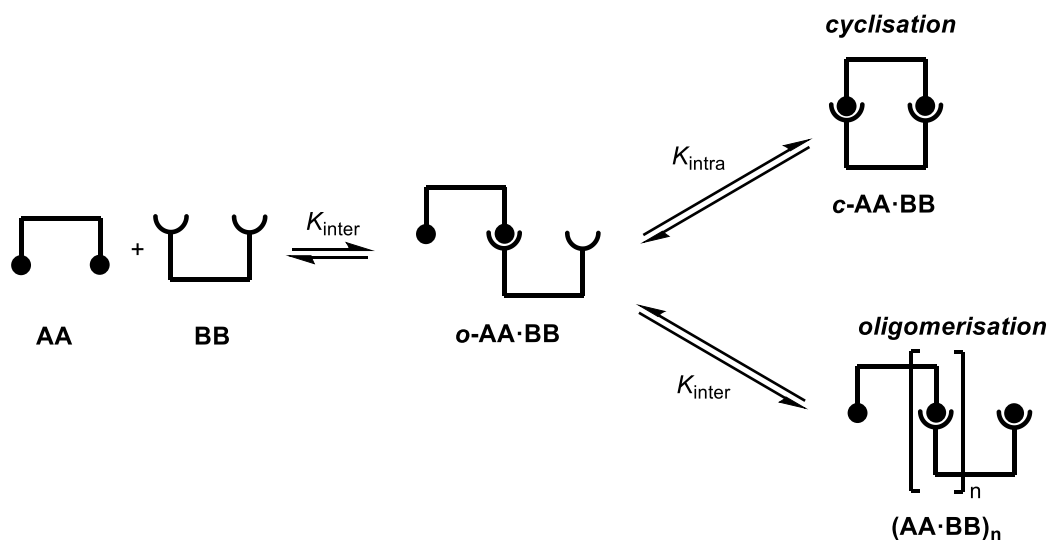
Figure 4.1. Schematic representation of chelate cooperativity in the *c*-AA•BB complex. The first binding is always intermolecular. The second binding is either intramolecular cyclisation or intermolecular interaction resulting in oligomerisation.

Effective molarity is defined by Equation 4.1.

$$\text{EM} = \frac{K_{intra}}{K_{inter}} \tag{4.1}$$

The literature provides a distribution of effective molarities in supramolecular systems. The median value is 100 mM and EMs greater than 10^2 M are considered to be extremely high, since less than 5% of the reviewed supramolecular systems reached this value.[2]

Porphyrin nanorings from the Anderson group are examples of such system with exceptionally high values of EM. The highest value has been found for complex **6-ring•T** (Figure 4.2). The Anderson group used a series of ligands with two, three, four and five pyridine binding sites to determine stepwise EMs for each binding interaction in the hexamer.[3] The value of EM for the first intramolecular binding interaction is 100 mM, which is comparable to the value found for the majority of supramolecular complexes. However, all four subsequent intramolecular binding interactions have exceptionally high values of EM of 10^3 M.
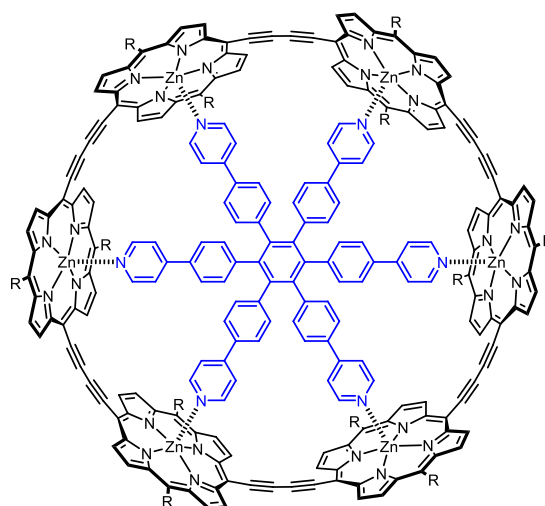
Figure 4.2. Complex of **6-ring** (black) with hexadentate ligand **T** (blue). R is a substituent.

The goal of this project was to test if the extreme values of effective molarity found for the **6-ring** can stabilise a weakly-interacting H-bonded system inside the **6-ring** cavity. This should provide new insights into the extreme values of effective molarities and answer if the additional flexibility and different nature of the hexadentate supramolecular ligand system can be beneficial or not compared to the hexadentate covalent ligand. The H-bonded system would keep the pyridine units as the molecular recognition for the zinc porphyrins (Figure 4.3).
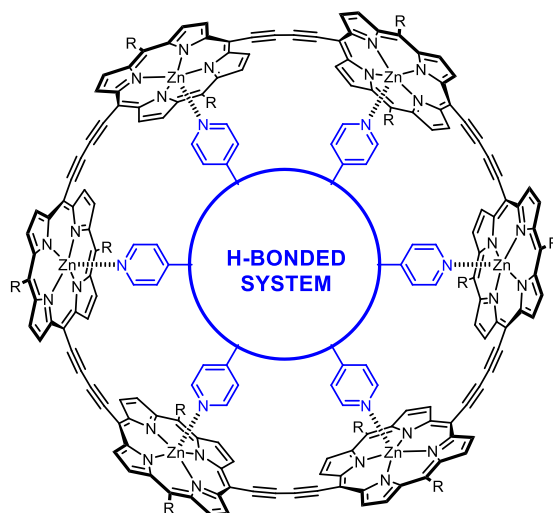
Figure 4.3. H-bonded supramolecular system inside the porphyrin nanoring. R is a substituent.

4.2. Approach

The initial idea for the supramolecular system was to utilise small molecules based on pyridine that would contain simple H-bond acceptors and donors units. The strength of the H-bonding interactions can be predicted by using the molecular recognition toolbox.[4] It is possible to quantify the free energy of a solution phase intermolecular interaction in defined solvent S by using Equation 4.2.

$$\Delta G°_{pred} = -(\alpha - \alpha_s)(\beta - \beta_s) + 6 \text{ kJ} \cdot \text{mol}^{-1} \qquad (4.2)$$

where α and β describe the H-bond donor and acceptor properties, respectively, S is an annotation for solvent and the value $6 \text{ kJ} \cdot \text{mol}^{-1}$ is the free energy cost of the bimolecular association.

Then, an association constant K_f for the process can be predicted by Equation 4.3.

$$K_{f,pred} = e^{\frac{-\Delta G°_{pred}}{RT}} \qquad (4.3)$$

Since phosphine oxides and phenols should produce the strongest H-bonding ($\beta = 10$ and $\alpha = 4$, respectively), these were the functional groups chosen to start with. Figure 4.4 shows two supramolecular systems using different bisphosphine oxides and commercially available pyridine-3,5-diol (**pyridinediol**). In addition, we also wanted to test systems that utilise weaker H-bonding acceptors to investigate the influence of H-bonding strength on the formation of the target system inside **6-ring**. From the β scale for H-bonding acceptors,[4] two

initial candidates were selected: a sulfoxide and an amide, both of which should still be reasonably strong H-bond acceptors (with $\beta = 9$ and with $\beta = 8$, respectively). The amide seemed the best candidate because of its synthetic accessibility. A supramolecular system inside the porphyrin nanoring cavity based on the different H-bonding acceptor and **pyridinediol** is shown in Figure 4.4c. It can be noted that these molecules are technically imides rather than amides and they should provide the optimal geometry for the target supramolecular system thanks to the preorganisation.
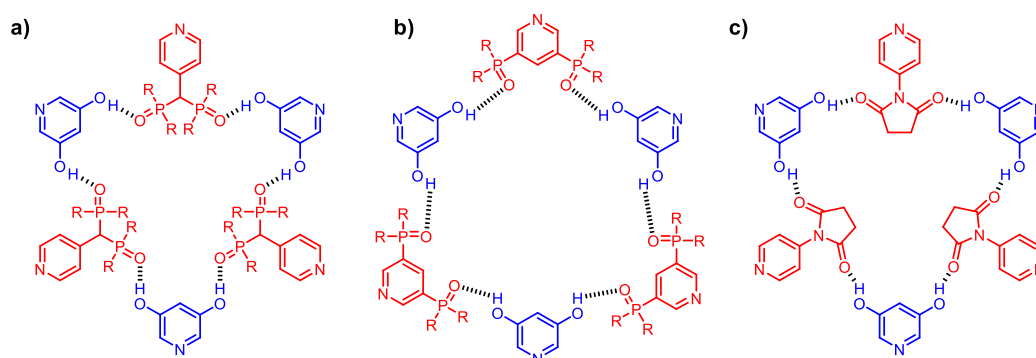
Figure 4.4. Supramolecular H-bonded system based on (a) (b) bisphosphine oxides and (c) imides. R is a solubilising group.

This approach would also allow us to construct a range of lower valency ligands by combining mono and bisphosphine oxides and phenols. An example based on **pyridinediol** and mono phosphine oxide is shown in Figure 4.5b.
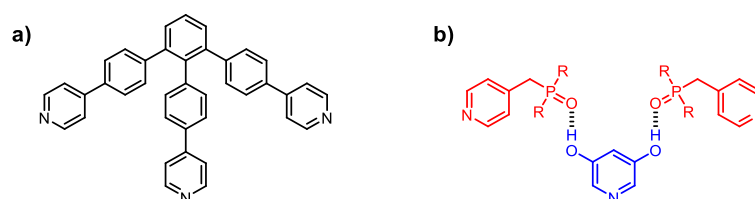
Figure 4.5. (a) Linear covalent template and (b) its supramolecular equivalent (R is a solubilising group).

To study the supramolecular system, a non-polar solvent has to be used, as these H-bonded systems would be disrupted in polar solvents such as methanol. We decided to employ chloroform and toluene.[4]

4.3. Modelling

Computational chemistry was used to test the different designs described in Figure 4.4. DFT calculations cannot be used for conformational searches for these systems due to the large number of atoms. Molecular mechanics cannot be used for these systems, because they contain both H-bonding and zinc-pyridine interactions, which are not parameterised well. Herein, we describe a strategy to overcome these issues.

We took ligand **T** from the X-ray structure of the **6-ring •T** (Figure 4.6) and used it as a template.[5] For molecular modelling calculations, we constrained the coordinates of the nitrogen atoms and the carbon atoms in the position 4 (Figure 4.7). With this, the conformational search could rotate the pyridines freely around their axes. In addition, this modelling does not employ **6-ring.** This method lowers the calculations costs, but it does not find all the possible structures, since the porphyrin units of **6-ring** can rotate in the real structures.
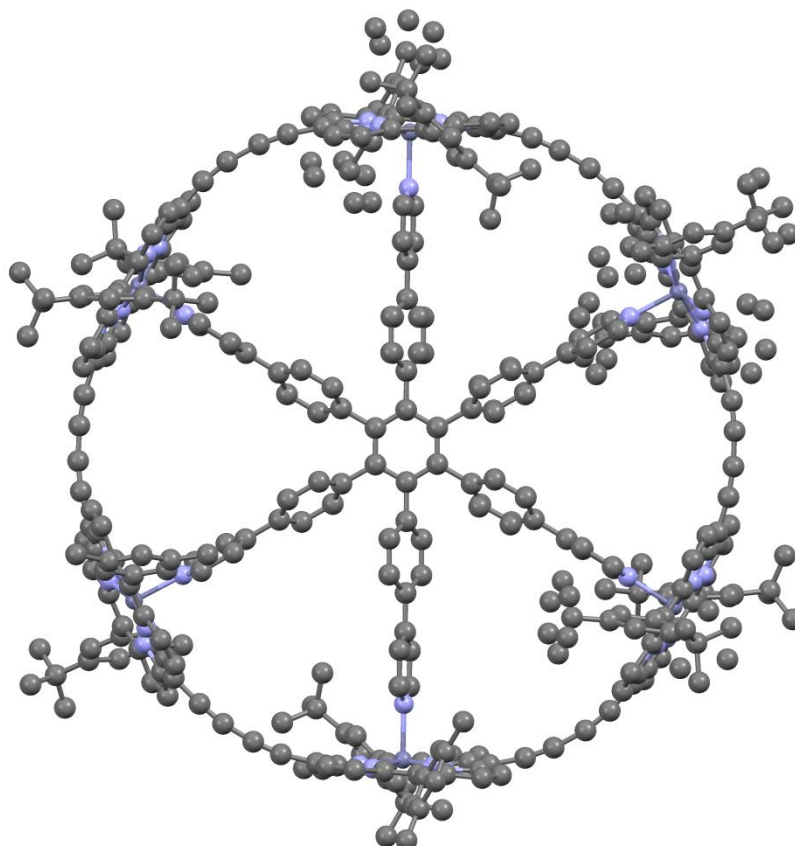
Figure 4.6. X-ray structure of the **6ring•T** complex.[5]
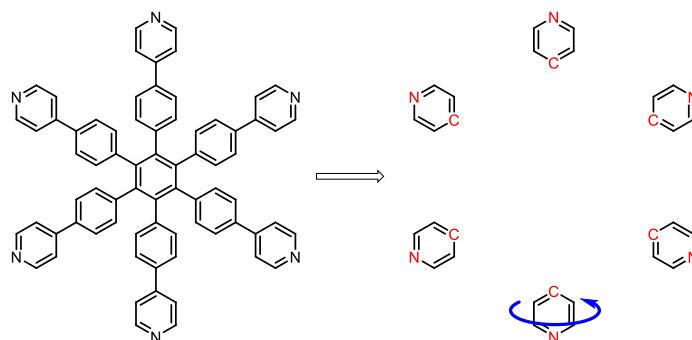
Figure 4.7. Template **T** as a template for molecular modelling calculations. The atoms in red were constrained for the calculations to allow rotation around the pyridine axis (one is highlighted in blue).

With this simplified method in hand, we were able to model the systems proposed in Figure 4.4. The restricted conformational search provided structures with either 5 or 6 H-bonds connecting the ligands of these systems as shown in Figure 4.8. The system based on bisphosphine oxide shown in Figure 4.8a provided a structure that is not fully connected by H-bonding. This does not mean that the proposed system cannot be formed inside the porphyrin nanoring, since the search was restricted as stated above. The other two systems from Figure 4.4, based on a different bisphosphine oxide and imide, provided lowest energy structures that are connected together by 6 H-bonds. This showed that it should be possible to obtain the target H-bonded supramolecular systems inside the cavity of porphyrin nanoring.
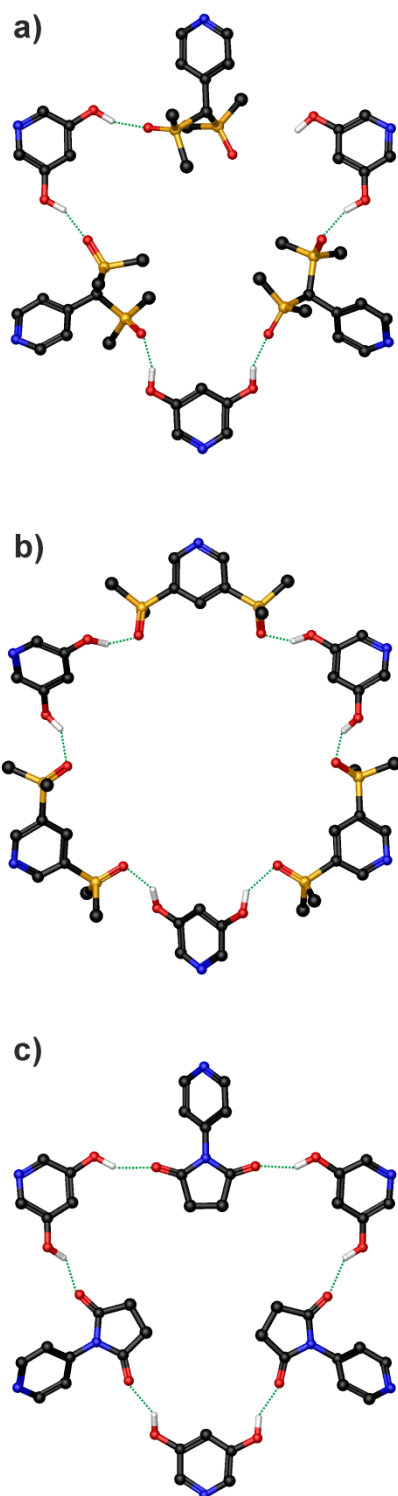
Figure 4.8. Lowest energy structures from restricted molecular mechanics conformational search of H-bonded supramolecular systems based on (a) and (b) bisphosphine oxides and (c) imines using **T** as a template. The coordinates of nitrogen atoms and carbon atoms in the position 4 were constrained (See Figure 4.7). Hydrogen atoms that do not contribute to H-bonding were omitted for clarity; colouring of atoms: C (black), N (blue), O (red), P (yellow), H (white); green dashed line is the H-bond.

4.4. Synthesis

4.4.1. Synthesis of porphyrin nanoring

First of all, a porphyrin nanoring had to be synthesised. To do that, a porphyrin monomer and a suitable template had to be prepared.[3,6] The synthesis of porphyrin monomer **M** was accomplished in seven steps (Scheme 4.1). Dipyrromethane **1** was prepared from pyrrole on a multigram scale with a yield of 35%. Also on a multigram scale, the substituted benzaldehyde **2** was synthesised by radical bromination of substituted toluene and a subsequent Sommelet reaction. The reaction of **1** and **2** with trifluoroacetic acid followed by an *in-situ* reaction with DDQ provided a porphyrin that was immediately treated with zinc acetate to generate zinc porphyrin **3** in 28% yield. The bromination of this porphyrin with NBS produced the dibromo porphyrin **4** with a yield of 83%. Trihexylsilyl acetylene **5** was prepared in 95% yield from ethynylmagnesium bromide. The Sonogashira coupling of **4** with **5** produced the THS-protected *meso*-alkynyl porphyrin **6** with a yield of 96%. In the last step, **6** was deprotected by TBAF to obtain the target porphyrin monomer **M** in 80% yield.
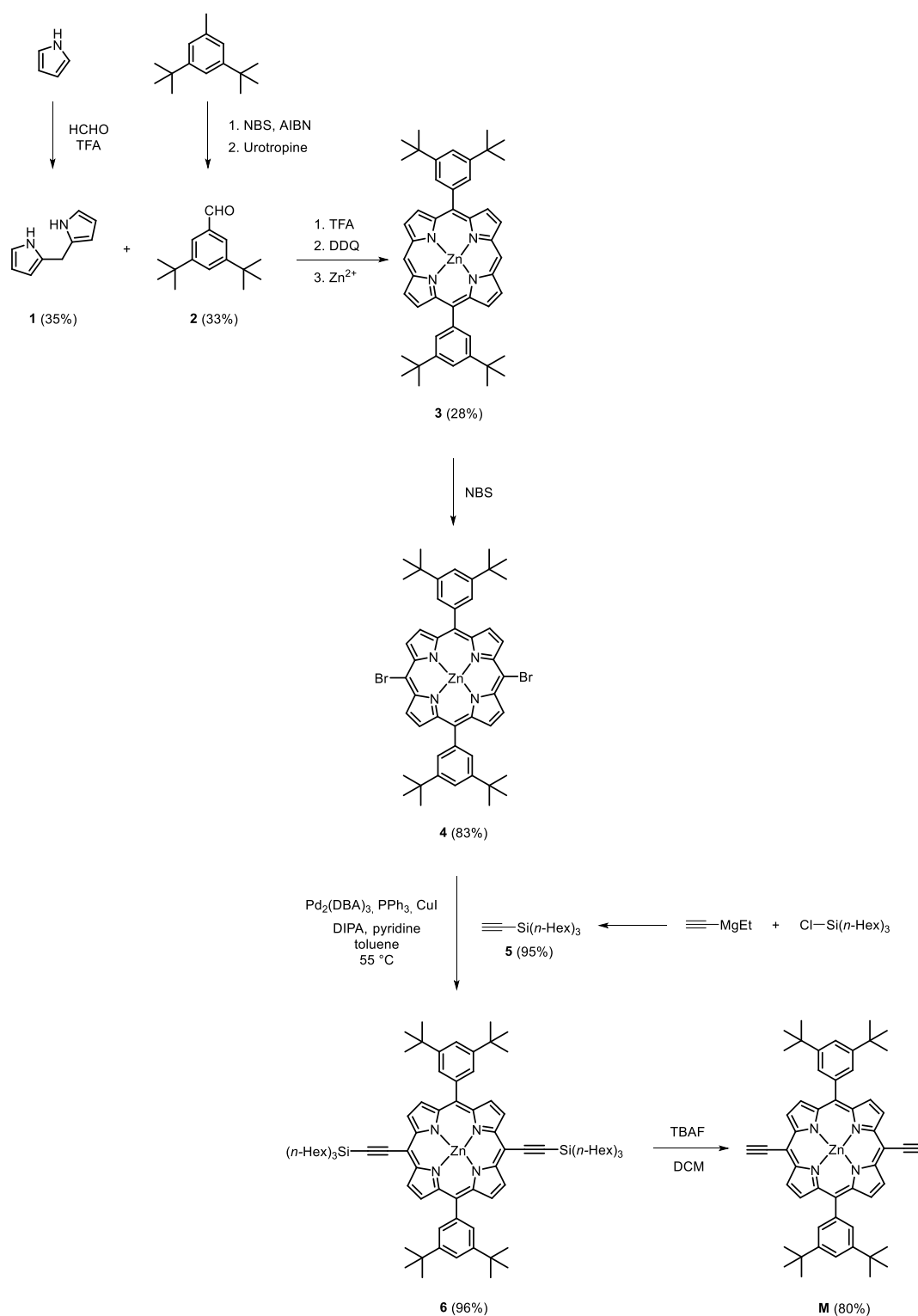
Scheme 4.1. Synthesis of porphyrin monomer **M**.[3]

The template **T** was prepared in two steps (Scheme 4.2). The bromination of hexaphenylbenzene with neat bromine provided hexabromo-hexaphenylbenzene **7** in a 82% yield. The subsequent six fold Suzuki coupling provided template **T** with a yield of 42% (average 87% yield for each coupling).
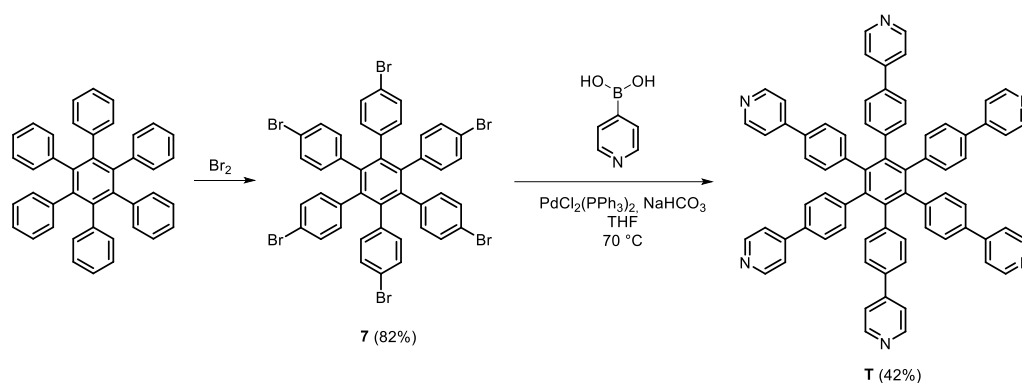
Scheme 4.2. Synthesis of template **T**.[6]

Having both porphyrin monomer **M** and template **T** in hand, the next step was the synthesis of porphyrin nanoring complex **6-ring•T** by oxidative coupling (Scheme 4.3). The crucial aspect of this preparation is the work-up since 6-ring, 12-ring and higher oligomers and polymers are all formed in this reaction and have to be separated. Particularly, the 6-ring and 12-ring are similar and therefore more difficult to separate from each other. The published procedure used size exclusion chromatography for this purification. However, nowadays the Anderson group uses preparative GPC. With the aid of GPC, the **6-ring•T** was prepared in 16% yield and only traces (<1 mg) of the 12-ring were detected. However, we found a new more straightforward method for the isolation of **6-ring**. This method is based solely on the use of alumina plugs and column chromatography on silica. With the aid of this new purification method, **6-ring•T** was prepared in 22% yield. The column chromatography is actually just a simple filtration, since the **6-ring•T** is eluted in approximately 30% hexane in toluene, whereas the 12-ring and polymers stay at the top of the column with this solvent system and are eluted only upon using 100% toluene. This significant difference could permit the porphyrin nanoring synthesis on a large scale since the loading amounts of GPC are limited and it should be easy to scale this new method up.

Template **T** binds extremely well to the **6-ring** and therefore drastic conditions have to be used to obtain the template-free porphyrin nanoring **6-ring** from **6-ring•T**. One possible method is the treatment of **6-ring•T** with trifluoroacetic acid which removes zinc from the porphyrins and thus removes the template **T** as well. The obtained free base porphyrin ring has to be treated with zinc acetate again to produce template-free zinc porphyrin nanoring **6-ring**. The yield of this two-step procedure was 35% (Scheme 4.3).

6-ring·T (22%)

6-ring (35%)
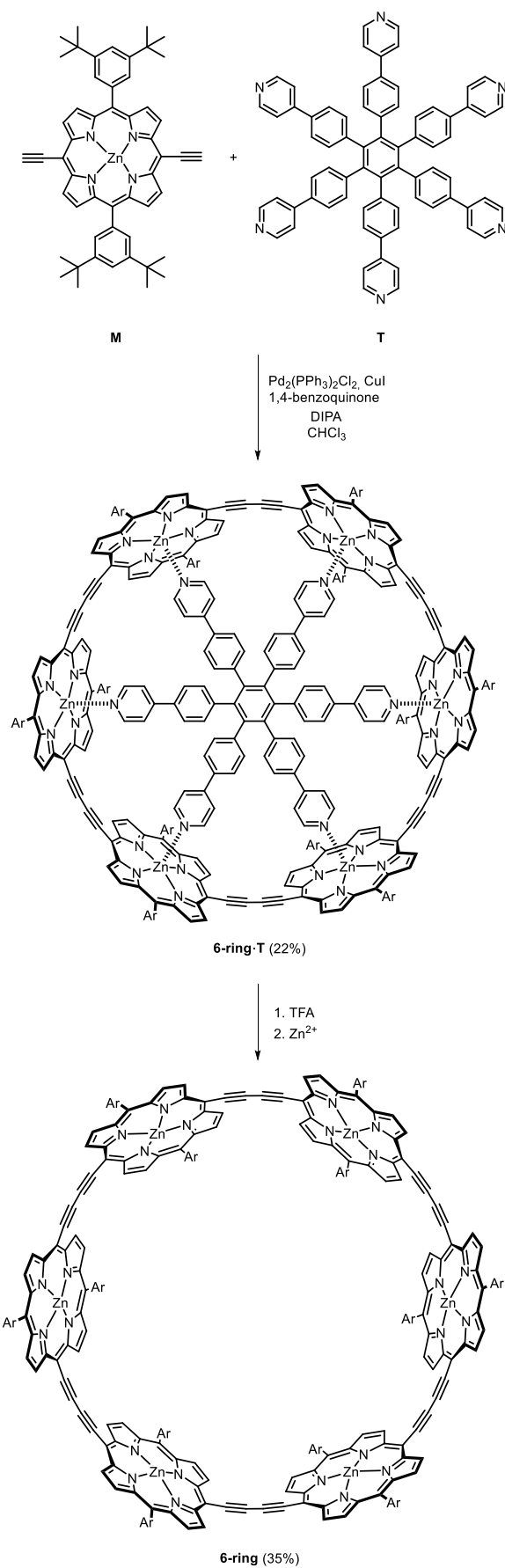
Scheme 4.3. Synthesis of **6-ring** (Ar = 3,5-bis(*t*-butyl)phenyl).[6]

4.4.2. Synthesis of ligands

After the successful preparation of **6-ring**, the synthesis of the proposed ligands from Figure 4.4 and Figure 4.5 was undertaken. The simplest molecule **8** was synthesised first (Scheme 4.4). Lithiation of 4-methylpyridine with *n*-butyllithium, followed by a reaction with a chlorodialkylphosphine and finally *in-situ* oxidation of the obtained phosphine produced phosphine oxides **8a** and **8b** in good yields (53% and 73%, respectively).

8a R = *t*Bu (53%)
8b R = *i*Pr (73%)
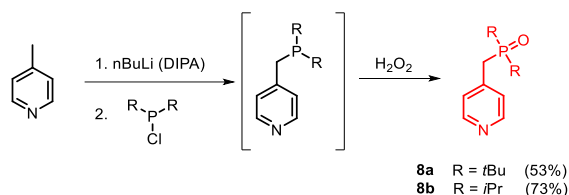
Scheme 4.4. Synthesis of ligands **8a-b**.

Next, the synthesis of the more complex ligands based on bisphosphine oxides (Figure 4.4a) was attempted. Firstly, the same methodology employed for the preparation of the mono phosphine oxides **8** was used (Scheme 4.5). Unlike in the previous examples, the reaction did not proceed, probably due to the bulkiness of alkyl groups on the phosphorus atom, which could have severely limited access of the base to the methylene group.
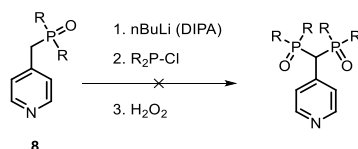
Scheme 4.5. Attempted synthesis of bisphosphine oxides (R is a solubilising group).

A different approach for the synthesis of the desired bisphosphine oxides was proposed. It entailed the preparation of bisphosphine oxide scaffold first by oxidation of commercially available bisphosphine to produce **9** (Scheme 4.6). Several different reaction conditions were tested to prepare the target compound from **9**.[7,8] Again, all attempts failed.

Conditions: A) Pd(OAc)$_2$, Xantphos, NaOEt, CPME, 110 °C
B) Pd(OAc)$_2$, Xantphos, NaH, CPME, 110 °C
C) Cs$_2$CO$_3$, CuI, 2-piconilic acid, THF, 130 °C
D) Cs$_2$CO$_3$, CuI, 2-piconilic acid, TEBAC, THF/ACN, 130 °C
E) Cs$_2$CO$_3$, CuI, TEBAC, ACN, 130 °C
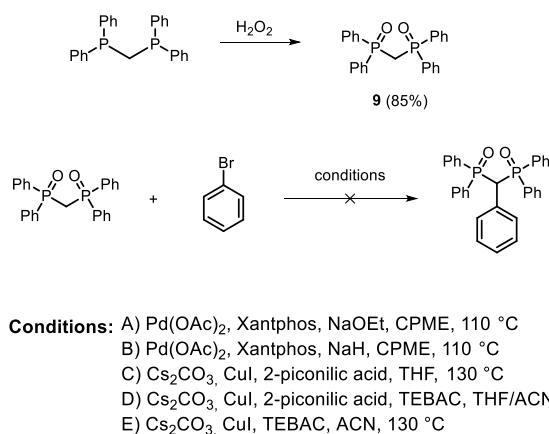
Scheme 4.6. Different approach for the synthesis of target bisphosphine oxides.

Since we did not succeed in the preparation of the compound shown in Figure 4.4a, we resorted to preparation of the ligand from Figure 4.4b. The synthesis for a phosphonate diester based on this structure is known.[9] Phosphonate diesters are just slightly worse hydrogen-bond acceptors (with β = 8.9) than phosphine oxides,[4] therefore we employed this procedure to obtain **10** in a 57% yield (Scheme 4.7).
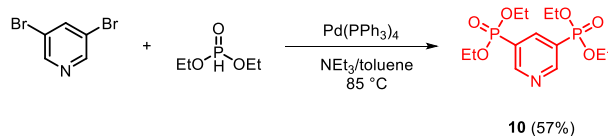
Scheme 4.7. Synthesis of **10**.

Finally, to explore the system that uses a different H-bonding acceptor shown in Figure 4.4c, cyclic imide **11** was prepared by a reaction of 4-aminopyridine with succinic anhydride as shown in Scheme 4.8.
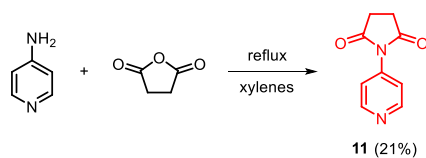
Scheme 4.8. Synthesis of imide **11**.

4.5. Titrations

Firstly, the H-bonding properties of the ligands were obtained by NMR titrations in d^8-toluene. For all the H-bond acceptors, 4-methylphenol (**P**) was used as the H-bond donor, since all the proposed systems utilise **pyridinediol** as the second partner (Figure 4.4).

As an example of a phosphine oxide, **8a** was used (Figure 4.9). Equations 4.1 and 4.2 predict an association constant of 540 M^{-1} for the formation of complex between **8a** ($\beta = 9.9$) and **P** ($\alpha = 3.8$) in toluene ($\alpha_S = 1.0$; $\beta_S = 2.2$). The ^{31}P NMR signal of the phosphine atom shifts significantly upon formation of H-bond, therefore it was easy to follow the change (Figure 4.9b) and use a 1:1 binding isotherm to fit the experimental data (Figure 4.9c). The association constant was determined to be 302 ± 51 M^{-1}.
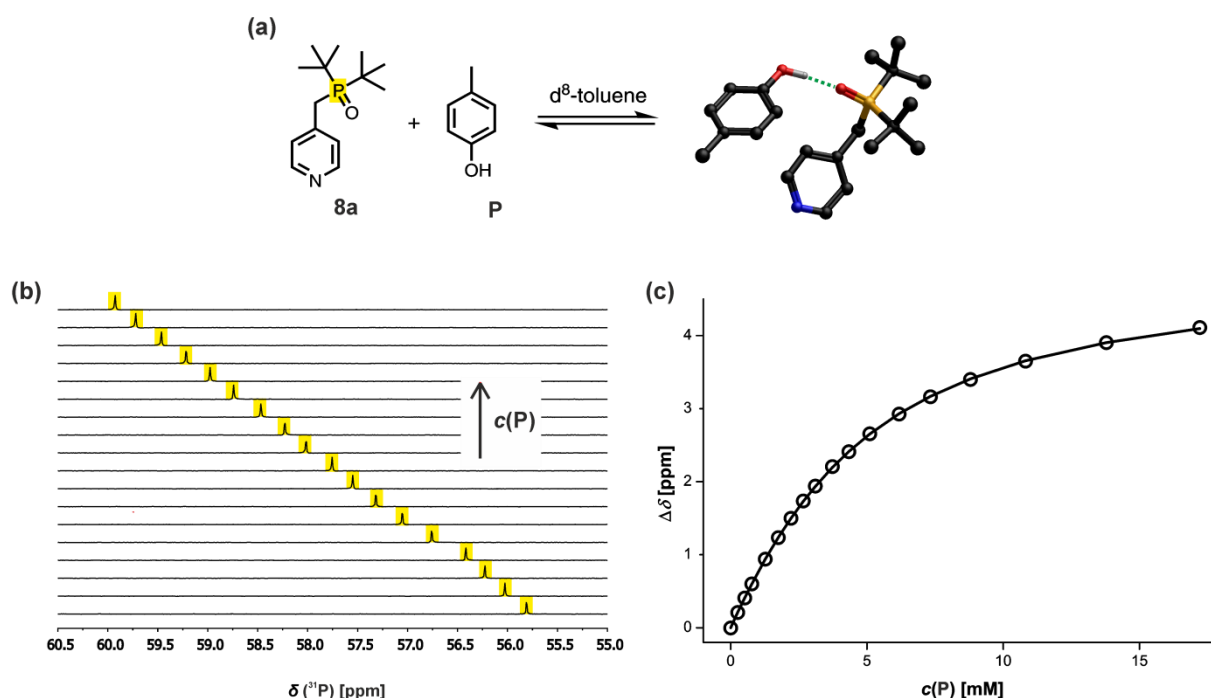
Figure 4.9. ^{31}P NMR (162 MHz, d^8-toluene, 298 K) titration of **P** into **8a** (3mM). (a) Structure of the complex optimised by molecular modelling; hydrogen atoms that do not contribute to H-bonding were omitted for clarity; colouring of atoms: C (black), N (blue), O (red), P (yellow), H (grey); green dashed line is the H-bond; (b) change of ^{31}P chemical shift upon addition of **P** in d^8-toluene at 298 K; (c) experimental data (circles) and calculated values (lines) based on a 1:1 binding isotherm.

Commercially available lactam **L** was used as a model for imide ligand **11**, (Figure 4.10). Equations 4.1 and 4.2 predict an association constant for the complex **L·P** in toluene as 90 M^{-1} (using $\alpha(\mathbf{P}) = 3.8$ and $\beta(\mathbf{L}) = 8.3$). The addition of **L** to a solution of **P**

resulted in a significant change of the Ar-O$\underline{H}$ chemical shift (Figure 4.10b). A 1:1 binding isotherm was used to fit the titration data (Figure 4.10c) and the association constant was determined to be 16 ± 1 M^{-1}. This value is an order of magnitude lower than that determined for phosphine oxide **8a**, which was also true for the values predicted from Equations 4.1 and 4.2.
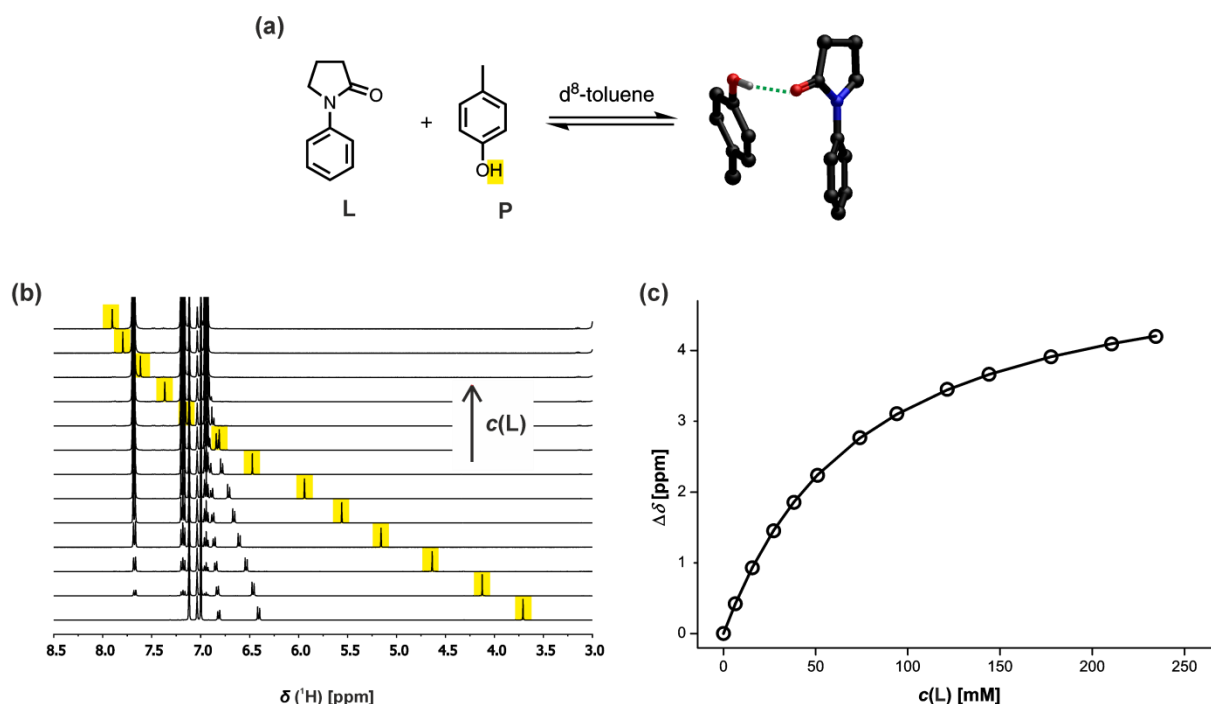
Figure 4.10. ^{1}H NMR (400 MHz, d^8-toluene, 298 K) titration of **P** into **8a** (11 mM). (a) Structure of the complex optimised by molecular modelling; hydrogen atoms that do not contribute to H-bonding were omitted for clarity; colouring of atoms: C (black), N (blue), O (red), H (grey); green dashed line is the H-bond; (b) change of ^{1}H chemical shift of –O$\underline{H}$ upon addition of **L** in d^8-toluene at 298 K; (c) experimental data (circles) and calculated values (lines) based on a 1:1 binding isotherm.

4.6. Mixing experiments

Next, we investigated the formation of the target supramolecular systems inside **6-ring**. Unfortunately, a major problem appeared – it was realised that **pyridinediol** is insoluble in both toluene and chloroform. Therefore, it had to be added as a solution in methanol to an empty NMR tube. Afterwards, methanol was removed and all the remaining compounds were added. We assumed that the solubility issue would be overcome in the final mixture due to pyridine–zinc porphyrin and H-bonding interaction that would dissolve

pyridinediol. Since the **6-ring** solutions are dark brown colour, it was hard to judge if **pyridinediol** dissolved after the addition of all remaining compounds. An example of these NMR mixing experiments is depicted in Figure 4.11. When the NMR tube was cleaned afterwards, it was noticed that there is probably still some undissolved solid at the bottom. These mixing NMR experiments thus did not provide any useful information as it was hard to judge if all the compounds dissolved as well as bound to **6-ring**. The insolubility of **pyridinediol** also resulted in impossibility to conduct any direct formation titrations (both NMR and UV-vis-NIR). Therefore the only feasible additional experiment was a displacement UV-vis-NIR titration with either quinuclidine or pyridine. Unfortunately, it was not possible to obtain any titration curves, because even a small initial addition changed the spectra completely and there was no observable change after further additions as seen in Figure 4.12. Additionally, we realised that both quinuclidine and pyridine are also H-bond acceptors, and by that, they can disrupt the target H-bonded system. For the correct execution of the displacement titrations, it is desired that the displacement happens only at the zinc porphyrin sites, which means that the displacement titrations cannot be used to study this system also.
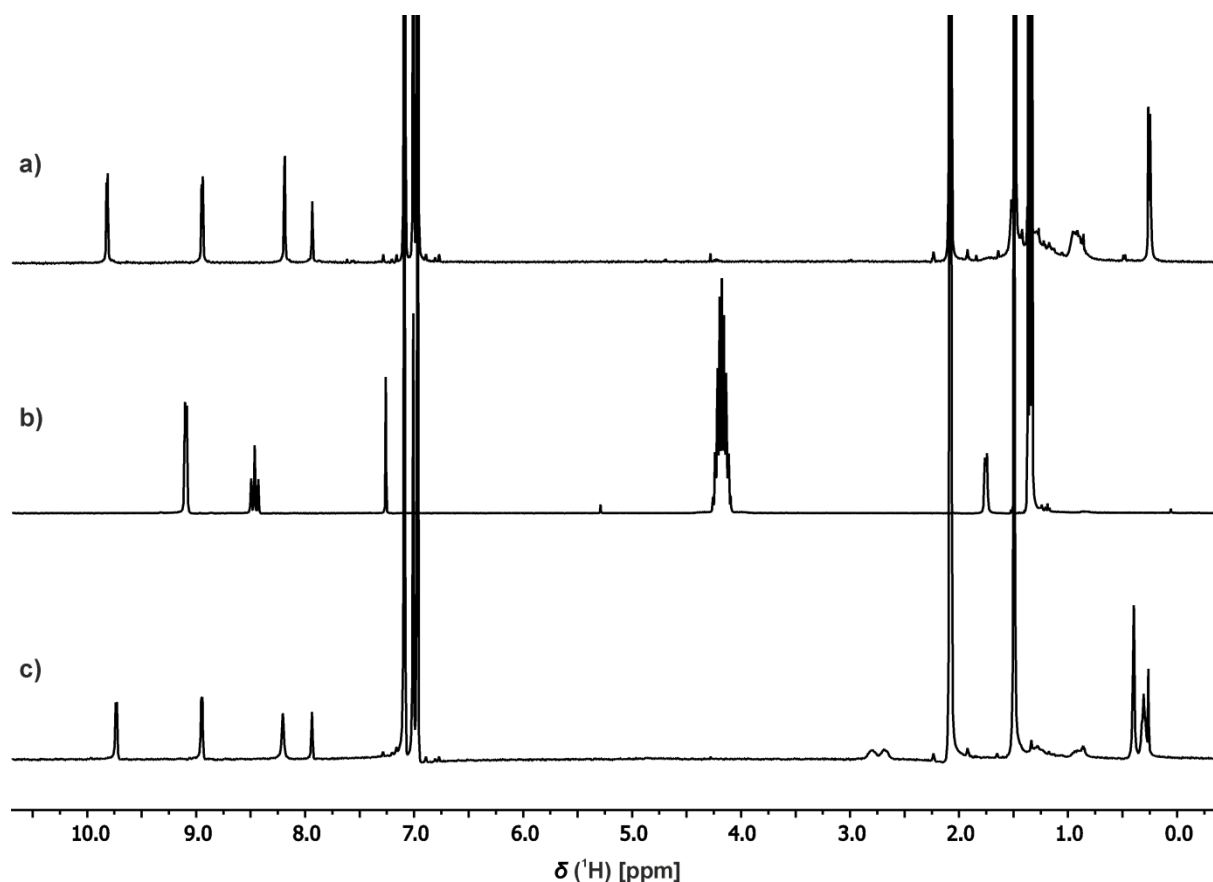
Figure 4.11. ^{1}H NMR spectra of (a) **6-ring** (400 MHz, d[8]-toluene), (b) **10** (400 MHz, CHCl$_3$) and (c) mixture of **6-ring**, **pyridinediol** and **10** in a 1:3:3 ratio (400 MHz, d[8]-toluene).
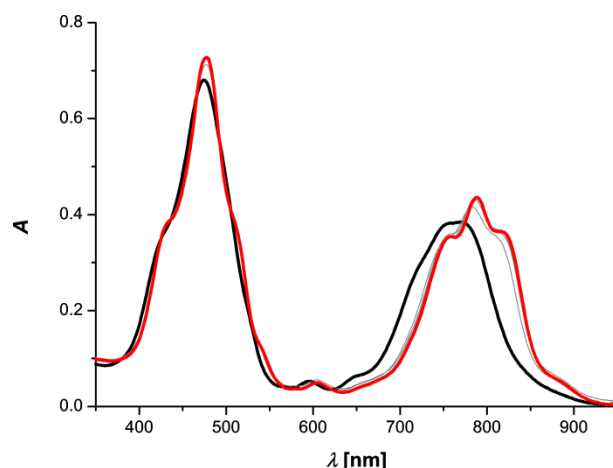
Figure 4.12. UV-vis-NIR titration of quinuclidine to **6-ring**, **pyridinediol** and **10** in a 1:3:3 ratio taken from a NMR stock solution. The spectra are shown on the left with the spectrum of the complex in thick black line and the end spectrum in red thick line.

4.7. Conclusion

Different pyridine ligands based on phosphine oxides and an imide were prepared. Their H-bond properties were investigated by ^{1}H NMR titrations. We attempted to use these molecules to prepare a supramolecular system inside a porphyrin nanoring, but all the attempts failed, mostly due to the insolubility of **pyridinediol** in solvents used (chloroform and toluene). Because of this, the work on this project was terminated. However, recently, we realized a possible solution to overcome the solubility issue. The synthesis of pyridinediol (Figure 4.13) with R = tert-butyldimethylsilyl is known. If a different solubilizing group, such as trihexylsilyl and citronellyl, is used, the solubility of the pyridinediol should increase significantly in non-polar solvents. This has not been explored so far, as a completely different system was proposed, which is described in the following Chapter.
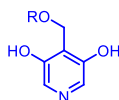
Figure 4.13. Proposed more soluble pyridinediol (R is a solubilizing group).

4.8.   Experimental section

4.8.1. General

The majority of chemicals were bought from commercial suppliers and used without further purifications unless stated otherwise. 3,5-Di-*tert*-butyltoluene was synthesised in the lab of Prof H. Anderson. Solvents were either distilled before use or used as obtained; the Grubb's quality solvents were used for sensitive reactions. For chromatography, automatic chromatography systems CombiFlash® R_f^+ and CombiFlash® R_f^+ Lumen™ (with UV light detection: 254 nm and 500 nm for porphyrin nanorings, and evaporative light scattering detector for Lumen) with pre-packed puriFlash® columns from Interchim (silica, 25 μm; 15 μm for porphyrin nanorings) with an absorption of mixtures on Celite® were used. For plugs, silica gel 60 (Merck, 40–63 μm) and alumina (either Aluminium oxide 90 standardised from Merck or Aluminium oxide, activated, basic, Brockmann I, standard grade from Sigma-Aldrich) were used. The reactions were monitored by glass TLC plates coated with silica gel 60 F_{254} (Merck) and the plates were inspected by UV light (254 nm). For GPC, recycling Shimadzu Prominence GPC with UV light detection (500 nm) with a set of columns JAIGEL 3H (20 × 600 nm) and JAIGEL 4H (20 × 600 nm) were used.

^{1}H, ^{13}C, ^{31}P NMR spectra were recorded on Bruker 400 MHz Avance III HD Spectrometers at 400 MHz for ^{1}H, 101 MHz for ^{13}C and 252 MHz for ^{31}P. All chemicals shift are quoted in ppm and were referenced to residual peaks of CDCl$_3$ (^{1}H: 7.26 ppm; ^{13}C: 77.00 ppm). Coupling constants *J* are stated in Hz. FT-IR spectra were measured on a Bruker Alpha spectrometer. HR-MS spectra were obtained on a Waters Xevo® G2-S by electrospray ionisation of samples. Melting points were recorder on a Mettler-Toledo MP90 system.

4.8.2. Synthesis

Synthesis of **1**
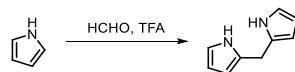
Formaldehyde (37% in water, 9.7 mL, 130 mmol) was added to pyrrole (200 mL, 2.84 mol) and the solution was degassed by the vaccum/Ar cycle (5×). The flask was covered with aluminium foil and trifluroacetic acid (99%, 1.1 mL, 14 mmol) was added by syringe under vigorous stirring. After 6 minutes, CH_2Cl_2 (200 mL) was added, followed immediately by saturated solution of Na_2CO_3 (200 mL). The organic phase was separated and washed with the saturated solution of Na_2CO_3 (2 × 200 mL), water (200 mL) and dried over Na_2SO_4. The volatiles were removed under reduced pressure (up to 70 °C and 9mBar to remove unreacted pyrrole). The Kugelrohr distillation (130 °C, 1 mBar) of the residue produced the title compound as yellowish solid (6.1 g, 35% crude yield). The compound was used in the next step without any additional purification.

^{1}H NMR (CDCl₃, 400 MHz, 298 K): 7.63 (br, 2H), 6.62–6.61 (m, 2H), 6.20–6.18 (m, 2H), 6.09–6.06 (m, 2H), 3.94 (s, 2H).

The observed data was in agreement with the previously reported values.[10]

Synthesis of **2**
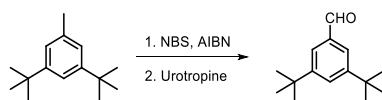
3,5-Di-*tert*-butyltoluene (25.0 g, 123 mmol), *N*-bromosuccinimide (33.0 g, 185 mmol) and azobisisobutyronitrile (0.90 g, 5.5 mmol) in benzene (50 mL) were heated slowly to reflux. Then it was refluxed gently for 4 hours. After this time, the mixture was cooled to room temperature and the precipitate was filtered off over filtrate paper and the solvent was removed under reduced pressure. The residue was dissolved in a mixture of EtOH/H_2O (1:1, 70 mL) and urotropine (50.0 g, 357 mmol) was added. The mixture was then refluxed for 4 hours. HCl (37%, 21 mL) was added and the mixture was refluxed for additional 30 minutes. The mixture was cooled and ethanol was removed under reduced pressure (40 °C, 125 mBar). The residue was then extracted with diethyl ether (1 × 300 mL, 2 × 200 mL). The collected organic phases were then dried over Na_2SO_4 and the solvent was removed under reduced pressure. Recrystallisation from EtOH afforded the title compound as white crystals (8.89 g, 33% yield).

^{1}H NMR (CDCl$_3$, 400 MHz, 298 K): δ 10.01 (s, 1H), 7.75–7.69 (m, 3H), 1.37 (s, 18H).

The observed data was in agreement with the previously reported values.[11]

Synthesis of **3**
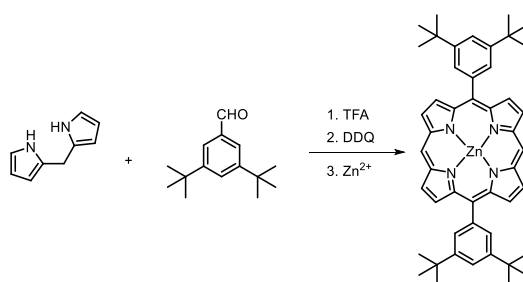
1 (1.88 g, 12.9 mmol) and **2** (2.81 g, 12.9 mmol) were placed into a freshly open Winchester bottle of CH_2Cl_2 (2.5 L) and the solution was degassed by the vacuum/Ar cycle (3×). Trifluoroacetic acid (0.62 mL, 8.0 mmol) was added rapidly and the Winchester bottle was covered with aluminium foil. The reaction mixture was then stirred for 3.5 hours and 2,3-dichloro-5,6-dicyano-1,4-benzoquinone (DDQ, 4.38 g, 19.3 mmol) was added and stirring was continued for 30 minutes. Triethylamine (12.5 mL) was then added and the mixture was concentrated to a volume of about 300 mL by reduced pressure. Then it was passed over a large silica plug with CH_2Cl_2 and washed thoroughly (4×, after each run the volume was concentrated to approximately 300 mL). The solvent was removed by reduced pressure and the residue was dissolved in fresh CH_3Cl (300 mL). $Zn(OAc)_2 \cdot 2H_2O$ (3.17 g, 14.4 mmol) was dissolved in methanol (30 mL) and added to the CH_3Cl solution. The reaction mixture was stirred for 1 hour. The mixture was then passed over medium-size silica plug with CH_2Cl_2. The solvents were removed by reduced pressure and the residue was recrystallised by layer addition (CH_2Cl_2/ CH_3OH) at fridge and then dried under high vacuum overnight to obtain a purple powder (1.28 g, 28% yield).

The procedure was repeated at the same scale and smaller scale (with 1.55 g of dipyrromethane) with the same yields (29% and 28%, respectively).

^{1}H NMR (CDCl$_3$ + 1% d^5-pyridine, 400 MHz, 298 K): δ 10.19 (s, 2H), 9.36 (d, J = 4.5 Hz, 4H), 9.11 (d, J = 4.5 Hz, 4H), 8.10 (d, J = 2.0 Hz, 4H), 7.79 (t, J = 2.0 Hz, 2H), 1.55 (s, 36H).

The observed data was in agreement with the reported values.[12]

Synthesis of **4**
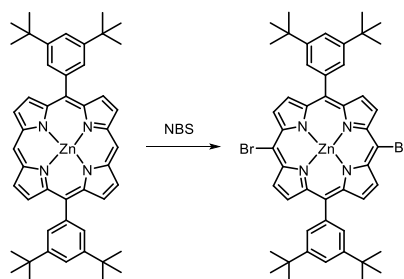
To a solution of zinc porphyrin **3** (1.06 g, 1.41 mmol) in CH_2Cl_2 (175 mL) and pyridine (2.9 mL) was added *N*-bromosuccinimide (*freshly recrystallised*, 505 mg, 2.84 mmol) at −10 °C. After stirring for 10 minutes at −10 °C, the cooling bath was removed and the reaction flask was covered by aluminium foil and the reaction mixture was left heated slowly to room temperature. After 1.5 hours, hexane (180 mL) was added and the reaction mixture was passed over medium-size silica plug, which was previously treated with a mixture of CH_2Cl_2/hexane/pyridine (1:1:0.08, 0.5 L). Then the mixture of CH_2Cl_2/hexane was used for washing the plug. The solvents were removed under reduced pressure and then toluene (30 mL) was added and subsequently removed under reduced pressure three times to help to remove pyridine. The residue was dissolved in the mixture of CH_2Cl_2 (150 mL) and pyridine (4 drops). Then methanol (400 mL) was added as a second layer and the slow crystallisation at fridge provided purple solid that was washed with plenty of methanol and dried under high vacuum to obtain a purple powder (1.07 g, 83% yield).

^{1}H NMR (CDCl$_3$, 400 MHz, 298 K): δ 9.64 (d, J = 4.5 Hz, 4H), 8.89 (d, J = 4.5 Hz, 4H), 7.97 (d, J = 2.0 Hz, 4H), 7.78 (t, J = 2.0 Hz, 2H), 1.53 (s, 36H).

R_f (CH$_2$Cl$_2$/hexane 1:1; silica): 0.62.

The observed data was in agreement with the reported values.[13]

Synthesis of **5**
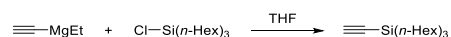
Chlorotrihexylsilane (97%, 10.0 g, 30.4 mmol) was added dropwise to a stirred solution of ethynylmagnesium bromide (0.5 in THF, 100 mL, 50 mmol) under N_2. The mixture was refluxed for 2 hours. To a cooled down solution, HCl (aq., 10%, 80 mL) was added and the organic phase was washed with water (80 mL), dried over $MgSO_4$ and evaporated to obtain the title product (8.88 g, 95% yield) as yellowish liquid.

^{1}H NMR (CDCl$_3$, 400 MHz, 298 K): δ 2.36 (s, 1H), 1.41 − 1.21 (m, 24H), 0.89 (t, $J = 7.0$ Hz, 9H), 0.67 − 0.55 (m, 6H).

The observed data was in agreement with the reported values.[14]

Synthesis of **6**
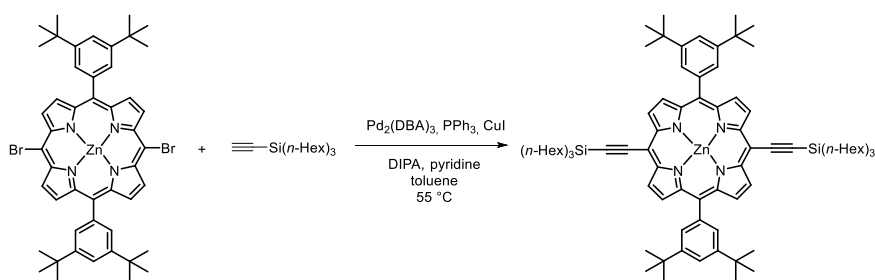
Triphenylphosphine (59 mg, 0.23 mmol), CuI (46 mg, 0.24 mmol), *tris*(dibenzylideneacetone)-dipalladium (105 mg, 0.10 mmol) and dibromoporphyrin **4** (1.05 g, 1.15 mmol) were placed in a flame-dried Schlenk tube under argon. Then toluene (74 mL), diisopropylamine (40 mL) and pyridine (2.1 mL) were added and the mixture was thoroughly deoxygenated by 4 freeze/pump/thaw cycles. After this, trihexylsilylacetylene **5** (1.4 mL, 3.6 mmol) was added by syringe through the septum. The reaction mixture was then heated at 55 °C for 90 minutes. The solvents were removed under reduced pressure and the residue was dissolved in CH_2Cl_2 and passed over silica plug and the solvent was reduced under reduced pressure again. Toluene (2 × 30 mL) was added and subsequently removed under reduced pressure to remove the remaining pyridine. The layer recrystallisation (CH_2Cl_2/CH_3OH) of the residue produced a green solid that was washed with plenty of methanol to produce the title product as a green solid (1.51 g, 96% yield).

^{1}H NMR (CDCl$_3$, 400 MHz, 298 K): δ 9.72 (d, J = 4.5 Hz, 4H), 8.96 (d, J = 4.5 Hz, 4H), 8.05 (d, J = 1.5 Hz, 4H), 7.82 (s, 2H), 1.82 − 1.69 (m, 12H), 1.54 (m, 48H), 1.46 − 1.23 (m, 24H), 1.06 − 0.97 (m, 12H), 0.89 (t, J = 7.0 Hz, 18H).

R_f (CH$_2$Cl$_2$/EtOAc/pyridine 10:1:1, silica): 0.92.

The observed data was in agreement with the reported values.[15]

Synthesis of **M**
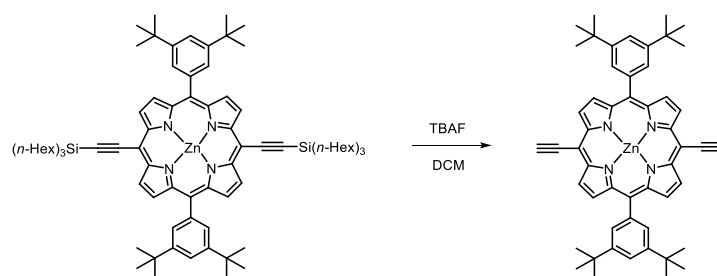
To a solution of THS-protected porphyrin **6** (600 mg, 0.44 mmol) in CH_2Cl_2 (60 mL), TBAF (4.2 mL, 1.0M solution in THF, 4.2 mmol) was added in one portion. After 15 minutes, the mixture was passed over silica plug ($CHCl_3$/pyridine 100:1). The solvent was removed under reduced pressure and toluene (2×100 mL) was added and subsequently removed under reduced pressure to remove the remaining pyridine. A layer recrystallisation (CH_2Cl_2/CH_3OH) produced a dark violet solid that was washed with CH_3OH (3×40 mL) and dried under high vacuum overnight to yield the title compound as a violet solid (280 mg, 80% yield).

^{1}H NMR (CDCl$_3$ + 1% d^5-Py, 400 MHz, 298 K): δ 9.67 (d, J = 4.5 Hz, 4H), 8.91 (d, J = 4.5 Hz, 4H), 8.00 (d, J = 2.0 Hz, 4H), 7.79 (t, J = 2.0 Hz, 2H), 4.14 (s, 2H), 1.54 (s, 36H).

The observed data was in agreement with the reported values.[15]

Synthesis of **8**
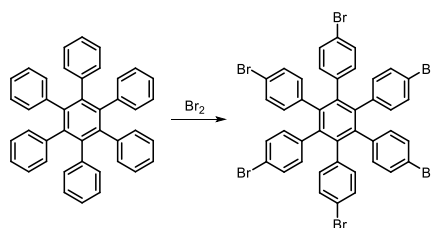
To a finely ground hexaphenylbenzene (1.07 g, 2.00 mmol), neat bromine (3 mL) was added. After 30 minutes of stirring, additional bromine (1 mL) was added. After additional 30 minutes, additional bromine (1 mL; altogether 5 mL, 194 mmol) was added. The reaction mixture was stirred for 1 hour and then cooled to –78 °C by a dry-ice/acetone bath and ethanol (20 mL) was added in two parts. The precipitate was collected at room temperature by filtration and washed with EtOH (2 × 20 mL) and water (2 × 20 mL), then was stirred with CH_2Cl_2 (10 mL) for 10 minutes and the supernatant solution was pipetted off. This procedure was repeated several times with CH_3OH (5–10 mL), CH_2Cl_2 (5–10 mL) to remove the yellowish colour from the solution phase. The remaining white solid was then dried under high vacuum overnight to yield title product as a white solid (1.65 g, 82% yield).

^{1}H NMR (CDCl$_3$, 400 MHz, 298 K): δ 7.05 (d, J = 8.5 Hz, 1H), 6.61 (d, J = 8.5 Hz, 1H).

MP: > 400 °C

The observed data was in agreement with the reported values.[16]

Synthesis of **T**
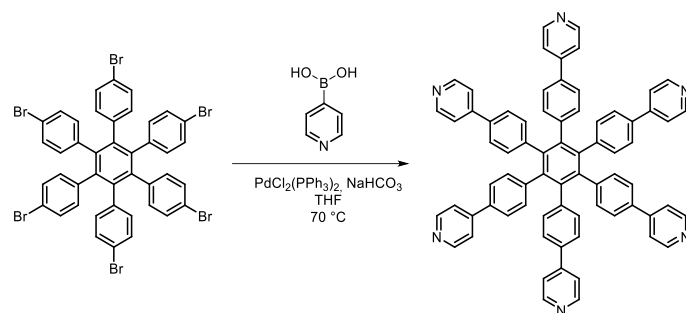
8 (600 mg, 0.60 mmol) was placed into a big Schlenk flask. Dimethoxyethane (18 mL), THF (42 mL) and PdCl$_2$(PPh$_3$)$_2$ (80 mg, 0.11 mmol) were added. NaHCO$_3$ (900 mg, 10.7 mmol) and hydrate of 4-pyridineboronic acid (2.17 g, 15 mmol) were partially dissolved in water (*HPLC quality*, 26 mL) and transferred into the Schlenk flask. Additional NaHCO$_3$ (90 mg, 1 mmol) was added. The mixture was thoroughly deoxygenated by 4 freeze/pump/thaw cycles. The mixture was then heated at 70 °C with stirring for 5 days. Additional PdCl$_2$(PPh$_3$)$_2$ (35 mg, 0.05 mmol; altogether 115 mg, 0.16 mmol), NaHCO$_3$ (350 mg, 4.2 mmol; altogether 1340 mg, 16 mmol) and hydrate of 4-pyridineboronic acid (450 mg, 3.0 mmol; altogether 2.62 g, 18 mmol) were added and the heating was continued for additional 2 days. Solvents were then removed under reduced pressure. CombiFlash of the residue on silica (CH$_2$Cl$_2$/Et$_3$N/CH$_3$OH 100:0.25:0%→10%) provided white solid that was partially dissolved in small amount of freshly open CHCl$_3$ and a large quantity of CH$_3$OH was added. The precipitated solid was washed with excess of CH$_3$OH and dried under high vacuum to obtain the title product as a white crystalline solid (251 mg; 42% yield).

^{1}H NMR (CDCl$_3$, 400 MHz, 298 K): δ 8.53 (dd, J = 5.0, 1.5 Hz, 12H), 7.32 (dd, J = 5.0 Hz, J = 1.5 Hz, 12H), 7.25 (borderline d/dd hidden under solvent, 12H), 7.02 (d, J = 8.0 Hz, 12H).

MP: > 400 °C

The observed data was in agreement with the reported values.[6]

Synthesis of **6-ring•T**
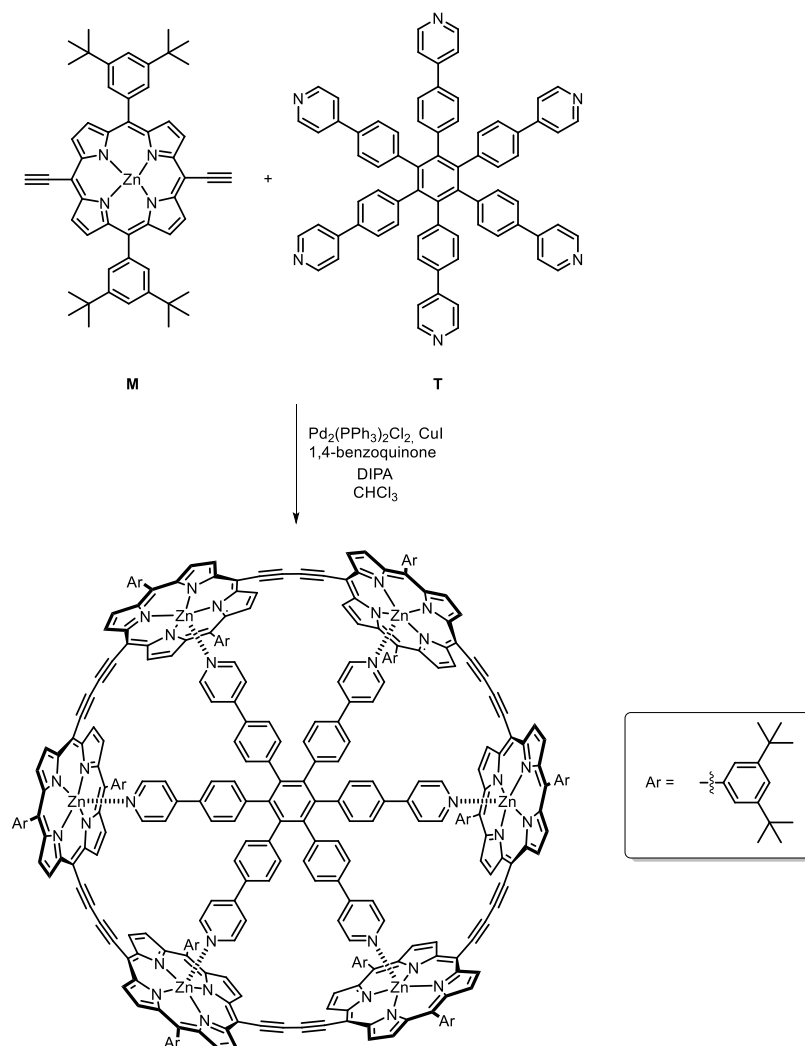
With GPC work-up:

Template **T** (64 mg, 64 µmol) and porphyrin monomer **M** (200 mg, 251 µmol) and freshly opened $CHCl_3$ (280 mL) were sonicated for 2 hours. In the meantime, a solution of catalyst was prepared by mixing dichlorobis(triphenylphosphine)-palladium(II) (58 mg, 83 µmol), CuI (79 mg, 415 µmol), 1,4-benzoquinone (184 mg, 1.7 mmol) and freshly opened $CHCl_3$ (80 mL), sonicating for 2 minutes and addition of freshly distilled diisopropylamine (0.5 mL). Both solutions were cooled to room temperature and the solution of catalyst was added to the mixture of template and porphyrin under vigorous stirring. The flask was closed with septum and covered with aluminium foil. The mixture was stirred vigorously for 18 hours and afterwards it was filtered over basic alumina plug that was then washed with additional $CHCl_3$ and 1% pyridine in $CHCl_3$. The solvents were removed under reduced pressure and the residue was dissolved in 1% pyridine in toluene (10 mL). SEC chromatography of this

solution on Biobeads™ SX-1 (Bio-Rad[®]) using 1% pyridine in toluene as an eluent removed the rest of benzoquinone. Again, solvents were removed under reduced pressure and the residue was dissolved in 1% pyridine in toluene (4 mL) and filtered over a PTFE filter (0.20 μm) and injected into GPC system. The recycling GPC with toluene and a flow rate of 8.5 mL/min provided a solution of the title compound where solvents were removed under reduced pressure and after drying under high vacuum overnight, the title compound was obtained as a brown solid (38 mg, 16% yield).

With CombiFlash work-up:

Template **T** (22 mg, 22 μmol) and porphyrin monomer **M** (67 mg, 85 μmol) and freshly opened CHCl$_3$ (150 mL) were sonicated for 2 hours. In the meantime, a solution of catalyst was prepared by mixing dichlorobis(triphenylphosphine)-palladium(II) (21 mg, 30 μmol), CuI (32 mg, 168 μmol), 1,4-benzoquinone (70 mg, 0.65 mmol) and freshly opened CHCl$_3$ (30 mL), sonicating for 2 minutes and addition of diisopropylamine (0.2 mL).

Both solutions were cooled to room temperature and the solution of catalyst was added to the mixture of template and porphyrin under vigorous stirring. The flask was covered with aluminium foil. The mixture was stirred vigorously for 18 hours and afterwards it was filtered over neutral alumina plug that was then washed with additional CHCl$_3$. The solvents were removed under reduced pressure and the residue was dissolved in 1% pyridine in toluene and filtered over a new neutral alumina plug. The solvents were removed under reduced pressure. CombiFlash of the residue on silica gel (hexane/toluene, toluene: 0%→30%→100%) followed by removing of solvents under reduced pressure and drying under high vacuum overnight provided the title compound as a brown solid (18 mg, 22% yield).

^{1}H NMR (CDCl$_3$, 400 MHz, 298 K): δ 9.57 (d, J = 4.5 Hz, 24H), 8.79 (d, J = 4.5 Hz, 24H), 8.03 (s, 12H), 7.85 (s, 12H), 7.79 (s, 12H), 5.51 (d, J = 9.0 Hz, 12H), 5.46 (d, J = 9.0 Hz, 12H), 4.99 (d, J = 7.0 Hz, 12H), 2.31 (d, J = 7.0 Hz, 12H), 1.56 (s, 108H), 1.52 (s, 108H).

The observed data was in agreement with reported values.[6]

Synthesis of **6-ring**
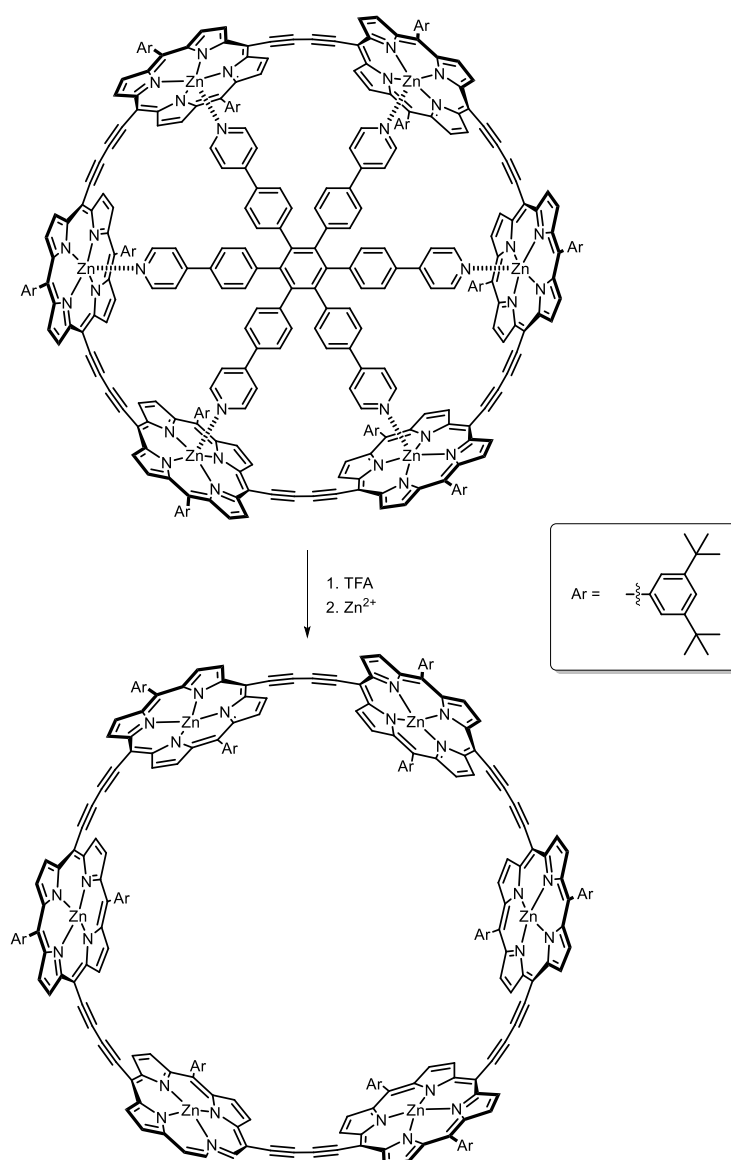
To a solution of **6-ring•T** (8.7 mg, 1.5 µmol) in CH_2Cl_2 (9 mL), trifluoroacetic acid (90 µL, 1.2 µmol) was added in one portion. After 5 minutes of vigorous stirring, pyridine (1.5 mL) was added. The mixture was filtered over a silica plug previously pre-treated with 1% pyridine in CH_2Cl_2. The filtrate was absorbed on Celite and CombiFlashed on silica (petrol ether/CH_2Cl_2, CH_2Cl_2: 0%→100%). Afterwards, the solvents were removed under reduced pressure. The residue was dissolved in CH_2Cl_2 (20 mL) and $Zn(OAc)_2$•$2H_2O$ (96 mg; 437 µmol) in CH_3OH (4 mL) was added. The mixture was stirred overnight and then filtered over a small silica plug and the filtrate was absorbed on Celite®. CombiFlash on silica (EtOAc) provided a solid that was recrystallised from CH_2Cl_2/CH_3OH and dried under high vacuum to obtain the title compound as a brown solid (2.5 mg, 35% yield).

^{1}H NMR (CDCl$_3$, 400 MHz, 298 K): δ 9.70 (d, J = 4.5 Hz, 24H), 8.88 (d, J = 4.5 Hz, 24H), 7.96 (d, J = 1.5 Hz, 24H), 7.78 (t, J = 1.5 Hz, 24H), 1.50 (s, 216H).

The observed data was in agreement with the reported values.[6]

Synthesis of **8**
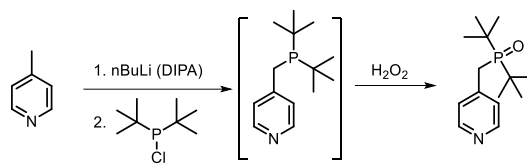
To a solution of 4-methylpyridine (300 μL, 3.08 mmol, 1 eq.), diisopropylamine (450 μL, 3.21 mmol, 1.05 eq.) in THF (10 mL) under N_2 atmosphere was added *n*BuLi (1.6M in hexanes, 2.4 mL, 1.25 eq.) dropwise at –78 °C (colour changed to orange). The mixture was then stirred for 1.5 hours at –78 °C, di-*tert*-butylchlorophosphane (96%, 1.2 mL, 6.06 mmol, 2 eq.) was added dropwise at –78 °C (colour changed to yellow). Then the mixture was stirred for 1.5 hours at –78 °C and left heated to room temperature. Then the reaction mixture was stirred at this temperature for 1 hour and solvents were removed under reduced pressure. To the residue CH_3OH (10 mL) was added, and H_2O_2 (20%, 1.5 mL, 8.82 mmol, 3 eq.) was slowly added and the reaction mixture was stirred for 4 hours. Then brine solution (2 mL) and water (10 mL) were added and the mixture was extracted with CH_2Cl_2 (2×40 mL) and EtOAC (40 mL), dried with anhydrous $MgSO_4$ and solvents were removed under reduced pressure. CombiFlash of the residue on silica gel (CH_2Cl_2/CH_3OH, CH_3OH: 0%→5%→10%) provided the title compound as a white solid (416 mg, 53% yield). The compound can be recrystallised from the mixture of CH_3CN/EtOAc/MTBE with a large loss of material providing white crystalline solid.

^{1}H NMR (CDCl$_3$, 400 MHz, 298 K): δ 8.49 (d, J = 5.5 Hz, 2H), 7.39 (d, J = 5.0 Hz, 2H), 3.09 (d, J = 10.5 Hz, 2H), 1.23 (d, J = 13.5 Hz, 18H).

^{13}C NMR (CDCl$_3$, 101 MHz, 298 K): δ 149.4 (d, J = 1.0 Hz), 144.1 (d, J = 6.5 Hz), 125.6 (d, J = 4.5 Hz), 36.5 (d, J = 59.0 Hz), 28.6 (d, J = 48.5 Hz), 26.9.

^{31}P NMR (CDCl$_3$, 252 MHz, 298 K): δ 58.0.

HR-MS (ESI): Calculated for $C_{14}H_{25}NOP$ [M+H]$^+$ 254.1674, found: 254.1679 (Δ = 1.9 ppm).

FT-IR (thin film): 2991, 2952, 2912, 2781, 1599, 1476, 1418, 1157, 1136, 992, 839 cm^{-1}.

MP: 189–190 °C

R_f (EtOAC/CH$_3$OH 1:1; silica): 0.57.

^{1}H NMR

8.49
8.48

7.40
7.39
7.26

3.10
3.08

1.24
1.21

1.99   2.00   2.20   18.40

10.0 9.5 9.0 8.5 8.0 7.5 7.0 6.5 6.0 5.5 5.0 4.5 4.0 3.5 3.0 2.5 2.0 1.5 1.0 0.5 0.0
f1 (ppm)

^{31}P NMR

250 200 150 100 50 0 -50 -100 -150 -200
f1 (ppm)
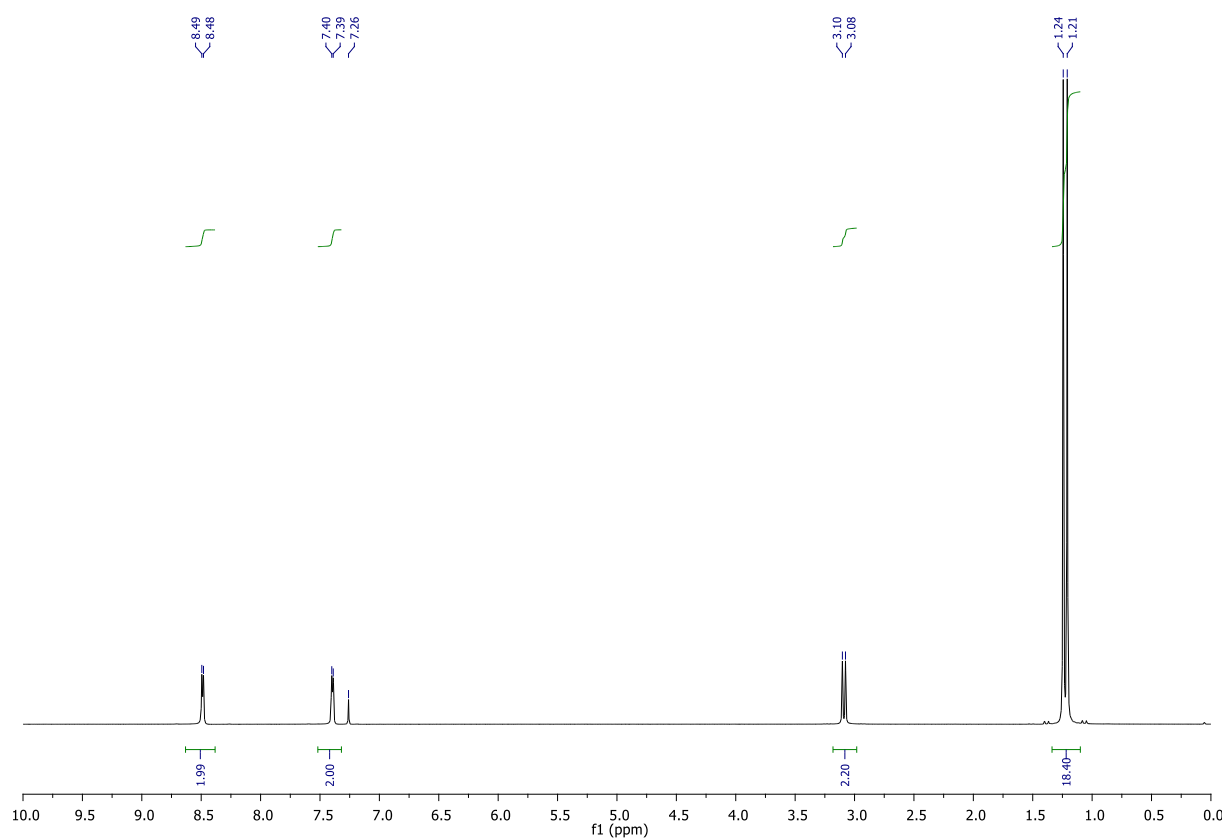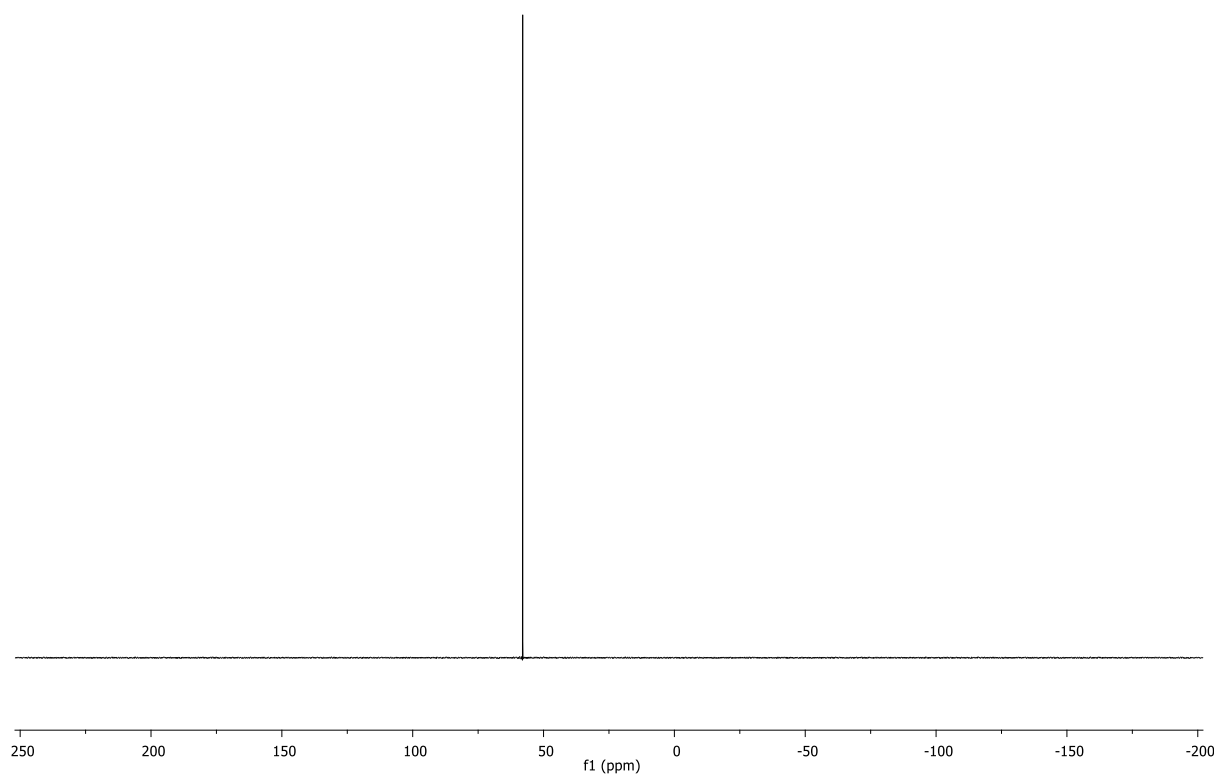
^{13}C NMR
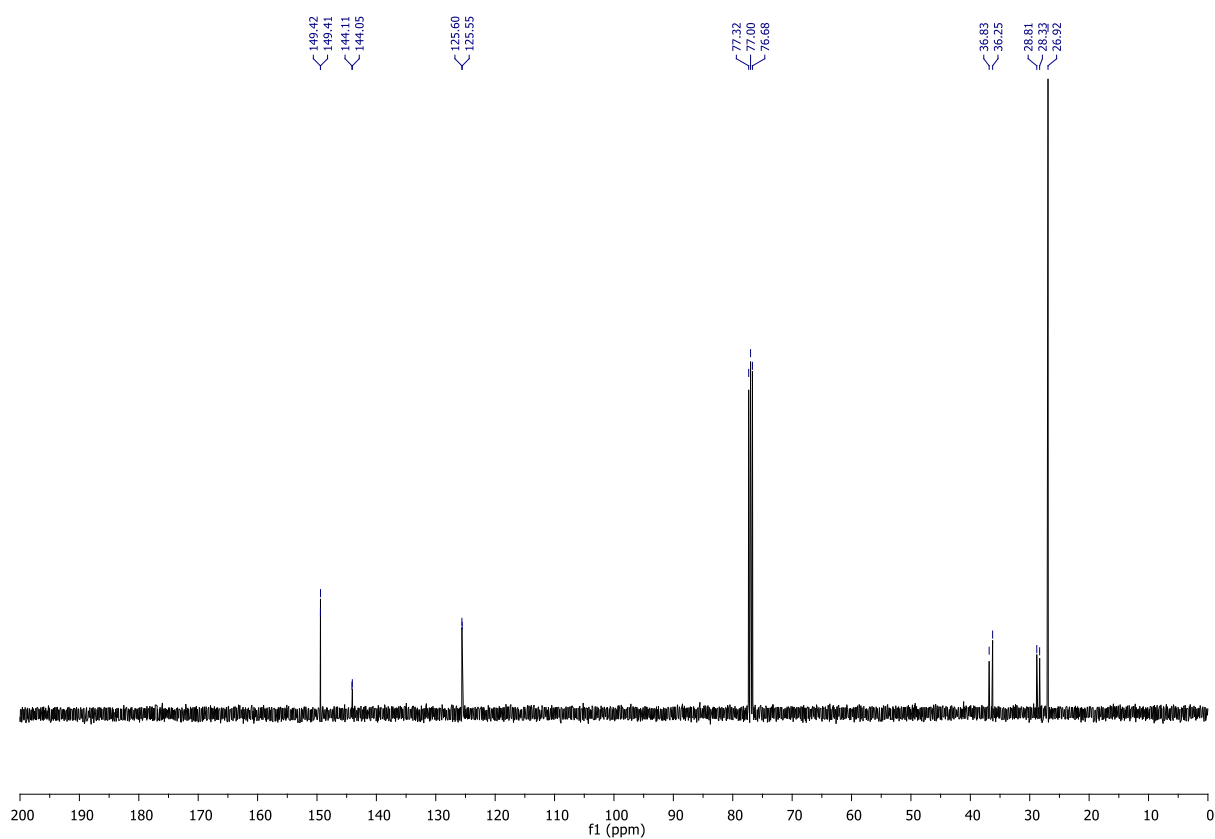
^{13}C DEPT NMR
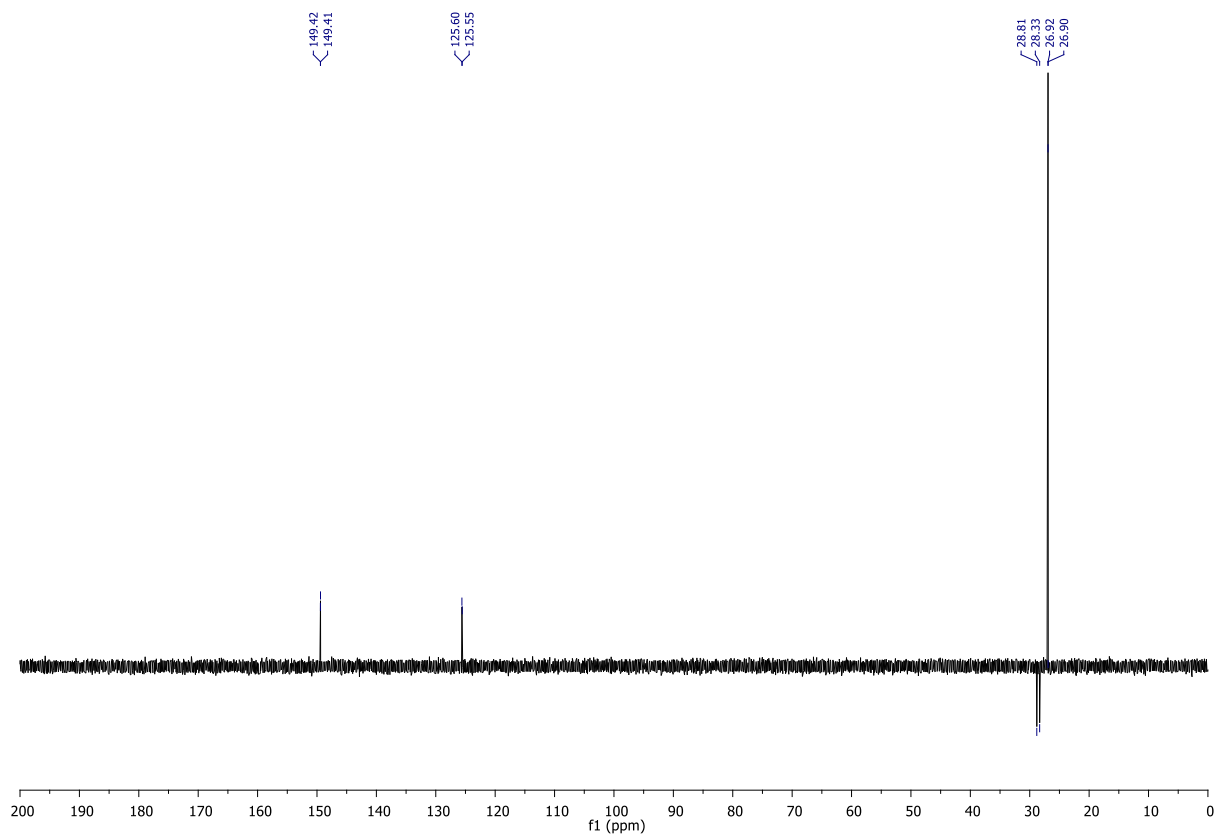
Synthesis of **8b**
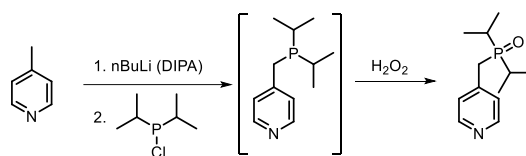
To a solution of 4-methylpyridine (300 μL, 3.08 mmol, 1 eq.), diisopropylamine (1.35 mL, 9.63 mmol, 3 eq.) in THF (10 mL) under N_2 atmosphere was added nBuLi (1.6M in hexanes, 2.4 mL, 1.25 eq.) dropwise at −78 °C (colour changed to orange). The mixture was then stirred for 1.5 hours at −78 °C, diisopropylchlorophosphane (96%, 1.0 mL, 6.03 mmol, 2 eq.) was added dropwise at −78 °C (colour changed to yellow). Then the mixture was stirred for 1.5 hours at −78 °C and left heated to room temperature. Then the reaction mixture was stirred at this temperature for 1 hour and solvents were removed under reduced pressure. To the residue, CH_3OH (10 mL) was added, and H_2O_2 (20%, 1.5 mL, 8.82 mmol, 3 eq.) was slowly added and the reaction mixture was stirred for 1 hours. Then brine solution (2 mL) and water (10 mL) were added and the reaction mixture was extracted with the mixture of CH_2Cl_2 and EtOAc (1:1, 3×50 mL), dried with anhydrous $MgSO_4$ and solvents were removed under reduced pressure. CombiFlash of the residue on silica gel (CH_2Cl_2/CH_3OH, CH_3OH: 0%→5%→10%) provided the title compound as sticky oil (505 mg, 73% yield).

¹H NMR (CDCl₃, 400 MHz): δ 8.49 (d, J = 5.5 Hz, 2H), 7.29 (d, J = 4.5 Hz, 2H), 3.03 (d, J = 12.0 Hz, 2H), 2.08 – 1.88 (m, 2H), 1.17 – 1.10 (m, 12H).

¹³C NMR (CDCl₃, 101 MHz): δ 149.7 (d, J = 1.5 Hz), 142.4 (d, J = 7.0 Hz), 125.1 (d, J = 4.5 Hz), 31.2 (d, J = 53.0 Hz), 25.9 (d, J = 64.5 Hz), 15.9 (dd, J = 14.5, J = 3.0 Hz).

³¹P NMR (CDCl₃, 252 MHz): δ 53.7.

HR-MS (ESI): Calculated for $C_{12}H_{21}NOP$ [M+H]⁺ 226.1361, found: 226.1361 (Δ = 0 ppm).

FT-IR (thin film): 3384, 2967, 2938, 2876, 1602, 1465, 1420, 1173, 1150, 1123, 1028, 886, 841 cm⁻¹.

^{1}H NMR

^{31}P NMR

^{13}C NMR

149.73
149.72
142.45
142.38
125.07
125.03
77.32
77.00
76.68
31.43
30.90
26.22
25.58
16.00
15.97
15.86
15.83

200 190 180 170 160 150 140 130 120 110 100 90 80 70 60 50 40 30 20 10 0
f1 (ppm)

^{13}C DEPT NMR

149.73
149.72
125.07
125.03
31.43
30.90
26.22
25.58
16.00
15.98
15.86
15.83

200 190 180 170 160 150 140 130 120 110 100 90 80 70 60 50 40 30 20 10 0
f1 (ppm)
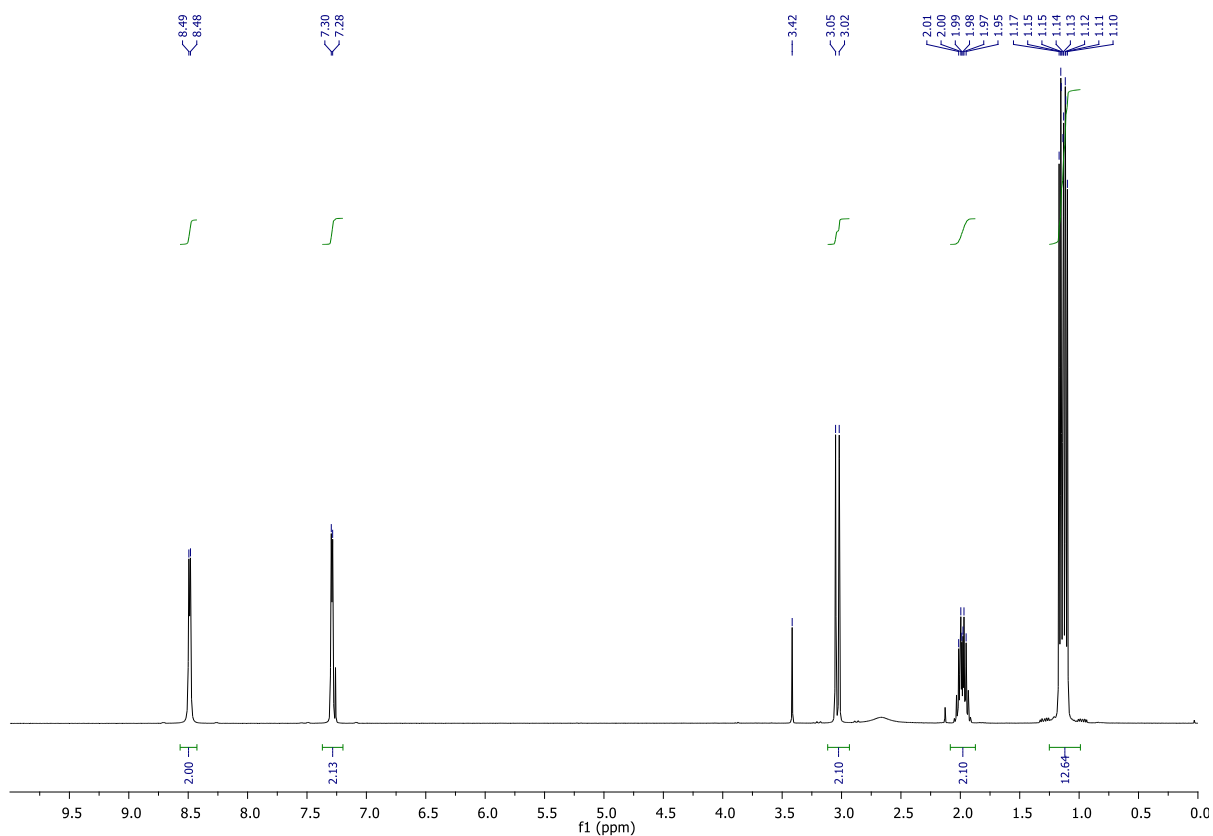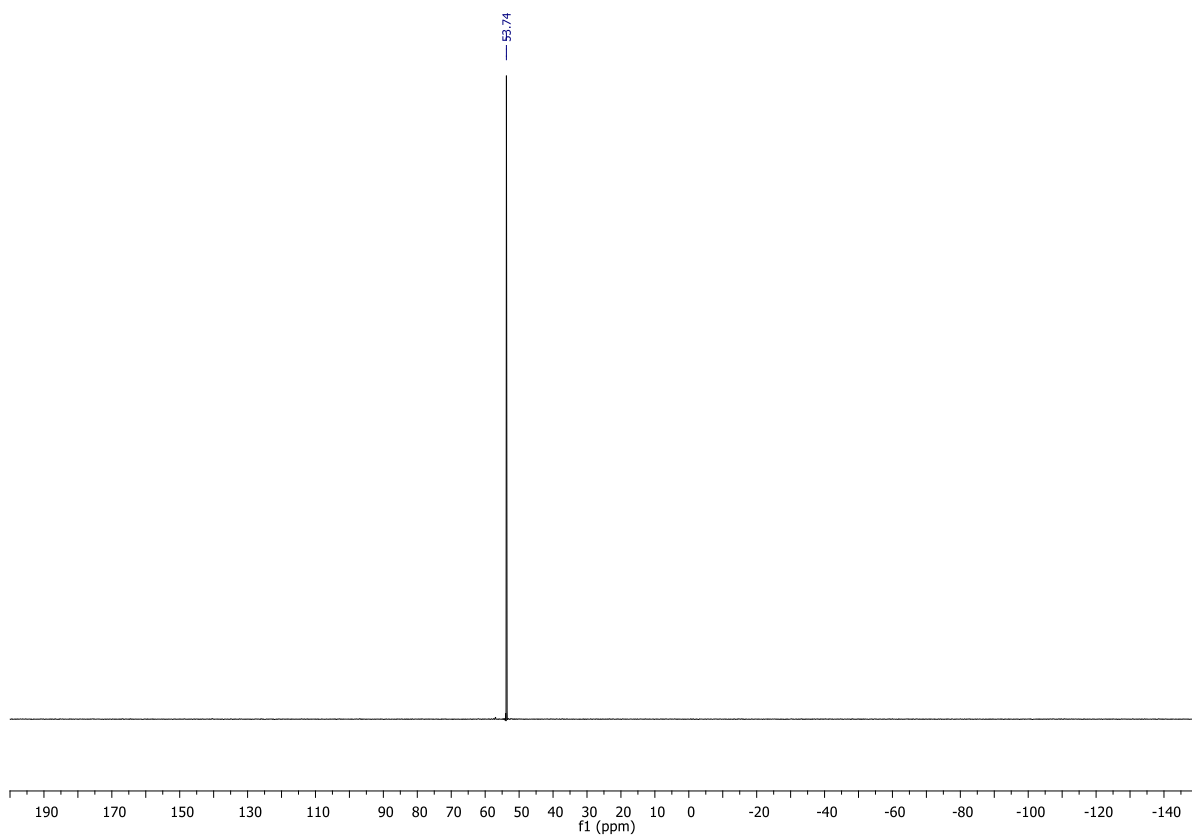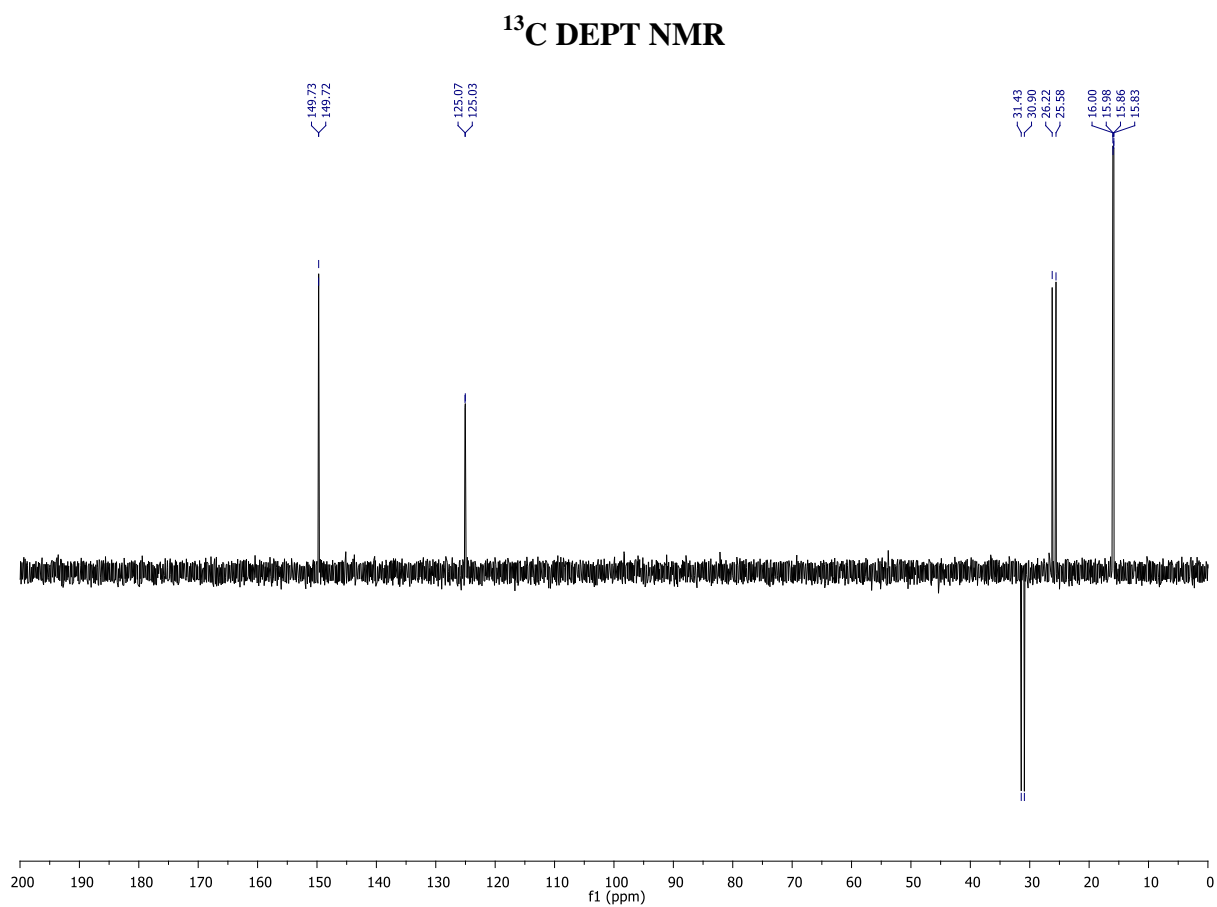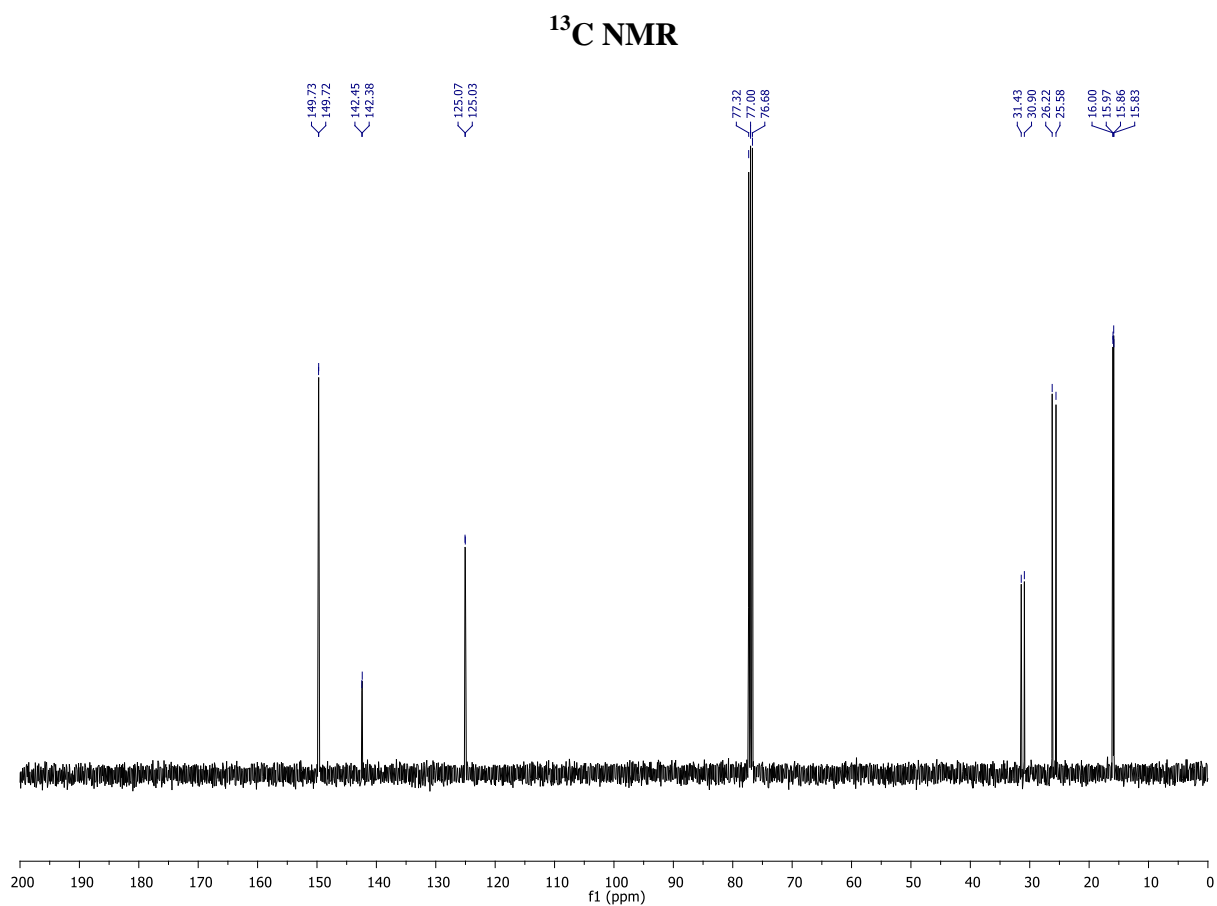
Synthesis of **9**
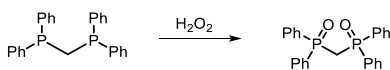
To a solution of bis(dimethylphosphanyl)methane (97%, 1.37 g, 3.46 mmol, 1 eq.) in CH_2Cl_2 (15 mL) at RT was H_2O_2 added (20%, 16 mL, 94 mmol, 27 eq.). After 4 hours of stirring, organic phase was separated, washed with water (10 mL), dried with anhydrous $MgSO_4$, and the solvent was removed under reduced pressure to produce the title compound as a white crystalline solid (1.22 g, 85%).

^{1}H NMR (CDCl$_3$, 400 MHz, 298 K): δ 7.76–7.70 (m, 8H), 7.44–7.31 (m, 12H), 3.52 (t, J = 14.5 Hz, 2H).

^{31}P NMR (CDCl$_3$, 252 MHz, 298 K): δ 24.7.

MP: 186 – 187 °C

R_f (CH$_2$Cl$_2$, silica): 0.05.

The data was in agreement with previously published values.[16,17]

Synthesis of **10**
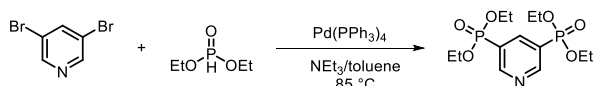
Synthesis according to the published procedure.[9] 57% yield (transparent oil)

^{1}H NMR (CDCl$_3$, 400 MHz, 298 K): δ 9.11 – 9.08 (m, 2H), 8.46 (tt, J = 13.0, 2.0 Hz, 1H), 4.26 – 4.10 (m, 8H), 1.35 (t, J = 7.0 Hz, 12H).
^{31}P NMR (CDCl$_3$, 252 MHz, 298 K): δ 14.2 (s)

The data was in agreement with previously published data.[9]

Synthesis of **11**
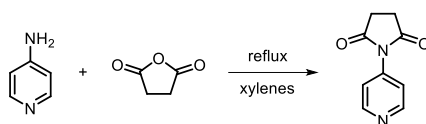
4-Aminopyridine (1.00 g, 10.6 mmol) and succinic anhydride (1.08 g, 10.8 mmol) in xylenes (50 mL) were refluxed in Dean-Stark apparatus for 29 hours. After cooling down, the solid was collected with the aid of petrol ether (2 × 100 mL) and petrol ether was then removed under reducer pressure. The solid was extracted with CH_2Cl_2 (2 × 200 mL) at reflux for 30 minutes and directly filtered. The solvent was removed under reducer pressure and the residue was recrystallised from EtOH to produce the title product as a white crystalline solid (406 mg, 21% yield).

^{1}H NMR (CDCl$_3$, 400 MHz, 298 K): δ 8.73 (dd, J = 5.0 Hz, J = 1.5 Hz, 2H), 7.41 (dd, J = 5.0 Hz, J = 1.5 Hz, 2H), 2.92 (s, 4H).

^{13}C NMR (CDCl$_3$, 101 MHz, 298 K): δ 175.0, 150.8, 139.5, 119.9, 28.4.

HR-MS (ESI): Calculated for $C_9H_9N_2O_2$ [M+H]$^+$ 177.0664, found: 177.0663 (Δ = 0.56 ppm).

FT-IR (thin film): 2952, 2922, 2853, 1727, 1705, 1590, 1461, 1390, 1191 cm^{-1}.

MP: 232 – 234 °C (decomposing)

^{1}H NMR

8.74
8.73
8.73
8.72

7.42
7.41
7.41
7.40
7.26

2.92

2.00

1.98

4.14

10.0 9.5 9.0 8.5 8.0 7.5 7.0 6.5 6.0 5.5 5.0 4.5 4.0 3.5 3.0 2.5 2.0 1.5 1.0 0.5 0.0
f1 (ppm)

^{13}C NMR

175.00

150.80

139.51

119.93

77.32
77.00
76.68

28.35

200 190 180 170 160 150 140 130 120 110 100 90 80 70 60 50 40 30 20 10 0
f1 (ppm)
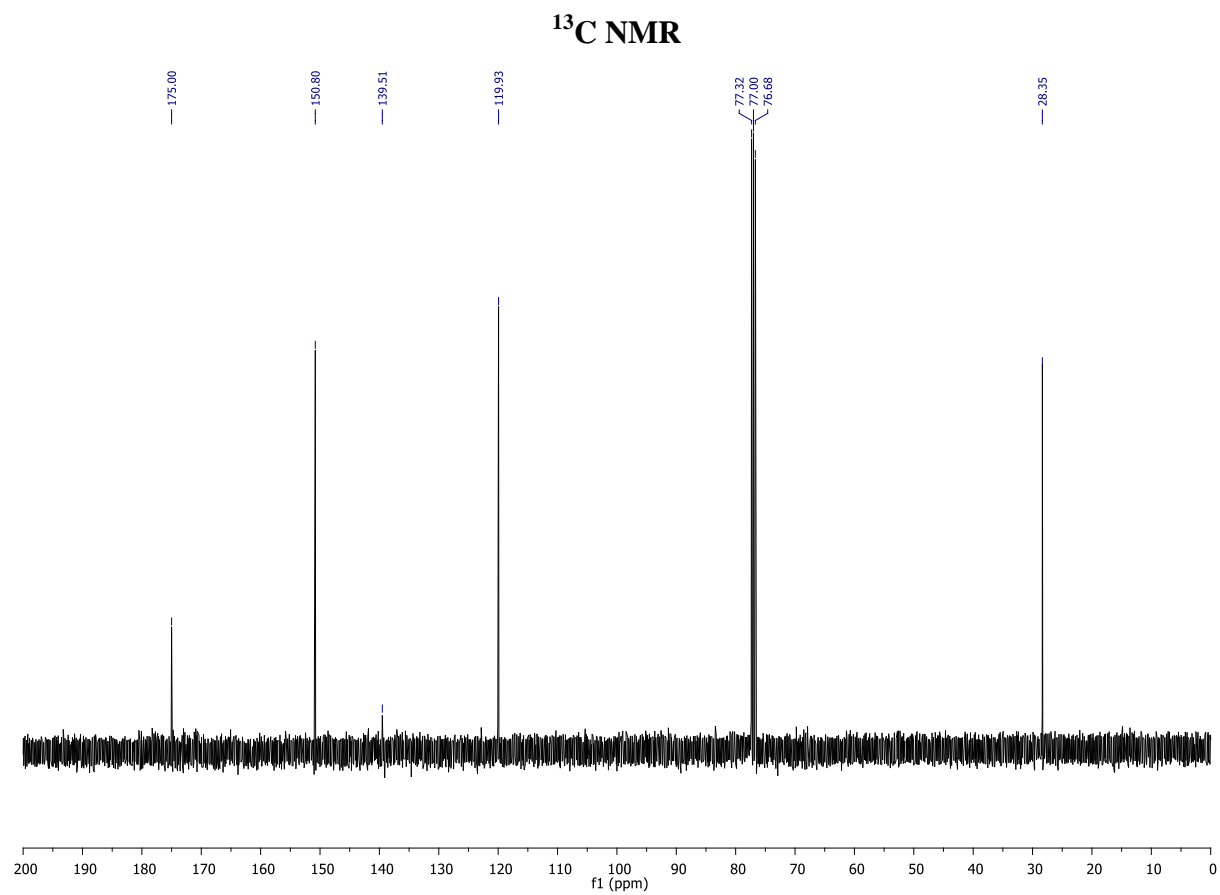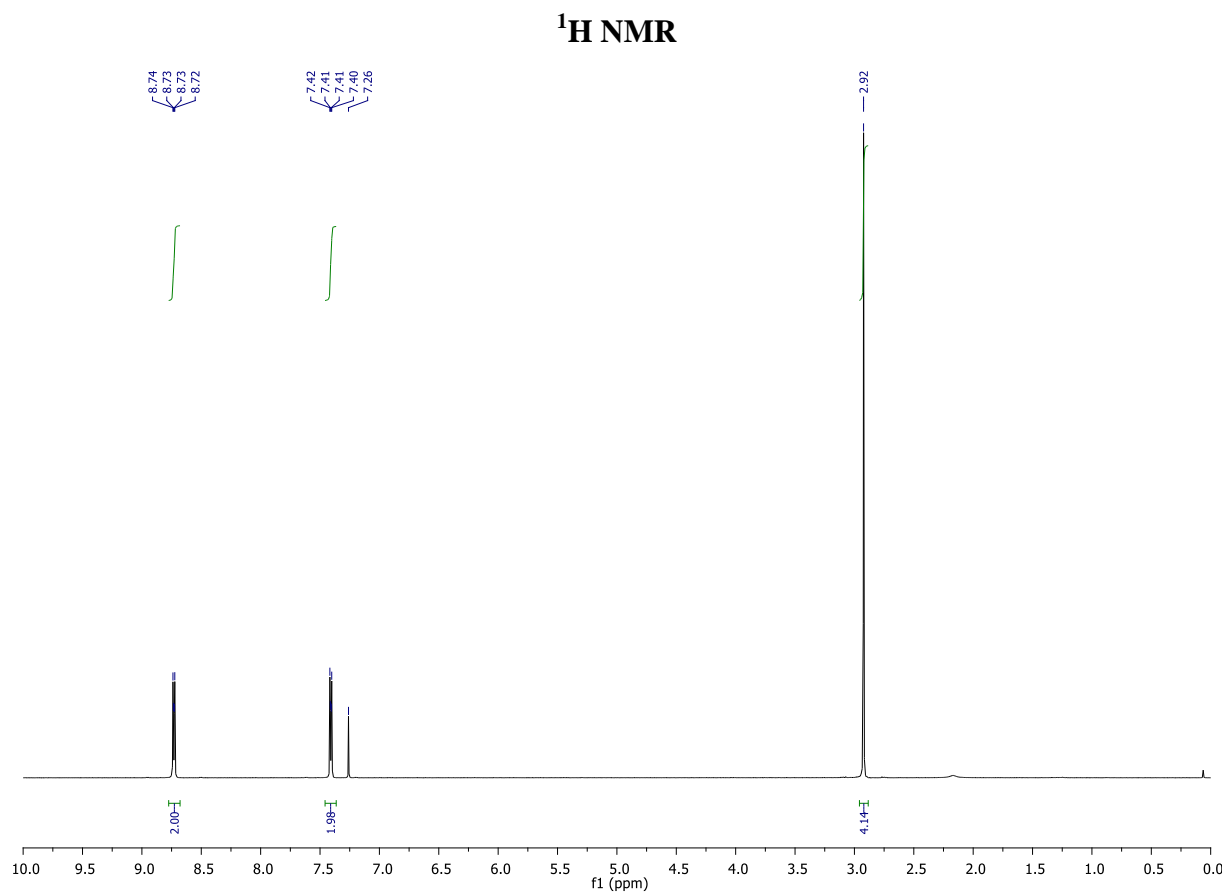
4.8.3. Modelling

The structures of H-bonded complexes were optimised by molecular mechanics in Schrödinger Suite 2016-4 using MacroModel suite. A global minimum structure was found by conformational search using OPLS3 as a force field without any solvent model and no cut-off for non-covalent interactions.

4.8.4. NMR titrations

The NMR titrations were recorded on a Bruker 400 MHz Avance III HD Smart Probe Spectrometer at 298 K. As a solvent, d^8-toluene was used. A host solution with known concertation was prepared and fraction of this solution (0.6 mL) was transferred into a NMR tube. Then, the guest solution was prepared by dissolving a known amount of guest in the host stock solution in a volumetric flask. A change of chemicals shifts of either ^1H or ^{31}P upon addition of aliquots of guest solution were followed. The d^8-toluene residual peak was used for reference (CH_3: 2.11 ppm). The observed changes of chemical shifts were analysed using a purpose-written fitting macro in Microsoft Excel (written by Prof Hunter). A 1:1 binding isotherm was used to fit the experimental data. The experiments were measured at least two times on at least two different days in order to eliminate possible systematic errors. The results are stated as average values and errors are quoted as two times the standard deviation.

4.9. References

(1)   Hunter, C. A.; Anderson, H. L. *Angew. Chem. Int. Ed.* **2009**, *48*, 7488-7499.

(2)   Motloch, P.; Hunter, C. A. *Adv. Phys. Org. Chem.* **2016**, *50*, 77-118.

(3)   Hogben, H. J.; Sprafke, J. K.; Hoffmann, M.; Pawlicki, M.; Anderson, H. L. *J. Am. Chem. Soc.* **2011**, *133*, 20962-20969.

(4)   Hunter, C. A. *Angew. Chem. Int. Ed.* **2004**, *43*, 5310-5324.

(5)   Sprafke, J. K.; Kondratuk, D. V.; Wykes, M.; Thompson, A. L.; Hoffmann, M.; Drevinskas, R.; Chen, W.-H.; Yong, C. K.; Kärnbratt, J.; Bullock, J. E.; Malfois, M.; Wasielewski, M. R.; Albinsson, B.; Herz, L. M.; Zigmantas, D.; Beljonne, D.; Anderson, H. L. *J. Am. Chem. Soc.* **2011**, *133*, 17262-17273.

(6)   Hoffmann, M.; Kärnbratt, J.; Chang, M.-H.; Herz, L. M.; Albinsson, B.; Anderson, H. L. *Angew. Chem. Int. Ed.* **2008**, *47*, 4993-4996.

(7)   Montel, S.; Jia, T.; Walsh, P. J. *Org. Lett.* **2014**, *16*, 130-133.

(8)   Yip, S. F.; Cheung, H. Y.; Zhou, Z.; Kwong, F. Y. *Org. Lett.* **2007**, *9*, 3469-3472.

(9)   Zon, J.; Videnova-Adrabinska, V.; Janczak, J.; Wilk, M.; Samoc, A.; Gancarz, R.; Samoc, M. *CrystEngComm* **2011**, *13*, 3474-3484.

(10)   Littler, B. J.; Miller, M. A.; Hung, C.-H.; Wagner, R. W.; O'Shea, D. F.; Boyle, P. D.; Lindsey, J. S. *J. Org. Chem.* **1999**, *64*, 1391-1396.

(11)   Megiatto, J. D.; Schuster, D. I.; Abwandner, S.; de Miguel, G.; Guldi, D. M. *J. Am. Chem. Soc.* **2010**, *132*, 3847-3861.

(12)   Shediac, R.; Gray, M. H. B.; Uyeda, H. T.; Johnson, R. C.; Hupp, J. T.; Angiolillo, P. J.; Therien, M. J. *J. Am. Chem. Soc.* **2000**, *122*, 7017-7033.

(13)   Cheng, F.; Zhang, S.; Adronov, A.; Echegoyen, L.; Diederich, F. *Chem. Eur. J.* **2006**, *12*, 6062-6070.

(14)   Lehnherr, D.; Gao, J.; Hegmann, F. A.; Tykwinski, R. R. *Org. Lett.* **2008**, *10*, 4779-4782.

(15)   Taylor, P. N.; Anderson, H. L. *J. Am. Chem. Soc.* **1999**, *121*, 11538-11545.

(16)   Rathore, R.; Burns, C. L.; Deselnicu, M. I. *Org. Lett.* **2001**, *3*, 2887-2890.

(17)   Petersson, M. J.; Loughlin, W. A.; Jenkins, I. D. *Chem. Commun.* **2008**, 4493-4494.

V

Supramolecular system inside porphyrin nanoring

5.1. Introduction

Most biological systems are multivalent.[1] The product of multiple bindings is usually not just a simple sum of individual binding contributions because of cooperativity.[2] In multivalent supramolecular systems, two types of cooperativity exist – allosteric and chelate cooperativity. Allosteric cooperativity occurs when the first binding influences the strength of the second binding. Chelate cooperativity originates from the binding between a multivalent host and guest, where the local "effective concentration" is increased for the second binding. Such increase is quantified through effective molarity (EM).

The literature provides a distribution of effective molarities in supramolecular systems. The median value is 100 mM and EM > 10^2 M is considered to be extremely high, since less than 5% of the reviewed supramolecular systems showed the values of this magnitude.[3] Porphyrin nanorings from the Anderson group show exceptionally high values of EM. The highest value has been found for complex **6-ring•T** (Figure 5.1a).[4] The Anderson group used a series of ligands with two, three, four and five pyridine binding sites to determine stepwise EMs for each binding interaction in the hexamer.[5] The value of EM for the first intramolecular binding interaction is 100 mM, which is comparable to the value found for the majority of supramolecular complexes. However, all four subsequent intramolecular binding interactions have exceptionally high values of EM of 10^3 M. Another system that shows high degree of chelate cooperativity is the H-bonded rosette motif (Figure 5.1b) with EM = 2 M.[6]
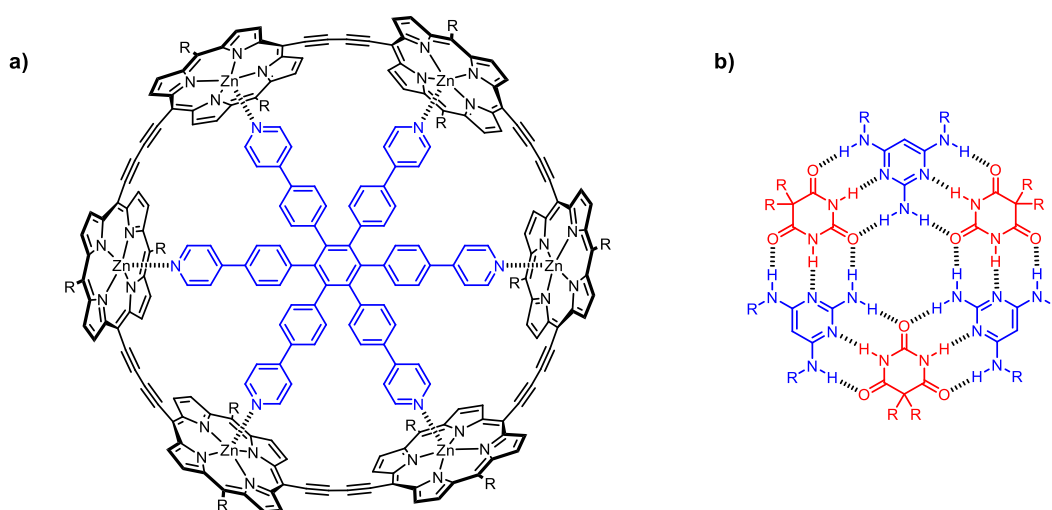
Figure 5.1. Two supramolecular systems with high effective molarity. (a) Complex of **6-ring** (black) with hexadentate ligand **T** (blue) and (b) rosette motif using pyrimidines (blue) and barbiturates (red). R is a substituent.

The goal of this work was to test if the extreme values of effective molarity found for **6-ring** and the rosette motif can be joined together to prepare a system that contains both of them to study whether there are any synergistic effect in the assembly. Anderson and co-workers stated that the size of template **T** is actually smaller than what would be optimal for the binding to **6-ring** based on results of the X-ray crystallography.[7] This means that the target supramolecular H-bonded system might be a better fit thanks to its flexibility compared to the covalent hexadentate template **T**. On the other hand, there are much higher entropic costs associated with the assembly of supramolecular system inside the **6-ring** cavity. The interplay between those two effects will decide if the target H-bonded system can be formed inside a porphyrin nanoring.

5.2. Approach

To be able to prepare a supramolecular system based on the rosette motif inside a porphyrin nanoring, the rosette building blocks (barbiturate and pyrimidines) have to be coupled to pyridine units that would work as the molecular recognition for the zinc porphyrins of **6-ring**. We decided to test barbiturate-pyridines and pyrimidine-pyridines with a different substitution positions on the pyridine and different linker lengths to increase the probability to find the optimal system. Two barbiturate-pyridine ligands **3B3** and **4B3**, and four different pyrimidine-pyridine ligands **3P1**, **3P2**, **4P1** and **4P2** are depicted in Figure 5.2. The alkyl substituents should increase the solubility in non-polar solvents that will be used for the study, such as chloroform.
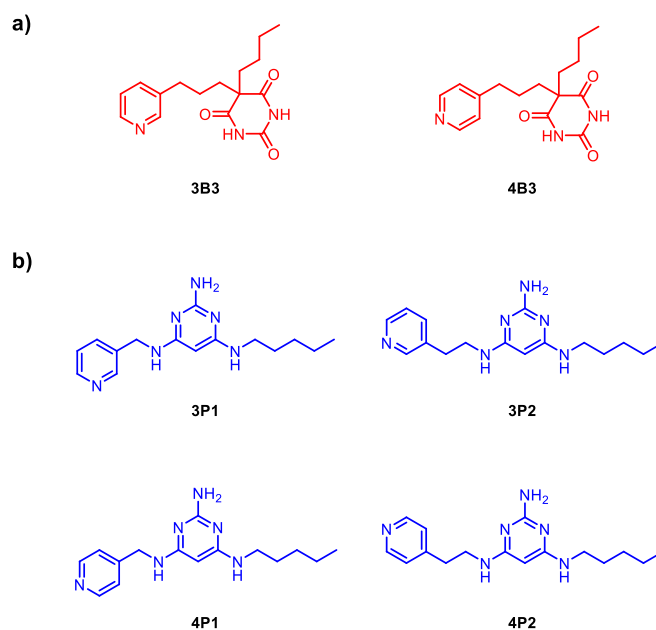
Figure 5.2. Building blocks for rosettes equipped with pyridine ligands; (a) barbiturate-pyridines **3B3** and **4B3** and (b) pyrimidine-pyridines **3P1**, **3P2**, **4P1** and **4P2**.

The association constant for the formation of the supramolecular system based on the rosette inside **6-ring** (Figure 5.3 and Figure 5.4) is given by Equation 5.1.

$$K_\mathrm{f} = K_\mathrm{rosette} \times K_\mathrm{Py,1}^3 \times K_\mathrm{Py,2}^3 \times \overline{\mathrm{EM}}^5 \qquad (5.1)$$

where K_rosette is an association constant for the formation of the rosette (Figure 5.3), $K_\mathrm{Py,1}$ and $K_\mathrm{Py,2}$ are association constant for the binding of the pyridine units of the ligands to **6-ring** and $\overline{\mathrm{EM}}$ is the geometric average of effective molarities of sequential binding of the rosette to **6-ring**, thus $\overline{\mathrm{EM}} = \sqrt[5]{\mathrm{EM}_1 \cdot \mathrm{EM}_2 \cdot \mathrm{EM}_3 \cdot \mathrm{EM}_4 \cdot \mathrm{EM}_5}$ as shown in Figure 5.4. If the statistical factor K_σ is included,[8-10] the statistically corrected value of $\overline{\mathrm{EM}}_\mathrm{s}$ can be determined by Equation 5.2

$$K_\mathrm{f} = K_\sigma \times K_\mathrm{rosette} \times K_\mathrm{Py,1}^3 \times K_\mathrm{Py,2}^3 \times \overline{\mathrm{EM}}_\mathrm{s}^5 \qquad (5.2)$$

The macroscopic K_rosette was determined previously as $(6.25 \pm 0.09) \times 10^{15}$ M^{-5}.[6] $K_\mathrm{Py,1}$ and $K_\mathrm{Py,2}$ will be measured with the aid of suitable model pyridine compounds. By measuring K_f, we will be able to determine $\overline{\mathrm{EM}}_\mathrm{s}$ and compare it to the values obtained with covalent hexadentate ligand **T**.
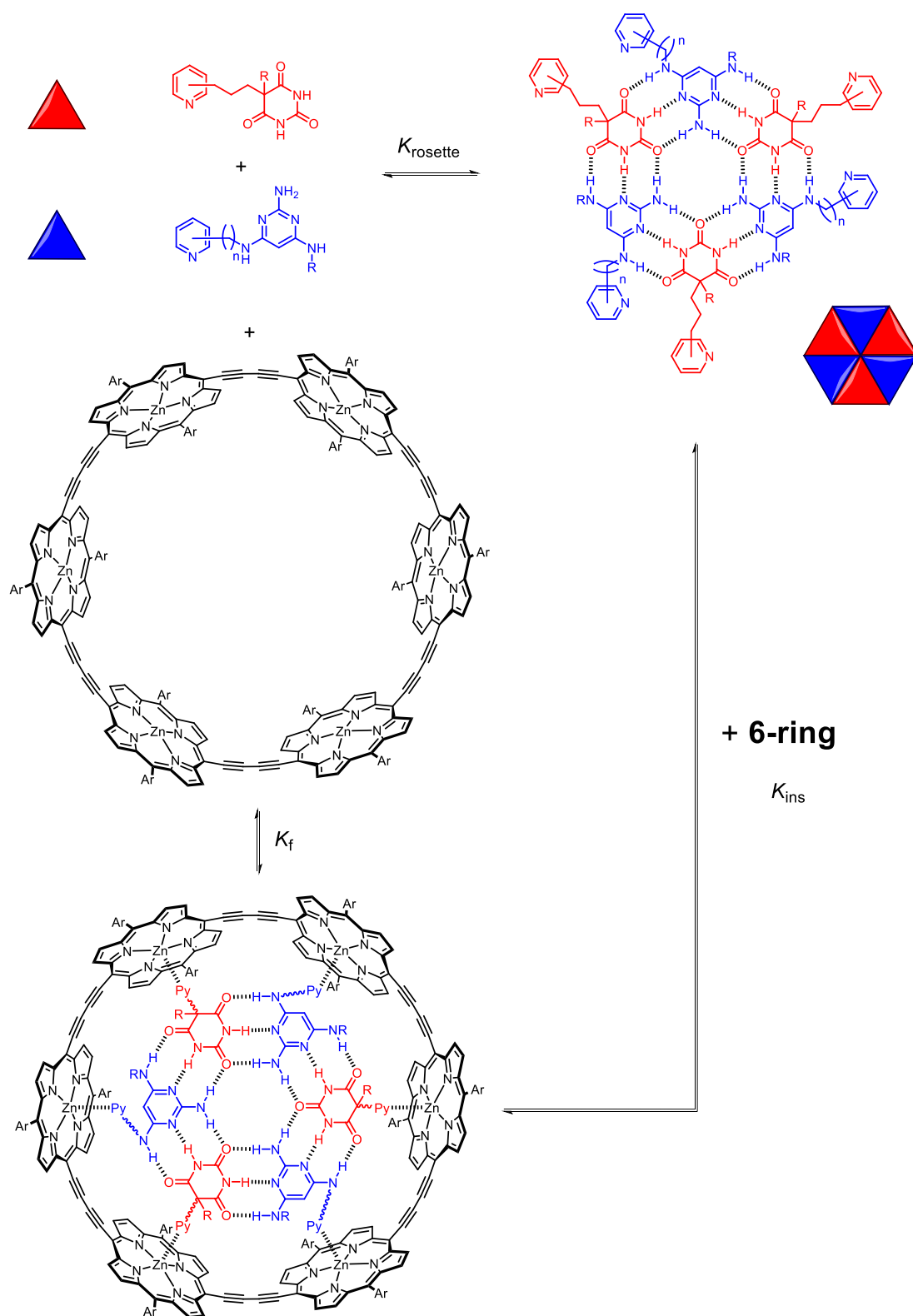
Figure 5.3. Thermodynamic cycle for the formation of the rosette supramolecular system inside **6-ring** from barbiturate-pyridines and pyrimidine-pyridines. R is a solubilising group, Ar = 3,5-bis(*t*-butyl)phenyl, n is 1 or 2, Py is a pyridine unit.
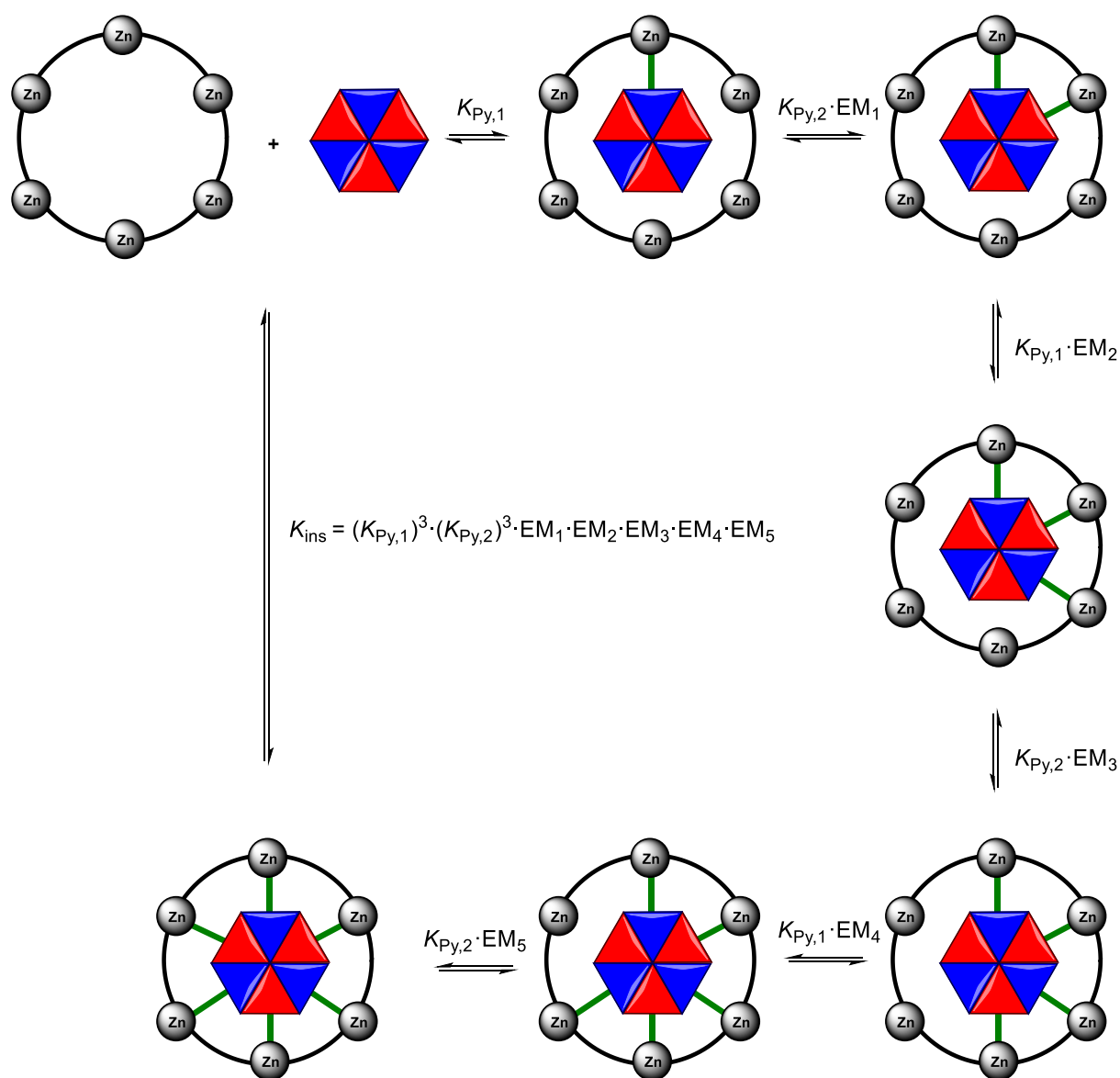
Figure 5.4. Schematic representation of sequential binding of the rosette (red and blue hexagone) to **6-ring** (black circle), green line denotes pyridine–zinc porphyrin interaction. First binding is intermolecular, all the remaining are intramolecular.

5.3. Modelling

All the possible combinations (namely **3B3₃•3P1₃**, **3B3₃•3P2₃**, **3B3₃•4P1₃**, **3B3₃•4P2₃**, **4B3₃•3P1₃**, **4B3₃•3P2₃**, **4B3₃•4P1₃**, **4B3₃•4P2₃**) were investigated by a conformational search using molecular mechanics in the absence of **6-ring**. The structure of **T** from the X-ray structure of **6-ring•T** was used as a template,[7] where the coordinates of the nitrogen atoms and carbon atoms in the position 4 were constrained. The rest of the molecules were then built from these fragments. With this, the conformational search could rotate the pyridine units freely around their axes. This modelling does not employ **6-ring**, which has both benefits and drawbacks. The main benefits are lower calculation costs, and the main drawback is that this method does not find all the possible structures, since the real structure can have the pyridines tilted from the fixed axis taken from the X-ray structure and there can be also some movement of the porphyrin units of **6-ring**. On the other hand, when it provides the desired conformation, the probability of obtaining this architecture should be high. It has to be noted that the conformational search was done without the solubilising alkyl groups on barbiturate as well as pyrimidine to decrease the computational costs. Only complex **3B3₃•3P2₃** provided a structure containing the rosette motif as shown in Figure 5.5.
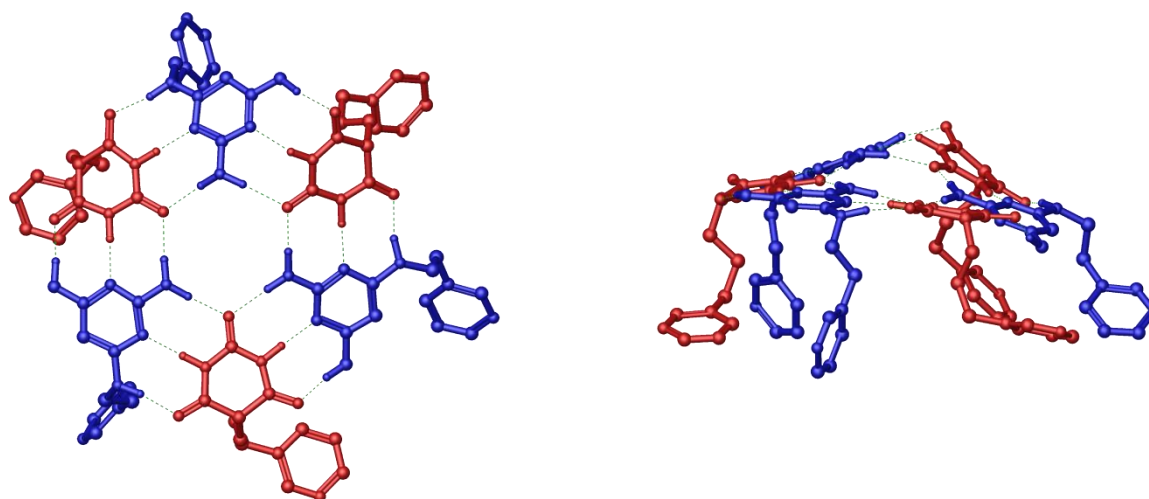
Figure 5.5. Lowest energy structure of **3B3₃•3P2₃** rosette system from a conformational search using molecular modelling (OPLS3/no solvent) and **T** as a template, where the coordinates of the nitrogen atoms and carbon atoms in the position 4 of pyridine units were constrained (the alkyl groups of both barbiturate-pyridines and pyrimidine-pyridines were replaced by hydrogen atoms in the calculations). Hydrogen atoms that do not contribute to H-bonding were omitted for clarity; colouring: **3B3** in red, **3P2** in blue, green dashed line is the H-bond.

Then, the optimised structure of **3B3$_3$•3P2$_3$** was placed inside **6-ring** and further optimised by semi-empirical method PM6 as depicted in Figure 5.6b (the 3,5-bis(*t*-butyl)phenyl groups were replaced by hydrogen atoms in the calculations). As stated above, the restricted conformational search does not explore all the possibilities, therefore we modelled all the possible complexes by using different starting structures. In this way, it was possible to find structures containing the rosette motif for all the complexes based on **3B3** (Figure 5.6). No structures containing the rosette motif were found for the complexes based on **4B3**. This modelling showed that rosette systems **3B3$_3$•3P1$_3$** and **3B3$_3$•3P2$_3$** fit well into **6-ring** as depicted in Figures 5.6a and 5.6b. In comparison, some porphyrin units had to rotate significantly in the **3B3$_3$•4P1$_3$** and **3B3$_3$•4P2$_3$** systems to be able to accommodate them inside the cavity as depicted in Figures 5.6c and 5.6d.
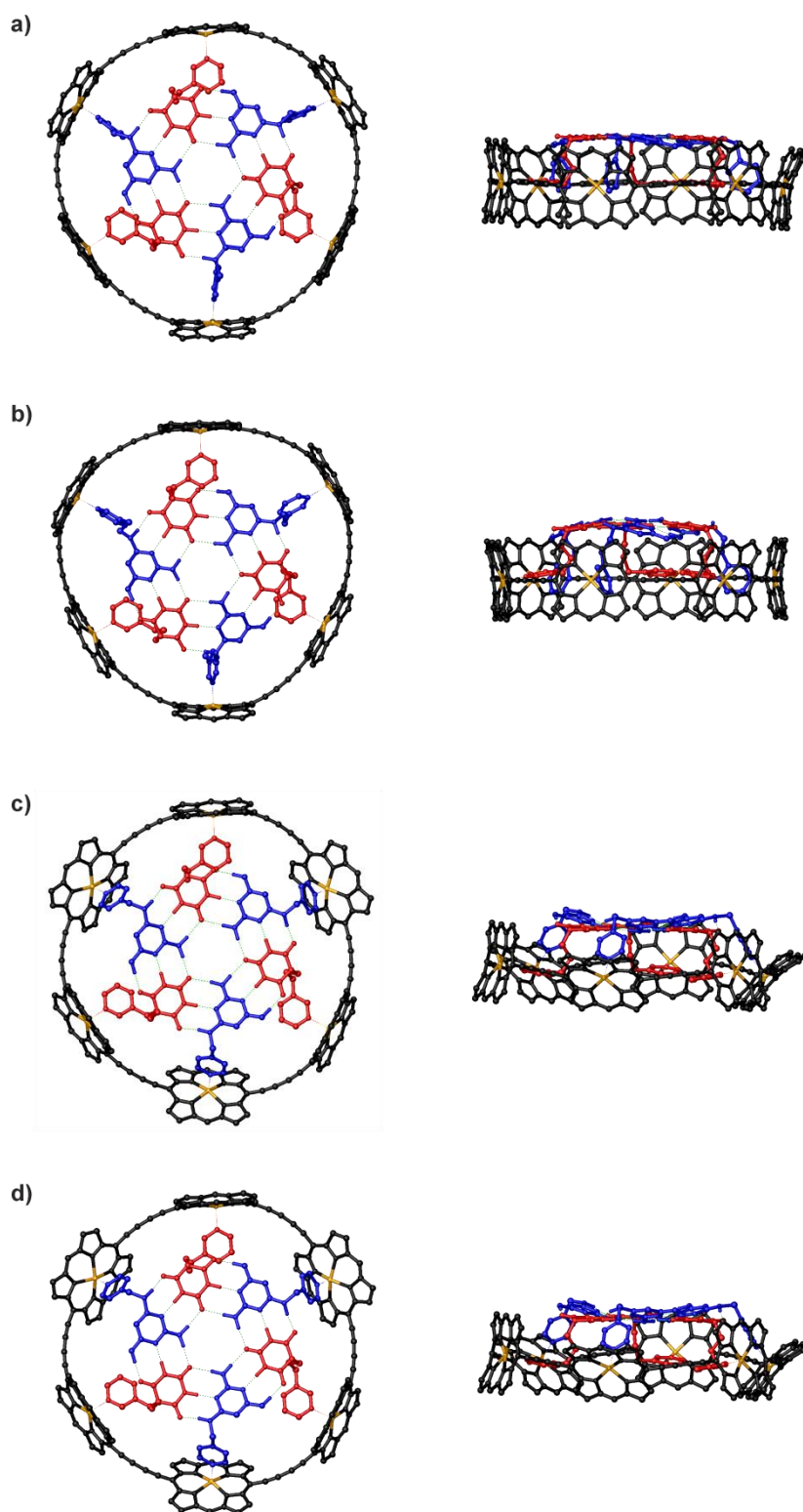
Figure 5.6. PM6-optimised structures of the H-bonded rosettes (a) **3B3$_3$•3P1$_3$**, (b) **3B3$_3$•3P2$_3$**, (c) **3B3$_3$•4P1$_3$**, (d) **3B3$_3$•4P2$_3$** bound inside the **6-ring** (alkyl groups on barbiturate-pyridines and pyrimidine-pyridines as well as 3,5-bis(*t*-butyl)phenyl on **6-ring** were replaced by hydrogen atoms in the calculations). Hydrogen atoms that do not contribute to H-bonding were omitted for clarity. Colouring: **6-ring** in black with highlighted Zn atoms in yellow, barbiturate-pyridines in red, pyrimidine-pyridines in blue, green dashed line is the H-bond.

145

5.4. Synthesis

The synthesis of **6-ring** was described in Chapter IV. Pyrimidine-pyridines **3P1**, **3P2**, **4P1** and **4P2** were synthesised in two steps from the commercially available 4,6-dichloropyrimidin-2-amine in good to excellent yields as shown in Scheme 5.1. The first reaction provided singly substituted products that were easily isolated by precipitation. These were then converted to the final products in neat *n*-pentylamine at 150 – 160 °C.
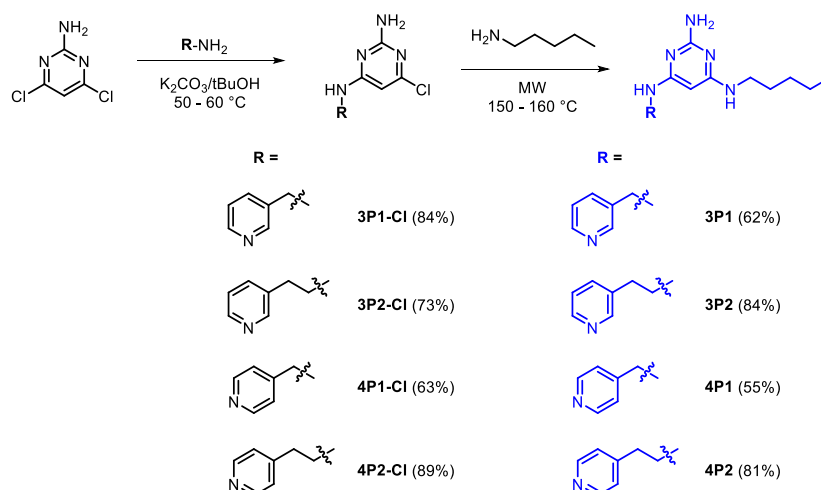
Scheme 5.1. Synthesis of pyrimidine-pyridines **3P1**, **3P2**, **4P1** and **4P2**.

The barbiturate-pyridines **3B3** and **4B3** were synthesised starting from commercially available (3-pyridin-3-yl)propan-1-ol and (3-pyridin-4-yl)propan-1-ol, respectively, as shown in Scheme 5.2. Firstly, the hydroxyl group was transformed to a mesylate, followed by the protection of the nucleophilic pyridine nitrogen atoms with $BH_3 \cdot SMe_2$ in excellent yields in order to avoid mixtures of alkylation products.[11] The protected mesylates were then reacted with *n*-butyl diethylmalonate to produce malonates **c** that were obtained both as protected (majority) and deprotected (⅓ to ½) forms. The target barbiturate-pyridines were obtained directly from the deprotected malonate **c** by a reaction with urea in DMF as shown on **4B3** or from the protected malonate **c-BH₃** by the same reaction that provided again protected and unprotected target product as shown on **3B3**. The final deprotection was achieved by HCl in methanol.
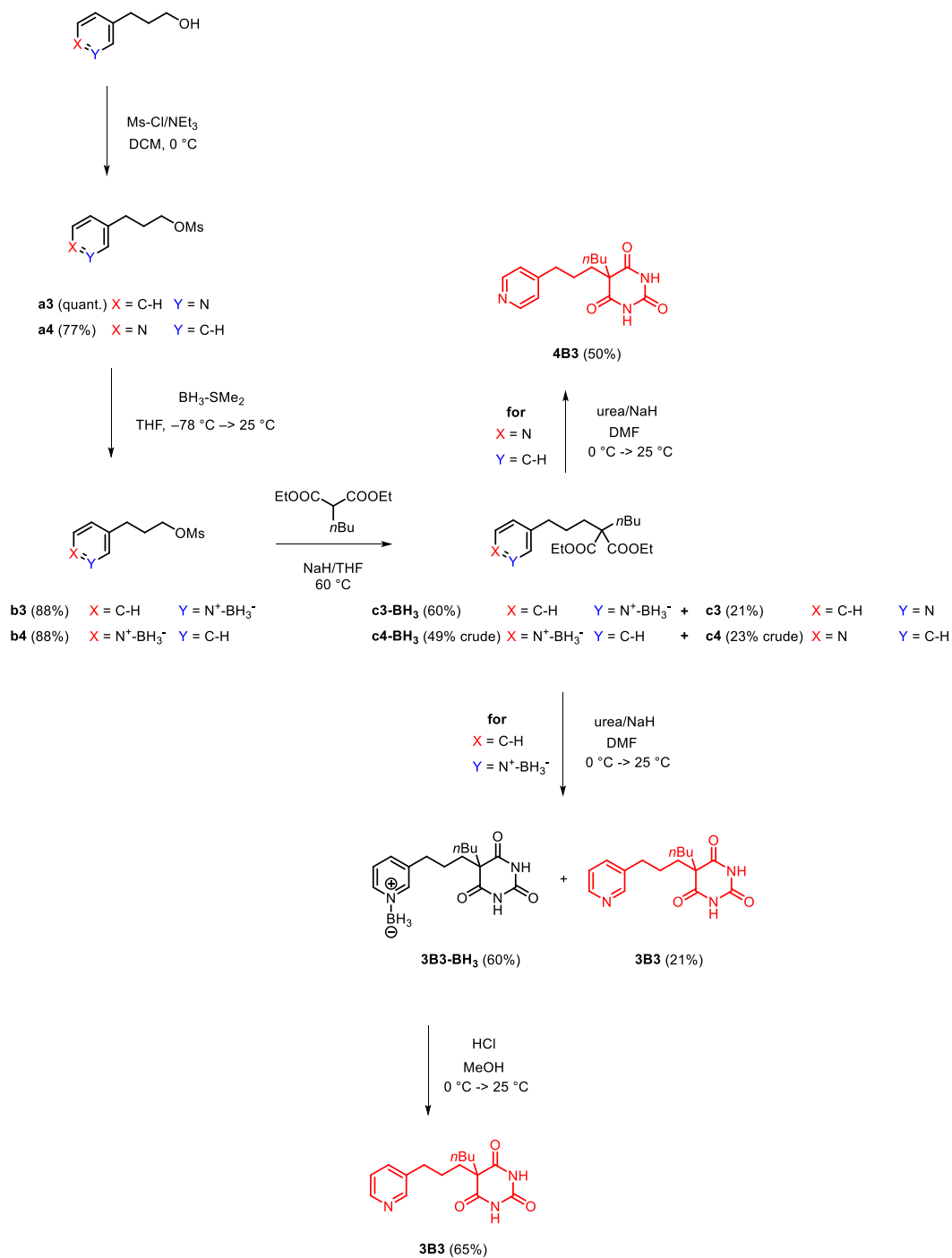
Scheme 5.2. Synthesis of barbiturate-pyridines **3B3** and **4B3**.

5.5. UV-vis-NIR titrations

Firstly, a reference association constant of binding of a pyridine unit to a zinc porphyrin had to be measured. Since we used compounds based on 3-pyridinyl as well as 4-pyridinyl, we decided to use 3-methylpyridine (**3Py**) and 4-methylpyridine (**4Py**) to obtain the association constants. The UV-vis-NIR titration of **3Py** to **6-ring** in chloroform at 298 K is depicted in Figure 5.7. To fit the experimental data with a 1:1 binding isotherm, we assumed that all six porphyrin units act independently and identically. This leads to the description of each pyridine–zinc porphyrin coordination event independently. The apparent 1:1 association constants measured for the pyridine–zinc porphyrin interaction are outlined in Table 5.1. The **4Py** binds slightly stronger to **6-ring** than **3Py**.
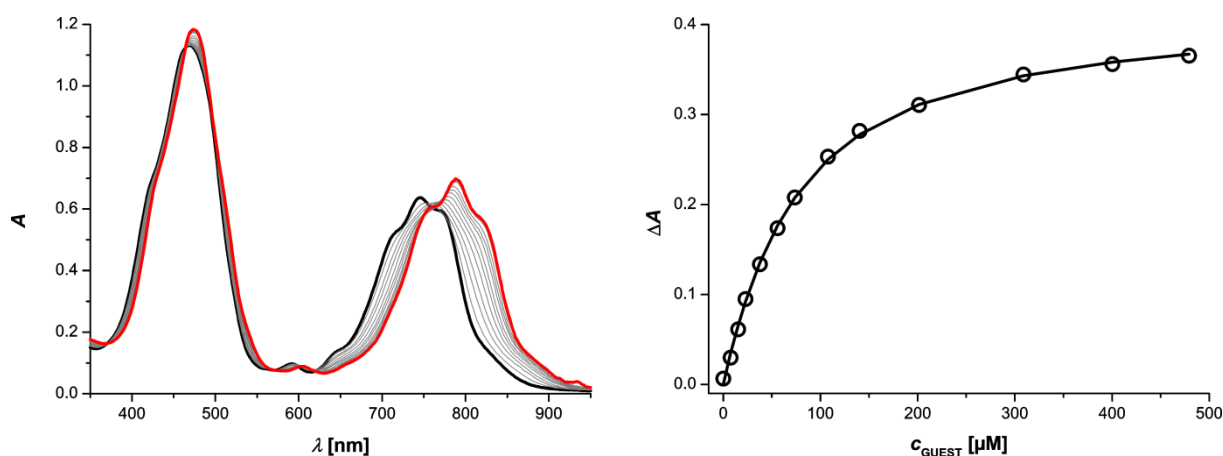
Figure 5.7. UV-vis-NIR titration (CHCl$_3$, 298 K) of **3Py** to **6-ring**. UV-vis-NIR spectra are shown on the left with the spectrum of unbound **6-ring** in thick black line and the end spectrum in red thick line. On the right are shown the experimental data at 833 nm (circles) and calculated values (line) based on a 1:1 binding isotherm assuming that the six porphyrin units of **6-ring** act identically and independently while the host concentration was also allowed to change upon fitting.

Then we investigated the binding of the prepared barbiturate-pyridine and pyrimidine-pyridine compounds to **6-ring** again by UV-vis-NIR titrations in chloroform at 298 K using the same fitting method as stated above. The results are shown in Table 5.1. The determined apparent association constants are all higher by average an order of magnitude than the reference association constants for methylpyridines **3Py** and **4Py**. Although these systems cannot form rosettes, multiple H-bonding interactions are still possible as shown on the example of a system based on **3B3** in Figure 5.8 that was optimised by PM6.

Table 5.1. Apparent 1:1 association constants measured by UV-vis-NIR titrations in CHCl$_3$ at 298 K for the pyridine–zinc porphyrin interaction using **6-ring** as the host. Errors are quoted as two times the standard deviation based on two repetitions.
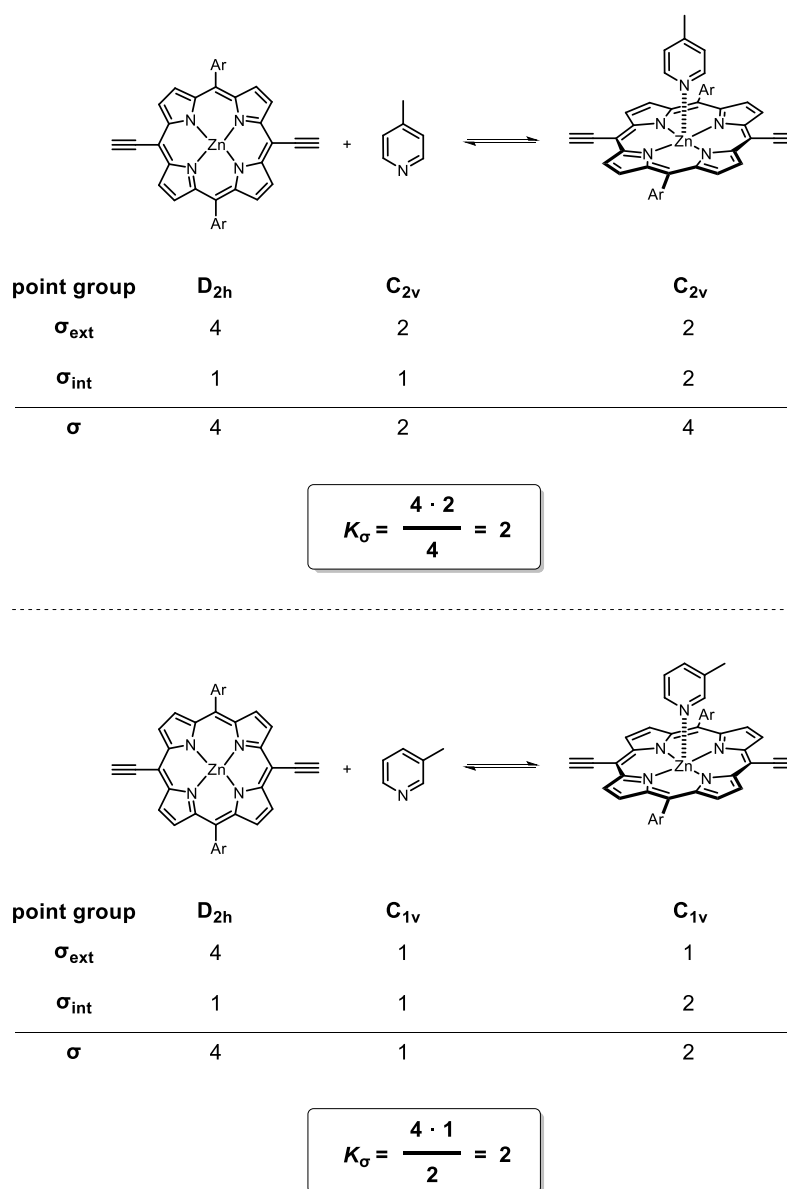
Guest	log K / M^{-1}	Guest mixture (1:1)	log K / M^{-1}	Guest mixture (1:1)	log K / M^{-1}
3Py	4.2 ± 0.1				
4Py	4.4 ± 0.1				
3B3	4.7 ± 0.1	**3B3** + **P**	4.6 ± 0.3		
4B3	5.2 ± 0.1	**4B3** + **P**	5.3 ± 0.1		
3P1	5.2 ± 0.3	**3P1** + **B**	5.6 ± 0.1	**3P1** + **C**	5.6 ± 0.1
3P2	5.4 ± 0.2	**3P2** + **B**	5.5 ± 0.1	**3P2** + **C**	5.5 ± 0.1
4P1	5.2 ± 0.1	**4P1** + **B**	5.4 ± 0.5	**4P1** + **C**	5.5 ± 0.3
4P2	5.2 ± 0.5	**4P2** + **B**	5.5 ± 0.1	**4P2** + **C**	5.9 ± 0.4
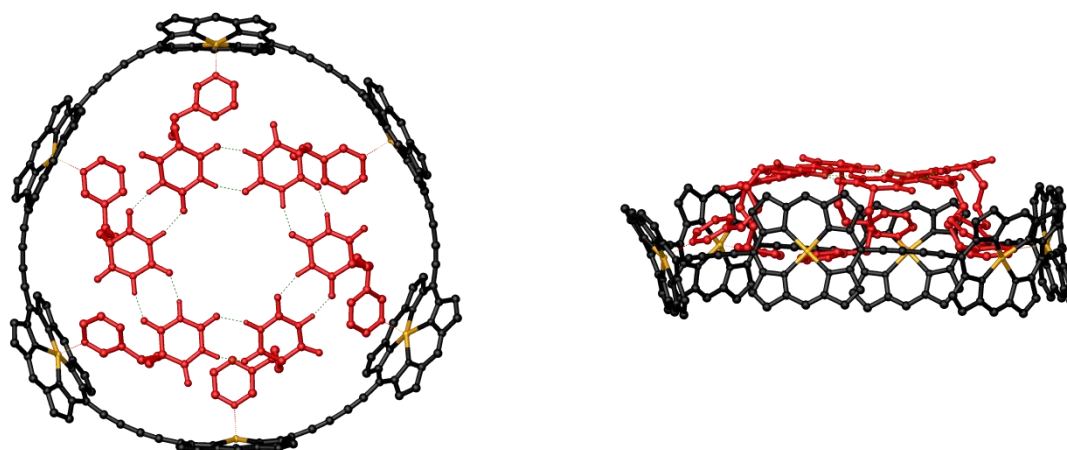
Figure 5.8. PM6-optimised structure of **3B3** ligands bound to **6-ring** showing H-bonding interactions between the ligands (alkyl groups on **3B3** and 3,5-bis(*t*-butyl)phenyl on **6-ring** were replaced by hydrogen atoms in the calculations). Hydrogen atoms that do not contribute to H-bonding were omitted for clarity. Colouring: **6-ring** in black with highlighted Zn atoms in yellow, **3B3** in red, green dashed line is the H-bond.

Next, we investigated the complexes in which one of the rosette building blocks contained the pyridine unit and the second was the corresponding rosette partner without any pyridine (see Figure 5.9). We decided to include also a cyanurate partner that should form more stable rosettes.[12] We conducted UV-vis-NIR titrations by an addition of the mentioned two rosette components in a 1:1 ratio as the guest solution into **6-ring** in CHCl$_3$ at 298 K. A 1:1 binding isotherm was used to fit the experimental data assuming that all six porphyrin

units of **6-ring** coordinate a pyridine ligand and act identically and independently. By that, we determined apparent 1:1 association constants for the pyridine–zinc porphyrin interaction and they are depicted in Table 5.1. All the titrations can be found in the Experimental section. Within the experimental error, all of these complexes showed the same stability as the ligands on their own. In the absence of any increased stability due to the presence of the rosette patterns, there is no evidence for a rosette formation.
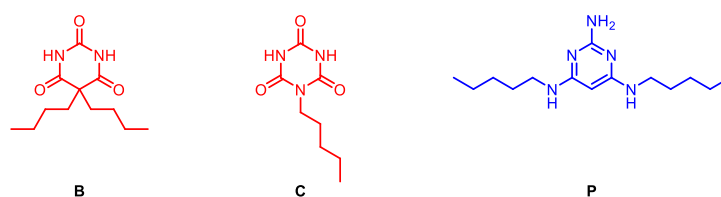
Figure 5.9. Barbiturate **B**, cyanurate **C** and pyrimidine **P**.

Next, we investigated the complexes in which both of the rosette components contained the pyridine unit. We determined apparent 1:1 association constants for the pyridine–zinc porphyrin interaction by UV-vis-NIR titrations in $CHCl_3$ at 298 K by titrating a solution of barbiturate-pyridine and pyrimidine-pyridine in a 1:1 ratio to **6-ring**. A significant difference could be observed when the mixture was used compared to the separate ligands as shown in Figure 5.10. A 1:1 binding isotherm was used to fit the experimental data assuming that all six porphyrin units of **6-ring** coordinate a pyridine ligand and act identically and independently, and using the total concentration of pyridine units as the guest concentration. All the titrations can be found in the Experimental part. The results are shown in Table 5.2.

To quantify the difference between a mixture and ligands, a cooperativity factor **COOP** defined by Equation 5.3 was used. Two systems (**3B3 + 3P1** and **3B3 + 4P1**) showed an order of magnitude higher cooperativity factor compared to the other systems.

$$\mathbf{COOP} = \frac{K_{(1:1\ \text{mixture})}}{K_{\text{ligand,1}} \times K_{\text{ligand,2}}} \tag{5.3}$$
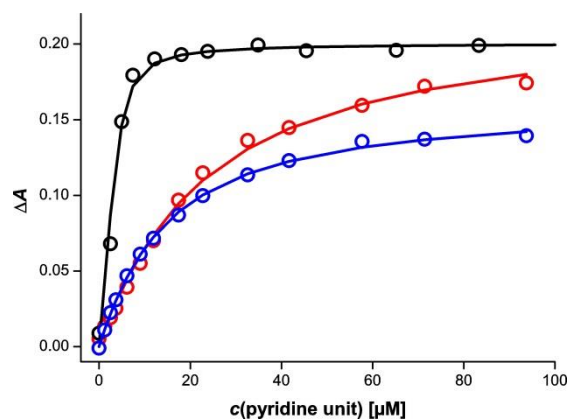
Figure 5.10. UV-vis-NIR titration (CHCl$_3$, 298 K) of **3B3** (red), **3P1** (blue) and a 1:1 mixture of **3B3** and **3P1** (black) to **6-ring** (0.8 μM) showing the experimental data at 838 nm (circles) and calculated values (lines) based on a 1:1 binding isotherm assuming that the six porphyrin units of **6-ring** act identically and independently while the host concentration was also allowed to change upon fitting.

Table 5.2. Apparent 1:1 association constants measured by UV-vis-NIR titrations in CHCl$_3$ at 298 K for the pyridine–zinc porphyrin interaction using **6-ring** as the host. Errors are quoted as two times the standard deviation based on two repetitions.

Guest	log K / M^{-1}	Guest	log K / M^{-1}	Guest mixture (1:1)	log K / M^{-1}	COOP / M
3B3	4.7 ± 0.1	**3P1**	5.2 ± 0.3	**3B3** + **3P1**	7.2 ± 0.2	150
3B3	4.7 ± 0.1	**3P2**	5.4 ± 0.2	**3B3** + **3P2**	6.6 ± 0.2	30
3B3	4.7 ± 0.1	**4P1**	5.2 ± 0.1	**3B3** + **4P1**	7.5 ± 0.5	300
3B3	4.7 ± 0.1	**4P2**	5.2 ± 0.5	**3B3** + **4P2**	6.5 ± 0.1	30
4B3	5.2 ± 0.1	**3P1**	5.2 ± 0.3	**4B3** + **3P1**	6.6 ± 0.2	30
4B3	5.2 ± 0.1	**3P2**	5.4 ± 0.2	**4B3** + **3P2**	7.1 ± 0.1	60
4B3	5.2 ± 0.1	**4P1**	5.2 ± 0.1	**4B3** + **4P1**	6.7 ± 0.3	30
4B3	5.2 ± 0.1	**4P2**	5.2 ± 0.5	**4B3** + **4P2**	6.8 ± 0.1	40

These results allowed us to calculate **6-ring** effective molarities for the rosette complexes from Equations 5.1 and 5.2, assuming $K_f = K^6$, where K is an apparent 1:1 association constants for the pyridine–zinc porphyrin interaction for the formation of rosette complexes inside **6-ring** depicted in Table 5.2; using $K_{rosette}$ as $(6.25 \pm 0.09) \times 10^{15} \, M^{-5}$, and $K_{Py,1}$ and $K_{Py,2}$ from the reference methylpyridine UV-vis-NIR titrations (Table 5.1). The determination of statistical factors for the formation of the rosette complexes inside **6-ring** is shown in Figure 5.11 and the determination of statistical factors for the reference pyridine complexes that has to be taken into account is shown in Figure 5.12. The determined **6-ring** effective molarities for the binding of H-bonded rosette systems are depicted in Table 5.3.

point group	C$_1$	C$_1$	D$_{6h}$	C$_3$
σ_{ext}	1	1	12	3
σ_{int}	1	1	2^6	1
σ	1	1	728	3

$$K_\sigma = \frac{728 \cdot 1^3 \cdot 1^3}{3} = \frac{728}{3}$$
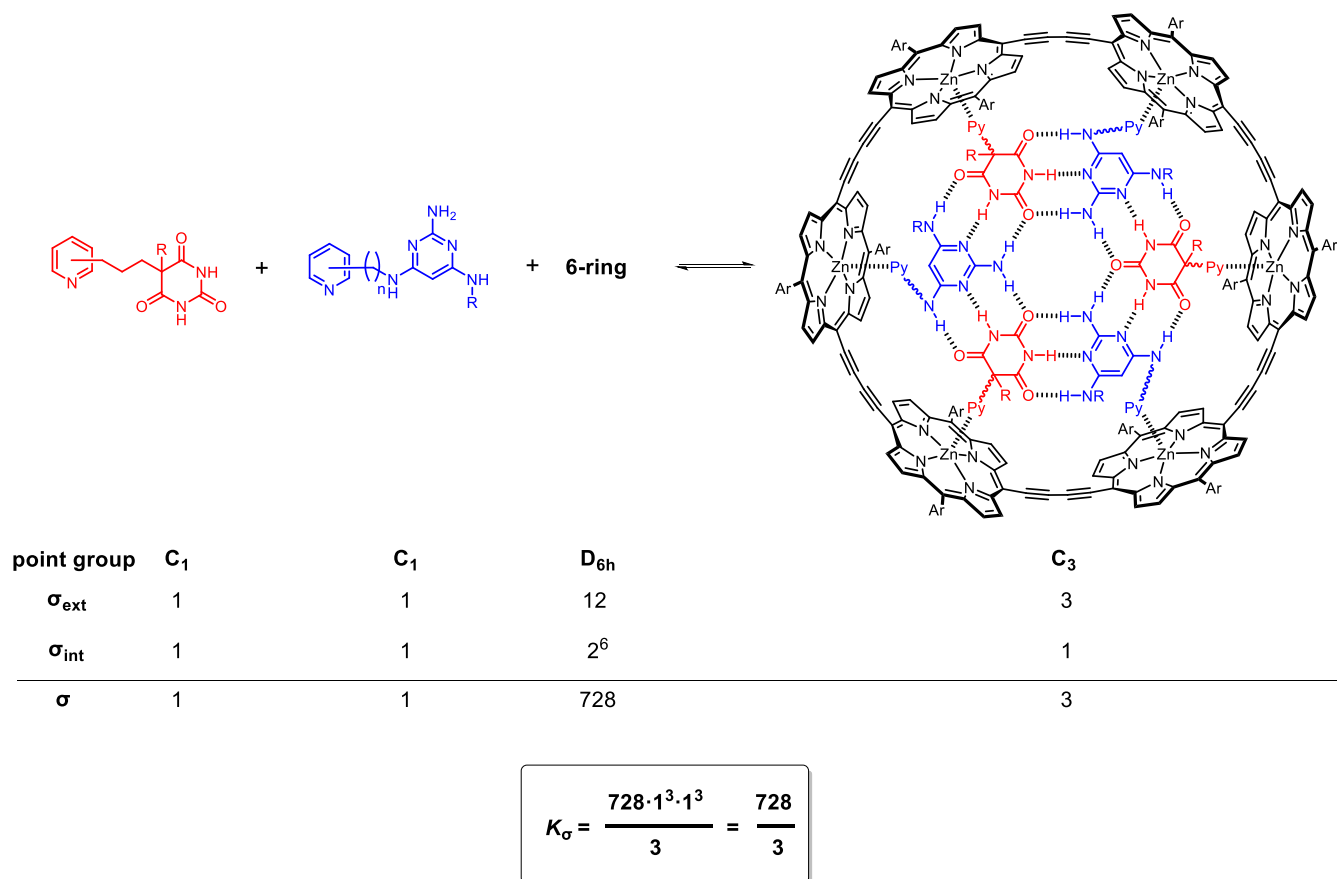
Figure 5.11. Statistical factor K_σ for the rosette assembly inside **6-ring** (R is a solubilising group, Ar = 3,5-bis(*t*-butyl)phenyl, n is 1 or 2, Py is a pyridine unit). Using higher external symmetry for ligands based on 4-pyridyl would not change the overall statistical factors as the internal and external statistical factors of the ligands and complex would cancel each other out as described in detail in Figure 5.12 below for simpler systems.

point group	D_{2h}	C_{2v}	C_{2v}
σ_{ext}	4	2	2
σ_{int}	1	1	2
σ	4	2	4

$$K_\sigma = \frac{4 \cdot 2}{4} = 2$$

point group	D_{2h}	C_{1v}	C_{1v}
σ_{ext}	4	1	1
σ_{int}	1	1	2
σ	4	1	2

$$K_\sigma = \frac{4 \cdot 1}{2} = 2$$

Figure 5.12. Statistical factor K_σ for the reference methylpyridine complexes **4Py** (top) and **3Py** (bottom).

Table 5.3. Geometric averages of effective molarity for a sequential binding of H-bonded rosette system to **6-ring** in CHCl$_3$ at 298 K. Errors are quoted as two times the standard deviation.

Ligand system (1:1)	$\overline{\text{EM}}$ [M]	$\overline{\text{EM}}_s$ [M]
3B3 + **3P1**	6.3 ± 3.7	2.1 ± 1.2
3B3 + **3P2**	1.2 ± 0.6	0.40 ± 0.20
3B3 + **4P1**	11 ± 15	3.7 ± 4.8
3B3 + **4P2**	0.69 ± 0.14	0.23 ± 0.05
4B3 + **3P1**	0.91 ± 0.55	0.30 ± 0.18
4B3 + **3P2**	3.6 ± 0.5	1.2 ± 0.2
4B3 + **4P1**	0.91 ± 0.66	0.30 ± 0.22
4B3 + **4P2**	1.2 ± 0.2	0.40 ± 0.08

The determined effective molarities cluster around the value of 1 M with systems **3B3 + 3P1**, **3B3 + 4P1** and **4B3 + 3P2** showing the highest values (> 1 M) and system **3B3 + 4P2** being the lowest. All these values are significantly lower (at least two orders of magnitude) than the reference system based on hexadentate ligand **T** (126 M).[5] On the other hand, the determined values of effective molarities can still be considered high compared to the other supramolecular systems.[3] Moreover, the alkyl chains between the pyridine and barbiturate units in **3B3** and **4B3** are quite long and it is known that the introduction of each additional rotor decrease the value of effective molarity in supramolecular systems.[13] Therefore, the optimisation of the linker length could lead to a significantly more cooperative system since the effect would be cubic.

5.6. NMR experiments

We conducted ^{1}H NMR experiments to further characterise the complexes in solution. To do that, we chose systems with highest and lowest effective molarities (namely **3B3** + **3P1**, **3B3** + **4P1**, **4B3** + **3P2** and **3B3** + **4P2**). As an example, the system **3B3** + **3P1** is discussed here and the rest can be found in the Experimental section. A 1:3:3 mixture of **6-ring**, **3B3** and **3P1** resulted in highly complicated ^{1}H NMR spectra with broad peaks as seen in Figure 5.13c, especially when compared to the ^{1}H NMR spectra of separate **6-ring** and a 1:1 mixture of **3B3** and **3P1** at the same concentrations (Figure 5.13a-b). This is probably due to an intermediate exchange of the free components and assemblies on the ^{1}H NMR time-scale. A very broad N-H rosette peak was observable, what points out to the rosette assembly.
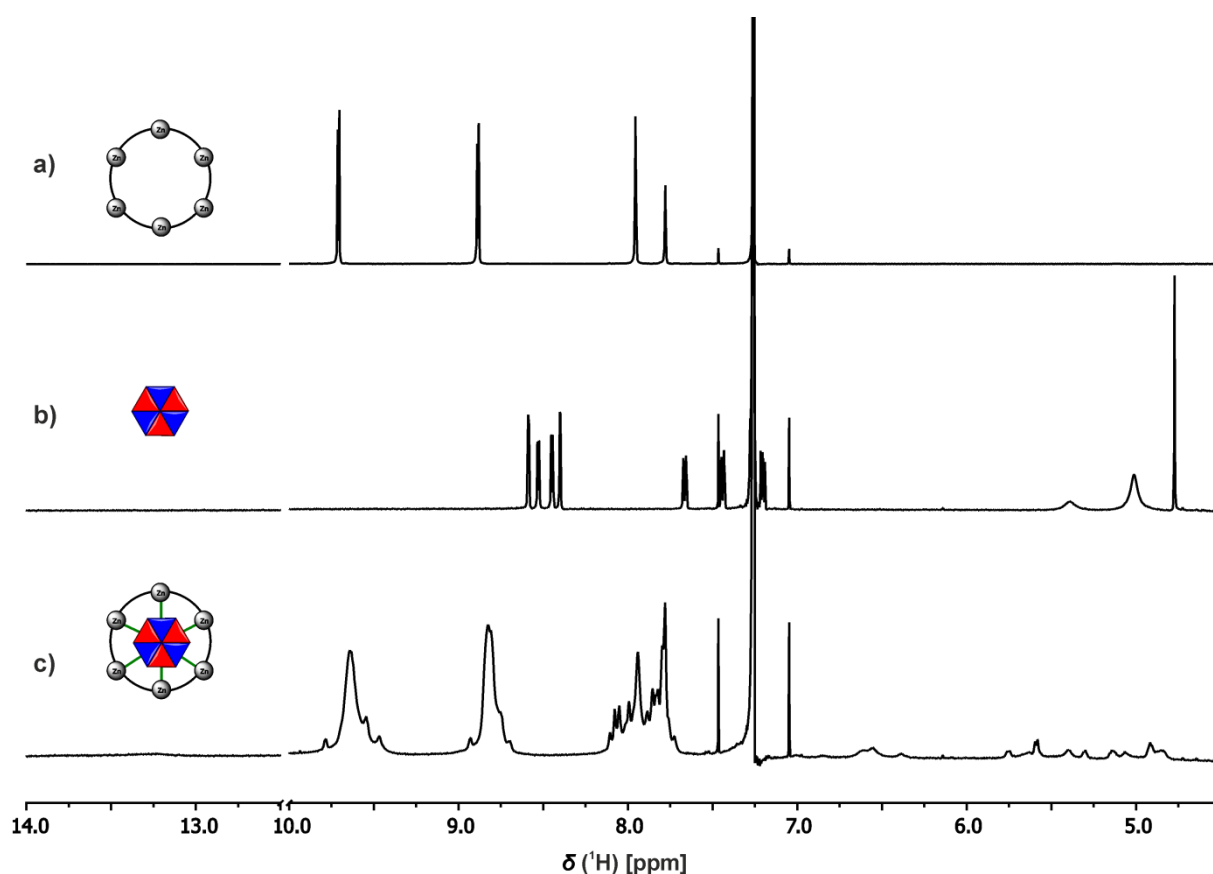
Figure 5.13. Partial ^{1}H NMR (500 MHz, CDCl$_3$, 298 K) spectra of (a) **6-ring** (0.16 mM), (b) mixture of **3B3** (0.48 mM) and **3P1** (0.48 mM) and (c) mixture of **6-ring** (0.16 mM), **3B3** (0.48 mM) and **3P1** (0.48 mM).

155

5.7. Conclusion and future work

In this chapter, we designed and prepared H-bonded rosette systems using various barbiturate-pyridine and pyrimidine-pyridine ligands with different linker lengths and different position of nitrogen atom of pyridine. We used UV-vis-NIR titrations in chloroform to show that these systems assemble inside **6-ring** in a cooperative fashion. The effective molarities of sequential binding of the rosette systems to **6-ring** were determined to range from 0.23 to 3.7 M, which is significantly lower (two to three orders of magnitude) compared to the reference **6-ring•T** complex, probably due to ligands being too floppy. On the other hand, the determined values of effective molarity are still high compared to other supramolecular systems from the literature.

The results from this study could be used for the application of the H-bonded rosette system as an easily-removable supramolecular template for the synthesis of **6-ring**. After the reaction, a simple change of the solvent could disrupt the H-bonded system and remove the rosette from **6-ring**, which would overcome the issues connected with using the original covalent hexadentate template **T**. This could potentially show a new way for the construction of advanced molecular architectures where covalent templates are difficult or even impossible to remove. This supramolecular templating by a supramolecular template is very scarce in the literature.[14]

5.8. Experimental section

5.8.1. General

The syntheses of **B**, **C** and **P** were described in the Chapter III and the synthesis of **6-ring** was described in the Chapter IV. The chemicals were bought from commercial suppliers and used without further purifications unless stated otherwise. Solvents were either distilled before use or used as obtained. For chromatography, automatic chromatography systems CombiFlash R_f^+ and CombiFlash R_f^+ Lumen (with UV light detection at 254 nm and 280 nm and evaporative light scattering detector for Lumen) with pre-packed puriFlash columns from Interchim (silica, 25 μm) with a loading of mixtures on Celite were used. The microwave used was Biotage Initiator$^+$. The reactions were monitored either by glass TLC plates coated with silica gel 60 F_{254} (Merck) and the plates were inspected by UV light (254 nm) or by LSMS Waters Acquity H-class UPLC coupled with a single quadrupole Waters SQD2 with the conditions as follows: UPLC Column (see below), solvent A: Water + 0.1% formic acid; solvent B: acetonitrile od THF (see below) + 0.1% formic acid; gradient and flow rate (see below); column temperature of 40 °C, the signal was monitored at 254 nm and 280 nm.

Columns

  Col1: ACQUITY UPLC CSH C18 Column, 130Å, 1.7 μm, 2.1 mm X 50 mm
  Col3: ACQUITY UPLC HSS T3 Column, 100Å, 1.8 μm, 2.1 mm X 50 mm

Methods

  MeCN-FAST: Gradient: $0 - 2$ minutes $5\% - 100\%$B + 1 minute 100%B
   Flow rate: 0.6 ml/min
  MeCN-SLOW: Gradient: $0 - 4$ minutes $5\% - 100\%$B + 1 minute 100%B
   Flow rate: 0.6 ml/min
  THF-FAST: Gradient: $0 - 2$ minutes $5\% - 80\%$B + 1 minute 80%B
   Flow rate: 0.4 ml/min
  THF-SLOW: Gradient: $0 - 4$ minutes $5\% - 80\%$B + 1 minute 80%B
   Flow rate: 0.4 ml/min
  THF_FAST_5%-35%: Gradient of 0-2 minutes $5\% - 35\%$B + 1 minute 100%B
   Flow rate: 0.4 ml/min

^{1}H and ^{13}C NMR spectra were recorded on Bruker 400 MHz Avance III HD SmartProbe Spectrometers at 400 MHz for ^{1}H, 128 MHz for ^{11}B, 101 MHz for ^{13}C or on a Bruker 500 MHz AVIII HD SmartProbe Spectrometer at 500 MHz for ^{1}H and 126 MHz for ^{13}C. All chemicals shift are quoted in ppm and were referenced to the residual peaks of used solvents: CDCl$_3$ (^{1}H: 7.26 ppm; ^{13}C: 77.00 ppm), CD$_3$OD (^{1}H: 3.31 ppm; ^{13}C: 49.00 ppm), d^6-DMSO (^{1}H: 2.50 ppm; ^{13}C: 39.52 ppm). Coupling constants J are stated in Hz. FT-IR spectra were measured on a Bruker Alpha spectrometer. HR-MS spectra were obtained on a Waters Xevo G2-S, Waters Vion IMS Qtof or Waters LCT Premier by electrospray-ionisation of samples. Melting points were recorder on a Mettler-Toledo MP90 system. Elemental analysis was performed by the Microanalysis facility at the Department of Chemistry at the University of Cambridge.

5.8.2. Synthesis

Synthesis of a3
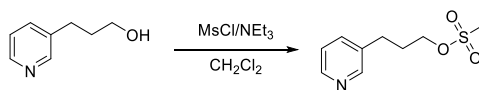
To a solution of 3-(pyridin-3-yl)propan-1-ol (1 mL, 1.06 g, 7.7 mmol) and NEt$_3$ (3 mL) in CH$_2$Cl$_2$ (50 mL) was added methanesulfonyl chloride (0.8 mL, 10.3 mmol, 1.4 eq) at 0 °C in small parts over the period of 90 minutes. The reaction mixture was stirred at 0 °C for additional 30 minutes and then diluted with CH$_2$Cl$_2$ (50 mL). The still-cool solution was washed with H$_2$O (2×30 mL) and brine (30 mL), dried with MgSO$_4$ and solvents were removed under reducer pressure (at no more than 30 °C). A combiflash of the residue on silica gel (PE/EtOAc, EtOAc: 0%→100%) provided the title compound as yellowish liquid (1.65 g; quant.)

(*This compound is quite unstable even when stored in fridge.*)

^{1}H NMR (CDCl$_3$, 400 MHz, 298 K): δ 8.53 – 8.42 (m, 2H), 7.52 (dt, J = 8.0 Hz, 2.0 Hz, 1H), 7.23 (dd, J = 8.0, 5.0 Hz, 1H), 4.24 (t, J = 6.0 Hz, 2H), 3.01 (s, 3H), 2.80 – 2.74 (t, J = 7.0 Hz, 2H), 2.13 – 2.05 (m, 2H).

^{13}C NMR (CDCl$_3$, 101 MHz, 298 K): 149.9, 147.9, 135.9, 135.6, 123.4, 68.6, 37.4, 30.4, 28.8.

¹H NMR

8.48
8.47
8.47
7.53
7.53
7.51
7.51
7.26
7.25
7.24
7.23
7.22
4.26
4.24
4.23
3.13
3.01
2.79
2.77
2.75
2.10
2.10
2.09
2.08
2.08
2.07
2.07
2.07

1.93
1.00
0.99
2.02
3.04
2.04
2.06

¹³C NMR

149.88
147.89
135.86
135.60
123.44
77.32
77.00
76.68
68.57
37.42
30.40
28.79
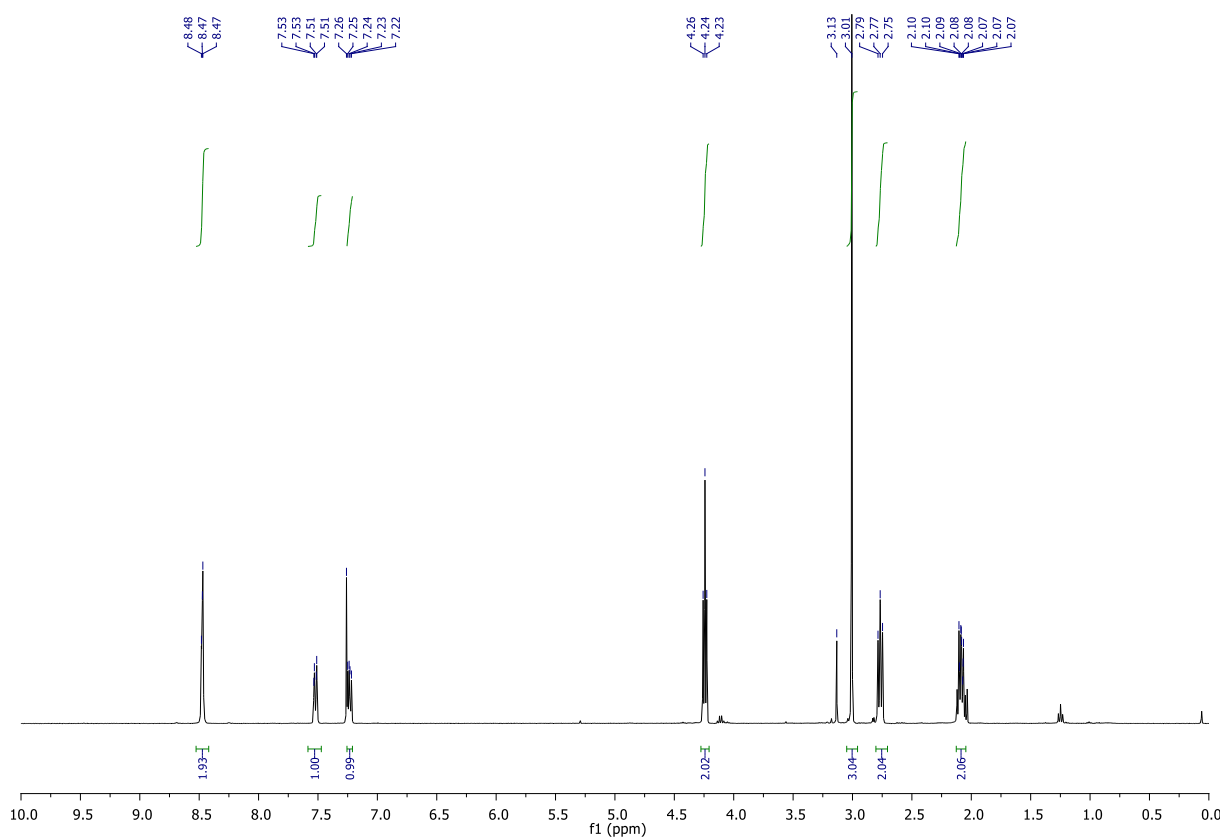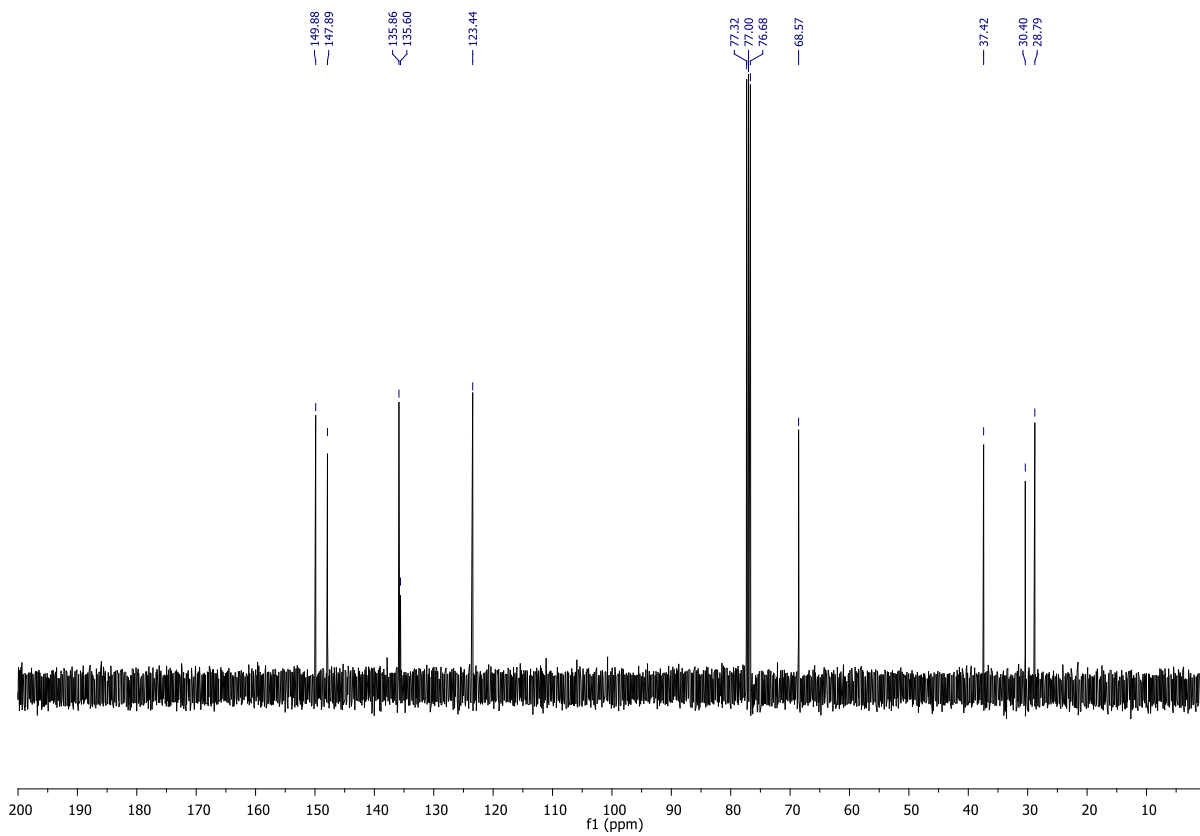
Synthesis of b3
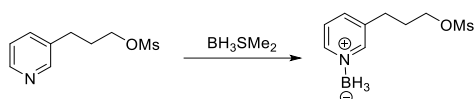
a3 (2.41 g, 11.1 mmol) was flushed with nitrogen. Then THF (20 mL) was added, which produced slurry solution. The reaction mixture was cooled to −78 °C. To this solution, $BH_3 \cdot SMe_2$ (6.0 mL, 2.0M solution in THF, 12 mmol) was added dropwise at −78 °C. After 30 minutes of stirring, the cooling bath was removed. After stirring at RT for 1 hour, the conversion was checked by TLC (10:1 EtOAc/MeOH) and additional $BH_3 \cdot SMe_2$ (1.0 mL, 2.0M solution in THF, 2 mmol; altogether 14 mmol) was added dropwise at −78 °C. The solution was stirred for 15 minutes and the cooling bath was removed. After additional 30 minutes of stirring, the mixture was cooled again to −78 °C and methanol (9 mL) was added dropwise. After 15 minutes, the cooling bath was removed and the mixture was allowed to heat to room temperature and then solvents were removed under reduced pressure. A combiflash of the residue on silica (Celite loading, PE/EtOAc; EtOAc: 0%→100%) provided the title compound (2.25 g, 88% yield) as transparent oil, which crystalise upon standing in a freezer over a couple of days/weeks to form a white solid.

^{1}H NMR (CDCl$_3$, 400 MHz, 298 K): δ 8.45 − 8.43 (m, 2H), 7.78 (d, J = 8.0 Hz, 1H), 7.45 (dd, J = 8.0, 6.0 Hz, 1H), 4.25 (td, J = 6.0, 1.0 Hz, 2H), 3.02 (d, J = 1.0 Hz, 3H), 2.84 (t, J = 8.0 Hz, 2H), 2.75 − 2.15 (br, 3H), 2.16 − 2.02 (m, 2H).
^{1}H NMR (CDCl$_3$, 400 MHz, 298 K, ^{11}B decoupled): δ 8.45 − 8.43 (m, 2H), 7.78 (d, J = 8.0 Hz, 1H), 7.45 (dd, J = 8.0, 6.0 Hz, 1H), 4.24 (t, J = 6.0 Hz, 2H), 3.02 (d, J = 1 Hz, 3H), 2.83 (t, J = 8.0 Hz, 2H), 2.55 (s, 3H), 2.16 − 2.02 (m, 2H).
^{13}C NMR (CDCl$_3$, 101 MHz, 298 K): δ 147.2, 145.4, 139.2, 138.5, 125.2, 68.11, 37.4, 29.9, 28.6.
^{11}B NMR (CDCl$_3$, 128 MHz, 298 K, normal glass): δ −12.4 (d, J = 88 Hz)

HR-MS (ESI): Calculated for $C_9H_{15}BNO_3S$ [M–H]$^+$ 228.0866, found: 228.0865 (Δ = 0.4 ppm)

FT-IR (thin film): 2936, 2360, 2310, 2271, 1620, 1585, 1486, 1443, 1346, 1331, 1164.

MP: 51 − 53 °C

LCMS Method: Col1-MeCN-FAST

^{1}H NMR

^{1}H NMR (^{11}B decoupled)

^{13}C NMR

147.18
145.40
139.16
138.46
125.17
77.32
77.00
76.68
68.11
37.41
29.89
28.63

f1 (ppm)

^{11}B NMR (normal glass)

-12.07
-12.75

f1 (ppm)
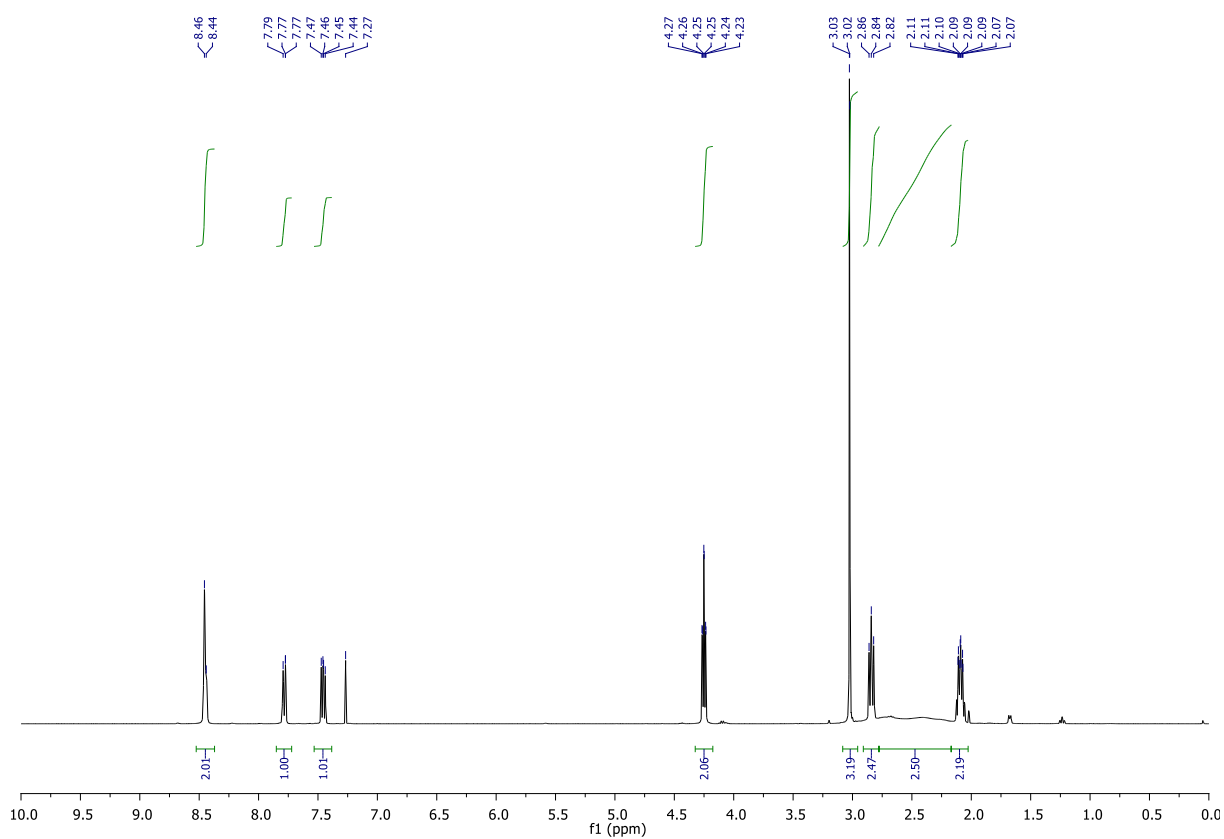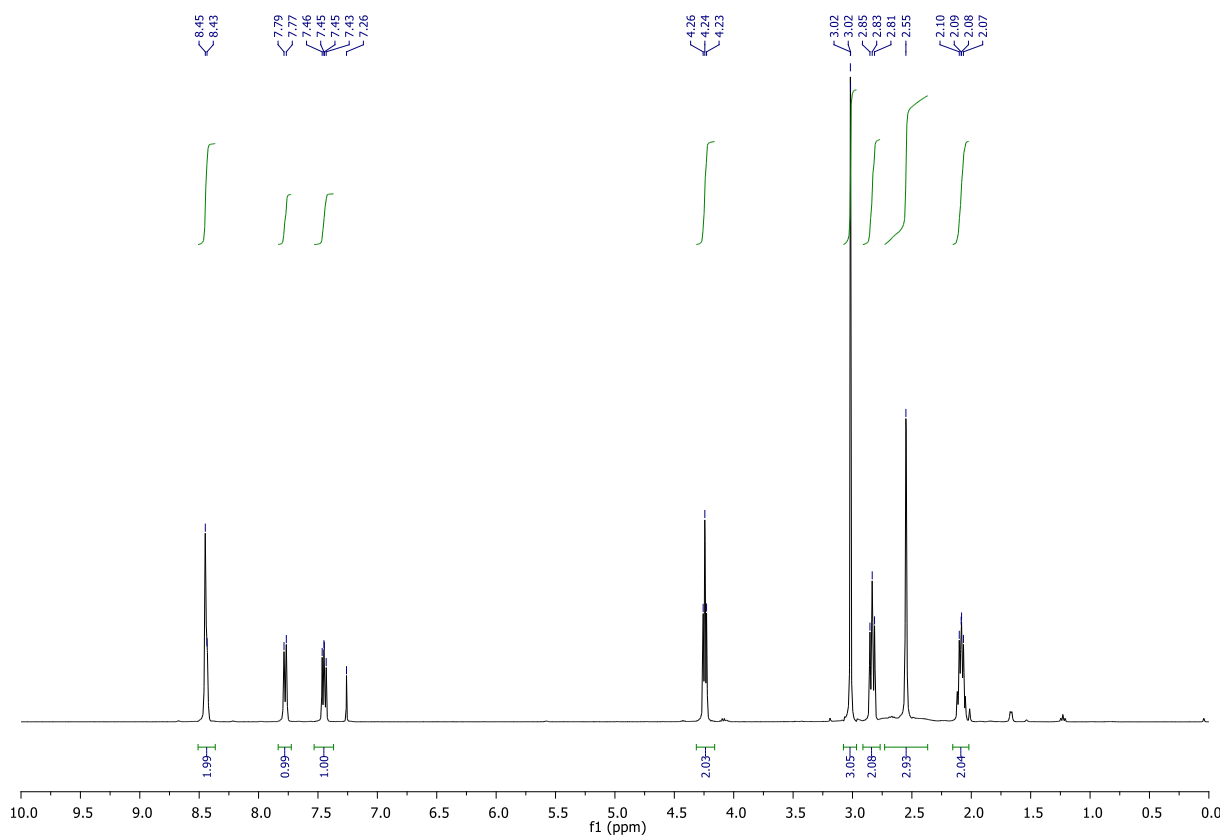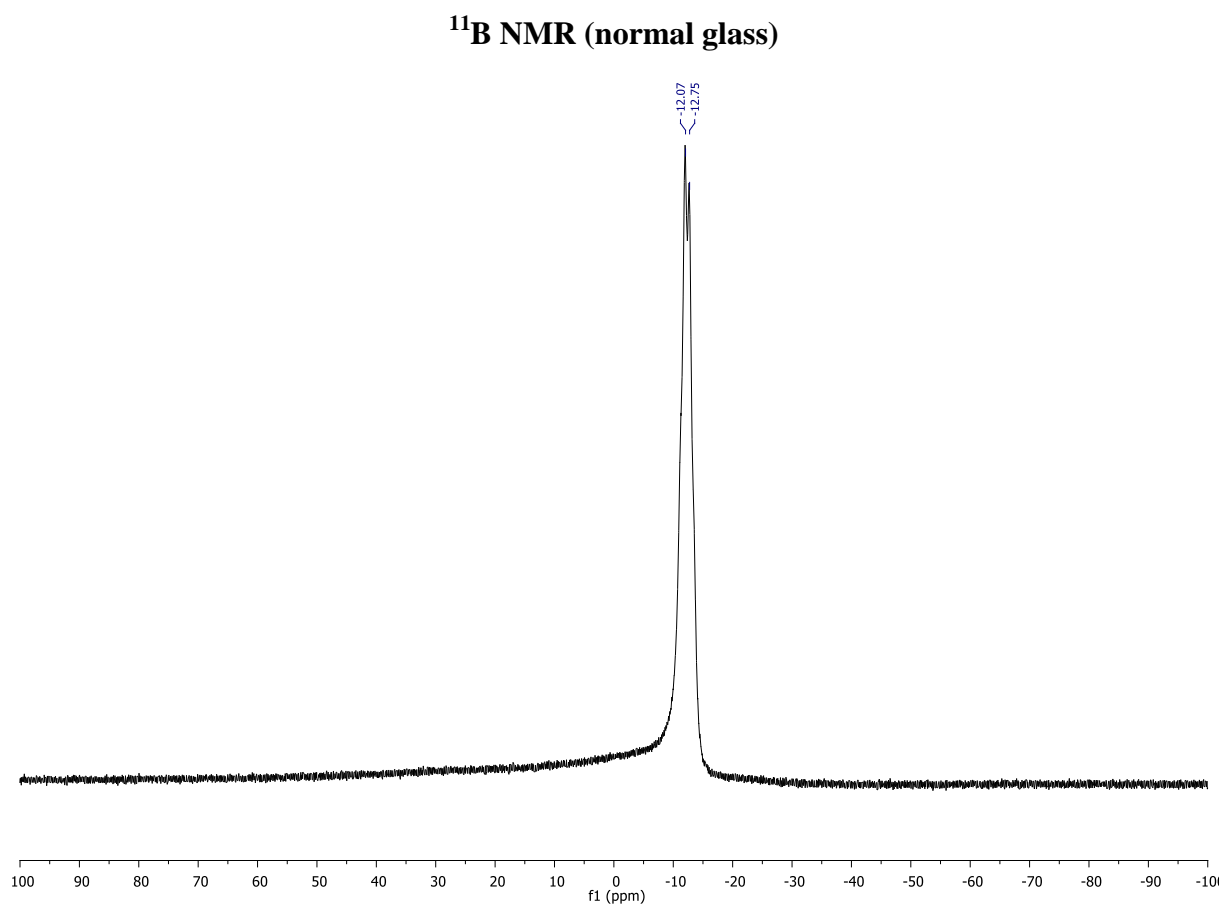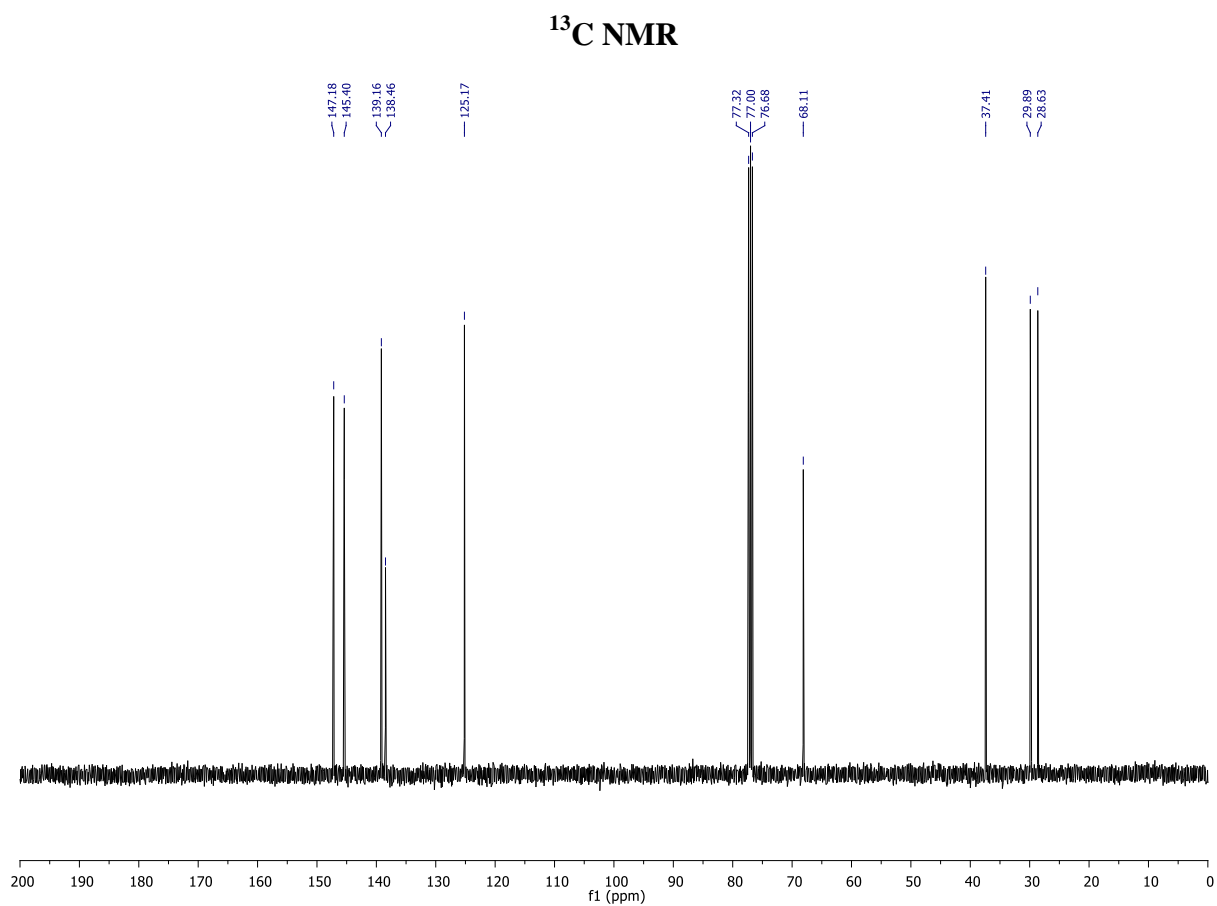
Synthesis of c3-BH₃ and c3
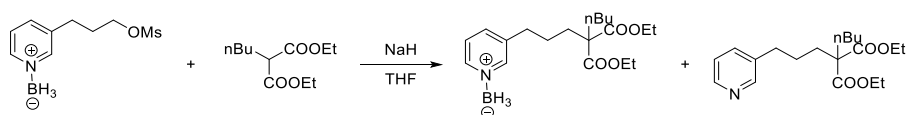
NaH (60% in mineral oil, 255 mg, 6.38 mmol) was flushed with nitrogen. THF (10 mL) was added and the mixture was cooled to 0 °C. Then diethyl-2-butylmalonate (1.45 mL, 6.52 mmol) was added dropwise (the solution became clear after the addition). **b3** (718 mg, 3.13 mmol) was added as a solid. After 1 hour of stirring, the cooling bath was removed. The mixture was heated at 60 °C for 4 hours and after cooling to RT, water (20 mL) was added and the mixture was extracted with dichloromethane (4 × 30 mL). The organic phase was dried over MgSO₄ and the solvents were removed under reduced pressure. A combiflash of the residue on silica (Celite loading, PE/EtOAc, EtOAc: 0%→50%) provided after drying in vacuum oven overnight products **c3-BH₃** (655 mg, 60% yield) and **c3** (219 mg, 21% yield) as transparent dense liquids (**c3-BH₃** crystalise upon storage in freezer over a couple of weeks).

LCMS Method: Col1-MeCN-SLOW

Compound **c3-BH₃**:

^{1}**H NMR (CDCl₃, 400 MHz, 298 K)**: δ 8.42 − 8.40 (m, 2H), 7.70 (d, J = 8.0 Hz, 1H), 7.40 (dd, J = 8.0, 6.0 Hz, 1H), 4.21 − 4.06 (m, 4H), 3.00 − 2.11 (br, 3H), 2.66 (t, J = 8.0 Hz, 2H), 1.91 − 1.78 (m, 4H), 1.59 − 1.46 (m, 2H), 1.32 − 1.23 (m, 2H), 1.20 (t, J = 7.0 Hz, 6H), 1.11 − 1.03 (m, 3H), 0.85 (t, J = 7.0 Hz, 3H).

^{1}**H NMR (CDCl₃, 400 MHz, 298 K, ^{11}B decoupled)**: δ 8.42 − 8.40 (m, 2H), 7.70 (d, J = 8.0 Hz, 1H), 7.40 (dd, J = 8.0, 6.0 Hz, 1H), 4.21 − 4.08 (m, 4H), 2.66 (t, J = 8.0 Hz, 2H), 2.55 (s, 3H), 1.92 − 1.77 (m, 4H), 1.60 − 1.45 (m, 2H), 1.34 − 1.23 (m, 2H), 1.20 (t, J = 7.0 Hz, 6H), 1.15 − 1.01 (m, 2H), 0.86 (t, J = 7.0 Hz, 3H).

^{13}**C NMR (CDCl₃, 101 MHz, 298 K)**: δ 171.4, 147.1, 145.1, 139.6, 138.8, 124.9, 61.1, 57.2, 32.8, 32.2, 31.7, 26.1, 25.1, 22.8, 14.00, 13.8.

^{11}**B NMR (CDCl₃, 128 MHz, 298 K, normal glass)**: δ −12.4 (d, J = 79 Hz)

HR-MS: Calculated for C₂₁H₃₄BN₂O₄ [M+CH₃CN–H]$^+$ 389.2612, found: 389.2627 (Δ = 3.9 ppm)

FT-IR (thin film): 2959, 2935, 2872, 2371, 1725, 1619, 1484, 1463, 1444 cm^{-1}.

MP: 37 – 40 °C

Compound **c3**:

^{1}H NMR (CDCl$_3$, 400 MHz, 298 K): δ 8.38 – 8.36 (m, 2H), 7.41 (d, J = 8.0 Hz, 1H), 7.13 (dd, J = 8.0, 5.0 Hz, 1H), 4.09 (q, J = 7.0 Hz, 4H), 2.56 (t, J = 7.5 Hz, 2H), 1.91 – 1.71 (m, 4H), 1.55 – 1.37 (m, 2H), 1.28 – 1.17 (m, 2H), 1.14 (t, J = 7.0 Hz, 6H), 1.06 – 0.98 (m, 2H), 0.81 (t, J = 7.5 Hz, 3H).

^{13}C NMR (CDCl$_3$, 101 MHz, 298 K): δ 171.5, 149.8, 147.3, 136.8, 135.6, 123.1, 60.9, 57.2, 32.9, 31.9, 31.5, 25.9, 25.4, 22.7, 13.9, 13.7.

HR-MS: Calculated for C$_{19}$H$_{30}$NO$_4$ [M+H]$^+$ 336.2175, found: 336.2173 (Δ = 0.6 ppm)

FT-IR (thin film): 2958, 2935, 2872, 1725, 1575, 1478, 1463, 1423 cm^{-1}.

c3-BH₃: ¹H NMR

c3-BH₃: ¹H NMR (¹¹B decoupled)

165

c3-BH$_3$: ^{13}C NMR

171.43

147.14
145.08
139.59
138.83

124.89

77.32
77.00
76.68

61.09
57.16

32.77
32.19
31.68
26.07
25.06
22.79

13.99
13.76

f1 (ppm)
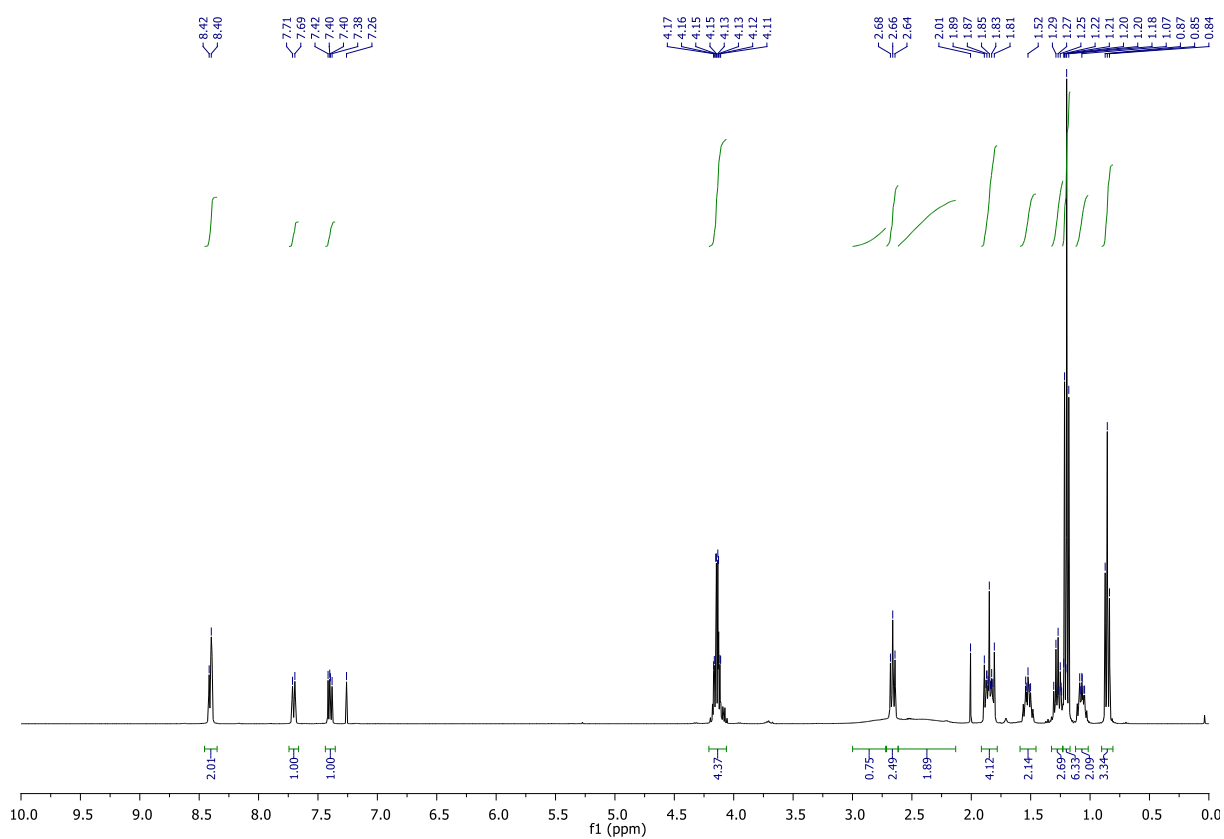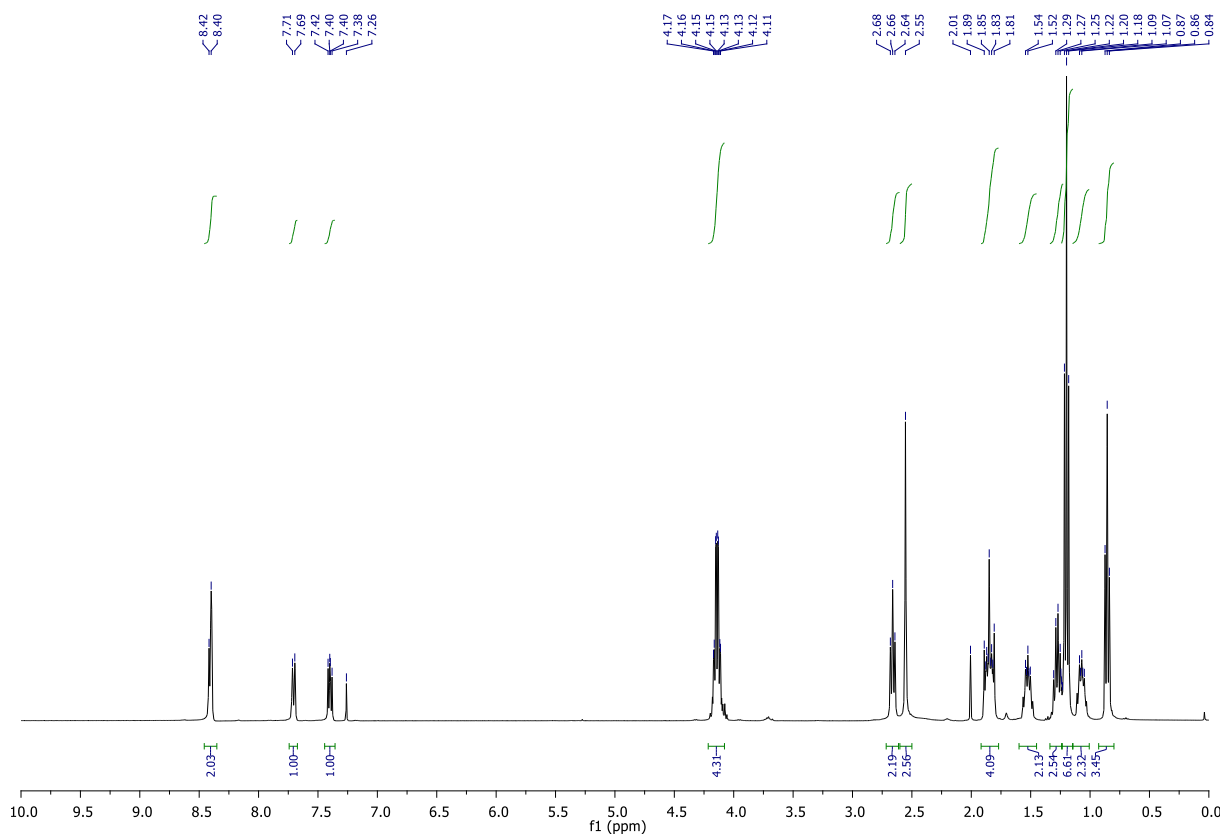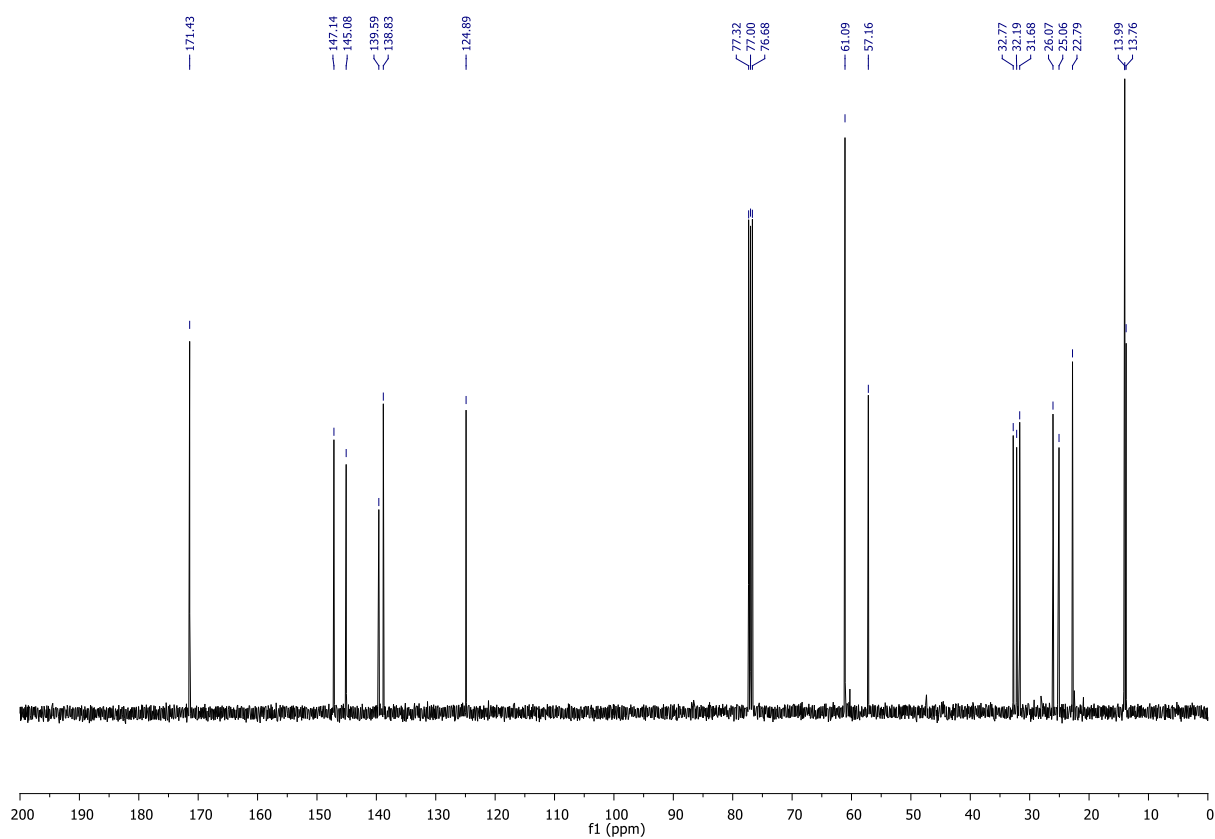
c3-BH$_3$: ^{11}B (normal glass)

-12.13
-12.75

f1 (ppm)
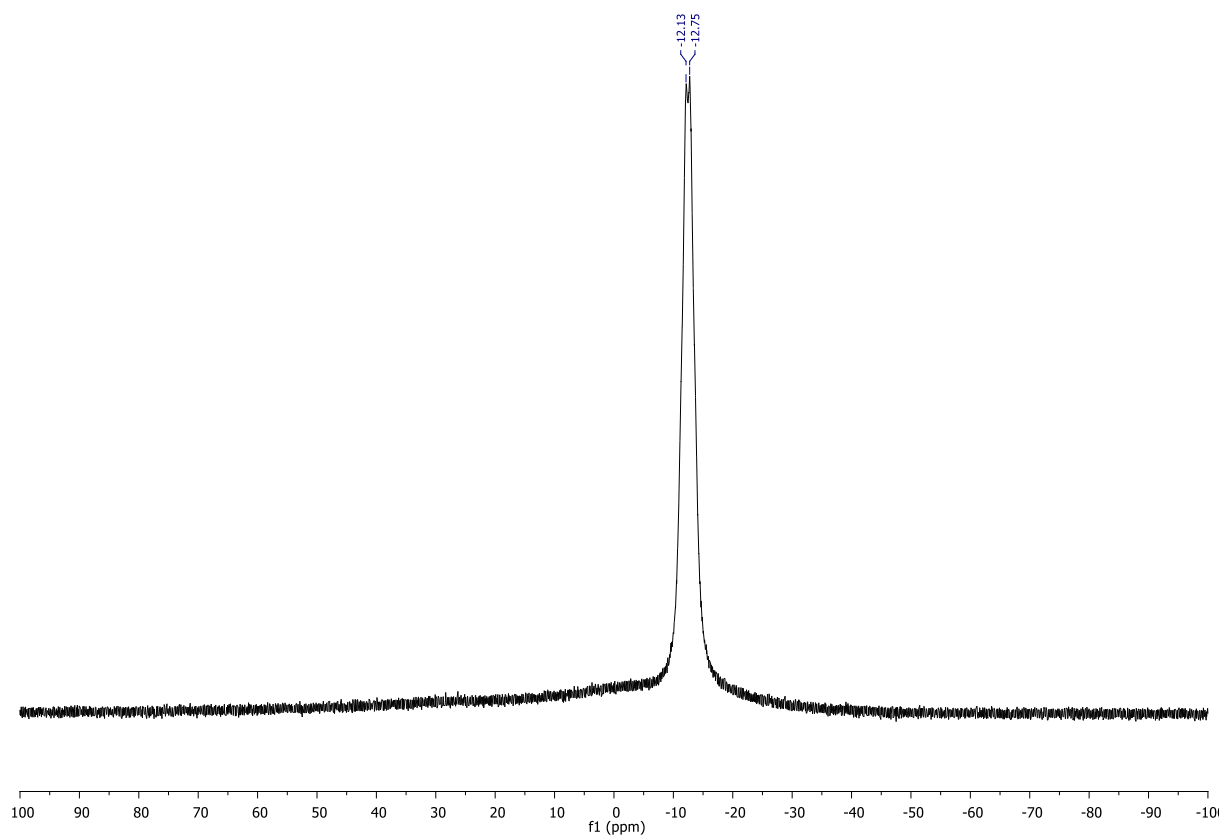
c3: ¹H NMR
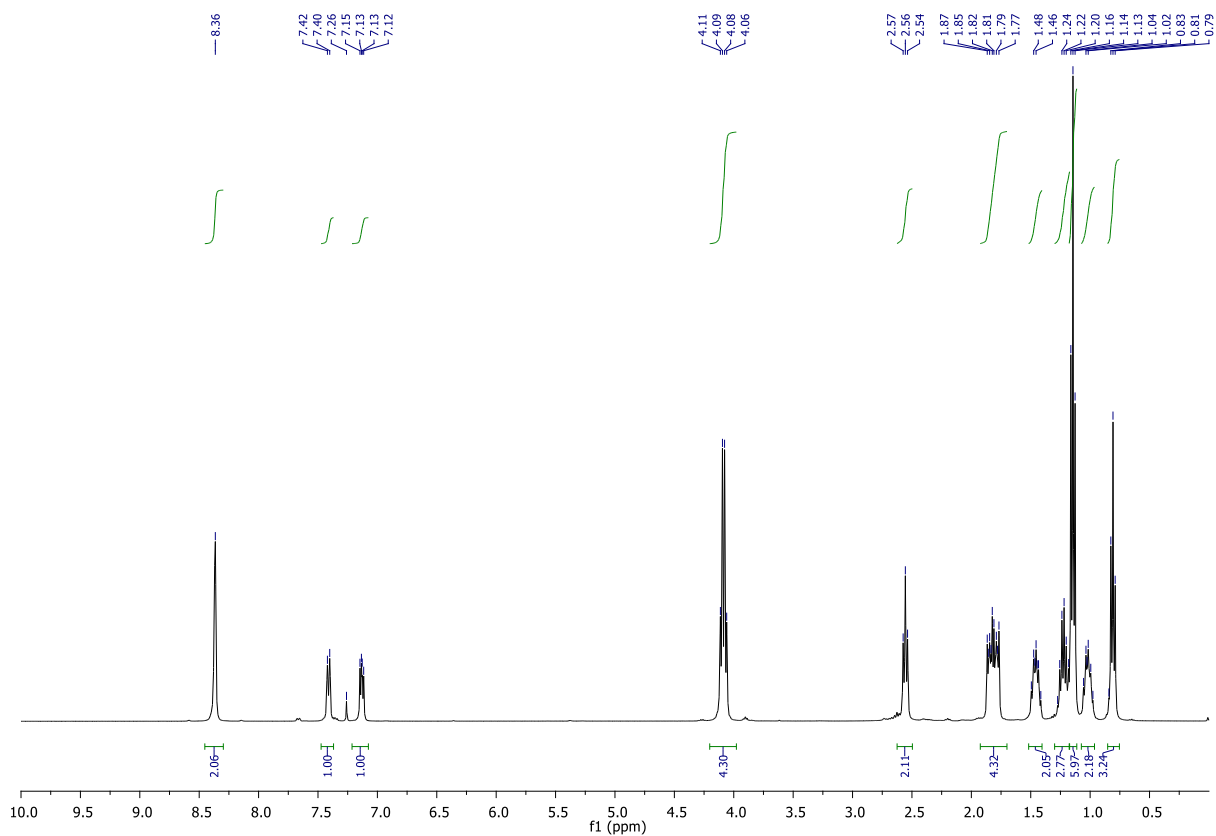
c3: ¹³C NMR
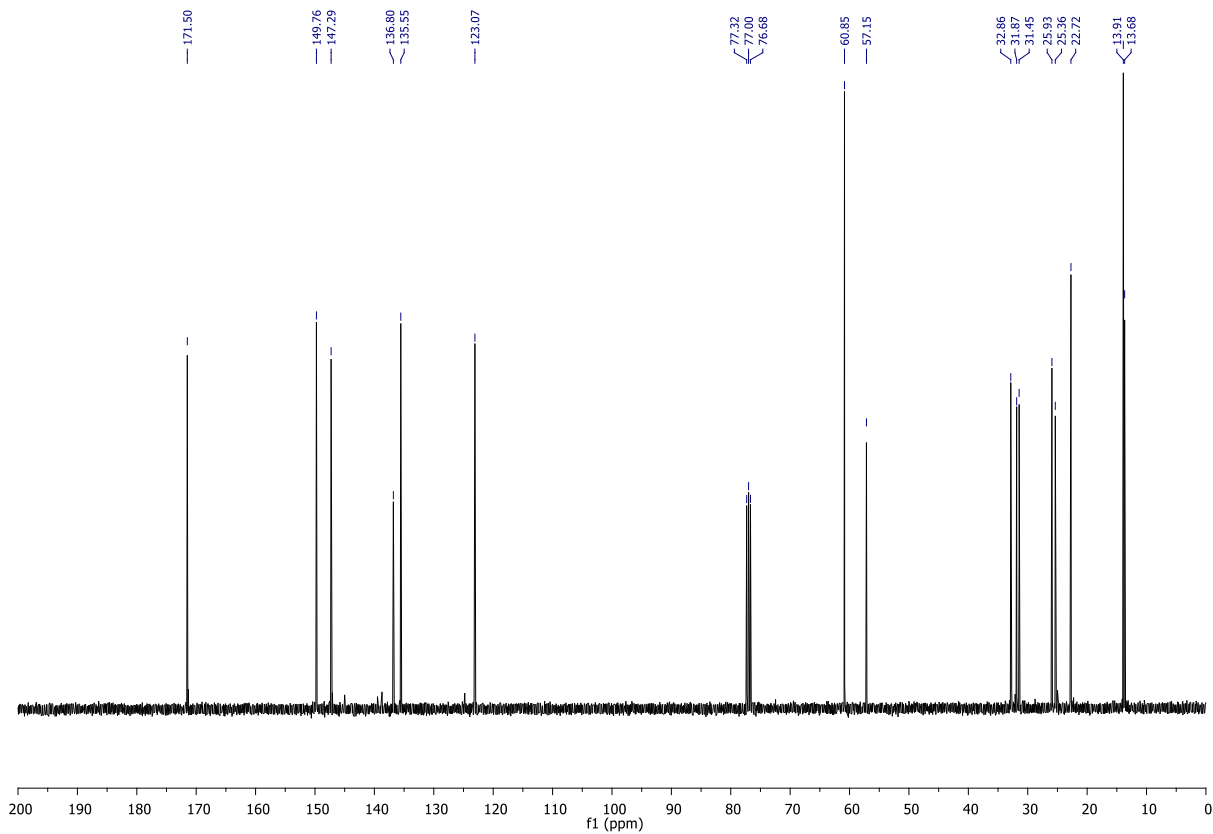
Synthesis of 3B3-BH₃ and 3B3
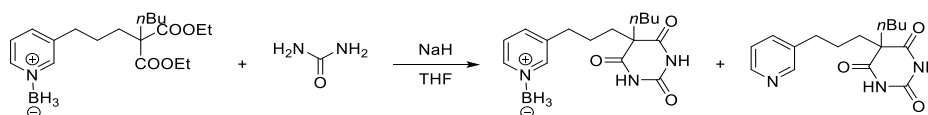
NaH (60% in mineral oil, 300 mg, 7.5 mmol) was flushed with nitrogen and DMF (6 mL) was added. The mixture was cooled to 0 °C and urea (1.18 g, 19.6 mmol) was added. After 2 hours of stirring, **c3-BH₃** (646 mg, 1.85 mmol) in DMF (7 mL) was added at 0 °C. The mixture was stirred overnight at RT and a saturated solution of NH₄Cl (5 mL) was added with cooling to 0 °C. Water (10 mL) was added and the mixture was extracted with dichloromethane (3 × 40 mL). The collected organic phase was dried over MgSO₄ and the solvents were removed under reduced pressure (60 °C, <14 mBar). A combliflash of residue on silica (Celite loading, PE/EtOAc, EtOAc: 0%→100%) provided after drying in vacuum oven overnight products **3B3-BH₃** (350 mg, 60% yield) and **3B3** (117 mg, 21% yield) as white crystalline solids.

LCMS Method: Col3-MeCN-FAST

Compound **3B3-BH₃**:

^{1}H NMR (CD₃OD, 400 MHz, 298 K): δ 8.42 (s, 2H), 7.88 (d, J = 8.0 Hz, 1H), 7.53 (dd, J = 8.0, 6.0 Hz, 1H), 2.95 – 2.09 (br, 3H), 2.69 (t, J = 7.5 Hz, 2H), 1.97 – 1.86 (m, 4H), 1.58 – 1.50 (m, 2H), 1.32 – 1.22 (m, 2H), 1.22 – 1.13 (m, 2H), 0.87 (t, J = 7.0 Hz, 3H).

^{1}H NMR (CD₃OD, 400 MHz, 298 K, ^{11}B decoupled): δ 8.42 (s, 2H), 7.88 (d, J = 8.0 Hz, 1H), 7.53 (dd, J = 8.0, 6.0 Hz, 1H), 2.69 (t, J = 7.5 Hz, 2H), 2.54 (s, 3H), 1.97 – 1.86 (m, 4H), 1.58 – 1.51 (m, 2H), 1.32 – 1.22 (m, 2H), 1.22 – 1.13 (m, 2H), 0.87 (t, J = 7.0 Hz, 3H).

^{13}C NMR (CD₃OD, 101 MHz, 298 K): δ 174.9, 151.2, 148.4, 146.4, 141.0, 140.6, 126.5, 56.7, 40.1, 38.6, 33.1, 28.1, 27.1, 23.6, 14.0.

^{11}B NMR (CD₃OD, 128 MHz, 298 K, normal glass): δ −12.6

HR-MS: Calculated for C₁₆H₂₃BN₃O₃ [M–H]$^+$ 316.1832, found: 316.1844 (Δ = 3.8 ppm)

FT-IR (thin film): 3326, 3104, 2959, 2931, 2860, 2368, 1753, 1699, 1619, 1585, 1486, 1441, 1421, 1384, 1335, 1336, 1321 cm^{-1}.

MP: > 161°C (decompose and produce gas)

Compound **3B3**:
This product is characterised below.

3B3-BH₃: ¹H NMR
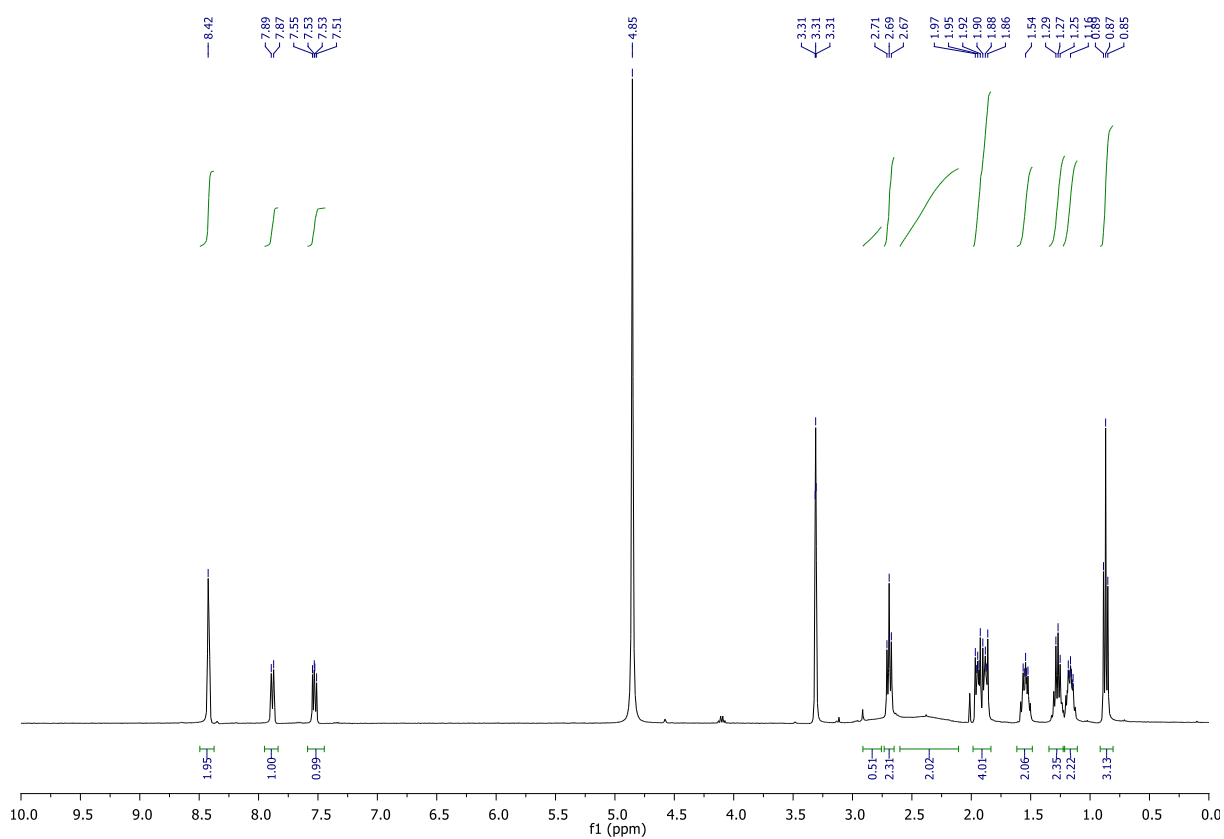
3B3-BH₃: ¹H NMR (¹¹B decoupled)

3B3-BH₃: ¹³C NMR

Peaks: 174.87, 151.22, 148.40, 146.43, 141.04, 140.56, 126.51, 56.86, 49.43, 49.00, 48.79, 48.57, 38.60, 33.09, 28.08, 27.05, 23.64, 13.97
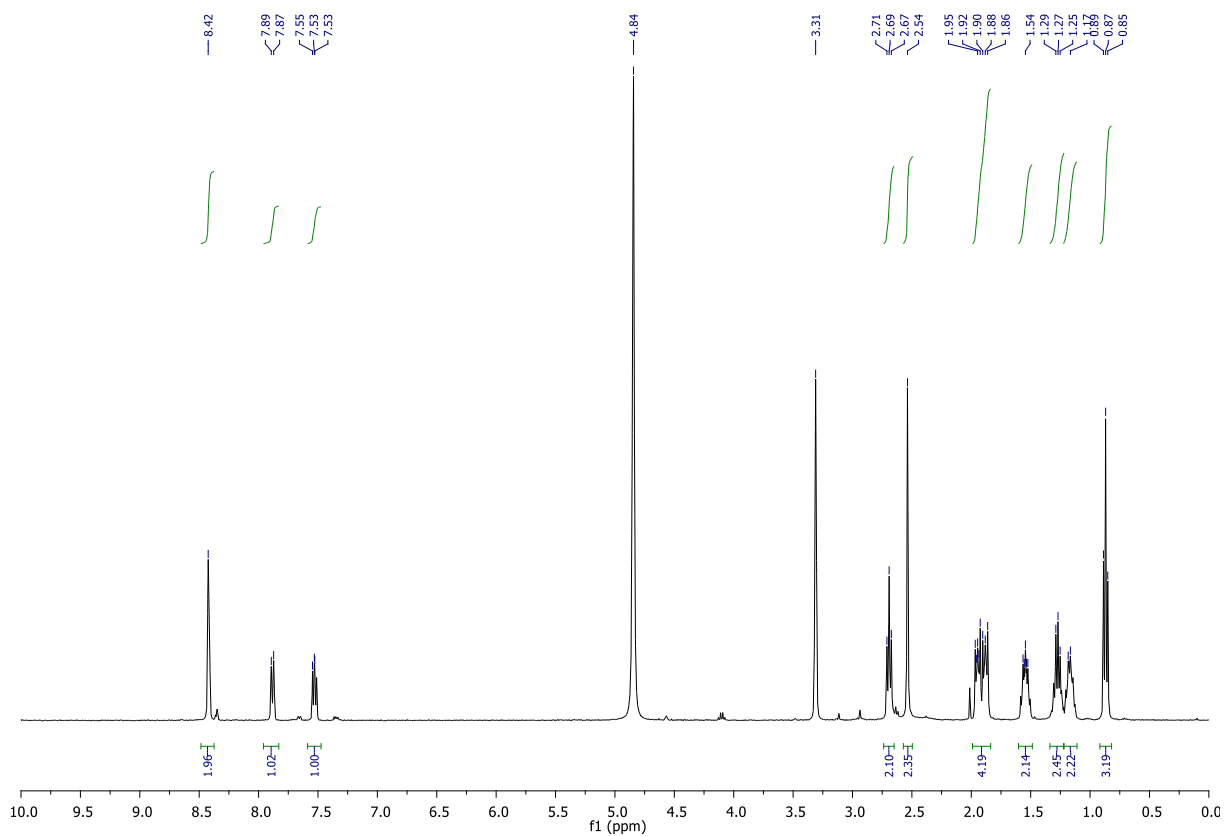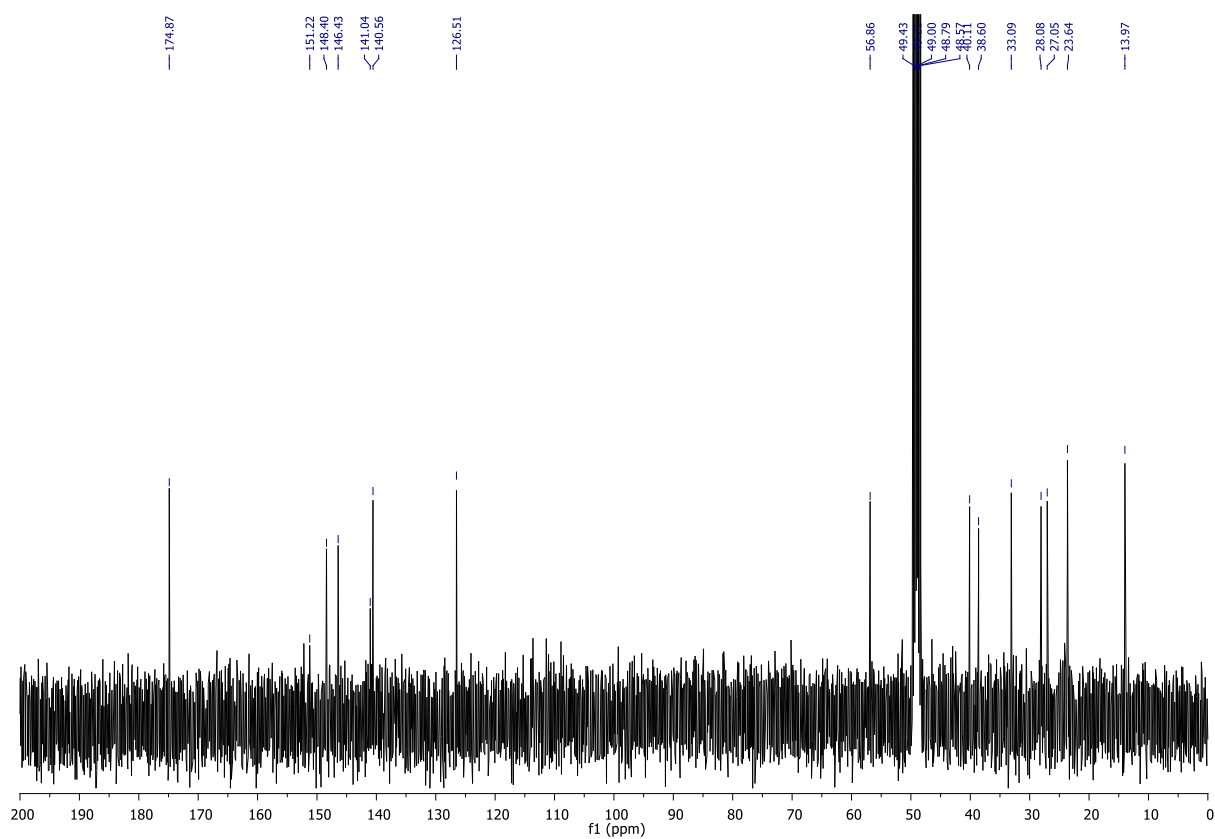
3B3-BH₃: ¹¹B (normal glass)

Peak: -12.16
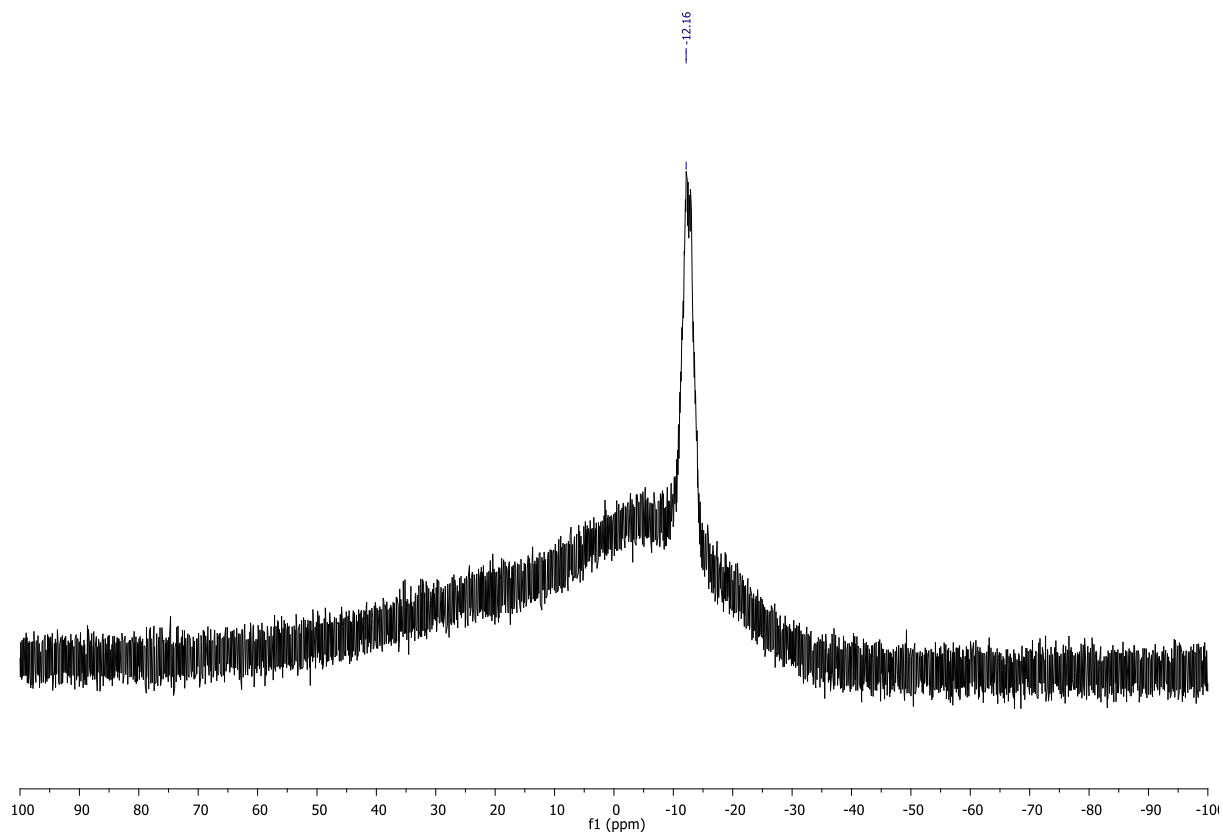
Synthesis of 3B3
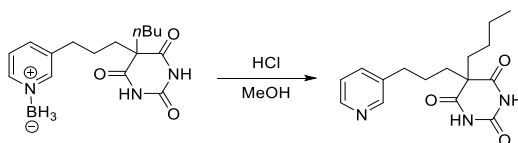
To a mixture of **3B3-BH$_3$** (274 mg, 0.86 mmol) and methanol (15 mL) [note: *not dissolved even at* RT] at 0 °C, HCl (*conc.*, 100 µL, 1.2 mmol) was added. After 15 minutes, the cooling bath was removed and the mixture was stirred at RT until full conversion was reached (2 hours), which was checked by LCMS. A saturated solution of NaHCO$_3$ (4 mL) was added (pH > 8) and then a saturated solution of NH$_4$Cl (30 mL) was added (pH < 7). The mixture was extracted with dichloromethane (4 × 50 mL), dried over MgSO$_4$, the solvents were removed under reducer pressure. A combiflash of the residue on silica (Celite loading, PE/EtOAc, EtOAc: 0%→100%) provided after drying in vacuum oven overnight the title compound (170 mg, 65% yield) as a white crystalline solid.

^{1}H NMR (CD$_3$OD, 400 MHz, 298 K): δ 8.37 – 8.35 (m, 2H), 7.67 – 7.64 (m, 1H), 7.35 (ddd, J = 8.0, 5.0, 1.0 Hz, 1H), 2.64 (t, J = 7.5 Hz, 2H), 2.00 – 1.85 (m, 4H), 1.58 – 1.50 (m, 2H), 1.33 – 1.22 (m, 2H), 1.21 – 1.10 (m, 2H), 0.86 (t, J = 7.0 Hz, 3H).

^{13}C NMR (CD$_3$OD, 101 MHz, 298 K): δ 175.0, 151.4, 150.0, 147.8, 139.0, 138.2, 125.2, 56.9, 40.0, 39.0, 33.4, 28.1, 27.4, 23.7, 14.0.

HR-MS (ESI): Calculated for C$_{16}$H$_{22}$N$_3$O$_3$ [M+H]$^+$ 304.1661, found: 304.1668 (Δ = 2.3 ppm)

FT-IR (thin film): 3222, 3103, 2959, 2930, 2859, 1698, 1596, 1580, 1413, 1385, 1357, 1325 cm^{-1}.

MP: 184 – 186 °C

EA: Required for C$_{16}$H$_{21}$N$_3$O$_3$: C 63.35, H 6.98, N 13.85; found: C 62.92, H 7.09, N 13.66.

LCMS Method: Col3-MeCN-FAST

^{1}H NMR
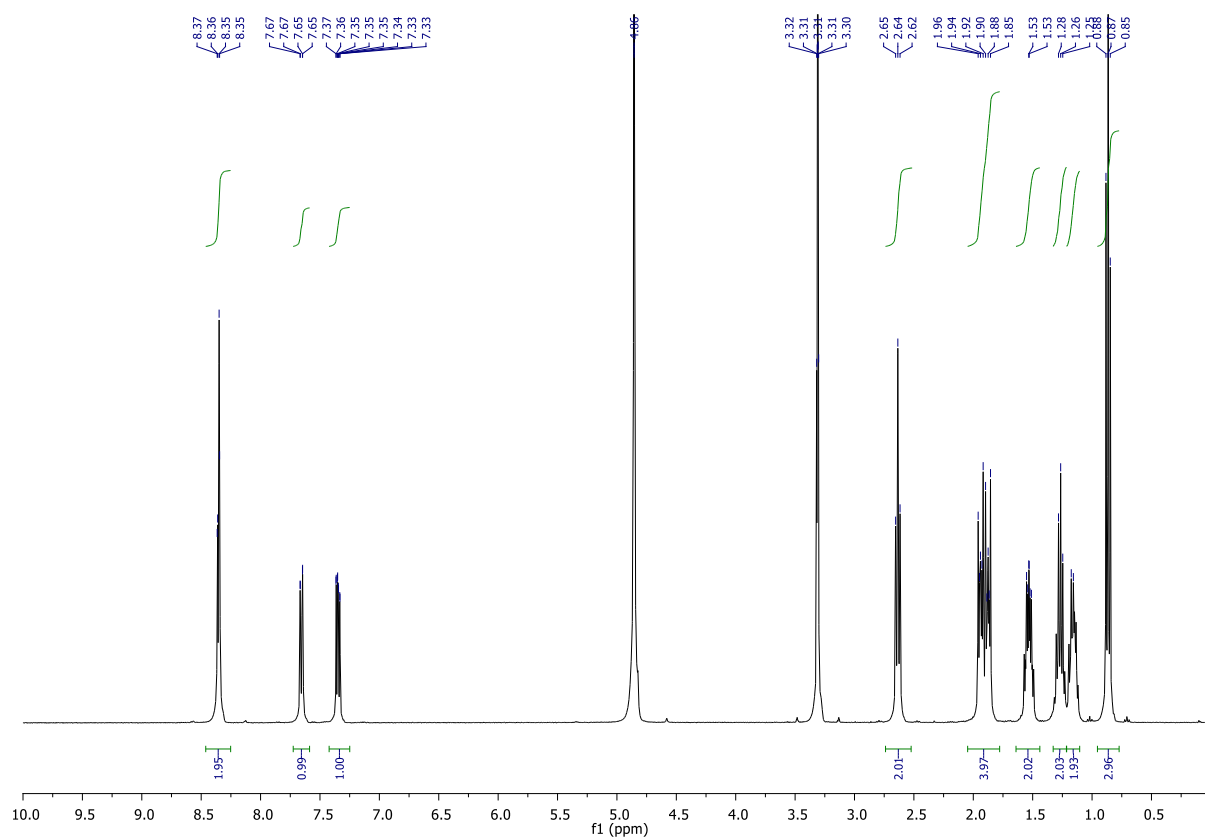
^{13}C NMR
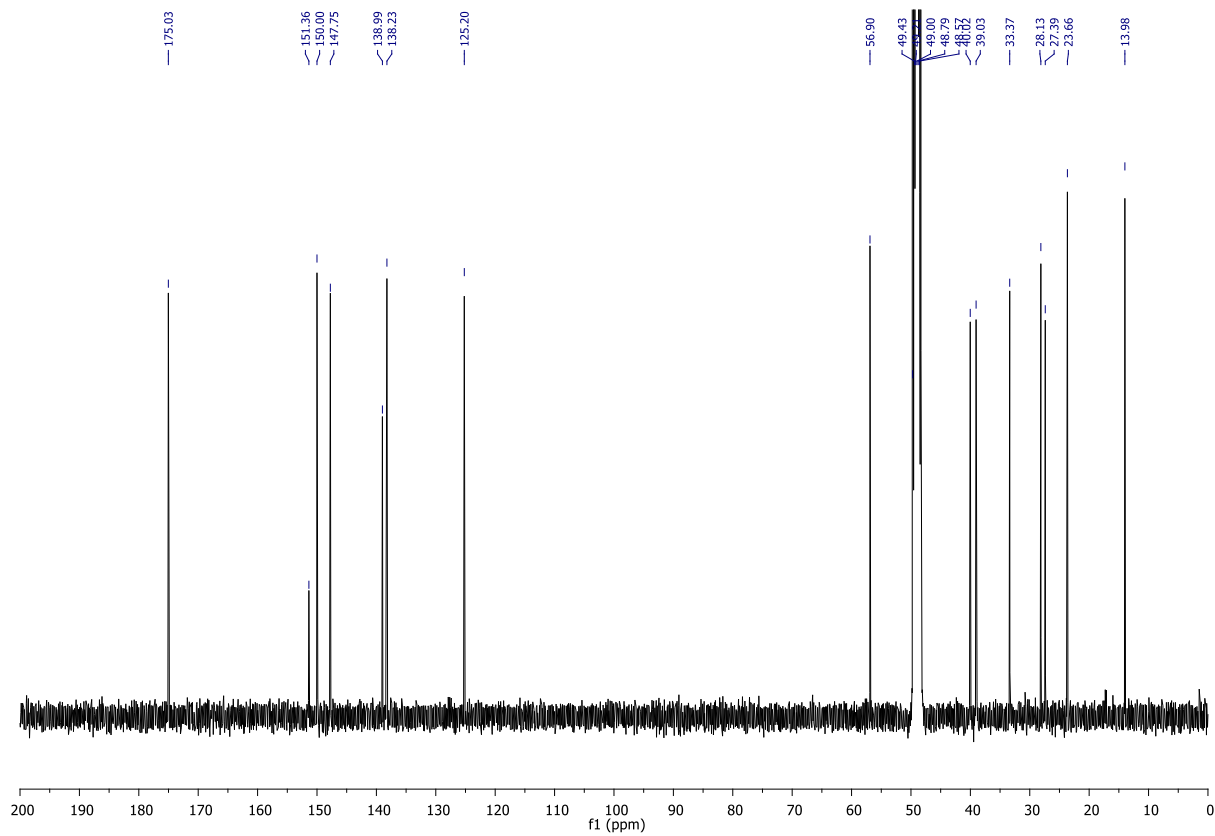
Synthesis of a4
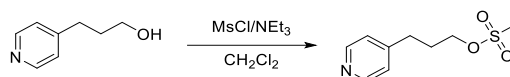
To a solution of 3-(pyridin-4-yl)propan-1-ol (1.29 g, 9.4 mmol) and NEt$_3$ (4 mL) in CH$_2$Cl$_2$ (50 mL) was added methanesulfonyl chloride (1.2 mL, 15.5 mmol, 1.6 eq) at 0 °C in small parts over the period of 90 minutes. The still-cool solution was washed with H$_2$O (50 mL) and brine (25 mL), dried with MgSO$_4$ and solvents were removed under reducer pressure (at no more than 30 °C). A combiflash of the residue on silica gel (PE/EtOAc, EtOAc: 0%→100%) provided the title compound as transparent oil (1.53 g, 77% yield).

^{1}H NMR (CDCl$_3$, 400 MHz, 298 K): δ 8.50 (dd, J = 4.5, 1.5 Hz, 2H), 7.11 (d, J = 6.0 Hz, 2H), 4.22 (t, J = 6.0 Hz, 2H), 2.99 (s, 3H), 2.76 – 2.72 (m, 2H), 2.11 – 2.04 (m, 2H).
^{13}C NMR (CDCl$_3$, 101 MHz, 298 K): δ 149.9, 149.2, 123.7, 68.5, 37.4, 30.9, 29.6.

^{1}H NMR

8.51
8.51
8.50
8.49

7.26
7.12
7.11

4.24
4.22
4.21

3.00
3.00
2.99
2.76
2.74
2.72
2.11
2.10
2.09
2.08
2.08
2.07
2.06
2.06
2.04
2.02

2.00
2.06
2.03
3.14
2.31
2.35

f1 (ppm)

^{13}C NMR

149.92
149.18

123.74

77.32
77.00
76.68
68.49

37.37

30.87
29.57

f1 (ppm)
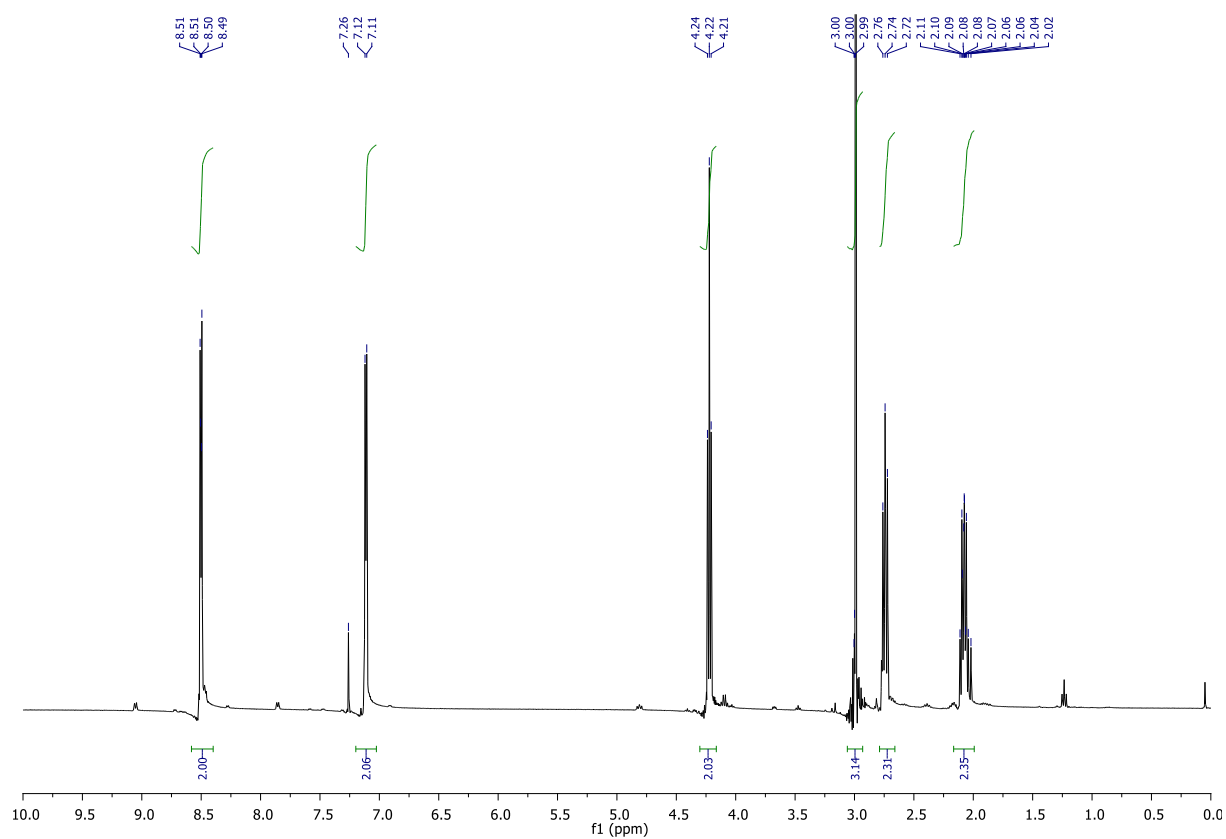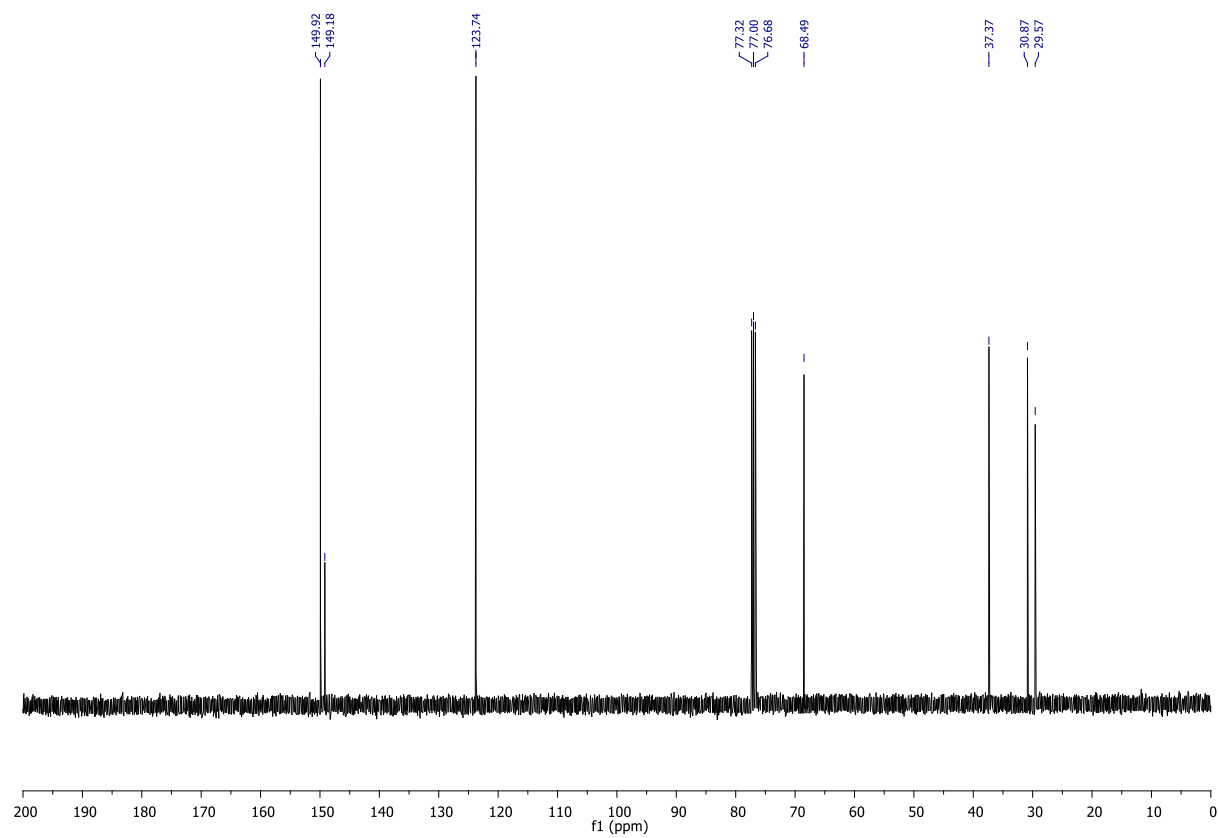
Synthesis of **b4**
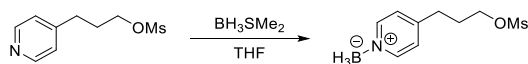
a4 (1.53 g, 7.11 mmol) was flushed with nitrogen. Then THF (10 mL) was added and the reaction mixture was cooled to −78 °C. To this solution, BH$_3$•SMe$_2$ (4.0 mL, 2.0M solution in THF, 8 mmol) was added dropwise at −78 °C. After 30 minutes of stirring, the cooling bath was removed. After stirring at RT for 2.5 hours, the mixture was cooled again to −78 °C and methanol (3 mL) was added dropwise. After 10 minutes, the cooling bath was removed and the mixture was allowed to heat to room temperature and then solvents were removed under reduced pressure. A combiflash of the residue on silica (Celite loading, PE/EtOAc; EtOAc: 0%→100%) provided the title compound (1.44 g, 88% yield) as transparent oil, which crystalise upon standing in the freezer over a couple of days/weeks to form a white solid.

^{1}H NMR (CDCl$_3$, 400 MHz, 298 K): δ 8.47 (d, J = 6.5 Hz, 2H), 7.34 (d, J = 6.5 Hz, 2H), 4.25 (t, J = 6.0 Hz, 2H), 3.02 (s, 3H), 2.90 − 2.86 (m, 2H), 2.63 (br, 3H), 2.14 − 2.07 (m, 2H).
^{1}H NMR (CDCl$_3$, 400 MHz, 298 K, ^{11}B decoupled): δ 8.47 (d, J = 6.0 Hz, 2H), 7.34 (d, J = 6.0 Hz, 2H), 4.25 (t, J = 6.0 Hz, 2H), 3.03 (s, 3H), 2.90 − 2.86 (m, 2H), 2.54 (s, 3H), 2.14 − 2.07 (m, 2H).
^{13}C NMR (CDCl$_3$, 101 MHz, 298 K): δ 153.7, 147.3, 125.3, 68.0, 37.5, 31.0, 29.2.
^{11}B NMR (CDCl$_3$, 128 MHz, 298 K, normal glass): δ −12.7 (d, J = 86 Hz).

HR-MS (ESI): Calculated for C$_9$H$_{15}$BNO$_3$S [M–H]$^+$ 228.0866, found: 228.0855 (Δ = 4.7 ppm)

FT-IR (thin film): 3021, 2938, 2361, 2312, 2282, 1631, 1349, 1170 cm^{-1}.

MP: 58 °C (melts and decomposes)

LCMS Method: Col3_ MeCN_FAST_5%-35%
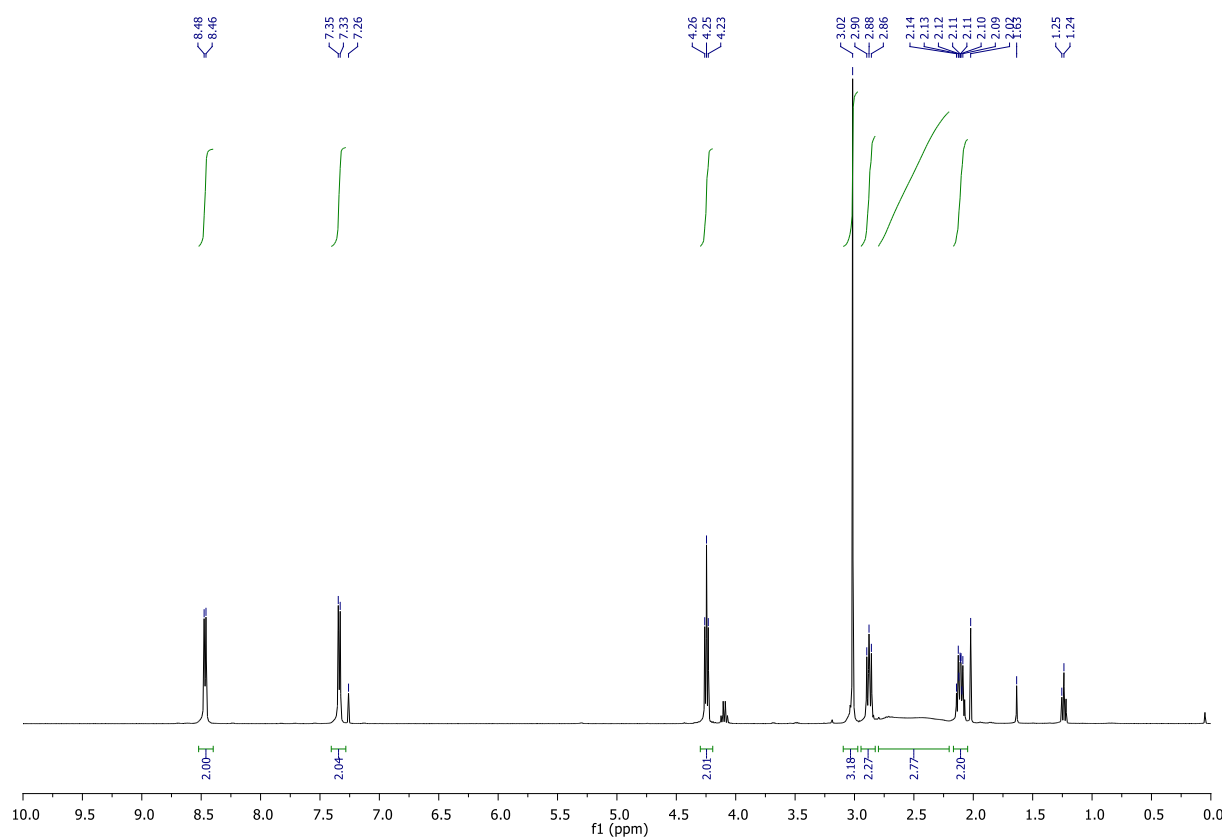
^{1}H NMR

^{1}H NMR (^{11}B decoupled)
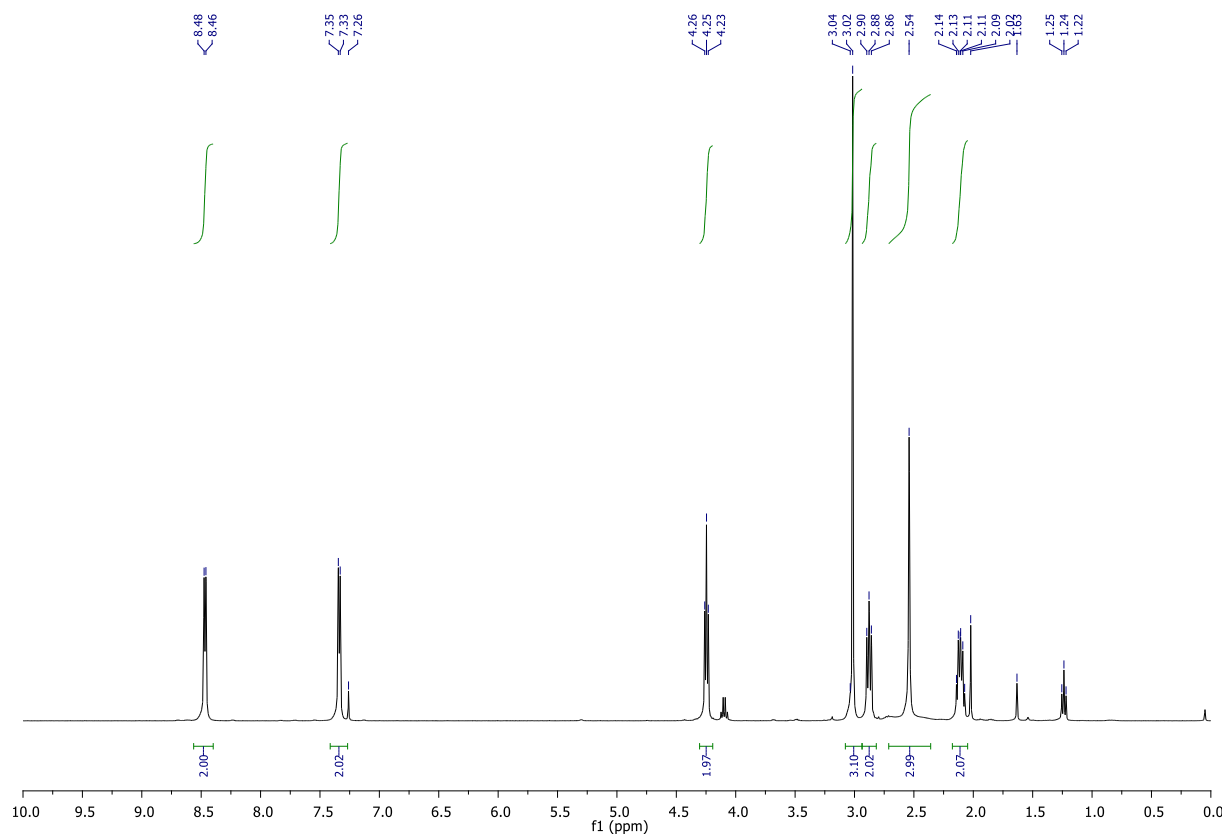
^{13}C NMR
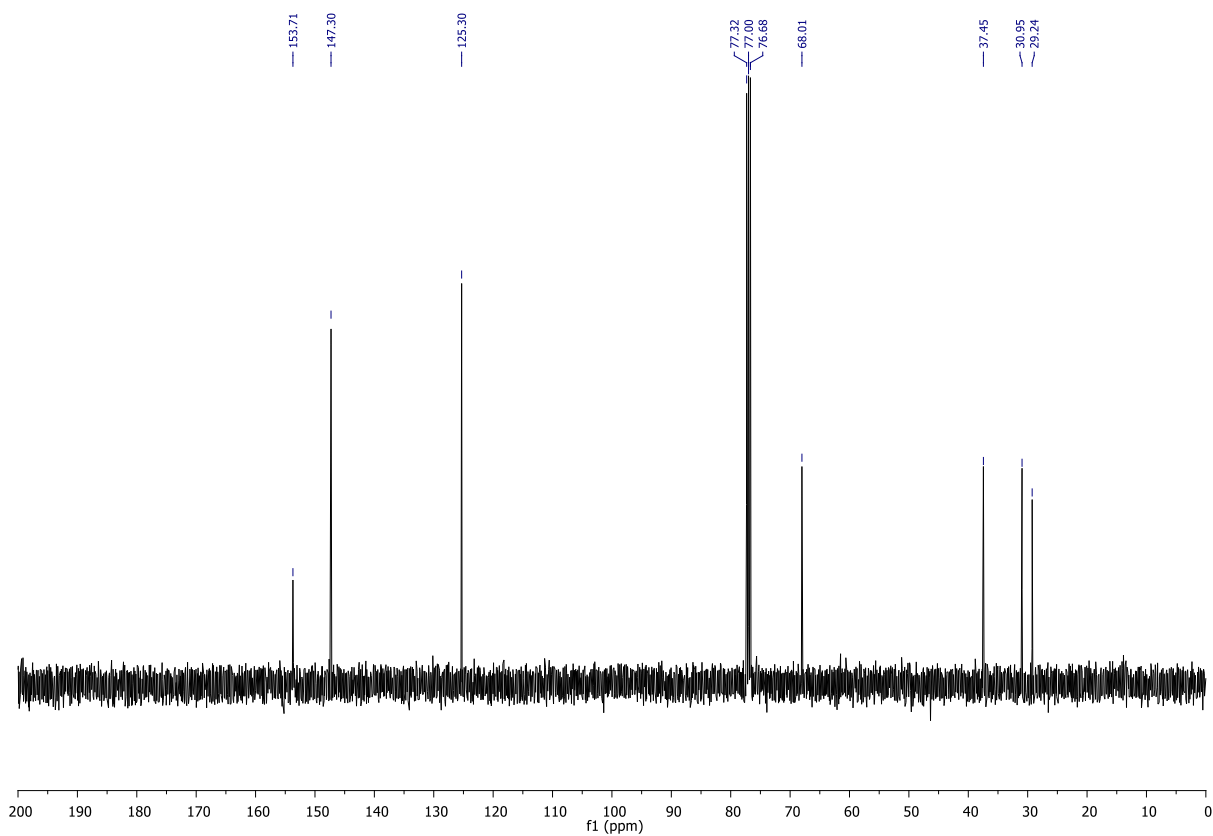
^{11}B NMR (normal glass)
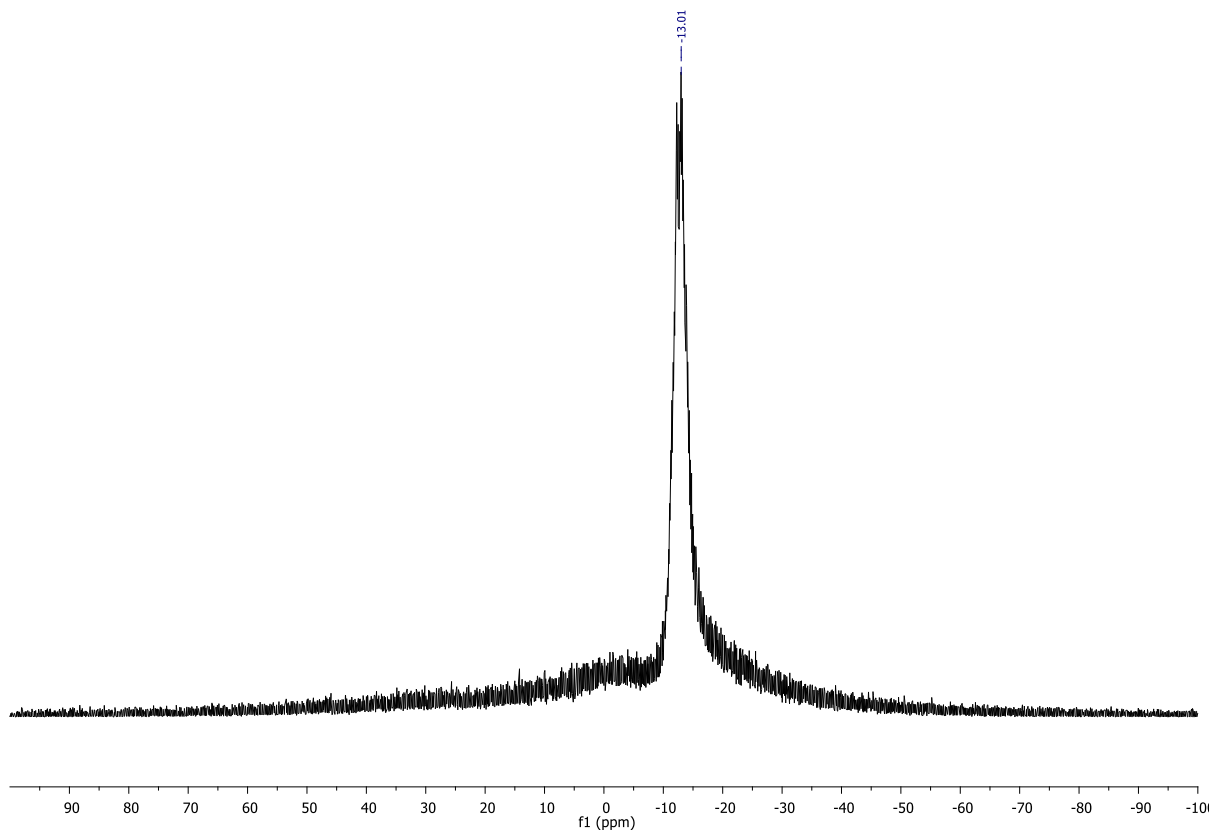
Synthesis of c4-BH$_3$ and c4
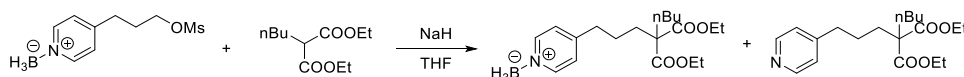
NaH (60% in mineral oil, 334 mg, 8.35 mmol) was flushed with nitrogen. THF (10 mL) was added and the mixture was cooled to 0 °C. Then diethyl-2-butylmalonate (1.9 mL, 8.54 mmol) was added dropwise. After 30 minutes of stirring **b4** (631 mg, 2.76 mmol) was added as a solid. The mixture was heated at 60 °C for 5 hours and then after cooling to RT, water (20 mL) was added and the mixture was extracted with dichloromethane (3 × 50 mL). The organic phase was dried over MgSO$_4$ and the solvents were removed under reduced pressure. A combiflash of the residue on silica (Celite loading, PE/EtOAc, EtOAc: 0%→50%) provided after drying in vacuum oven overnight products **c4-BH$_3$** (472 mg, 49% crude yield) as transparent oil and **c4** (110 mg, 23% crude yield) as yellowish oil. (*Both products contained an additional impurity and were used in the next reactions without further purification.*)

LCMS Method: Col1-MeCN-SLOW

Compound **c4-BH$_3$**:
^{1}H NMR (CDCl$_3$, 400 MHz, 298 K): δ 8.46 (d, J = 6.0 Hz, 2H), 7.29 (d, J = 6.5 Hz, 2H), 4.22 − 4.10 (m, 4H), 2.73 (t, J = 7.5 Hz, 2H), 1.90 − 1.83 (m, 4H), 1.62 − 1.54 (m, 2H), 1.33 − 1.25 (m, 2H), 1.22 (t, J = 7.0 Hz, 6H), 1.13 − 1.05 (m, 2H), 0.88 (t, J = 7.5 Hz, 3H).
^{1}H NMR (CDCl$_3$, 400 MHz, 298 K, ^{11}B decoupled): δ 8.46 (d, J = 6.0 Hz, 2H), 7.29 (d, J = 6.0 Hz, 2H), 4.21 − 4.10 (m, 4H), 2.73 (t, J = 7.5 Hz, 2H), 2.56 (s, 3H), 1.90 − 1.83 (m, 4H), 1.62 − 1.53 (m, 2H), 1.33 − 1.27 (m, 2H), 1.22 (t, J = 7.0 Hz, 6H), 1.12 − 1.05 (m, 2H), 0.88 (t, J = 7.3 Hz, 3H).
^{13}C NMR (CDCl$_3$, 101 MHz, 298 K): δ 171.5, 155.0, 147.2, 146.8, 125.2, 121.7, 61.2, 57.2, 35.2, 32.3, 31.8, 26.1, 24.3, 22.8, 14.1, 13.8.
^{11}B NMR (CDCl$_3$, 128 MHz, 298 K, normal glass): δ −13.0 (d, J = 93 Hz).

MS: 389.26 [M+CHC$_3$CN−H]$^+$

FT-IR (thin film): 2959, 2935, 2872, 2362, 2308, 2280, 1725, 1630, 1562, 1504, 1463, 1439, 1367, 1258, 1200, 1169, 1086, 1024 cm^{-1}.

Compound **c4**:

^{1}H NMR (CDCl$_3$, 400 MHz, 298 K): δ 8.48 (d, J = 5.5 Hz, 2H), 7.09 (d, J = 6.0 Hz, 2H), 4.19 – 4.12 (m, 4H), 2.61 (t, J = 7.5 Hz, 2H), 1.91 – 1.83 (m, 4H), 1.57 – 1.49 (m, 2H), 1.34 – 1.24 (m, 2H), 1.21 (t, J = 7.0 Hz, 6H), 1.11 – 1.03 (m, 2H), 0.88 (t, J = 7.5 Hz, 3H).

^{13}C NMR (CDCl$_3$, 101 MHz, 298 K): δ 171.7, 150.7, 149.7, 123.8, 61.1, 57.3, 35.2, 32.0, 31.6, 26.1, 24.6, 22.9, 14.1, 13.9.

MS: 336.22 [M+H]$^+$

FT-IR (thin film): 2958, 2936, 2872, 1728, 1601, 1464, 1415, 1367, 1257, 1200, 1160 cm^{-1}.

c4-BH$_3$: ^{1}H NMR
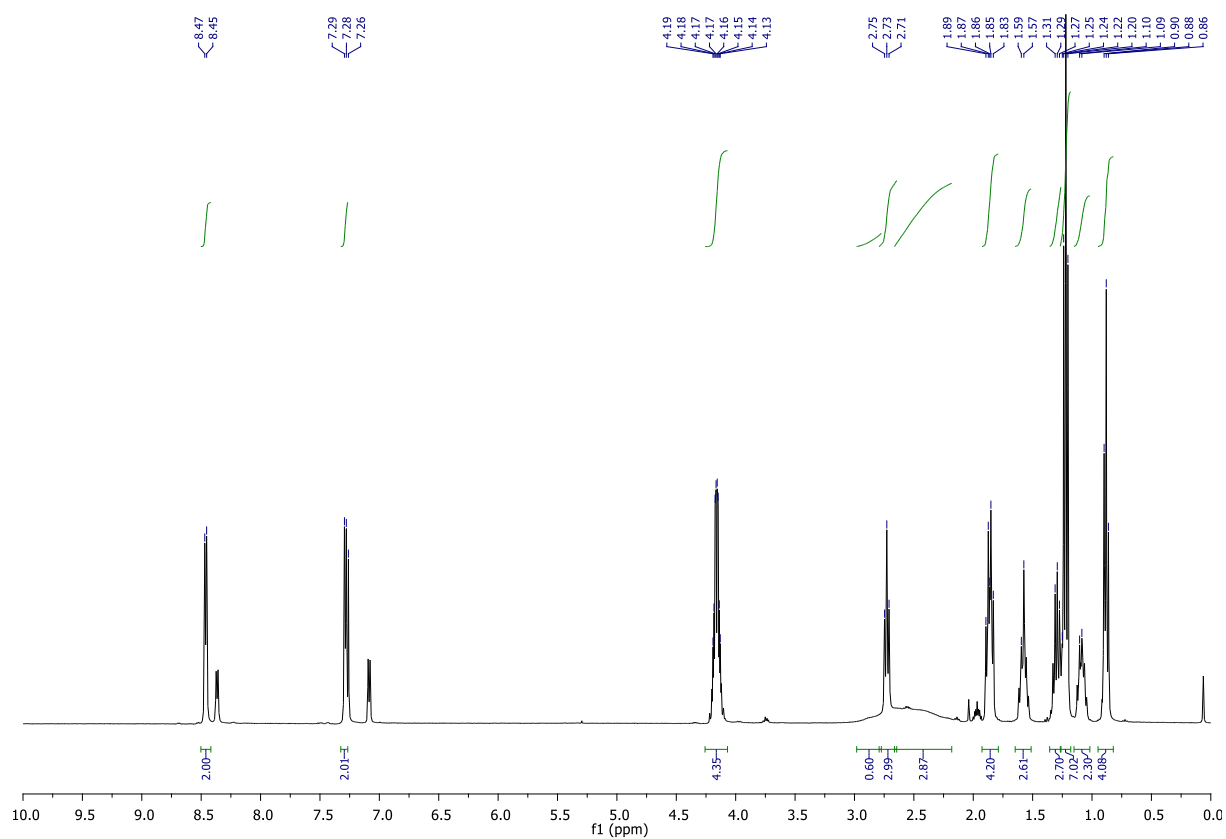
c4-BH$_3$: ^{1}H NMR (^{11}B decoupled)
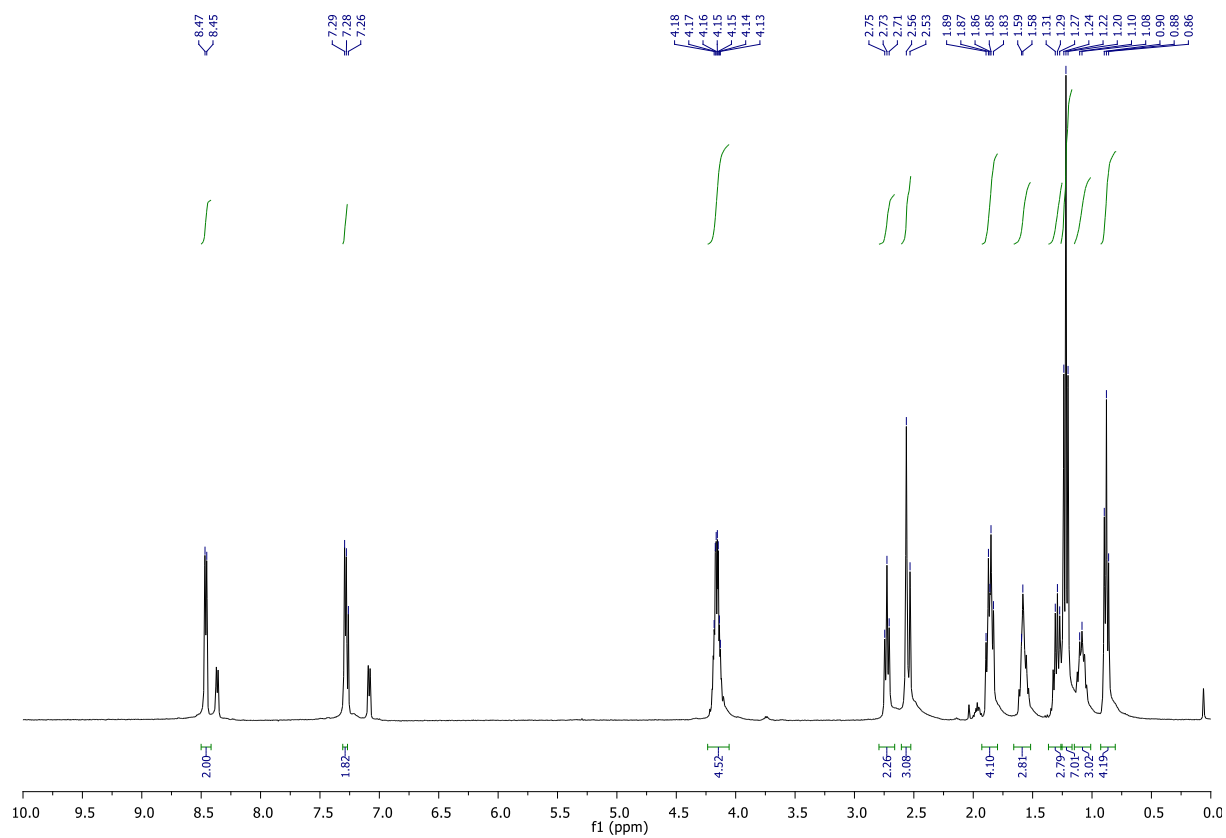
c4-BH₃: ¹³C NMR
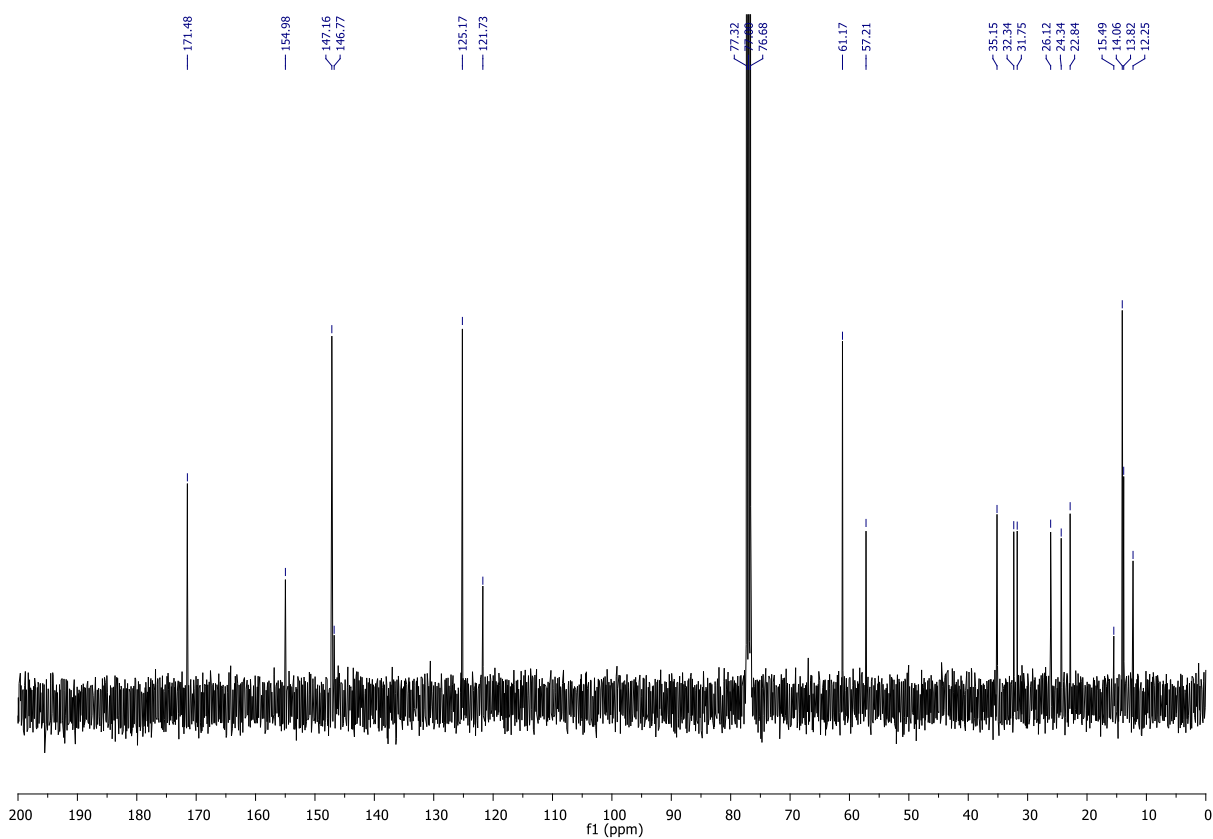
c4-BH₃: ¹¹B (normal glass)

c4: ^{1}H NMR

8.49
8.48
7.26
7.09
7.08
4.18
4.18
4.17
4.16
4.16
4.14
4.14
4.13
4.12
2.63
2.61
2.59
1.91
1.89
1.87
1.87
1.85
1.83
1.55
1.53
1.30
1.29
1.27
1.23
1.21
1.19
1.09
1.07
0.89
0.88
0.86

2.00
2.02
4.24
2.13
4.38
2.25
2.51
6.35
2.44
3.36

f1 (ppm)

c4: ^{13}C NMR

171.66
150.65
149.72
123.81
77.32
77.00
76.68
61.05
57.30
35.17
32.01
31.61
26.08
24.63
22.88
14.07
13.85

f1 (ppm)
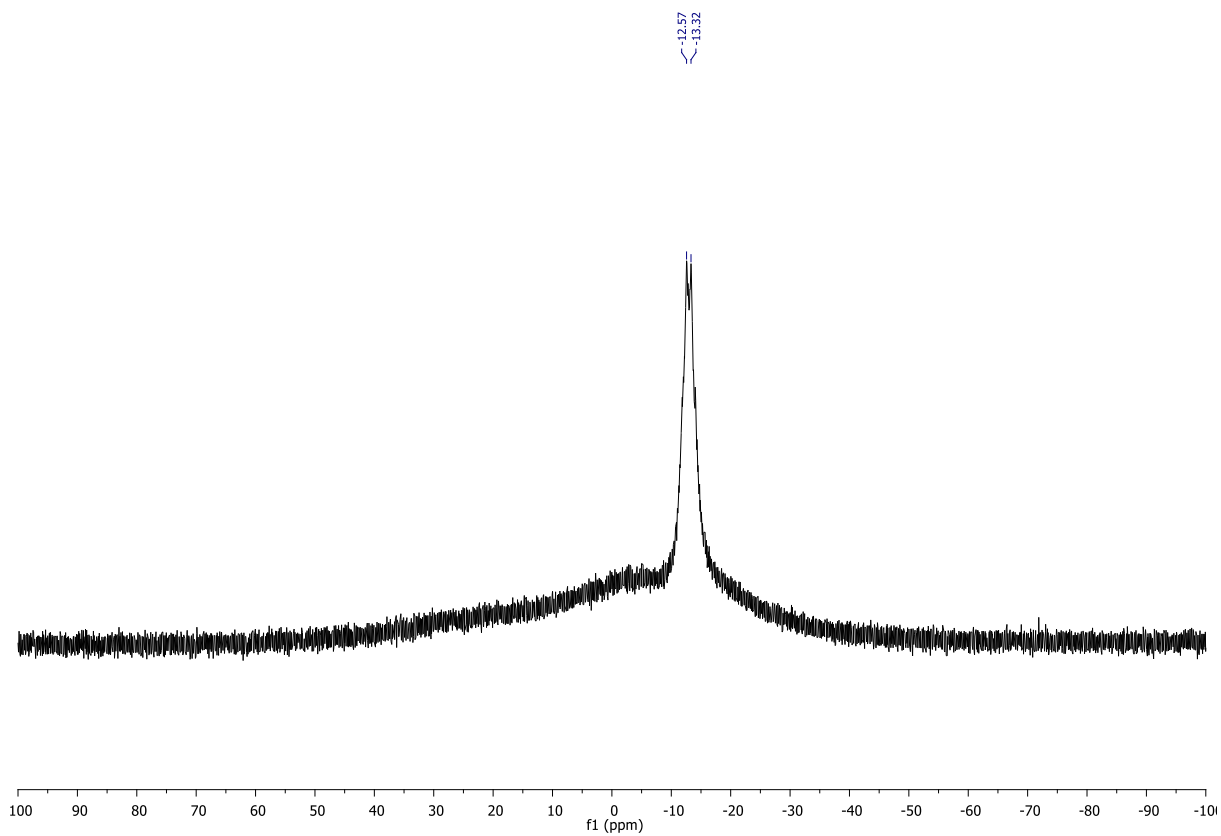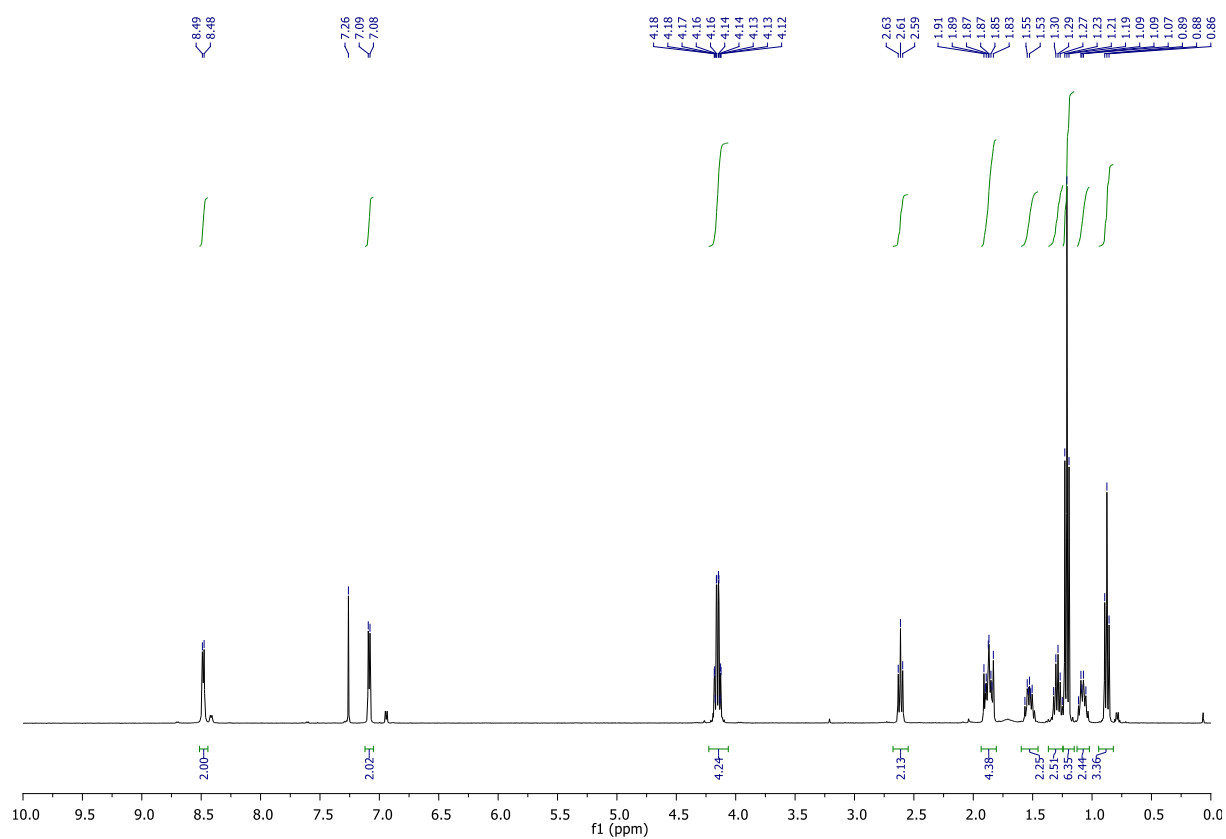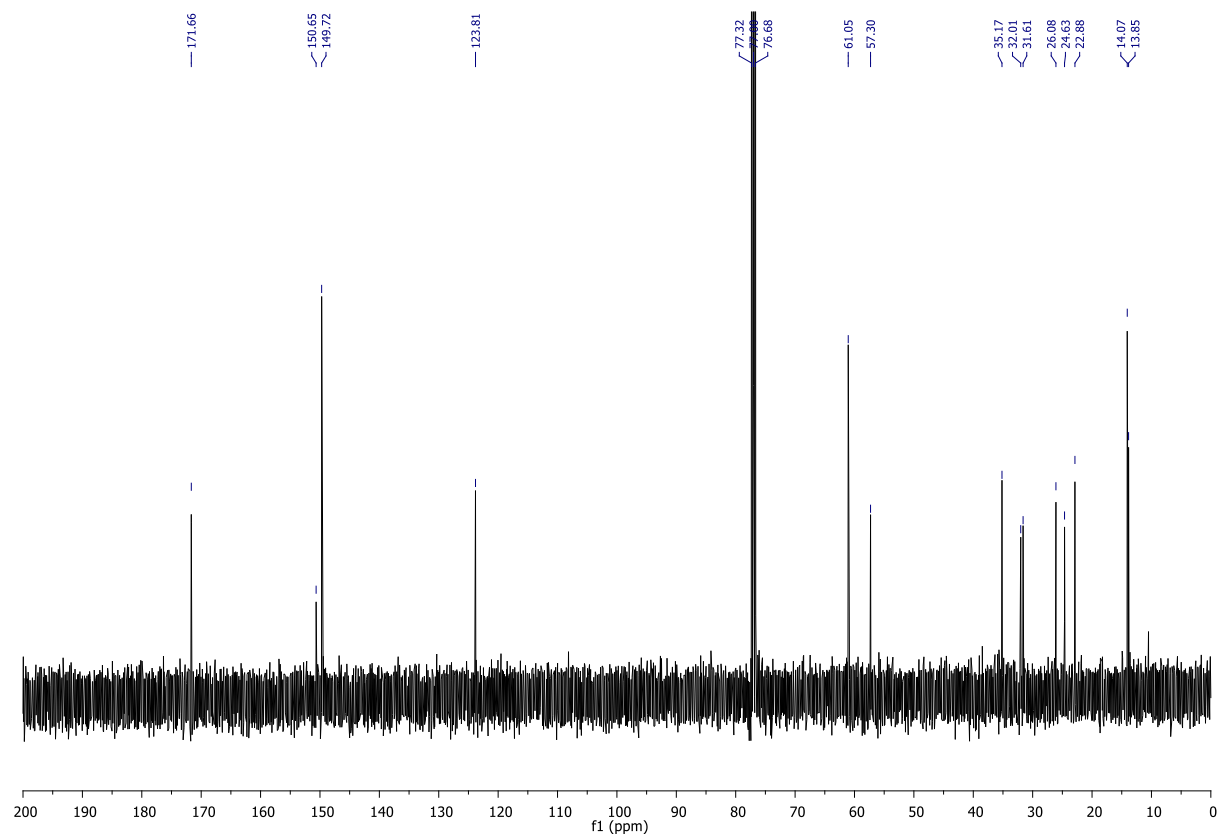
Synthesis of 4B3
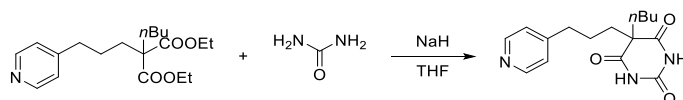
NaH (60% in mineral oil, 57 mg, 1.4 mmol) was flushed with nitrogen and DMF (2 mL) was added. The mixture was cooled to 0 °C and urea (197 mg, 3.28 mmol) was added. After 90 minutes of stirring, **c4** (102 mg, 0.30 mmol) in DMF (4 mL) was added at 0 °C. The mixture was stirred for 5 days at RT and a saturated solution of NH_4Cl (5 mL) was added with cooling to 0 °C. Water (10 mL) was added and the mixture was extracted with dichloromethane (3 × 50 mL). The collected organic phase was dried over $MgSO_4$ and the solvents were removed under reduced pressure (60 °C, <14 mBar). A combliflash of residue on silica (Celite loading, PE/EtOAc, EtOAc: 0%→100%) provided after drying in vacuum oven at 40 °C overnight the title product (350 mg, 50% yield) as a white crystalline solid.

^1H NMR (CD$_3$OD, 400 MHz, 298 K): δ 8.40 (dd, J = 4.5, 1.5 Hz, 2H), 7.25 (dd, J = 4.5, 1.5 Hz, 2H), 2.65 (t, J = 7.5 Hz, 2H), 1.95 − 1.92 (m, 2H), 1.90 − 1.85 (m, 2H), 1.60 − 1.51 (m, 2H), 1.33 − 1.23 (m, 2H), 1.20 − 1.12 (m, 2H), 0.87 (t, J = 7.0 Hz, 3H).

^{13}C NMR (CD$_3$OD, 101 MHz, 298 K): δ 175.0, 153.3, 149.9, 125.6, 56.9, 40.1, 39.0, 35.6, 28.1, 26.5, 23.7, 14.0.

HR-MS (ESI): Required for $C_{16}H_{22}N_3O_3$ $[M+H]^+$ 304.1656, found: 304.1644 (Δ = 3.91 ppm).

FT-IR (thin film): 3226, 3100, 2959, 2930, 2858, 1723, 1701, 1607, 1417, 1384, 1357, 1260, 1217 cm^{-1}.

MP: 174 − 176 °C

EA: Required for $C_{16}H_{21}N_3O_3$: C 63.35, H 6.98, N 13.85; found: C 62.67, H 7.01, N 13.44.

LCMS Method: Col3_ MeCN_FAST_5%-35%

^{1}H NMR

^{13}C NMR
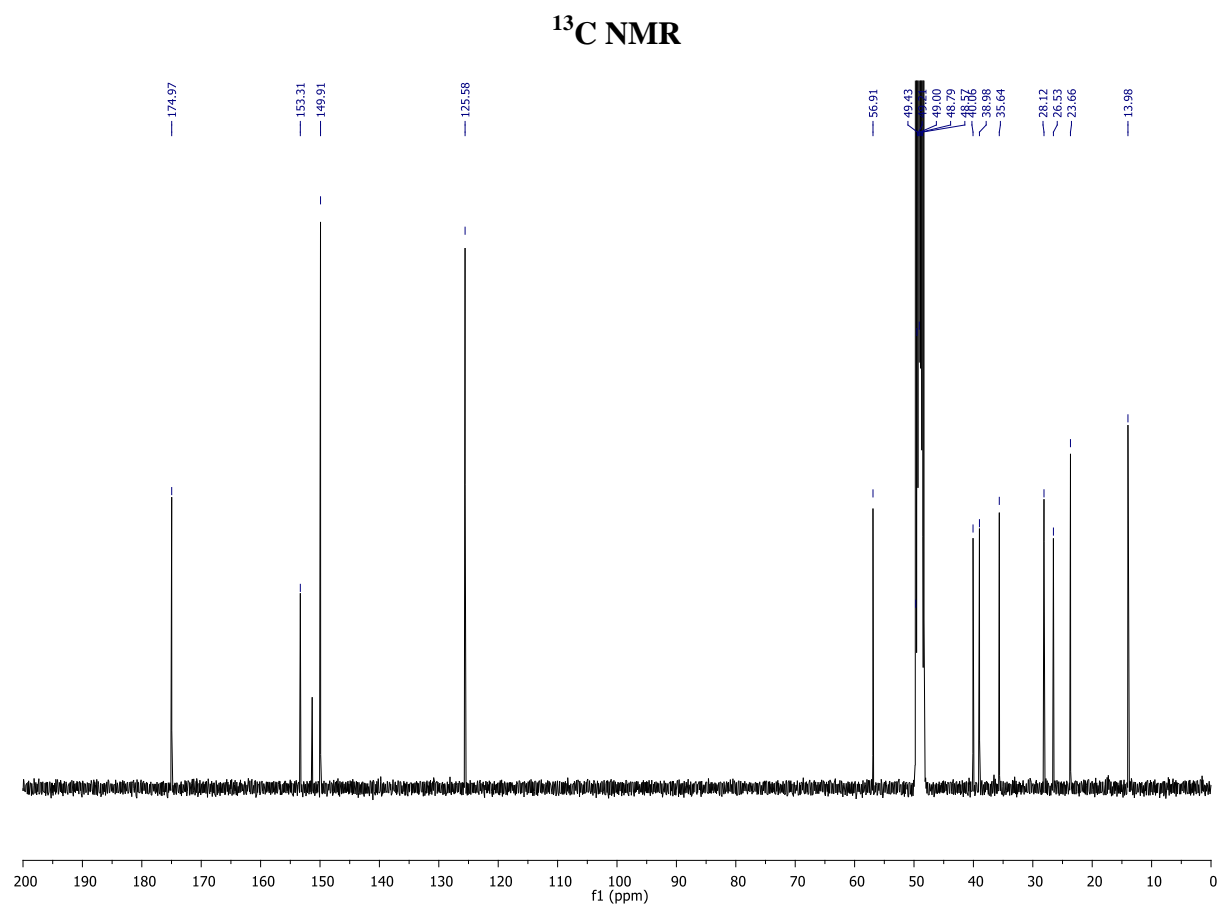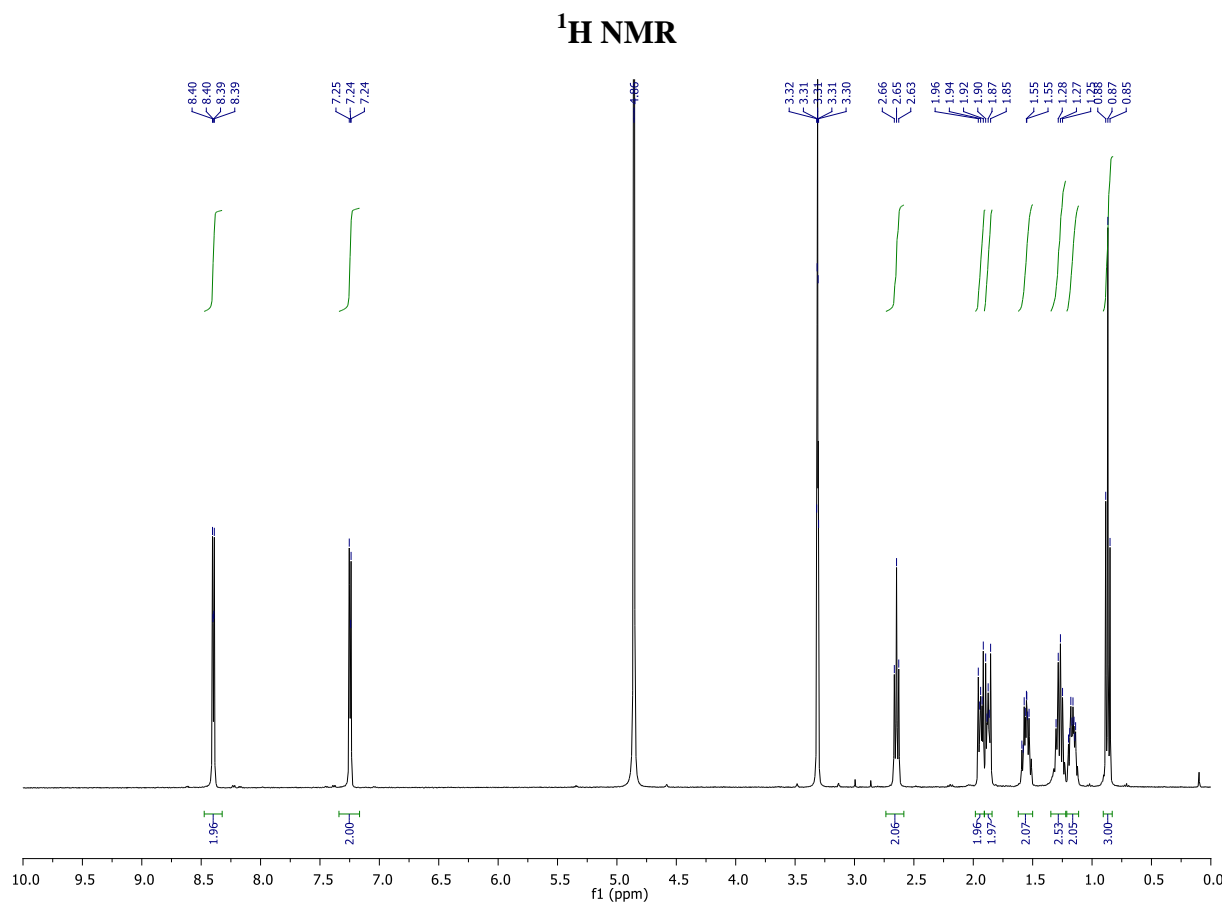
Synthesis of 3P1-Cl
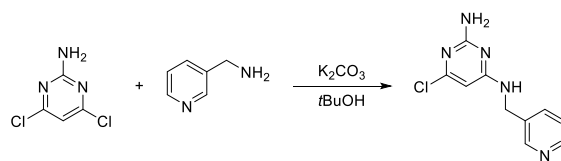
A mixture of 4,6-dichloropyrimidin-2-amine (689 mg, 4.20 mmol), 3-picolylamine (1 mL, 1 g, 9.8 mmol), K$_2$CO$_3$ (437 mg, 3.17 mmol) and tBuOH (15 mL) were heated at 50 °C for 4 days. The mixture was evaporated and water (20 mL) was added. The mixture was then sonicated for 2 minutes. The obtained solid was collected by suction and dried overnight in vacuum oven at 40 °C to provide the title compound (831 mg, 84% yield) as a white solid.

^{1}H NMR (CD$_3$OD/CDCl$_3$, 400 MHz, 298 K): δ 8.47 (d, J = 1.5 Hz, 1H), 8.39 (d, J = 3.5 Hz, 1H), 7.74 (d, J = 8.0 Hz, 1H), 7.33 (dd, J = 8.0, 5.0 Hz, 1H), 5.85 (s, 1H), 4.53 (s, 2H).
^{13}C NMR (d^6-DMSO, 126 MHz, 298 K): δ 164.0, 163.0, 157.6, 149.0, 148.2, 135.4, 135.2, 123.6, 92.8, 41.08.
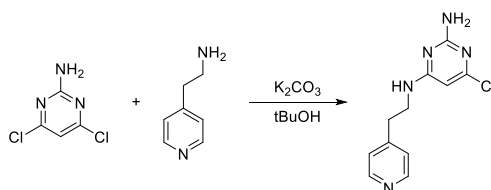
HR-MS (ESI): Calculated for C$_{10}$H$_{11}$N$_5$Cl [M+H]$^+$ 236.0703, found: 236.0693 (Δ = 4.2 ppm)

FT-IR (thin film): 1640, 1575, 1551, 1469, 1427, 1369, 1331, 1150 cm^{-1}.

MP: 198 – 200 °C

LCMS Method: Col3_ MeCN_FAST_5%-35%

^{1}H NMR

8.48
8.47
8.40
8.39
7.75
7.73
7.56
7.35
7.34
7.33
7.32
5.85
4.62
4.53
3.32
3.31
3.31
3.31
3.30

0.98
0.97
1.00
1.05
0.97
2.06

^{13}C NMR

164.02
162.98
157.64
148.97
148.18
135.38
135.17
123.62
92.79
41.08
40.11
40.02
39.94
39.85
39.78
39.61
39.52
39.44
39.35
39.19
39.02
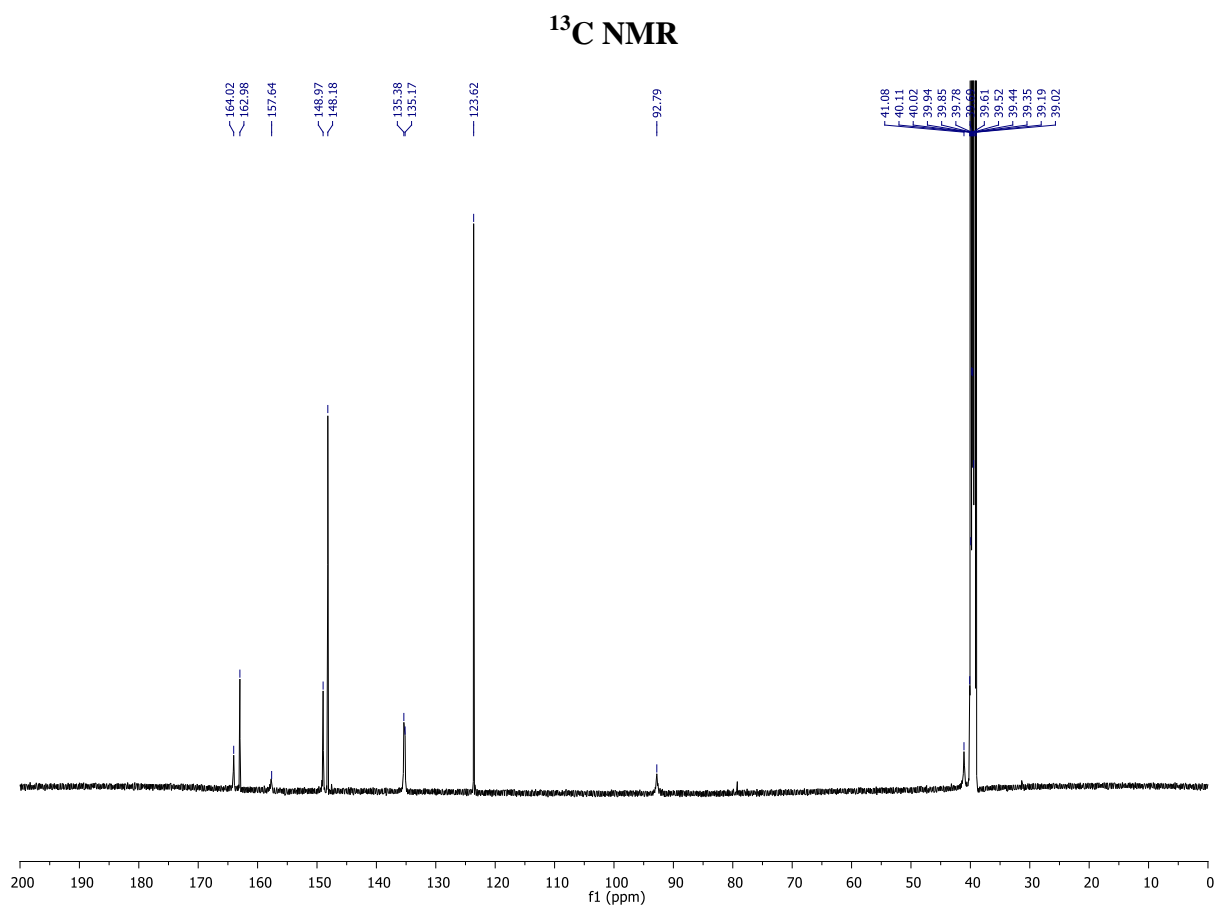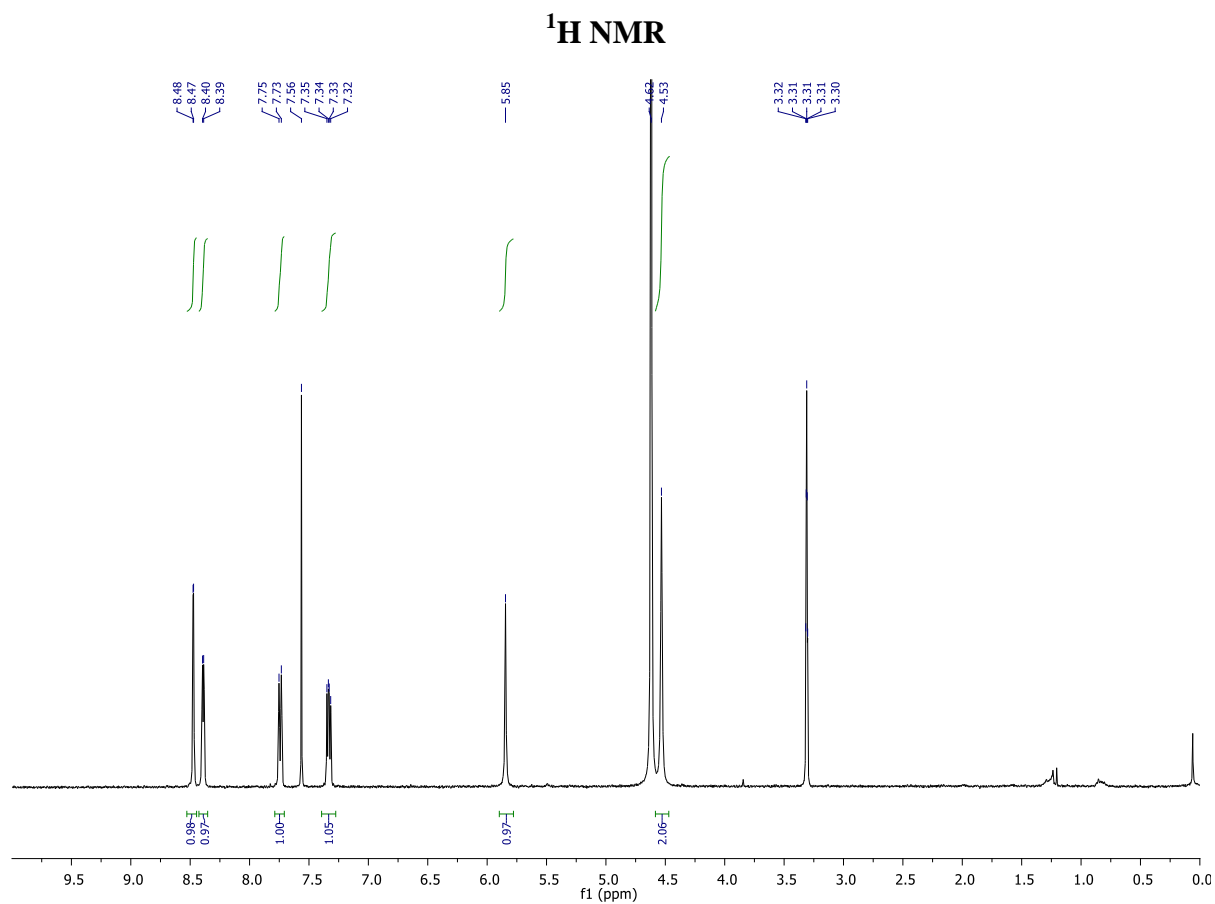
Synthesis of 3P2-Cl
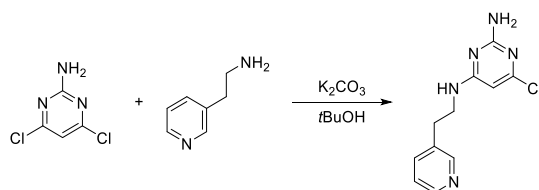
A mixture of 4,6-dichloropyrimidin-2-amine (776 g, 4.64 mmol), 3-(2-aminoethyl)pyridine (1 mL, 1 g, 7.5 mmol), K_2CO_3 (490 mg, 3.55 mmol) and tBuOH (18 mL) were heated at 50 °C for 2 days. The mixture was evaporated and water (20 mL) was added. The mixture was then sonicated for 30 minutes. The obtained solid was collected by suction and dried overnight in vacuum oven at 40 °C to provide the title compound (840 mg, 73% yield) as a pale yellow solid.

^{1}H NMR (CD$_3$OD, 400 MHz, 298 K): δ 8.41 (d, J = 2.0 Hz, 1H), 8.37 (dd, J = 5.0, 1.5 Hz, 1H), 7.74 (dt, J = 8.0, 1.5 Hz, 1H), 7.36 (dd, J = 8.0, 5.0 Hz, 1H), 5.78 (s, 1H), 3.59 (s, 2H), 2.92 (t, J = 7.0 Hz, 2H).

^{13}C NMR (d^6-DMSO, 126 MHz, 298 K): δ 164.1, 163.1, 157.3, 150.0, 147.5, 136.5, 135.1, 123.6, 92.8, 41.3, 32.0.

HR-MS (ESI): Calculated for $C_{11}H_{13}N_5Cl$ [M+H]$^+$ 250.0859, found: 250.0850 (Δ = 3.6 ppm)

FT-IR (thin film): 3276, 2371, 1575, 1478, 1425, 1362 cm^{-1}.

MP: 152 − 157 °C

LCMS Method: Col3_MeCN_FAST_5%-35%

^{1}H NMR

^{13}C NMR
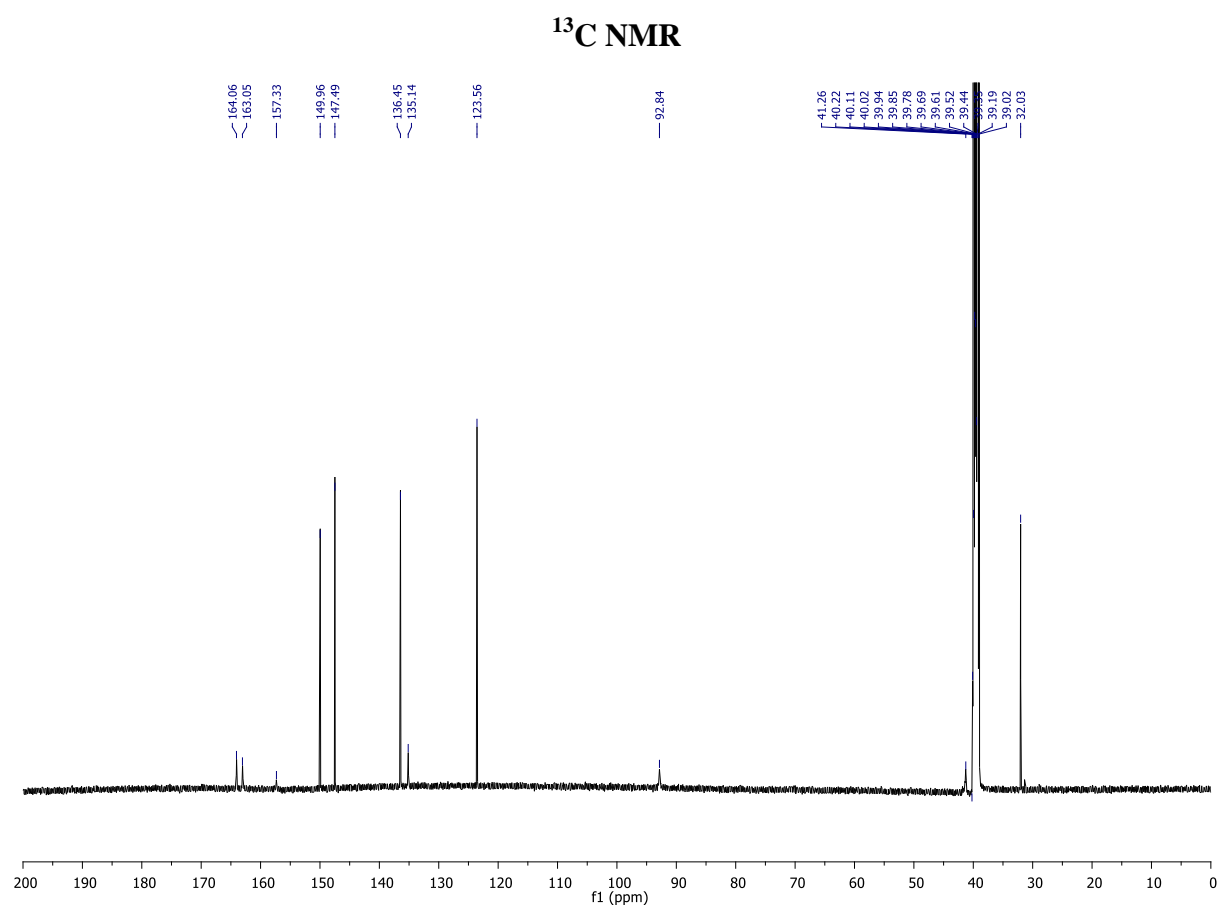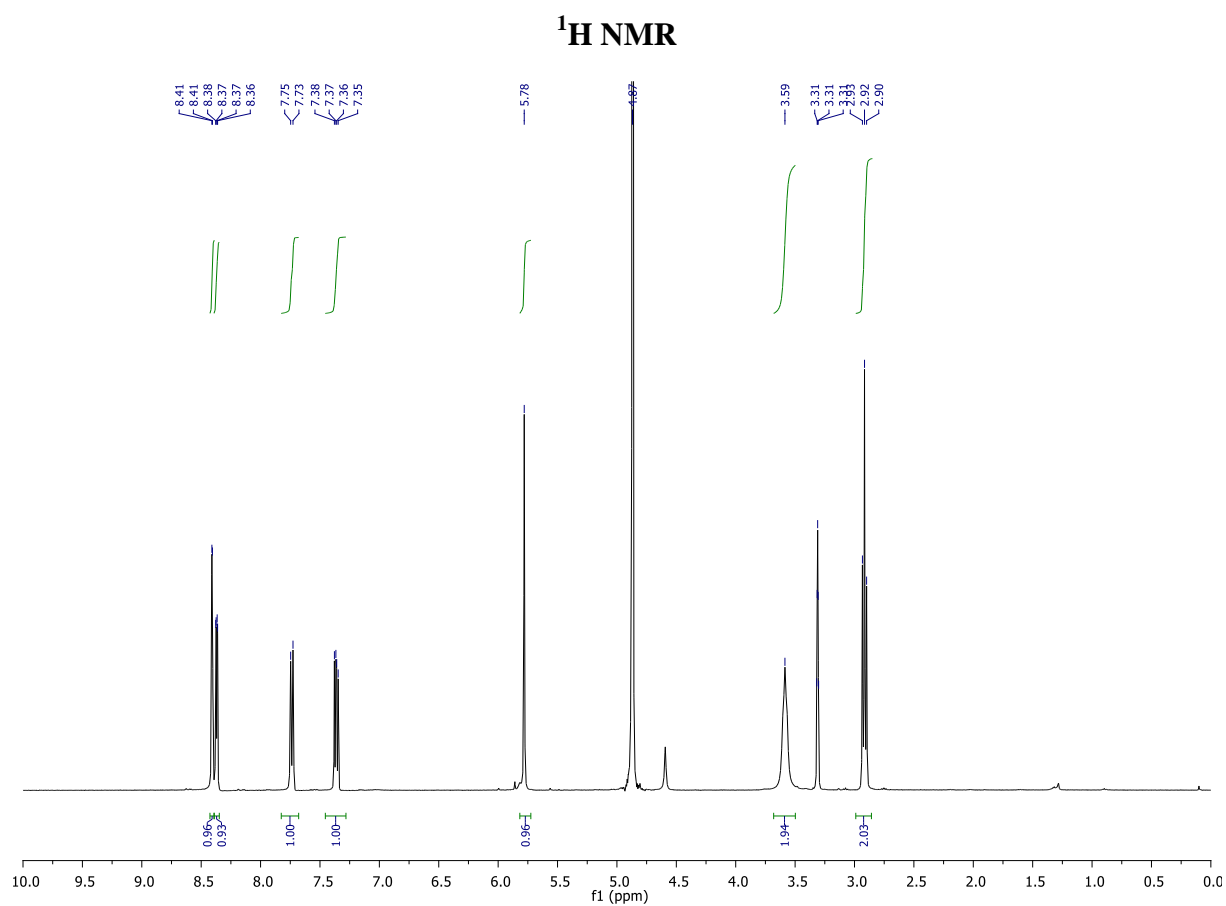
Synthesis of 4P1-Cl
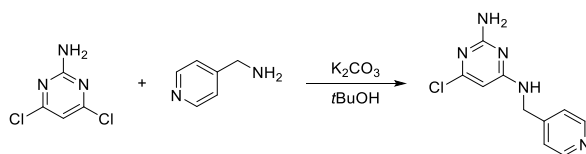
A mixture of 4,6-dichloropyrimidin-2-amine (800 mg, 4.88 mmol), 4-picolylamine (3 mL, 3.18 g, 29 mmol), K_2CO_3 (676 mg, 4.89 mmol) and tBuOH (15 mL) were heated at 60 °C overnight. The mixture was evaporated and water (30 mL) was added. The mixture was then sonicated for 30 minutes and the mixture dissolved. After standing, the form solid was collected and dried in the vacuum oven overnight to provid the title compound (727 mg, 63% yield) as a pale yellow solid.

^{1}H NMR (CD$_3$OD, 400 MHz, 298 K): δ 8.44 (d, J = 6.0 Hz, 2H), 7.35 (d, J = 6.0 Hz, 2H), 5.90 (s, 1H), 4.60 (s, 2H).

^{13}C NMR (d^6-DMSO, 126 MHz, 298 K): δ 164.2, 163.0, 157.8, 149.6, 148.9, 122.3, 92.8, 42.3.

HR-MS (ESI): Calculated for $C_{10}H_{11}N_5Cl$ [M+H]$^+$ 236.0697, found: 236.0694 (Δ = 1.5 ppm)

FT-IR (thin film): 3312, 3200, 2387, 1573, 1556, 1496, 1475, 1417, 1360, 1314, 1249 cm^{-1}.

MP: > 136 °C (carbonisation)

LCMS Method: Col3_ MeCN_FAST_5%-35%

^{1}H NMR

8.45
8.43

7.35
7.34

5.90

4.88
4.60

3.32
3.31
3.31
3.30

2.05
2.07
1.00
2.04

10.0 9.5 9.0 8.5 8.0 7.5 7.0 6.5 6.0 5.5 5.0 4.5 4.0 3.5 3.0 2.5 2.0 1.5 1.0 0.5 0.0
f1 (ppm)

^{13}C NMR

164.18
162.99
157.78
149.60
148.93

122.25

92.82

42.28
40.02
39.85
39.69
39.52
39.19
39.02
37.62
37.16
36.74

200 190 180 170 160 150 140 130 120 110 100 90 80 70 60 50 40 30 20 10 0
f1 (ppm)
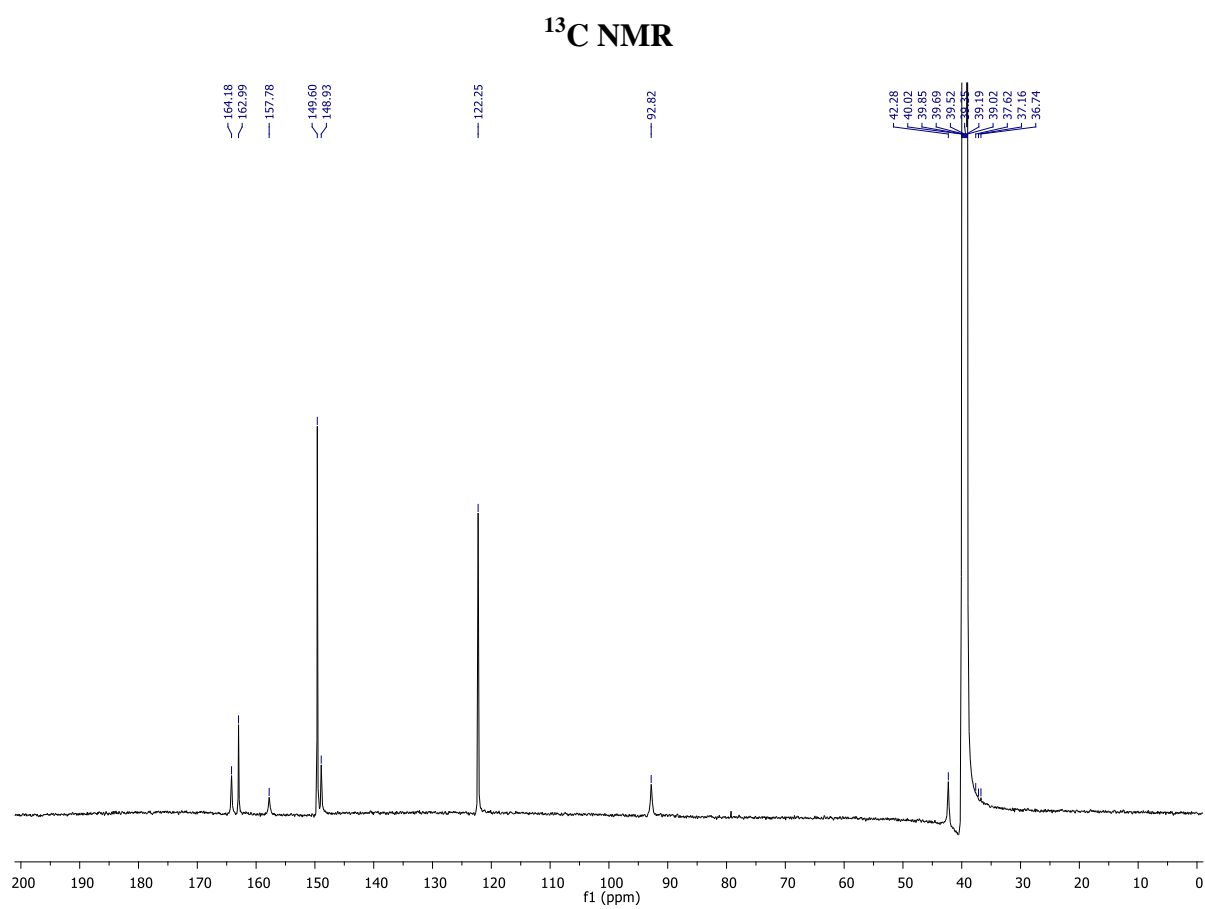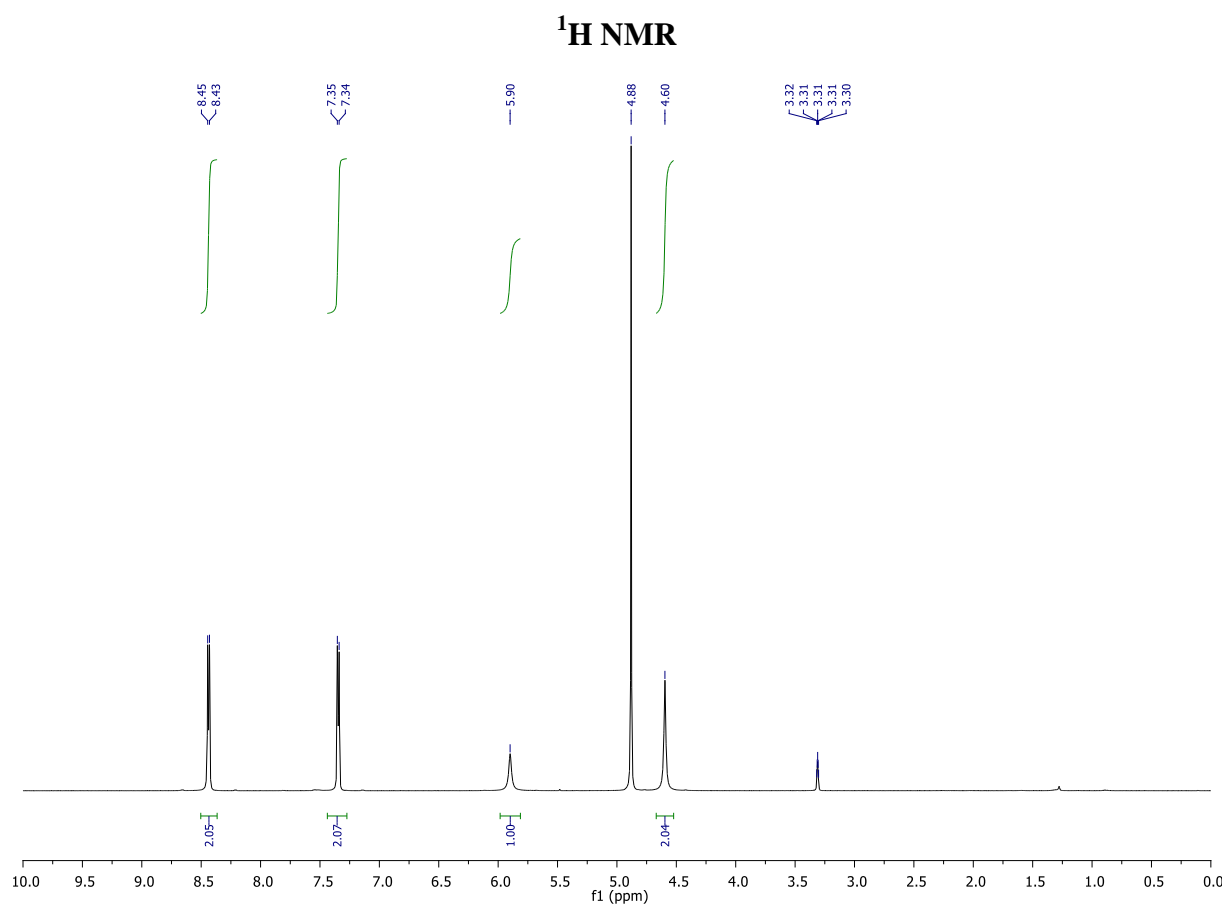
Synthesis of 4P2-Cl

A mixture of 4,6-dichloropyrimidin-2-amine (1.06 g, 6.46 mmol), 4-(2-aminoethyl)pyridine (1.2 mL, 1.2 g, 10 mmol), K_2CO_3 (0.76 g, 5.5 mmol) and *t*BuOH (15 mL) were heated at 50 °C for 3 days. The mixture was evaporated and water (30 mL) was added. The mixture was then sonicated for 20 minutes. The obtained solid was collected by suction and dried overnight in vacuum oven at 40 °C to provide the title compound (1.43 g, 89% yield) as a yellow solid.

^{1}H NMR (CD3OD, 400 MHz, 298 K): δ 8.43 − 8.42 (m, 2H), 7.33 (d, *J* = 6.0 Hz, 2H), 5.79 (s, 1H), 3.61 (s, 2H), 2.93 (t, *J* = 7.0 Hz, 2H).

^{13}C NMR (CD3OD, 101 MHz, 298 K): δ 165.7, 164.4, 162.8, 151.7, 149.9, 126.1, 94.8, 41.9, 35.8.

HR-MS (ESI): Calculated for $C_{11}H_{13}N_5Cl$ [M+H]$^+$ 250.0854, found: 250.0850 (Δ = 1.4 ppm)

FT-IR (thin film): 3277, 2397, 1574, 1481, 1420, 1362 cm^{-1}.

MP: 157 °C (carbonisation)

LCMS Method: Col3_MeCN_FAST_5%-35%

^{1}H NMR

^{13}C NMR
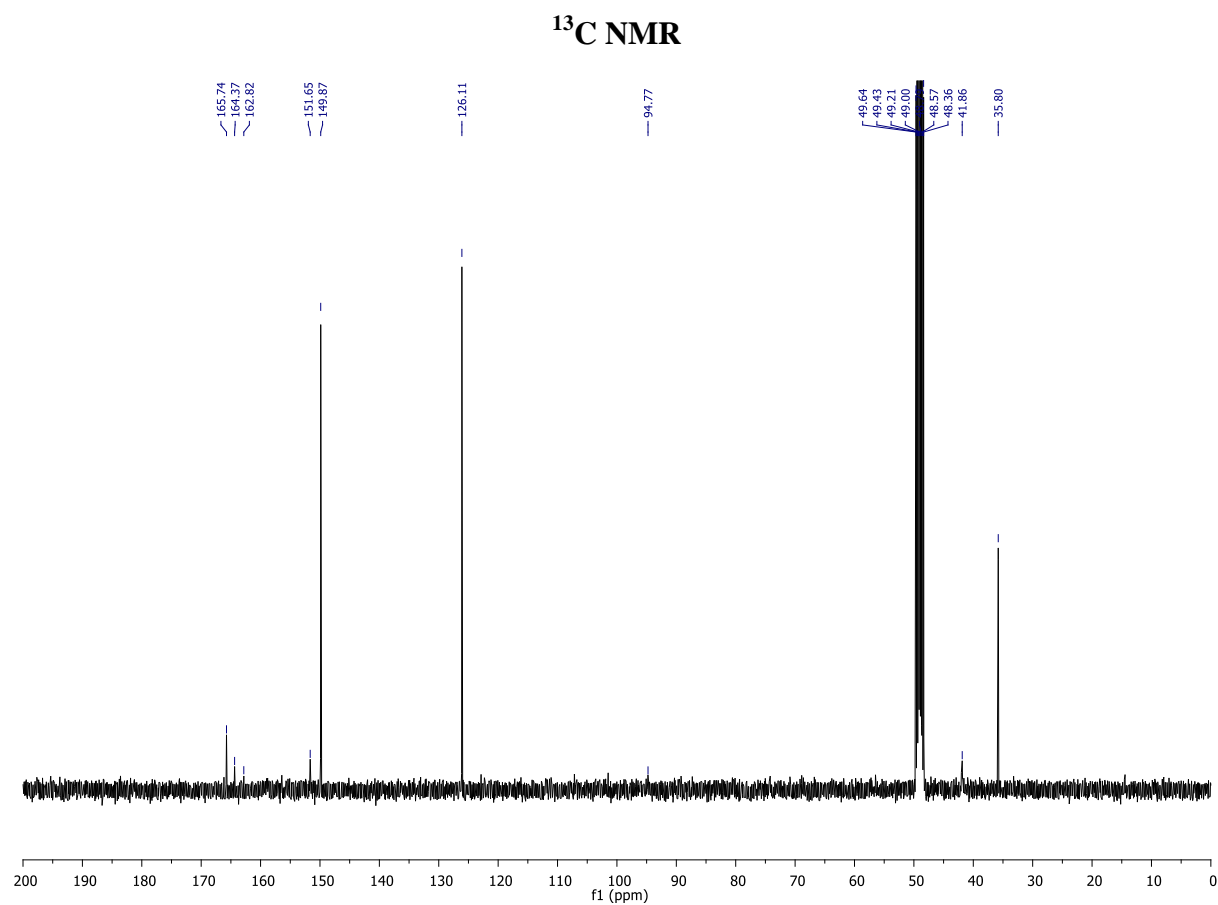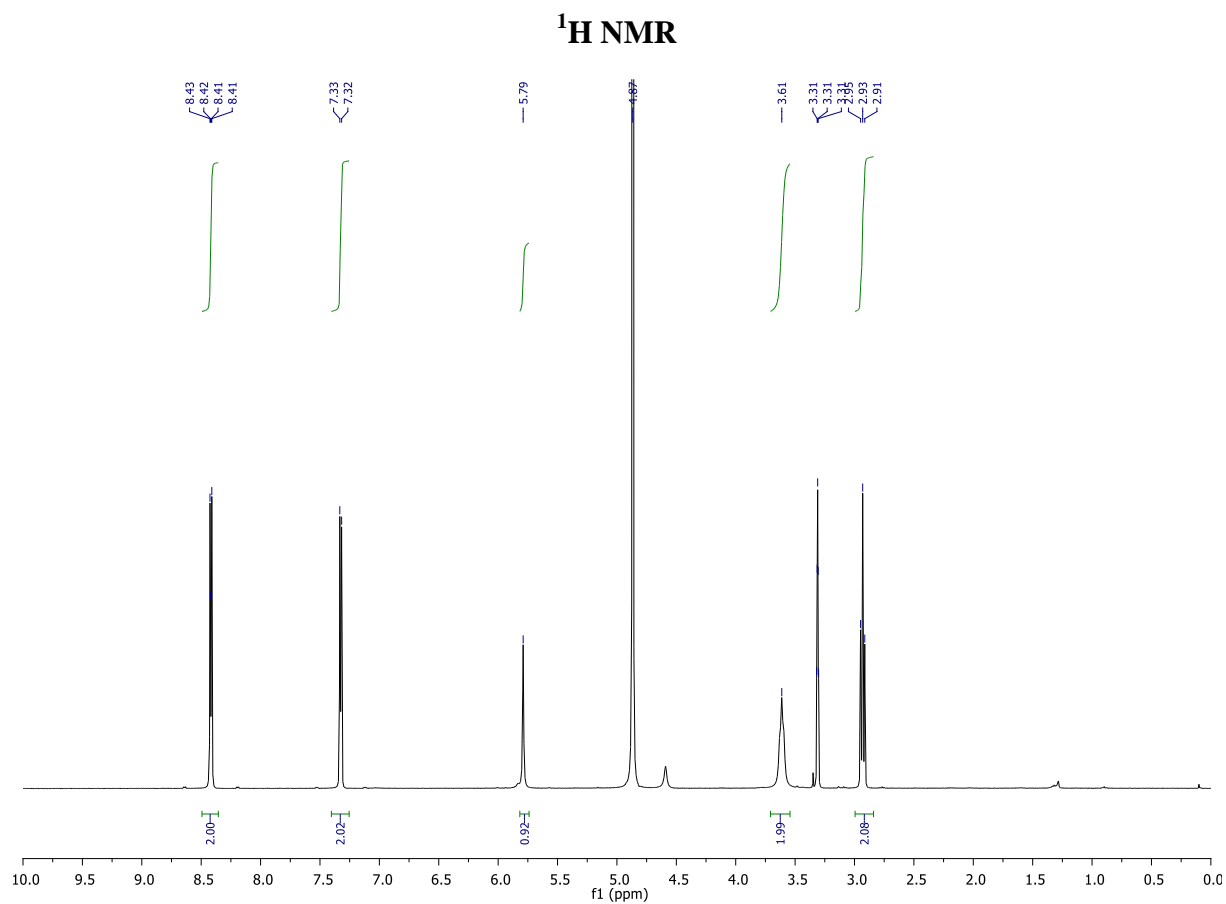
Synthesis of 3P1
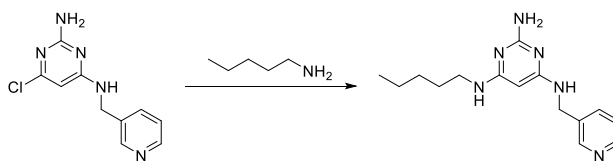
3P1-Cl (337 mg, 1.43 mmol) was flushed with nitrogen in a MW vial. *n*-Pentylamine (1 mL, 0.9 g, 10 mmol) was added and the mixture was heated in microwave at 160 °C for 2 hours. A saturated solution of $NaHCO_3$ (15 mL) was added and the mixture was extracted with CH_2Cl_2/MeOH (20:1, 2 × 50mL) and CH_2Cl_2 (2 × 50 mL). The organic phase was dried over $MgSO_4$, evaporated and loaded to Celite. A combiflash of the residue on silica (CH_2Cl_2/MeOH: MeOH 0%→20%) provided the title compound (253 mg, 62% yield) as yellowish oil.

^{1}H NMR (CD$_3$OD, 400 MHz, 298 K): δ 8.50 (s, 1H), 8.38 (d, J = 4.0 Hz, 1H), 7.77 (d, J = 7.5 Hz, 1H), 7.34 (dd, J = 7.0, 5.0 Hz, 1H), 4.89 (s, 1H), 4.46 (s, 2H), 3.08 (t, J = 7.0 Hz, 2H), 1.52 – 1.43 (m, 2H), 1.29 (d, J = 2.5 Hz, 4H), 0.88 (t, J = 6.0 Hz, 3H).

^{13}C NMR (CD$_3$OD, 101 MHz, 298 K): δ 165.2, 165.1, 164.0, 149.1, 148.4, 137.7, 137.1, 125.1, 74.0, 43.2, 42.3, 30.3, 30.1, 23.5, 14.4.

HR-MS (ESI): Calculated for $C_{15}H_{23}N_6$ [M+H]$^+$ 287.1979, found: 287.1976 (Δ = 0.98 ppm)

FT-IR (thin film): 3309, 2955, 2928, 2858, 1575, 1505, 1455, 1424, 1355 cm^{-1}.

LCMS Method: Col3_MeCN_FAST_5%-35%

^{1}H NMR

8.50
8.38
8.37
7.78
7.76
7.36
7.34
7.33
4.92
4.89
4.46
3.31
3.09
3.08
3.06
1.50
1.48
1.47
1.29
1.29
0.90
0.88
0.86

0.99 0.99 0.99 1.00 0.97 1.92 2.02 2.18 4.61 3.51

10.0 9.5 9.0 8.5 8.0 7.5 7.0 6.5 6.0 5.5 5.0 4.5 4.0 3.5 3.0 2.5 2.0 1.5 1.0 0.5 0.0
f1 (ppm)

^{13}C NMR

166.78
165.20
165.08
163.95
150.20
149.09
148.43
137.69
137.12
125.08
74.03
49.64
49.42
49.21
49.00
48.79
48.57
48.36
43.24
42.29
30.27
30.09
23.49
14.42

200 190 180 170 160 150 140 130 120 110 100 90 80 70 60 50 40 30 20 10 0
f1 (ppm)

Synthesis of 3P2
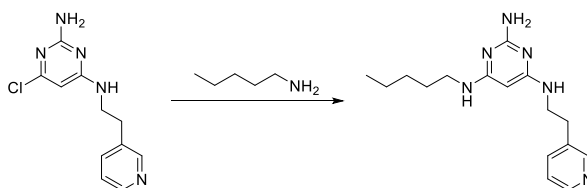
3P2-Cl (123 mg, 0.493 mmol) was flushed with nitrogen in a MW vial. *n*-Pentylamine (1 mL, 0.9 g, 10 mmol) was added and the mixture was heated in microwave at 150 °C for 7 hours. A saturated solution of NaHCO$_3$ (10 mL) was added and the mixture was extracted with dichloromethane (4 × 30 mL). The organic phase was dried over MgSO$_4$, evaporated and loaded to Celite. A combiflash of the residue on silica (CH$_2$Cl$_2$/MeOH: MeOH 0%→10%) provided the title compound (124 mg, 84% yield) as orange dense oil.

^{1}H NMR (CD$_3$OD, 400 MHz, 298 K): δ 8.41 (s, 1H), 8.36 (d, J = 4.0 Hz, 1H), 7.71 (d, J = 7.5 Hz, 1H), 7.33 (dd, J = 7.5, 5.0 Hz, 1H), 3.45 (t, J = 7.0 Hz, 2H), 3.12 (t, J = 7.0 Hz, 2H), 2.88 (t, J = 7.0 Hz, 2H), 1.56 − 1.53 (m, 2H), 1.35 − 1.30 (m, 4H), 0.91 (t, J = 6.0 Hz, 3H).

**^{13}C NMR (CD$_3$OD, 101 MHz, 298 K)**: δ 165.1, 165.0, 163.9, 150.4, 147.9, 138.7, 137.4, 125.1, 73.6, 43.2, 42.3, 33.8, 30.3, 30.2, 23.5, 14.4.

HR-MS (ESI): Calculated for C$_{16}$H$_{25}$N$_6$ [M+H]$^+$ 301.2141, found: 301.2142 (Δ = 0.3 ppm)

FT-IR (thin film): 3310, 3189, 2953, 2928, 2858, 1573, 1526, 1458, 1429, 1358 cm^{-1}.

LCMS Method: Col3_MeCN_FAST_5%-35%

195

^{1}H NMR

8.41
8.36
8.35
7.72
7.70
7.35
7.33
7.32
5.48
4.91
3.47
3.45
3.43
3.12
3.10
2.90
2.88
2.87
1.56
1.55
1.53
1.35
1.34
1.33
0.92
0.91
0.89

1.00
1.04
1.00
1.01
2.08
2.10
2.12
2.25
4.65
3.34

10.0 9.5 9.0 8.5 8.0 7.5 7.0 6.5 6.0 5.5 5.0 4.5 4.0 3.5 3.0 2.5 2.0 1.5 1.0 0.5 0.0
f1 (ppm)

^{13}C NMR

167.31
165.11
164.99
163.87
150.43
147.86
138.69
137.38
125.10
73.61
49.64
49.43
49.21
49.00
48.79
48.57
48.36
43.16
42.33
33.76
30.33
30.16
23.52
14.43

200 190 180 170 160 150 140 130 120 110 100 90 80 70 60 50 40 30 20 10 0
f1 (ppm)

Synthesis of 4P1

4P1-Cl (105 mg, 0.45 mmol) was flushed with nitrogen in a MW vial. *n*-Pentylamine (1 mL, 0.9 g, 10 mmol) was added and the mixture was heated in microwave at 160 °C for 3 hours. A saturated solution of NaHCO$_3$ (15 mL) was added and the mixture was extracted with CH$_2$Cl$_2$/MeOH (20:1, 2 × 50 mL) and CH$_2$Cl$_2$ (2 × 50 mL). The organic phase was dried over MgSO$_4$, evaporated and loaded to Celite. A combiflash of the residue on silica (CH$_2$Cl$_2$/MeOH: MeOH 0%→20%) provided the title compound (71 mg, 55% yield) as orange dense oil.

^{1}H NMR (CD$_3$OD, 400 MHz, 298 K): δ 8.42 (d, J = 5.5 Hz, 2H), 7.35 (d, J = 5.0 Hz, 2H), 4.86 (s, 1H), 4.47 (s, 2H), 3.08 (t, J = 7.0 Hz, 2H), 1.52 − 1.43 (m, 2H), 1.29 (d, J = 3.0 Hz, 4H), 0.88 (t, J = 6.5 Hz, 3H).

^{13}C NMR (CD$_3$OD, 101 MHz, 298 K): δ 165.2, 165.2, 163.9, 152.3, 149.9, 123.6, 74.0, 44.7, 42.3, 30.3, 30.1, 23.5, 14.4.

HR-MS (ESI): Calculated for C$_{15}$H$_{23}$N$_6$ [M+H]$^+$ 287.1979, found: 287.1975 (Δ = 1.26 ppm)

FT-IR (thin film): 3302, 3175, 2953, 2926, 2587, 1572, 1497, 1446, 1355, 1312, 1219, 1204 cm^{-1}.

LCMS Method: Col3_MeCN_FAST_5%-35%

^{1}H NMR

^{13}C NMR
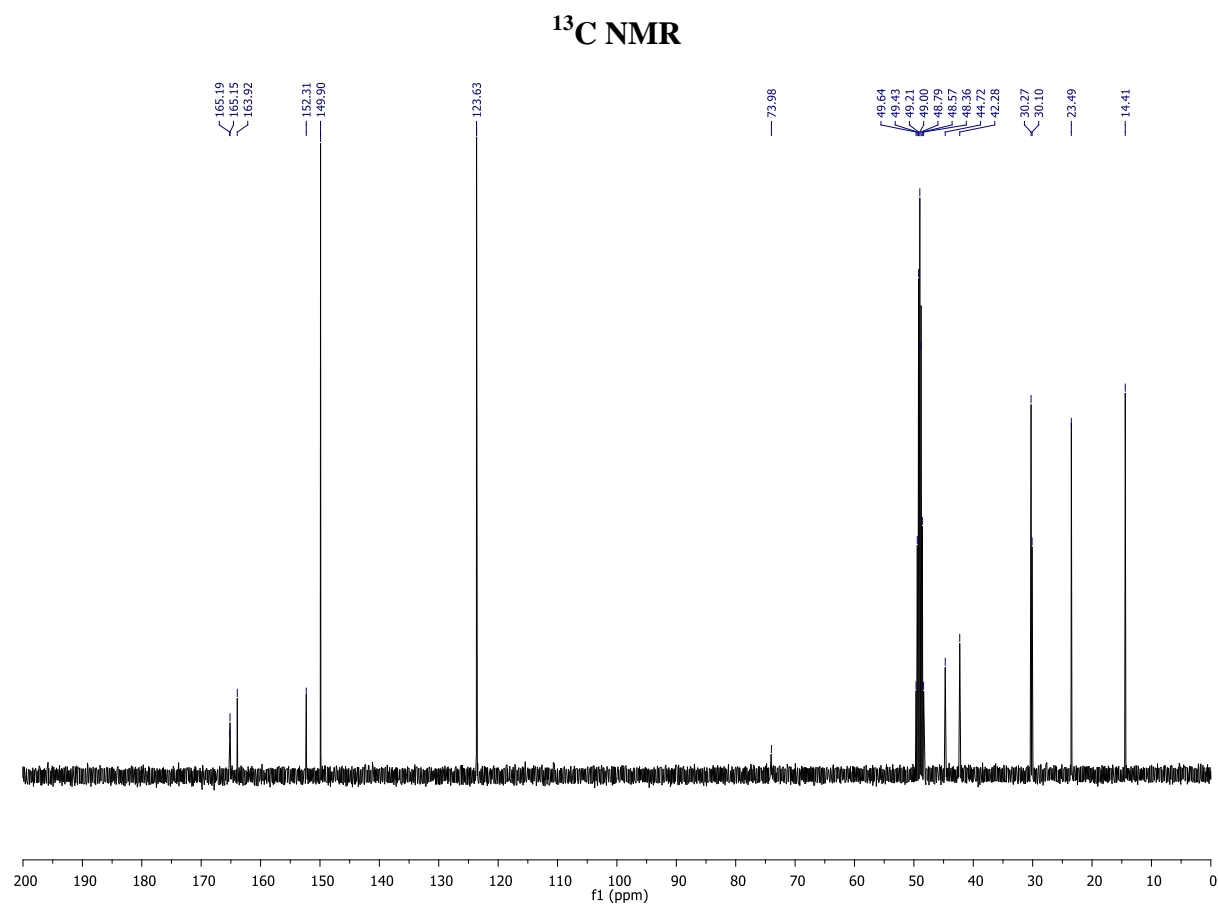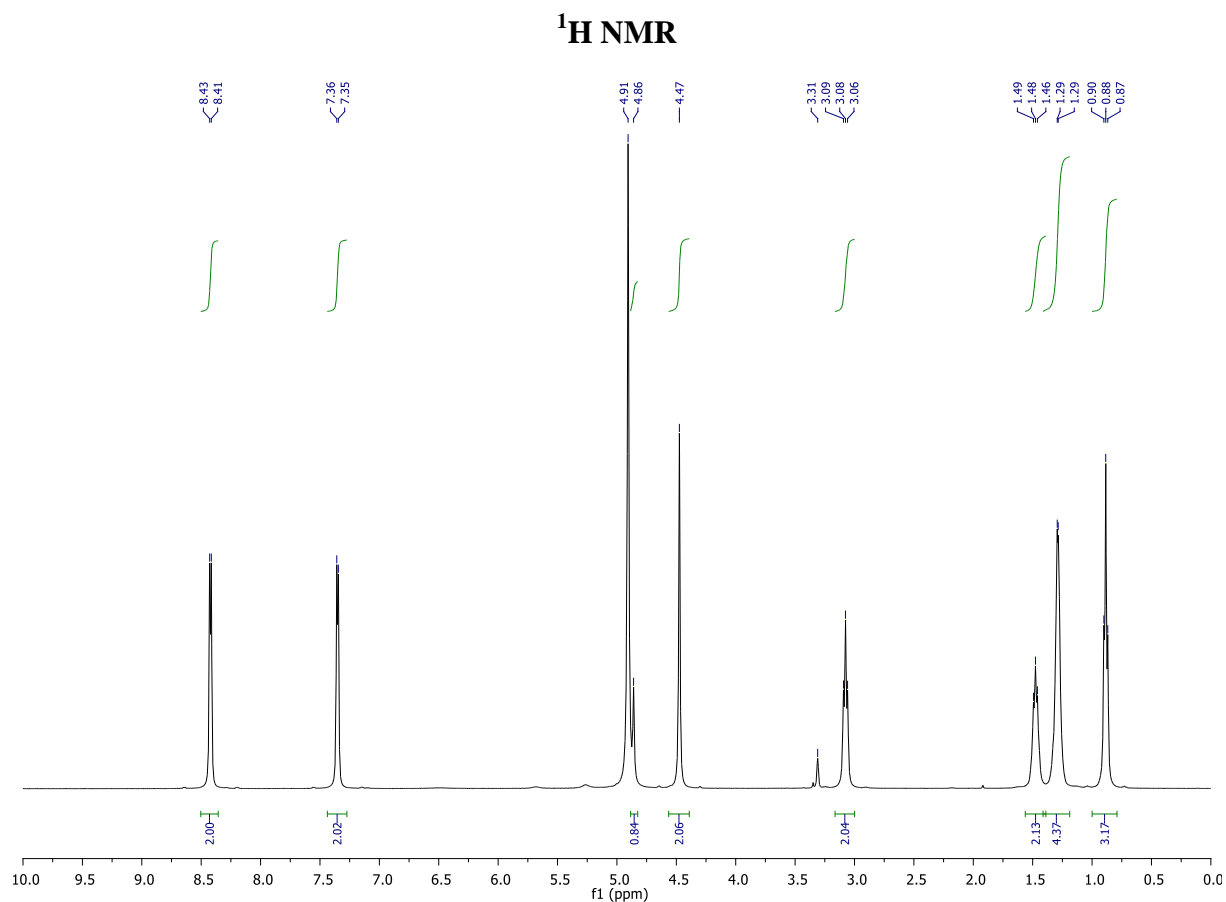
Synthesis of 4P2
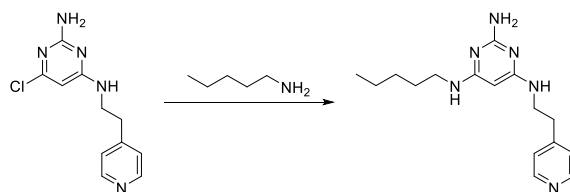
4P2-Cl (100 mg, 0.40 mmol) was flushed with nitrogen in a MW vial. *n*-Pentylamine (1 mL, 0.9 g, 10 mmol) was added and the mixture was heated in microwave at 160 °C for 5 hours. A saturated solution of NaHCO$_3$ (10 mL) and water (10 mL) were added and the mixture was extracted with CH$_2$Cl$_2$/MeOH (20:1, 50 mL) and CH$_2$Cl$_2$ (3 × 50 mL). The organic phase was dried over MgSO$_4$, evaporated and loaded to Celite. A combiflash of the residue on silica (CH$_2$Cl$_2$/MeOH: MeOH 0%→10%) provided the title compound (97 mg, 81% yield) as yellow oil.

^{1}H NMR (CDCl$_3$, 400 MHz, 298 K): δ 8.53 (d, J = 6.0 Hz, 2H), 7.15 (d, J = 6.0 Hz, 2H), 4.80 (s, 1H), 4.60 − 4.41 (m, 3H), 3.51 (dd, J = 13.0, 7.0 Hz, 2H), 3.13 (dd, J = 13.0, 7.0 Hz, 2H), 2.89 (t, J = 7.0 Hz, 2H), 1.61 − 1.54 (m, 2H), 1.39 − 1.30 (m, 4H), 0.90 (t, J = 7.0 Hz, 3H).

^{13}C NMR (CDCl$_3$, 101 MHz, 298 K): δ 164.1, 163.8, 162.2, 150.0, 148.0, 124.1, 72.5, 41.7, 41.7, 35.1, 29.1, 29.0, 22.4, 14.0.

HR-MS (ESI): Calculated for C$_{16}$H$_{25}$N$_6$ [M+H]$^+$ 301.2135, found: 301.2131 (Δ = 1.30 ppm)

FT-IR (thin film): 3310, 2954, 2927, 2857, 2421, 1555, 1494, 1455, 1430, 1417, 1357, 1219 cm^{-1}.

LCMS Method: Col3_MeCN_FAST_5%-35%

^{1}H NMR

^{13}C NMR
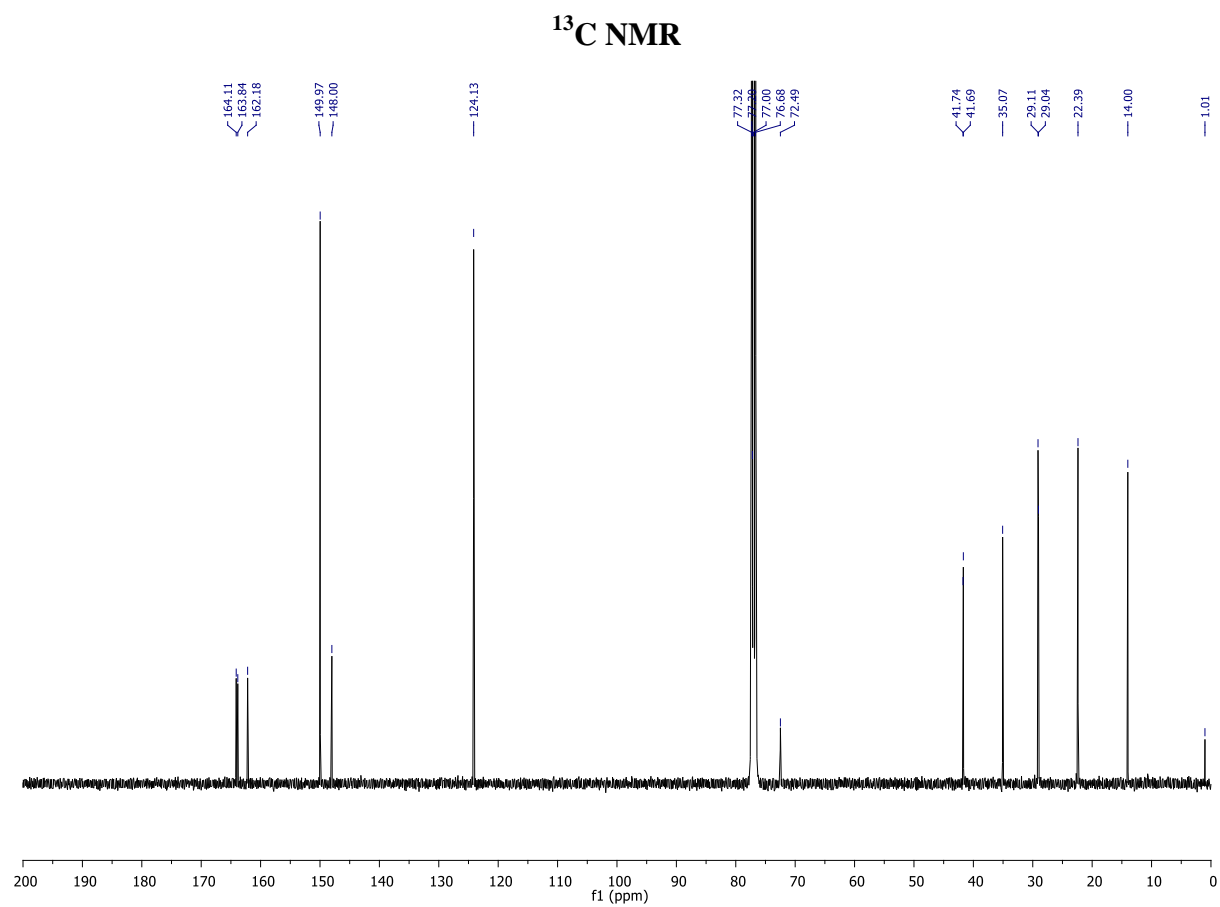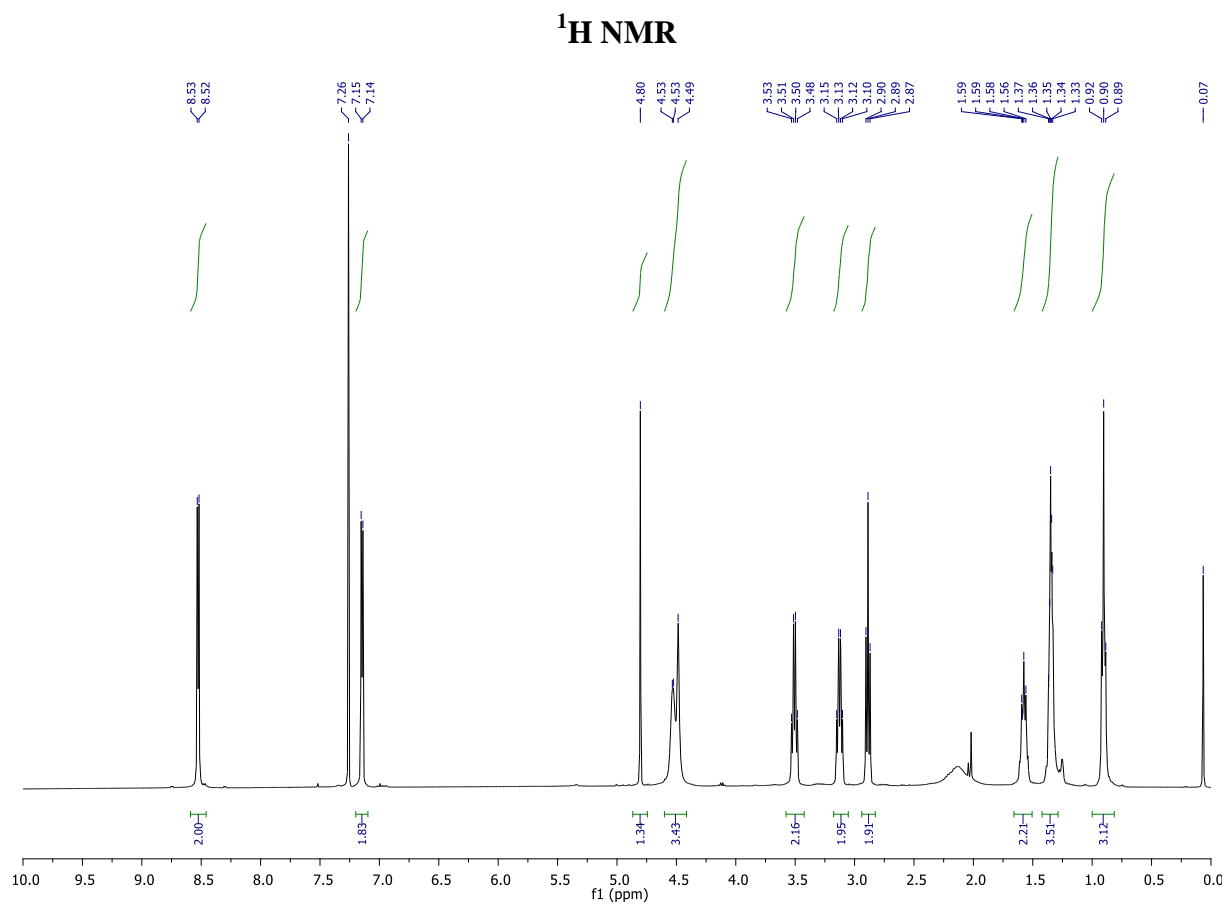
5.8.3. Modelling

The conformational search was done by molecular mechanics in Schrödinger Suite 2016-4 using MacroModel suite. A global minimum structure was found by conformational search using OPLS3 as a force field and without using any solvent model and with using no cut-off for non-covalent interactions. For semi-empirical calculations, PM6 as implemented in *Gaussian 09* was used.[15]

5.8.4. UV-vis-NIR titrations

General

The UV-vis-NIR titrations were recorded on a Cary 60 UV-Vis machine (Agilent Technologies) at 298 K. Freshly opened $CHCl_3$ (HPLC quality, stabilised with amylene) was used as a solvent and was filtered over basic alumina plug before use. A host solution with known concentration was prepared and fraction of this solution was transferred into a glass cuvette. Then, a guest solution with known concentration was prepared. A change of UV-vis-NIR absorption upon addition of aliquots of guest solution was followed. The observed changes of UV-vis-NIR absorbance were analysed using a purpose-written fitting macro in Microsoft Excel (written by Prof Hunter). A 1:1 binding isotherm was used to fit the experimental data assuming that all six porphyrin units of **6-ring** coordinate a pyridine ligand and act identically and independently. The concentration of host was allowed to change upon fitting. The experiments were measured at least two times on at least two different days with freshly prepared solutions in order to eliminate possible systematic errors. The results are stated as average values and errors are quoted as two times the standard deviation.

UV-vis-NIR titrations
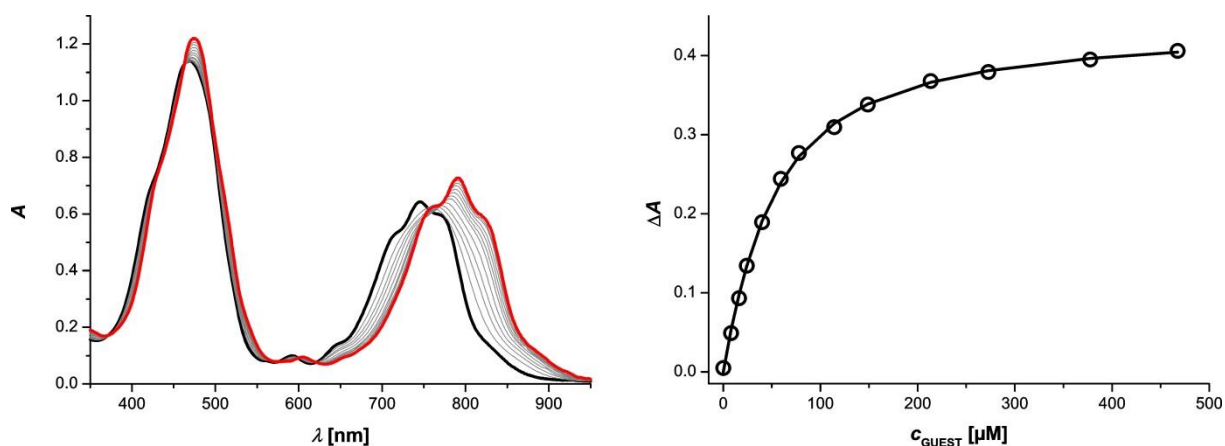
Figure 5.E1. UV-vis-NIR titration (CHCl$_3$, 298 K) of **4Py** to **6-ring**. UV-vis-NIR spectra are shown on the left with the spectrum of unbound **6-ring** in thick black line and the end spectrum in red thick line. On the right are shown the experimental data at 833 nm (circles) and calculated values (line) based on a 1:1 binding isotherm assuming that the six porphyrin units of **6-ring** act identically and independently.
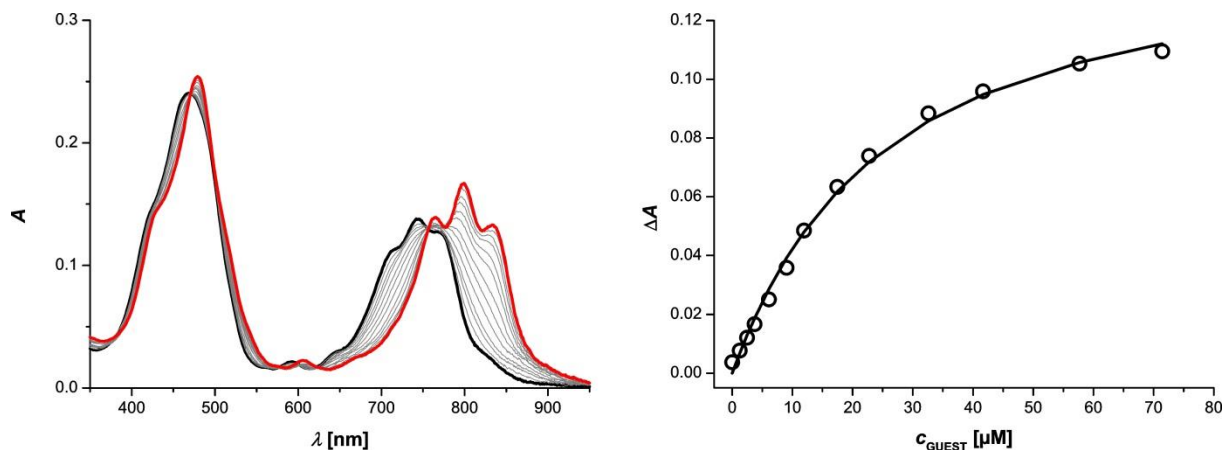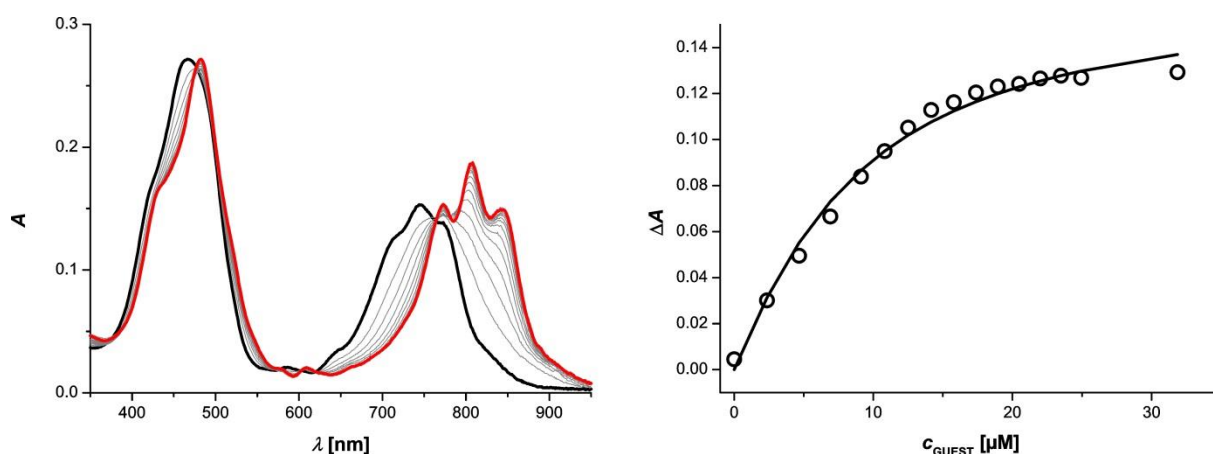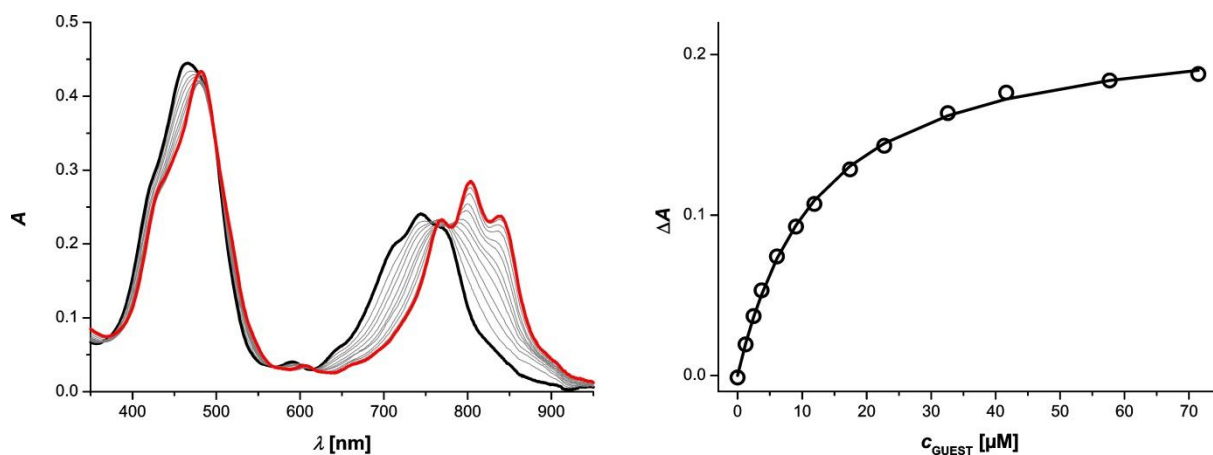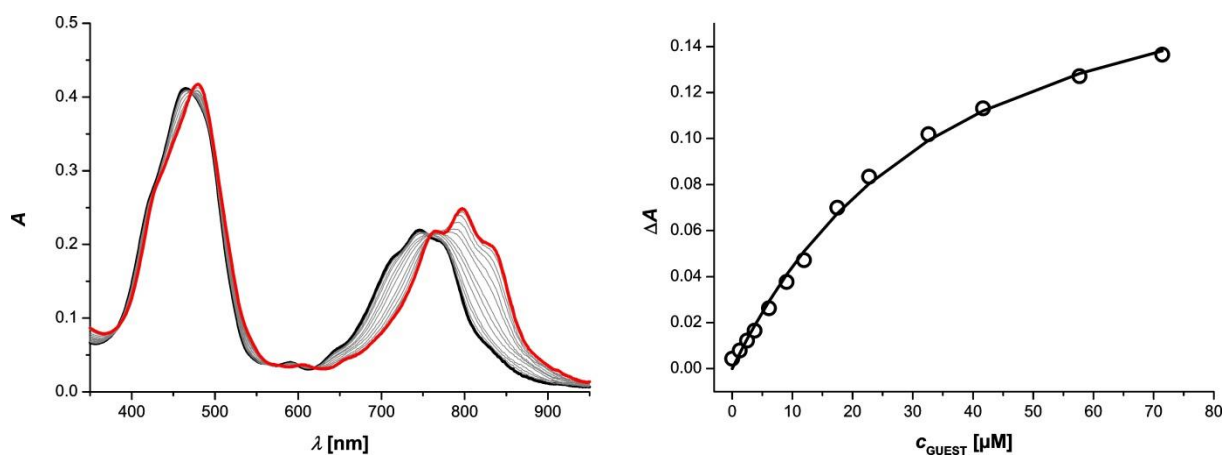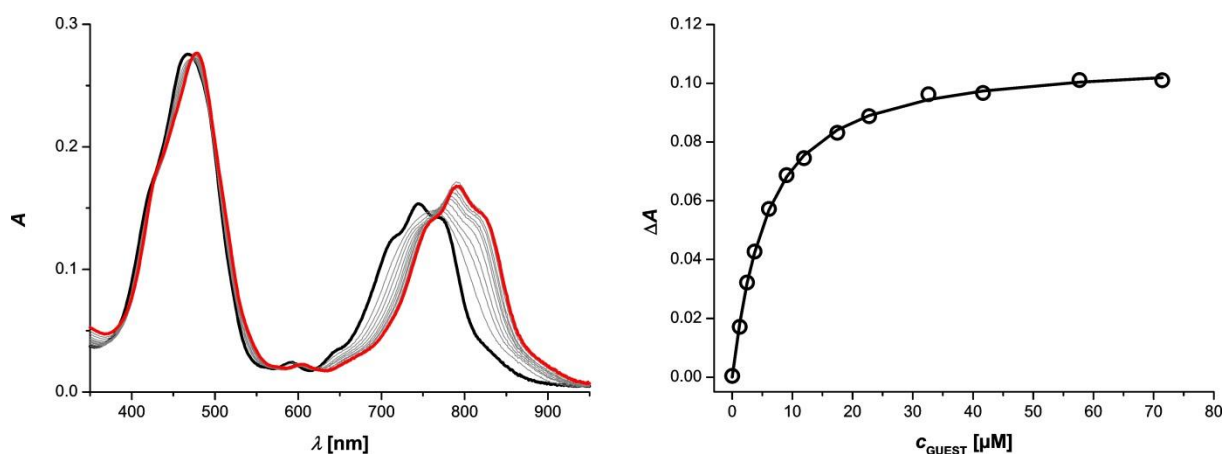

Figure 5.E2. UV-vis-NIR titration (CHCl$_3$, 298 K) of **3B3** to **6-ring**. UV-vis-NIR spectra are shown on the left with the spectrum of unbound **6-ring** in thick black line and the end spectrum in red thick line. On the right are shown the experimental data at 842 nm (circles) and calculated values (line) based on a 1:1 binding isotherm assuming that the six porphyrin units of **6-ring** act identically and independently.
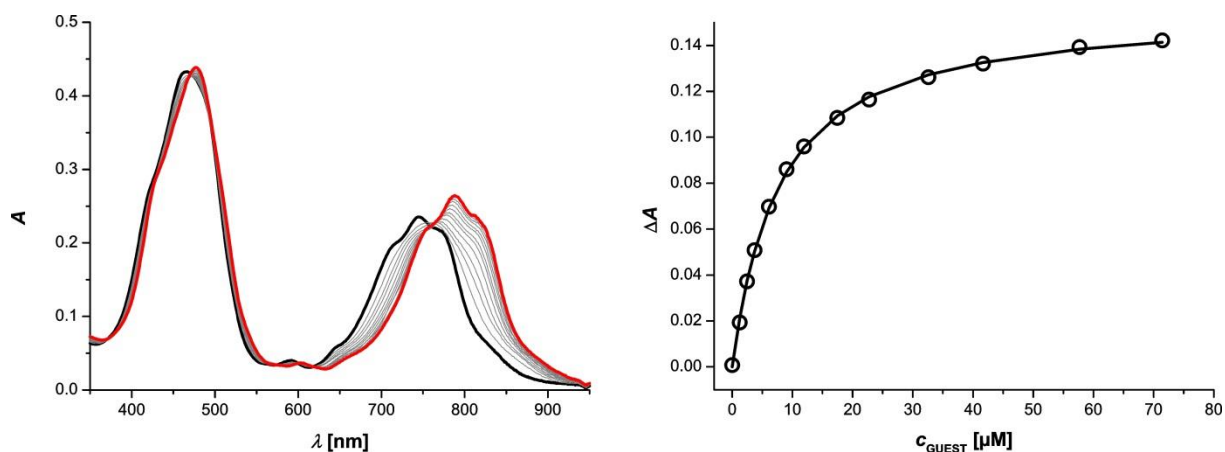
Figure 5.E3. UV-vis-NIR titration (CHCl$_3$, 298 K) of **4B3** to **6-ring**. UV-vis-NIR spectra are shown on the left with the spectrum of unbound **6-ring** in thick black line and the end spectrum in red thick line. On the right are shown the experimental data at 831 nm (circles) and calculated values (line) based on a 1:1 binding isotherm assuming that the six porphyrin units of **6-ring** act identically and independently.
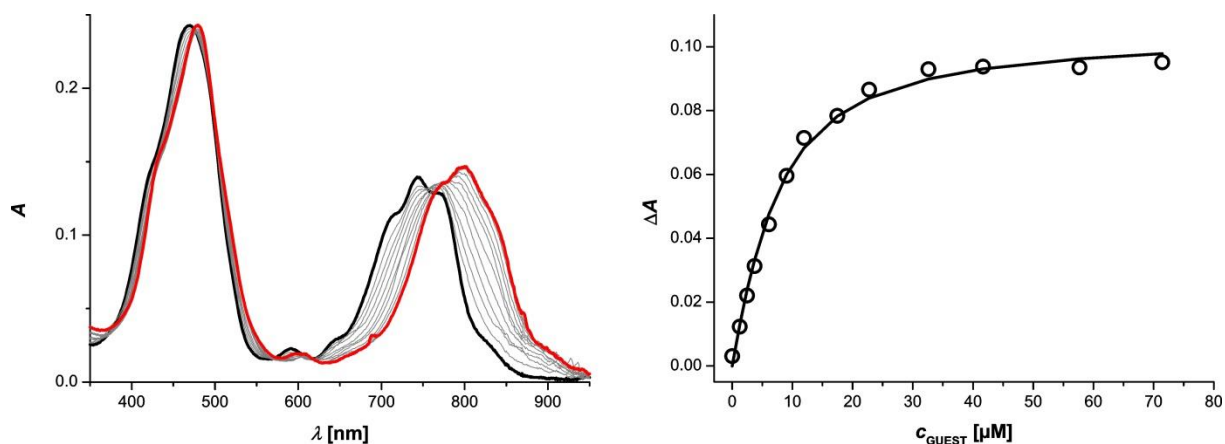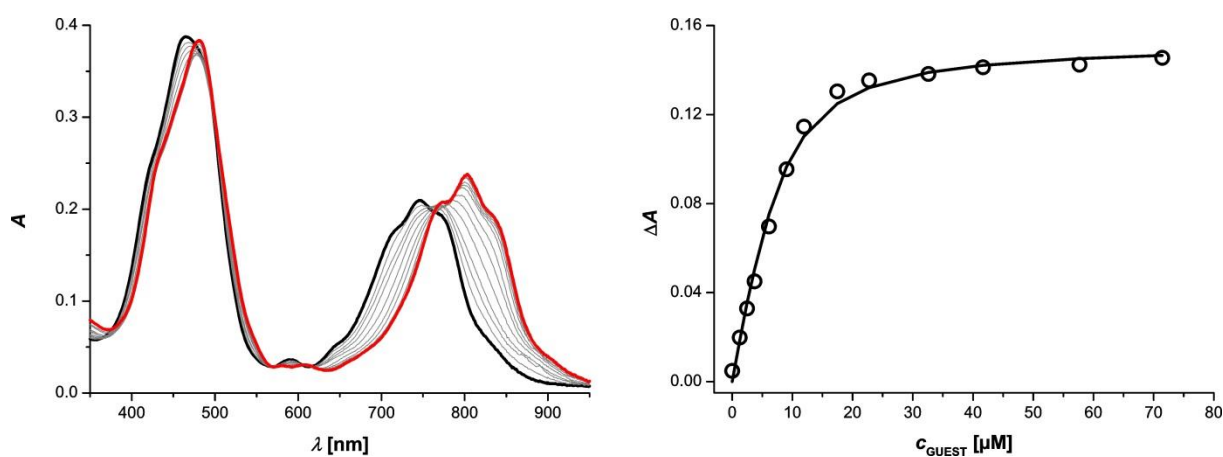

Figure 5.E4. UV-vis-NIR titration (CHCl$_3$, 298 K) of **3P1** to **6-ring**. UV-vis-NIR spectra are shown on the left with the spectrum of unbound **6-ring** in thick black line and the end spectrum in red thick line. On the right are shown the experimental data at 831 nm (circles) and calculated values (line) based on a 1:1 binding isotherm assuming that the six porphyrin units of **6-ring** act identically and independently.
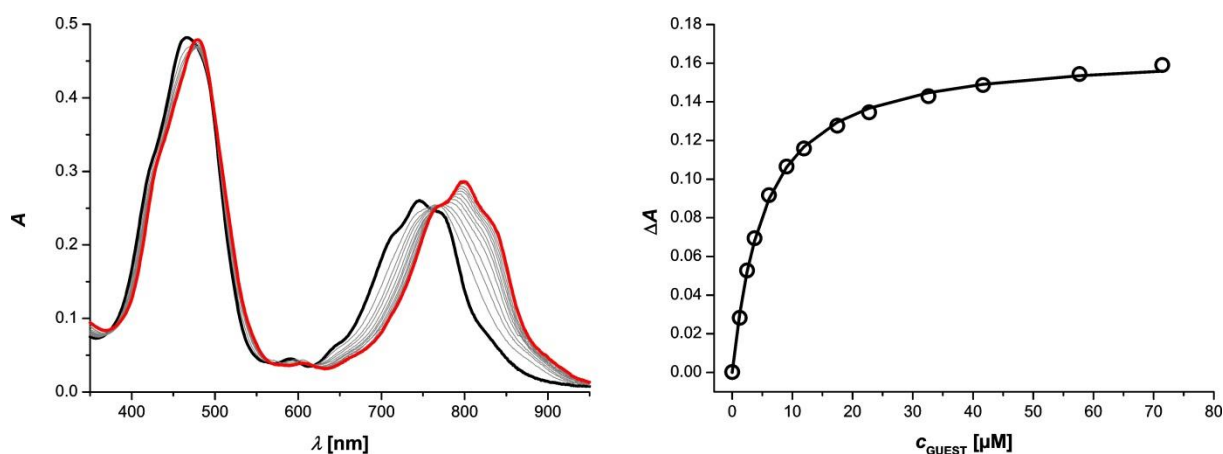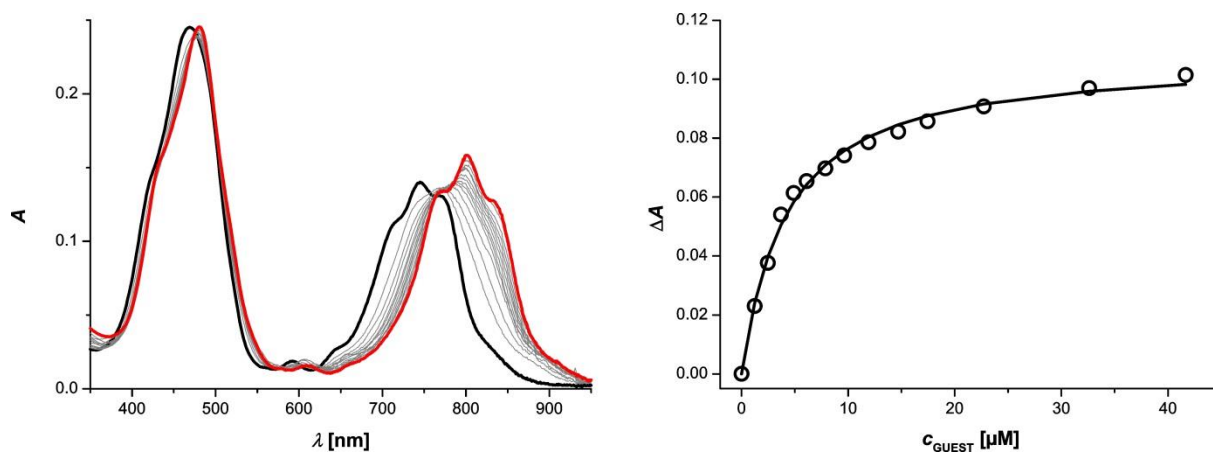
Figure 5.E5. UV-vis-NIR titration (CHCl$_3$, 298 K) of **3P2** to **6-ring**. UV-vis-NIR spectra are shown on the left with the spectrum of unbound **6-ring** in thick black line and the end spectrum in red thick line. On the right are shown the experimental data at 836 nm (circles) and calculated values (line) based on a 1:1 binding isotherm assuming that the six porphyrin units of **6-ring** act identically and independently.
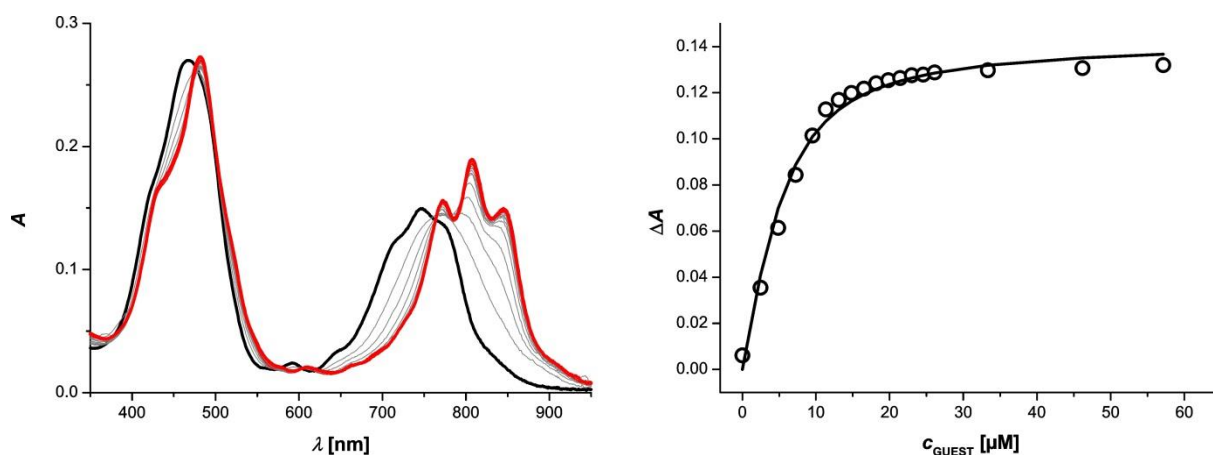

Figure 5.E6. UV-vis-NIR titration (CHCl$_3$, 298 K) of **4P1** to **6-ring**. UV-vis-NIR spectra are shown on the left with the spectrum of unbound **6-ring** in thick black line and the end spectrum in red thick line. On the right are shown the experimental data at 852 nm (circles) and calculated values (line) based on a 1:1 binding isotherm assuming that the six porphyrin units of **6-ring** act identically and independently. A 1:1 binding isotherm struggles to describe the experimental data correctly, but the concentration of ligand for half bound is 7 μM and the best fit for a 1:1 binding isotherm was used to compare this ligand with other systems.

Figure 5.E7. UV-vis-NIR titration (CHCl$_3$, 298 K) of **4P2** to **6-ring**. UV-vis-NIR spectra are shown on the left with the spectrum of unbound **6-ring** in thick black line and the end spectrum in red thick line. On the right are shown the experimental data at 843 nm (circles) and calculated values (line) based on a 1:1 binding isotherm assuming that the six porphyrin units of **6-ring** act identically and independently.
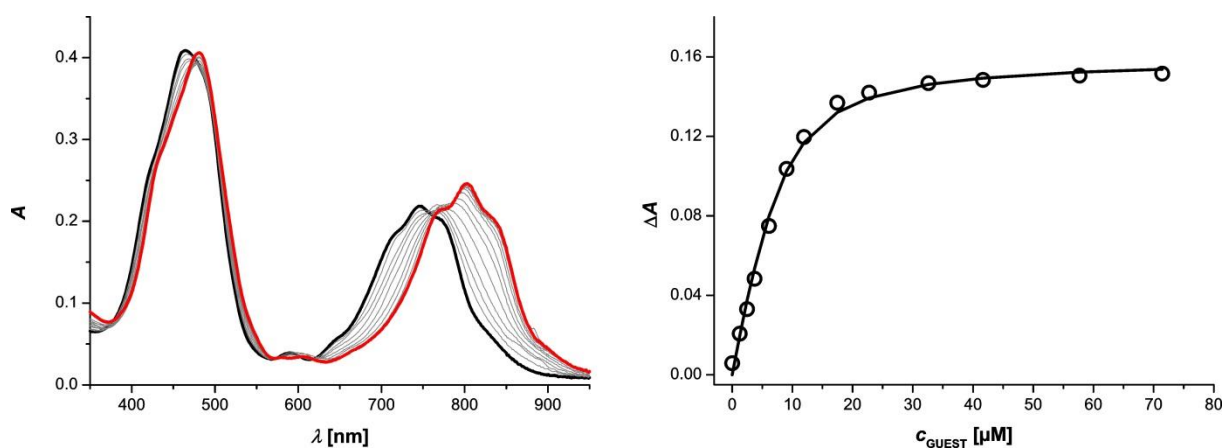

Figure 5.E8. UV-vis-NIR titration (CHCl$_3$, 298 K) of a 1:1 mixture of **P** and **3B3** to **6-ring**. UV-vis-NIR spectra are shown on the left with the spectrum of unbound **6-ring** in thick black line and the end spectrum in red thick line. On the right are shown the experimental data at 831 nm (circles) and calculated values (line) based on a 1:1 binding isotherm assuming that the six porphyrin units of **6-ring** act identically and independently.

Figure 5.E9. UV-vis-NIR titration (CHCl$_3$, 298 K) of a 1:1 mixture of **P** and **4B3** to **6-ring**. UV-vis-NIR spectra are shown on the left with the spectrum of unbound **6-ring** in thick black line and the end spectrum in red thick line. On the right are shown the experimental data at 831 nm (circles) and calculated values (line) based on a 1:1 binding isotherm assuming that the six porphyrin units of **6-ring** act identically and independently.
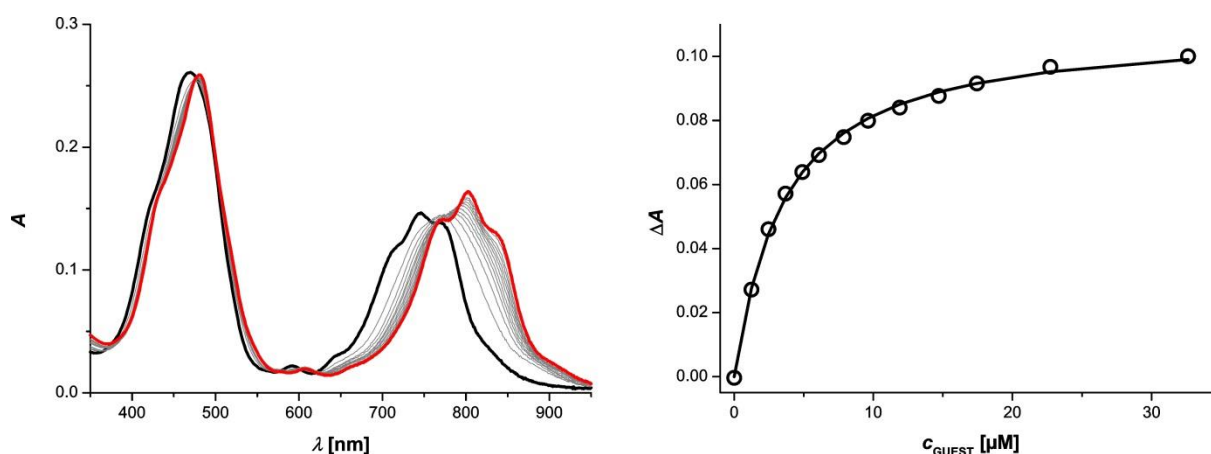

Figure 5.E10. UV-vis-NIR titration (CHCl$_3$, 298 K) of a 1:1 mixture of **B** and **3P1** to **6-ring**. UV-vis-NIR spectra are shown on the left with the spectrum of unbound **6-ring** in thick black line and the end spectrum in red thick line. On the right are shown the experimental data at 831 nm (circles) and calculated values (line) based on a 1:1 binding isotherm assuming that the six porphyrin units of **6-ring** act identically and independently.
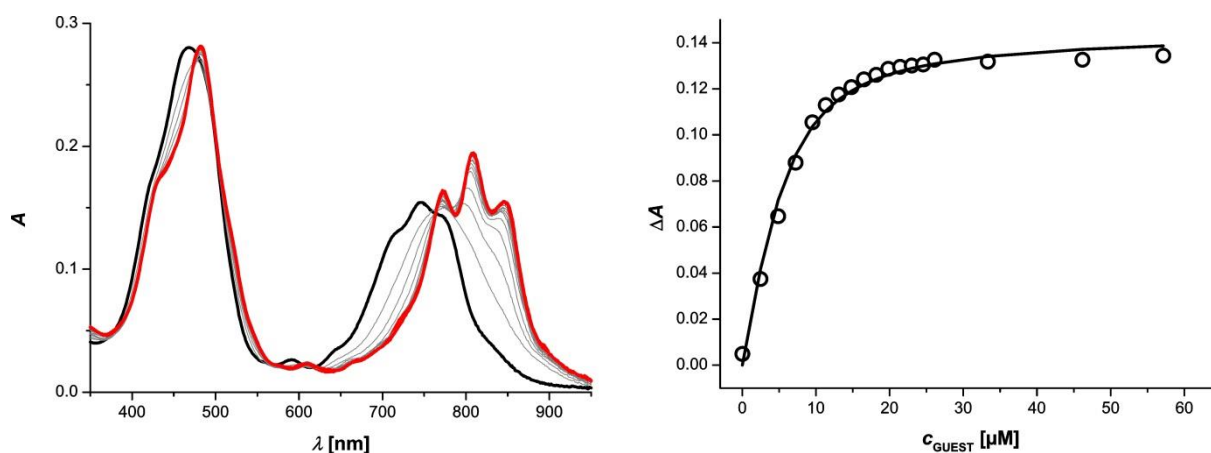
Figure 5.E11. UV-vis-NIR titration (CHCl$_3$, 298 K) of a 1:1 mixture of **B** and **3P2** to **6-ring**. UV-vis-NIR spectra are shown on the left with the spectrum of unbound **6-ring** in thick black line and the end spectrum in red thick line. On the right are shown the experimental data at 836 nm (circles) and calculated values (line) based on a 1:1 binding isotherm assuming that the six porphyrin units of **6-ring** act identically and independently.
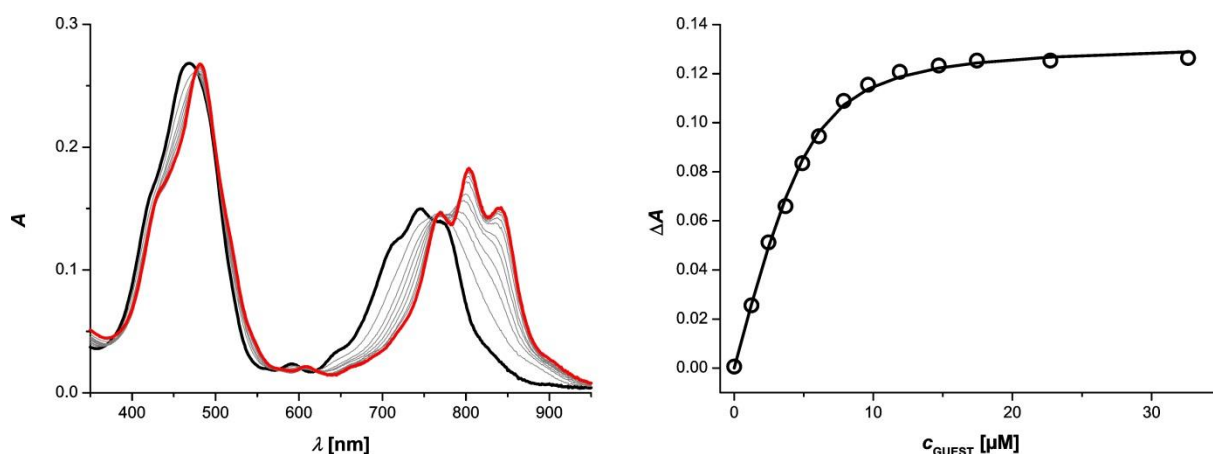

Figure 5.E12. UV-vis-NIR titration (CHCl$_3$, 298 K) of a 1:1 mixture of **B** and **4P1** to **6-ring**. UV-vis-NIR spectra are shown on the left with the spectrum of unbound **6-ring** in thick black line and the end spectrum in red thick line. On the right are shown the experimental data at 852 nm (circles) and calculated values (line) based on a 1:1 binding isotherm assuming that the six porphyrin units of **6-ring** act identically and independently.
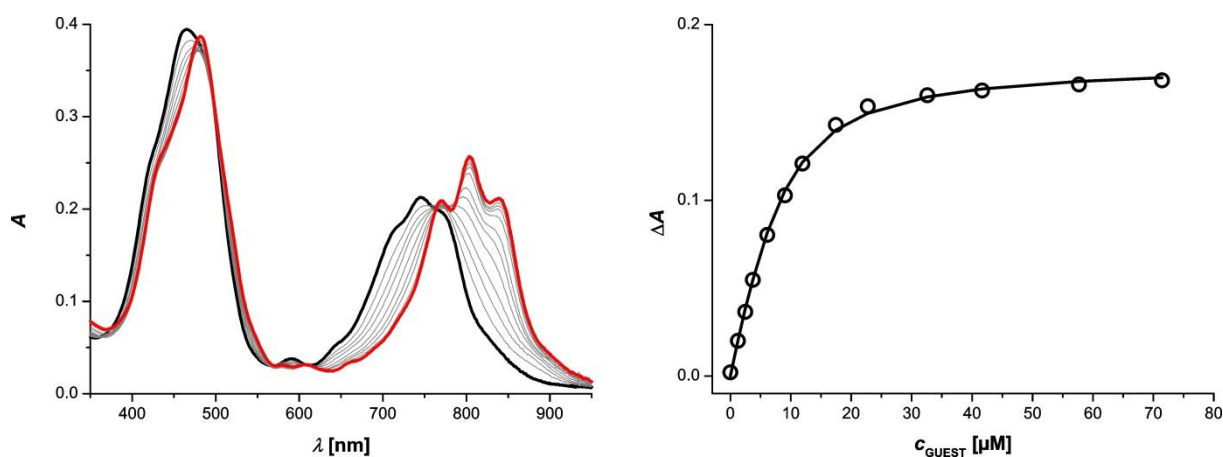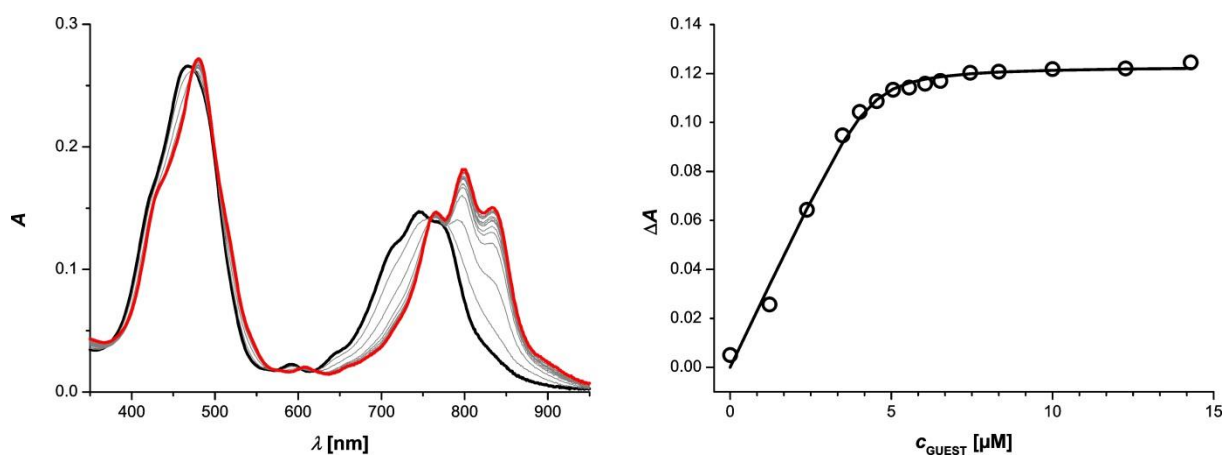
Figure 5.E13. UV-vis-NIR titration (CHCl$_3$, 298 K) of a 1:1 mixture of **B** and **4P2** to **6-ring**. UV-vis-NIR spectra are shown on the left with the spectrum of unbound **6-ring** in thick black line and the end spectrum in red thick line. On the right are shown the experimental data at 843 nm (circles) and calculated values (line) based on a 1:1 binding isotherm assuming that the six porphyrin units of **6-ring** act identically and independently.
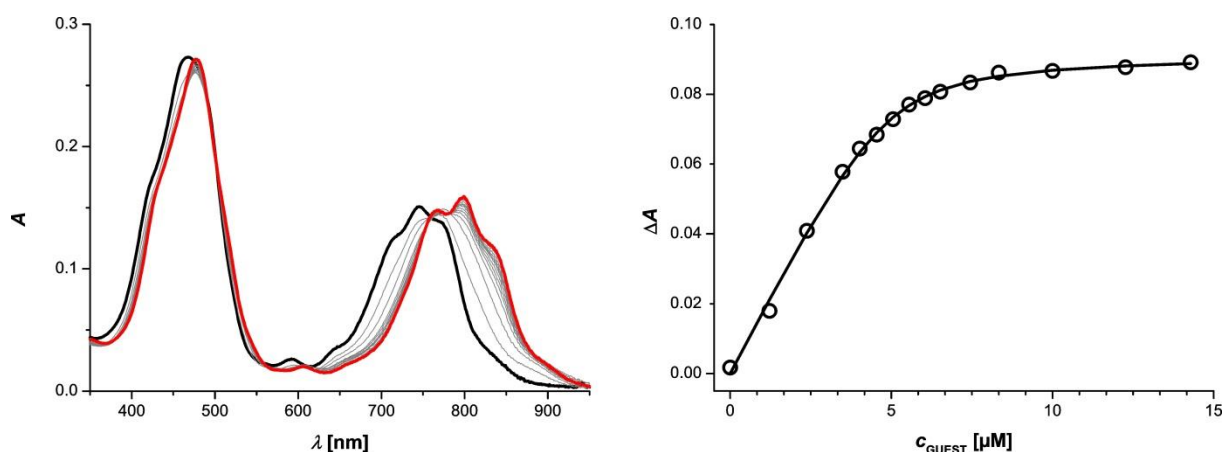

Figure 5.E14. UV-vis-NIR titration (CHCl$_3$, 298 K) of a 1:1 mixture of **C** and **3P1** to **6-ring**. UV-vis-NIR spectra are shown on the left with the spectrum of unbound **6-ring** in thick black line and the end spectrum in red thick line. On the right are shown the experimental data at 831 nm (circles) and calculated values (line) based on a 1:1 binding isotherm assuming that the six porphyrin units of **6-ring** act identically and independently.
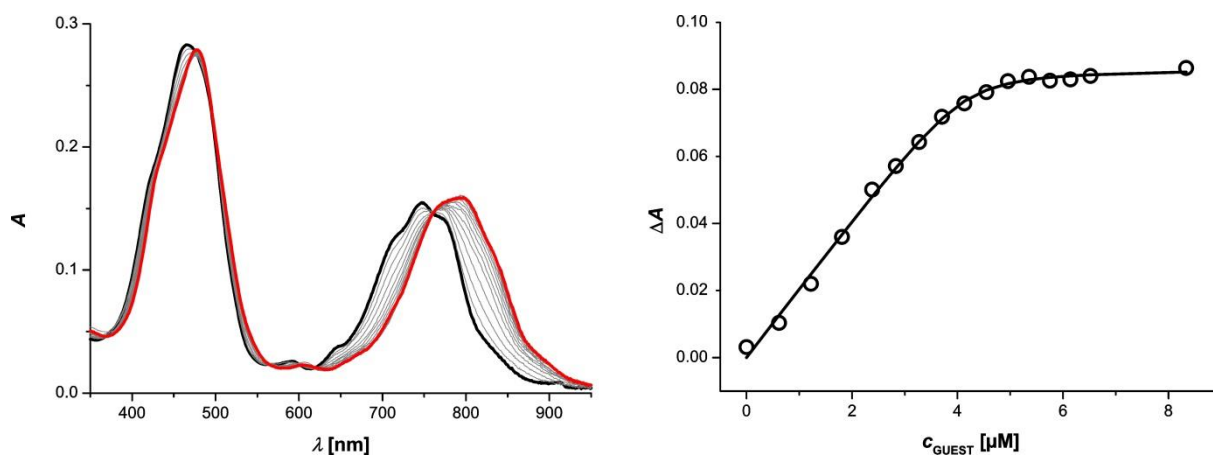
Figure 5.E15. UV-vis-NIR titration (CHCl$_3$, 298 K) of a 1:1 mixture of **C** and **3P2** to **6-ring**. UV-vis-NIR spectra are shown on the left with the spectrum of unbound **6-ring** in thick black line and the end spectrum in red thick line. On the right are shown the experimental data at 836 nm (circles) and calculated values (line) based on a 1:1 binding isotherm assuming that the six porphyrin units of **6-ring** act identically and independently.
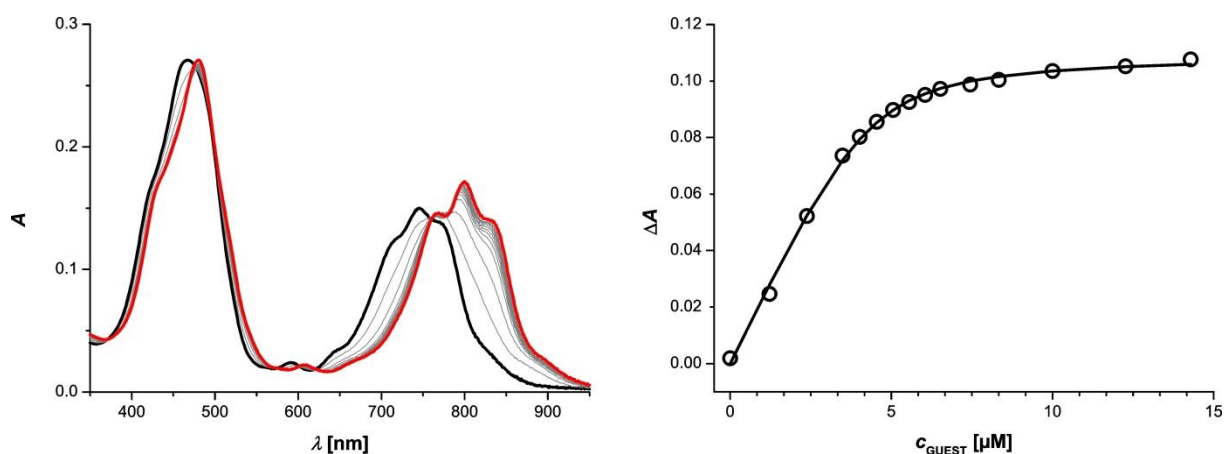

Figure 5.E16. UV-vis-NIR titration (CHCl$_3$, 298 K) of a 1:1 mixture of **C** and **4P1** to **6-ring**. UV-vis-NIR spectra are shown on the left with the spectrum of unbound **6-ring** in thick black line and the end spectrum in red thick line. On the right are shown the experimental data at 852 nm (circles) and calculated values (line) based on a 1:1 binding isotherm assuming that the six porphyrin units of **6-ring** act identically and independently.
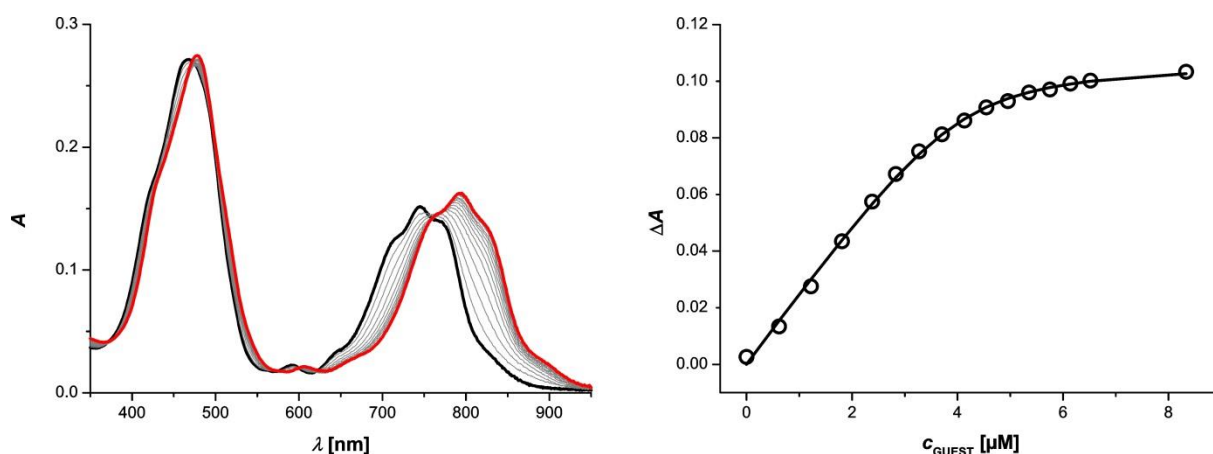
Figure 5.E17. UV-vis-NIR titration (CHCl₃, 298 K) of a 1:1 mixture of **C** and **4P2** to **6-ring**. UV-vis-NIR spectra are shown on the left with the spectrum of unbound **6-ring** in thick black line and the end spectrum in red thick line. On the right are shown the experimental data at 843 nm (circles) and calculated values (line) based on a 1:1 binding isotherm assuming that the six porphyrin units of **6-ring** act identically and independently.

Figure 5.E18. UV-vis-NIR titration (CHCl₃, 298 K) of a 1:1 mixture of **3B3** and **3P1** to **6-ring**. UV-vis-NIR spectra are shown on the left with the spectrum of unbound **6-ring** in thick black line and the end spectrum in red thick line. On the right are shown the experimental data at 835 nm (circles) and calculated values (line) based on a 1:1 binding isotherm assuming that the six porphyrin units of **6-ring** act identically and independently.
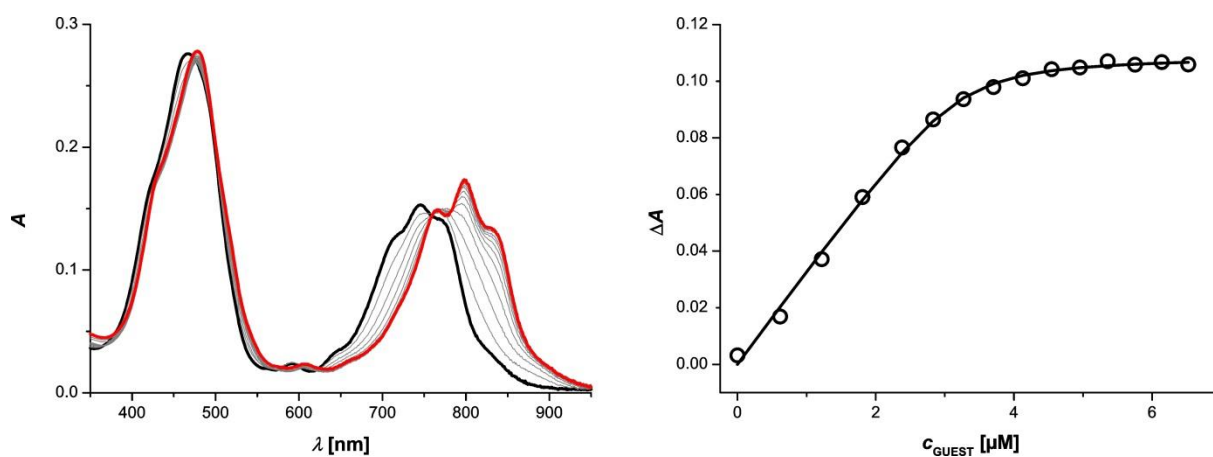
Figure 5.E19. UV-vis-NIR titration (CHCl$_3$, 298 K) of a 1:1 mixture of **3B3** and **3P2** to **6-ring**. UV-vis-NIR spectra are shown on the left with the spectrum of unbound **6-ring** in thick black line and the end spectrum in red thick line. On the right are shown the experimental data at 838 nm (circles) and calculated values (line) based on a 1:1 binding isotherm assuming that the six porphyrin units of **6-ring** act identically and independently.
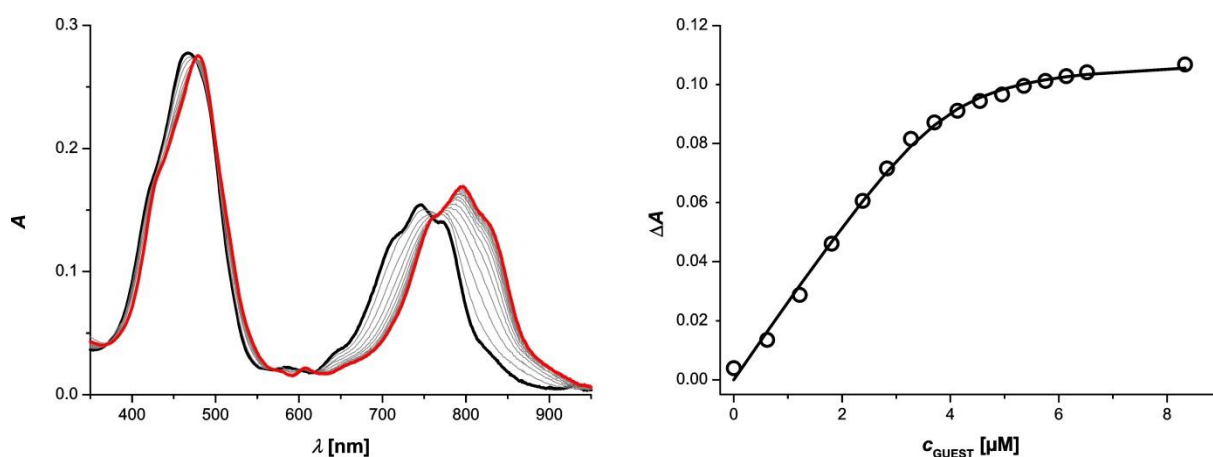

Figure 5.E20. UV-vis-NIR titration (CHCl$_3$, 298 K) of a 1:1 mixture of **3B3** and **4P1** to **6-ring**. UV-vis-NIR spectra are shown on the left with the spectrum of unbound **6-ring** in thick black line and the end spectrum in red thick line. On the right are shown the experimental data at 831 nm (circles) and calculated values (line) based on a 1:1 binding isotherm assuming that the six porphyrin units of **6-ring** act identically and independently.
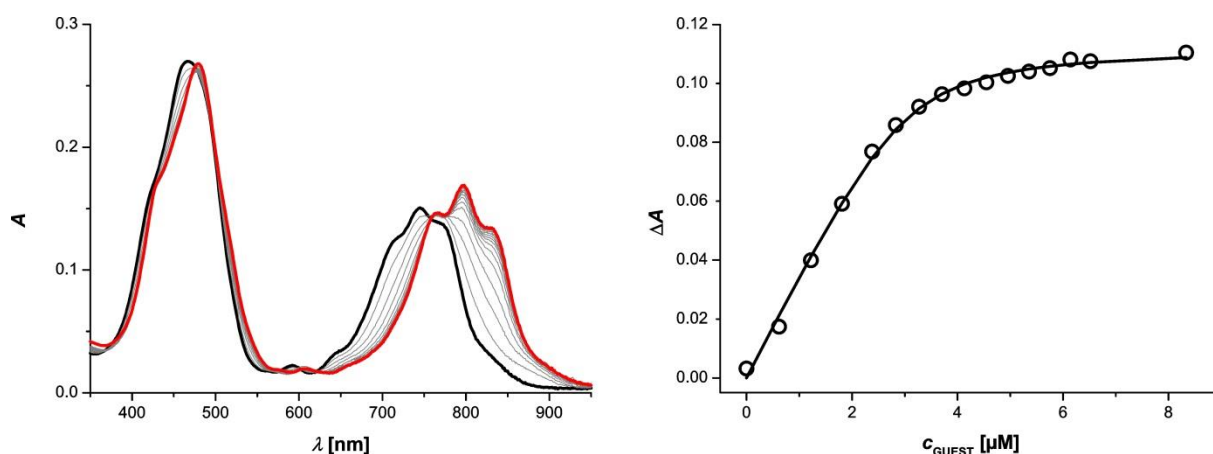
Figure 5.E21. UV-vis-NIR titration (CHCl$_3$, 298 K) of a 1:1 mixture of **3B3** and **4P2** to **6-ring**. UV-vis-NIR spectra are shown on the left with the spectrum of unbound **6-ring** in thick black line and the end spectrum in red thick line. On the right are shown the experimental data at 842 nm (circles) and calculated values (line) based on a 1:1 binding isotherm assuming that the six porphyrin units of **6-ring** act identically and independently.

Figure 5.E22. UV-vis-NIR titration (CHCl$_3$, 298 K) of a 1:1 mixture of **4B3** and **3P1** to **6-ring**. UV-vis-NIR spectra are shown on the left with the spectrum of unbound **6-ring** in thick black line and the end spectrum in red thick line. On the right are shown the experimental data at 831 nm (circles) and calculated values (line) based on a 1:1 binding isotherm assuming that the six porphyrin units of **6-ring** act identically and independently.

Figure 5.E23. UV-vis-NIR titration (CHCl$_3$, 298 K) of a 1:1 mixture of **4B3** and **3P2** to **6-ring**. UV-vis-NIR spectra are shown on the left with the spectrum of unbound **6-ring** in thick black line and the end spectrum in red thick line. On the right are shown the experimental data at 837 nm (circles) and calculated values (line) based on a 1:1 binding isotherm assuming that the six porphyrin units of **6-ring** act identically and independently.


Figure 5.E24. UV-vis-NIR titration (CHCl$_3$, 298 K) of a 1:1 mixture of **4B3** and **4P1** to **6-ring**. UV-vis-NIR spectra are shown on the left with the spectrum of unbound **6-ring** in thick black line and the end spectrum in red thick line. On the right are shown the experimental data at 834 nm (circles) and calculated values (line) based on a 1:1 binding isotherm assuming that the six porphyrin units of **6-ring** act identically and independently.

Figure 5.E25. UV-vis-NIR titration (CHCl$_3$, 298 K) of a 1:1 mixture of **4B3** and **4P2** to **6-ring**. UV-vis-NIR spectra are shown on the left with the spectrum of unbound **6-ring** in thick black line and the end spectrum in red thick line. On the right are shown the experimental data at 835 nm (circles) and calculated values (line) based on a 1:1 binding isotherm assuming that the six porphyrin units of **6-ring** act identically and independently.

5.8.5. NMR experiments
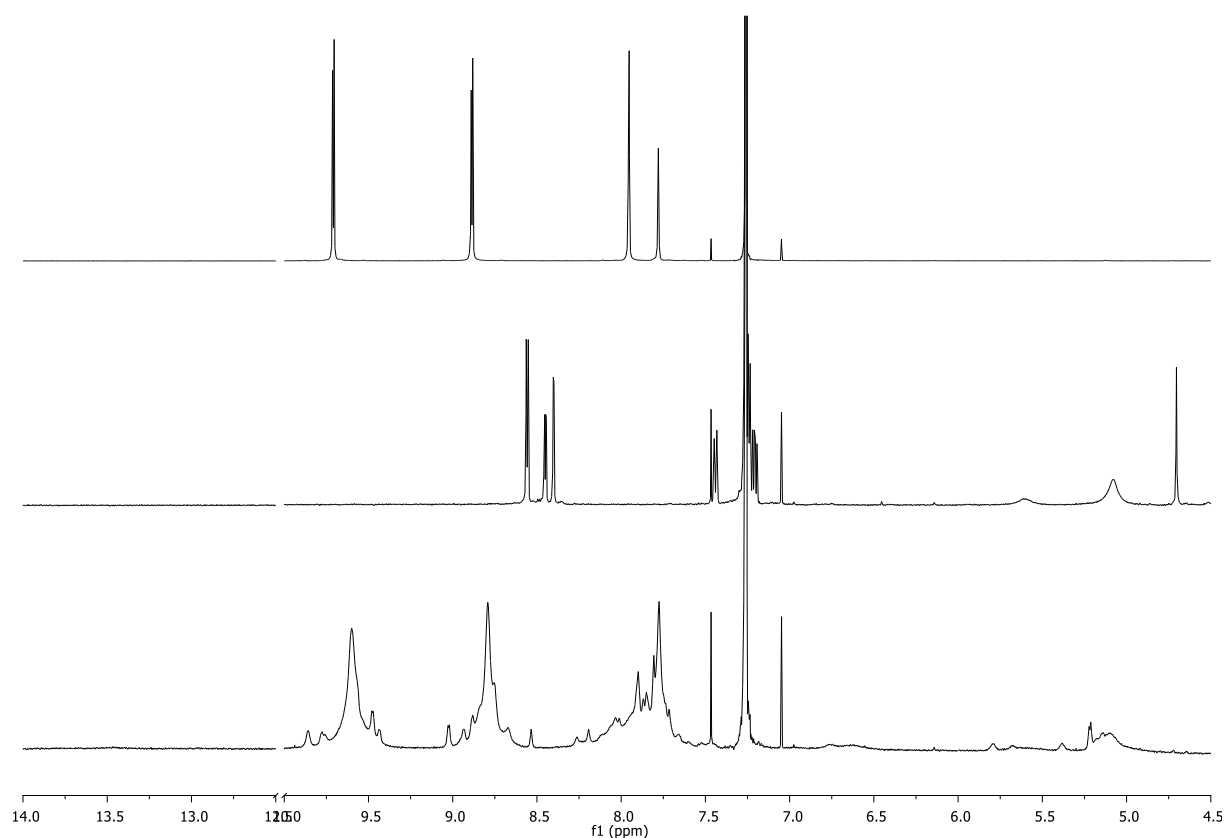
Figure 5.S26. Partial ^{1}H NMR (500 MHz, CDCl$_3$, 298 K) spectra of (a) **6-ring** (0.16 mM), (b) mixture of **3B3** (0.48 mM) and **4P1** (0.48 mM) and (c) mixture of **6-ring** (0.16 mM), **3B3** (0.48 mM) and **4P1** (0.48 mM).
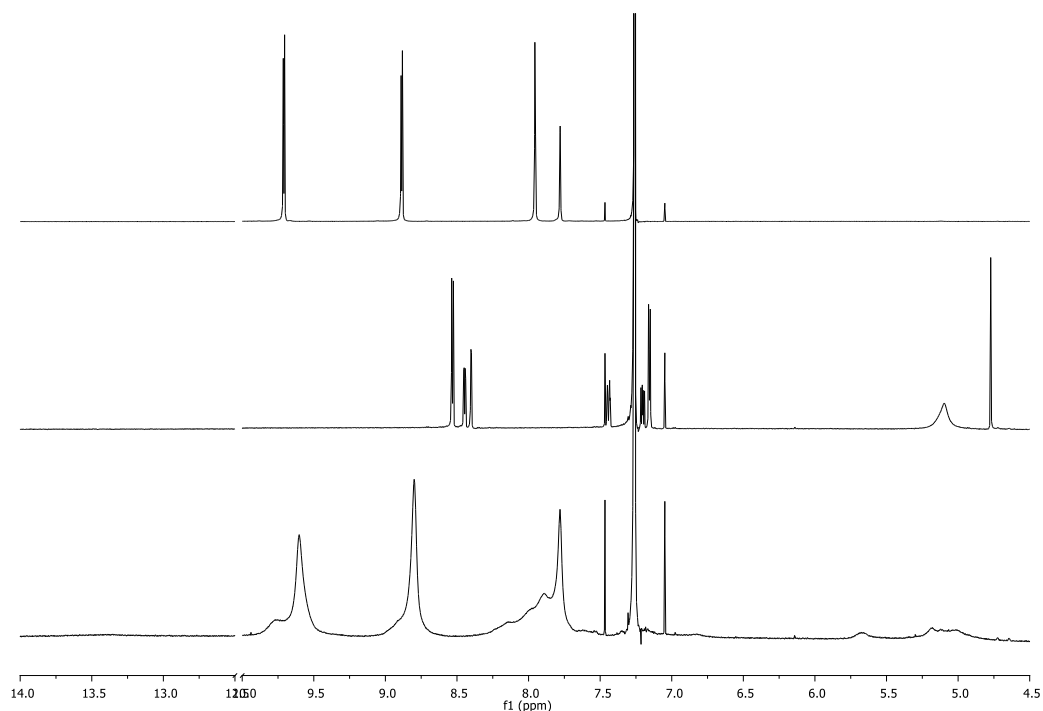
Figure 5.S27. Partial ^{1}H NMR (500 MHz, CDCl$_3$, 298 K) spectra of (a) **6-ring** (0.16 mM), (b) mixture of **3B3** (0.48 mM) and **4P2** (0.48 mM) and (c) mixture of **6-ring** (0.16 mM), **3B3** (0.48 mM) and **4P2** (0.48 mM).
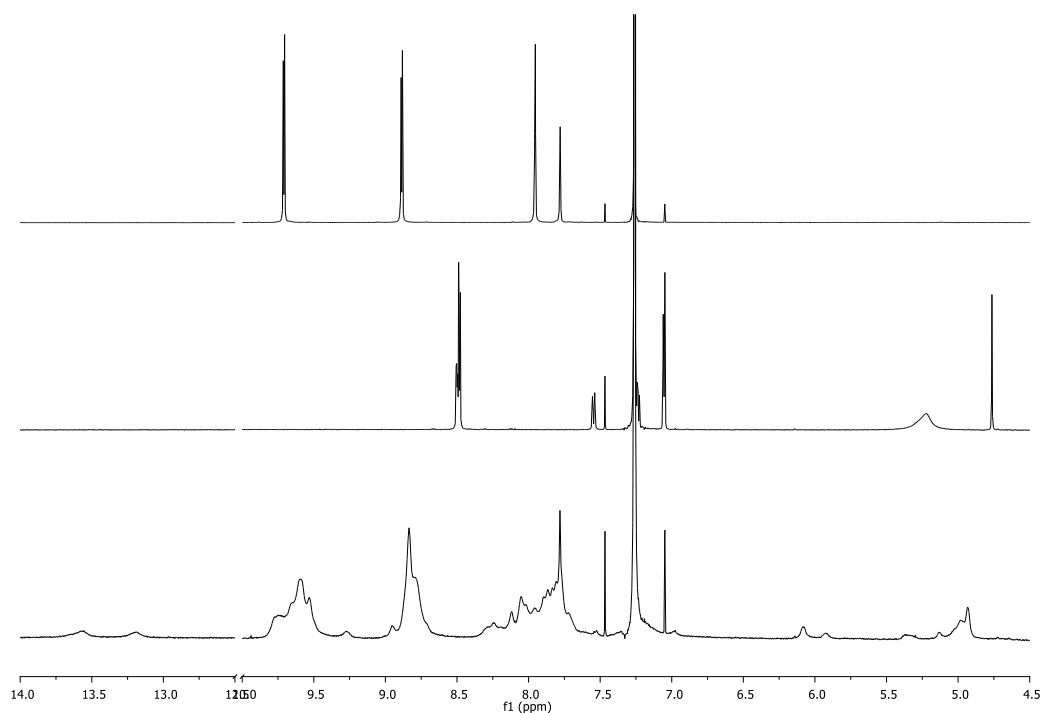
Figure 5.S28. Partial ^{1}H NMR (500 MHz, CDCl$_3$, 298 K) spectra of (a) **6-ring** (0.16 mM), (b) mixture of **4B3** (0.48 mM) and **3P2** (0.48 mM) and (c) mixture of **6-ring** (0.16 mM), **4B3** (0.48 mM) and **3P2** (0.48 mM).

215

5.9. References

(1)   Fasting, C.; Schalley, C. A.; Weber, M.; Seitz, O.; Hecht, S.; Koksch, B.; Dernedde, J.; Graf, C.; Knapp, E.-W.; Haag, R. *Angew. Chem. Int. Ed.* **2012**, *51*, 10472-10498.

(2)   Hunter, C. A.; Anderson, H. L. *Angew. Chem. Int. Ed.* **2009**, *48*, 7488-7499.

(3)   Motloch, P.; Hunter, C. A. *Adv. Phys. Org. Chem.* **2016**, *50*, 77-118.

(4)   Hoffmann, M.; Kärnbratt, J.; Chang, M.-H.; Herz, L. M.; Albinsson, B.; Anderson, H. L. *Angew. Chem. Int. Ed.* **2008**, *47*, 4993-4996.

(5)   Hogben, H. J.; Sprafke, J. K.; Hoffmann, M.; Pawlicki, M.; Anderson, H. L. *J. Am. Chem. Soc.* **2011**, *133*, 20962-20969.

(6)   Motloch, P., Chapter III, Ph.D. Thesis, University of Cambridge, 2019.

(7)   Sprafke, J. K.; Kondratuk, D. V.; Wykes, M.; Thompson, A. L.; Hoffmann, M.; Drevinskas, R.; Chen, W.-H.; Yong, C. K.; Kärnbratt, J.; Bullock, J. E.; Malfois, M.; Wasielewski, M. R.; Albinsson, B.; Herz, L. M.; Zigmantas, D.; Beljonne, D.; Anderson, H. L. *J. Am. Chem. Soc.* **2011**, *133*, 17262-17273.

(8)   Benson, S. W. *J. Am. Chem. Soc.* **1958**, *80*, 5151-5154.

(9)   Bishop, D. M.; Laidler, K. J. *J. Chem. Phys.* **1965**, *42*, 1688-1691.

(10)   Ercolani, G.; Piguet, C.; Borkovec, M.; Hamacek, J. *J. Phys. Chem. B* **2007**, *111*, 12195-12203.

(11)   Zajac, M. A. *J. Org. Chem.* **2008**, *73*, 6899-6901.

(12)   ten Cate, M. G. J.; Huskens, J.; Crego-Calama, M.; Reinhoudt, D. N. *Chem. Eur. J.* **2004**, *10*, 3632-3639.

(13)   Misuraca, M. C.; Grecu, T.; Freixa, Z.; Garavini, V.; Hunter, C. A.; van Leeuwen, P. W. N. M.; Segarra-Maset, M. D.; Turega, S. M. *J. Org. Chem.* **2011**, *76*, 2723-2732.

(14)   Rousseaux, S. A. L.; Gong, J. Q.; Haver, R.; Odell, B.; Claridge, T. D. W.; Herz, L. M.; Anderson, H. L. *J. Am. Chem. Soc.* **2015**, *137*, 12713-12718.

(15)   Frisch, M. J.; Trucks, G. W.; Schlegel, H. B.; Scuseria, G. E.; Robb, M. A.; Cheeseman, J. R.; Scalmani, G.; Barone, V.; Mennucci, B.; Petersson, G. A.; Nakatsuji, H.; Caricato, M.; Li, X.; Hratchian, H. P.; Izmaylov, A. F.; Bloino, J.; Zheng, G.; Sonnenberg, J. L.; Hada, M.; Ehara, M.; Toyota, K.; Fukuda, R.; Hasegawa, J.; Ishida, M.; Nakajima, T.; Honda, Y.; Kitao, O.; Nakai, H.; Vreven, T.; Montgomery Jr., J. A.; Peralta, J. E.; Ogliaro, F.; Bearpark, M. J.; Heyd, J.; Brothers, E. N.; Kudin, K. N.; Staroverov, V. N.; Kobayashi, R.; Normand, J.; Raghavachari, K.; Rendell, A. P.; Burant, J. C.; Iyengar, S. S.; Tomasi, J.; Cossi, M.; Rega, N.;

Millam, N. J.; Klene, M.; Knox, J. E.; Cross, J. B.; Bakken, V.; Adamo, C.; Jaramillo, J.; Gomperts, R.; Stratmann, R. E.; Yazyev, O.; Austin, A. J.; Cammi, R.; Pomelli, C.; Ochterski, J. W.; Martin, R. L.; Morokuma, K.; Zakrzewski, V. G.; Voth, G. A.; Salvador, P.; Dannenberg, J. J.; Dapprich, S.; Daniels, A. D.; Farkas, Ö.; Foresman, J. B.; Ortiz, J. V.; Cioslowski, J.; Fox, D. J.; Gaussian, Inc.: Wallingford, CT, USA, 2009.

VI

Hybrid hydrogen-bonded/
metal-coordinated cage

6.1. Introduction

Nature uses simple building blocks to assemble highly complex well-defined structures by multivalent non-covalent interactions.[1] The scientific community has found a large number of artificial systems that resemble these structures found in nature.[2] There are two main ways the synthetic systems are assembled: hydrogen-bonding and metal-coordination. The former is used in capsules and the latter in metal-coordinated cages. Cages are usually prepared by coordination of a metal to pyridines,[3-5] imines,[6] and other suitable ligands.[7] Capsules use the direction, polarity and self-complementarity of hydrogen bonds.[8] Both types have attracted substantial attention thanks to their host-guest and stimuli-responsive behaviour,[9,10] and sometimes just pure curiosity and sportsmanship.[11] Conversely, there are not many examples in which these two methods of assembly are utilised together in the self-assembly of well-defined discrete hybrid 3D structures.[12-14]

One of the hydrogen-bonded motifs that have been used in the formation of capsules as well as hybrid 2D structures is the rosette motif (Figure 6.1). The groups of Whitesides, Reindhout and others studied extensively the rosette self-assembly, crystal packing and kinetic stability.[15,16] The Reindhout group prepared a molecular container based on double rosettes using a calix[4]arene ditriaminotriazine.[17] They were able to use this system for the encapsulation of different guest molecules.
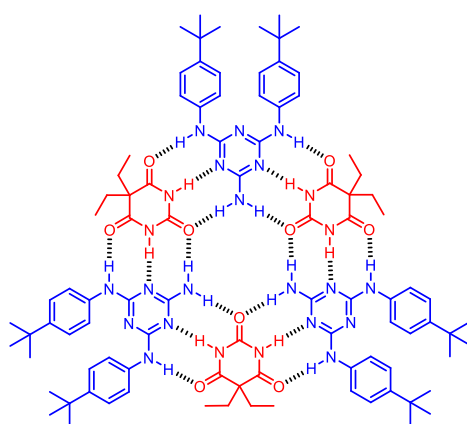
**Figure 6.1**. Rosette motif based on a barbiturate and triazine.

Several hybrid systems based on the rosette motif have been prepared. The Whitesides group synthesised a tris(triazine) hub containing imidazole groups on the periphery.[18] They were able to assemble them with zinc porphyrins to form hybrid systems as confirmed by ^{1}H NMR spectroscopy, ESI-MS and GPC. The Reinhout group used the rosette motif to prepare rosette metallo-dendrimers with molecular weights up to 28 kDa.[19] The group of Therrien used this motif to prepare supramolecular piano-stool complexes of Ru, Rh and Ir on the periphery of the rosette.[20] They extended this work to prepare heteronuclear supramolecular metalla-assemblies.[21]

All of the aforementioned examples of hybrid complexes based on rosette motif have one important thing in common: since the metal-coordinated fragment is always on the periphery, it is not a crucial part of the architecture of the complex. In other words, if the metallic part is removed, the main 3D structure of the complex remains the same. There is only one example of 3D hybrid architecture based on the rosette motif, where removing the metal part changes the 3D topology significantly: The group of Li prepared a strapped porphyrin cyanuric acid and mixed it with a triazine and pyridine-substituted barbiturate to prepare a hybrid cage structure.[22] The removal of metal-coordinated fragment from the double rosette complex would lead to the disassembly and produce a single rosette complex. Unfortunately, they characterised this cage only by simple ^{1}H NMR spectroscopy and did not explore the host-guest and stimuli-responsive behaviour. There are only a limited number of systems using different motifs that can be considered genuine hybrid hydrogen-bonded/metal-coordinated cages in the literature.

We hypothetised that the rosette motif could be employed for the preparation of a new discrete 3D hybrid hydrogen-bonded/metal-coordinated system. The design and assembly of such system is described in this chapter.

6.2. Approach

We decided to use the barbiturate-pyridine type of molecules explored in Chapter V to form the target hybrid cage by a coordination of a metal to pyridine units (Figure 6.2). The first choice was to employ palladium(II) salts because their pyridine complexes are well-defined, well-studied and easily prepared (usually by a simple mixing of compounds).[23] Another explored metal was platinum, due to the creation of more stable complexes compared to palladium.[24]
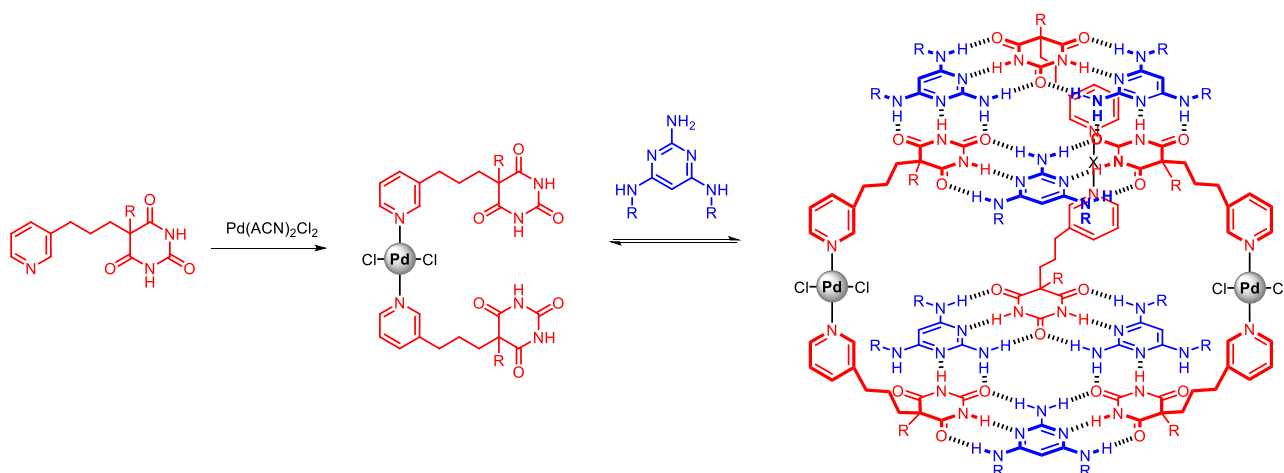
Figure 6.2. Hybrid hydrogen-bonded/metal-coordinated cage (R is a solubilising group).

The ultimate aim of this project was to fully characterise the target complex in solution and if possible also in solid state. For that, a detailed study by 2D NMR spectroscopy was conducted and different additional techniques tried. Moreover, the host-guest behaviour of the cage was explored. Since the target cage has hybrid character, it was shown that each of its parts was able to respond selectively to a different stimulus.

We tried to find the alkyl linkers between the barbiturate and the pyridine units that would provide the optimal geometry for the target cage complex: the barbiturate and pyridine units in perpendicular planes. The coordination of palladium(II) to the pyridine unit in *trans* fashion should then produce a complex with two parallel rosettes. A structure search of CCDC suggested two lead candidates (Figure 6.3); the first one without any alkyl linker between the barbiturate and pyridine units (**4B0)** and the second one with a -CH$_2$- linker (**4B1**).
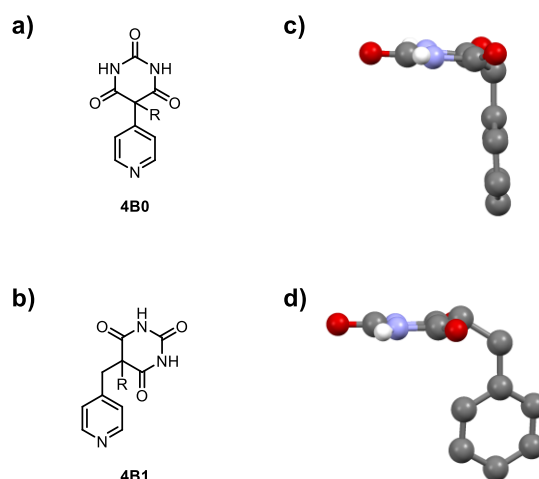
Figure 6.3. Barbiturate-pyridines (a) **4B0** and (b) **4B1** (R is a solubilising group) and X-ray structures of (c) CCDC 1549455 and (d) CCDC 217698 structures showing the right geometry for the target cage (other atoms of the molecules were removed for clarity). Colouring of atoms: C (grey), N (blue), O (red) and H (white).

As the second rosette component, different pyrimidines and triazines with substituents that should increase the probability of successful crystallisation were utilised (Figure 6.4).
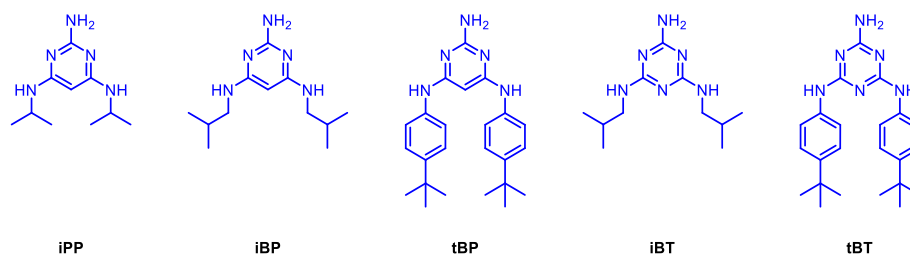

Figure 6.4. Pyrimidines and triazines used to form cages in this study.

6.3. Modelling

Firstly, we modelled the target hybrid cages based on both **4B0** and **4B1** computationally using semi-empirical method PM6. As the starting points, ideal cage structures similar to the one showed in Figure 6.2 were used. **tBP** was chosen as the second rosette component. Their optimisation provided possible structures of the target cages as depicted in Figure 6.5 (alkyl groups were replaced by hydrogen atoms to decrease the computational costs). The structure predicted for **4B1** is much more packed in comparison with **4B0**. In addition, the rosette of complex with **4B0** is much flatter that should correlate

with the stability.[15] In both cases, the large void volume inside the cages could result in problems with crystallisation.[25]
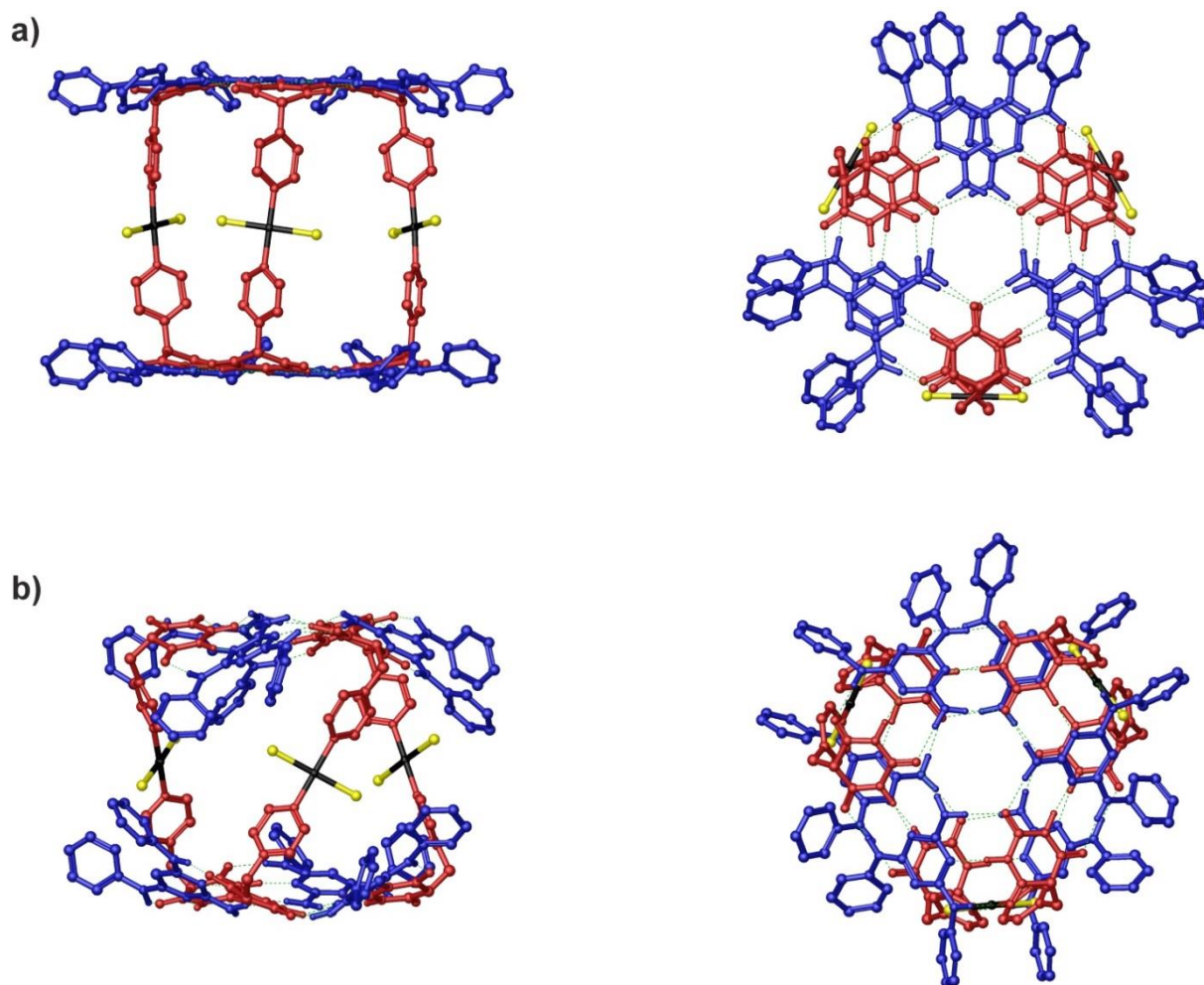
Figure 6.5. PM6 optimised possible structures of hybrid cages based on (a) **4B0** and (b) **4B1** using **tBP** as the second partner (alkyl groups were replaced by hydrogen atoms in the calculations). Hydrogen atoms that do not contribute to hydrogen-bonding were omitted for clarity. Colouring: barbiturate-pyridine in red, pyrimidine in blue, palladium atoms in black, chlorine atoms in yellow, green dashed line is the hydrogen-bond.

6.4. Synthesis of cage components

4B1 was synthesised using slightly altered literature procedure utilising DMF instead of ethanol for the second step that resulted in an increased yield (Scheme 6.1).
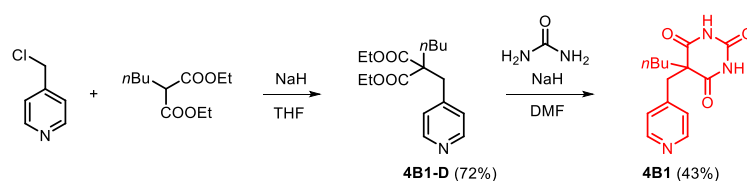
Scheme 6.1. Synthesis of barbiturate-pyridine **4B1**.

Pyrimidines containing isobutyl (**iBP**), isopropyl (**iPP**) and *tert*-butylphenyl (**tBP**) were synthesised in one step syntheses in excellent yields (Scheme 6.2). Triazines **iBT** and **tBT** were prepared in two steps using a literature procedure (Scheme 6.2).[26]
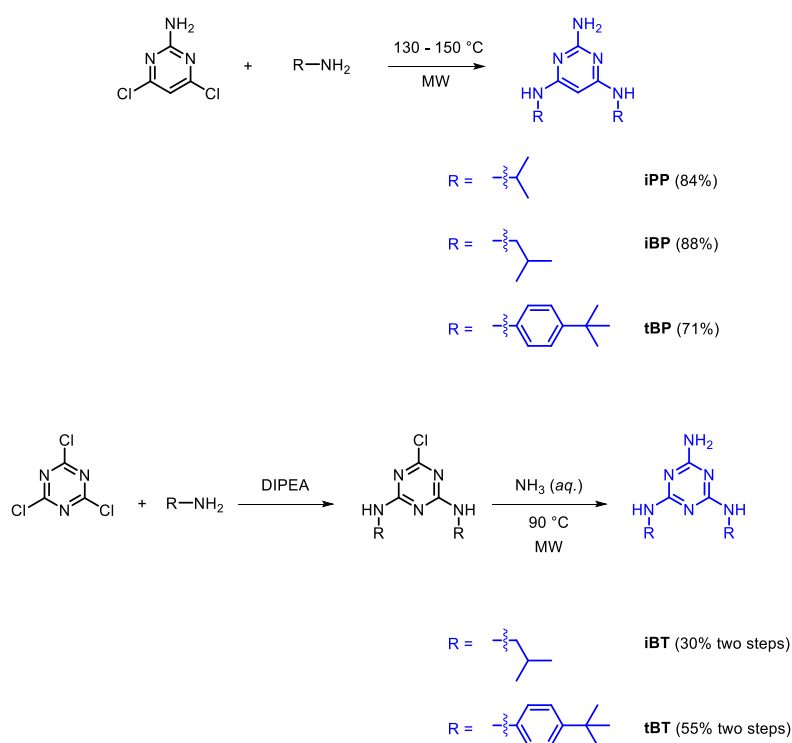
Scheme 6.2. Synthesis of pyrimidines **iPP**, **iBP** and **iBP** and triazines **iBT** and **tBT**.

Next, the palladium complex **Pd(4B1)₂Cl₂** was isolated as a solid by reacting **4B1** with Pd(ACN)₂Cl₂ (Scheme 6.3). The ^{1}H NMR and ^{13}C NMR spectra showed the expected downfield of the pyridine C-H as shown in Figure 6.6. HR-MS and elemental analysis additionally confirmed the stoichiometry (see the Experimental section).
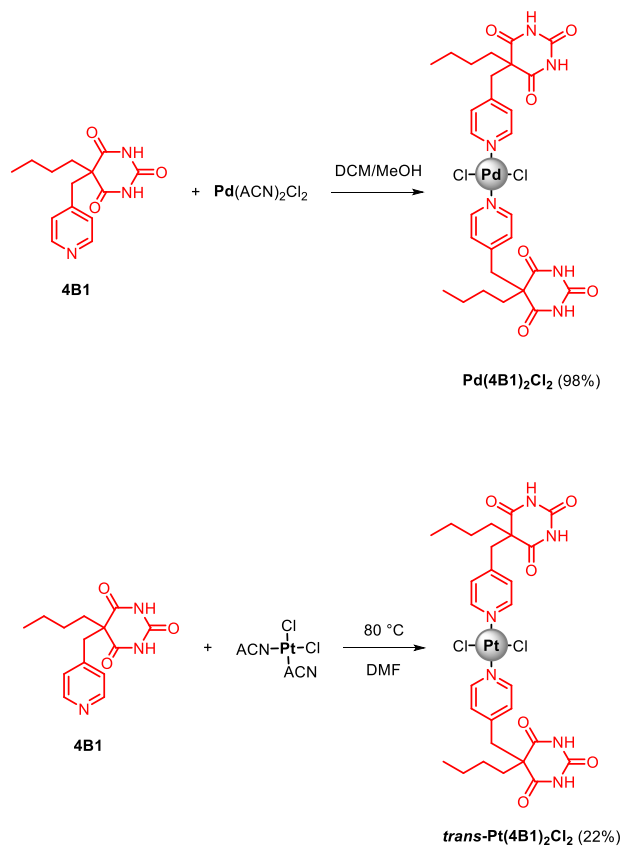
Scheme 6.3. Preparation of **Pd(4B1)₂Cl₂** and ***trans*-Pt(4B1)₂Cl₂**.
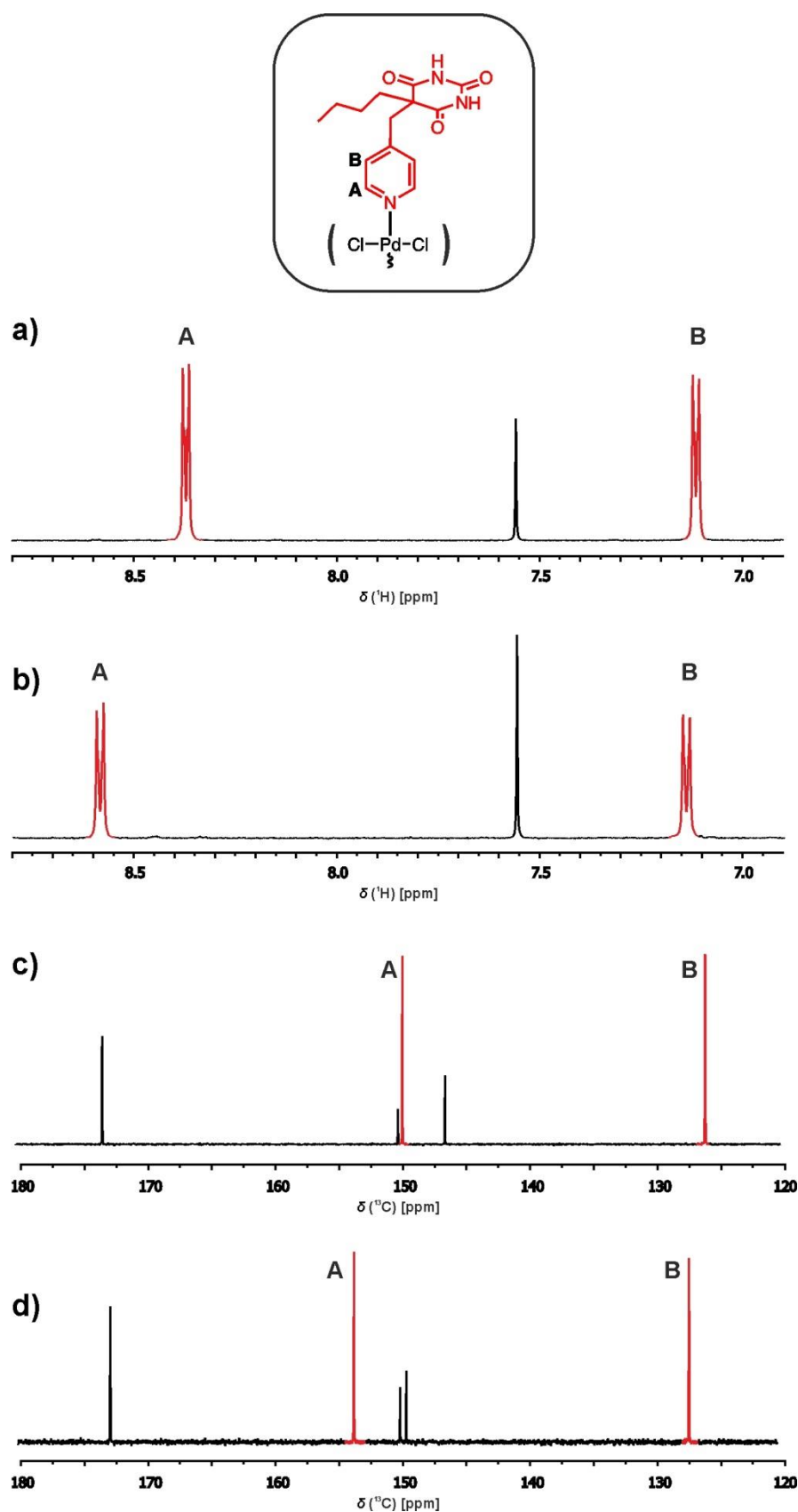
Figure 6.6. (a) (b) Partial ^{1}H NMR (400 MHz, CDCl$_3$/CD$_3$OD (1:1), 298 K) spectrum of (a) **4B1** and (b) **Pd(4B1)$_2$Cl$_2$**. (c) (d) Partial ^{13}C NMR (101 MHz, CDCl$_3$/CD$_3$OD (1:1), 298 K) spectrum of (c) **4B1** and (d) **Pd(4B1)$_2$Cl$_2$**. The selected peaks are assigned using the labelling scheme shown and coloured in red.

Then, the corresponding platinum complex was prepared. It is usually possible to isolate both *cis* and *trans* platinum complexes due to their different stabilities.[24] Conversely, palladium complexes have intermediate lability which prevents this. The *trans* platinum complexes are normally prepared at elevated temperatures, at which *cis* complexes isomerise into *trans* complexes.[24] For the target cage, *trans* configuration is desirable. We therefore prepared **trans-Pt(4B1)₂Cl₂** from *cis*-bis(acetonitrile)-dichloroplatinum in DMF at 80 °C (Scheme 6.3). The prepared complex was stable enough for purification by column chromatography. We were able to obtain an X-ray structure of this complex (Figure 6.7). The measurement and analysis was done by Dan-George Dumitrescu at Elettra-Sincrotrone Trieste. The structure showed the desired perpendicular architecture of two barbiturates. They were directed towards opposite sides, but it is expected that the -CH₂- linker would allow them to rotate.
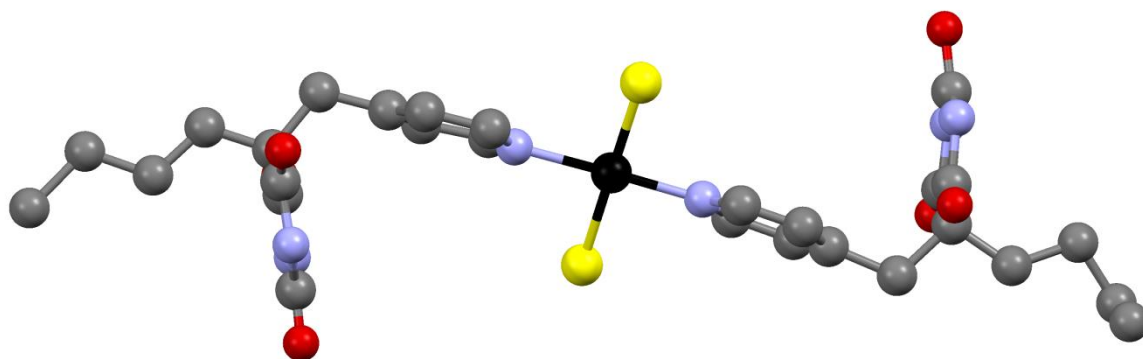
Figure 6.7. X-ray structure of **trans-Pt(4B1)₂Cl₂**. Only one molecule from the crystal lattice is shown. Water and hydrogens were removed for clarity. Colouring of atoms: C (grey), N (blue), O (red), Pt (black) and Cl (yellow).

6.5. Preparation of hybrid complexes

To prepare the rosette hybrid cage, **Pd(4B1)₂Cl₂** and pyrimidine **iPP** were added as solids to a Y-NMR tube, followed by the addition of CDCl₃. **Pd(4B1)₂Cl₂** is not soluble in CDCl₃, but it dissolved in the presence of **iPP**. This provided the first indication that the desired complex was forming as the solubility of rosette building blocks increases significantly when the rosette complex is formed.[15] In addition, ¹H NMR spectrum showed the formation of the well-defined characteristic rosette peaks of bound NH of barbiturate in the region of δ 14 – 15 ppm as well as bound NH and NH₂ from pyrimidine in the region of

δ 7 – 9 ppm (Figure 6.8a). Comparing this to premixed rosette **4B1•iPP** of the same concentration in CDCl$_3$ (Figure 6.8b), **Pd(4B1)$_2$Cl$_2$•iPP$_2$** showed the formation of much more stable rosette. When the palladium salt was added to the premixed rosette **4B1•iPP**, the formation of the same rosette complex was observed by ^{1}H NMR spectroscopy (Figure 6.8c). In addition, when all the compounds were mixed together in a one-pot fashion, the same ^{1}H NMR spectrum was obtained (Figure 6.8d).
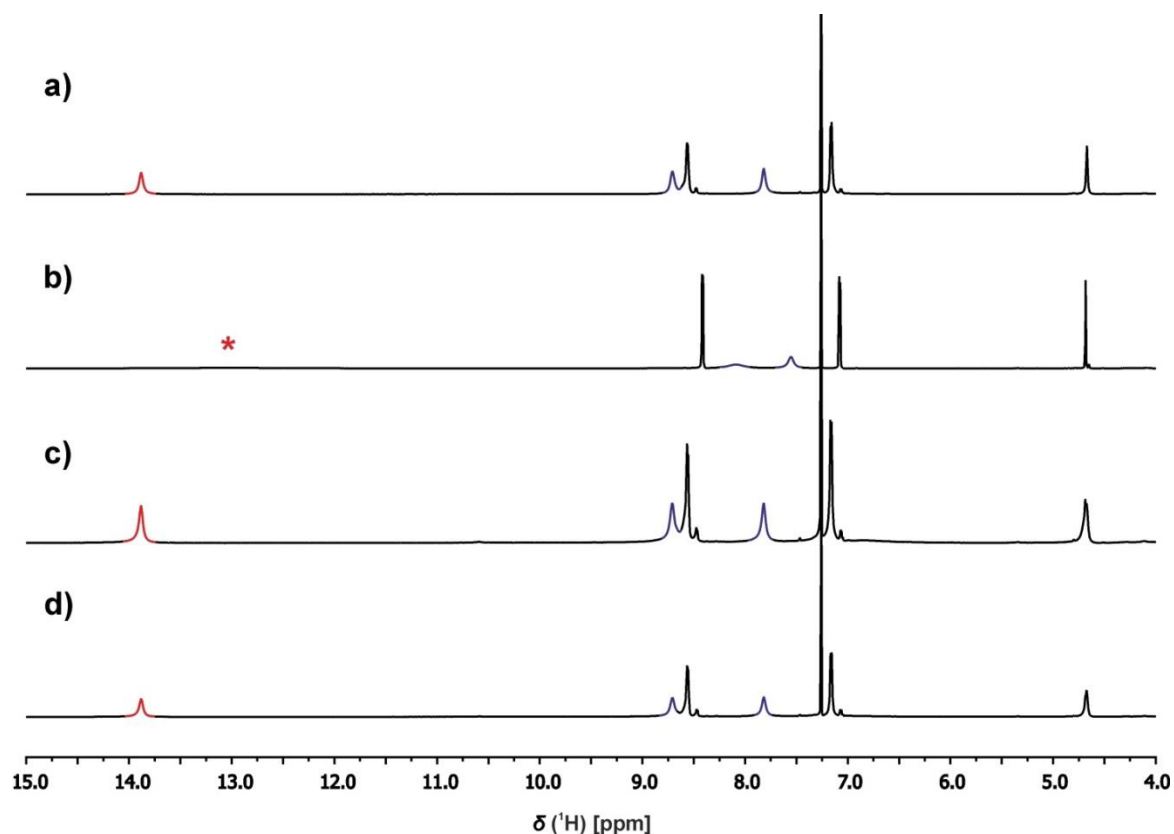
Figure 6.8. Partial ^{1}H NMR (500 MHz, CDCl$_3$, 298 K, [**iPP**] ~ 20 mM) spectra of (a) 1:2 mixture of **Pd(4B1)$_2$Cl$_2$** and **iPP** (b) 1:1 mixture of **4B1** and **iPP** (asterisk represents a broad peak), (c) adding a half equivalent of Pd(ACN)$_2$Cl$_2$ to the 1:1 mixture of **4B1** and **iPP** and (d) 2:2:1 mixture of **4B1**, **iPP** and Pd(ACN)$_2$Cl$_2$.Colouring of peaks: barbiturate N-H in red, pyrimidine NH/NH$_2$ in blue.

Similar results were obtained when **iBP** was used. Unfortunately, these complexes decomposed over time. **Pd(4B1)$_2$Cl$_2$•iBP** fully decomposed in three days, which was assessed by ^{1}H NMR spectra looking at the disappearance of characteristic rosette peaks and the change of the pyridine peaks and C-H of pyrimidine (Figure 6.9a). Moreover, the decomposition showed the same rate even when the cage was diluted 10-fold (Figure 6.9b).

^{13}C NMR spectroscopy did not provide useful information as most of the peaks were broad (see the Experimental section). We did not explore this further as a more suitable system was found (see below), but can be probably attributed to insertion of palladium into aromatic C-H of pyrimidines.
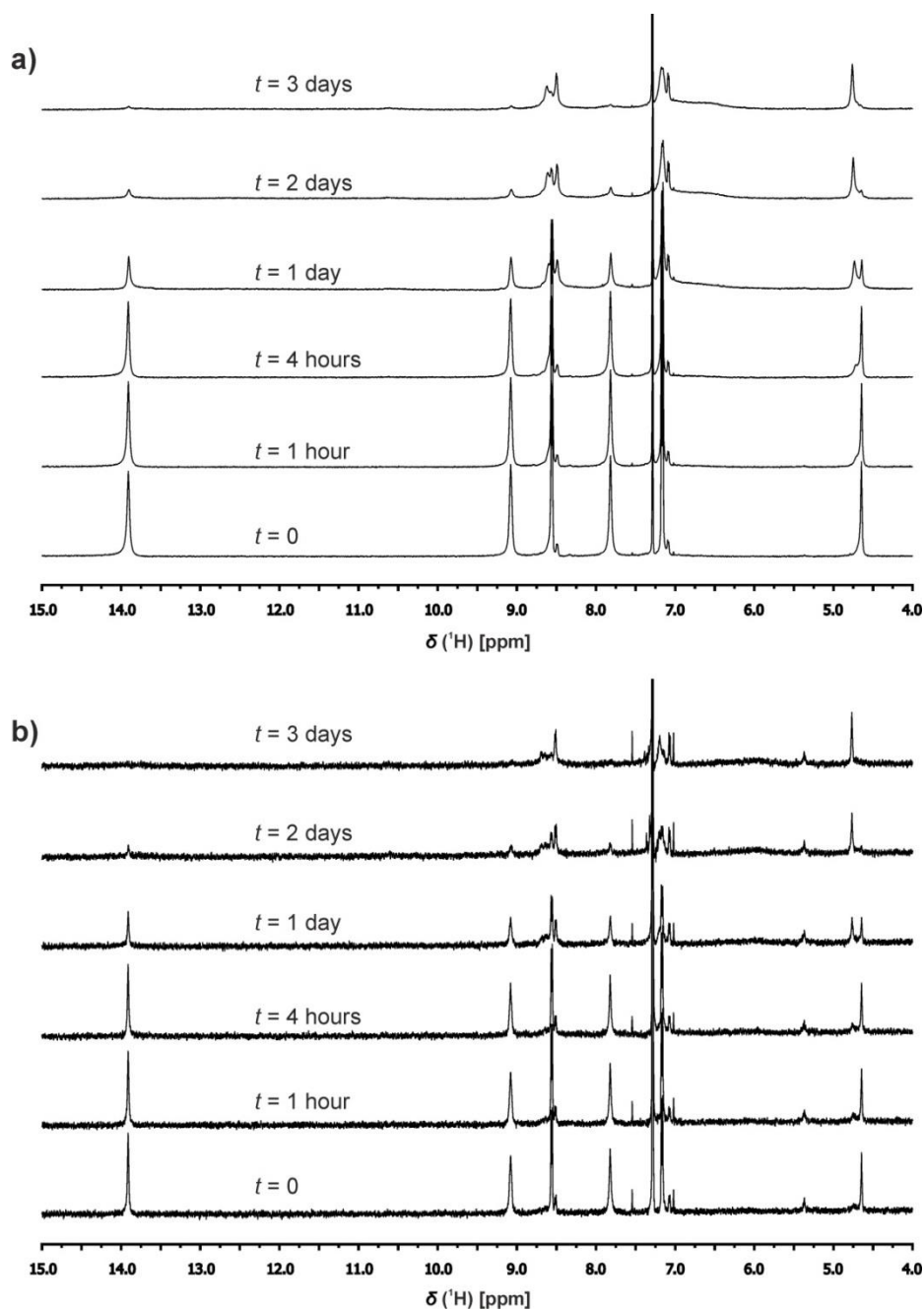
Figure 6.9. Partial ^{1}H NMR (400 MHz, CDCl$_3$, 298 K) spectra of the decomposition of complex **Pd(4B1)$_2$Cl$_2$•iBP$_2$** over time at the concentration of a) 12 mM and b) 1.2 mM.

When **iBT** was used, a solid precipitated from the mixture and using **tBP** led to the formation of a gel. Finally, using **tBT**, we were able to prepare a rosette complex that was

stable over a period of weeks as shown in Figure 6.10. Surprisingly, no coordination of palladium to triazine was observed. The bulkiness of **tBT** probably positively influences the rosette complex structure and prevents it from precipitation as compared to other systems.
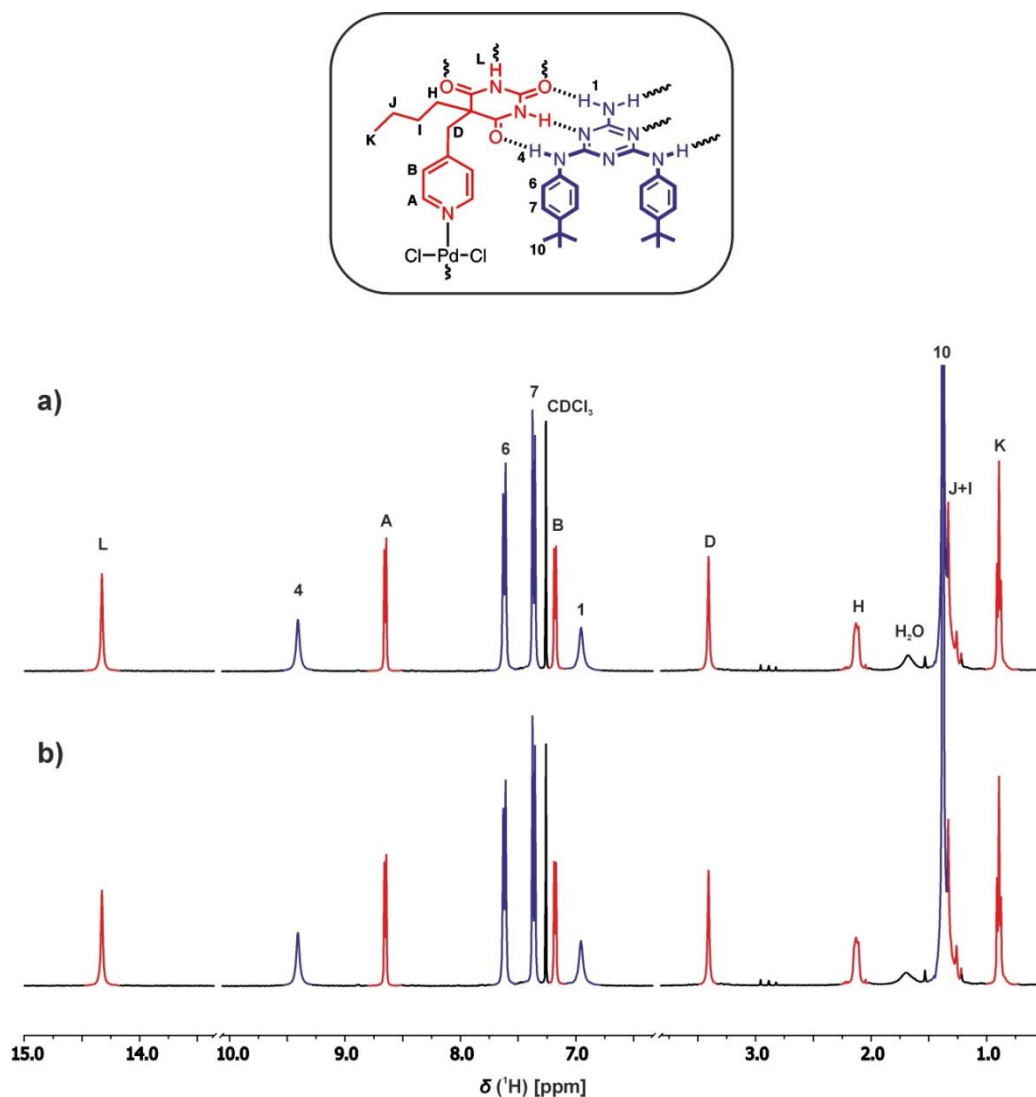
Figure 6.10. Partial ^{1}H NMR (400 MHz, CDCl$_3$, 298 K, 10 mM) spectra of complex **Pd(4B1)$_2$Cl$_2$•tBT$_2$** (a) immediately after mixing and (b) after 6 weeks. The peaks are assigned using the labelling scheme shown.

Next, we explored complexes based on platinum. As all of them produced gels or precipitated out of the solutions within a couple of hours/days, they will not be discussed here. This also prevented us from exploring if the complexes based on platinum are more stable than the ones based on palladium, as was hypothesised.

6.6. Characterisation of complexes

To characterise the 3D structure of **Pd(4B1)$_2$Cl$_2$•tBT$_2$** in solution, we applied NOESY NMR spectroscopy (Figure 6.11a). This experiment allowed us to see cross-peaks due to NOE between the N-H in both barbiturate and triazine (Figure 6.11b). The triazine NH$_2$ is close in space only to N-H in barbiturate and N-H in triazine. In comparison, triazine N-H has all the expected connections for the rosette structure. The same applies for the N-H of barbiturate.

Next, we applied DOSY NMR experiments to obtain the diffusion coefficients (*D*) of complex **Pd(4B1)$_2$Cl$_2$•tBT$_2$** and rosette **4B1•tBT** to compare them using mesitylene as an internal reference (Figure 6.12). The diffusion coefficient is related to a hydrodynamic radius (*R*) through Stokes-Einstein equation for spherical molecules (Equation 6.1).[27,28]

$$D = \frac{k_B\,T}{6 \times \pi \times \eta_0 \times R} \tag{6.1}$$

where k_B is the Boltzmann's constant, T is a temperature and η_0 is a viscosity of a solvent.

It is possible to estimate the hydrodynamic radius of the studied complex either directly, or by using an internal reference with known hydrodynamic radius. Mesitylene is often employed as such reference (with $R_{mesitylene} = 3.0$ Å).[28] The estimation is then given by Equation 6.2.
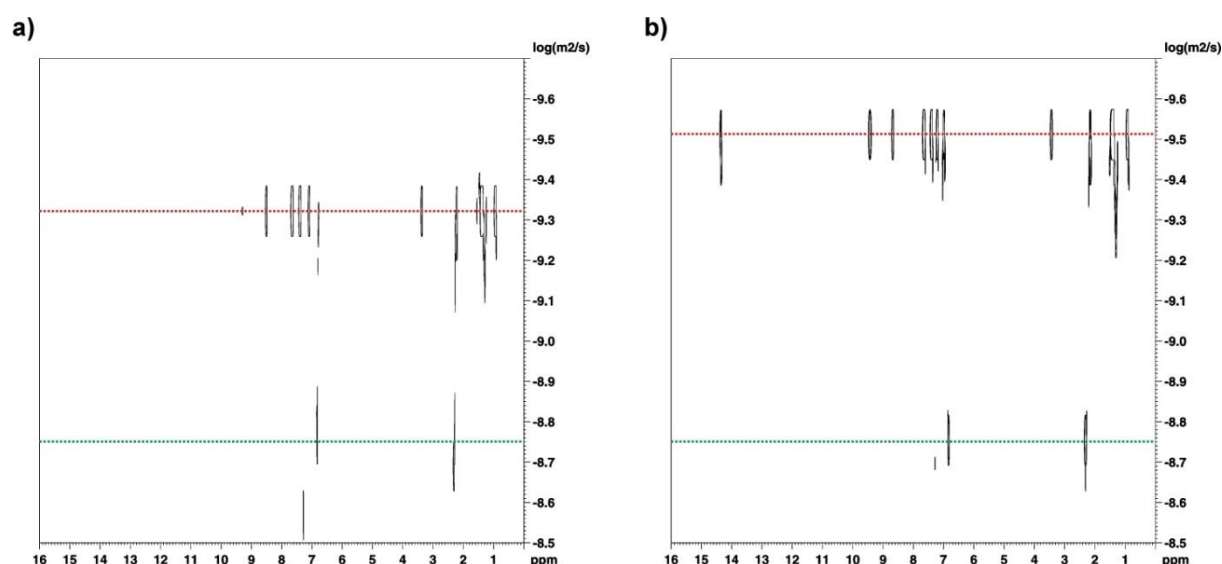
$$R = \frac{R_{mesitylene} \times D_{mesitylene}}{D} \tag{6.2}$$

This allowed us to determine the experimental hydrodynamic radii for **4B1•tBT** and **Pd(4B1)$_2$Cl$_2$•tBT$_2$** as 12 Å and 17 Å, respectively (Table 6.1).

a)

b)
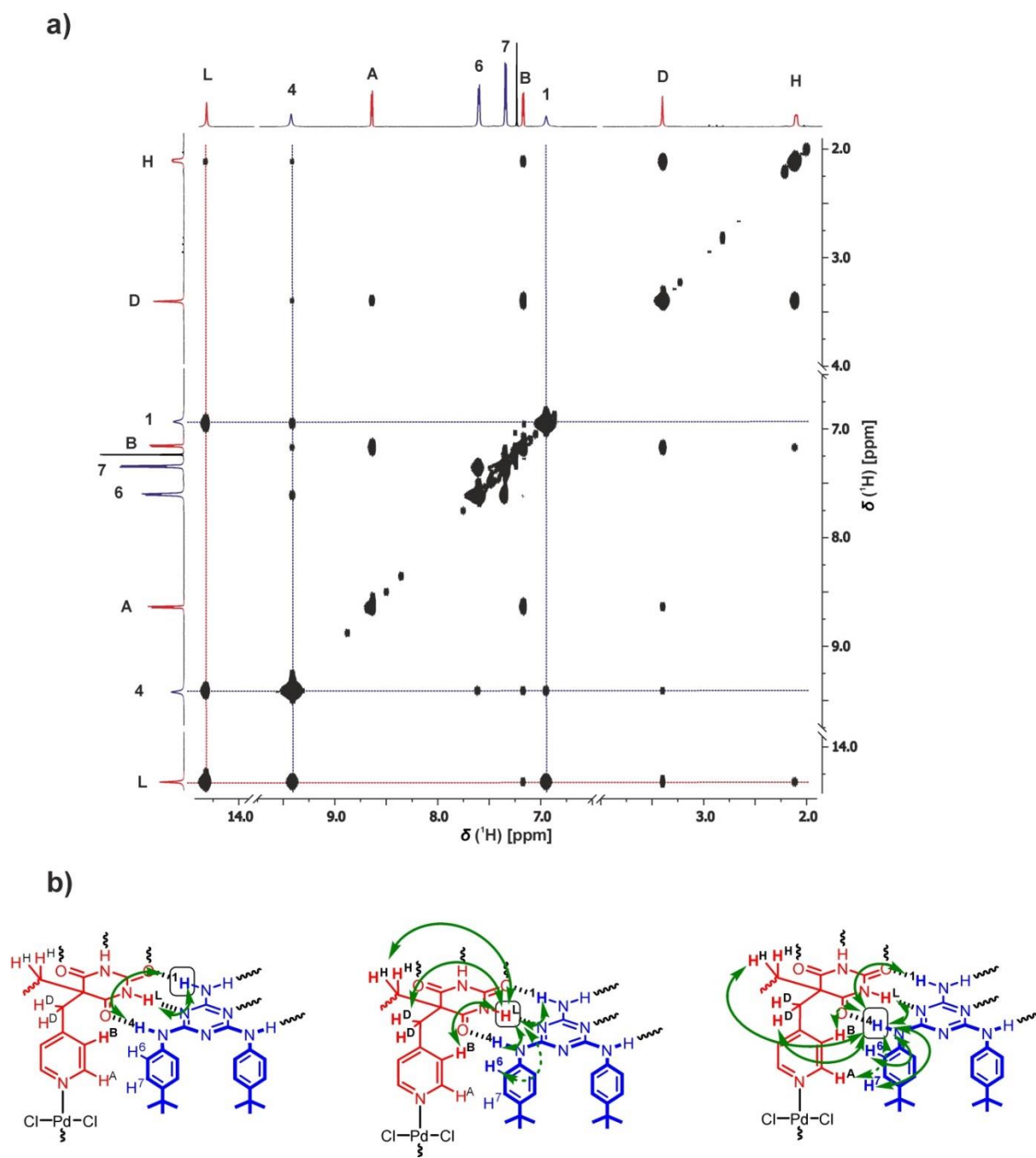
Figure 6.11. (a) Partial NOESY (700 MHz, CDCl$_3$, 298 K, 10 mM) spectrum of complex **Pd(4B1)$_2$Cl$_2$•tBT$_2$**, (b) NOE connections in **Pd(4B1)$_2$Cl$_2$•tBT$_2$** (dashed lines show less intense connections)

Figure 6.12. DOSY NMR (^{1}H, 400 MHz, CDCl$_3$, 298 K, [**tBT**] = 16 mM) spectra of (a) **4B1•tBT** (red line) and (b) **Pd(4B1)$_2$Cl$_2$•tBT$_2$** (red line) using mesitylene as an internal reference (green line).

Table 6.1. Diffusion coefficients and experimental and theoretical hydrodynamic radii.

	D [m^{2}s^{-1}]	R_{exp} [Å] [a]	R_{theo} [Å] [b]	R_{theo} [Å] [c]
mesitylene	1.65×10^{-9}	-	3	3
4B1•tBT	4.2×10^{-10}	12	15	12
Pd(4B1)$_2$Cl$_2$•tBT$_2$	2.9×10^{-10}	17	15/17 [d]	14/14 [d]

[a]From DOSY NMR experiments (CDCl$_3$, 298 K, [**tBT**] = 16 mM) using mesitylene ($R_{mesitylene}$ = 3.0 Å) as an internal reference.
[b]From PM6 optimised structures based on a radius (see Figure 6.13).
[c]From PM6 optimised structures using method of Timmerman *et al.* (see Figure 6.13).
[d]For two different optimised structures (see Figure 6.13).

To gain more insight into these values, we optimised all the structures by the semi-empirical method PM6 (Figure 6.13). Two different structures of **Pd(4B1)$_2$Cl$_2$•tBT$_2$** were found. The one being more open is about 10 kJ·mol^{-1} less stable as shown in Figure 6.13c-d. The hydrodynamic radius can be predicted by a radius of the studied molecule if the molecule is spherical. The results are depicted in Table 6.1. This provided a good agreement for mesitylene and **Pd(4B1)$_2$Cl$_2$•tBT$_2$**. The less stable structure of **Pd(4B1)$_2$Cl$_2$•tBT$_2$** as judged by PM6 energies provided an excellent agreement with the experimental value of hydrodynamic radii. PM6 is a semi-empirical method that does not take any solvent effects into account, therefore calculations using higher theory and including solvent models could predict this structure to be more stable. On the other hand, **4B1•tBT** was not described well

by the radius. This is not surprising, since this complex is not spherical as seen from the modelling in Figure 6.13b. Alternatively, Timmerman *et al.* showed a different way for the prediction of a hydrodynamic radius for non-spherical molecules by averaging the XYZ dimensions of the gas-phase optimised structures.[20] Such approach was successfully employed in various rosette assemblies. Following this method, we observed an excellent agreement of the predicted hydrodynamic radii for mesitylene and **4B1•tBT** with the experimental values (Table 6.1). However, this method did not provide a good description of the experimental data for either structure of **Pd(4B1)$_2$Cl$_2$•tBT$_2$**. In addition, the authors of the method stated that this procedure sometimes struggles to predict the hydrodynamic radius correctly and they were not able to explain for which systems this happens. Therefore we cannot exclude that one of such systems is **Pd(4B1)$_2$Cl$_2$•tBT$_2$**.
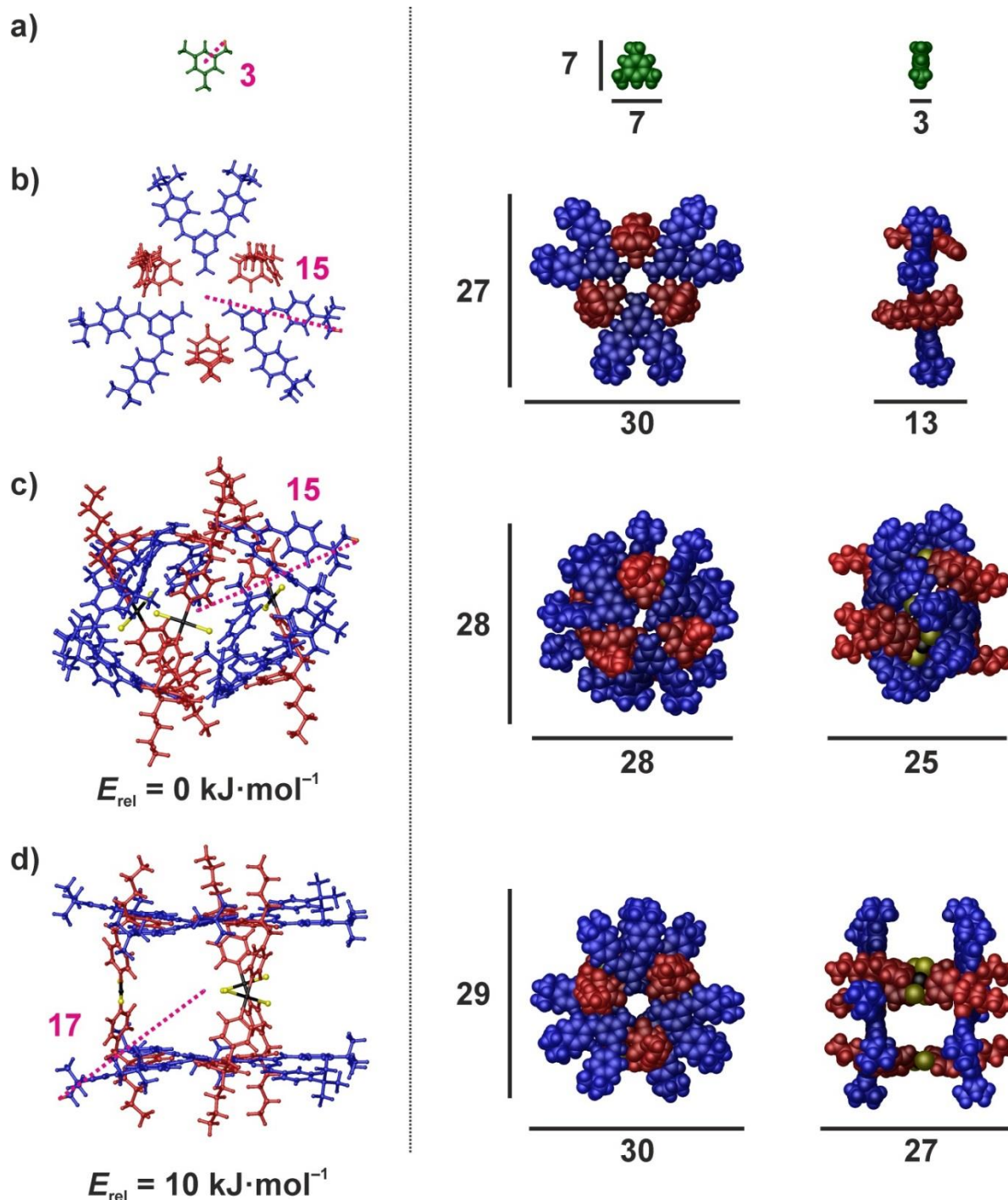
Figure 6.13. PM6 optimised structures of (a) mesitylene, (b) **4B1•tBT** and (c), (d) **Pd(4B1)₂Cl₂•tBT₂** (showing two different isomers with different relative energies). Colouring: mesitylene in green, **4B1** in red, **tBT** in blue, palladium atoms in black, chlorine atoms in yellow. The determination of radius is shown on left (dashed pink lines connect centroids of the molecules with the most distant atoms in orange), the determination of XYZ dimensions is shown on the right. All the distances are in Å.

Next, we conducted a dilution experiment of **Pd(4B1)$_2$Cl$_2$•tBT$_2$** in CDCl$_3$ at 298 K (Figure 6.14). It was possible to observe the characteristic rosette peaks at concentrations as low as 31 μM, which shows high stability of the complex.
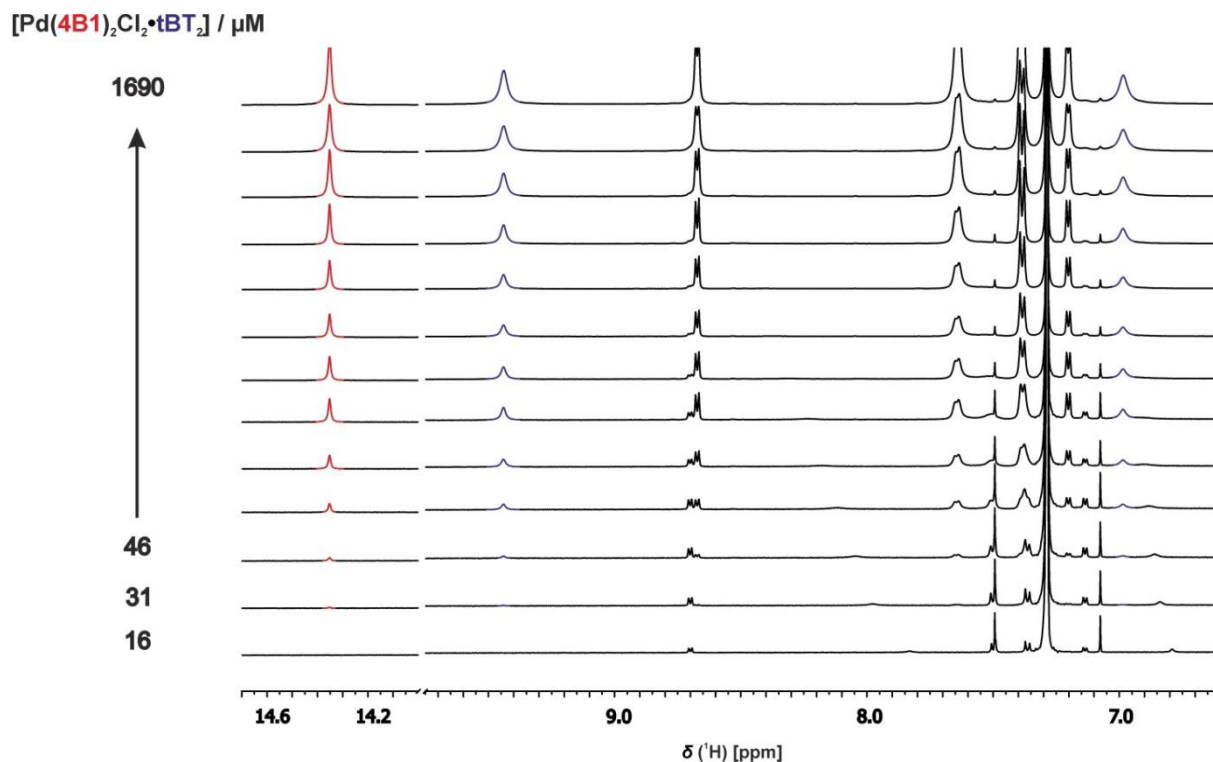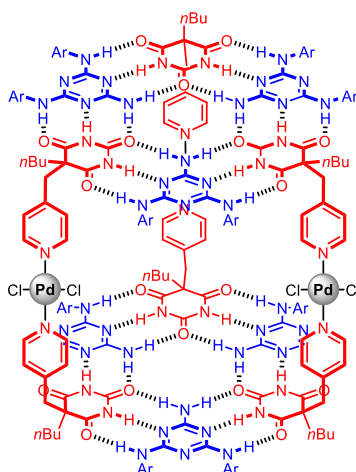
[Pd(**4B1**)$_2$Cl$_2$•t**BT**$_2$] / μM

Figure 6.14. ^{1}H NMR (500 MHz, CDCl$_3$, 298 K) dilution experiment of **Pd(4B1)$_2$Cl$_2$•tBT$_2$**. Colouring of peaks: barbiturate N-H in red, triazine NH/NH$_2$ in blue.

Unfortunately, we were not able to use the DMSO denaturation experiments employed by the Whitesides group and others to establish the hydrogen-bond stability of the cage,[28,29] because **Pd(4B1)$_2$Cl$_2$** was not stable in DMSO solutions as showed in Figure 6.15. This was confirmed by the appearance of multiple peaks in ^{1}H NMR spectra directly after DMSO addition and their change over time, and was probably due to the formation of Pd–DMSO complexes.

To conclude the characterisation section, combining all the inferences from different methods, there is a high probability that the structure of **Pd(4B1)$_2$Cl$_2$•tBT$_2$** in solution (CDCl$_3$, 298 K) is as suggested – the hybrid cage shown in Figure 6.16.
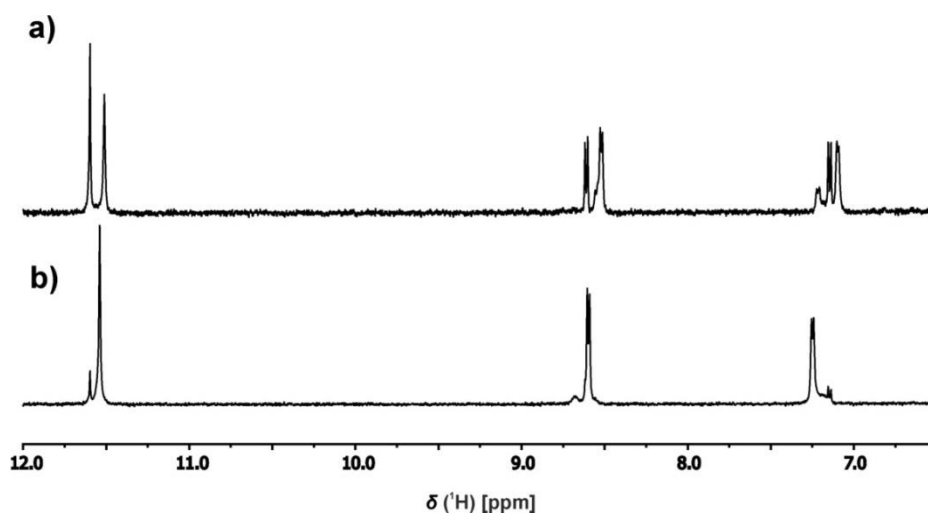
Figure 6.15. Partial ^{1}H NMR (400 MHz, d^6-DMSO, 298 K) spectra of **Pd(4B1)$_2$Cl$_2$** (a) directly after the addition of solvent and (b) after 1 day.

**Figure 6.16**. Postulated structure of **Pd(4B1)$_2$Cl$_2$•tBT$_2$** in CDCl$_3$ at 298 K (Ar = *p-tert-butylphenyl*).

To further characterise the complex, ESI-MS was used. Unfortunately, this method did not provide any additional information. It can be noted that it was difficult to obtain even the mass spectrum of **Pd(4B1)$_2$Cl$_2$**. Because of that, the Ag$^+$–labelling technique for MALDI MS will be explored.[30] Since **Pd(4B1)$_2$Cl$_2$•tBT$_2$** contains chlorine atoms, the successful characterisation of the complex by this method might be hampered by AgCl precipitation. A large number of different conditions for the crystallisation were explored and several crystals were submitted for an X-ray analysis.

6.7. Host-guest and stimuli-responsive behaviour of hybrid cage

The cavity of the cage is quite large as was shown in Figure 6.13. This led us to explore the cage ability to encapsulate fullerenes. Adding fullerenes C_{60} and C_{70} as solids to $CDCl_3$ or $CDCl_3/d^8$-toluene mixtures of the cage did not result in their dissolving, which would show the formation of the host-guest complex. In addition, no change was observed in the ^1H NMR spectra.

The mixed architecture of the prepared complexes should provide different platforms for various stimuli as shown in Figure 6.17. A stronger ligand (such as phosphine) should remove the metal from the pyridine unit, and by that also change the double rosette complex to a single rosette. A cyanurate (such as **cya**) should replace the barbiturate in the rosette since it forms stronger complexes and by that release **Pd(4B1)₂Cl₂** from the complex.[17]
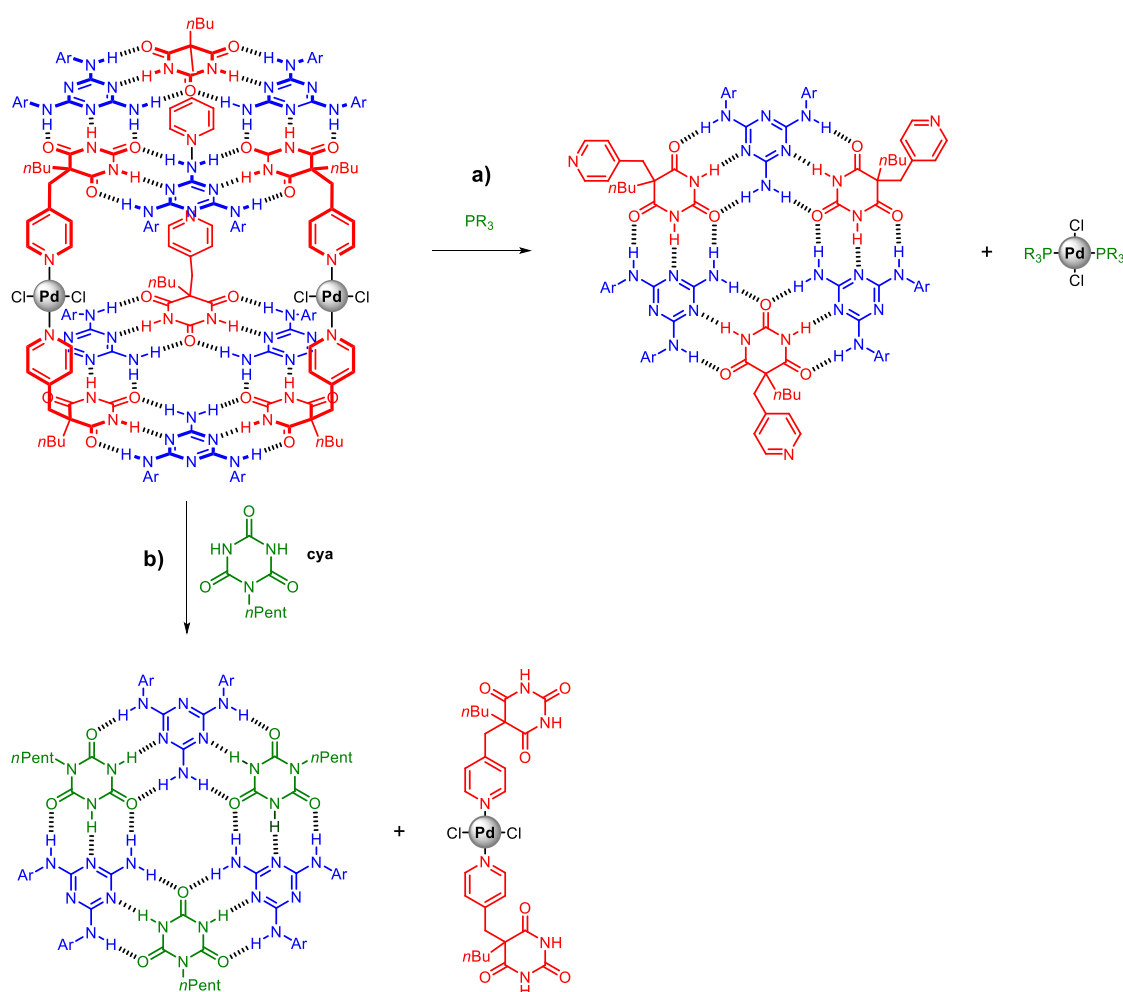

Figure 6.17. Responsive behaviour of hybrid cage **Pd(4B1)₂Cl₂•tBT₂** to different stimuli: (a) phosphine and (b) a cyanurate **cya** (Ar = *p-tert*-butylphenyl).

To test our hypotheses, we added PPh$_3$ to the **Pd(4B1)$_2$Cl$_2$•tBT$_2$** solution, which resulted in the removal of palladium from pyridine units as judged by the upfield movement of C-H of the pyridine unit of **4B1** as well as significant broadening of characteristic rosette peaks in ^{1}H NMR spectra (see Figure 6.18a-b), that is comparable to single rosettes. Additionally, ^{31}P NMR spectra showed a formation of Pd(PPh$_3$)$_2$Cl$_2$.[31] When we tried to recover the cage by the addition of Pd(ACN)$_2$Cl$_2$, we observed the formation of mixed pyridine–phosphine–palladium species by ^{1}H NMR and ^{31}P NMR spectroscopy (Figure 6.18c). This was corroborated by mixing **4B1**, PPh$_3$ and Pd(ACN)$_2$Cl$_2$ separately that resulted in the corresponding ^{1}H NMR and ^{31}P NMR spectra as seen in Figure 6.18d.

When a more bulky phosphine bis(diphenylphosphino)ferrocene (**dppf**) was used, the displacement of palladium worked in the same fashion as for PPh$_3$ (Figure 6.19a-b). Then it was possible to recover the hybrid cage by the addition of Pd(ACN)$_2$Cl$_2$ that produced the same ^{1}H NMR spectrum as for the starting complex with additional Pd(**dppf**)Cl$_2$ peaks as depicted in Figure 6.19c. Moreover, no change in ^{31}P NMR spectra was observed in this case, which provided an additional proof.

Finally, we explored the possibility of exchanging the barbiturate in the rosette with a cyanuarate. Adding **cya** to the solution of **Pd(4B1)$_2$Cl$_2$•tBT$_2$** led to the precipitation of the solid inside the NMR tube. This was probably **Pd(4B1)$_2$Cl$_2$** that is not soluble in CDCl$_3$. It was possible to observe the formation of **cya•tBT** rosette and the disappearance of the aromatic signals of the **4B1**-unit in the remaining solution by ^{1}H NMR spectra as shown in Figure 6.20.
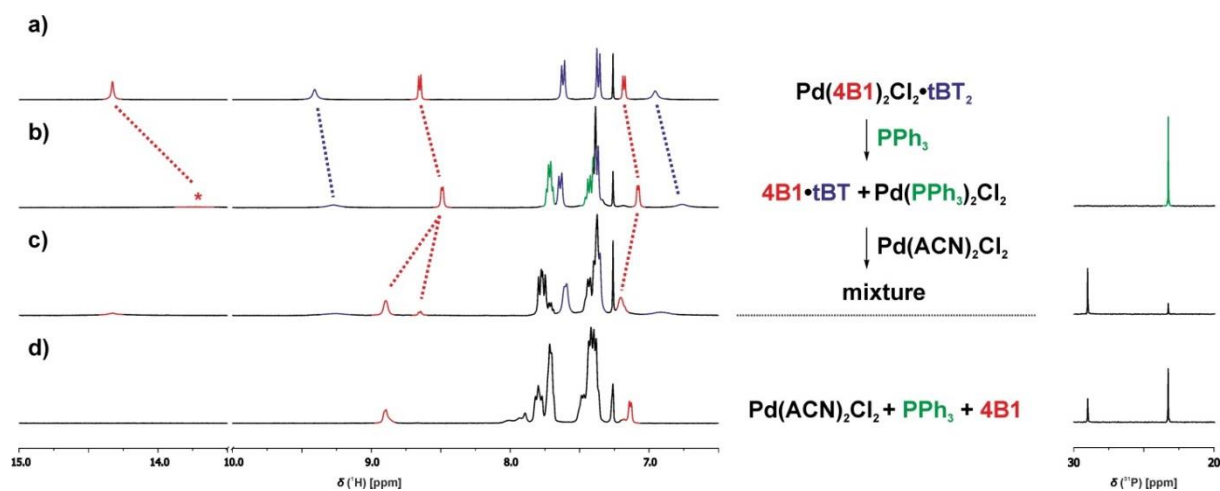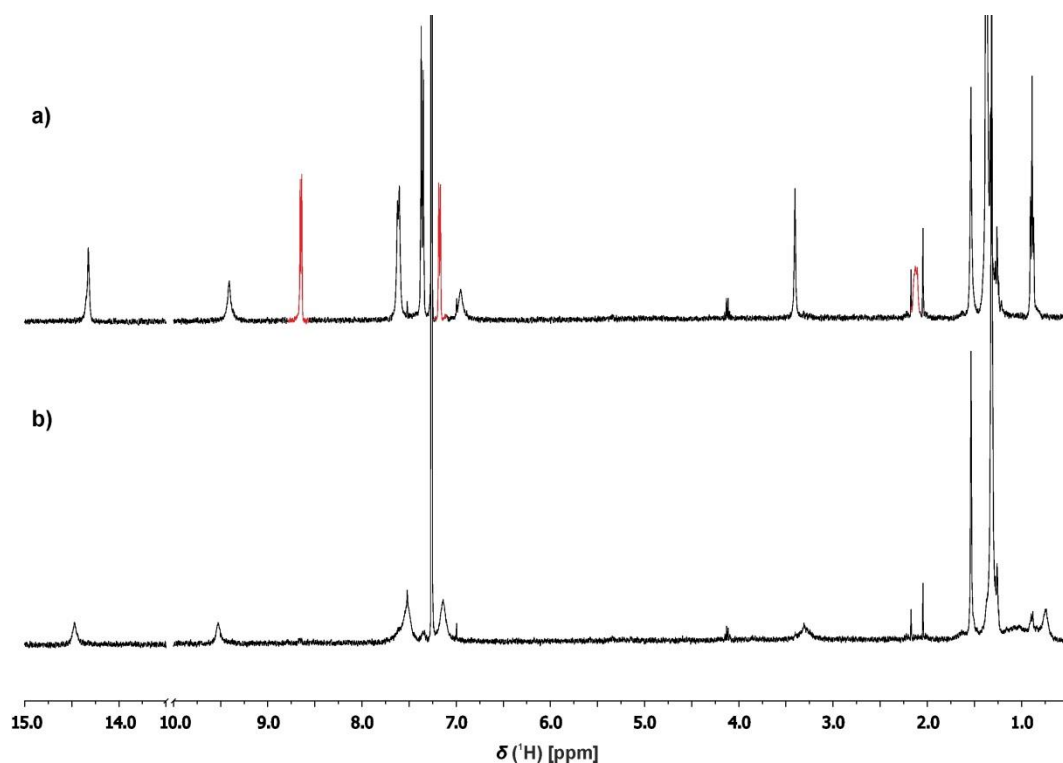
Figure 6.18. Partial ^{1}H NMR (400 MHz, CDCl$_3$, 298 K) spectra (left) and partial ^{31}P NMR (162 MHz, CDCl$_3$, 298 K) spectra (right) of (a) complex **Pd(4B1)$_2$Cl$_2$•tBT$_2$** (10 mM), (b) after addition of PPh$_3$ (asterisk represents a broad peak), (c) followed by addition of Pd(ACN)$_2$Cl$_2$; (d) separate mixture of Pd(ACN)$_2$Cl$_2$, PPh$_3$ and **4B1**. Colouring of peaks: **4B1** in red, **tBT** in blue and PPh$_3$ in green.
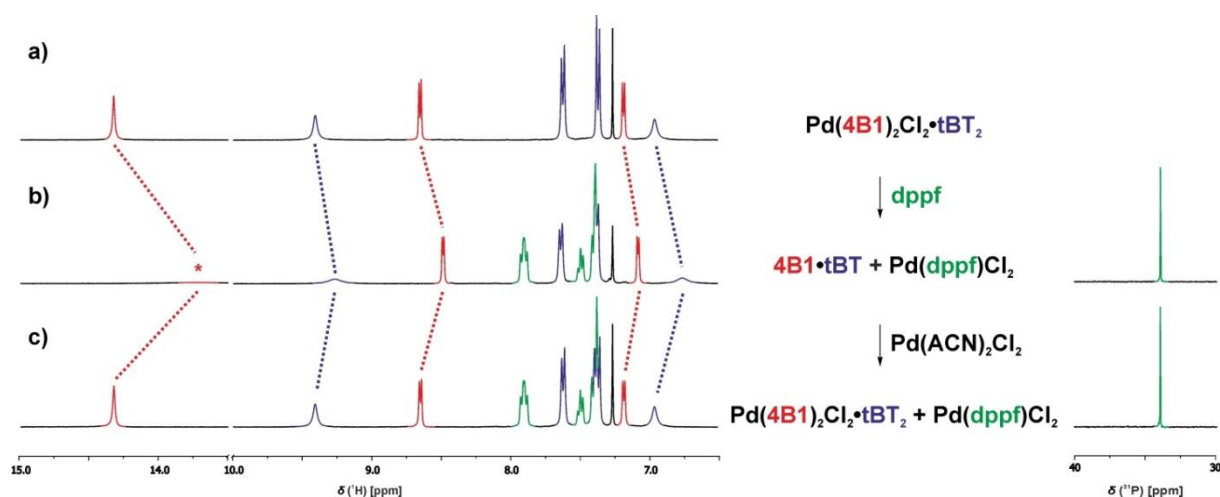
Figure 6.19. Partial ^{1}H NMR (400 MHz, CDCl$_3$, 298 K) spectra (left) and partial ^{31}P NMR (162 MHz, CDCl$_3$, 298 K) spectra (right) of (a) complex **Pd(4B1)$_2$Cl$_2$•tBT$_2$** (8 mM), (b) after addition of **dppf** (asterisk represents a broad peak), (c) followed by addition of Pd(ACN)$_2$Cl$_2$. Colouring of peaks: **4B1** in red, **tBT** in blue and **dppf** in green.

Figure 6.20. Partial ^{1}H NMR (400 MHz, CDCl$_3$, 298 K) spectra of (a) **Pd(4B1)$_2$Cl$_2$•tBT$_2$** (1.2 mM; selected peaks of the **4B1**-part are highlighted in red), (b) after addition of **cya**.

6.8. Conclusion and future work

In this chapter, we designed and prepared hybrid hydrogen-bonded/metal-coordinated cages using barbiturate-pyridines, pyrimidines or triazines and palladium or platinum salts. These complexes are a rare example of architectures where both hydrogen-bonding and metal-coordination form the crucial part of the topology of the complex, since if either is removed, the architecture changes drastically. Most of the prepared cages decomposed, produced gels or precipitated out of the CDCl$_3$ solutions over time. The most stable system was **Pd(4B1)$_2$Cl$_2$•tBT$_2$**. They were characterised in solution by ^{1}H NMR, ^{13}C NMR and 2D NMR spectroscopy experiments (including NOESY and DOSY) to establish their structure in solution. Due to their mixed character, they show unusual dynamic behaviour as both of their parts response selectively to different stimuli such as phosphine and cyanurate. This research could be extended to prepare well-defined discrete heterometal assemblies by preparing metal complexes from pyridine derivatives of pyrimidines or triazines in corresponding fashion. An example of such platinum-palladium system is shown in Figure 6.21.
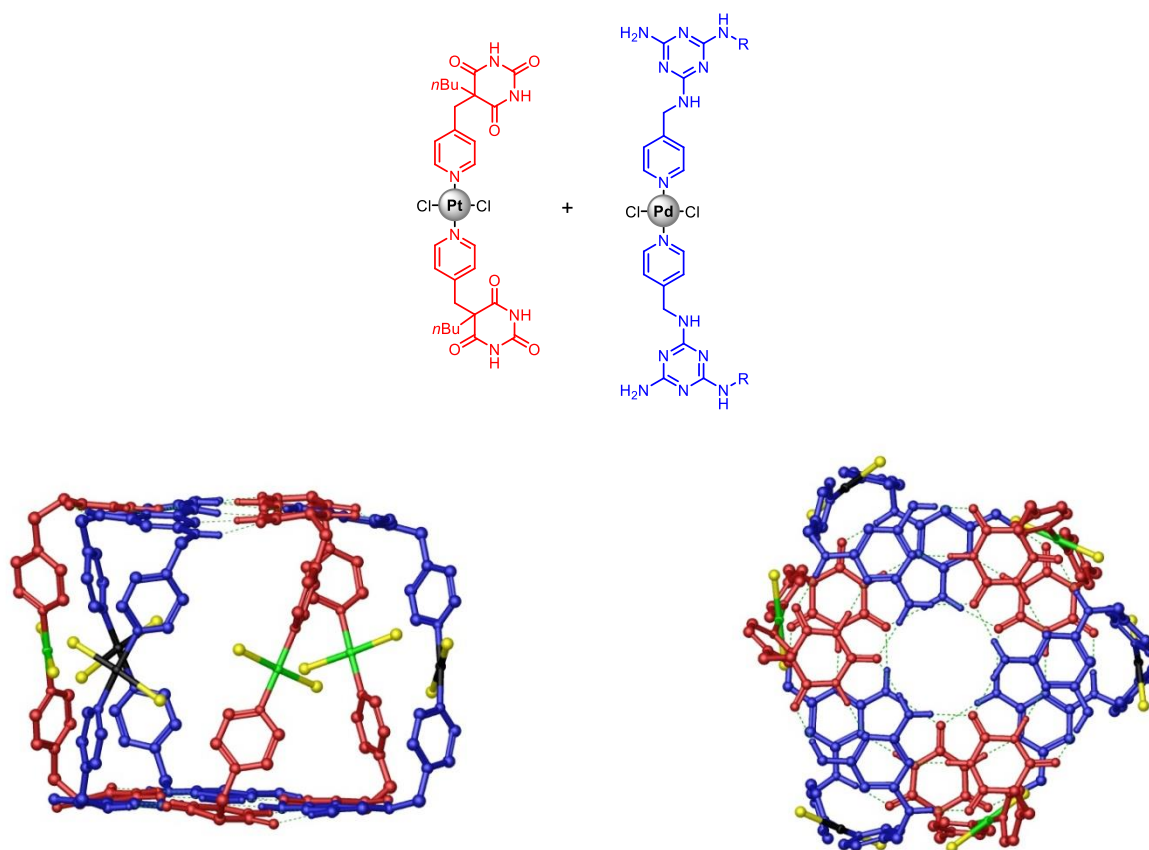
Figure 6.21. Possible future direction to prepare heterometalic hybrid cages using pyridine-substituted pyrimidine as the second partner (R is a solubilising group). The structure was optimised by PM6 (alkyl groups were replaced by hydrogen in the calculations). Hydrogen atoms that do not contribute to hydrogen-bonding were omitted for clarity. Colouring: barbiturate-pyridine in red, pyrimidine-pyridine in blue, palladium atoms in black, platinum atoms in green, chlorine atoms in yellow, green dashed line is the hydrogen-bond.

6.9.   Experimental section

6.9.1. General

The synthesis of **cya** was described in Chapter III. The chemicals were bought from commercial suppliers and used without further purifications unless stated otherwise. Solvents were either distilled before use or used as obtained. For chromatography, automatic chromatography systems CombiFlash R_f^+ and CombiFlash R_f^+ Lumen (with UV light detection at 254 nm and 280 nm and evaporative light scattering detector for Lumen) with pre-packed puriFlash columns from Interchim (silica, 25 μm) with a loading of mixtures on Celite were used. The microwave used was Biotage Initiator$^+$. The reactions were monitored by LSMS Waters Acquity H-class UPLC coupled with a single quadrupole Waters SQD2 with the conditions as follows: UPLC Column (see below), solvent A: Water + 0.1% formic acid; solvent B: acetonitrile od THF (see below) + 0.1% formic acid; gradient and flow rate (see below); column temperature of 40 °C, the signal was monitored at 254 nm and 280 nm.

Columns

      Col1: ACQUITY UPLC CSH C18 Column, 130Å, 1.7 μm, 2.1 mm X 50 mm
      Col3: ACQUITY UPLC HSS T3 Column, 100Å, 1.8 μm, 2.1 mm X 50 mm

Methods

      MeCN-FAST: Gradient: 0 – 2 minutes 5% – 100%B + 1 minute 100%B
         Flow rate: 0.6 ml/min
      MeCN-SLOW: Gradient: 0 – 4 minutes 5% – 100%B + 1 minute 100%B
         Flow rate: 0.6 ml/min
      THF-FAST: Gradient: 0 – 2 minutes 5% – 80%B + 1 minute 80%B
         Flow rate: 0.4 ml/min
      THF-SLOW: Gradient: 0 – 4 minutes 5% – 80%B + 1 minute 80%B
         Flow rate: 0.4 ml/min
      THF_FAST_5%-35%: Gradient of 0-2 minutes 5% – 35%B + 1 minute 100%B
         Flow rate: 0.4 ml/min

^{1}H and ^{13}C NMR spectra were recorded on Bruker 400 MHz Avance III HD SmartProbe Spectrometers at 400 MHz for ^{1}H and 101 MHz for ^{13}C or on a Bruker 500 MHz Avance TCI CryoProbe Spectrometer and Bruker 500 MHz AVIII HD SmartProbe Spectrometer at 500 MHz for ^{1}H and 126 MHz for ^{13}C, or on a Bruker 700 MHz Avance II+ TXO Cryoprobe Spectrometer at 700 MHz for ^{1}H and 176 MHz for ^{13}C.

All chemicals shift are quoted in ppm and were referenced to the residual peaks of used solvents: $CDCl_3$ (^{1}H: 7.26 ppm; ^{13}C: 77.00 ppm), CD_3OD (^{1}H: 3.31 ppm; ^{13}C: 49.00 ppm), d^6-DMSO (^{1}H: 2.50 ppm; ^{13}C: 39.52 ppm). Coupling constants J are stated in Hz. NOESY spectra were recorded on Bruker 700 MHz Avance II+ TXO Cryoprobe Spectrometer. DOSY NMR experiments were conducted on a Bruker 400 MHz Avance III HD SmartProbe Spectrometer. FT-IR spectra were measured on a Bruker Alpha spectrometer. HR-MS spectra were obtained on a Waters Xevo G2-S, Waters Vion IMS Qtof or Waters LCT Premier by electrospray-ionisation of samples. Melting points were recorder on a Mettler-Toledo MP90 system. Elemental analysis was performed by the Microanalysis facility at the Department of Chemistry at the University of Cambridge. The X-ray measurement and analysis of *trans*-**Pt(4B1)$_2$Cl$_2$** was done by Dan-George Dumitrescu at Elettra-Sincrotrone Trieste.

6.9.2. Modelling

For semi-empirical calculations, PM6 as implemented in *Gaussian 09* was used.[32]

6.9.3. Synthesis

Synthesis of **4B1-D**
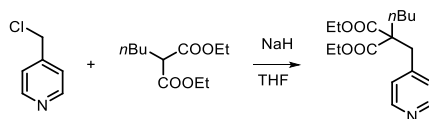
NaH (60% in mineral oil, 1.13 g, 28.3 mmol) was flushed with N_2 and THF (60 mL) was added. Diethyl 2-butylmalonate (4.5 mL, 4.4 g, 20 mmol) was then added at 0 °C. After stirring at RT for 30 minutes, 4-(chloromethyl)pyridine (97%, 1.65 g, 12.5 mmol) was then added. The mixture was refluxed overnight. A saturated solution of NaCl (20 mL) and water (10 mL) were added the mixture was extracted with dichloromethane (4 × 50 mL). The collected organic phase was dried over $MgSO_4$ and the solvents were removed under reduced pressure. A combliflash of residue on silica (Celite loading, PE/EtOAc, EtOAc: 0%→100%) provided the title product (2.75 g, 72% yield) as yellowish liquid.

**^{1}H NMR (CDCl$_3$, 400 MHz, 298 K)**: δ 8.50 (dd, J = 4.5, 1.5 Hz, 2H), 7.05 (dd, J = 4.5, 1.5 Hz, 2H), 4.26 – 4.11 (m, 4H), 3.23 (s, 2H), 1.88 – 1.72 (m, 2H), 1.39 – 1.29 (m, 4H), 1.25 (t, J = 7.0 Hz, 6H), 0.93 (t, J = 7.0 Hz, 3H).

The observed data was in agreement with the reported values.[20]

Synthesis of **4B1**
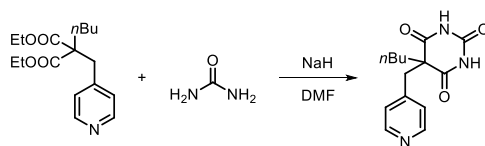
NaH (60% in mineral oil, 1.4 g, 35 mmol) was flushed with N_2 and DMF (40 mL) was added. Urea (5.0 g, 83 mmol) was then added at 0 °C. After 30 minutes, the ice bath was removed. After additional stirring for 1 hour, **4B1-D** (2.4 g, 7.8 mmol) was added at 0 °C. The mixture was then stirred at 40 °C for 2 days. A saturated solution of NH_4Cl (100 mL) and ethyl acetate (150 mL) were added. The organic phase was separated, washed with water (3 × 50 mL) and dried over $MgSO_4$ and the solvents were removed under reduced pressure. A combliflash of residue on silica (Celite loading, PE/EtOAc, EtOAc: 0%→100%) provided the title product (0.92 g, 43% yield) as a white crystalline solid.

^{1}H NMR (CDCl$_3$, 400 MHz, 298 K): δ 8.50 (dd, J = 4.5, 1.5 Hz, 2H), 7.83 (s, 2H), 7.04 (dd, J = 4.5, 1.4 Hz, 2H), 3.27 (s, 2H), 2.19 – 2.09 (m, 2H), 1.38 – 1.29 (m, 2H), 1.28 – 1.18 (m, 2H), 0.89 (t, J = 7.0 Hz, 3H).

^{13}C NMR (CDCl$_3$, 101 MHz, 298 K): δ 171.0, 150.2, 147.0, 143.7, 124.6, 58.0, 42.8, 39.9, 27.0, 22.5, 13.6.

MP: 252 – 254 °C

EA: Required for $C_{14}H_{17}N_3O_3$: C 61.08, H 6.22, N 15.26; found: C 61.21, H 6.26, N 15.13.

The observed data was in agreement with the reported values.[20]

Synthesis of **iPP**
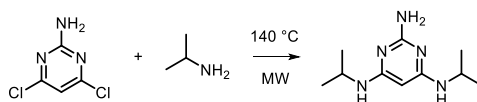
4,6-Dichloropyrimidin-2-amine (317 mg, 1.89 mmol) was flushed with nitrogen in a MW vial. Isopropylamine (2.3 mL, 1.6 g, 27 mmol) was added and the mixture was heated in microwave at 140 °C for 25 hours. A saturated solution of $NaHCO_3$ (20 mL) was added and the mixture was extracted with CH_2Cl_2/MeOH (10:1; 3 × 50 mL) and CH_2Cl_2 (50 mL). The organic phase was dried over $MgSO_4$, evaporated and loaded to Celite. A combiflash of the residue on silica (CH_2Cl_2/MeOH: MeOH 0%→10%) provided the title compound (334 mg, 84% yield) as a pale-orange solid.

^{1}H NMR (CD$_3$OD, 400 MHz, 298 K): δ 4.90 (s, 1H), 3.83 − 3.73 (m, 2H), 1.17 (d, J = 6.5 Hz, 12H).

^{13}C NMR (CDCl$_3$, 101 MHz, 298 K): δ 163.3, 162.5, 72.6, 42.7, 22.9.

HR-MS (ESI): Required for $C_{10}H_{20}N_5$ [M+H]$^+$ 210.1719, found: 210.1713 (Δ = 2.9 ppm).

FT-IR (thin film): 3314, 2968, 2930, 2872, 1572, 1521, 1494, 1365, 1337, 1192, 1125 cm^{-1}.
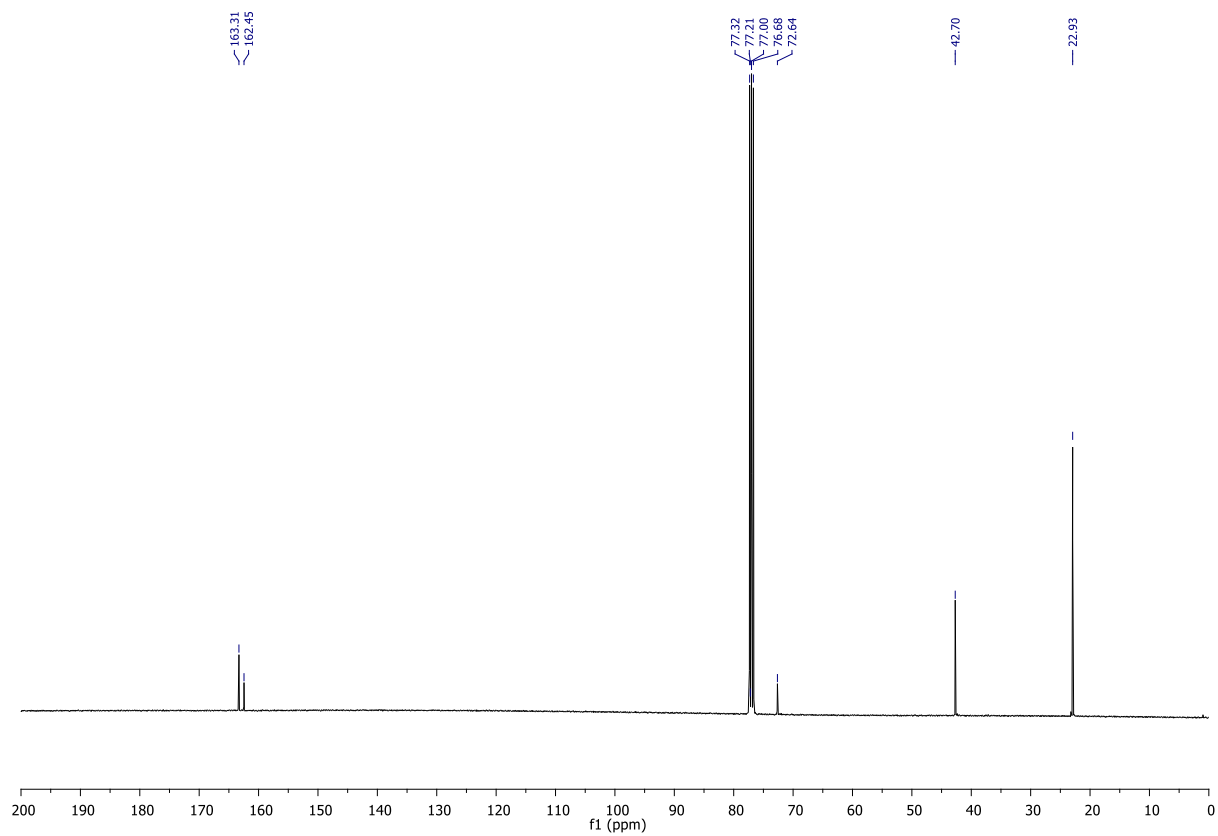
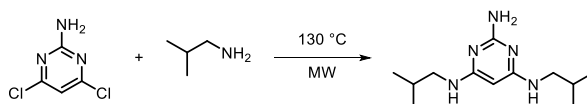**MP**: 128 − 131 °C

LCMS Method: Col3-MeCN-SLOW

^{1}H NMR
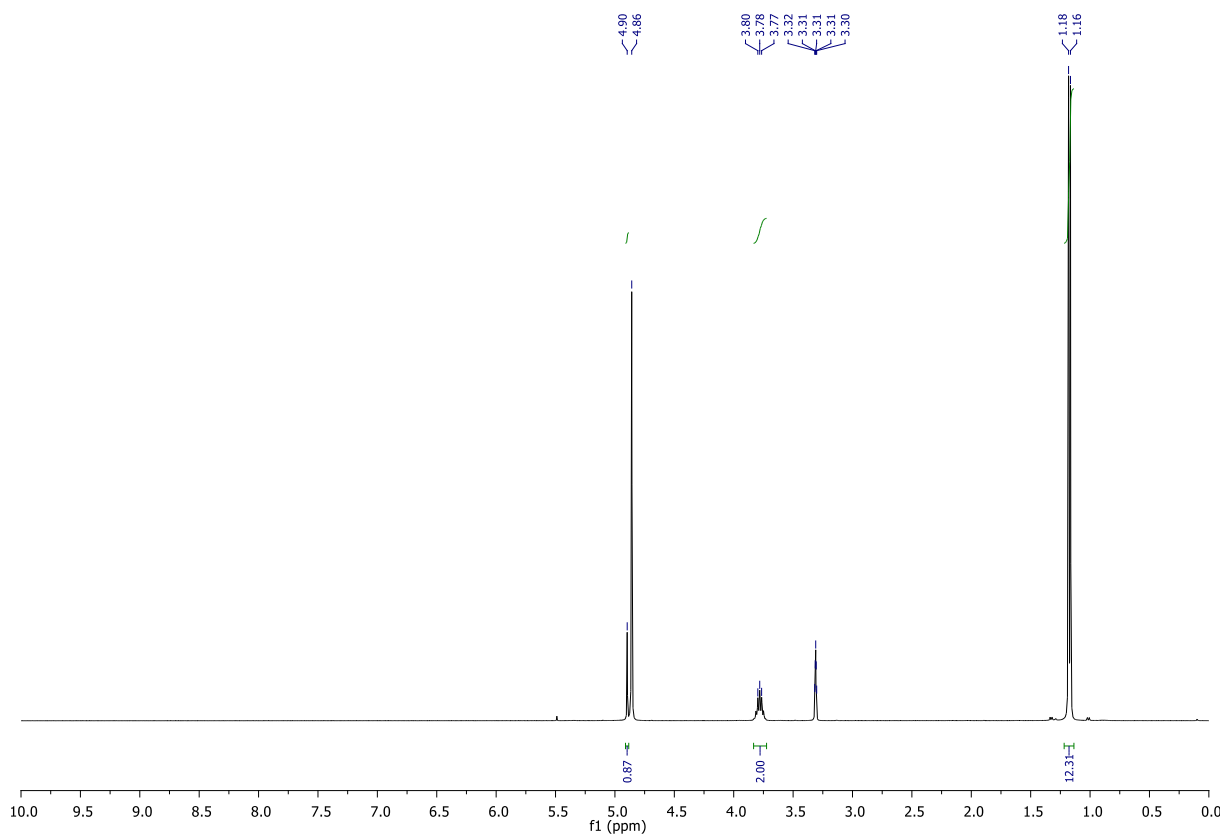
^{13}C NMR

Synthesis of **iBP**

4,6-Dichloropyrimidin-2-amine (307 mg, 1.87 mmol) was flushed with nitrogen in a MW vial. Isopropylamine (2 mL, 18.8 mmol) was added and the mixture was heated in microwave at 130 °C for 18 hours. The remaining amine was removed under reduced pressure and the residue was loaded on Celite. A combiflash of the residue on silica (EtOAc/MeOH: MeOH 0%→5%→10%) provided the title compound (392 mg, 88% yield) as a yellowish solid.

^{1}H NMR (CDCl$_3$, 400 MHz, 298 K): δ 4.79 (s, 1H), 4.57 (s, 2H), 4.46 (s, 2H), 3.00 – 2.93 (m, 4H), 1.90 – 1.78 (m, 2H), 0.95 (d, J = 6.5 Hz, 12H).
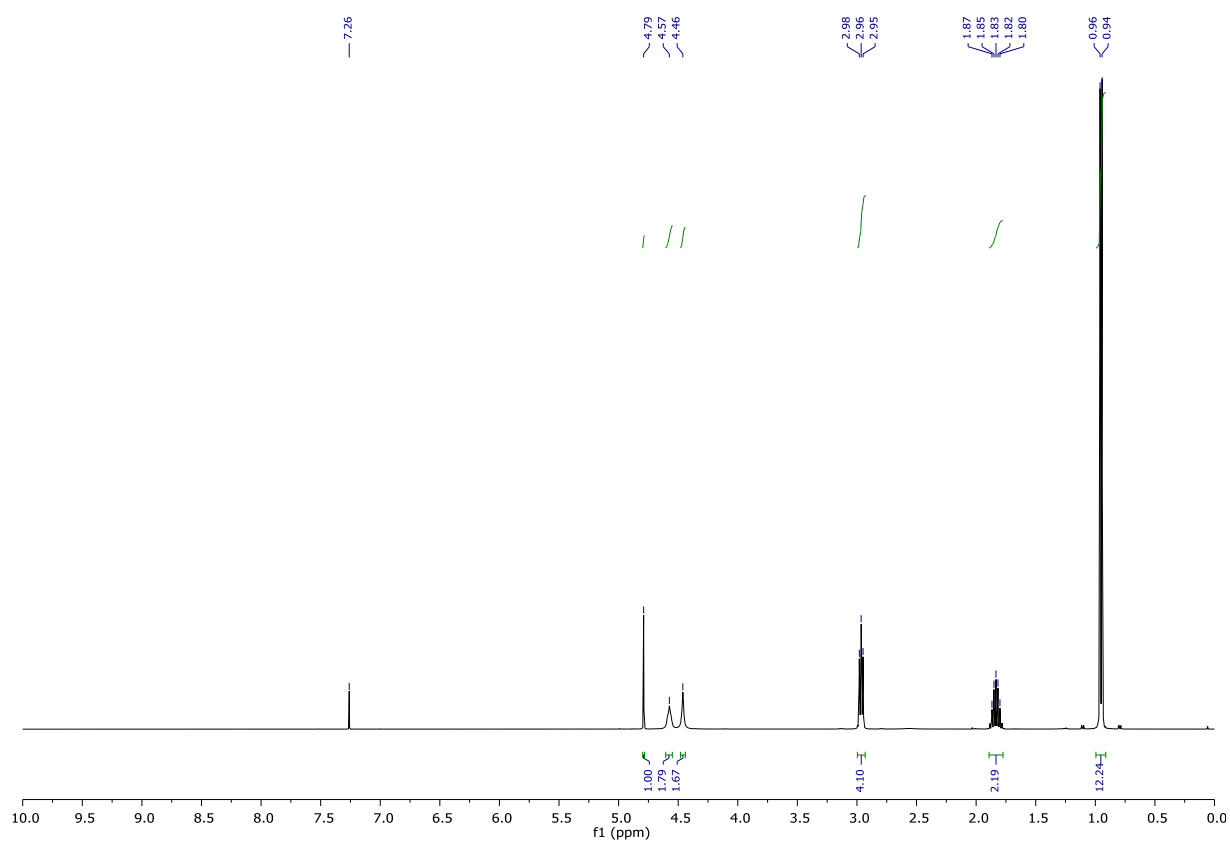**^{13}C NMR (CDCl$_3$, 101 MHz, 298 K)**: δ 164.4, 162.4, 71.9, 49.4, 28.3, 20.3.

HR-MS (ESI): Calculated for C$_{12}$H$_{24}$N$_5$ [M+H]$^+$ 238.2032, found: 238.2035 (Δ = 1.3 ppm)

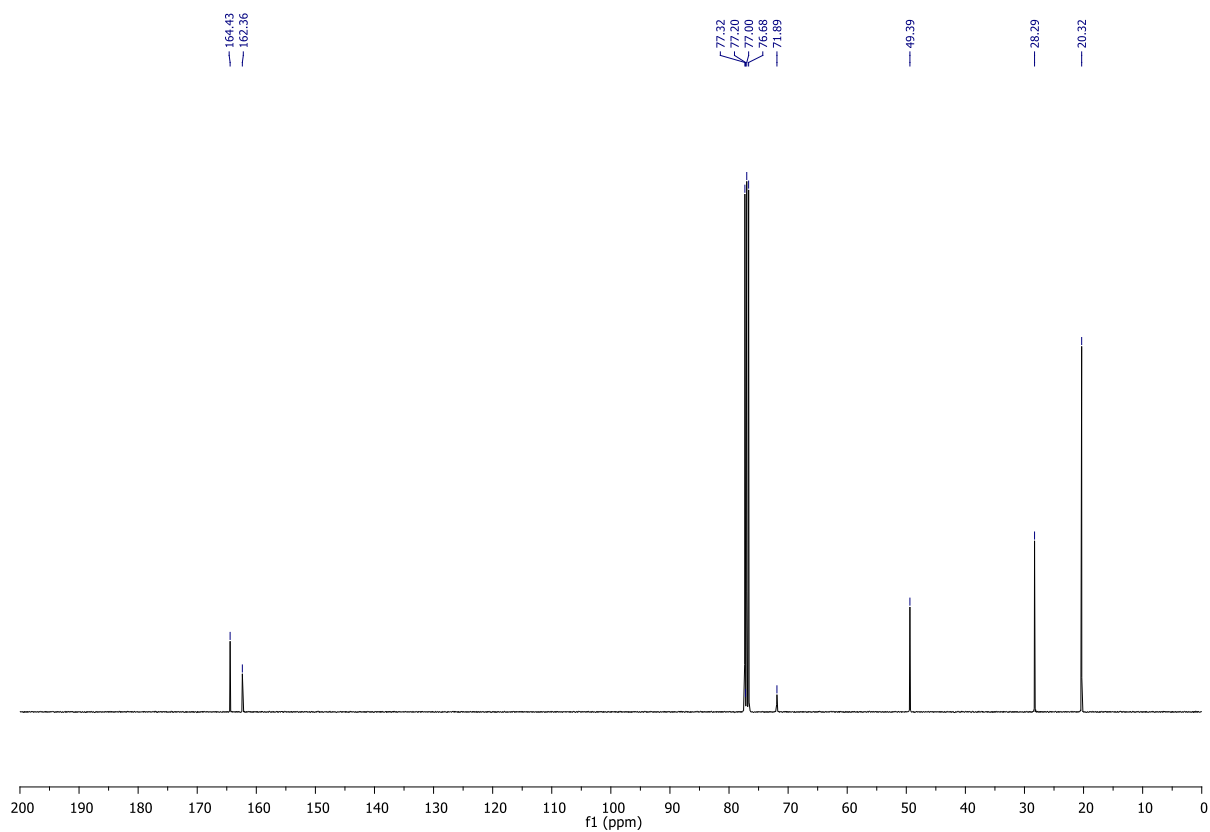**FT-IR (thin film)**: 3453, 3264, 3104, 2960, 2868, 2402, 1578, 1428 cm^{-1}.
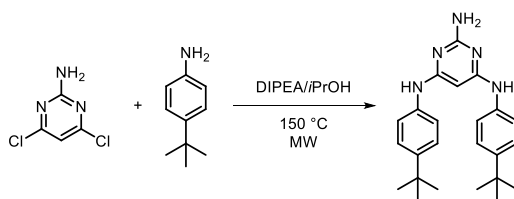
MP: 151 – 153 °C

LCMS Method: Col3-MeCN-SLOW

^{1}H NMR

^{13}C NMR

251

Synthesis of **tBP**

4,6-Dichloropyrimidin-2-amine (178 mg, 1.06 mmol) was flushed with nitrogen in a MW vial. N,N-diisopropylethylamine (0.5 mL, 2.48 mmol), isopropyl alcohol (1.0 mL) and 4-tertbutylaniline (0.6 mL, 562 mg, 3.77 mmol) were added and the mixture was heated in microwave at 150 °C for 1 hours. Then, additional 4-*tert*-butylaniline (0.5 µL, 467 mg, 3.14 mmol) was added under nitrogen atmosphere and the mixture was heated in microwave at 170 °C for 10 hours. A saturated solution of $NaHCO_3$ (20 mL) and water (20 mL) were added and the mixture was extracted with CH_2Cl_2/MeOH (10:1; 2×50 mL) and CH_2Cl_2 (2×50 mL). The organic phase was dried over $MgSO_4$, evaporated and loaded to Celite. A combiflash of the residue on silica (CH_2Cl_2/MeOH: MeOH 0%→10%) provided the title compound (294 mg, 71% yield) as a pale-pink solid.

^{1}H NMR (d^6-DMSO, 400 MHz, 298 K): δ 8.52 (s, 2H), 7.44 (d, J = 8.5 Hz, 4H), 7.25 (d, J = 8.5 Hz, 4H), 5.80 (s, 2H), 5.50 (s, 1H), 1.26 (s, 18H).

MP: 281 – 284 °C

LCMS Method: Col3-MeCN-SLOW

The observed data was in agreement with the reported values.[30]

Synthesis of **iBT**

Synthesis according to the published procedure using isobutylamine.[26] Pale yellowish solid, 463 mg (30% yield).

^{1}H NMR (CDCl$_3$/CD$_3$OD, 400 MHz, 298 K): δ 5.22 – 4.62 (m, 4H), 2.07 – 1.82 (m, 2H), 1.07 (d, J = 6.5 Hz, 12H). (*referenced to CD$_3$OD*)

MP: 129 – 131 °C

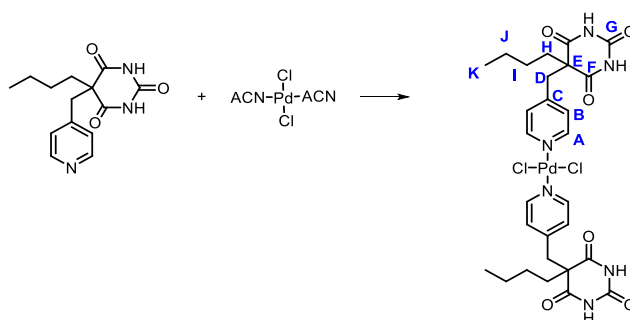The data was in agreement with previously published data.[33]

Synthesis of **tBT**

Synthesis according to the published procedure.[26] White solid, 1.4 g (55 % yield).

^{1}H NMR (CDCl$_3$/CD$_3$OD, 400 MHz, 298 K): δ 7.41 (d, J = 8.5 Hz, 4H), 7.29 (d, J = 8.5 Hz, 4H), 1.28 (s, 18H). (*referenced to CD$_3$OD*)

MP: 287 – 289 °C

The data was in agreement with previously published data.[26]

Synthesis of **Pd(4B1)₂Cl₂**

4B1 (78.30 mg, 284 μmol) and Pd(ACN)₂Cl₂ (36.85 mg, 142 μmol) in DCM (10 mL) and MeOH (10 mL) were sonicated for 5 minutes and the solvents were removed under reduced pressure. This provided the title product (101 mg, 98% yield) as a pale yellow solid.

^{1}H NMR (CDCl₃/CD₃OD, 400 MHz, 298 K): δ 8.58 (d, J = 6.5 Hz, 4H, A), 7.13 (d, J = 6.5 Hz, 4H, B), 3.26 (s, 4H, D), 2.04 – 2.00 (m, 4H, H), 1.32 – 1.18 (m, 8H, J + I), 0.86 (t, J = 7.0 Hz, 6H, K). (*referenced to CD₃OD*)

^{13}C NMR (CDCl₃/CD₃OD, 126 MHz, 298 K): δ 172.9 (F), 153.6 (A), 150.0 (G), 149.5 (C), 127.1 (B), 57.8 (E), 41.7 (D), 41.2 (H), 27.4 (I), 23.1 (J), 13.9 (K). (*referenced to CD₃OD*)

HR-MS (ESI): Required for $C_{28}H_{34}N_6O_6{}^{35}Cl_2Na^{106}Pd$ [M+Na]$^+$ 749.0844, found: 749.0833 (Δ = 1.5 ppm).

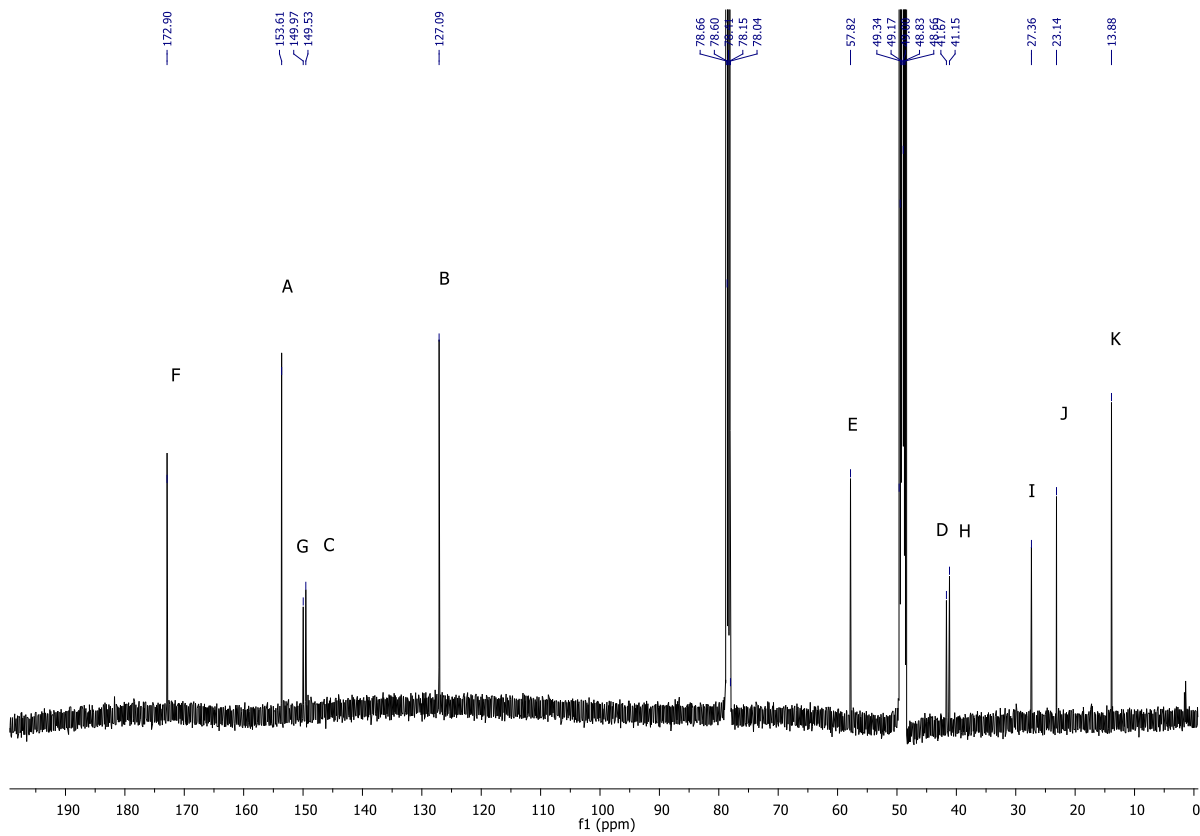**FT-IR (thin film)**: 3227, 3105, 2958, 2932, 2856, 1708, 1619, 1409, 1324, 1260, 1070 cm^{-1}.
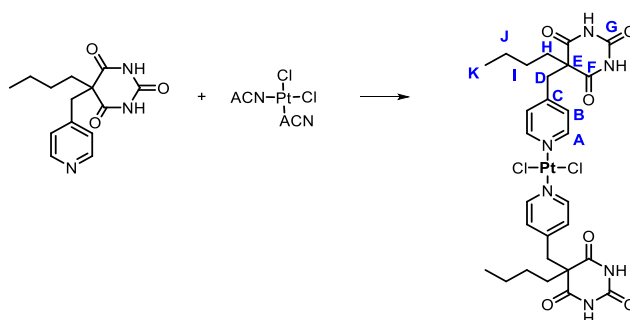
MP: 324 °C (transition/carbonisation)

EA: Required for $C_{28}H_{34}Cl_2N_6O_6Pd$: C 46.20, H 4.71, N 11.55; found: C 46.13, H 4.75, N 11.30.

^{1}H NMR
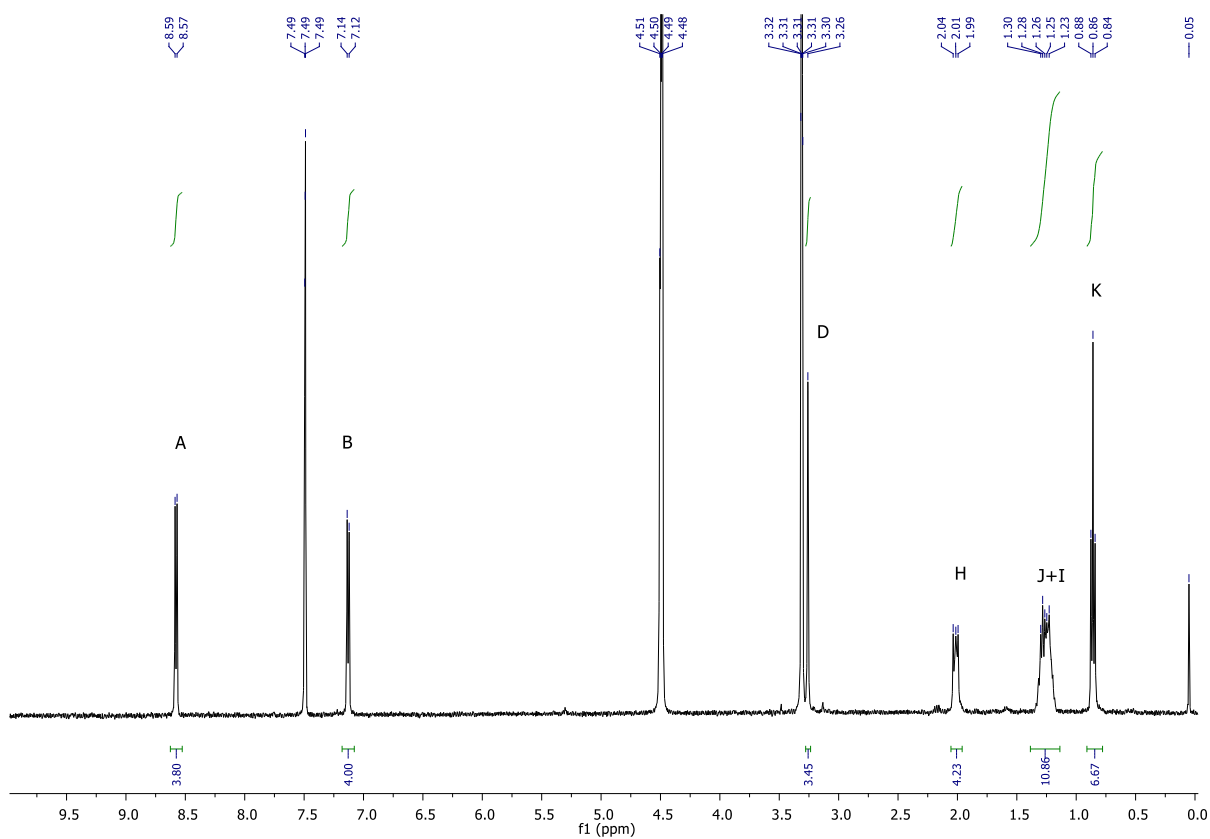
^{13}C NMR

Synthesis of *trans*-**Pt(4B1)$_2$Cl$_2$**

4B1 (58.81 mg, 214 μmol) and *cis*-bis(acetonitrile)dichloroplatinum (37.3 mg, 107 μmol) in DMF (4 mL) were stirred at 80 °C under N$_2$ for 4 days. The solvent was then evaporated and a combliflash of residue on silica (Celite loading, DCM/MeOH, MeOH: 0%→10%) provided the title product (19 mg, 22% yield) as a yellowish solid.

^{1}H NMR (CDCl$_3$/CD$_3$OD, 400 MHz, 298 K): δ 8.66 (d, J = 6.5 Hz, 4H, A), 7.11 (d, J = 6.5 Hz, 4H, B), 3.28 (s, 4H, D), 2.08 – 1.98 (m, 4H, H), 1.36 – 1.17 (m, 8H, J + I), 0.87 (t, J = 7.0 Hz, 6H, K). (*referenced to CD$_3$OD*)

^{13}C NMR (CDCl$_3$/CD$_3$OD, 126 MHz, 298 K): δ 172.7 (F), 153.8 (A), 149.8 (G), 149.0 (C), 127.2 (B), 57.6 (E), 41.4 (D), 41.1 (H), 27.2 (I), 23.0 (J), 13.8 (K). (*referenced to CD$_3$OD*)

HR-MS (ESI): Required for C$_{28}$H$_{35}$N$_6$O$_6$^{35}Cl$_2$^{195}Pt [M+H]$^+$ 816.1642, found: 816.1638 (Δ = 0.5 ppm).

FT-IR (thin film): 2956, 2918, 2851, 1704, 1621, 1410, 1324, 1245, 771 cm^{-1}.

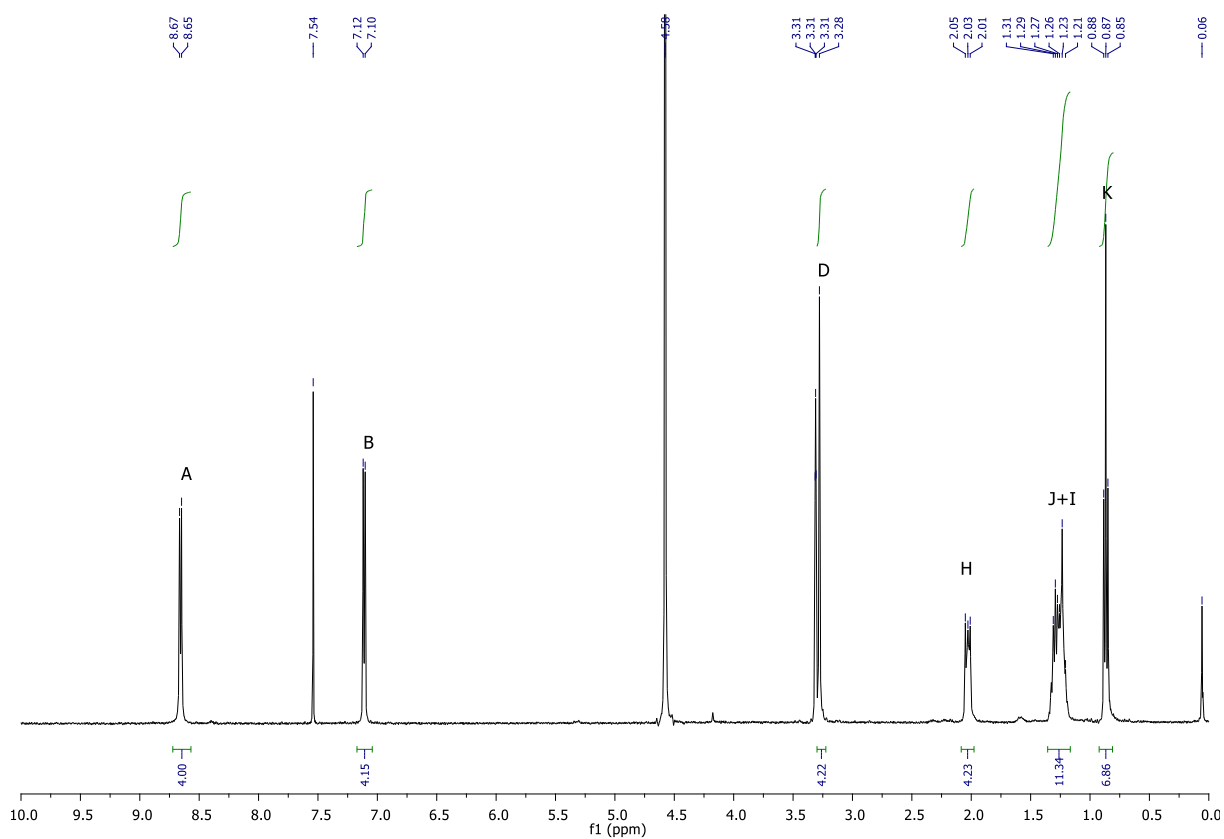**EA:** Required for C$_{28}$H$_{34}$Cl$_2$N$_6$O$_6$Pt: C 41.18, H 4.20, N 10.29; found: C 40.25, H 4.02, N 9.73.

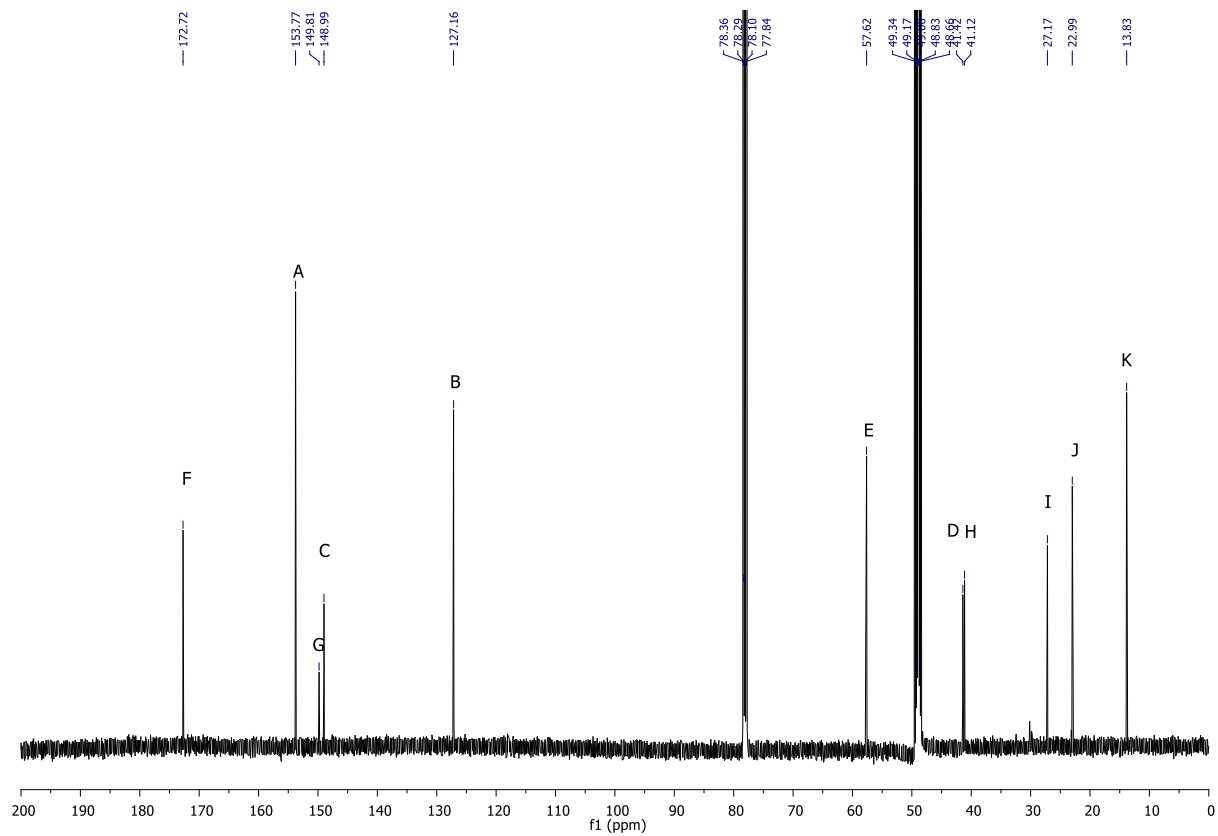A single crystal was grown by a slow evaporation of DCM/MeOH solution at room temperature.

CCDC: Pending.

^{1}H NMR

8.67
8.65
7.54
7.12
7.10
4.59
3.31
3.31
3.31
3.28
2.05
2.03
2.01
1.31
1.29
1.27
1.26
1.23
1.21
0.88
0.87
0.85
0.06

A
B
D
K
J+I
H

4.00 4.15 4.22 4.23 11.34 6.86

10.0 9.5 9.0 8.5 8.0 7.5 7.0 6.5 6.0 5.5 5.0 4.5 4.0 3.5 3.0 2.5 2.0 1.5 1.0 0.5 0.0
f1 (ppm)

^{13}C NMR

172.72
153.77
149.81
148.99
127.16
78.36
78.29
78.10
77.84
57.62
49.34
49.17
48.83
48.66
41.42
41.12
27.17
22.99
13.83

A
F
B
C
G
E
D H
I
J
K

200 190 180 170 160 150 140 130 120 110 100 90 80 70 60 50 40 30 20 10 0
f1 (ppm)

257

Preparation of **Pd(4B1)$_2$Cl$_2$•iPP$_2$**

Step-wise

4B1 (5.64 mg, 20.5 μmol) and Pd(ACN)$_2$Cl$_2$ (2.68 mg, 10.3 μmol), were added to a Y-NMR tube as solids. CDCl$_3$ (0.6 mL) was added and the mixture was sonicated and shaken for 5 minutes, which resulted in precipitation. Then, **iPP** (4.16 mg, 20.0 μmol) as a solid and additional CDCl$_3$ (0.4 mL) were added and the mixture was shaken until everything dissolved.

From **4B1•iPP**

4B1 (5.70 mg, 20.7 μmol) and **iPP** (4.38 mg, 20.9 μmol) were added to a Y-NMR tube as solids and CDCl$_3$ (0.6 mL) was added. Afterwards, Pd(ACN)$_2$Cl$_2$ (2.72 mg, 10.5 μmol) as a solid and additional CDCl$_3$ (0.4 mL) were added and the mixture was shaken until everything dissolved.

One-pot

Pd(ACN)$_2$Cl$_2$ (2.80 mg, 10.8 μmol), **4B1** (5.98 mg, 21.7 μmol) **iPP** (4.57 mg, 21.9 μmol) were added to a Y-NMR tube as solids. CDCl$_3$ (1 mL) was added and the mixture was sonicated and shaken for 10 minutes until everything dissolved.

Preparation of **Pd(4B1)$_2$Cl$_2$•iBP$_2$**

Pd(ACN)$_2$Cl$_2$ (2.99 mg, 11.5 μmol), **4B1** (5.98 mg, 23.1 μmol) **iBP** (5.45 mg, 23.0 μmol) were added to a Y-NMR tube as solids. CDCl$_3$ (1 mL) was added and the mixture was sonicated and shaken for 10 minutes until everything dissolved.
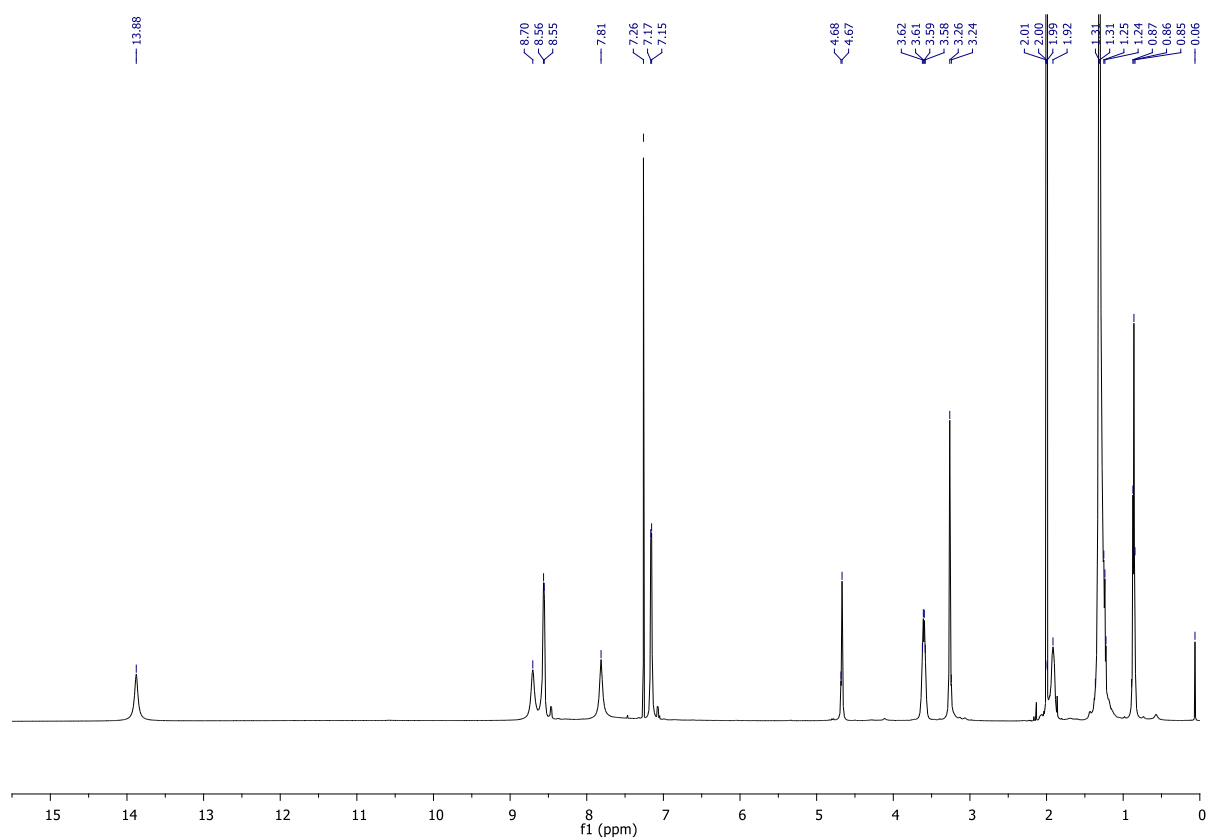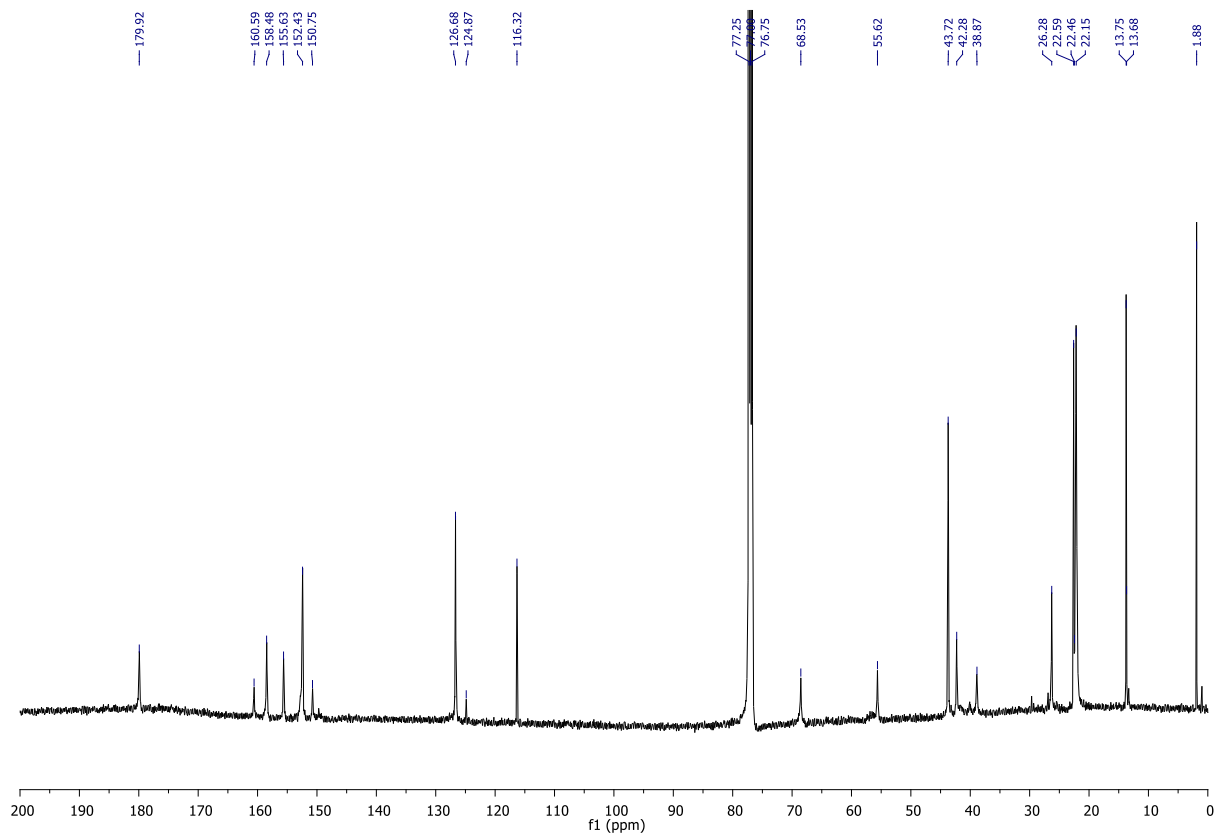
The 10-fold diluted sample was prepared as follow:

0.1 mL of the above final solution was transferred to a NMR tube and additional CDCl$_3$ (0.9 mL) was added and the mixture was well mixed.
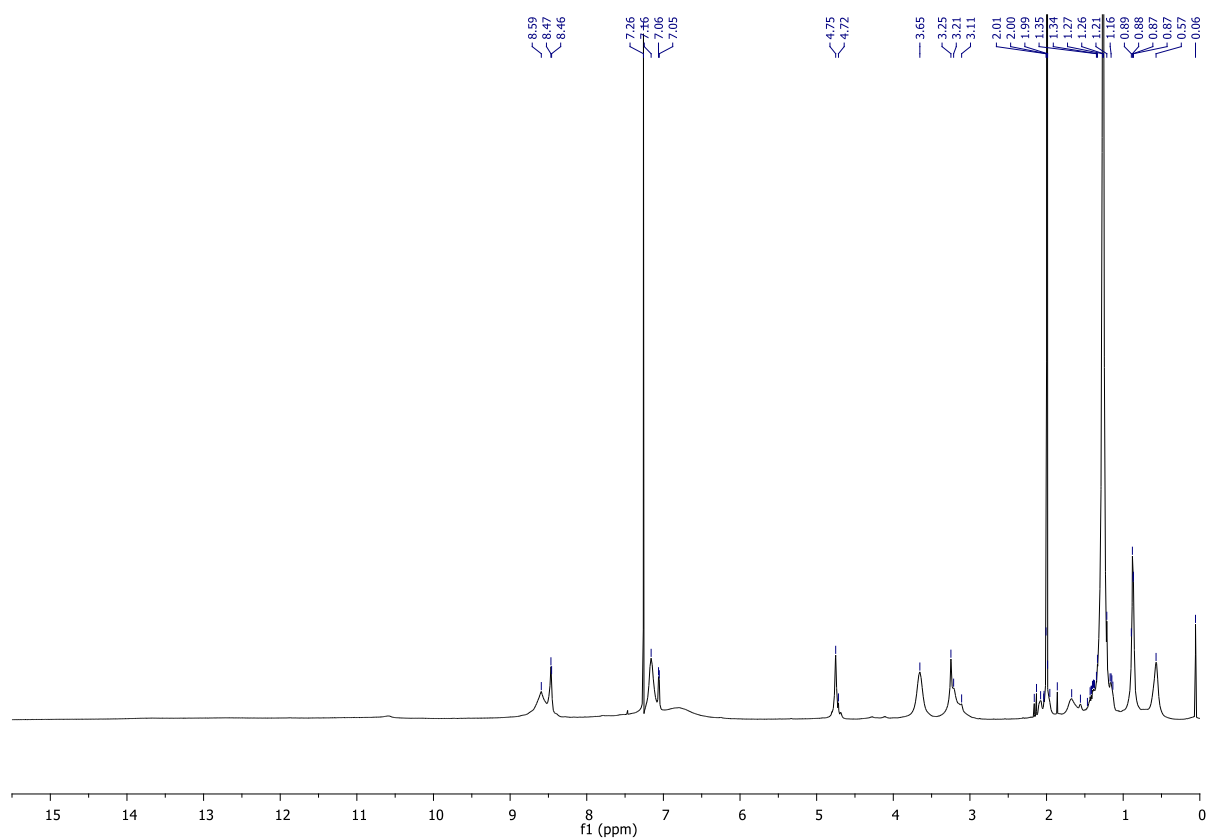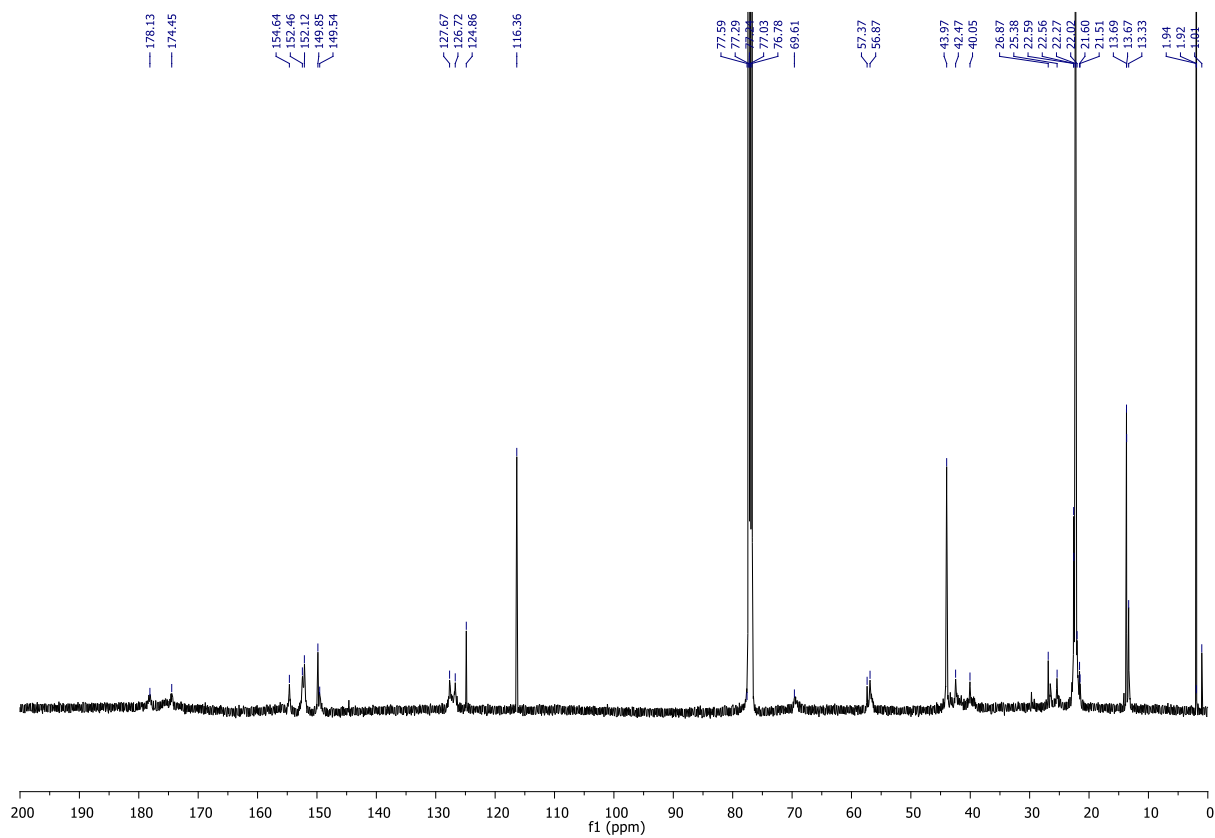
Pd(4B1)$_2$Cl$_2$•iBP$_2$: ^{1}H NMR

Pd(4B1)$_2$Cl$_2$•iBP$_2$: ^{13}C NMR

decomposed Pd(4B1)$_2$Cl$_2$•iBP$_2$: ^{1}H NMR

decomposed Pd(4B1)$_2$Cl$_2$•iBP$_2$: ^{13}C NMR

261

Preparation of **Pd(4B1)$_2$Cl$_2$•tBT$_2$**
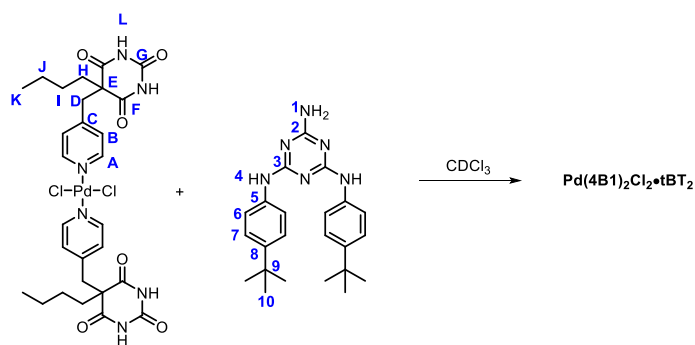
To a Y-NMR tube, **Pd(4B1)$_2$Cl$_2$** (6.04 mg, 8.31 μmol) and **tBT** (6.53 mg, 16.7 μmol) were added as solids. CDCl$_3$ (0.8 mL) was added and the mixture was sonicated and shaken for 5 minutes until everything dissolved.

^{1}H NMR (CDCl$_3$, 400 MHz, 298 K): δ 14.33 (s, 12H, L), 9.41 (s, 24H, 4), 8.65 (d, J = 6.5 Hz, 12H, A), 7.62 (d, J = 8.5 Hz, 24H, 6), 7.37 (d, J = 8.5 Hz, 24H, 7), 7.18 (d, J = 6.5 Hz, 12H, B), 6.96 (s, 24H, 1), 3.41 (s, 12H, D), 2.19 − 2.08 (m, 12H, H), 1.38 (s, 108H, 10), 1.3 (m, 24H, J + I, covered by *tert*-butyl), 0.89 (t, J = 7.0 Hz, 18H, K).

^{13}C NMR (CDCl$_3$, 126 MHz, 298 K): δ 174.7 (F), 165.7 (2), 163.4 (3), 153.3 (A), 153.0 (G), 148.0 (C), 146.3 (8), 136.3 (5), 126.7 (B), 125.3 (7), 121.8 (6), 57.2 (E), 42.7 (H), 38.5 (D), 34.3 (9), 31.5 (10), 26.2 (I), 22.4 (J), 13.6 (K).

¹H NMR

¹³C NMR

263
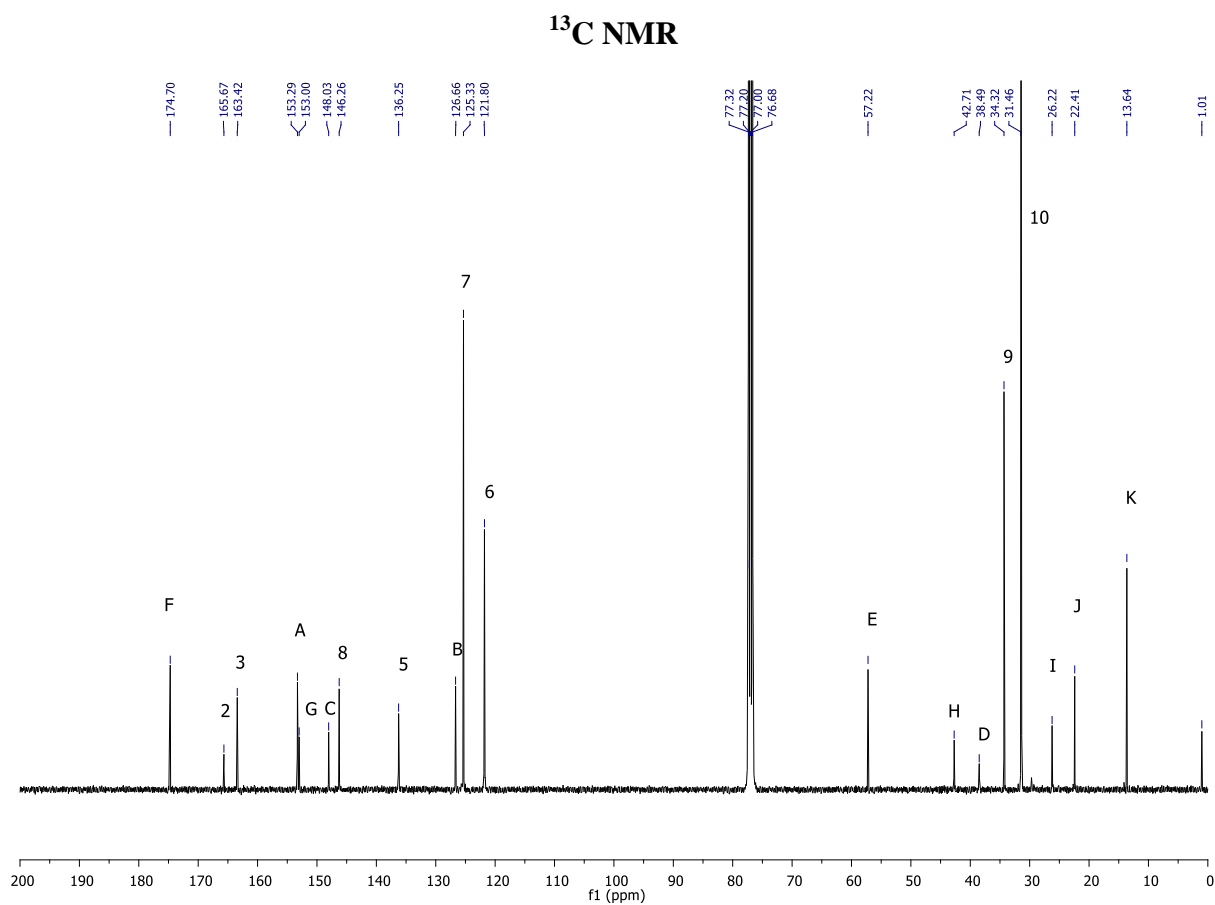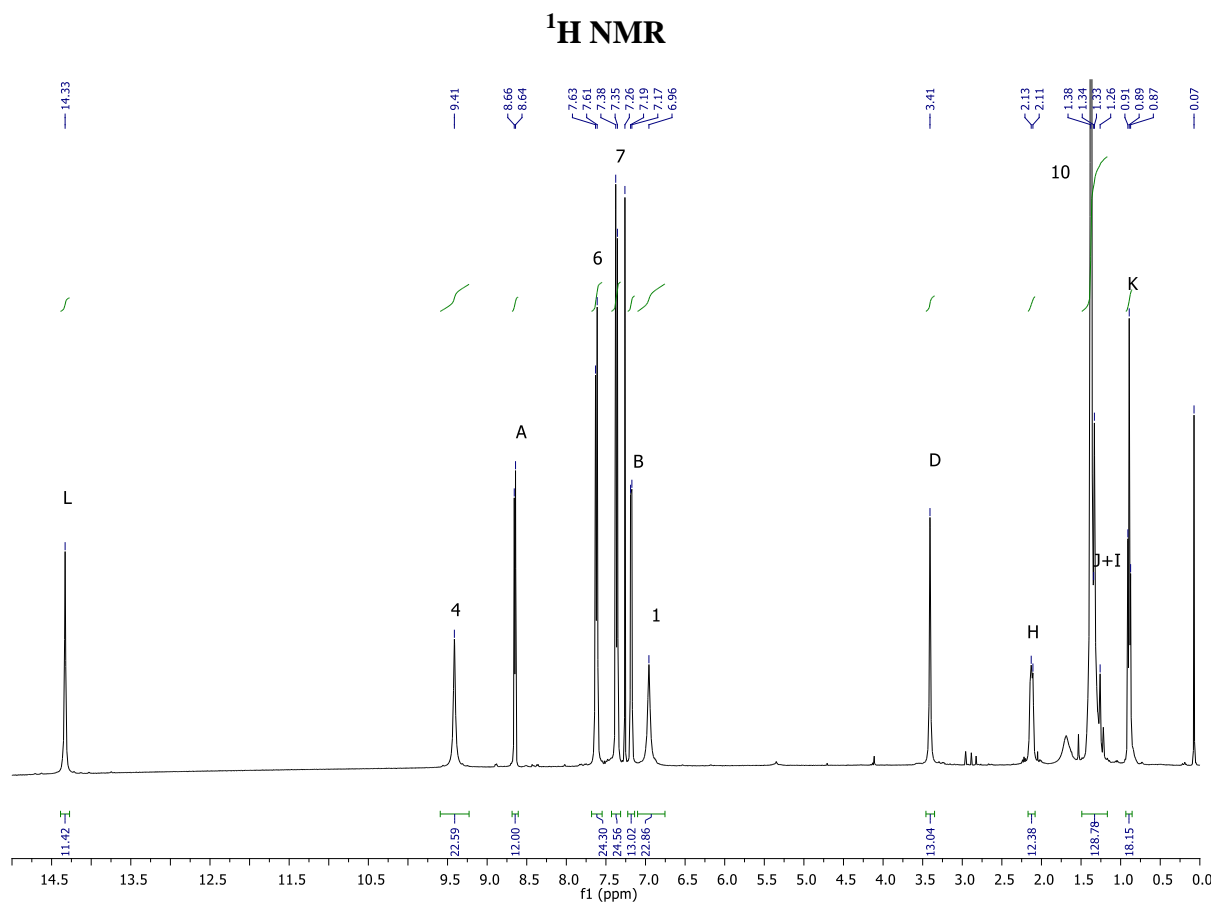
6.9.4. Stimuli-responsive behaviour

Response to PPh₃

•Addition of PPh₃

To a Y-NMR tube, **Pd(4B1)₂Cl₂** (7.37 mg, 10.1 µmol) and **tBT** (6.53 mg, 20.1 µmol) were added as solids. CDCl₃ (0.7 mL) was added and the mixture was sonicated and shaken for 5 minutes until everything dissolved. PPh₃ (5.32 mg, 20.3 µmol) as a solid and additional CDCl₃ (0.1 mL) were added and the mixture was shaken for 2 minutes.

•Recovery of the cage after addition of PPh₃

To the solution above, Pd(ACN)₂Cl₂ (2.66 mg, 10.3 µmol) as a solid and additional CDCl₃ (0.2 mL) were added and the mixture was shaken for 5 minutes.

•Separate experiment to prove the formation of mixed pyridine–phosphine–palladium species

To a Y-NMR tube, Pd(ACN)₂Cl₂ (5.68 mg, 21.6 µmol), **4B1** (6.06 mg, 22.0 µmol) and PPh₃ (5.74 mg, 21.9 µmol) were added as solids. CDCl₃ (0.8 mL) was added and the mixture was sonicated and shaken for 2 minutes until everything dissolved.

Response to dppf

•Addition of **dppf**

To a Y-NMR tube, **Pd(4B1)₂Cl₂** (6.05 mg, 8.3 µmol) and **tBT** (6.67 mg, 17.1 µmol) were added as solids. CDCl₃ (0.7 mL) was added and the mixture was sonicated and shaken for 5 minutes until everything dissolved. **dppf** (4.60 mg, 8.3 µmol) as a solid and additional CDCl₃ (0.1 mL) were added and the mixture was shaken for 2 minutes.

•Recovery of the cage after addition of **dppf**

To the solution above, Pd(ACN)₂Cl₂ (2.16 mg, 8.3 µmol) as a solid and additional CDCl₃ (0.1 mL) were added and the mixture was shaken for 5 minutes.

Response to cya

Pd(4B1)₂Cl₂ (10.55 mg, 14.5 µmol), **tBT** (11.46 mg, 29.3 µmol) and CDCl₃ (2 mL) were sonicated for 10 minutes. 0.1 mL of this solution was then transferred to a Y-NMR tube and additional CDCl₃ (0.5 mL) was added. To this solution, **cya** (0.30 mg, 1.5 µmol) was added as a solid.

6.10. References

(1)   Mateu, M. G. *Arch. Biochem. Biophys.* **2013**, *531*, 65-79.

(2)   Ballester, P.; Fujita, M.; Rebek, J. *Chem. Soc. Rev.* **2015**, *44*, 392-393.

(3)   Fujita, M.; Tominaga, M.; Hori, A.; Therrien, B. *Acc. Chem. Res.* **2005**, *38*, 369-378.

(4)   Seidel, S. R.; Stang, P. J. *Acc. Chem. Res.* **2002**, *35*, 972-983.

(5)   Han, M.; Engelhard, D. M.; Clever, G. H. *Chem. Soc. Rev.* **2014**, *43*, 1848-1860.

(6)   Nitschke, J. R. *Acc. Chem. Res.* **2007**, *40*, 103-112.

(7)   Smulders, M. M. J.; Riddell, I. A.; Browne, C.; Nitschke, J. R. *Chem. Soc. Rev.* **2013**, *42*, 1728-1754.

(8)   Conn, M. M.; Rebek, J. *Chem. Rev.* **1997**, *97*, 1647-1668.

(9)   McConnell, A. J.; Wood, C. S.; Neelakandan, P. P.; Nitschke, J. R. *Chem. Rev.* **2015**, *115*, 7729-7793.

(10)   Rebek, J. J. *Chem. Commun.* **2000**, 637-643.

(11)   Fujita, D.; Ueda, Y.; Sato, S.; Mizuno, N.; Kumasaka, T.; Fujita, M. *Nature* **2016**, *540*, 563.

(12)   Galindo, M. A.; Amantia, D.; Clegg, W.; Harrington, R. W.; Eyre, R. J.; Goss, J. P.; Briddon, P. R.; McFarlane, W.; Houlton, A. *Chem. Commun.* **2009**, 2833-2835.

(13)   Kokan, Z.; Kovačević, B.; Štefanić, Z.; Tzvetkova, P.; Kirin, S. I. *Chem. Commun.* **2018**, *54*, 2094-2097.

(14)   Alam, M. A.; Nethaji, M.; Ray, M. *Angew. Chem. Int. Ed.* **2003**, *42*, 1940-1942.

(15)   Whitesides, G. M.; Simanek, E. E.; Mathias, J. P.; Seto, C. T.; Chin, D.; Mammen, M.; Gordon, D. M. *Acc. Chem. Res.* **1995**, *28*, 37-44.

(16)   Timmerman, P.; Prins, Leonard J. *Eur. J. Org. Chem.* **2001**, *2001*, 3191-3205.

(17)   Kerckhoffs, J. M. C. A.; van Leeuwen, F. W. B.; Spek, A. L.; Kooijman, H.; Crego-Calama, M.; Reinhoudt, D. N. *Angew. Chem. Int. Ed.* **2003**, *42*, 5717-5722.

(18)   Simanek, E. E.; Isaacs, L.; Li, X.; Wang, C. C. C.; Whitesides, G. M. *J. Org. Chem.* **1997**, *62*, 8994-9000.

(19)   Huck, W. T. S.; Hulst, R.; Timmerman, P.; van Veggel, F. C. J. M.; Reinhoudt, D. N. *Angew. Chem. Int. Ed.* **1997**, *36*, 1006-1008.

(20)   Zhang, F.; Therrien, B. *Eur. J. Inorg. Chem.* **2017**, *2017*, 3214-3221.

(21)   Zhang, F.; Therrien, B. *Eur. J. Inorg. Chem.* **2018**, *2018*, 2399-2407.

(22)   Shao, X.-B.; Jiang, X.-K.; Zhu, S.-Z.; Li, Z.-T. *Tetrahedron* **2004**, *60*, 9155-9162.

(23)   Chakrabarty, R.; Mukherjee, P. S.; Stang, P. J. *Chem. Rev.* **2011**, *111*, 6810-6918.

(24)   Kukushkin, Y. N. *Platinum Metals Rev.* **1991**, *35*, 28-31.

(25)   Santolini, V.; Tribello, G. A.; Jelfs, K. E. *Chem. Commun.* **2015**, *51*, 15542-15545.

(26)   Mathias, J. P.; Simanek, E. E.; Zerkowski, J. A.; Seto, C. T.; Whitesides, G. M. *J. Am. Chem. Soc.* **1994**, *116*, 4316-4325.

(27)   Timmerman, P.; Weidmann, J.-L.; Jolliffe, K. A.; Prins, L. J.; Reinhoudt, D. N.; Shinkai, S.; Frish, L.; Cohen, Y. *J. Chem. Soc., Perkin Trans. 2* **2000**, 2077-2089.

(28)   Montoro-García, C.; Camacho-García, J.; López-Pérez, A. M.; Bilbao, N.; Romero-Pérez, S.; Mayoral, M. J.; González-Rodríguez, D. *Angew. Chem. Int. Ed.* **2015**, *54*, 6780-6784.

(29)   Mammen, M.; Simanek, E. E.; Whitesides, G. M. *J. Am. Chem. Soc.* **1996**, *118*, 12614-12623.

(30)   Timmerman, P.; Jolliffe, K. A.; Crego Calama, M.; Weidmann, J.-L.; Prins, L. J.; Cardullo, F.; Snellink-Ruël, B. H. M.; Fokkens, R. H.; Nibbering, N. M. M.; Shinkai, S.; Reinhoudt, D. N. *Chem. Eur. J.* **2000**, *6*, 4104-4115.

(31)   Li, J.; Fu, H.; Hu, P.; Zhang, Z.; Li, X.; Cheng, Y. *Chem. Eur. J.* **2012**, *18*, 13941-13944.

(32)   Frisch, M. J.; Trucks, G. W.; Schlegel, H. B.; Scuseria, G. E.; Robb, M. A.; Cheeseman, J. R.; Scalmani, G.; Barone, V.; Mennucci, B.; Petersson, G. A.; Nakatsuji, H.; Caricato, M.; Li, X.; Hratchian, H. P.; Izmaylov, A. F.; Bloino, J.; Zheng, G.; Sonnenberg, J. L.; Hada, M.; Ehara, M.; Toyota, K.; Fukuda, R.; Hasegawa, J.; Ishida, M.; Nakajima, T.; Honda, Y.; Kitao, O.; Nakai, H.; Vreven, T.; Montgomery Jr., J. A.; Peralta, J. E.; Ogliaro, F.; Bearpark, M. J.; Heyd, J.; Brothers, E. N.; Kudin, K. N.; Staroverov, V. N.; Kobayashi, R.; Normand, J.; Raghavachari, K.; Rendell, A. P.; Burant, J. C.; Iyengar, S. S.; Tomasi, J.; Cossi, M.; Rega, N.; Millam, N. J.; Klene, M.; Knox, J. E.; Cross, J. B.; Bakken, V.; Adamo, C.; Jaramillo, J.; Gomperts, R.; Stratmann, R. E.; Yazyev, O.; Austin, A. J.; Cammi, R.; Pomelli, C.; Ochterski, J. W.; Martin, R. L.; Morokuma, K.; Zakrzewski, V. G.; Voth, G. A.; Salvador, P.; Dannenberg, J. J.; Dapprich, S.; Daniels, A. D.; Farkas, Ö.; Foresman, J. B.; Ortiz, J. V.; Cioslowski, J.; Fox, D. J.; Gaussian, Inc.: Wallingford, CT, USA, 2009.

(33)   Irikura, T.; Abe, Y.; Okamura, K.; Higo, K.; Maeda, A.; Morinaga, F.; Shirai, G.; Hatae, S. *J. Med. Chem.* **1970**, *13*, 1081-1089.

Acknowledgments

(in ± order of appearance)

Main actors

my brother	for all your great help before, through and after my Ph.D.
Chris (Hunter)	for giving me the chance to do a Ph.D. in your group and to learn a lot about science and life in general thanks to you and the people in your group
Filip	for all your help, stories, wine, dinners, …
Mark W	for always being super nice
Ana	for being extremely enthusiastic and stealing almost all my tweezers (does it correlate…?!)
Mike	for always being super nice
Leonard Prins and others	for setting up and organization of MULTI-APP
Pavle	for being my lab older brother and a great support
Jorge	for the friendship and all the great time together
Harry Anderson and his group	for your help and nice time in Oxford
Stefan	for breakfasts, talks and mostly fun
Yudi	for being Yudí
Elena	for never giving up
Istvan	for your scientific drive
Gloria	for completely unexpected support

Supporting acts

Giulia, Geneva, Carlos, Cristina N, James, Elkin, Maria, Nicola, Jon, Mark D, Flore, Sarah, Loren, Peter, Ennio, Judith, Carlo, Luca, Vytautas, Marion, Maria Chiara, Lucia, Lucas, Francesco

it was (mostly) fun to have you around!

Funding

$$^{\ddagger}\text{EM} = 1.25$$

(from Equation 1.5)